NASA TR R-6

NATIONAL AERONAUTICS AND SPACE ADMINISTRATION

TECHNICAL REPORT
R-6

EXPERIMENTAL AND THEORETICAL STUDIES OF AXISYMMETRIC FREE JETS

By EUGENE S. LOVE, CARL E. GRIGSBY, LOUISE P. LEE, and MILDRED J. WOODLING

1959

For sale by the Superintendent of Documents, U.S. Government Printing Office, Washington 25, D.C. Yearly subscription, $10; foreign, $13; single copy price varies according to size - - - - - - - - - Price $2.25

ERRATA

NASA Technical Report R-6

By Eugene S. Love, Carl E. Grigsby, Louise P. Lee,
and Mildred J. Woodling
1959

Page 108:

In the key at the top of figure 20, a solid line should appear opposite the word "Experiment."

Page 116:

The line keys above figure 23 should be corrected as follows:

———————— Characteristic boundary

- - - - - - - - Circular-arc, satisfying δ_j and $\left(\frac{y}{r_j}\right)_{max}$

——— - ——— Circular-arc, $\frac{\rho_o}{d_j}$

Issued 2-10-61

NASA - Langley Field, Va.

TECHNICAL REPORT
R-6

EXPERIMENTAL AND THEORETICAL STUDIES OF AXISYMMETRIC FREE JETS

By EUGENE S. LOVE, CARL E. GRIGSBY, LOUISE P. LEE, and MILDRED J. WOODLING

Langley Research Center
Langley Field, Va.

CONTENTS

TECHNICAL REPORT R-6

EXPERIMENTAL AND THEORETICAL STUDIES OF AXISYMMETRIC FREE JETS [1]

By Eugene S. Love, Carl E. Grigsby, Louise P. Lee, and Mildred J. Woodling

SUMMARY

Some experimental and theoretical studies have been made of axisymmetric free jets exhausting from sonic and supersonic nozzles into still air and into supersonic streams with a view toward problems associated with propulsive jets and the investigation of these problems.

For jets exhausting into still air, consideration is given to the effects of jet Mach number, nozzle divergence angle, and jet static-pressure ratio upon jet structure, jet wavelength, and the shape and curvature of the jet boundary. Studies of the effects of the ratio of specific heats of the jets are included as are observations pertaining to jet noise and jet simulation.

For jets exhausting into supersonic streams, an attempt has been made to present primarily theoretical curves of the type that may be useful in evaluating certain jet interference effects and in formulating experimental studies. The primary variables considered are jet Mach number, free-stream Mach number, jet static-pressure ratio, ratio of specific heats of the jet, nozzle exit angle, and boattail angle. The simulation problem and the case of a hypothetical hypersonic vehicle are examined. A few experimental observations are included.

INTRODUCTION

The increasing interest in the problems associated with the use of propulsive jets has in recent years brought about the compilation of several summaries and bibliographies on jets and related subjects—for example, reference 1, chapter IX of reference 2, and the summary studies of reference 3. From these compilations and from numerous investigations of more recent origin the need for further study of free jets is evident.

This report presents results of some experimental and theoretical studies of axisymmetric free jets exhausting from sonic and supersonic nozzles into still air and into supersonic streams with a view toward problems associated with propulsive jets and the investigation of these problems. The first part of this report deals with jets exhausting into still air; the second part deals with jets exhausting into supersonic streams.

SYMBOLS

A	exit area of nozzle
A_t	throat area of nozzle
$\frac{A_t}{A}$	nozzle area ratio, $M\left(\frac{\frac{\gamma+1}{2}}{1+\frac{\gamma-1}{2}M^2}\right)^{\frac{\gamma+1}{2(\gamma-1)}}$
$C_{p,b}$	base pressure coefficient, $\frac{p_b-p_\infty}{q_\infty}$
d_b	diameter of base
d_j	diameter of jet exit
l	distance along jet axis from plane of jet exit to shock intersection or to Riemann wave
M	Mach number

[1] Supersedes declassified NACA Research Memorandum L54L31 by Eugene S. Love and Carl E. Grigsby, 1955; NACA Research Memorandum L55J14 by Eugene S. Love, 1956; NACA Research Memorandum L56G18 by Eugene S. Love, Mildred J. Woodling, and Louise P. Lee, 1956; and NACA Technical Note 4195 by Eugene S. Love and Louise P. Lee, 1958.

M_j jet Mach number at nozzle exit; for a divergent nozzle, value at nozzle lip

M_∞ free-stream Mach number; Mach number on boattail surface; Mach number ahead of exit shock or ahead of shock at beginning of separation

P Busemann's pressure number

p static pressure

p_b base pressure

p_j jet static pressure at nozzle exit; for a divergent nozzle, value at nozzle lip

p_t stagnation pressure

p_∞ ambient or free-stream static pressure; also pressure ahead of exit shock or ahead of shock at beginning of separation

p'_∞ static pressure of external flow existing immediately ahead of jet exit and behind exit shock, or pressure in region of separated flow immediately ahead of jet exit

$\frac{p}{p_t}=\left(1+\frac{\gamma-1}{2}M^2\right)^{-\frac{\gamma}{\gamma-1}}$

q dynamic pressure

R distance from source

r_j radius of jet exit

S diameter of Riemann wave

V local velocity

V_l limiting velocity

$\frac{V}{V_l}$ limiting velocity ratio, $\sqrt{1-\left(\frac{p}{p_t}\right)^{\frac{\gamma-1}{\gamma}}}$

w primary wavelength of jet

x distance from plane of nozzle exit measured parallel to jet axis

y perpendicular distance from jet axis

β boattail angle immediately ahead of jet exit

$\beta_j=\sqrt{M_j^2-1}$

γ ratio of specific heats

δ two-dimensional turning angle through an oblique shock

δ_j angle between jet axis and tangent to free jet boundary at nozzle lip, that is, initial inclination of mixing boundary (positive when it diverges with respect to jet axis)

θ direction of velocity with respect to jet axis

θ_N exit angle of nozzle with respect to jet axis, or divergence angle of conical nozzle

λ Kawamura parameter, $\frac{1}{\gamma}(\sin\mu\cos\mu)$

μ Mach angle

ν Prandtl-Meyer turning angle from sonic velocity

ξ shock inclination

ρ average radius of curvature of jet boundary

ρ_o initial radius of curvature of jet boundary (at $x=0$)

Subscripts:

j jet, unless more explicitly defined, generally value at nozzle surface immediately ahead of jet exit (j', local value in free jet at jet boundary)

max maximum value

N nozzle

∞ free stream or value at boattail surface immediately ahead of jet exit (∞', local value at jet boundary)

I. JETS EXHAUSTING INTO STILL AIR

INTRODUCTION

Although considerable effort has been devoted to the study of free jets exhausting from sonic and supersonic nozzles into still air, there is still much room for additional study of the effects of the variables involved. Consider the general sketch in figure 1(a) of the first portion of the nonviscous boundary of a jet exhausting supersonically into still air. The well-known characteristic curvature of the boundary is obviously brought about by the requirement that the pressure along the boundary must be constant. The shape and curvature of the inviscid boundary is dependent upon a number of variables; these include ratio of specific heats of the jet, Mach number of the jet, divergence angle of the nozzle or nozzle geometry in general, and jet pressure ratio.[2] However, the variation in shape and curvature of the boundary with most of these variables has not been studied except for a few specific and unrelated cases. It

[2] Throughout this paper the term "jet pressure ratio" refers to the ratio of jet static pressure at exit to the ambient or free-stream static pressure. Static-pressure ratio has been used in preference to total-pressure ratio since the latter rarely permits presentation of data in a form that facilitates comparison, does not lend to the elimination of variables, and thereby often obscures conclusions.

might be stated that figure 1(a) is an illustrative sketch of a sonic jet operating at some jet pressure ratio greater than 1 as shown in figure 1(b), a conically divergent nozzle operating at a jet pressure ratio less than 1 as shown in figure 1(c), or a number of combinations of variables involved. The jet structure, that is, type of shock or expansion pattern within the jet, would of course be dependent upon these combinations. The exact structure and boundary shape would be unique for a particular combination; but without further study of the effects of the variables involved, the implication of the uniqueness in terms of large or small differences in structure and boundary shape is not clear.

The broadening in recent years of the probable fields of application of free-jet characteristics has pointed up, in particular, the need for additional knowledge of boundary shape and curvature. In all such applications the condition of constant pressure along the jet boundary must be a permissible assumption in order to use the characteristics of the jet exhausting into still air. Perhaps the most direct application is in assessing the deflections of the external stream caused by a propulsive jet exhausting from an aircraft flying at low or moderate subsonic speeds as illustrated in figure 2(a). Another application is in the performance of ejectors when the interaction between the primary jet and the subsonic secondary air flow may be assumed to take place at or near constant pressure (fig. 2(b)). A third probable application is in the prediction of the pressure on the base annulus separating an exhausting jet from an external supersonic stream when the ratio of jet exit diameter to base diameter is not very near 1 (fig. 2(c)). In reference 4 a method based upon the peak-pressure-rise coefficient associated with the separation of a turbulent boundary layer was proposed for predicting the pressure on a two-dimensional base separating supersonic streams having different Mach numbers and pressures. Reference 5, which includes a detailed description of this method, presents results for a two-dimensional base that show this prediction to be satisfactory. For the base annulus, the two-dimensional approach would be expected to be satisfactory when the ratio of the jet exit diameter to the base diameter approaches 1 since the curvatures of the free boundaries involved are essentially eliminated. This is illustrated in figure 3 which presents the two-dimensional prediction and three experimental curves obtained by Edgar M. Cortright, Jr., and Fred D. Kochendorfer of the Lewis Flight Propulsion Laboratory. The two-dimensional approach can obviously not be applied to thick base annuli such as illustrated in figure 2(c) without a knowledge of the curvature of the boundaries, the most important of which is the curvature of the jet boundary.

Besides the interest in jet-boundary curvature, there is also interest in the effects of various parameters upon jet structure. Both combustion problems and problems dealing with jet noise and screech have been shown to be associated with jet structure, in particular with the existence and location of shocks within the free jet. A conference on jet noise held in England led to the conclusion that theories of jet noise cannot make much further headway without a better knowledge of jet structure.

This part of the paper will present the results of theoretical and experimental studies of jets exhausting into still air and will cover the effects of jet Mach number, nozzle divergence angle, and jet pressure ratio upon such characteristics as jet structure, wavelength, and shape and curvature of the jet boundary. Studies of the effects of the ratio of specific heats of the jet will be included as will be observations pertaining to noise and to simulation of one jet by another.

EXPERIMENTAL STUDIES

Models.—Twenty-one steel nozzles of identical external geometry were constructed for the experimental studies. A sketch of a typical divergent nozzle installed in the air supply conduit is shown in figure 4. The throat of each nozzle was rounded and smoothly faired, and the interior surface was polished from the start of the convergence to the exit. Sixteen nozzles of the conically divergent type were designed with exit (i.e., divergence) angles θ_N of 5°, 10°, 15°, and 20° for each of four exit Mach numbers M_j of 1.50, 2.00, 2.50, and 3.00. Four nozzles were designed for these same Mach numbers to give $\theta_N=0°$ at the exit. These four nozzles had contoured profiles that gave essentially isentropic flow throughout and parallel flow at the jet exit. One convergent nozzle was designed for an exit Mach number of 1.00 ($\theta_N=0°$). All nozzles were designed with $\gamma_j=1.400$.

Tests.—The experimental study was confined to schlieren observations. Insofar as possible the tests were conducted with the mixing-zone apparatus (see ref. 5) of the Langley 9-Inch Tunnel Section in order to take advantage of its double-image schlieren apparatus which permits both vertical and horizontal density gradients to be recorded separately on a single negative for one spark of the source light. In these tests the nozzles exhausted to atmospheric pressure. Because the tests employed the dry-air supply system of the Langley 9-inch supersonic tunnel which is limited to a maximum storage pressure of 500 lb/sq in., supplementary tests for the higher jet Mach numbers and jet pressure ratios were made in the Langley 9-inch supersonic tunnel in which the tunnel was employed as a vacuum box. The schlieren system of the tunnel was used in these tests; consequently, the observations were confined to vertical density gradients. For the sonic nozzle only, tests were also made with the tunnel schlieren system but with the nozzle exhausting to atmospheric pressure.

For each nozzle, several preliminary tests were made during which the behavior of the jet with varying pressure was observed but not photographed. Based on these tests the intervals were selected for schlieren photography. The stagnation pressure of the jet was measured by means of a mercury manometer or precision high pressure gages. Calibration tests with the sonic nozzle indicated that the pressure tap shown in figure 4 gave an accurate measurement of stagnation pressure.

Since numerous tests have shown that the pressures in conically divergent nozzles of the type employed in these tests follow closely the theoretical expansion (see ref. 6, for example) and because the nozzles were machined within 0.001 inch of the specified dimensions, no Mach number calibration was made of the conically divergent nozzles. Calibrations were made, however, of the four supersonic nozzles having $\theta_N=0°$. With the exception of the $M_j=2.50$ nozzle which was within ± 0.01 of its design value, these nozzles had a maximum Mach number deviation of about -0.04 from their design value. This deviation was felt to be minor for the purpose of these tests, and the static pressure on the nozzle wall just prior to exit p_j was calculated for all nozzles from the measured total pressure and the design Mach number.

RESULTS AND DISCUSSION

Schlieren photographs.—Since it was impractical to include all photographs taken in this investigation, only a few representative ones are presented. Figure 5 presents an illustrative sequence of double-image schlieren photographs wherein for a given value of p_j/p_∞ the upper left-hand image accentuates the vertical gradients (horizontal knife edge) and the other image accentuates the horizontal gradients (vertical knife edge).

Jet structure.—The gaseous jet exhausting supersonically into still air has been known to exhibit a periodic or chain-like structure at least as early as the observations of Rayleigh in 1879. (See summary of studies presented in ref. 3.) Rayleigh and many others (see section VI, ref. 1, for example) have offered explanations for and elaborated upon the manner in which the expansion and compression waves within a free jet form the periodic patterns at low jet pressure ratios and the not so periodic patterns at high jet pressure ratios. References 7 to 14 include both theoretically and experimentally deduced explanations for the occurrence of shock waves in jets and their change and growth with varying jet pressure ratio. Reference 10 includes excellent photographs by the Riemann mirror method of the variation in the structure and shock pattern with jet pressure ratio for an axisymmetric jet exhausting sonically. Reference 11 includes characteristic calculations for a two-dimensional jet ($M_j=1.50$, $\theta_N=0°$) that show clearly how the coalescence of the characteristic lines creates shock waves within the jet; with increasing jet pressure ratio, these shocks are shown to grow in strength and extent from a faintly discernible compression to intersecting shocks and then to strong shocks of large curvature requiring a Mach reflection. Other calculations of the shock formation that deal in particular with point of origin, factors favoring shock formation, and focusing effects for two-dimensional and axisymmetric jets are given in references 12 to 14. For axisymmetric jets the same general phenomena occur as in two-dimensional jets but at lower jet pressure ratios. In order to distinguish the circular, dish-shaped, normal shocks that occur in axisymmetric jets

from the analogous normal shocks associated with the Mach reflection in two-dimensional jets, the former are, in jet studies, often referred to as "Riemann waves." (Rigorously, the term is applicable to all normal shocks.) This term is adopted herein.

Qualitatively, the present studies showed no significant deviations in jet structure or shock patterns that would not be expected. Although a few previous studies include photographs which show that the shock phenomenon begins with a Riemann wave pattern, decays to an intersecting shock pattern, thence to no shocks, and then goes through the well-known reverse variation, one is likely to gain the incorrect impression from most past studies that the initial variation begins with the shock-free condition. The decay in shock strength is confined to a narrow range of jet pressure ratios immediately after starting and was observed to take place at all Mach numbers of these tests. Once the Riemann wave reappears the general shock pattern does not change with increasing jet pressure ratio. These variations will become more apparent in the quantitative results to be presented in the sections that follow.

Primary wavelength.—Since the observations of Rayleigh mentioned in the previous section, several theories have been advanced for the prediction of the primary wavelength or the length of the first periodic segment of the free jet and the secondary wavelength or the length of succeeding periodic segments, which are known to differ from the primary, particularly at the higher jet pressure ratios. The predominant interest has been centered upon primary wavelength. An excellent summary of jet wavelength theories in existence prior to 1949 is given in reference 3. Since that time Wada (ref. 7), Pack (ref. 8), and others have added to earlier contributions or have advanced new theories. Little has been added, however, to the old and very limited experimental information, most of which is confined to sonic exits and jet pressure ratios of the order of 3 or less.

Figure 6 presents a double-image schlieren photograph in which the primary wavelength w is designated. Figure 7 presents the nondimensional primary wavelength w/d_j as a function of jet pressure ratio p_j/p_∞ for all values of M_j and θ_N of these tests. It will be noted that there are more experimental data for $M_j=1.00$ than for the other Mach numbers at any given value of θ_N. The data for $M_j=1.00$ represent values measured from shadowgraphs, schlierens, repeat tests, and photographic enlargements of different sizes. Within the accuracy of the measurements there was no apparent difference in the data from these sources. In general, however, the accuracy of all measurements from any source tended to decrease slightly as p_j/p_∞ increased as a result of the decrease in definition caused by the increased turbulence surrounding the jet. As expected, at a constant value of p_j/p_∞ and θ_N, the experimental results show that the wavelength increases with increasing Mach number. In addition, divergence angle θ_N is indicated to be of secondary importance within the range of 0° to 20°. There tends to be a decrease in wavelength with increasing θ_N; the exceptions to this behavior might be attributable to experimental accuracy. From a consideration of the increasing shock losses within the jet (increasing entropy) that occur with increasing θ_N, one might expect increasing θ_N to cause the wavelength to decrease.

Two of the methods which have had some success in predicting the wavelength were used to calculate the upper and lower curves shown in figure 7(a) for $M_j=1.00$. The method of Pack (ref. 8) has been advanced as being applicable to all Mach numbers. It is based upon linear theory (and therefore subject to the restrictions of linear theory) and is a correction of Prandtl's formula which is known to be in error. (See refs. 3 and 8, for example.) The older method of Hartmann and Lazarus (ref. 9) is proposed for sonic jets only. This latter method is semiempirical, as are most of the others except those of Prandtl and Pack mentioned above, and it involves constants determined from experimental results for low values of p_j/p_∞. It is not surprising, therefore, to find that both methods are not satisfactory except at very low jet pressure ratios. (See fig. 7(a).) Because of the inadequacy at $M_j=1.00$, no comparison has been made between the method of Pack and the present results for higher Mach numbers; furthermore, the assumption of the method that w/d_j is independent of M_j and a function only of the ratio of jet stagnation pressure to the ambient pressure can be shown from these results to be insufficient.

On the basis of these experimental data an attempt was made to derive a seimempirical relation for the variation of w/d_j with p_j/p_∞ that would apply to $\theta_N=0°$ and varying M_j. For axisymmetric jets the only inviscid solution to w/d_j not requiring the combined treatment of a characteristics net and the shock equations is for $\theta_N=0°$ and $p_j/p_\infty=1$. For this condition only, the solution is the same for two-dimensional and axisymmetric jets and is $w/d_j=\beta_j$, where $\beta_j=\sqrt{M_j^2-1}$. Outside of satisfying this condition and the equally simple requirement that the value of p_j/p_∞ for $w/d_j=0$ must lie to the right of the theoretical value of p_j/p_∞ for starting (denoted by arrows on the abscissas in the figures and is equal to 1 for $M_j=1.00$), the solutions were derived so as to fit best the results for $M_j=1.00$ in preference to the other Mach numbers. Consequently, the abrupt change in the variation of w/d_j with p_j/p_∞ that accompanies the reappearance of the Riemann wave within the jet occurs at about $p_j/p_\infty=2$. This well-known feature has been treated for sonic jets by many authors (refs. 7 to 11, for example). The two semiempirical relations thus derived are as follows:

For $\frac{p_j}{p_\infty}\lessapprox 2$

$$\frac{w}{d_j}=1.55\sqrt{M_j^2\left(\frac{p_j}{p_\infty}\right)-1}-0.55\beta_j \qquad (1)$$

and for $\frac{p_j}{p_\infty}\gtrapprox 2$

$$\frac{w}{d_j}=1.52\left(\frac{p_j}{p_\infty}\right)^{0.437}+1.55(\sqrt{2M_j^2-1}-1)-0.55\beta_j +0.5\left[\frac{1}{1.55}\sqrt{\left(\frac{p_j}{p_\infty}-2\right)\beta_j}-1\right] \qquad (2)$$

The curves given by these equations are shown by the solid lines in figure 7. It is interesting to note that the theoretical inviscid value of β_j for $p_j/p_\infty=1$ is in close agreement with the experimental results for all values of M_j. Although equations (1) and (2) generally give a fair prediction of the experimental results, there is a tendency at the higher jet pressure ratios to overpredict the wavelength at low Mach numbers and to underpredict at the higher Mach numbers. An inherent shortcoming of these equations lies in the assumption that the abrupt change in the variation of wavelength with jet pressure ratio occurs at $p_j/p_\infty=2$, regardless of the value of M_j. In the following section this region of abrupt change will be shown to vary with M_j.

Existence, location, and diameter of Riemann wave.—Figure 8 presents the nondimensional distance from the plane of the jet exit, measured along the jet axis, to the focal point of the intersecting shock pattern or to the Riemann wave. This distance l/d_j increases with increasing p_j/p_∞ and M_j as would be expected. There is a tendency for l/d_j to decrease as θ_N increases for a given value of p_j/p_∞.

Figure 9 presents the nondimensional diameter of the Riemann wave S/d_j. As p_j/p_∞ increases from the condition of a Riemann wave at the jet exit (starting value of p_j/p_∞ is indicated in the figures), the Riemann wave first decreases in diameter and for the lower values of θ_N gives way to an intersecting shock pattern ($S/d_j=0$). With further increases in p_j/p_∞ the Riemann wave increases in diameter, or reappears if a condition of $S/d_j=0$ had been reached, and continues to increase.

From the curves of figure 9, the range of M_j and p_j/p_∞ in which no Riemann wave occurs can be found for a given value of θ_N. The results are shown in figure 10 for $\theta_N=0°$, 5°, and 10°; there were insufficient data to determine the boundaries of the regions for $\theta_N=15°$ and 20° but it is evident from figure 9 that for these values of θ_N the Riemann wave is always present for $M_j=2.00$, 2.50, and 3.00. From figure 10, the effect of increasing θ_N is to reduce significantly the range in which no Riemann wave occurs. The true effect of M_j is not clear in the lower range of M_j; but, for the higher range of M_j, increasing M_j increases the range of p_j/p_∞ in which no Riemann wave occurs. There is little doubt that an intersecting shock pattern is restricted to low jet pressure ratios. The dashed line to the left of the left-hand boundary for $\theta_N=0°$ represents the theoretical starting condition (the Riemann wave at the jet exit) and is in fair agreement with the trend of the experimentally determined boundary.

The abrupt change in the variation of wavelength with jet pressure ratio that is associated with the reappearance of the Riemann wave mentioned in the previous section was assumed to take

place at $p_j/p_\infty \approx 2$ for $M_j=1(\theta_N=0°)$ in developing equations (1) and (2). Although figure 10 shows this to be a fair assumption for $M_j=1$, it also indicates indirectly that this region of abrupt change varies with M_j.

Initial inclination of jet boundary.—When a jet exhausts from a nozzle into still air, it will undergo a two-dimensional expansion or compression exactly at the nozzle lip dependent only upon whether $p_j/p_\infty>1$ or $p_j/p_\infty<1$, respectively. The degree of the expansion (or compression) is a function of p_j/p_∞, M_j, and γ_j. For the pressure ratios of predominant interest ($p_j/p_\infty>1$), it is instructive to consider the magnitude of the expansion or the initial inclination of the jet boundary that may occur. The calculated initial inclinations for $\theta_N=0°$ and $\gamma_j=1.400$ are presented in figure 11. For $\theta_N\neq 0°$, the value of θ_N is added to the value of δ_j given by the curves. With the large power sources (rockets) now available and under development, the curves of figure 11 imply that the likelihood of encountering initial inclinations near 90° may not be too remote. If extreme pressure ratios are encountered, large initial inclinations will occur as is indicated by the schlieren photograph in figure 12.

In view of the number of current applications of sonic exits, the variation of δ_j with p_j/p_∞ for $M_j=1.00$ is presented to enlarged scale in figure 13 for $\gamma_j=1.115$, 1.400, and 1.667. The upper and lower values of γ_j represent the probable limits encountered in both practical and experimental applications. The effects of decreasing γ_j is to increase δ_j, and this effect increases as p_j/p_∞ increases.

Preliminary calculations by method of characteristics.—Several preliminary calculations were made by the method of characteristics to obtain the shape of the jet boundary and to observe the formation of the jet structure. The salient features of these calculations are given in appendix A. The characteristic nets are shown in figure 14. Points on the boundary in the region of "foldback" have been circled for clarity.

Figure 14(a) presents the nets at $p_j/p_\infty=2$, 10, and 20 for $M_j=1.01$, $\theta_N=0°$, and $\gamma_j=1.400$ (essentially a sonic jet). The errors in the nets for $M_j=1.01$ are discussed in appendix A and, by mere observation, are obviously not negligible in the vicinity of the jet axis. The boundary shape and the general coalescence of the characteristics, also discussed in appendix A, are nevertheless sufficiently accurate to be of value. At $p_j/p_\infty=2$, there is no indicated presence of a shock within the jet, but, if the calculations were carried further, an intersection of like characteristics would probably be realized before the axis is crossed. At $p_j/p_\infty=10$ and 20, the manner in which the intersection of like characteristics defines the presence of a shock within the jet is clearly illustrated.

Figure 14(b) presents the nets for $M_j=1.50$ to 3.00, $\theta_N=0°$, and $\gamma_j=1.400$ at $p_j/p_\infty=2$. No shocks are indicated to be present within the jets, but, again, the tendency toward intersection of like characteristics would suggest that shocks might appear for all values of M_j before the axis is reached if the calculations were continued.

Figures 14(c) to 14(f) present the nets for $M_j=1.50$ to 3.00, $\theta_N=0°$, and $\gamma_j=1.400$ at $p_j/p_\infty=10$ and 20. All nets indicate that shocks have formed within the jets.

Figure (14g) presents nets for $M_j=2.00$ at $p_j/p_\infty=1$ to show the effects of nozzle divergence angle θ_N for $\gamma_j=1.400$ and to show the effects of γ_j for $\theta_N=10°$. The indicated effect of increasing θ_N is to promote the formation of shocks within the jet. The effect of increasing γ_j from 1.200 to 1.400 to 1.667 is also to favor the formation of shocks within the jet. This effect of γ_j is somewhat understandable from consideration of the effect that γ has in simple two-dimensional flow upon the maximum turning angle of the flow δ_{max} through an attached shock. This effect, as well as the effect upon the inclination ξ_{max} of the associated shock, is shown in figure 15. Since at Mach numbers other than 1 the value of δ_{max} decreases noticeably with increasing γ, it is logical to expect that at high values of γ compressions of the same family introduced in a flow will, for a given amount of turning, result in an earlier appearance of a shock brought about by the coalescence of these compressions than might occur at lower values of γ.

Although the effect of M_j and p_j/p_∞ (for $\theta_N=0°$ and $\gamma_j=1.400$) upon the shape of the boundary may be observed directly from the nets, this effect is perhaps better illustrated in figure 16 which reproduces these boundaries and compares them directly. Figure 17 shows the effect of M_j and p_j/p_∞ upon the maximum height $(y/r_j)_{max}$ reached

by the boundary and upon its location as estimated by replacing the straight line segments with a smoothly faired curve through the calculated boundary points in the vicinity of $(y/r_j)_{max}$, at the same time being guided by the sign and value of θ for the last two points on the boundary. Since the values for $M_j=2.50$ and $p_j/p_\infty=20$ did not agree closely with the trend established by the other boundaries, there is apparently some error in the calculations of this net and therefore the data for this condition were not used in preparing figure 17. The curves of figure 17(a) appear to indicate that beyond $M_j\approx3$ the increase of $(y/r_j)_{max}$ with M_j will be small at all values of p_j/p_∞. The theoretical curve for $p_j/p_\infty=1$ is obviously a straight line for which $(y/r_j)_{max}$ is always 1. The curves of figure 17(b) indicate that as M_j is increased the location of $(y/r_j)_{max}$ continues to increase at all values of p_j/p_∞. The theoretical curve for $p_j/p_\infty\rightarrow1$ is half the wavelength and, therefore, equal to β_j.

Figure 18(a) affords a direct comparison of the boundary shapes for varying θ_N. The increase in $(y/r_j)_{max}$ with θ_N is observed to be almost linear within this range of θ_N (0° to 20°). Figure 18(b) presents a comparison of the boundaries for a particular condition of varying γ_j. The ordinate scale has been enlarged in this figure for clarity; consequently, the local slopes of the boundaries are considerably exaggerated, as can be seen by referring to figure 18(a) ($\theta_N=10°$). From figure 18(b), the effect of increasing γ_j is very small and amounts essentially to a slight increase in y/r_j as x/r_j increases. As $x/r_j\rightarrow0$, it is obvious that the effect of γ_j will vanish. Emphasis should be placed on the fact that the particular set of initial conditions used in this study of the effects of γ_j were selected to explore what might be considered a sort of "minimum effect" of γ_j on the boundary: namely, $p_j/p_\infty=1$ and $M_j=2$. (In the vicinity of $M_j=2$, the ratio of static pressure to stagnation pressure p/p_t is relatively insensitive to γ.) Consequently, the effects of γ_j on the boundary for other initial conditions may be considerably different from those shown here, as will be illustrated directly in a subsequent section of this report.

The following section on boundary curvature will show indirectly that the theoretical nonviscous boundaries calculated by the method of characteristics agree satisfactorily with the observed experimental boundaries in the schlieren photographs. This favorable agreement has been noted previously at low jet pressure ratios (3 or less), for example, in reference 15. The fact that this agreement extends to high jet pressure ratios is particularly encouraging from the viewpoint of continuous calculation by machine in that the use of foldback as employed herein permits continuous calculation off the axis. No schlieren photograph was available for $p_j/p_\infty=20$, the highest jet pressure ratio of these calculations; however, a comparison between the calculated results at $p_j/p_\infty=20$ and the experimental results at $p_j/p_\infty=21.9$ for $M_j=1.50$, $\theta_N=0°$, and $\gamma_j=1.400$ presented in figure 19 shows sufficient agreement to indicate that the procedure is satisfactory for predicting both boundary and shock. The difference between the experimental and predicted shock and boundary is in the direction to be accounted for by the difference between the theoretical and experimental values of p_j/p_∞. In addition, mixing tends to diffuse the experimental boundary prior to reaching the theoretically predicted maximum diameter of the jet.

Average and initial curvature of jet boundary.—An examination of the schlieren photographs of these tests indicated that the shape of the portion of the jet boundary from its start to the vicinity of the maximum diameter of the jet (within the primary wavelength) could be fairly well approximated by a circular arc. The radius of this circular arc will, for convenience, be called the average radius of curvature ρ of the jet boundary and, as shown in the sketch in figure 20(a), is laid off along the normal to the free jet boundary at the exit. Figures 20 and 21 present the results of the experimental measurements in nondimensional form ρ/d_j as a function of p_j/p_∞ to show the effects of M_j and θ_N, respectively. Random examples of the applicability of these experimental curves are given in figure 22 which presents the circular-arc boundary and the normal to the free boundary at the exit superposed on schlieren photographs.

An assessment was also made of the similarity of the boundaries given by the characteristics calculations to a circular-arc boundary passing through $(y/r_j)_{max}$ given by the characteristic solution and having its radius laid off along the normal to the free jet boundary at the exit. The

circular-arc boundary thus defined was in all cases found to be a good approximation of the characteristic boundary; a typical example of this may be seen in figure 23. The values of ρ/d_j obtained from the characteristic solutions in this manner are designated by the symbols in figures 20(a) and 21(b). These values show surprisingly close agreement with the experimental curves even at low jet pressure ratios where the experimental results would be expected to be less accurate. For $M_j=2.50$ and $p_j/p_\infty=20$ (fig. 20(a)) a corrected and an uncorrected value are shown; the suspected error in the characteristic solution for these conditions was mentioned earlier. The corrected value for $(y/r_j)_{max}$ was determined from the faired curve of figure 17(a).

In reference 14, Johannesen and Meyer have obtained a solution for the initial curvature of the axially symmetric free jet boundary (i.e., the curvature at $x=0$). This solution and its method of application are summarized in appendix B. The nondimensional initial radius of curvature ρ_o/d_j given by the Johannesen-Meyer solution has been calculated for the same jet conditions for which characteristic nets were calculated ($\gamma_j=1.400$ only). The results are shown in figure 24. In reference 2, the value of ρ_o/d_j obtained from the Johannesen-Meyer solution was shown to be in close agreement with the value of ρ_o/d_j obtained from the polynomial satisfying the first few points on a boundary calculated by the method of characteristics. It is of interest for practical application, however, to obtain an idea of how far along the characteristic boundary the circular-arc boundary given by ρ_o/d_j will continue to hold good. Comparisons showed that, except at values of $p_j/p_\infty<2$, the boundary given by ρ_o/d_j is applicable only to regions in close proximity to the exit as illustrated in figure 23. The effects of M_j, p_j/p_∞, and θ_N upon the extent of applicability of ρ_o/d_j are indicated indirectly in figure 25 where the ratio ρ/ρ_o is presented. The values of ρ in this ratio are those corresponding to the circular-arc boundary through $(y/r_j)_{max}$. For $\theta_N>0°$ the extent of applicability is severely restricted even at $p_j/p_\infty=1$.

From the above results and the fitting of polynomials to the characteristic points on the boundary as in reference 2, the exact boundary is seen to decrease in curvature in proceeding outward along the boundary from the exit toward the maximum diameter of the jet.

Additional calculations of boundaries by method of characteristics for conically divergent nozzles.—Some time after the completion of the preliminary studies of boundaries discussed in the preceding sections of this report, an extensive program was undertaken to calculate the boundaries of supersonic axisymmetric jets exhausting from conically divergent nozzles. The purpose of this program was to extend the preliminary calculations of boundaries for conically divergent nozzles to a wide range of variables and to present these boundaries in a form convenient for practical use. Other than the calculations by Johannesen (ref. 2), reproduced in figure 26 herein, practically no information could be found for $p_j/p_\infty>1$. In the present program, a total of 2,960 boundaries were calculated. These calculations were made for all combinations of the following variables: values of M_j of 1.5, 2.0, 2.5, and 3.0; values of γ_j of 1.115, 1.200, 1.300, 1.400, and 1.667; values of θ_N of 5°, 10°, 15°, and 20°; and values of p_j/p_∞ of 1 to 10 in increments of 0.25. Some comments on the method and accuracy of these calculations are given in the first part of appendix C. The boundaries obtained and some observations drawn from them are presented in the next four sections of this report.

Presentation of boundaries for conically divergent nozzles.—The 2,960 calculated boundaries are presented in figures 27 to 30. Each group of boundaries corresponds to a variation of p_j/p_∞ from 1 to 10 for a particular combination of M_j, θ_N, and γ_j. The solid boundaries denote changes in p_j/p_∞ of 1; the three dashed boundaries between the solid boundaries correspond to changes in p_j/p_∞ of 0.25 and are also calculated, not interpolated, boundaries. For clarity, a number of the groups have insets covering the lower range of x/r_j in which the ordinate y/r_j is shown to twice scale. The order of presentation of these groups of boundaries is as follows:

Figure	M_j
27	1.5
28	2.0
29	2.5
30	3.0

For figures 27 to 30, parts (a), (b), (c), and (d) are for θ_N of 5°, 10°, 15°, and 20°, respectively. Each figure subdivision contains five groups of boundaries corresponding to the five values of γ_j, and these five groups are presented in the order of ascending values of γ_j, that is, from $\gamma_j=1.115$ to 1.667.

Effects of variables for conically divergent nozzles.—The effect of increasing jet pressure ratio p_j/p_∞ is obvious from figures 27 to 30. Effects of the other variables at a jet pressure ratio of 5 (arbitrarily chosen) are shown in figure 31. At this jet pressure ratio, the effect of increasing M_j (fig. 31(a)) is to decrease the initial inclination of the boundary, to increase the maximum diameter of the free jet, and to move the maximum diameter farther away from the plane of the jet exit. The effect of increasing γ_j (fig. 31(b)) is to decrease the initial inclination of the boundary, to decrease the maximum diameter of the free jet, and to move the maximum diameter closer to the plane of the jet exit. The effect of increasing θ_N (fig. 31(c)) is to increase the initial inclination of the boundary, to increase the maximum diameter of the free jet, and to move the maximum diameter closer to the plane of the jet exit. A brief examination at other values of p_j/p_∞ indicated that these effects are apparently typical of all pressure ratios; however, there might be exceptions which were not disclosed by this examination.

Simulation of one jet boundary by another for conically divergent nozzles.—In figures 27 to 31 it may be noted that the initial inclination of the boundary varies with every variable. When jet boundaries are simulated, the initial inclination is, perhaps, the most important property to be duplicated. For this reason and because of the problems confronted in jet simulation, it is of interest to examine the degree of boundary simulation that may be achieved by simulating initial inclination only through a variation of p_j/p_∞ only and, in addition, to determine whether complete simulation is possible through a variation of all variables.

In order to aid in the selection of values of p_j/p_∞ that give the same initial inclination δ_j, figure 32 has been prepared which gives the variation with p_j/p_∞ of the initial inclination for a jet exhausting from a nozzle having zero divergence angle ($\theta_N=0°$). The value of δ_j at any finite value of θ_N is simply the sum of θ_N plus the value of δ_j for $\theta_N=0°$.

Figure 33 presents some typical examples of boundary simulation. Random examples of the boundary simulation that may be expected by duplication of δ_j only are shown in figures 33(a) to 33(d). In these examples M_j and θ_N remain constant and p_j/p_∞ is allowed to vary so that the value of δ_j is the same for both values of γ_j. (See fig. 32.) In essence, a boundary given by an air jet ($\gamma_j=1.400$, dashed boundary) is compared with a boundary given by a jet of another gas or by a heated air jet ($\gamma_j<1.400$). The results indicate that the differences between the boundaries thus simulated can be attributed primarily to differences in γ_j and that differences in γ_j of the order of 0.1 or less create negligibly small differences in the boundary when the initial inclination is duplicated. This observation also implies that, insofar as the effects of boundary shape are concerned, air jets heated to the order of 2,500° R or lower can be satisfactorily simulated by cold air jets by altering the pressure ratio to give the same initial inclination.

Figure 33(e) gives an example which illustrates the point that, in general, the boundary of most jets may be satisfactorily simulated by an air jet by allowing a freedom of choice of the variables for the air jet. Extremely large values of p_j/p_∞ would, of course, produce exceptions. (It will be noted that the boundaries of figure 33 are, as before, given in the discontinuous-slope form. This form tends to exaggerate the differences in the lower range of x/r_j, particularly at the first calculated point on the boundary.)

Figure 33(f) illustrates that, for a particular value of γ_j, there are a number of combinations of M_j, θ_N, and p_j/p_∞ that produce essentially the same boundary.

Interpolation and extrapolation of calculated boundaries for conically divergent nozzles.—Interpolation and cross-plotting can be used to obtain a reliable boundary within the range of any of the variables covered by these calculations. The reliability of a boundary necessitating the use of extrapolation to cover a variable the magnitude of which places it outside the range of these calculations is not readily apparent. A cursory

examination, however, gave the following indications. Extrapolations of p_j/p_∞ should not exceed values of p_j/p_∞ of about 14 and probably less; extrapolations below $p_j/p_\infty=1$ are not recommended. Extrapolations to $\theta_N=0°$ are of particular interest since the nozzle having parallel flow at the exit is often encountered. This extrapolation may be made with good results as indicated by the example given in figure 34 where an extrapolated boundary for $\theta_N=0°$ is shown to be in good agreement with the calculated boundary for $\theta_N=0°$. Extrapolations to values of θ_N in excess of about 25° are not recommended. Extrapolations of M_j to $M_j=1$ ($\theta_N=0°$) appear permissible, and extrapolations to $M_j\approx3.5$ or slightly higher appear within reason. The necessity for extrapolations of γ_j beyond the range of these calculations appears remote; however, should the need arise, the extrapolation could in all likelihood be made with confidence.

Calculations of initial portion of boundary for large values of p_j/p_∞.—After the programing and completion of the calculations for the conically divergent nozzles covered in the preceding sections, the need for information on boundaries at large jet pressure ratios stimulated an additional set of calculations. This need arises from the fact that in the proposed trajectories of most rocket-propelled hypersonic vehicles, the rocket propulsion unit will remain in operation long enough for the exhausting jet to encounter the very low pressures of high altitudes. When this condition occurs, p_j/p_∞ becomes very large, and as a result the free jet expands greatly. More will be said about this in the second part of this report. With the hope of gaining some familiarity with the size of the free jet, a number of calculations were made at large values of p_j/p_∞ of the initial portion of the boundary for the case of $\theta_N=15°$ and $M_j=2.5$. Some comments on the procedure and accuracy of these calculations are given in the second part of appendix C.

The choice of jet pressure ratios for the calculations was influenced to some extent by an examination of the variation of the initial inclination of the jet boundary δ_j with jet pressure ratio p_j/p_∞. This variation is presented in figure 35 for the values of the ratio of specific heats γ_j used in the boundary calculations. It is interesting to note first the magnitude of δ_j for the nozzle with a sonic exit ($M_j=1$ and $\theta_N=0°$), since at very large values of p_j/p_∞ this nozzle gives the largest possible values of δ_j (fig. 35). By comparison with these values for the sonic nozzle, the values of δ_j for the nozzle of this study ($M_j=2.5$ and $\theta_N=15°$) are significantly lower at very large values of p_j/p_∞, and this difference increases with decreasing γ_j. Of course at very low values of p_j/p_∞ any conically divergent nozzle will produce a value of δ_j greater than that for the sonic nozzle, since $\delta_j=\theta_N$ at $p_j/p_\infty=1$; in this instance, $\delta_j=\theta_N=15°$ for $p_j/p_\infty=1$.

The curves of figure 35 illustrate that, at large values of p_j/p_∞, conically divergent nozzles likely to be encountered in practical applications may produce large initial inclinations of the boundary. For rockets where γ_j is of the order of 1.2 and sometimes less, this initial inclination may easily exceed 90°, and at extremely large pressure ratios it is not inconceivable for the free-jet flow at the jet boundary to be directed initially almost 180° opposite to the direction of flow along the jet axis. Thus, to the general objective of gaining some familiarity with the size and shape of free jets at large pressure ratios was added the objective of calculating some boundaries for which δ_j exceeded 90°. In addition, boundaries for which a comparison would show the effects of γ_j for similar values of p_j/p_∞ and for similar values of δ_j were desired.

The curves of figure 35 show that the variation of δ_j with p_j/p_∞ is such that at p_j/p_∞ of the order of 10^8 for $\gamma_j=1.667$ and of the order of 10^{22} for $\gamma_j=1.200$, the initial inclination has approached closely its maximum value. Consequently, if calculations could be made near these values of p_j/p_∞ (or higher), they should be sufficient for most purposes to represent jets operating in the range from these values to infinity. Unfortunately, although solutions were attempted for these extremely large pressure ratios, satisfactory results could not be obtained without successive refinements and reprograming of the automatic calculations. For these reasons and because of other commitments of the electronic calculators, the boundaries at these extremely large pressure ratios were not obtained. The values of p_j/p_∞, and the corresponding values of δ_j, for which

boundaries were calculated for the case of $M_j=2.5$ and $\theta_N=15°$ are given in the following table:

p_j/p_∞	δ_i, deg
$\gamma_j=1.677$	
59.92	48.55
569.2	57.72
1,618	60.74
$\gamma_j=1.400$	
81.94	60.02
1,346	75.59
2,692	78.53
$\gamma_j=1.200$	
76.58	70.99
1,303	94.51
9,776	107.6
41,820	115.6

The exact values of p_j/p_∞ used in the calculations were determined by the arbitrary condition of terminating the expansion at one of the manually calculated characteristic lines from the center of expansion.

Presentation of boundaries for large values of p_j/p_∞.—The calculated boundaries, together with the indicated position of the shock formed within the jet (given by the intersection and coalescence of characteristic lines of the same family), are shown separately for each value of p_j/p_∞ in figures 36 to 38. For $\gamma_j=1.200$, only the boundary for $p_j/p_\infty=76.58$ is presented separately (fig. 38) inasmuch as only a minute segment of the jet shock was indicated in the inadvertently shortened calculation at $p_j/p_\infty=1{,}303$, and none was indicated at the higher values of p_j/p_∞. All boundaries for $\gamma_j=1.200$, as well as for the other values of γ_j, are presented together subsequently. At first glance the results for all values of γ_j give indication of a tendency for the jet shock to be eliminated with increasing p_j/p_∞ at very large values of p_j/p_∞. It would, however, appear debatable as to whether a valid indication of such an occurrence could be substantiated by these calculations, inasmuch as an inherent stretching of the meshes within the characteristic net occurs with increasing p_j/p_∞ in these calculations. Nevertheless, it may be reasoned that for $p_j/p_\infty=\infty$ the velocity at the boundary is radial; that is, the characteristic line is in the same direction as the direction of the velocity, which is the direction of the boundary. Consequently, the only coalescence of the characteristic lines occurs on the boundary. It follows that if at $p_j/p_\infty=\infty$ this coalescence were indicative of a shock, the shock would coincide with the boundary. However, since a shock must have a pressure rise across it, the existence of a shock on the boundary represents an impossible condition for $p_j/p_\infty=\infty$ in view of the following: First, a pressure rise cannot exist across a boundary and, second, the existence of a pressure rise at $p_j/p_\infty=\infty$ would imply that, in expanding to a vacuum, the jet flow has expanded to a pressure less than a vacuum and thus requires a pressure rise at the boundary to restore its pressure to the ambient vacuum, a clearly impossible situation. Thus, it appears that at $p_j/p_\infty=\infty$ no jet shock will be present, and an indication of the elimination of the jet shock with increasing p_j/p_∞ may, at large values of p_j/p_∞, be reasonable.

In figure 39, the boundaries for each value of γ_j are presented compositely to show more readily the effect of increasing p_j/p_∞. Included are boundaries for $p_j/p_\infty=1$ and 10 calculated previously. The enormous size that the free jet may attain at large pressure ratios is readily apparent, particularly for $\gamma_j=1.200$ (fig. 39(c)) when the initial inclination of the boundary approaches and exceeds the vertical.

Effect of γ_j for large values of p_j/p_∞.—Some idea of the effect of γ_j at large pressure ratios upon the shape of the boundary for essentially equal values of p_j/p_∞ may be obtained by comparing the boundary for $\gamma_j=1.400$ with that for $\gamma_j=1.200$ at $p_j/p_\infty\approx1{,}300$ as shown in figure 40. (Actually, for $\gamma_j=1.400$, $p_j/p_\infty=1{,}346$ and for $\gamma_j=1.200$, $p_j/p_\infty=1{,}303$.) In spite of the short extent of the boundary for $\gamma_j=1.200$, the comparison shown in figure 40 is sufficient to point up the large effect that γ_j has upon boundary shape at large pressure ratios.

At low values of p_j/p_∞ (of the order of 10), the procedure of simulating a jet of one value of γ_j by a jet of another value of γ_j through duplication of δ_j by changing the value of p_j/p_∞ is a useful

artifice in many experimental investigations. An examination of the adequacy of this procedure at large pressure ratios is of interest. Figure 41 compares the boundary of the jet for $\gamma_j=1.400$ with the boundary for $\gamma_j=1.667$, both having an initial inclination of about 60° but widely different values of p_j/p_∞. (The value of p_j/p_∞ for $\gamma_j=1.667$ is about 20 times that for $\gamma_j=1.400$.) The comparison is sufficient to show that this procedure does not yield accurate simulation of the boundary at large pressure ratios but might give first-order simulation of interference effects. For extremely large values of p_j/p_∞ the curves of figure 35 serve to demonstrate that simulation by this procedure is impossible for the case of primary interest, namely, simulation of a jet having a low value of γ_j by a jet having a higher value of γ_j (with significant differences in γ_j, of course, say of the order of 0.1 or more). For example, it is impossible for the jet of this study with $\gamma_j=1.400$ to duplicate the value of δ_j for the jet with $\gamma_j=1.200$ when the latter jet operates at values of p_j/p_∞ greater than about 10^4.

Observations on jet breakdown and jet noise.—Within the range of observation of the schlieren photographs, the jet structure for all Mach numbers and divergence angles of these tests deflected from the axis of the jet in an alternate fashion as the jet flow proceeded downstream. Example of this phenomenon for $M_j=1.00$ may be seen in figure 42. Examination of the present results indicates that the jet breaks down into a vortex pattern closely resembling a vortex street and thereafter into a region of wide turbulent diffusion. This alternate deflection of the jet structure has been noted by Alan Powell of England in his studies of the relation between the degeneration of the jet, jet structure, and sound generation.

The type of sound wave that may be observed to be generated by the jet was found to be dependent to some degree on the sensitivity setting of the optical system. For example, the strong, lower frequency sound waves which Powell has described as having their effective source in the region of disintegration of the jet structure, and which are emitted in the upstream direction in an alternate manner according to the degeneration of jet structure, may be seen in the photographs in figure 43 but not in the photographs in figure 42 for which the schlieren system had a less sensitive setting. Examination of photographs taken at a higher sensitivity setting showed that both the structure of the jet and the sound waves moving upstream tend to become masked by turbulence surrounding the jet and, to some extent, by sound waves having their apparent source in the vicinity of the jet exit and at the initial appearance of turbulence on the free jet boundary not far from the exit. These observations seem to indicate that the apparent discrepancies that exist in some previous studies of sound waves associated with jets may be due in part to the different sensitivities of the optical systems employed. The degeneration of the jet is, of course, a highly unstable phenomenon and the apparent source of the sound waves associated with degeneration of jet structure varies accordingly.

At jet pressure ratios slightly greater than that for the reappearance of the Riemann wave, the sound waves associated with the degeneration of jet structure become less prominent, and the sound waves associated with smaller scale turbulence and the initial appearance of turbulence on the jet boundary are observed to predominate. Examples of this are given in figure 44. The photographs of figure 44 also show that as p_j/p_∞ increases, the more intense sound waves coming from the vicinity of the jet exit tend to be more directional and to lie roughly in a band inclined some 30° to 45° with respect to the jet axis in the downstream direction. This directional trend is in agreement with sound measurements from several investigations. (See ref. 16, for example.)

From the concept of eddy convection velocity as advanced by Lighthill (ref. 17), one would expect the sound waves in the ambient air to change in shape as M_j increases. This concept has its basis in the idea that small vortices or eddies at the jet boundary are convected downstream at some velocity and, as Lighthill states, "not in the sense that eddies are convected downstream with this velocity unchanged, but that they alter slowest when viewed by an observer moving with this velocity." If this convection velocity is supersonic with respect to the ambient air, oblique compression waves must be expected to arise from the jet boundary and to be inclined in the manner of a nose shock or bow wave common to an object in

502683 O—59——2

supersonic flight. Consequently, the shape of the sound (or compression) waves emitted in a downstream direction may be expected to change from spherical (subsonic eddy convection velocity) to conical (supersonic eddy convection velocity), or as observed in the schlieren photographs, from circular to straight oblique, as the jet velocity at the jet boundary increases. The present tests indicated that the shape of the sound waves was a function of the variables M_j, p_j/p_∞, and θ_N. In general, however, with increasing jet velocity at the boundary, the circular sound waves did tend to give way to oblique compression waves. An example of these oblique waves may be seen in figure 45. In figure 21(a) of reference 5, similar waves may be observed for a two-dimensional jet (M_j=3.36).

From the work of Powell, Lighthill, and others the sound intensity and source of generation, and in fact nearly all sound phenomena associated with jets, are known to be primarily dependent upon jet structure. The significant effects that M_j, p_j/p_∞, and θ_N may have upon the structure have been shown in some of the previous sections by experimental and theoretical results for air jets (γ_j=1.40). In addition, significant effects of γ_j upon boundary shape have been shown theoretically. In the generation of jet noise, the effects of γ_j would appear to be of major importance. For example, light gases such as helium are sometimes employed in jet studies to obtain high sonic velocities comparable to those of a hot jet. In so doing, the proper order of magnitude of the eddy convection velocity may be duplicated and this source of sound and compression wave generation is essentially reproduced. However, the shock structure within the jet will be considerably different because of the large differences in γ_j; consequently, one of the predominant sources of sound—that of passage of turbulence through shock patterns—will not be properly duplicated. Conversely, duplication of γ_j satisfies the shock structure within the jet, but eddy convection (and turbulence) at the boundary may or may not be duplicated, although this is felt to be less important. Another factor to consider is that a jet having a high sonic velocity may exhaust through a convergent nozzle at $p_j/p_\infty < 1$ and create supersonic eddy convection velocities (with respect to the ambient air), whereas the jet itself is obviously subsonic with respect to itself and therefore free of shocks.

From the previous discussion the importance of considering separately the effects of γ_j, temperature of the jet, and sonic velocity of the jet in the problem of jet noise becomes obvious. It follows that the general observations on this problem made from the present experimental studies will have limited applicability. Although investigations of jet noise with small models are known to be subject to scale effects, these effects are essentially concerned with turbulence and have no significant effect upon jet structure.

II. JETS EXHAUSTING INTO SUPERSONIC STREAMS

INTRODUCTION

Probably the predominant interest in jets exhausting into supersonic streams is in the aerodynamic interference they may create. Numerous investigations have been made and much effort is presently being devoted to the study of jet interference upon surfaces in close proximity to the jet exit, such as the base annulus, boattail surface, tail surfaces, and the like. Relatively little has been done to explore the jet interference on surfaces considerably downstream of the exit or far removed from the jet axis. An experimental study in this direction is given in reference 18.

Consider an aircraft of the type illustrated in figure 46 in which only that portion of the flow field created by jet operation has been included. Here many variables complicate the problem, but there is no doubt that the rear of the fuselage as well as the tail surfaces may be subjected to significant interference pressure fields. These interference fields would begin approximately at the intersection of the exit shock and the fuselage and extend rearward. For a given aircraft configuration the inclination of this exit shock would, excluding viscous effects which are usually minor in this regard, be determined by the combined action of the free-stream variables and of all the influencing variables common to a jet exhausting into still air. For the general configuration, the importance of geometry and the relation of the aircraft components to the interference problem is readily apparent. The interference pressure

fields downstream of the exit shock are determined by boundary curvature, jet structure and the rate of decay of jet structure, the type of mixing zone (subsonic or supersonic), and viscous mixing at the jet boundary. At the present time there is a noticeable lack of information applicable to interference problems of this type.

This part of the paper will present primarily theoretical curves of the type that may be useful in evaluating jet interference effects for varying jet Mach number, free-stream Mach number, ratio of specific heats of the jet, and jet pressure ratio. These calculations will touch upon one phase of the base-pressure problem (effects of γ_j), the initial inclination of the jet boundary, the initial inclination of the exit shock, the jet structure, simulation of jet boundary and associated pressure fields, some results of experimental observations, and a cursory examination of the behavior of a jet exhausting from a hypothetical hypersonic vehicle.

EXPERIMENTAL STUDIES

In the course of this portion of the study, a minor experimental investigation was conducted in the Langley 9-inch supersonic tunnel to obtain schlieren photographs of the behavior of the jets exhausting into supersonic streams over a wide field of observation in comparison with the base diameter. A sketch of the model is shown in figure 47. Tests were conducted at free-stream Mach numbers of 1.62, 1.94, and 2.41 and over a wide range of jet pressure ratios. Two jet nozzles were employed, one having a sonic exit ($\theta_N=0°$) and the other having a design area ratio for a Mach number of 2.50 with $\theta_N=10°$. The ratio of jet-exit diameter to base diameter was 0.75 for both nozzles.

RESULTS AND DISCUSSION

The theoretical calculations included in the sections to follow do not form a complete coverage of what might be considered the current range of interest. The number of parameters involved and their possible combinations preclude such consideration herein. The calculations are intended to be illustrative examples, and the conclusions drawn from them are subject to these limitations.

Variation in basic flow parameters with γ.—Inasmuch as the ratio of specific heats γ will be one of the prime variables considered, a review of the effects of γ upon the ratio of static pressure to stagnation pressure p/p_t and upon the Prandtl-Meyer turning angle from sonic velocity ν appears worthwhile. Figure 48 presents the variation of ν with M for several values of γ and shows the decrease in ν that accompanies an increase in γ at constant M. Figure 49 presents the variation of p/p_t with M for the same values of γ and shows that at $M\approx2.25$, γ has a negligible effect on p/p_t. Below $M\approx2.25$ an increase in γ decreases p/p_t, whereas the reverse is true above $M\approx2.25$.

Effects of γ_j upon jet interference on base pressure.—There is a particular interest in determining to what extent cold air jets, or unheated gas jets having a value of γ_j simulating hot jets, may be used in experimental studies. Cortright and Kochendorfer have studied the effects of many of the influencing variables associated with jet interference on boattail and base pressures, and have presented a procedure for correcting the base-pressure data for one value of γ_j to other values of γ_j. In this procedure, the jet total pressures that produce the same base pressure for various values of γ_j and any given nozzle-afterbody combination are assumed to be those that yield the same value of δ_j. Alternatively stated, the procedure is one for correcting the jet pressure ratio for fixed known values of p_b/p_∞ and δ_j. From the comparisons that have been made by Cortright and Kochendorfer, and others, this procedure appears suitable for obtaining, at least, a first-order approximation of the effects of γ_j upon the base pressure and boattail pressures.

Figure 50 presents curves obtained directly from the calculations of figures 48 and 49 that may be used in applying the procedure just mentioned. In figure 50, the values of p/p_t from figure 49 are designated as $p_j/p_{t,j}$ or $p_b/p_{t,j}$ and the values of ν from figure 48 are designated as ν_j or $(\nu_j+\delta_j)$. With the value of ν_j corresponding to M_j at the desired value of γ_j determined and with the value of δ_j given, the value of $(\nu_j+\delta_j)$ at the desired value of γ_j, that is, the amount of expansion necessary to reach $p_b/p_{t,j}$, is known. The value of $p_b/p_{t,j}$ may thus be read from figure 50 at the desired value of γ_j. Division of the known fixed value of p_b/p_∞ by this value of $p_b/p_{t,j}$ gives the corrected jet total-pressure ratio

$p_{t,j}/p_\infty$, which when multiplied by $p_j/p_{t,j}$ corresponding to M_j at the desired value of γ_j gives the corrected jet pressure ratio p_j/p_∞. For $M_j=1$ the dashed lines (fig. 50) are ignored and the curves are used directly since ν_j becomes zero. For $M_j>1$ the value of δ_j must be measured from a base line corresponding to the value of M_j considered (for which $\delta_j=0°$), such as indicated by the dashed lines. A detailed examination of the curves of figure 50 indicated that at a fixed value of p_j/p_∞ (1 or greater) the base pressure will apparently always increase with decreasing γ_j. (Emphasis is placed on the fact that the foregoing conclusion is in terms of jet static-pressure ratio which is used throughout in this paper. In terms of jet total-pressure ratio, no such conclusion may be drawn since the reversal in the effect of γ upon p/p_t with varying M (fig. 49) that occurs near $M\approx2.25$ may or may not reverse the effects of γ_j upon base pressure beyond $M_j\approx2.25$. Below $M_j\approx2.25$ the effects of γ_j upon base pressure are apparently the same in terms of either total- or static-pressure ratio.)

The possibility of misuse of the curves of figure 50 in experimental studies bears some note. For $M_j=1$, the curves have a certain uniqueness in that the nozzle area ratio for $M_j=1$ is independent of γ_j. For $M_j>1$ the nozzle area ratio is, of course, a function of γ_j as shown in figure 51, and the use of a scale model of a prototype nozzle in experimental studies employing cold air, for example, results in a different value of M_j from that of the prototype. The correction for γ_j would be incorrect if this different value of M_j were employed to obtain the corrected jet pressure ratio. The preceding statement should not be construed as implying that M_j per se has a significant effect on the variation of base pressure with jet pressure ratio; experimental results obtained to date show that M_j has only small effect on this variation. Of course the nozzle of a model could be designed with the experimental value of γ_j to give the same value of M_j (by varying throat area only) as obtained by the prototype with its value of γ_j.

Initial inclination of jet boundary for constant M_j, $\theta_N=0°$, and $\beta=0°$.—Figures 52 (a), (b), and (c) present for $\gamma_j=1.115$, 1.400, and 1.667, respectively, the effects for a sonic exit ($M_j=1.00$ and $\theta_N=0°$) of increasing jet pressure ratio p_j/p_∞ upon the initial boundary inclination δ_j at several values of free-stream Mach number M_∞. (These calculations, as well as others to follow, correspond to a base annulus thickness of zero and zero boattailing and are for $\gamma_\infty=1.400$ unless otherwise specified.) The curves indicate that for a given value of γ_j the variation of δ_j with p_j/p_∞ experiences small effects from varying M_∞. A comparison of figures 52 (a), (b), and (c) for a constant value of M_∞ shows that for a given jet pressure ratio, decreasing γ_j causes an increase in δ_j. Figures 53 (a), (b), and (c) are cross plots of the respective parts of figure 52 and show the variation of p_j/p_∞ with M_∞ for several values of δ_j. From both figures 52 and 53 the effect of increasing M_∞ is seen to be negligible for values of p_j/p_∞ of the order of 2 or less.

A comparison of these calculations (figs. 52 and 53) with those for $M_\infty=0$ (fig. 13) illustrates the large effect that external supersonic flow has in reducing δ_j for a given jet pressure ratio as a result of the presence of the exit shock. As an example, for $\gamma_j=1.400$ and $p_j/p_\infty\approx8$ the value of δ_j is approximately 37.3° for $M_\infty=0$ (fig. 13), whereas for $M_\infty=3$ the value of δ_j is about 17.1° (fig. 52(b)). It is obvious from the outset, therefore, that inclinations of the external flow in the vicinity of the jet boundary caused by jet operation will, for a given value of p_j/p_∞ and γ_j, be considerably less for supersonic external flow than for subsonic external flow.

Initial inclination of jet boundary for constant M_∞, $\theta_N=0°$, and $\beta=0°$.—Figure 54 presents for $\gamma_j=1.115$, 1.300, 1.400, and 1.667 some examples of the effects of M_j upon p_j/p_∞ for several values of δ_j. The data of figure 54(a) are for $M_\infty=1.30$ whereas those of figure 54(b) are for $M_\infty=2.00$. All calculations were made with $\theta_N=0°$ and $\beta=0°$. Examination of the curves again indicates that for any value of M_j the effect of decreasing γ_j at constant p_j/p_∞ is to cause an increase in δ_j. Further, the minimum in the curves that occurs between $M_j=1$ and about 1.5 indicates that for a given value of p_j/p_∞ the effect of increasing M_j is to increase δ_j initially and thereafter to decrease δ_j.

Initial inclination of the exit shock for varying M_∞ and M_j, $\theta_N=0°$, and $\beta=0°$.—The data of figure 54 may be used to calculate the initial inclination of the exit shock of the type illustrated in figure 46. The results are presented in figures

55 (a) and (b) for $M_\infty = 1.30$ and 2.00, respectively. Again, all calculations were made with $\theta_N = 0°$ and $\beta = 0°$. The effects of p_j/p_∞ upon ξ are shown for $\gamma_j = 1.115$, 1.300, 1.400, and 1.667 at each of several values of M_j from 1.00 to 4.00. These curves indicate the significant effect that γ_j may have upon the approximate upstream limit (i.e., the exit shock) of the interference pressure field created by a jet as a result of the change in shock inclination. The duplication of γ_j in experimental studies of jet interference upon surfaces as shown in figure 46 would, therefore, in many instances appear desirable. However, in experimental studies of jet interference, the duplication of γ_j is sometimes not practical or possible. In such instances, curves of the type given in figures 52 to 55 may be used to convert the values of p_j/p_∞ corresponding to the experimental value of γ_j to values of p_j/p_∞ for simulated γ_j. For example, consider the case of $M_j = 2.00$, $M_\infty = 2.00$, and experimental values of $p_j/p_\infty = 20$ and $\gamma_j = 1.667$. A simulation for $\gamma_j = 1.300$ is desired. From figure 55(b) the shock inclination ξ for the experimental conditions is about 59.4°; the experimental conditions represent, therefore, a value of $p_j/p_\infty \approx 12$ for $\gamma_j = 1.300$. Although this procedure may be used in experimental work to give duplication of the exit shock inclination and δ_j without duplication of γ_j, it is important to note that the jet structure and, consequently, the interference pressure field downstream of the exit shock is not exactly duplicated, although it may be adequately duplicated for the purpose of the investigation. Some aspects of this problem will be considered next.

Examination of simulation of jet boundary and ambient wave interference field.—Because of the negligibly small differences found in the boundaries of supersonic jets exhausting into still air for differences in γ_j of the order of 0.1, provided the initial inclination is duplicated, an attempt was made to determine whether equally small differences in the boundary shape and, of equal importance, in the ambient wave interference field could be expected for supersonic jets exhausting into supersonic streams under the same conditions of simulation (identical δ_j). At the outset, there are reasons for suspecting that the effect of a given change in γ_j would have less effect upon the jet-boundary shape for jets exhausting expansively into supersonic streams as compared with jets exhausting into still air at the same value of p_j/p_∞. For example, for the same value of p_j/p_∞ the jet exhausting into the supersonic stream undergoes considerably less expansion than the jet exhausting into still air because of the pressure rise across the exit shock generated in the supersonic stream. Thus, effectively, the first portion of the issuing jet flow for the jet exhausting into the supersonic stream resembles that which occurs for a jet exhausting into still air at a significantly lower value of p_j/p_∞. For jets exhausting into still air it has already been shown that the lower the value of p_j/p_∞, the less the effect of γ_j; moreover, at $p_j/p_\infty = 1$ changes in γ_j greater than 0.4 were shown to have negligible effect upon the boundary shape of jets exhausting into still air.

The structure of an axisymmetric supersonic jet and the wave interference field it creates in the ambient supersonic stream may be calculated by the method of characteristics (see refs. 19 and 20). However, the complexities involved discourage even machine calculations with the procedures presently available. Of the few calculations that have been made, one of the most complete appears to be that of Schäfer (ref. 20). This calculation was made for a jet having $M_j = 2.37$, $\gamma_j = 1.405$, and $\theta_N = 12.5°$ and exhausting at $p_j/p_\infty \approx 8.9$ into an ambient stream having a Mach number of 3.24 and a ratio of specific heats of 1.405 (same as the jet); the exterior surface ahead of the jet exit had a boattail angle of 9°. The net for this calculation is reproduced in figure 56. In reference 21, the isobars for this calculation have been computed and the calculation is presented in isobar-streamline form. The Schäfer calculation has been repeated with the initial variables remaining the same except for γ_j, which was changed to 1.300, and p_j/p_∞, which was reduced so that the initial inclination of the mixing boundary was duplicated. This new calculation was carried to the maximum diameter of the jet. The boundary shape and the interference isobars in the ambient stream obtained in this calculation could not be distinguished from those shown in reference 21. Thus, the conclusion drawn for jets exhausting into still air would appear to apply as well to jets exhausting into supersonic streams, namely, differences in γ_j of the order of at least 0.1 create negligibly small differences when the initial inclination of the jet

boundary is duplicated.

Initial inclination of jet boundary for varying M_∞, M_j, θ_N, and β.—On the basis of the results shown in the preceding section, cold air jets may be expected to yield satisfactory results in many studies of jet interference by duplication of δ_j (or ξ) only. Thus far, the curves that might be used for simulation purposes have been restricted to $\theta_N=0°$ and $\beta=0°$. It appears desirable, therefore, to examine the case of finite θ_N and β, particularly for the case where cold-air-jet simulation would amount to a difference in γ_j from the hot jet of the order of 0.1. Calculations were made of the initial boundary inclination δ_j for $\gamma_\infty=1.400$ and $\gamma_j=1.286$ (or 9/7). This value of γ_j is generally representative of many hot jets; furthermore, some of the required flow properties for the calculations were available for this value. The calculations cover ambient-stream Mach numbers of 1.2, 1.5, 2.0, 2.5, and 3.0 at the boattail surface immediately ahead of the exit, jet exit Mach numbers of 1.0, 1.5, 2.0, 2.5, and 3.0, values of θ_N and β ranging from 0° to 20° immediately ahead of the exit, and values of p_j/p_∞ within the approximate inviscid limits for supersonic flow, except at the higher values of M_∞ and M_j where the calculations were terminated somewhat short of these limits. Appendix D gives additional details on these calculations. Note that θ_N and β in these calculations refer to conditions immediately upstream of the jet exit.

The results of the calculations are presented in figures 57 to 61. The curves for all values of M_j are shown together for a particular value of M_∞ and a particular combination of β and θ_N. The curves for a particular combination of β and θ_N can be simply converted to those applicable to the infinite number of combinations of β and θ_N that may be formed to give the same sum of $\beta+\theta_N$, provided both β and θ_N remain positive according to the original convention. For example, curves for $\beta=10°$ and $\theta_N=0°$ can be made applicable to $\beta=8°$ and $\theta_N=2°$, $\beta=5°$ and $\theta_N=5°$, $\beta=0°$ and $\theta_N=10°$, and so forth, because by maintaining the sum of $\beta+\theta_N$ constant, one is merely rotating the infinitesimally small fragment of the boattail and nozzle surface just ahead of the exit (see appendix D) about a point formed by the juncture of the boattail and nozzle surfaces, and is therefore not altering the other initial quantities. Accordingly, the value of p_j/p_∞ remains unchanged, and the value of δ_j changes by the amount that β (or θ_N) was changed. For example, if β were decreased 5°, δ_j would increase 5°. The expressions in appendix D for determining the type of disturbance phenomenon are also applicable to these converted values of β, θ_N, and δ_j.

The present results for finite θ_N and β show a similiarity to those given earlier for $\theta_N=0°$ and $\beta=0°$ in indicating a small effect of M_j and, therefore, by the reversibility of the problem, an equally small effect of M_∞. Although the present calculations were based on a base annulus of zero thickness, results shown previously herein and in reference 5 would appear to indicate that the results of the present calculations could be satisfactorily applied to configurations having thin base annuli.

The present calculations may also be used to obtain an idea of the order of magnitude of p_j/p_∞ associated with the separation of a turbulent boundary layer on the boattail surface or on the nozzle surface. If the value of $(\delta_j+\beta)>0$ and exceeds the critical turning angle associated with separation (of the order of that shown in ref. 22) for the same initial conditions that exist on the boattail just ahead of the jet exit, then separation may occur on the boattail surface. In like manner if the value of $(\delta_j-\theta_N)<0$ and if $|\delta_j-\theta_N|$ exceeds the critical angle associated with separation for the same initial conditions that exist on the nozzle just ahead of the jet exit, then separation may occur on the nozzle surface.

Basic considerations of jet structure.—From figure 56 the indication is obtained that, theoretically, a supersonic outer stream will permit an intersecting shock pattern to exist within the jet at much higher jet pressure ratios before giving way to a Riemann wave than would be the case for a subsonic outer stream. Previous experimental observations such as presented in reference 23, for example, support this indication.

For a supersonic outer stream, wavelength ceases to be a function of jet properties only and is subject to the additional effects of the outer stream variables. However, when the mixing boundary between the jet and outer stream is subsonic, the jet does tend to exhibit periodic structure, as has been shown experimentally. So long as the mixing boundary remains subsonic, the

shocks which occur within the jet must obviously be reflected at the subsonic boundary and cannot penetrate into the outer stream. Nevertheless, the jet structure and the pressure fields in the outer stream are interrelated because of the pressure balance that must take place at the mixing boundary. When the mixing boundary is supersonic throughout, the shocks which occur within the jet are not reflected upon reaching the mixing boundary but continue through the boundary and into the outer stream and are bent or deflected without discontinuity according to the Mach number distribution and direction of flow in the mixing boundary and outer stream. Examples of shocks passing through the boundary have been observed in several jet studies; an excellent photograph of this phenomenon for two-dimensional flow may be seen in figure 36 of reference 24.

The possibility exists for the case of a supersonic mixing boundary that as the shock from within the jet traverses the mixing boundary, the so-called second-family characteristic or Mach lines having their origins along the portion of the shock within the mixing boundary may diverge, creating an expansion, or may form an envelope thereby creating a weak secondary shock within the jet which has the appearance of a reflected shock. The manner in which this occurs is somewhat analagous to the interaction of incident shocks with the supersonic portions of boundary layers, as described in reference 25. If a secondary shock (or expansion) occurs, the phenomenon may repeat itself when the secondary shock (or expansion) traverses the mixing boundary and will continue in this fashion until the compressions (or expansions) within the jet are eliminated.

If all initial conditions for which a secondary shock occurs are assumed to remain invariant and the supersonic mixing boundary is pictured as being compressed to zero thickness, the shock from within the jet will have a discontinuity in slope at the point where it crosses the boundary and the secondary shock will have its origin at this point. Thus, the conditions become those amenable to inviscid theoretical treatment, namely, supersonic streams separated by a supersonic interface. A two-dimensional study by Kawamura (ref. 26) of the supersonic interface and wave patterns in the two-dimensional supersonic compound jet will be considered in the following section.

Kawamura analysis.—The analysis of Kawamura (ref. 26) is applicable to low jet pressure ratios only, but the results are indicative of what might be expected to occur at much higher jet pressure ratios. In this analysis Kawamura develops expressions for the changes in flow direction and pressure and establishes the type of secondary or so-called reflected wave and the jet structure on the basis of the parameter $\lambda=\frac{1}{\gamma}(\sin \mu \cos \mu)$. It is shown that if at the supersonic interface the difference between local values of λ for the free jet and the outer stream $\lambda_{j'}-\lambda_{\infty'}$ is positive, a compression wave (or expansion wave) passing from the jet through the supersonic interface and into the outer stream will cause a compression wave (or expansion wave) to be reflected into the jet; that is, the reflected wave is of the same type as the wave which passes through the boundary. If $\lambda_{j'}-\lambda_{\infty'}$ is negative the reflected wave is of opposite type. As the jet structure decays in passing downstream, Kawamura shows that the wave pattern composing this structure is of the same type (compressive or expansive) throughout the jet if $\lambda_{j'}-\lambda_{\infty'}$ is positive and of alternating type if $\lambda_{j'}-\lambda_{\infty'}$ is negative.

The values of the basic Kawamura parameter λ have been computed for $M=1.0$ to 3.0 and $\gamma=1.100$ to 1.667. The results are given in figure 62. Values of the difference parameter $\lambda_{j'}-\lambda_{\infty'}$ have also been computed and are presented in figure 63 as a function of $M_{j'}$ for varying γ_j and $M_{\infty'}$. The primes again denote local values at the interface. The values of λ and $\lambda_{j'}-\lambda_{\infty'}$ given by these curves may be used to obtain flow direction and pressures by substitution in the expressions given in reference 26. The curves in figure 63 are of particular significance to the problem of jet interference in that they show the degree of importance of simulation of γ_j in experimental studies which are concerned with jet structure and the changes in the pressure fields of the outer stream that are caused by the jet. One might expect the indication that the greater the difference between the experimental value of γ_j and the value for true simulation, the greater the error in jet structure and

in the interference pressure fields created by the jet. Not so obvious, however, is the indication that it is possible for differences in γ_j to result in a type of jet structure and ambient pressure field that is opposite from that for true simulation.

In applying the procedures of Kawamura and in studies of shocks within the jet, a knowledge of the effect of γ upon shock inclination ξ is helpful. Calculations have been made of the variation of ξ with δ for $M=1.50$ to 5.00 and $\gamma=1.115$ to 1.667. Since (excluding $\gamma=1.400$) this information is not generally available, it is presented in figure 64.

Conditions for no reflection at supersonic interface.—In reference 25, Barry has shown for the case of two supersonic flows separated by a supersonic interface and having identical values of γ that, if the difference between the Mach numbers of the two flows is small, there will be no reflection at the interface from the passage of a shock through the interface when the average Mach number of the two flows equals $\sqrt{2}$. From the work of Kawamura discussed in the previous section, no reflection would be expected from the passage of compression or expansion waves through a supersonic interface when $\lambda_f-\lambda_{\infty'}=0$. Figure 65 presents the variation of $M_{\infty'}$ with M_f for no reflection at several values of γ_j as determined from the calculations for figure 63. The 45° line for $\gamma_j=1.400$ is the trivial solution for $\gamma_j=\gamma_\infty$ and $M_f=M_{\infty'}$. A confirmation of Barry's solution becomes readily apparent at the intersection of the curves for $\gamma_j=1.400$. Perhaps the most important conclusion to be drawn from figure 65 is that the condition of no reflection is one which may occur often in practical applications even from a nonviscous consideration. The inclusion of viscous effects, and therefore a mixing boundary of finite thickness, would tend to weaken a reflection since the origin of the reflections is not confined to a point. Accordingly, reflections within jets having supersonic mixing boundaries would be expected to have a much lesser interference effect upon the pressure fields in the outer stream than the waves which give rise to these reflections, and to eliminate themselves rapidly within the course of a few additional reflections.

Experimental observations.—The schlieren observations of references 5 and 27 demonstrate, for a two-dimensional jet with a supersonic mixing boundary, the weakness of the reflection associated with the passage of a strong shock from within the jet into the outer stream. Also illustrated is the very rapid elimination of reflections (ref. 27, in particular). In no instance could more than two reflections be detected within the jet, and in most instances only one.

For axisymmetric jets, the schlieren observations of several studies never show more than three reflections when a strong shock from within the jet passes through a supersonic boundary into the outer stream. In most instances, there is only one visible reflection and, in some instances, no reflections are visible. The pressure measurements of reference 18 also indicate the rapid elimination of and attenuation in strength of such reflections.

In order to observe the reflections, jet structure, and disturbances introduced into the outer stream at distances considerably farther downstream and away from the jet axis than was possible in the investigation just mentioned, the minor investigation described earlier in this part of the paper was undertaken. With the support arrangement employed (see fig. 47), the results of reference 23 indicate that some interference upon the jet from the side strut is to be expected; however, this interference is not believed to affect the qualitative results of the tests. Some examples of the schlieren photographs obtained in these tests are shown in figures 66, 67, and 68. In none of the photographs could more than one reflection be detected, after which the jet continued downstream with only small spreading. For a given pressure ratio, the jet for $M_j=2.50$ did not dissipate so readily in moving downstream as did the jet for $M_j=1.00$. From these tests, indications are that for jets with supersonic mixing boundaries the reflections associated with the passage of the shock from within the jet into the outer stream may be assumed to have negligible interference effects upon the ambient stream. Downstream of the region where the jet shock passes through the mixing boundary, it appears permissible to assume for interference studies that the jet is cylindrical in shape; this is in agreement with the pressure surveys of reference 23. Insofar as axisymmetric jets are concerned, the main disturbances introduced into the outer stream will, for supersonic mixing boundaries, apparently be

the exit shock (or expansion) and the shock from within the jet.

From available experimental results, the presence or absence of a Riemann wave within a jet bounded by a supersonic stream is indicated to be a function of the base and afterbody geometry as well as the flow variables of the jet and free stream. In general, however, the Riemann wave occurring at low values of p_j/p_∞ gives way to an intersecting shock pattern at higher values of p_j/p_∞ than for the same jet exhausting into still air. Once the intersecting shock pattern occurs within a jet bounded by a supersonic stream, the present results indicate that it will remain to a value of p_j/p_∞ many times that for which the Riemann wave would reappear in the same jet exhausting into still air; after the Riemann wave reappears, its growth with p_j/p_∞ is much less for the jet bounded by a supersonic stream.

Comments on boundaries at large values of p_j/p_∞.—From the calculated boundaries presented in the first part of this paper for a jet exhausting into still air at large values of p_j/p_∞, it is apparent that a rocket-propelled hypersonic vehicle may encounter serious jet interference problems if it encounters the large values of p_j/p_∞ that are likely to occur at high altitudes. These problems arise from the presence of the large, bulbous, free jet of gases immediately downstream of the nozzle exit, and are, in the main, twofold. First, the large deflections of the free-stream flow caused by the jet flow may result in major aerodynamic interference upon nearby surfaces; for example, large regions of separated flow may occur on the vehicle surface ahead of the rocket exit. Second, the heat existing in the core of this large mass of gases may at hypersonic speeds introduce direct heating problems through radiation by causing the temperatures of the nearby surfaces which are already experiencing high aerodynamic heating to exceed the critical values. None of the aerodynamic interference effects can be estimated with any reliability without some knowledge of the magnitude of the region encompassed by the free jet, the initial inclination of the jet boundary, the shape of the boundary, and the applicability of the results for exhaust into still air at large values of p_j/p_∞. Since these problems now confront the designer, a few comments on a jet issuing from a hypothetical ground-launched hypersonic vehicle seem in order.

Figure 69 presents an assumed speed-altitude variation for this hypothetical hypersonic vehicle. For simplicity a single rocket is assumed to provide power for the vehicle and the rocket is assumed to operate at design value at sea level (that is, at $p_j/p_\infty=1$); in practical applications the value of p_j/p_∞ at sea level is usually less than 1.0 if the rocket is to encounter high altitudes.

The variation of p_j/p_∞ with altitude was calculated with p_∞ assumed equal to the pressure at altitude and with the pressure at altitude varying according to the ICAO standard atmosphere (ref. 28) with extensions to higher altitudes. The value of p_j was assumed to be invariant with altitude. The variation thus obtained is shown by the solid curve in figure 70 and represents the conditions shown in sketch 1. It is important to

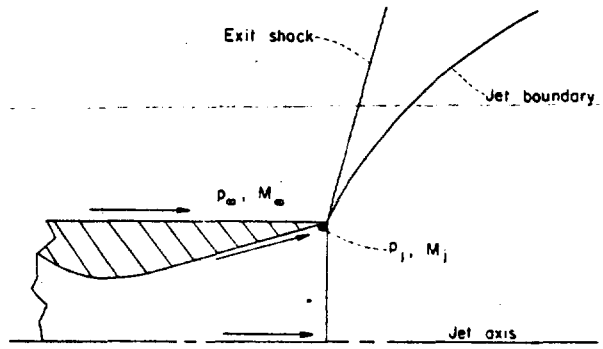

Sketch 1.

note that the solid-line curve in figure 70 is independent of the value of M_∞ at altitude; the speed of the ambient flow could be zero at all altitudes or could vary in some arbitrary manner as in figure 69.

In order to examine the effect of speed-altitude variation of the hypothetical vehicle (fig. 69) on the initial inclination of the jet boundary δ_j, consideration must be given to the pressure rise through the shock in the ambient flow. For large pressure ratios, separation will undoubtedly occur on the external surface ahead of the base because the boundary layer will not withstand a pressure rise of the magnitude necessary to turn the flow through the large initial deflections of the jet boundary. Sketch 2 probably represents a more realistic representation of the phenomena. Little

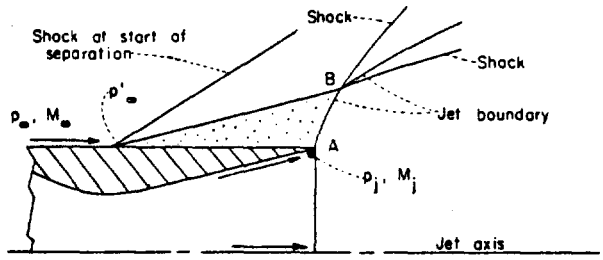

Sketch 2.

is known at present about the pressure rise associated with separation at hypersonic speeds; consequently two conditions have been examined. For one condition a pressure rise p'_∞/p_∞ corresponding to a 30° turning of the flow through an oblique shock at separation is assumed to occur; for the other condition, in order to have a quasi-limiting condition, the pressure rise through a normal shock is assumed to have taken place ahead of the separated region. In the determination of the resulting values of p_j/p'_∞, the pressure p'_∞ is assumed to hold throughout the separated region. The curves corresponding to the oblique shock with 30° turning and to the normal shock are shown in figure 70. Of course the portions of the curves at very low values of p_j/p'_∞ have no meaning since a 30° deflection of the external flow by the jet would be impossible at these low values. For large pressure ratios, however, the oblique-shock curve should give a reasonable first-order indication of the values of p_j/p'_∞ that would be encountered, and the fact that the normal-shock curve is not greatly removed from the oblique-shock curve is believed to indicate that values of δ_j calculated from the oblique-shock curve could not be greatly different from those that are experienced with practical configurations.

Since the curves of figure 70 are independent of γ_j, θ_N, and M_j, they may be applied to the nozzle of the still-air study having $M_j=2.5$, $\theta_N=15°$, and varying values of γ_j. Values of the initial inclination of the jet boundary δ_j for this nozzle have been determined with the aid of figures 35 and 70 and the results are shown plotted against geopotential altitude in figure 71. The solid-line curves are for $M_\infty=0$, and the dashed-line curves are for the speed-altitude variation of figure 69 with the oblique-shock separation of the boundary layer. Although only the curves for $\gamma_j=1.200$ may be considered applicable to the rocket-propulsion unit of the hypothetical vehicle, the curves for the other values of γ_j have been included to point up the effect of γ_j and for possible information on the behavior of jets on reaction controls. Again the lower portions of the dashed-line curves (small δ_j) have no meaning. The difference between the solid-line curve and the dashed-line curve at a particular γ_j shows the effect that the presence of supersonic ambient flow, defined according to figure 69 and with separation ahead of the base, has in reducing the initial deflection of the boundary. As the extremely large pressure ratios of high altitude are approached (fig. 71), the effects of the ambient flow may be readily deduced from these curves to be secondary in determining the value of δ_j. Of particular importance is the indication that feasible rocket-propelled hypersonic vehicles may encounter, within their range of operation, initial inclinations of the jet boundary approaching and exceeding 90°; consequently, large regions of separated flow, together with large aerodynamic and possible aerothermal interference effects, may occur on these vehicles.

The indication that the effects of the ambient flow are secondary at extremely large pressure ratios in determining the value of δ_j does not imply that the shape of the boundary will not be significantly affected by the ambient flow at lower pressure ratios. No reason is apparent why the procedure employed at low pressure ratios for determining the shape of the portion of the jet boundary that bounds the region of separation (from point A to point B in sketch 2) should not be useful at large pressure ratios; in this procedure this portion of the boundary is determined by employing the boundary of the jet exhaustign into still air at a pressure ratio equal to p_j/p'_∞. However, at point B of sketch 2, where the separated region ends and the jet flow and ambient flow interact directly, a large and abrupt turning of the boundary may be expected at large pressure ratios and hypersonic speeds, if the flow deflections accompanying separation at these speeds are of the order of 30° (turbulent boundary layer preceding separation). Beyond point B the ambient flow will have significant influence on the boundary shape in the same manner as it does at low pressure ratios and supersonic speeds.

CONCLUDING REMARKS

Some experimental and theoretical studies have been made of axisymmetric free jets exhausting from sonic and supersonic nozzles into still air and into supersonic streams with a view toward problems associated with propulsive jets and the investigation of these problems. The scope and results of these studies are divided into two sections.

JETS EXHAUSTING INTO STILL AIR

For jets exhausting into still air, the primary variables considered were jet Mach number, nozzle divergence angle, jet static-pressure ratio, and the ratio of specific heats of the jet. The effects of most of these variables upon jet structure, primary wavelength, and the shape and curvature of the jet boundary were studied. Observations were also made of features pertaining to jet noise and jet simulation. Some of the results and conclusions follow:

1. Divergence angle of the nozzle (0° to 20°) has a small effect upon the primary wavelength of the jet. Existing methods for predicting the wavelength of an axisymmetric jet are inadequate above a jet static-pressure ratio of about 2. Semiempirical relations are presented which give fair predictions of experimental results for jet Mach numbers from 1 to 3.

2. Curves defining the existence as well as the location and diameter of the Riemann wave are presented. Increasing nozzle divergence angle reduces significantly the range of jet static-pressure ratios in which no Riemann wave occurs. The effect of jet Mach number is not clear in the lower range of jet Mach numbers, but for the higher range of jet Mach numbers an increase in jet Mach number increases the range of jet static-pressure ratios in which no Riemann wave occurs. An intersecting shock pattern is clearly restricted to low jet static-pressure ratios.

3. A tabulated solution of the expansive flow field calculated by the method of characteristics is presented for the jet with sonic exit. Calculations by the method of characteristics employing the procedure of foldback appear adequate for predicting both jet boundary shape and shock location within the jet, provided the calculations are not carried too near the end of the first wavelength of the jet.

4. A circular-arc boundary is a satisfactory prediction, both theoretically and experimentally, of the first portion of the jet boundary from the jet exit to the vicinity of the maximum diameter of the jet. The range of applicability of the Johannesen-Meyer solution for the initial curvature of the boundary is, as the solution implies, restricted to regions in very close proximity to the exit. Values of the integrals for general use of the Johannesen method of characteristics are presented for a broad range of application.

5. Approximately 3,000 calculated boundaries are presented. These boundaries cover jet static-pressure ratios from 1 to about 42,000, values of ratio of specific heats of the jet from 1.115 to 1.667, nozzle divergence angles from 0° to 20°, and jet Mach numbers from 1.0 to 3.0. Most of these boundaries (2,960) comprise a systematic study in the static-pressure range from 1 to 10 for conically divergent nozzles, and are presented in a form that facilitates practical use. From these calculations, a random selection of boundaries is used to show the effects of the several variables involved.

6. The possibility of interpolating and extrapolating boundaries is discussed, and the feasibility of simulating one supersonic jet by another supersonic jet is examined. With regard to simulation, the results indicate that the differences between boundaries for jets having different ratios of specific heats, but the same jet Mach number and nozzle divergence angle, are negligibly small when the initial inclination of the boundary is duplicated and when the difference in the ratios of specific heats is not much greater than about 0.1. Cold air jets thus offer the possibility of satisfactory simulation in many investigations.

7. Observations of the sound waves generated by the jet indicated that the type of sound wave that may be observed is dependent upon the sensitivity of the optical system employed; therein may lie the apparent discrepancies between some of the visual studies of sound waves associated with jets. The present observations tended to confirm in general the hypotheses of Powell and Lighthill regarding sound waves associated with degeneration of jet structure and with eddy convection velocity, respectively.

JETS EXHAUSTING INTO SUPERSONIC STREAMS

For jets exhausting into supersonic streams, an attempt was made to present primarily theoretical curves of the type that may be useful in evaluating certain jet interference effects and in formulating experimental studies. The primary variables considered were jet Mach number, free-stream Mach number, jet static-pressure ratio, the ratio of specific heats of the jet, nozzle exit angle, and boattail angle. The simulation problem was examined as was the case of a hypothetical hypersonic vehicle. A few experimental observations were made. A summary of the types of curves which have been presented and some of the indicated conclusions follow:

1. Curves of the type applicable to the Cortright-Kochendorfer method for correcting base-pressure data for one value of the ratio of specific heats of the jet to other values are given for a broad range of operation. Apparently the base pressure for a given value of jet static-pressure ratio will always increase with decreasing ratio of specific heats of the jet.

2. A number of curves are presented for the case of zero exit angle of the nozzle and zero boattail angle to show the effects of other variables upon the initial inclination of the jet boundary. At a constant jet Mach number of 1 (sonic exit), the variation of the initial inclination of the boundary with jet static-pressure ratio experiences small effects from varying free-stream Mach number; these effects are negligible below a jet static-pressure ratio of about 2. For a given free-stream Mach number, increasing jet Mach number at a fixed value of jet static-pressure ratio first increases the initial inclination of the jet boundary (jet Mach number near 1) and thereafter decreases the initial inclination of the boundary (jet Mach numbers of the order of 1.5 and greater). For a given value of jet static-pressure ratio and fixed jet properties, the initial inclination of the jet boundary is always less for a supersonic than for a subsonic ambient stream.

3. Decreasing the ratio of specific heats of the jet always increases the initial inclination of the jet boundary. The ratio of specific heats of the jet can have a significant effect upon the initial inclination of the exit shock in the ambient supersonic stream and, therefore, upon the upstream limit of the interference pressure field created by the jet. The type of curves presented to show these effects may be used to achieve simulation of initial inclination of the boundary and initial inclination of the exit shock in experimental studies without simulation of the ratio of specific heats of the jet. (Jet structure is not simulated.) An illustrative calculation shows that this simulation also gives adequate simulation of the boundary shape and of the ambient wave interference field created by the jet provided that (as in the case of jets exhausting into still air) the difference between the ratios of specific heats for the simulated jet and the prototype jet is of the order of 0.1 or less.

4. Curves are presented that give the initial inclination of the jet boundary for varying boattail angles and nozzle exit angles. For these curves, the ratio of specific heats for the free stream is 1.400 and that for the jet is 1.286. Nozzle exit angles range from 0° to 20°, boattail angles from 0° to 20°, jet Mach numbers from 1 to 3, and free-stream Mach numbers on the boattail surface from 1.2 to 3.0. Both jet Mach number and, by the reversibility of the problem, Mach number on the boattail surface have in general a small effect upon the results.

5. Consideration is given to jet structure and the phenomena to be expected in the presence of subsonic and supersonic mixing boundaries. Curves are presented of the basic Kawamura parameter and of the difference parameter, from which the importance of the ratio of specific heats of the jet to the jet structure and ambient pressure field may be gathered. Curves showing the effects of the ratio of specific heats upon shock inclination are included.

6. In practical application, it is quite possible to have a condition of no reflection from the passage of a shock from within the jet through a supersonic mixing boundary and into the outer stream. Experimental observations indicate that when such reflections do occur they are weak and eliminate themselves rapidly. For jet interference studies, it appears permissible to assume that the jet is cylindrical downstream of the region where the shock arising from within the jet passes through the mixing boundary.

7. A cursory examination of the behavior of the propulsive jet on a hypothetical rocket-propelled

hypersonic vehicle indicates that feasible hypersonic vehicles may encounter, within their range of operation, initial inclinations of the jet boundary approaching and exceeding 90°. Consequently, large regions of separated flow may occur on such vehicles, together with large aerodynamic and possible aerothermal interference effects. When extremely large pressure ratios are encountered at high altitude, the effects of the ambient flow are indicated to be secondary in determining the initial inclination of the jet boundary.

LANGLEY RESEARCH CENTER,
NATIONAL AERONAUTICS AND SPACE ADMINISTRATION,
LANGLEY FIELD, VA., *August 22, 1958.*

APPENDIX A

CALCULATIONS BY METHOD OF CHARACTERISTICS

BASIC CONSIDERATIONS

For several years, the Langley Bell Computing Section has had established procedures for characteristic calculations, by machine, of the lattice-point type which do not require iterations in the point-to-point flow-field calculations. The characteristic nets thus calculated must, therefore, be somewhat more dense than those employing iterative methods for comparable accuracy. (See refs. 19 and 29 for descriptions of lattice-point type of characteristic calculations.) Insofar as possible the present investigation utilized the procedures of the Langley Bell Computing Section. Nevertheless, certain complications arose in the calculations. They were as follows:

(1) The solution for points on and near the jet axis which must be confronted regardless of the type of characteristic calculation employed

(2) The choice of procedure to follow when intersecting characteristics of the same family indicated the presence of a shock

(3) The solution for divergent nozzles which the existing lattice-point procedures could handle only by time-consuming additions to the calculations

(4) The solution for the sonic exit

These four subjects will be covered in the sections to follow.

POINTS ON AND NEAR THE AXIS

The characteristic calculations for a given set of initial conditions were originally proposed to be carried through only until the maximum height of the jet boundary was reached. This limit was selected for two reasons: First, the boundary shape beyond the maximum height usually has little practical value, and, second, the number of solutions required on the jet axis would be reduced. Although the latter would not be encountered at the higher values of M_j and θ_N (this accounts for the continuance of some of the calculations for $\theta_N \neq 0°$), they would cause considerable delay in the overall program in that they required transcalculation from machine to manual to machine. The frequency with which this transcalculation is required becomes increasingly severe as M_j decreases. Several procedures are available for refining the calculations near the axis, most of which are discussed in reference 19. The method of successive approximations as described in reference 29 was used in the present calculations with at least two approximations being made for the first point on each first-family characteristic leaving the axis. This procedure gave satisfactory results for all nets except those for $M_j = 1.01$ as can be observed in figure 14(a) where the change in slope of the second-family characteristics reverses sign in reaching the axis, an obvious indication of appreciable error. Calculations at higher values of M_j have shown that surprisingly large errors in the flow field near the axis can be present without seriously affecting the shape of the portion of the jet boundary considered herein or the coalescence of characteristics (shock growth) near the boundary. An indication of the error on the axis and its effect on boundary shape for the most critical condition ($M_j = 1$) will be covered in the section on the solution for the sonic exit.

INTERSECTION OF LIKE CHARACTERISTICS AND SHOCK GROWTH

The occurrence of a shock is first indicated by the intersection of the last expansion characteristic from the lip of the nozzle and the first reflected characteristic from the boundary. Successive intersections of the same type indicate a growth in strength of the shock and define its shape and location. Several procedures are available for handling the occurrence of a shock. The rigorous solution is to combine the shock equations and the characteristic equations. The ensuing computations become so complicated, however, that this approach is rarely used except to demonstrate the procedure. To date, no satisfactory method has been found to incorporate the procedure in machine calculations; consequently, it was not considered for use. Of the remaining

procedures, all require transcalculation except the use of a foldback procedure which permits the machine to make continuous calculations from the axis to the boundary. From a cursory examination, none of the remaining procedures appear to give accuracy better than that obtained with foldback, and some are inferior. For the above reasons, the foldback procedure was used in the present calculations as shown by the characteristic nets in figure 14. This procedure is given this name because of the manner in which the characteristic net folds back upon itself as the calculations proceed beyond the point for the occurrence of a shock within the jet. In essence the characteristic equations are permitted to handle their own difficulties by ignoring the intersection of characteristics of the same family. The location of the shock is established by the inner envelope of the intersections of like characteristics, clear examples of which may be seen at $p_j/p_\infty=10$ and 20 in figure 14(a). The jet flow field between the shock and the jet boundary is defined by the net remaining after the foldback portion of the net is deleted. Thus the method of foldback predicts boundary and shock location and actually gives the type of discontinuities in velocity and direction that occur in crossing a shock.

SOLUTION FOR DIVERGENT NOZZLES

As mentioned previously, the lattice-point procedures available for machine computations at the time of these calculations were not amenable to ready solutions for θ_N other than zero. The centered-expansion characteristic method of Johannesen and Meyer (refs. 2 and 14) is readily applicable to any free jet problem ($p_j/p_\infty \geqq 1$) but this procedure was not available for machine computation nor had the integrals (see appendix B) been evaluated at the time of these calculations except for the range of $M_j=2.73$ to 3.89 ($\gamma_j=1.400$) and for the intervals given in references 2 and 14. In order to take advantage of the existing procedure available for machine, the properties of the leading characteristic were calculated by the Johannesen-Meyer method and used as a base from which the calculations were continued in the same manner as employed for $\theta_N=0°$. A brief description of the calculation of the leading characteristic by this method follows.

Consider a conically divergent nozzle assumed to give pure source flow and the polar and Cartesian coordinates as shown in sketch 3. The

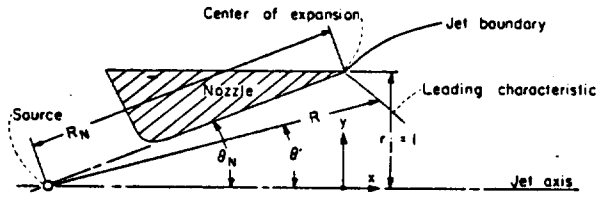

Sketch 3.

initial properties of the flow at the nozzle lip just prior to exit are given, namely, M_j, μ_j, γ_j, and θ_N. From the initial conditions and the relation

$$R=C\left(1+\frac{2}{\gamma-1}\sin^2\mu\right)^{\frac{\gamma_j+1}{4(\gamma_j-1)}}(\sin\mu)^{-\frac{1}{\gamma_j-1}} \qquad \text{(A1)}$$

the constant C may be determined. With P representing Busemann's pressure number and $t=1{,}000-P$, the relation $dt=-2d\theta$ allows the value of R to be evaluated for any value of $\theta=\theta_N+d\theta$. The flow properties for a given point on the leading characteristics are thus determined and the Cartesian coordinates of the point are

$$\left.\begin{aligned} x&=R\cos\theta-R_N\cos\theta_N \\ y&=R\sin\theta \end{aligned}\right\} \qquad \text{(A2)}$$

The relation between P and μ was only available for $\gamma_j=1.4$. Consequently, tables and charts showing this relation for other values of γ_j were prepared for these calculations. Inasmuch as these data are not generally available, they are presented in table I.

An idea of the curvature of the leading characteristic may be gained from reference 2 where an expression for the point of inflexion has been derived in terms of γ_j and the local Mach number on the leading characteristic. This is

$$M=\sqrt{\frac{3}{2-\gamma_j}} \qquad \text{(A3)}$$

The curve given by this relation is shown in figure 72. For a constant value of γ_j, the leading characteristic will be concave to the jet axis for values of

M above the curve and convex to the axis for values below.

SOLUTION FOR THE SONIC EXIT

A solution to the sonic exit for M_j exactly equal to 1 is difficult since the slope of the leading characteristic is infinite. The usual procedure is to select a value of M_j slightly greater than 1 with the implicit assumption that the difference in this solution from that for M_j exactly equal to 1 is negligible. The first solutions for the sonic exit (fig. 14(a)) were calculated for $M_j=1.01$ ($\mu_j=81.93°$). The errors in the calculations near the axis have been discussed and shown to be significant. The advantages of having a so-called universal solution for the expansive flow field leaving a sonic exit for which the errors in the region of the axis are small and for which the properties of the expansive flow field are tabulated have been recognized in the past. Such a solution would not only be valuable to jet studies but to any axisymmetric problem involving flow from a sonic orifice (for example, in the design of axisymmetric nozzles for supersonic wind tunnels). By using iterative procedures, Owen and Thornhill (ref. 30) have made a characteristic calculation of the flow into a vacuum for $M_j=1.0038$ ($\mu_j=85°$) with special consideration being given to the flow near the axis of symmetry. The properties of the flow field off the axis are not given; consequently, the additional universal applicability that this solution might otherwise have is lacking. This additional applicability would be somewhat limited, however, since the method employed, although very accurate, gave large mesh size to the characteristic net. The points defining the flow field are, therefore, few.

In an effort to obtain a solution for the sonic exit that would have the flow field defined in small increments and to assess the effect of errors near the axis upon the jet boundary, the initial conditions of Owen and Thornhill ($M_j=1.0038$, $\mu_j=85°$) were utilized in a calculation of an exceptionally dense net for $p_j/p_\infty=2$ with a second approximation being carried out for each axis point by trans-calculation. The results of these calculations are given in table II for the expansion portion of the flow field only. A comparison of the characteristic net at the axis and the boundary shape with the solution for $M_j=1.01$ (from fig. 14(a)) is shown in figure 73. Figure 74 presents, to a sensitive ordinate scale, a comparison of the nondimensional velocity distributions along the axis for several conditions. A comparison of the results for $p_j/p_\infty=2$ in figures 73 and 74 shows that appreciable errors in the characteristic net near the axis and, therefore, in the velocity along the axis, may have negligibly small effects upon the boundary shape through the maximum value of y/r_j even for the critical condition of $M_j\approx 1$. The initial portions of the velocity distributions for $p_j/p_\infty=10$ and 20 and $M_j=1.01$ are included in figure 74 to illustrate the effects of further increasing the mesh size (see fig. 14(a)). From the comparisons of the calculations for $p_j/p_\infty=2$, the errors in the boundaries for $p_j/p_\infty=10$ and 20 may be expected to be small.

The calculation of Owen and Thornhill and the present calculation ($M_j=1.0038$) of the velocity along the axis are in good agreement (fig. 74). This agreement would appear to indicate that even near $M=1$ the simpler noniterative procedure of the present calculation may be expected to give results equally as satisfactory as those of the more tedious iterative procedures if the net is dense. Experimental measurements of the velocity along the axis have been made by a number of methods. (See refs. 9, 10, and 31.) The probe results of reference 10 and the interferometric studies of reference 31 appear to contain least error and it is from a comparison with these results that Owen and Thornhill concluded that the agreement between experiment and their calculation was good. For a given accuracy in measuring pressure, the use of total-pressure probes to determine Mach number and velocity introduces large errors as the Mach number decreases from about 1.2 to 1; consequently, for values of x/r_j less than about 0.45, the probe results are subject to question. The interferometric measurements (ref. 31) are subject only to the accumulative errors in reducing the data; these results are shown by the hatched band in figure 74 where the width of the band denotes the scatter and probable error. Measurements have been made by Mr. R. M. O'Donnell of the Langley Aeronautical Laboratory utilizing the mixing zone apparatus of the Langley 9-Inch Tunnel Section.

In order to avoid probe interference and the inaccuracies near $M=1$, a splitter-plate technique was used with orifices installed on the plate surface along the jet axis. The results of these measurements are also indicated in figure 74. A comparison of the experimental results with the theoretical calculations would appear to indicate that the expansive flow field properties included in table II are sufficiently accurate to expect good results in application to other problems.

802688 O—59——3

APPENDIX B

CALCULATION OF INITIAL CURVATURE OF A JET BOUNDARY BY USE OF THE METHOD OF JOHANNESEN AND MEYER

Johannesen and Meyer (ref. 14) have obtained an approximate solution for the axially symmetrical flow of a perfect gas in the region of an expansion around a corner. This solution, which is in the form of an expansion in powers of the distance from the corner, replaces the conventional method of characteristics in such a region. An application is made to a jet discharging into still air where the static pressure in the jet nozzle is higher than ambient pressure. A formula is presented for the initial curvature, at the lip of the nozzle, of a jet boundary.

With the use of the notation of reference 14 (given at the end of this appendix), the initial curvature is given by

$$\left(\frac{d\theta}{d\bar{R}}\right)_{R=0}-\left(\frac{1}{q_F}\right)\cot\mu_F\left(\frac{dq}{d\bar{R}}\right)_{R=0} =\frac{-[q_F\sin\theta_J\sin^2\mu_F+u_1(\phi_F)]}{q_F\sin^2\mu_F} \quad \text{(B1)}$$

Now on the jet boundary, $\frac{dq}{d\bar{R}}=0$ and

$$\left(\frac{d\theta}{d\bar{R}}\right)_{R=0}=\frac{-[q_F\sin\theta_J\sin^2\mu_F+u_1(\phi_F)]}{q_F\sin^2\mu_F} \quad \text{(B2)}$$

(The initial radius of curvature in the symbolism of the text is ρ_o/d_j and is equal to $\frac{1}{2}\left(\frac{dR}{d\theta}\right)_{R=0}$.)

Each of the quantities of equation (B2) except $u_1(\phi_F)$ may be easily determined once the initial characteristics of the jet flow are given. The velocity component $u_1(\phi_F)$ is given by

$$u_1(\phi)=K(\phi)\Big[I_1(\phi)\cos\beta_o+I_2(\phi)\sin\beta_o -\lambda I_3(\phi)\cos\beta_o+\lambda I_4(\phi)\sin\beta_o+C_2\Big] \quad \text{(B3)}$$

where $K(\phi)=-\frac{a_j}{2\lambda}(1-z^2)^2\sqrt{z}$

and the integrals $I_1(\phi)\ldots I_4(\phi)$ can be written as

$$\left.\begin{aligned} I_1(\phi)&=\int\frac{\cos(\lambda^{-1}\sin^{-1}z)}{(1-z^2)^2\sqrt{z}}\,dz\\ I_2(\phi)&=\int\frac{\sin(\lambda^{-1}\sin^{-1}z)}{(1-z^2)^2\sqrt{z}}\,dz\\ I_3(\phi)&=\int\frac{\sin(\lambda^{-1}\sin^{-1}z)}{(1-z^2)^{3/2}z^{3/2}}\,dz\\ I_4(\phi)&=\int\frac{\cos(\lambda^{-1}\sin^{-1}z)}{(1-z^2)^{3/2}z^{3/2}}\,dz \end{aligned}\right\} \quad \text{(B4)}$$

The limits of integration are determined from the values of z corresponding to ϕ_L and ϕ_F (the values which ϕ takes on the leading and final Mach lines, respectively, at the lip). The relation between z and ϕ is given as

$$z=\sin\lambda(\phi+\beta_o) \quad \text{(B5)}$$

where

$$\beta_o=\mu_L-\pi-\phi_c+\frac{1}{\lambda}\cot^{-1}\left(\frac{1}{\lambda}\tan\mu_L\right) \quad \text{(B6)}$$

It will be noted that β_o is also given by the Busemann "pressure number" minus 1,000.

The integrals of equation (B4) have been computed for $\gamma=1.400$ over a large range of values of $z(1.0\lessapprox M_F\lessapprox 5.2)$ and are tabulated in table III. The value of each integral given in table III represents the integral between the limits $z=0.03$ and the value of z listed in the table. Thus in applying these results to the calculation of the initial curvature of a jet boundary, it is necessary only to obtain z_L and z_F corresponding to the given jet flow boundaries. The corresponding values of $I_1(\phi)\ldots I_4(\phi)$ can be obtained from table III and the difference between the integrals for z_F and z_L represents the desired solution to equation (B4).

In equation (B3), C_2 is an arbitrary constant and, since the integrals of equation (B4) are zero

for $z=z_L$, it is given by

$$C_2=\frac{u_1(\phi_L)}{K(\phi_L)} \tag{B7}$$

It will be noted that the solutions to equation (B4) given in table III are useful not only in the previously discussed application, but also in the much broader application of the characteristic calculation of the jet flow field as discussed in reference 2.

NOTATION FROM REFERENCE 14

(All distances made nondimensional with respect to radius of jet at exit)

a_* critical speed of sound

$I_1(\phi) \ldots I_4(\phi)$ integrals defined by equation (B4)

M Mach number

R, ϕ polar coordinates in meridian plane with origin at center of expansion

q velocity magnitude

u, v velocity components in direction of R and ϕ increasing

θ angle between downstream direction on axis and local stream direction

$\lambda=\sqrt{\frac{\gamma-1}{\gamma+1}}$

μ local Mach angle

Subscripts:

c limiting value as center is approached along boundary streamline from upstream

F limiting value as center is approached along final Mach line in region of centered expansion

J limiting value as center is approached along boundary streamline from downstream

L limiting value as center is approached along leading Mach line in region of centered expansion

APPENDIX C

METHOD AND ACCURACY OF CALCULATIONS FOR CONICALLY DIVERGENT NOZZLES

CALCULATIONS FOR p_j/p_∞ OF 1 TO 10

The method of characteristics was used throughout, and the procedure was similar to that described in the section of appendix A entitled "Solution for Divergent Nozzles." The leading characteristic lines and the initial values for the characteristic lines from the center of expansion were computed manually. The characteristic nets were determined on a card-programed electronic calculator.

The calculations were proposed to be carried through only until the maximum diameter of the jet boundary was reached, since the shape beyond the maximum diameter has little practical value. It will be noted, however, that a number of the boundary calculations extend beyond the maximum diameter. This random extension results from a random continuance of the calculations; since these additional points on the boundary were available, they have been included. For those boundaries that extend well beyond the maximum diameter, the boundary shape in the neighborhood of the final calculated point on the boundary may be subject to small errors that the foldback method of characteristics can introduce in this region. (See appendix A.) A few of the boundary calculations at $M_j=1.5$ were inadvertently terminated slightly short of the maximum diameter. In all the present calculations the first-family characteristic line determining the final point on the boundary had its origin on the leading-characteristic line. Consequently, the leading-characteristic line was terminated short of the jet axis, and the complications of calculations coming off the axis were not encountered. (See appendix A.) Inasmuch as the accuracy of the boundary calculations is closely related to the density of the characteristic net, some idea of the number of points contained in a typical characteristic net may be of interest. For every increase in p_j/p_∞ of 0.25, an additional characteristic line from the center of expansion was introduced. Thus, a relatively uniform accuracy was maintained as p_j/p_∞ was increased. For example, at $M_j=1.5$, $\theta_N=15°$, and $\gamma_j=1.400$, there are 28 points in the calculation at $p_j/p_\infty=1$ and 288 points in the calculation at $p_j/p_\infty=10$.

The calculated boundaries are presented in discontinuous-slope form, which is compatible with the lattice-point characteristic method (that is, calculated points on boundary joined by straight lines). In practical application a smooth curve is, of course, fitted to the discontinuous-slope form of the boundary, particular care being given to maintain the initial inclination of the boundary.

CALCULATIONS FOR LARGE VALUES OF p_j/p_∞

The procedure was, in general, the same as that described in the preceding section. For expediency, only the boundary points and a portion of the characteristic net sufficient to define the jet shock (by the foldback method of characteristics) were retained in the print-out phase of the automatic calculations.

Although considerable experience had been obtained in the previous calculations for jet pressure ratios of the order of 10 and lower, no information was available for determining beforehand the increments between the characteristic lines introduced from the center of expansion that should be used to insure a reliable boundary solution for the large pressure ratios. A similar situation existed as regards the spacing of the points along the leading characteristic line. After some trial calculations of boundaries, it was decided to introduce a new characteristic line from the center of expansion for approximately every degree of expansion. The spacing of the points along the leading characteristic line was selected on the basis of additional trial calculations and other factors, some of which are discussed subsequently. However, it may be noted here that points along the leading characteristic line were calculated for increments in x/r_j of 0.02, and

this spacing is recommended for the range of pressure ratios covered by this study. For values of M_j and θ_N greatly different from the values used herein ($M_j=2.5$, $\theta_N=15°$), and for pressure ratios greater than those covered in this study (of the order of 42,000), the rate at which the characteristic lines were introduced from the center of the expansion and the point spacing used along the leading characteristic line might not be adequate. With regard to the latter, the shape and inclination of the leading characteristic line have, in general, first-order dependence upon M_j and θ_N.

In the presentation of the boundaries, it will be noted in two cases that two boundaries and two shocks are shown. In both cases these two boundaries and shocks represent the examination of the effect of point spacing along the leading characteristic line upon the shape and position of the calculated boundary and the jet shock. This examination was primarily an outgrowth of the desire to retain a programing capacity (30 points along the leading characteristic) for the automatic calculations that had been used in the previous studies at lower pressure ratios and, at the same time, to obtain, if possible, a significant portion of the boundary and jet shock without incurring large errors. The shorter boundaries and jet shocks correspond to calculations made by the use of the first 30 points along the leading characteristic (that is, increments in x/r_j maintained standard at 0.02). The longer boundaries and jet shocks correspond to results obtained by use of every other point of the first 30 calculated points on the leading characteristic (increments in x/r_j of 0.04), every third point of the second 30 calculated points (increments in x/r_j of 0.06), and every fourth point of an additional 20 calculated points (increments in x/r_j of 0.08). The results show that the errors associated with the larger point spacing are small; consequently, this spacing was used in most of the calculations. A few of the boundaries do not have the extent to be expected from this point spacing. For these boundaries, difficulties encountered in the automatic phase of the calculation shortened the calculations. Since with one or two exceptions the completed portions of the boundaries for these shortened calculations are believed to convey adequately the shape of the boundary over a considerable distance from the jet exit, no effort was made to continue these calculations. As before, the boundaries are presented in discontinuous-slope form.

APPENDIX D

ADDITIONAL DETAILS ON CALCULATIONS OF δ_j FOR VARYING θ_N AND β

Consider the segment of the general boattailed fuselage or nacelle shown in figure 75(a). The rigorous point of analysis covers the infinitesimal region immediately upstream of the jet exit and adjacent to the boattail and nozzle surfaces, and immediately downstream of the jet exit; the initial values must conform to these conditions in using the results. The point of analysis is magnified in figure 75(b) and indicates the initial ratio of specific heats, Mach number, and static pressure of the ambient flow and of the jet flow. Only positive values of β and θ_N will be considered, positive β denoting convergence of the boattail and positive θ_N denoting divergence of the nozzle in the conventional sense as indicated in the figure. The initial conditions imply, of course, that the ambient flow is inclined at the angle β and that the jet flow is inclined at the angle θ_N. The sign convention for the initial deflection of the jet boundary δ_j is also indicated in figure 75(b).

The value of the initial deflection δ_j is a function only of the initial properties introduced above. If β and θ_N are both zero, one may visualize that when $p_j/p_\infty > 1$ a shock originating at the jet exit is introduced into the ambient stream (excluding $M_\infty = 1$) and an expansion centered at the jet exit is introduced into the jet; the converse is true for $p_j/p_\infty < 1$ (excluding $M_j = 1$). Exactly at $p_j/p_\infty = 1$, the jet and ambient flows are free of these distrubances, and $\delta_j = 0$. However, if β and/or θ_N are not zero, then the value of δ_j at $p_j/p_\infty = 1$ is also not zero, and a disturbance is always introduced in the jet or in the ambient flow or in both. The type of disturbance phenomenon that originates at the jet exit and is introduced in the jet and/or in the ambient flow may be logically reasoned as follows.

In ambient flow:

$$\left.\begin{array}{ll} (\delta_j+\beta)>0 & \text{Shock} \\ (\delta_j+\beta)=0 & \text{None} \\ (\delta_j+\beta)<0 & \text{Expansion} \end{array}\right\} \qquad \text{(D1)}$$

In jet flow:

$$\left.\begin{array}{ll} (\delta_j-\theta_N)>0 & \text{Expansion} \\ (\delta_j-\theta_N)=0 & \text{None} \\ (\delta_j-\theta_N)<0 & \text{Shock} \end{array}\right\} \qquad \text{(D2)}$$

With increasing values of p_j/p_∞ the general phenomena for finite β and/or θ_N vary in the following manner, the first given phenomenon pertaining to the jet and the second to the ambient stream: shock-expansion, shock-none, shock-shock, none-shock, and expansion-shock. (The special cases of M_j or $M_\infty = 1$ offer exceptions.)

The determination of the value of δ_j is based upon the requirement that the static pressures on both sides of the mixing boundary must be equal. For a given set of initial conditions there is no explicit solution for δ_j. In the present calculations values of flow deflection were assumed and applied to the jet or ambient stream as indicated in the preceding paragraph. Essentially, therefore, values of δ_j were assumed and values of p_j/p_∞ were calculated for various initial values of M_j, M_∞, β, and θ_N by appropriate use of the shock and expansion equations and by rotation of axes (parallel to θ_N or to β).

REFERENCES

1. Krzywoblocki, M. Z.: Jets. NOTS TM No. 1576, U.S. Naval Ord. Test Station (Inyokern, Calif.), Sept. 1953.
2. Johannesen, N. H.: Ejector Theory and Experiments. A.T.S. No. 1, Trans. Danish Acad. of Tech. Sci. (Copenhagen), 1951.
3. Oudart, Adalbert: L'Étude des jets et la mécanique théorique des fluides. Ministère de l'air. Publications Scientifiques et Techniques No. 234, 1949.
4. Love, Eugene S.: Base Pressure at Supersonic Speeds on Two-Dimensional Airfoils and on Bodies of Revolution With and Without Fins Having Turbulent Boundary Layers. NACA TN 3819, 1957. (Supersedes NACA RM L53C02.)
5. Coletti, Donald E.: Measurements and Predictions of Flow Conditions on a Two-Dimensional Base Separating a Mach Number 3.36 Jet and a Mach Number 1.55 Outer Stream. NACA RM L54C08, 1954.
6. Foster, Charles R., and Cowles, Frederick B.: Experimental Study of Gas-Flow Separation in Overexpanded Exhaust Nozzles for Rocket Motors. Progress Rep. No. 4–103 (Contract No. W–04–200–ORD–455, Ord. Dept.), Jet Propulsion Lab., C.I.T., May 9, 1949.
7. Wada, Yoshimasa: On the Recurrent Figure of a Jet. Jour. Phys. Soc. of Japan, vol. 7, no. 2, Mar.-Apr. 1952, pp. 211–214.
8. Pack, D. C.: A Note on Prandtl's Formula for the Wave-Length of a Supersonic Gas Jet. Quarterly Jour. Mech. and Appl. Math., vol. III, pt. 2, June 1950, pp. 173–181.
9. Hartmann, Jul., and Lazarus, Freimut: The Air-Jet With a Velocity Exceeding That of Sound. Phil. Mag. and Jour. Sci., ser. 7, vol. 31, no. 204, Jan. 1941, pp. 35–50.
10. Hartmann, Jul.: The Acoustic Air-Jet Generator. Ingeniørvidenskabelige Skrifter, Nr. 4, Akademiet for de Tekniske Videnskaber og Dansk Ingeniørforening (Copenhagen), 1939.
11. Pack, D. C.: On the Formation of Shock-Waves in Supersonic Gas Jets (Two-Dimensional Flow). Quarterly Jour. Mech. and Appl. Math., vol. I, pt. 1, Mar. 1948, pp. 1–17.
12. Meyer, R. E.: The Method of Characteristics for Problems of Compressible Flow Involving Two Independent Variables.
    Part I. The General Theory. (Appendix II by S. Goldstein.) Quarterly Jour. Mech. and Appl. Math., vol. I, pt. 2, June 1948, pp. 196–219.
    Part II. Integration Along a Mach Line. The Radial Focusing Effect in Axially Symmetrical Flow. Quarterly Jour. Mech. and Appl. Math., vol. I, pt. 4, Dec. 1948, pp. 451–469.
13. Meyer, R. E.: Focusing Effects in Two-Dimensional, Supersonic Flow. Phil. Trans. Roy. Soc. (London), ser. A, vol. 242, no. 844, Dec. 20, 1949, pp. 153–171.
14. Johannesen, N. H., and Meyer, R. E.: Axially-Symmetrical Supersonic Flow Near the Centre of an Expansion. Aero. Quarterly, vol. II, pt. II, Aug. 1950, pp. 127–142.
15. Rousso, Morris D., and Kochendorfer, Fred D.: Velocity and Temperature Fields in Circular Jet Expanding From Choked Nozzle into Quiescent Air. NACA RM E51F18, 1951.
16. Hubbard, Harvey H.: A Survey of the Aircraft-Noise Problem With Special Reference to Its Physical Aspects. NACA TN 2701, 1952.
17. Lighthill, M. J.: On Sound Generated Aerodynamically—II. Turbulence as a Source of Sound. Proc. Roy. Soc. (London), ser. A, vol. 222, no. 1148, Feb. 23, 1954, pp. 1–32.
18. Bressette, Walter E.: Investigation of the Jet Effects on a Flat Surface Downstream of the Exit of a Simulated Turbojet Nacelle at a Free-Stream Mach Number of 2.02. NACA RM L54E05a, 1954.
19. Isenberg, J. S.: The Method of Characteristics in Compressible Flow. Part I (Steady Supersonic Flow). Tech. Rep. No. F-TR-1173A-ND, ATI No. 26341, Air Materiel Command, U.S. Air Force, Dec. 1947.
20. Schäfer, M.: Steady Supersonic Flows. British M.A.P. Völkenrode. Reps. and Translations No. 995, Apr. 15, 1948. Reps. and Translations No. 996, May 1, 1948.
21. Love, Eugene S.: Supersonic Wave Interference Affecting Stability. NACA TN 4358, 1958. (Supersedes NACA RM L55L14a.)
22. Love, Eugene S.: Pressure Rise Associated With Shock-Induced Boundary-Layer Separation. NACA TN 3601, 1955.
23. Rousso, Morris D., and Baughman, L. Eugene: Spreading Characteristics of a Jet Expanding From Choked Nozzels at Mach 1.91. NACA TN 3836, 1956. (Supersedes NACA RM E51L19.)
24. Liepmann, H. W., Roshko, A., and Dhawan S.: On Reflection of Shock Waves From Boundary Layers. NACA Rep. 1100, 1952. (Supersedes NACA TN 2334.)
25. Barry, Frank W.: Interaction of an Oblique Shock Wave With a Boundary Layer on a Flat Plate. D.Sc. Thesis, M.I.T., 1950.
26. Kawamura, Ryuma: Reflection of a Wave at an Interface of Supersonic Flows and Wave Patterns in a Supersonic Compound Jet. Jour. Phys. Soc. of Japan, vol. 7, no. 5, Sept.–Oct. 1952, pp. 482–485.
27. Wilder, John G., Jr.: Part I of Final Report on Phase I of the Study of Air Exchange Problems in Supersonic Tunnels. Rep. No. AD–570–A–5 (Contract No. W33–038 ac–21809), Cornell Aero. Lab., Inc., Jan. 1949.

28. Anon.: Standard Atmosphere—Tables and Data for Altitudes to 65,800 Feet. NACA Rep. 1235, 1955. (Supersedes NACA TN 3182.)
29. Ferri, Antonio: Elements of Aerodynamics of Supersonic Flows. The Macmillan Co., 1949.
30. Owen, P. L., and Thornhill, C. K.: The Flow in an Axially Symmetric Supersonic Jet From a Nearly Sonic Orifice Into a Vacuum. Rep. No. 30/48 (Theo. Res. Rep. No. 5/48), Ministry of Supply, Armament Res. Establishment (British), Sept. 1948.
31. Ladenburg, R., Van Voorhis, C. C., and Winckler, J.: Interferometric Study of Supersonic Phenomena: Part I. A Supersonic Air Jet at 60 lb/in² Tank Pressure. NAVORD Rep. 69-46, Bur. Ordnance, Navy Dept., Apr. 17, 1946.

TABLE I.—RELATION BETWEEN BUSEMANN'S PRESSURE NUMBER, MACH ANGLE, AND MACH NUMBER FOR SEVERAL VALUES OF THE RATIO OF SPECIFIC HEATS

$$\left[P=1090^\circ-\mu-\left(\frac{\gamma+1}{\gamma-1}\right)^{\frac{1}{2}}\cot^{-1}\left[\left(\frac{\gamma+1}{\gamma-1}\right)^{\frac{1}{2}}\tan\mu\right]\right]$$

M	μ	P for—				
		$\gamma=1.200$	$\gamma=1.300$	$\gamma=1.400$	$\gamma=1.500$	$\gamma=1.667$
1.00	90.00	1000.00	1000.00	1000.00	1000.00	1000.00
1.05	72.25	999.46	999.48	999.51	999.53	999.56
1.10	65.38	998.53	998.60	998.66	998.72	998.81
1.15	60.41	997.37	997.50	997.62	997.73	997.89
1.20	56.44	996.06	996.27	996.46	996.62	996.87
1.25	53.13	994.60	994.89	995.16	995.40	995.75
1.30	50.28	993.09	993.49	993.84	994.16	994.62
1.35	47.79	991.50	992.01	992.46	992.86	993.44
1.40	45.58	989.85	990.48	991.04	991.53	992.24
1.45	43.60	988.14	988.90	989.57	990.16	991.00
1.50	41.81	986.40	987.31	988.09	988.79	989.78
1.55	40.18	984.65	985.70	986.62	987.42	988.56
1.60	38.68	982.87	984.09	985.14	986.05	987.35
1.65	37.31	981.08	982.47	983.65	984.69	986.14
1.70	36.03	979.30	980.86	982.19	983.35	984.96
1.75	34.85	977.49	979.24	980.72	982.01	983.79
1.80	33.75	975.70	977.64	979.28	980.68	982.64
1.85	32.72	973.90	976.04	977.84	979.38	981.50
1.90	31.76	972.11	974.45	976.41	978.08	980.38
1.95	30.85	970.32	972.87	975.01	976.81	979.28
2.00	30.00	968.55	971.32	973.63	975.57	978.22
2.05	29.20	966.77	969.77	972.25	974.33	977.16
2.10	28.44	965.02	968.24	970.90	973.12	976.12
2.15	27.72	963.28	966.74	969.57	971.93	975.12
2.20	27.04	961.55	965.25	968.26	970.77	974.13
2.25	26.39	959.83	963.78	966.98	969.62	973.16
2.30	25.77	958.15	962.34	965.72	968.51	972.22
2.35	25.18	956.47	960.91	964.47	967.41	971.30
2.40	24.62	954.80	959.50	963.25	966.32	970.40
2.45	24.09	953.16	958.11	962.05	965.27	969.52
2.50	23.58	951.53	956.74	960.87	964.23	968.65
2.55	23.09	949.93	955.40	959.72	963.22	967.81
2.60	22.62	948.36	954.09	958.59	962.23	967.00
2.65	22.17	946.78	952.78	957.47	961.26	966.19
2.70	21.74	945.22	951.49	956.37	960.30	965.40

TABLE I.—RELATION BETWEEN BUSEMANN'S PRESSURE NUMBER, MACH ANGLE, AND MACH NUMBER FOR SEVERAL VALUES OF THE RATIO OF SPECIFIC HEATS—Concluded

$$\left[P=1090°-\mu-\left(\frac{\gamma+1}{\gamma-1}\right)^{\frac{1}{2}}\cot^{-1}\left[\left(\frac{\gamma+1}{\gamma-1}\right)^{\frac{1}{2}}\tan\mu\right]\right]$$

M	μ	P for—				
		$\gamma=1.200$	$\gamma=1.300$	$\gamma=1.400$	$\gamma=1.500$	$\gamma=1.667$
2.75	21.32	943.71	950.25	955.32	959.38	964.65
2.80	20.92	942.20	949.01	954.27	958.47	963.90
2.85	20.54	940.70	947.78	953.22	957.56	963.16
2.90	20.17	939.24	946.59	952.22	956.69	962.45
2.95	19.81	937.78	945.40	951.22	955.83	961.74
3.00	19.47	936.36	944.25	950.25	955.00	961.07
3.05	19.14	934.95	943.11	949.30	954.17	960.40
3.10	18.82	933.54	941.98	948.35	953.36	959.74
3.15	18.51	932.18	940.88	947.44	952.58	959.10
3.20	18.21	930.82	939.80	946.54	951.80	958.48
3.25	17.92	929.49	938.74	945.65	951.05	957.87
3.30	17.64	928.17	937.69	944.78	950.30	957.27
3.35	17.37	926.87	936.67	943.93	949.58	956.69
3.40	17.10	925.58	935.65	943.09	948.86	956.12
3.45	16.85	924.34	934.67	942.28	948.18	955.56
3.50	16.60	923.07	933.67	941.46	947.48	955.01
3.55	16.36	921.84	932.73	940.69	946.82	954.48
3.60	16.13	920.66	931.79	939.91	946.17	953.96
3.65	15.90	919.47	930.86	939.16	945.52	953.45
3.70	15.68	918.28	929.94	938.40	944.89	952.94
3.75	15.47	917.13	929.05	937.67	944.27	952.45
3.80	15.26	916.00	928.17	936.96	943.67	951.97
3.85	15.05	914.88	927.31	936.26	943.08	951.51
3.90	14.86	913.77	926.45	935.56	942.49	951.04
3.95	14.66	912.68	925.62	934.89	941.93	950.60
4.00	14.48	911.60	924.79	934.21	941.36	950.14
4.05	14.29	910.54	923.98	933.57	940.81	949.72
4.10	14.12	909.49	923.18	932.92	940.27	949.28
4.15	13.94	908.48	922.41	932.29	939.75	948.88
4.20	13.77	907.44	921.62	931.66	939.21	948.46
4.25	13.61	906.46	920.88	931.06	938.71	948.06
4.30	13.45	905.46	920.13	930.45	938.21	947.66
4.35	13.29	904.49	919.40	929.87	937.72	947.28
4.40	13.14	903.54	918.68	929.30	937.24	946.91
4.45	12.99	902.59	917.96	928.72	936.76	946.53
4.50	12.84	901.66	917.27	928.16	936.29	946.17
4.55	12.70	900.75	916.59	927.62	935.84	945.81
4.60	12.56	899.83	915.90	927.07	935.39	945.46
4.65	12.42	898.95	915.24	926.55	934.95	945.12
4.70	12.28	898.10	914.61	926.05	934.54	944.80
4.75	12.15	897.23	913.97	925.53	934.11	944.46
4.80	12.02	896.36	913.32	925.02	933.68	944.13

TABLE II.—EXPANSIVE FLOW FIELD OBTAINED BY CHARACTERISTIC CALCULATIONS FOR JET FLOW FROM NEAR-SONIC EXIT ($M_i=1.0038$; $\mu_i=85°$)

x/r_i	y/r_i	θ, radians	μ, radians	V/V_i
0. 0000000	1. 000000	0. 0000000	1. 483530	0. 4095466
. 0000000	1. 000000	$.1570796\times10^{-3}$	1. 466077	. 4101196
. 0000000	1. 000000	$.3665190\times10^{-3}$	1. 448624	. 4107984
. 0000000	1. 000000	$.6108651\times10^{-3}$	1. 431171	. 4115834
. 0000000	1. 000000	$.9948375\times10^{-3}$	1. 413715	. 4124758
. 0000000	1. 000000	$.1361357\times10^{-2}$	1. 396262	. 4134764
. 0000000	1. 000000	$.1919861\times10^{-2}$	1. 378809	. 4145861
. 0000000	1. 000000	$.2443460\times10^{-2}$	1. 361357	. 4158062
. 0000000	1. 000000	$.3141592\times10^{-2}$	1. 343903	. 4171382
. 0000000	1. 000000	$.4014256\times10^{-2}$	1. 326450	. 4185834
. 0000000	1. 000000	$.4886921\times10^{-2}$	1. 308997	. 4201434
. 0000000	1. 000000	$.6108651\times10^{-2}$	1. 291544	. 4218200
. 0000000	1. 000000	$.7330381\times10^{-2}$	1. 274091	. 4236149
. 0000000	1. 000000	$.8726645\times10^{-2}$	1. 256638	. 4255301
. 0000000	1. 000000	$.1029744\times10^{-1}$	1. 239183	. 4275681
. 0000000	1. 000000	$.1204277\times10^{-1}$	1. 221729	. 429/307
. 0000000	1. 000000	$.1413716\times10^{-1}$	1. 204276	. 4320205
. 0000000	1. 000000	$.1623156\times10^{-1}$	1. 186824	. 4344399
. 0000000	1. 000000	$.1867502\times10^{-1}$	1. 169370	. 4369920
. 0000000	1. 000000	$.2129301\times10^{-1}$	1. 151916	. 4396794
. 0000000	1. 000000	$.2426007\times10^{-1}$	1. 134464	. 4425051
. 0000000	1. 000000	$.2740166\times10^{-1}$	1. 117010	. 4454728
. 0000000	1. 000000	$.3089232\times10^{-1}$	1. 099557	. 4485856
. 0000000	1. 000000	$.3473204\times10^{-1}$	1. 082104	. 4518470
. 0000000	1. 000000	$.3874630\times10^{-1}$	1. 064650	. 4552610
. 0000000	1. 000000	$.4328415\times10^{-1}$	1. 047197	. 4588314
. 0000000	1. 000000	$.4799654\times10^{-1}$	1. 029744	. 4625626
. 0000000	1. 000000	$.5305800\times10^{-1}$	1. 012291	. 4664589
. 0000000	1. 000000	$.5864305\times10^{-1}$	. 9948374	. 4705248
. 0000000	1. 000000	$.6457717\times10^{-1}$	. 9773841	. 4747653
. 0000000	1. 000000	$.7103489\times10^{-1}$	. 9599308	. 4791852
. 0000000	1. 000000	$.7784167\times10^{-1}$	. 9424776	. 4837899
. 0000000	1. 000000	$.8517205\times10^{-1}$	. 9250244	. 4885848
. 0000000	1. 000000	$.9285150\times10^{-1}$	. 9075712	. 4935756
. 0000000	1. 000000	. 1012291	. 8901177	. 4987684
. 0000000	1. 000000	. 1101303	. 8726642	. 5041691
. 0000000	1. 000000	. 1195550	. 8552110	. 5097841
. 0000000	1. 000000	. 1296779	. 8377581	. 5156200
. 0000000	1. 000000	. 1403245	. 8203046	. 5216837
. 0000000	1. 000000	. 1516691	. 8028511	. 5279822
. 0000000	1. 000000	. 1638864	. 7853980	. 5345225
. 0000000	1. 000000	. 1766272	. 7679447	. 5413120
. 0000000	1. 000000	. 1902408	. 7504914	. 5483583
. 0000000	1. 000000	. 2047270	. 7330381	. 5556689
. 0000000	1. 000000	. 2200859	. 7155847	. 5632514

TABLE II.—EXPANSIVE FLOW FIELD OBTAINED BY CHARACTERISTIC CALCULATIONS FOR JET FLOW FROM NEAR-SONIC EXIT ($M_i = 1.0038$; $\mu_i = 85°$)—Continued

x/r_i	y/r_i	θ, radians	μ, radians	V/V_i
0.8748868×10^{-2}	0.9000000	0.0000000	1.483530	0.4095466
$.9555603 \times 10^{-2}$	.9092211	$.1446463 \times 10^{-3}$	1.463211	.4102238
$.1031396 \times 10^{-1}$	.9162524	$.3427840 \times 10^{-3}$	1.444355	.4109805
$.1102749 \times 10^{-1}$	.9218810	$.5896295 \times 10^{-3}$	1.427030	.4117854
$.1170429 \times 10^{-1}$	.9265757	$.9433881 \times 10^{-3}$	1.407850	.4128000
$.1234886 \times 10^{-1}$	.9305198	$.1328176 \times 10^{-2}$	1.391373	.4137761
$.1296833 \times 10^{-1}$	.9339613	$.1856349 \times 10^{-2}$	1.372823	.4149921
$.1356240 \times 10^{-1}$	.9369516	$.2415849 \times 10^{-2}$	1.356551	.4161617
$.1413793 \times 10^{-1}$	.9396278	$.3119539 \times 10^{-2}$	1.339143	.4175210
$.1469872 \times 10^{-1}$	.9420389	$.3972444 \times 10^{-2}$	1.321153	.4190446
$.1524232 \times 10^{-1}$	.9442070	$.4889666 \times 10^{-2}$	1.304468	.4205672
$.1577920 \times 10^{-1}$	.9462136	$.6056157 \times 10^{-2}$	1.285959	.4223814
$.1630253 \times 10^{-1}$	.9480419	$.7297595 \times 10^{-2}$	1.268739	.4241893
$.1681743 \times 10^{-1}$	.9497379	$.8709333 \times 10^{-2}$	1.251399	.4261289
$.1732503 \times 10^{-1}$	.9513189	$.1029699 \times 10^{-1}$	1.234031	.4281934
$.1782630 \times 10^{-1}$	.9527994	$.1206632 \times 10^{-1}$	1.216703	.4303770
$.1832639 \times 10^{-1}$	.9542041	$.1411304 \times 10^{-1}$	1.198692	.4327803
$.1881765 \times 10^{-1}$	.9555173	$.1626392 \times 10^{-1}$	1.181620	.4351867
$.1930905 \times 10^{-1}$	.9567735	$.1870457 \times 10^{-1}$	1.164032	.4377994
$.1979706 \times 10^{-1}$	.9579674	$.2135203 \times 10^{-1}$	1.146674	.4405136
$.2028628 \times 10^{-1}$	.9591157	$.2430263 \times 10^{-1}$	1.129012	.4434169
$.2077330 \times 10^{-1}$	.9602138	$.2747403 \times 10^{-1}$	1.111633	.4464162
$.2126247 \times 10^{-1}$	.9612757	$.3096321 \times 10^{-1}$	1.094076	.4495936
$.2175437 \times 10^{-1}$	.9623052	$.3477736 \times 10^{-1}$	1.076417	.4529425
$.2224544 \times 10^{-1}$	.9632974	$.3883547 \times 10^{-1}$	1.059087	.4563820
$.2274390 \times 10^{-1}$	.9642718	$.4332415 \times 10^{-1}$	1.041362	.4600609
$.2324242 \times 10^{-1}$	.9652153	$.4807383 \times 10^{-1}$	1.023995	.4638276
$.2374527 \times 10^{-1}$	.9661386	$.5318255 \times 10^{-1}$	1.006649	.4677544
$.2425671 \times 10^{-1}$	.9670509	$.5874897 \times 10^{-1}$	.9890757	.4719052
$.2477335 \times 10^{-1}$	.9679471	$.6469384 \times 10^{-1}$	.9716050	.4762087
$.2529941 \times 10^{-1}$	.9688358	$.7111609 \times 10^{-1}$	.9540084	.4807267
$.2583159 \times 10^{-1}$	.9697124	$.7793801 \times 10^{-1}$	.9365624	.4853933
$.2637412 \times 10^{-1}$	.9705850	$.8525964 \times 10^{-1}$	.9190589	.4902683
$.2692374 \times 10^{-1}$	.9714492	$.9300398 \times 10^{-1}$	.9017302	.4952906
$.2748861 \times 10^{-1}$	.9723189	.1013614	.8842062	.5005740
$.2806548 \times 10^{-1}$	.9731895	.1102556	.8667195	.5060573
$.2865502 \times 10^{-1}$	.9740628	.1197001	.8492890	.5117393
$.2926174 \times 10^{-1}$	.9749463	.1297983	.8317795	.5176710
$.2988259 \times 10^{-1}$	.9758361	.1404767	.8143727	.5237977
$.3052228 \times 10^{-1}$	.9767399	.1518400	.7969420	.5301691
$.3118559 \times 10^{-1}$	.9776651	.1639926	.7793900	.5368312
$.3186586 \times 10^{-1}$	.9786032	.1767755	.7619984	.5436835
$.3257201 \times 10^{-1}$	.9795677	.1903837	.7445404	.5508208
$.3330541 \times 10^{-1}$	.9805613	.2048371	.7270520	.5582385
$.3406764 \times 10^{-1}$	.9815874	.2201551	.7095602	.5659332

TABLE II.—EXPANSIVE FLOW FIELD OBTAINED BY CHARACTERISTIC CALCULATIONS FOR JET FLOW FROM NEAR-SONIC EXIT (M_i=1.0038; μ_i=85°)—Continued

x/r_i	y/r_i	θ, radians	μ, radians	V/V_i
0.1749774×10^{-1}	0.8000000	0.0000000	1.483530	0.4095466
$.1922838\times10^{-1}$	.8197816	$.1510528\times10^{-3}$	1.462410	.4102535
$.2078493\times10^{-1}$	.8341065	$.3561345\times10^{-3}$	1.443067	.4110367
$.2219101\times10^{-1}$	.8450858	$.6104594\times10^{-3}$	1.425413	.4118659
$.2359168\times10^{-1}$	.8546931	$.9737907\times10^{-3}$	1.405951	.4129075
$.2483346\times10^{-1}$	.8622030	$.1368151\times10^{-2}$	1.389276	.4139074
$.2609680\times10^{-1}$	.8691397	$.1908553\times10^{-2}$	1.370534	.4151507
$.2723855\times10^{-1}$	.8748201	$.2480129\times10^{-2}$	1.354114	.4163453
$.2838181\times10^{-1}$	.8800755	$.3198335\times10^{-2}$	1.336568	.4177317
$.2951298\times10^{-1}$	.8848843	$.4067796\times10^{-2}$	1.318447	.4192844
$.3057419\times10^{-1}$	.8890703	$.5001940\times10^{-2}$	1.301650	.4208349
$.3167195\times10^{-1}$	.8931291	$.6189036\times10^{-2}$	1.283029	.4226807
$.3270836\times10^{-1}$	.8967120	$.7451460\times10^{-2}$	1.265714	.4245190
$.3373199\times10^{-1}$	.9000492	$.8885938\times10^{-2}$	1.248283	.4264902
$.3474248\times10^{-1}$	.9031649	$.1049835\times10^{-1}$	1.230834	.4285869
$.3574002\times10^{-1}$	.9060823	$.1229410\times10^{-1}$	1.213429	.4308037
$.3675098\times10^{-1}$	.9088947	$.1437000\times10^{-1}$	1.195342	.4332426
$.3772357\times10^{-1}$	.9114702	$.1655031\times10^{-1}$	1.178202	.4356838
$.3870814\times10^{-1}$	.9139638	$.1902332\times10^{-1}$	1.160550	.4383330
$.3968146\times10^{-1}$	.9163234	$.2170453\times10^{-1}$	1.143132	.4410842
$.4066361\times10^{-1}$	.9186084	$.2469127\times10^{-1}$	1.125413	.4440262
$.4163592\times10^{-1}$	.9207817	$.2790017\times10^{-1}$	1.107983	.4470645
$.4261623\times10^{-1}$	.9228918	$.3142865\times10^{-1}$	1.090375	.4502826
$.4360393\times10^{-1}$	.9249417	$.3528425\times10^{-1}$	1.072668	.4536734
$.4458426\times10^{-1}$	.9269063	$.3938457\times10^{-1}$	1.055295	.4571552
$.4558644\times10^{-1}$	.9288497	$.4391830\times10^{-1}$	1.037528	.4608784
$.4658284\times10^{-1}$	.9307207	$.4871368\times10^{-1}$	1.020123	.4646897
$.4758792\times10^{-1}$	.9325520	$.5386963\times10^{-1}$	1.002741	.4686622
$.4861403\times10^{-1}$	.9343686	$.5948550\times10^{-1}$	.9851338	.4728605
$.4964915\times10^{-1}$	.9361508	$.6548096\times10^{-1}$	.9676321	.4772124
$.5070513\times10^{-1}$	.9379218	$.7195563\times10^{-1}$	.9500062	.4817805
$.5177143\times10^{-1}$	.9396655	$.7883079\times10^{-1}$	.9325335	.4864982
$.5285950\times10^{-1}$	.9414032	$.8620683\times10^{-1}$	.9150035	.4914261
$.5395981\times10^{-1}$	.9431214	$.9400620\times10^{-1}$	.8976505	.4965021
$.5509334\times10^{-1}$	.9448548	.1024201	.8801025	.5018416
$.5625070\times10^{-1}$	.9465899	.1113714	.8625933	.5073825
$.5743312\times10^{-1}$	.9483301	.1208740	.8451427	.5131234
$.5865110\times10^{-1}$	.9500923	.1310312	.8276143	.5191161
$.5989669\times10^{-1}$	.9518664	.1417682	.8101875	.5253057
$.6118066\times10^{-1}$	.9536693	.1531901	.7927370	.5317423
$.6251329\times10^{-1}$	.9555169	.1654019	.7751659	.5384721
$.6387916\times10^{-1}$	.9573893	.1782429	.7577551	.5453941
$.6529787\times10^{-1}$	.9593157	.1919091	.7402784	.5526036
$.6677184\times10^{-1}$	.9613012	.2064194	.7227692	.5600967
$.6830406\times10^{-1}$	.9633523	.2217934	.7052569	.5678695

TABLE II.—EXPANSIVE FLOW FIELD OBTAINED BY CHARACTERISTIC CALCULATIONS FOR JET FLOW FROM NEAR-SONIC EXIT (M_i=1.0038; μ_i=85°)—Continued

x/r_i	y/r_i	θ, radians	μ, radians	V/V_i
0.2624660×10^{-1}	0.7000000	0.0000000	1.483530	0.4095466
$.2893369\times10^{-1}$	.7307138	$.1583478\times10^{-3}$	1.461485	.4102879
$.3130918\times10^{-1}$	.7523903	$.3710463\times10^{-3}$	1.441619	.4111006
$.3342216\times10^{-1}$	.7687039	$.6334703\times10^{-3}$	1.423617	.4119564
$.3555932\times10^{-1}$	.7831830	$.1006987\times10^{-2}$	1.403861	.4130274
$.3740747\times10^{-1}$	.7942188	$.1411383\times10^{-2}$	1.386974	.4140532
$.3932387\times10^{-1}$	.8046081	$.1964559\times10^{-2}$	1.368036	.4153261
$.4102068\times10^{-1}$	.8129446	$.2548770\times10^{-2}$	1.351464	.4165474
$.4273893\times10^{-1}$	.8207462	$.3281926\times10^{-2}$	1.333773	.4179631
$.4444764\times10^{-1}$	.8279228	$.4168522\times10^{-2}$	1.315520	.4195469
$.4603281\times10^{-1}$	.8341023	$.5120240\times10^{-2}$	1.298611	.4211269
$.4769823\times10^{-1}$	.8401893	$.6328608\times10^{-2}$	1.279881	.4230062
$.4925383\times10^{-1}$	.8455071	$.7612560\times10^{-2}$	1.262469	.4248768
$.5079232\times10^{-1}$	.8504680	$.9070455\times10^{-2}$	1.244949	.4268813
$.5231164\times10^{-1}$	.8551027	$.1070791\times10^{-1}$	1.227415	.4290125
$.5381138\times10^{-1}$	.8594433	$.1253051\times10^{-1}$	1.209931	.4312645
$.5533934\times10^{-1}$	.8636510	$.1463636\times10^{-1}$	1.191772	.4337406
$.5679911\times10^{-1}$	.8674782	$.1684683\times10^{-1}$	1.174567	.4362181
$.5828285\times10^{-1}$	.8711997	$.1935260\times10^{-1}$	1.156850	.4389058
$.5974741\times10^{-1}$	.8747166	$.2206788\times10^{-1}$	1.139373	.4416960
$.6122868\times10^{-1}$	.8781307	$.2509120\times10^{-1}$	1.121600	.4446785
$.6269242\times10^{-1}$	.8813725	$.2833785\times10^{-1}$	1.104119	.4477577
$.6417022\times10^{-1}$	.8845252	$.3190624\times10^{-1}$	1.086465	.4510180
$.6566015\times10^{-1}$	.8875906	$.3580388\times10^{-1}$	1.068714	.4544523
$.6713615\times10^{-1}$	.8905233	$.3994708\times10^{-1}$	1.051300	.4579778
$.6864879\times10^{-1}$	.8934321	$.4452600\times10^{-1}$	1.033495	.4617471
$.7014983\times10^{-1}$	.8962276	$.4936738\times10^{-1}$	1.016054	.4656045
$.7166413\times10^{-1}$	.8989644	$.5457069\times10^{-1}$	.9986399	.4696243
$.7321219\times10^{-1}$	.9016833	$.6023588\times10^{-1}$	.9810016	.4738718
$.7477322\times10^{-1}$	.9043502	$.6628181\times10^{-1}$	.9634712	.4782739
$.7636689\times10^{-1}$	.9070026	$.7280859\times10^{-1}$	.9458196	.4828937
$.7797522\times10^{-1}$	.9096132	$.7973626\times10^{-1}$	.9283209	.4876643
$.7961709\times10^{-1}$	.9122162	$.8716646\times10^{-1}$	.9107685	.4926464
$.8127664\times10^{-1}$	.9147891	$.9502022\times10^{-1}$	.8933950	.4977777
$.8298789\times10^{-1}$	.9173874	.1034898	.8758271	.5031747
$.8473521\times10^{-1}$	.9199887	.1124976	.8582998	.5087745
$.8652037\times10^{-1}$	.9225981	.1220566	.8408310	.5145760
$.8835997\times10^{-1}$	.9252419	.1322705	.8232859	.5206315
$.9024122\times10^{-1}$	.9279038	.1430644	.8058437	.5268853
$.9218093\times10^{-1}$	.9306101	.1545428	.7883776	.5333884
$.9419511\times10^{-1}$	.9333850	.1668113	.7707916	.5401872
$.9625939\times10^{-1}$	.9361974	.1797078	.7533653	.5471800
$.9840438\times10^{-1}$	.9390921	.1934286	.7358731	.5544630
.1006337	.9420770	.2079926	.7183484	.5620323
.1029517	.9451616	.2234182.	.7008191	.5698843

TABLE II.—EXPANSIVE FLOW FIELD OBTAINED BY CHARACTERISTIC CALCULATIONS FOR JET FLOW FROM NEAR-SONIC EXIT (M_i=1.0038; μ_i=85°)—Continued

x/r_i	y/r_i	θ, radians	μ, radians	V/V_i
0.3499547×10^{-1}	0.6000000	0.0000000	1.483530	0.4095466
$.3867622\times10^{-1}$	.6420716	$.1668802\times10^{-3}$	1.460426	.4103278
$.4189340\times10^{-1}$	.6711468	$.3878676\times10^{-3}$	1.439972	.4111742
$.4472931\times10^{-1}$	.6927650	$.6587788\times10^{-3}$	1.421589	.4120600
$.4761713\times10^{-1}$	.7120619	$.1042986\times10^{-2}$	1.401523	.4131633
$.5008229\times10^{-1}$	.7265769	$.1457836\times10^{-2}$	1.384418	.4142175
$.5266212\times10^{-1}$	.7403686	$.2024218\times10^{-2}$	1.365275	.4155226
$.5492242\times10^{-1}$	.7513222	$.2621446\times10^{-2}$	1.348547	.4167728
$.5722406\times10^{-1}$	.7616329	$.3370106\times10^{-2}$	1.330714	.4182198
$.5951836\times10^{-1}$	.7711436	$.4274451\times10^{-2}$	1.312328	.4198367
$.6163473\times10^{-1}$	.7792893	$.5244187\times10^{-2}$	1.295309	.4214483
$.6387540\times10^{-1}$	.7873778	$.6474402\times10^{-2}$	1.276469	.4233633
$.6595720\times10^{-1}$	.7944091	$.7780502\times10^{-2}$	1.258963	.4252680
$.6801737\times10^{-1}$	.8009748	$.9262501\times10^{-2}$	1.241356	.4273076
$.7005237\times10^{-1}$	.8071119	$.1092587\times10^{-1}$	1.223742	.4294749
$.7206108\times10^{-1}$	.8128611	$.1277601\times10^{-1}$	1.206185	.4317638
$.7411297\times10^{-1}$	.8184504	$.1491218\times10^{-1}$	1.187952	.4342794
$.7606651\times10^{-1}$	.8235182	$.1715325\times10^{-1}$	1.170684	.4367952
$.7805628\times10^{-1}$	.8284574	$.1969240\times10^{-1}$	1.152907	.4395231
$.8001887\times10^{-1}$	.8331229	$.2244248\times10^{-1}$	1.135377	.4423539
$.8200610\times10^{-1}$	.8376582	$.2550274\times10^{-1}$	1.117550	.4453789
$.8396814\times10^{-1}$	.8419619	$.2878747\times10^{-1}$	1.100021	.4485009
$.8595049\times10^{-1}$	.8461510	$.3239600\times10^{-1}$	1.082322	.4518054
$.8794995\times10^{-1}$	.8502267	$.3633555\times10^{-1}$	1.064528	.4552854
$.8992890\times10^{-1}$	.8541233	$.4052162\times10^{-1}$	1.047077	.4588566
$.9195961\times10^{-1}$	.8579936	$.4514601\times10^{-1}$	1.029236	.4626737
$.9397297\times10^{-1}$	.8617107	$.5003307\times10^{-1}$	1.011763	.4665793
$.9600427\times10^{-1}$	.8653507	$.5528355\times10^{-1}$	.9943193	.4706482
$.9808241\times10^{-1}$	.8689702	$.6099781\times10^{-1}$	.9766532	.4749467
.1001777	.8725207	$.6709356\times10^{-1}$	.9590975	.4794009
.1023177	.8760539	$.7367184\times10^{-1}$	.9414226	.4840743
.1044770	.8795313	$.8065158\times10^{-1}$	.9239040	.4888993
.1066820	.8830001	$.8813468\times10^{-1}$	.9063316	.4939376
.1089104	.8864287	$.9604133\times10^{-1}$	.8889401	.4991261
.1112094	.8898936	.1045653	.8713565	.5045823
.1135572	.8933633	.1136275	.8538146	.5102429
.1159561	.8968447	.1232410	.8363320	.5161067
.1184289	.9003736	.1335098	.8187742	.5222265
.1209579	.9039273	.1443581	.8013205	.5285461
.1235663	.9075417	.1558909	.7838440	.5351168
.1262757	.9112495	.1682129	.7662470	.5419861
.1290528	.9150082	.1811616	.7488100	.5490510
.1319394	.9188786	.1949334	.7313068	.5564087
.1349405	.9228712	.2095466	.7137706	.5640554
.1380618	.9269987	.2250195	.6962298	.5719874

TABLE II.—EXPANSIVE FLOW FIELD OBTAINED BY CHARACTERISTIC CALCULATIONS FOR JET FLOW FROM NEAR-SONIC EXIT (M_i=1.0038; μ_i=85°)—Continued

x/r_i	y/r_i	θ, radians	μ, radians	V/V_i
0.4374434×10^{-1}	0.5000000	0.0000000	1.483530	0.4095466
$.4846100\times10^{-1}$	.5539121	$.1769778\times10^{-3}$	1.459177	.4103753
$.5254666\times10^{-1}$	.5904221	$.4070187\times10^{-3}$	1.438074	.4112601
$.5612414\times10^{-1}$	.6173017	$.6869535\times10^{-3}$	1.419284	.4121795
$.5977866\times10^{-1}$	.6413480	$.1082254\times10^{-2}$	1.398890	.4133188
$.6287288\times10^{-1}$	.6592853	$.1507881\times10^{-2}$	1.381555	.4144042
$.6612807\times10^{-1}$	.6764208	$.2088014\times10^{-2}$	1.362207	.4157441
$.6896147\times10^{-1}$	.6899463	$.2698652\times10^{-2}$	1.345323	.4170256
$.7185592\times10^{-1}$	.7027234	$.3463248\times10^{-2}$	1.327346	.4185064
$.7474510\times10^{-1}$	.7145302	$.4385822\times10^{-2}$	1.308833	.4201587
$.7740083\times10^{-1}$	.7246116	$.5373993\times10^{-2}$	1.291702	.4218042
$.8022549\times10^{-1}$	.7346720	$.6626444\times10^{-2}$	1.272754	.4237574
$.8284144\times10^{-1}$	.7433932	$.7955135\times10^{-2}$	1.255155	.4256985
$.8543118\times10^{-1}$	.7515427	$.9461532\times10^{-2}$	1.237464	.4277756
$.8798959\times10^{-1}$	.7591641	$.1115108\times10^{-1}$	1.219771	.4299813
$.9051491\times10^{-1}$	.7663059	$.1302927\times10^{-1}$	1.202143	.4323092
$.9309869\times10^{-1}$	.7732625	$.1519639\times10^{-1}$	1.183843	.4348662
$.9555355\times10^{-1}$	.7795588	$.1746859\times10^{-1}$	1.166515	.4374222
$.9805710\times10^{-1}$	.7857050	$.2004151\times10^{-1}$	1.148683	.4401924
.1005254	.7915096	$.2282650\times10^{-1}$	1.131099	.4430661
.1030266	.7971580	$.2592415\times10^{-1}$	1.113225	.4461355
.1054948	.8025166	$.2924732\times10^{-1}$	1.095652	.4493022
.1079898	.8077361	$.3289624\times10^{-1}$	1.077912	.4526529
.1105070	.8128170	$.3687826\times10^{-1}$	1.060083	.4561801
.1129972	.8176732	$.4110714\times10^{-1}$	1.042597	.4597991
.1155546	.8225015	$.4577706\times10^{-1}$	1.024726	.4636658
.1180889	.8271374	$.5071022\times10^{-1}$	1.007226	.4676211
.1206461	.8316785	$.5600762\times10^{-1}$	.9897562	.4717411
.1232636	.8361971	$.6177063\times10^{-1}$	.9720677	.4760924
.1259026	.8406303	$.6791599\times10^{-1}$	.9544913	.4806003
.1285988	.8450441	$.7454492\times10^{-1}$	.9367972	.4853293
.1313192	.8493886	$.8157598\times10^{-1}$	.9192626	.4902105
.1340979	.8537241	$.8911124\times10^{-1}$	.9016766	.4953066
.1369059	.8580101	$.9706993\times10^{-1}$	.8842714	.5005539
.1398041	.8623437	.1056470	.8666767	.5060709
.1427642	.8666847	.1147623	.8491248	.5117938
.1457892	.8710415	.1244286	.8316339	.5177214
.1489083	.8754596	.1347503	.8140683	.5239070
.1520988	.8799099	.1456506	.7966075	.5302938
.1553901	.8844381	.1572345	.7791243	.5369339
.1588101	.8890853	.1696070	.7615211	.5438751
.1623162	.8937976	.1826045	.7440788	.5510132
.1659616	.8986520	.1964235	.7265701	.5584467
.1697527	.9036618	.2110815	.7090277	.5661719
.1736970	.9088429	.2265971	.6914804	.5741848

TABLE II.—EXPANSIVE FLOW FIELD OBTAINED BY CHARACTERISTIC CALCULATIONS FOR JET FLOW FROM NEAR-SONIC EXIT (M_i=1.0038; μ_i=85°)—Continued

x/r_i	y/r_i	θ, radians	μ, radians	V/V_i
0.5249321×10^{-1}	0.4000000	0.0000000	1.483530	0.4095466
$.5829498\times10^{-1}$	.4663154	$.1892671\times10^{-3}$	1.457683	.4104328
$.6328018\times10^{-1}$	.5102741	$.4288965\times10^{-3}$	1.435842	.4113629
$.6762103\times10^{-1}$	.5423475	$.7180689\times10^{-3}$	1.416603	.4123207
$.7206156\times10^{-1}$	.5710534	$.1124717\times10^{-2}$	1.395870	.4135001
$.7579934\times10^{-1}$	.5923424	$.1561331\times10^{-2}$	1.378302	.4146199
$.7974398\times10^{-1}$	.6127506	$.2155338\times10^{-2}$	1.358749	.4159981
$.8316185\times10^{-1}$	.6287947	$.2779654\times10^{-2}$	1.341710	.4173135
$.8666033\times10^{-1}$	.6439889	$.3560444\times10^{-2}$	1.323594	.4188308
$.9015518\times10^{-1}$	.6580482	$.4501390\times10^{-2}$	1.304953	.4205215
$.9336009\times10^{-1}$	.6700310	$.5508342\times10^{-2}$	1.287719	.4222032
$.9677905\times10^{-1}$	.6820305	$.6783516\times10^{-2}$	1.268668	.4241970
$.9993860\times10^{-1}$	.6924155	$.8135174\times10^{-2}$	1.250983	.4261768
.1030671	.7021261	$.9666313\times10^{-2}$	1.233212	.4282938
.1061581	.7112121	$.1138255\times10^{-1}$	1.215448	.4305400
.1092090	.7197296	$.1328895\times10^{-1}$	1.197754	.4329093
.1123340	.7280379	$.1548740\times10^{-1}$	1.179393	.4355101
.1152990	.7355502	$.1779083\times10^{-1}$	1.162009	.4381087
.1183254	.7428920	$.2039773\times10^{-1}$	1.144126	.4409235
.1213085	.7498263	$.2321800\times10^{-1}$	1.126497	.4438421
.1243329	.7565793	$.2635318\times10^{-1}$	1.108580	.4469581
.1273166	.7629857	$.2971503\times10^{-1}$	1.090969	.4501715
.1303336	.7692297	$.3340455\times10^{-1}$	1.073195	.4535704
.1333782	.7753107	$.3742883\times10^{-1}$	1.055334	.4571472
.1363893	.7811225	$.4170062\times10^{-1}$	1.037820	.4608159
.1394834	.7869056	$.4641547\times10^{-1}$	1.019923	.4647346
.1425488	.7924577	$.5139394\times10^{-1}$	1.002399	.4687420
.1456422	.7978984	$.5673795\times10^{-1}$	.9849107	.4729149
.1488097	.8033152	$.6254921\times10^{-1}$	.9672045	.4773210
.1520035	.8086308	$.6874335\times10^{-1}$	.9496129	.4818847
.1552675	.8139254	$.7542225\times10^{-1}$	.9319064	.4866710
.1585608	.8191381	$.8250338\times10^{-1}$	.9143605	.4916105
.1619253	.8243421	$.9008921\times10^{-1}$	.8967649	.4967665
.1653256	.8294877	$.9809850\times10^{-1}$	.8793534	.5020743
.1688362	.8346931	.1067266	.8617523	.5076541
.1724224	.8399091	.1158930	.8441961	.5134411
.1760879	.8451458	.1256096	.8267019	.5194343
.1798684	.8504583	.1359815	.8091342	.5256874
.1837360	.8558114	.1469309	.7916717	.5321431
.1877270	.8612601	.1585628	.7741886	.5388540
.1918753	.8668545	.1709824	.7565855	.5458684
.1961290	.8725292	.1840245	.7391430	.5530812
.2005530	.8783775	.1978861	.7216345	.5605918
.2051553	.8844156	.2125846	.7040924	.5683963
.2099451	.8906628	.2281373	.6865449	.5764911

TABLE II.—EXPANSIVE FLOW FIELD OBTAINED BY CHARACTERISTIC CALCULATIONS FOR JET FLOW FROM NEAR-SONIC EXIT ($M_i=1.0038$; $\mu_i=85°$)—Continued

x/r_i	y/r_i	θ, radians	μ, radians	V/V_t
0.6124208×10^{-1}	0.3000000	0.0000000	1.483530	0.4095466
$.6818709\times10^{-1}$	.3793820	$.2046700\times10^{-3}$	1.455848	.4105046
$.7410973\times10^{-1}$	.4307716	$.4539568\times10^{-3}$	1.433143	.4114894
$.7924108\times10^{-1}$	.4679374	$.7521654\times10^{-3}$	1.413425	.4124916
$.8449095\times10^{-1}$	.5011833	$.1169917\times10^{-2}$	1.392335	.4137164
$.8888973\times10^{-1}$	.5257342	$.1617429\times10^{-2}$	1.374541	.4148742
$.9354089\times10^{-1}$	.5493280	$.2225322\times10^{-2}$	1.354791	.4162941
$.9755704\times10^{-1}$	.5678273	$.2863299\times10^{-2}$	1.337606	.4176465
.1016731	.5853805	$.3660290\times10^{-2}$	1.319359	.4192033
.1057869	.6016422	$.4619959\times10^{-2}$	1.300604	.4209350
.1095527	.6154870	$.5645864\times10^{-2}$	1.283275	.4226555
.1135784	.6293890	$.6943925\times10^{-2}$	1.264133	.4246928
.1172928	.6414088	$.8318573\times10^{-2}$	1.246370	.4267141
.1209713	.6526554	$.9874819\times10^{-2}$	1.228529	.4288733
.1246058	.6631845	$.1161785\times10^{-1}$	1.210701	.4311626
.1281933	.6730591	$.1355278\times10^{-1}$	1.192950	.4335757
.1318706	.6827029	$.1578292\times10^{-1}$	1.174536	.4362226
.1353564	.6914182	$.1811804\times10^{-1}$	1.157107	.4388658
.1389166	.6999439	$.2075924\times10^{-1}$	1.139181	.4417275
.1424253	.7079981	$.2361493\times10^{-1}$	1.121514	.4446933
.1459840	.7158474	$.2678776\times10^{-1}$	1.103561	.4478583
.1494941	.7232950	$.3018798\times10^{-1}$	1.085920	.4511210
.1530444	.7305578	$.3391800\times10^{-1}$	1.068118	.4545704
.1566279	.7376344	$.3798433\times10^{-1}$	1.050233	.4581991
.1601714	.7443983	$.4229866\times10^{-1}$	1.032698	.4619198
.1638142	.7511336	$.4705846\times10^{-1}$	1.014782	.4658925
.1674226	.7576006	$.5208180\times10^{-1}$	.9972434	.4699541
.1710646	.7639398	$.5747163\times10^{-1}$	.9797411	.4741822
.1747950	.7702547	$.6333010\times10^{-1}$	.9620242	.4786455
.1785567	.7764534	$.6957195\times10^{-1}$	.9444241	.4832671
.1824019	.7826305	$.7629980\times10^{-1}$	.9267116	.4881128
.1862819	.7887137	$.8342972\times10^{-1}$	.9091618	.4931126
.1902467	.7947891	$.9106489\times10^{-1}$	.8915638	.4983303
.1942540	.8007980	$.9912289\times10^{-1}$	.8741514	.5037007
.1983926	.8068797	.1078003	.8565517	.5093451
.2026211	.8129759	.1170153	.8389974	.5151981
.2069439	.8190985	.1267798	.8215065	.5212587
.2114035	.8253123	.1371988	.8039429	.5275812
.2159669	.8315757	.1481939	.7864864	.5341075
.2206771	.8379536	.1598703	.7690086	.5408908
.2255745	.8445050	.1723332	.7514124	.5479799
.2305974	.8511529	.1854155	.7339768	.5552688
.2358232	.8580072	.1993149	.7164755	.5628577
.2412614	.8650870	.2140484	.6989406	.5707428
.2469232	.8724153	.2296329	.6813999	.5789202

502683 O—59——4

TABLE II.—EXPANSIVE FLOW FIELD OBTAINED BY CHARACTERISTIC CALCULATIONS FOR JET FLOW FROM NEAR-SONIC EXIT (M_i=1.0038; μ_i=85°)—Continued

x/r_i	y/r_i	θ, radians	μ, radians	V/V_i
0.6999094×10^{-1}	0.2000000	0.0000000	1.483530	0.4095466
$.7814935\times10^{-1}$	.2932515	$.2247088\times10^{-3}$	1.453487	.4105986
$.8505892\times10^{-1}$	.3519959	$.4821653\times10^{-3}$	1.429748	.4116522
$.9101575\times10^{-1}$	.3940939	$.7881754\times10^{-3}$	1.409518	.4127066
$.9710577\times10^{-1}$	.4317140	$.1216019\times10^{-2}$	1.388083	.4139827
.1021880	.4594072	$.1673625\times10^{-2}$	1.370074	.4151829
.1075677	.4860763	$.2294754\times10^{-2}$	1.350148	.4166487
.1121998	.5069522	$.2945972\times10^{-2}$	1.332837	.4180413
.1169509	.5267952	$.3758884\times10^{-2}$	1.314481	.4196408
.1217005	.5452002	$.4736880\times10^{-2}$	1.295630	.4214169
.1260422	.5608616	$.5781489\times10^{-2}$	1.278224	.4231790
.1306907	.5766236	$.7102420\times10^{-2}$	1.259009	.4252627
.1349745	.5902456	$.8500224\times10^{-2}$	1.241187	.4273279
.1392172	.6030010	$.1008146\times10^{-1}$	1.223291	.4295321
.1434093	.6149500	$.1185140\times10^{-1}$	1.205415	.4318671
.1475471	.6261626	$.1381485\times10^{-1}$	1.187620	.4343266
.1517909	.6371252	$.1607636\times10^{-1}$	1.169165	.4370226
.1558109	.6470301	$.1844303\times10^{-1}$	1.151703	.4397131
.1599187	.6567285	$.2111829\times10^{-1}$	1.133746	.4426244
.1639668	.6658933	$.2400926\times10^{-1}$	1.116052	.4456400
.1680739	.6748313	$.2721963\times10^{-1}$	1.098076	.4488565
.1721244	.6833140	$.3065816\times10^{-1}$	1.080414	.4521708
.1762224	.6915909	$.3442824\times10^{-1}$	1.062595	.4556734
.1803594	.6996596	$.3853618\times10^{-1}$	1.044695	.4593565
.1844498	.7073737	$.4289255\times10^{-1}$	1.027148	.4631316
.1886564	.7150602	$.4769630\times10^{-1}$	1.009223	.4671611
.1928230	.7224419	$.5276399\times10^{-1}$	.9916790	.4712791
.1970289	.7296808	$.5819882\times10^{-1}$	.9741735	.4755647
.2013382	.7368956	$.6410367\times10^{-1}$	.9564550	.4800874
.2056841	.7439802	$.7039212\times10^{-1}$	.9388551	.4847692
.2101275	.7510433	$.7716695\times10^{-1}$	.9211450	.4896769
.2146117	.7580012	$.8434381\times10^{-1}$	.9035992	.4947394
.2191948	.7649533	$.9202616\times10^{-1}$	.8860077	.5000212
.2238276	.7718315	.1001310	.8686035	.5054562
.2286136	.7787963	.1088551	.8510128	.5111674
.2335046	.7857805	.1181159	.8334690	.5170887
.2385057	.7927976	.1279254	.8159898	.5232186
.2436665	.7999223	.1383884	.7984393	.5296123
.2489486	.8071068	.1494258	.7809963	.5362110
.2544021	.8144258	.1611428	.7635334	.5430684
.2600741	.8219473	.1736441	.7459518	.5502340
.2658930	.8295828	.1867621	.7285314	.5576004
.2719490	.8374589	.2006942	.7110456	.5652689
.2782534	.8455980	.2154575	.6935263	.5732356
.2848195	.8540266	.2310674	.6760010	.5814967

TABLE II.—EXPANSIVE FLOW FIELD OBTAINED BY CHARACTERISTIC CALCULATIONS FOR JET FLOW FROM NEAR-SONIC EXIT ($M_i=1.0038$; $\mu_i=85°$)—Continued

x/r_i	y/r_i	θ, radians	μ, radians	V/V_i
0.7436538×10^{-1}	0.1500000	0.0000000	1.483530	0.4095466
$.8317474\times10^{-1}$	.2506917	$.2386524\times10^{-3}$	1.451882	.4106636
$.9060919\times10^{-1}$	.3130420	$.4982903\times10^{-3}$	1.427539	.4117602
$.9699916\times10^{-1}$	.3574981	$.8071739\times10^{-3}$	1.407067	.4128441
.1035258	.3972036	$.1239396\times10^{-2}$	1.385492	.4141482
.1089613	.4263999	$.1701726\times10^{-2}$	1.367401	.4153710
.1147162	.4545451	$.2329333\times10^{-2}$	1.347415	.4168611
.1196649	.4765663	$.2987052\times10^{-2}$	1.330061	.4182750
.1247419	.4975168	$.3807868\times10^{-2}$	1.311667	.4198972
.1298175	.5169622	$.4795145\times10^{-2}$	1.292788	.4216966
.1344541	.5335087	$.5849218\times10^{-2}$	1.275356	.4234807
.1394214	.5501795	$.7181786\times10^{-2}$	1.256122	.4255887
.1439965	.5645866	$.8591396\times10^{-2}$	1.238280	.4276770
.1485279	.5780827	$.1018549\times10^{-1}$	1.220369	.4299046
.1530053	.5907303	$.1196911\times10^{-1}$	1.202479	.4322636
.1574246	.6026027	$.1394722\times10^{-1}$	1.184673	.4347472
.1619583	.6142166	$.1622486\times10^{-1}$	1.166208	.4374687
.1662516	.6247101	$.1860736\times10^{-1}$	1.148736	.4401841
.1706396	.6349897	$.2130002\times10^{-1}$	1.130771	.4431212
.1749637	.6447058	$.2420885\times10^{-1}$	1.113070	.4461628
.1793514	.6541850	$.2743800\times10^{-1}$	1.095088	.4494063
.1836786	.6631828	$.3089573\times10^{-1}$	1.077422	.4527476
.1880569	.6719652	$.3468587\times10^{-1}$	1.059600	.4562779
.1924773	.6805290	$.3881461\times10^{-1}$	1.041699	.4599893
.1968479	.6887175	$.4319203\times10^{-1}$	1.024153	.4637926
.2013435	.6968795	$.4801800\times10^{-1}$	1.006230	.4678513
.2057962	.7047190	$.5310770\times10^{-1}$	.9886891	.4719985
.2102912	.7124086	$.5856505\times10^{-1}$	.9711876	.4763137
.2148974	.7200747	$.6449304\times10^{-1}$	.9534734	.4808670
.2195430	.7276040	$.7080453\times10^{-1}$	.9358805	.4855797
.2242934	.7351123	$.7760280\times10^{-1}$	.9181773	.4905191
.2290877	.7425102	$.8480291\times10^{-1}$	.9006386	.4956137
.2339883	.7499036	$.9250828\times10^{-1}$	.8830554	.5009283
.2389425	.7572198	.1006356	.8656597	.5063966
.2440612	.7646300	.1093821	.8480784	.5121421
.2492929	.7720624	.1186651	.8305447	.5180980
.2546430	.7795313	.1284958	.8130760	.5242634
.2601646	.7871167	.1389796	.7955368	.5306933
.2658167	.7947674	.1500364	.7781049	.5373289
.2716532	.8025630	.1617719	.7606537	.5442239
.2777245	.8105764	.1742904	.7430838	.5514283
.2839541	.8187130	.1874243	.7256758	.5588338
.2904386	.8271081	.2013705	.7082021	.5665424
.2971902	.8357857	.2161456	.6906951	.5745503
.3042234	.8447744	.2317650	.6731811	.5828536

TABLE II.—EXPANSIVE FLOW FIELD OBTAINED BY CHARACTERISTIC CALCULATIONS FOR JET FLOW FROM NEAR-SONIC EXIT (M_i=1.0038; μ_i=85°)—Continued

x/r_i	y/r_i	θ, radians	μ, radians	V/V_i
0.7873981×10^{-1}	0.1000000	0.0000000	1.483530	0.4095466
$.8822959\times10^{-1}$	.2084695	$.2556294\times10^{-3}$	1.449943	.4107434
$.9621177\times10^{-1}$	.2743377	$.5141673\times10^{-3}$	1.424918	.4118908
.1030506	.3210518	$.8245088\times10^{-3}$	1.404224	.4130064
.1100271	.3627573	$.1260242\times10^{-2}$	1.382538	.4143397
.1158255	.3934025	$.1726781\times10^{-2}$	1.364394	.4155859
.1219648	.4229777	$.2360357\times10^{-2}$	1.344369	.4171012
.1272373	.4461141	$.3024302\times10^{-2}$	1.326990	.4185370
.1326474	.4681468	$.3852923\times10^{-2}$	1.308578	.4201823
.1380558	.4886121	$.4849346\times10^{-2}$	1.289684	.4220056
.1429935	.5060287	$.5912788\times10^{-2}$	1.272240	.4238122
.1482860	.5235951	$.7256931\times10^{-2}$	1.252995	.4259453
.1531584	.5387772	$.8678228\times10^{-2}$	1.235144	.4280573
.1579842	.5530065	$.1028505\times10^{-1}$	1.217228	.4303091
.1627525	.5663467	$.1208232\times10^{-1}$	1.199330	.4326928
.1674589	.5788740	$.1407484\times10^{-1}$	1.181519	.4352014
.1722882	.5911355	$.1636853\times10^{-1}$	1.163051	.4379492
.1768602	.6022150	$.1876707\times10^{-1}$	1.145575	.4406900
.1815340	.6130738	$.2147700\times10^{-1}$	1.127609	.4436536
.1861396	.6233400	$.2440380\times10^{-1}$	1.109907	.4467218
.1908136	.6333596	$.2765189\times10^{-1}$	1.091928	.4499928
.1954230	.6428724	$.3112905\times10^{-1}$	1.074264	.4533615
.2000874	.6521604	$.3493948\times10^{-1}$	1.056444	.4569200
.2047971	.6612198	$.3908901\times10^{-1}$	1.038547	.4606604
.2094536	.6698838	$.4348733\times10^{-1}$	1.021005	.4644927
.2142441	.6785228	$.4833524\times10^{-1}$	1.003088	.4685814
.2189888	.6868218	$.5344646\times10^{-1}$	.9855518	.4727588
.2237790	.6949641	$.5892553\times10^{-1}$	.9680567	.4771047
.2286884	.7030838	$.6487617\times10^{-1}$	.9503516	.4816893
.2336401	.7110603	$.7121040\times10^{-1}$	.9327677	.4864337
.2387042	.7190166	$.7803149\times10^{-1}$	.9150741	.4914057
.2438154	.7268575	$.8525399\times10^{-1}$	.8975462	.4965332
.2490406	.7346955	$.9298199\times10^{-1}$	.8799746	.5018813
.2543234	.7424532	.1011313	.8625908	.5073834
.2597823	.7503128	.1098997	.8450224	.5131637
.2653624	.7581976	.1192035	.8275017	.5191553
.2710695	.7661229	.1290548	.8100463	.5253567
.2769604	.7741738	.1395581	.7925212	.5318236
.2829914	.7822958	.1506336	.7751036	.5384965
.2892199	.7905738	.1623862	.7576670	.5454298
.2957002	.7990851	.1749211	.7401124	.5526733
.3023504	.8077294	.1880694	.7227197	.5601183
.3092743	.8166504	.2020282	.7052613	.5678675
.3164847	.8258741	.2168137	.6877689	.5759170
.3239973	.8354310	.2324409	.6702701	.5842627

TABLE II.—EXPANSIVE FLOW FIELD OBTAINED BY CHARACTERISTIC CALCULATIONS FOR JET FLOW FROM NEAR-SONIC EXIT (M_i=1.0038; μ_i=85°)—Continued

x/r_i	y/r_i	θ, radians	μ, radians	V/V_i
0.8223936×10^{-1}	0.6000000×10^{-1}	0.0000000	1.483530	0.4095466
0.9230156×10^{-1}	.1750118	$.2728449\times10^{-3}$	1.448016	.4108239
.1007453	.2435908	$.5254415\times10^{-3}$	1.422354	.4120208
.1079591	.2920036	$.8354714\times10^{-3}$	1.401534	.4131627
.1153084	.3352248	$.1273159\times10^{-2}$	1.379806	.4145197
.1214059	.3669786	$.1742626\times10^{-2}$	1.361651	.4157847
.1278613	.3976561	$.2380778\times10^{-2}$	1.341628	.4173202
.1333997	.4216570	$.3049612\times10^{-2}$	1.324251	.4187736
.1390828	.4445335	$.3884348\times10^{-2}$	1.305843	.4204377
.1447637	.4657976	$.4887969\times10^{-2}$	1.286954	.4222805
.1499480	.4838975	$.5958929\times10^{-2}$	1.269514	.4241054
.1555067	.5021695	$.7312255\times10^{-2}$	1.250272	.4262591
.1606222	.5179644	$.8742921\times10^{-2}$	1.232426	.4283905
.1656888	.5327743	$.1035993\times10^{-1}$	1.214511	.4306622
.1706950	.5466643	$.1216819\times10^{-1}$	1.196618	.4330661
.1756362	.5597122	$.1417240\times10^{-1}$	1.178809	.4355951
.1807072	.5724894	$.1647885\times10^{-1}$	1.160345	.4383646
.1855072	.5840361	$.1889034\times10^{-1}$	1.142874	.4411261
.1904147	.5953574	$.2161420\times10^{-1}$	1.124912	.4441115
.1952506	.6060633	$.2455538\times10^{-1}$	1.107216	.4472015
.2001587	.6165155	$.2781881\times10^{-1}$	1.089241	.4504950
.2049990	.6264408	$.3131135\times10^{-1}$	1.071583	.4538864
.2098974	.6361344	$.3513791\times10^{-1}$	1.053771	.4574681
.2148437	.6455918	$.3930410\times10^{-1}$	1.035881	.4612322
.2197341	.6546380	$.4371924\times10^{-1}$	1.018347	.4650881
.2247659	.6636605	$.4858451\times10^{-1}$	1.000437	.4692015
.2297497	.6723292	$.5371339\times10^{-1}$	.9829109	.4734033
.2347817	.6808359	$.5921025\times10^{-1}$	.9654258	.4777740
.2399393	.6893212	$.6517869\times10^{-1}$	.9477298	.4823844
.2451417	.6976584	$.7153049\times10^{-1}$	.9301556	.4871550
.2504627	.7059762	$.7836962\times10^{-1}$	.9124741	.4921535
.2558336	.7141748	$.8560992\times10^{-1}$	.8949575	.4973079
.2613248	.7223721	$.9335522\times10^{-1}$	.8773974	.5026836
.2668769	.7304868	.1015214	.8600251	.5082135
.2726148	.7387098	.1103065	.8424698	.5140224
.2784807	.7469608	.1196270	.8249627	.5200427
.2844805	.7552559	.1294940	.8075212	.5262734
.2906744	.7636841	.1400123	.7900095	.5327704
.2970164	.7721883	.1511018	.7726063	.5394737
.3035670	.7808575	.1628676	.7551846	.5464379
.3103833	.7897730	.1754143	.7376447	.5537133
.3173794	.7988295	.1885726	.7202657	.5611906
.3246643	.8081781	.2025405	.7028223	.5689726
.3322520	.8178459	.2173331	.6853444	.5770556
.3401592	.8278651	.2329653	.6678605	.5854354

TABLE II.—EXPANSIVE FLOW FIELD OBTAINED BY CHARACTERISTIC CALCULATIONS FOR JET FLOW FROM NEAR-SONIC EXIT (M_i=1.0038; μ_i=85°)—Continued

x/r_i	y/r_i	θ, radians	μ, radians	V/V_i
0.8398913×10^{-1}	0.4000000×10^{-1}	0.0000000	1.483530	0.4095466
$.9435119\times10^{-1}$	.1584395	$.2836015\times10^{-3}$	1.446832	.4108741
.1030377	.2283162	$.5300123\times10^{-3}$	1.420832	.4120990
.1104461	.2775238	$.8392017\times10^{-3}$	1.399983	.4132539
.1179873	.3214634	$.1277553\times10^{-2}$	1.378266	.4146224
.1242382	.3537480	$.1748338\times10^{-2}$	1.360123	.4158966
.1308553	.3849577	$.2388767\times10^{-2}$	1.340118	.4174420
.1365294	.4093794	$.3059989\times10^{-2}$	1.322753	.4189042
.1423518	.4326681	$.3897827\times10^{-2}$	1.304358	.4205776
.1481717	.4543240	$.4905148\times10^{-2}$	1.285478	.4224302
.1534815	.4727609	$.5979965\times10^{-2}$	1.268049	.4242642
.1591757	.4913818	$.7338026\times10^{-2}$	1.248815	.4264282
.1644150	.5074801	$.8773406\times10^{-2}$	1.230975	.4285695
.1696042	.5225782	$.1039552\times10^{-1}$	1.213066	.4308513
.1747315	.5367415	$.1220948\times10^{-1}$	1.195179	.4332653
.1797922	.5500487	$.1421949\times10^{-1}$	1.177375	.4358049
.1849862	.5630832	$.1653241\times10^{-1}$	1.158914	.4385854
.1899022	.5748632	$.1895033\times10^{-1}$	1.141448	.4413576
.1949287	.5864157	$.2168122\times10^{-1}$	1.123491	.4443541
.1998818	.5973416	$.2462951\times10^{-1}$	1.105800	.4474553
.2049092	.6080103	$.2790045\times10^{-1}$	1.087830	.4507604
.2098670	.6181424	$.3140083\times10^{-1}$	1.070177	.4541633
.2148846	.6280394	$.3523550\times10^{-1}$	1.052370	.4577568
.2199514	.6376966	$.3941006\times10^{-1}$	1.034485	.4615330
.2249610	.6469347	$.4383367\times10^{-1}$	1.016957	.4654009
.2301157	.6561501	$.4870760\times10^{-1}$	.9990534	.4695269
.2352212	.6650049	$.5384508\times10^{-1}$	.9815326	.4737413
.2403763	.6736951	$.5935046\times10^{-1}$	.9640532	.4781248
.2456604	.6823645	$.6532786\times10^{-1}$	.9463645	.4827482
.2509906	.6908834	$.7168892\times10^{-1}$	.9287973	.4875318
.2564426	.6993835	$.7853689\times10^{-1}$	.9111227	.4925439
.2619459	.7077625	$.8578595\times10^{-1}$	.8936131	.4977120
.2675727	.7161411	$.9354010\times10^{-1}$	.8760607	.5031015
.2732621	.7244361	.1017149	.8586966	.5086453
.2791424	.7328427	.1105084	.8411490	.5144686
.2851540	.7412788	.1198369	.8236498	.5205035
.2913034	.7497607	.1297116	.8062167	.5267491
.2976521	.7583797	.1402373	.7887130	.5332612
.3041528	.7670773	.1513335	.7713183	.5399799
.3108678	.7759447	.1631054	.7539044	.5469598
.3178556	.7850650	.1756576	.7363728	.5542513
.3250282	.7943305	.1888208	.7190026	.5617448
.3324975	.8038959	.2027927	.7015672	.5695433
.3402780	.8137890	.2175884	.6840981	.5776431
.3483869	.8240429	.2332230	.6666225	.5860399

TABLE II.—EXPANSIVE FLOW FIELD OBTAINED BY CHARACTERISTIC CALCULATIONS FOR JET FLOW FROM NEAR-SONIC EXIT (M_i=1.0038; μ_i=85°)—Continued

x/r_i	y/r_i	θ, radians	μ, radians	V/V_i
0.8573891×10^{-1}	0.2000000×10^{-1}	0.0000000	1.483530	0.4095466
$.9640913\times10^{-1}$	.1419617	$.2957617\times10^{-3}$	1.445495	.4109313
.1053469	.2130881	$.5327943\times10^{-3}$	1.419124	.4121878
.1129557	.2630474	$.8407074\times10^{-3}$	1.398279	.4133552
.1206934	.3076758	$.1279626\times10^{-2}$	1.376596	.4147346
.1271007	.3404757	$.1751733\times10^{-2}$	1.358486	.4160176
.1338823	.3722060	$.2394370\times10^{-2}$	1.338508	.4175728
.1396945	.3970407	$.3067911\times10^{-2}$	1.321163	.4190438
.1456583	.4207365	$.3908738\times10^{-2}$	1.302786	.4207266
.1516193	.4427803	$.4919721\times10^{-2}$	1.283923	.4225890
.1570566	.4615510	$.5998251\times10^{-2}$	1.266506	.4244323
.1628884	.4805185	$.7361128\times10^{-2}$	1.247287	.4266066
.1682533	.4969190	$.8801193\times10^{-2}$	1.229456	.4287578
.1735669	.5123044	$.1042857\times10^{-1}$	1.211557	.4310497
.1788170	.5267407	$.1224802\times10^{-1}$	1.193678	.4334741
.1839989	.5403071	$.1426407\times10^{-1}$	1.175882	.4360241
.1893178	.5535987	$.1658363\times10^{-1}$	1.157431	.4388156
.1943515	.5656123	$.1900813\times10^{-1}$	1.139970	.4415985
.1994987	.5773964	$.2174599\times10^{-1}$	1.122020	.4446063
.2045707	.5885429	$.2470155\times10^{-1}$	1.104336	.4477187
.2097190	.5994290	$.2798032\times10^{-1}$	1.086373	.4510354
.2147960	.6097688	$.3148850\times10^{-1}$	1.068726	.4544499
.2199345	.6198701	$.3533131\times10^{-1}$	1.050926	.4580554
.2251236	.6297280	$.3951431\times10^{-1}$	1.033048	.4618438
.2302541	.6391590	$.4394629\times10^{-1}$	1.015526	.4657240
.2355336	.6485683	$.4882919\times10^{-1}$	.9976309	.4698625
.2407628	.6576101	$.5397533\times10^{-1}$	.9801170	.4740896
.2460429	.6664849	$.5948947\times10^{-1}$	.9626444	.4784860
.2514554	.6753397	$.6547586\times10^{-1}$	.9449635	.4831226
.2569153	.6840416	$.7184545\times10^{-1}$	.9274036	.4879198
.2625002	.6927254	$.7870217\times10^{-1}$	.9097362	.4929457
.2681379	.7012863	$.8596008\times10^{-1}$	.8922349	.4981275
.2739025	.7098476	$.9372271\times10^{-1}$	.8746905	.5035312
.2797314	.7183244	.1019057	.8573346	.5090893
.2857563	.7269162	.1107078	.8397960	.5149270
.2919160	.7355390	.1200442	.8223060	.5209767
.2982172	.7442096	.1299266	.8048812	.5272372
.3047231	.7530213	.1404597	.7873875	.5337646
.3113852	.7619142	.1515623	.7700009	.5404989
.3182673	.7709818	.1633403	.7525964	.5474946
.3254297	.7803089	.1758979	.7350737	.5548023
.3327820	.7897855	.1890656	.7177124	.5623122
.3404391	.7995700	.2030413	.7002863	.5701274
.3484158	.8096910	.2178394	.6828258	.5782444
.3567298	.8201823	.2334753	.6653590	.5866587

TABLE II.—EXPANSIVE FLOW FIELD OBTAINED BY CHARACTERISTIC CALCULATIONS FOR JET FLOW FROM NEAR-SONIC EXIT (M_i=1.0038; μ_i=85°)—Continued

x/r_i	y/r_i	θ, radians	μ, radians	V/V_i
0.8748868×10^{-1}	0.0000000	0.0000000	1.483530	0.4095466
$.9847630\times10^{-1}$	.1255896	$.5022097\times10^{-4}$	1.468986	.4100168
.1065861	.2050094	$.5568377\times10^{-3}$	1.419323	.4121774
.1142703	.2555404	$.8599938\times10^{-3}$	1.398091	.4133664
.1220925	.3006100	$.1296705\times10^{-2}$	1.376211	.4147606
.1285713	.3337110	$.1768165\times10^{-2}$	1.358007	.4160531
.1354303	.3657314	$.2410894\times10^{-2}$	1.337964	.4176172
.1413086	.3907899	$.3085008\times10^{-2}$	1.320581	.4190951
.1473411	.4147012	$.3926850\times10^{-2}$	1.302175	.4207848
.1533711	.4369481	$.4939281\times10^{-2}$	1.283291	.4226539
.1588711	.4558921	$.6019411\times10^{-2}$	1.265857	.4245033
.1647709	.4750381	$.7384276\times10^{-2}$	1.246624	.4266842
.1701982	.4915933	$.8826518\times10^{-2}$	1.228785	.4288414
.1755736	.5071256	$.1045614\times10^{-1}$	1.210876	.4311395
.1808850	.5217007	$.1227820\times10^{-1}$	1.192991	.4335700
.1861275	.5353986	$.1429698\times10^{-1}$	1.175190	.4361261
.1915088	.5488207	$.1661972\times10^{-1}$	1.156736	.4389237
.1966015	.5609525	$.1904735\times10^{-1}$	1.139273	.4417126
.2018092	.5728538	$.2178862\times10^{-1}$	1.121321	.4447266
.2069408	.5841118	$.2474766\times10^{-1}$	1.103634	.4478452
.2121498	.5951077	$.2803001\times10^{-1}$	1.085670	.4511683
.2172868	.6055522	$.3154209\times10^{-1}$	1.068024	.4545890
.2224860	.6157567	$.3538870\times10^{-1}$	1.050223	.4582011
.2277366	.6257158	$.3957580\times10^{-1}$	1.032346	.4619960
.2329280	.6352440	$.4401178\times10^{-1}$	1.014825	.4658827
.2382703	.6447510	$.4889869\times10^{-1}$	.9969308	.4700281
.2435617	.6538872	$.5404916\times10^{-1}$	.9794186	.4742618
.2489047	.6628551	$.5956781\times10^{-1}$	.9619493	.4786647
.2543819	.6718033	$.6555845\times10^{-1}$	.9442705	.4833083
.2599072	.6805974	$.7193277\times10^{-1}$	.9267138	.4881122
.2655591	.6893738	$.7879381\times10^{-1}$	.9090488	.4931453
.2712645	.6980264	$.8605600\times10^{-1}$	.8915508	.4983342
.2770985	.7066798	$.9382311\times10^{-1}$	.8740106	.5037450
.2829977	.7152482	.1020103	.8566582	.5093103
.2890955	.7239334	.1108162	.8391225	.5151557
.2953298	.7326504	.1201561	.8216353	.5212132
.3017075	.7414161	.1300423	.8042153	.5274813
.3082927	.7503249	.1405787	.7867253	.5340166
.3150361	.7593164	.1516847	.7693430	.5407587
.3220026	.7684848	.1634651	.7519420	.5477627
.3292530	.7779163	.1760256	.7344240	.5550785
.3366958	.7874995	.1891957	.7170672	.5625966
.3444474	.7973946	.2031729	.6996454	.5704203
.3525230	.8076305	.2179723	.6821891	.5785459
.3609406	.8182415	.2336091	.6647269	.5869688

TABLE II.—EXPANSIVE FLOW FIELD OBTAINED BY CHARACTERISTIC CALCULATIONS FOR JET FLOW FROM NEAR-SONIC EXIT (M_i=1.0038; μ_i=85°)—Continued

x/r_i	y/r_i	θ, radians	μ, radians	V/V_i
0. 1113133	0. 0000000	0. 0000000	1. 458017	0. 4104199
. 1226543	. 1001341	$.1093971\times10^{-3}$	1. 439118	. 4112127
. 1307679	. 1614455	$.9267815\times10^{-3}$	1. 388465	. 4139586
. 1398650	. 2110428	$.1330155\times10^{-2}$	1. 365541	. 4155035
. 1473816	. 2473901	$.1793538\times10^{-2}$	1. 347105	. 4168853
. 1553399	. 2826643	$.2437950\times10^{-2}$	1. 327019	. 4185345
. 1621432	. 3103040	$.3119146\times10^{-2}$	1. 309662	. 4200819
. 1691254	. 3367619	$.3973541\times10^{-2}$	1. 291315	. 4218428
. 1761033	. 3614450	$.5003369\times10^{-2}$	1. 272504	. 4237840
. 1824600	. 3824943	$.6102750\times10^{-2}$	1. 255139	. 4257004
. 1892846	. 4038321	$.7492855\times10^{-2}$	1. 235983	. 4279553
. 1955566	. 4223038	$.8961520\times10^{-2}$	1. 218210	. 4301822
. 2017686	. 4396642	$.1062050\times10^{-1}$	1. 200366	. 4325511
. 2079063	. 4559798	$.1247478\times10^{-1}$	1. 182543	. 4350534
. 2139641	. 4713352	$.1452821\times10^{-1}$	1. 164803	. 4376820
. 2201850	. 4864058	$.1688941\times10^{-1}$	1. 146408	. 4405562
. 2260694	. 5000380	$.1935564\times10^{-1}$	1. 129000	. 4434188
. 2320891	. 5134299	$.2213884\times10^{-1}$	1. 111103	. 4465099
. 2380207	. 5261101	$.2514135\times10^{-1}$	1. 093472	. 4497056
. 2440436	. 5385092	$.2846995\times10^{-1}$	1. 075564	. 4531082
. 2499831	. 5502965	$.3202882\times10^{-1}$	1. 057971	. 4566087
. 2559963	. 5618243	$.3592440\times10^{-1}$	1. 040224	. 4603026
. 2620702	. 5730853	$.4016213\times10^{-1}$	1. 022404	. 4641809
. 2680758	. 5838667	$.4464885\times10^{-1}$	1. 004938	. 4681508
. 2742584	. 5946346	$.4958879\times10^{-1}$	. 9871017	. 4723825
. 2803825	. 6049893	$.5479161\times10^{-1}$	. 9696460	. 4767024
. 2865678	. 6151608	$.6036287\times10^{-1}$	. 9522338	. 4811928
. 2929106	. 6253185	$.6640718\times10^{-1}$	. 9346141	. 4859263
. 2993106	. 6353084	$.7283452\times10^{-1}$	. 9171172	. 4908212
. 3058593	. 6452857	$.7974912\times10^{-1}$	. 8995153	. 4959470
. 3124716	. 6551289	$.8706345\times10^{-1}$	. 8820792	. 5012296
. 3192350	. 6649802	$.9488181\times10^{-1}$	. 8646014	. 5067360
. 3260760	. 6747410	. 1031187	. 8473129	. 5123973
. 3331501	. 6846423	. 1119731	. 8298427	. 5183413
. 3403852	. 6945867	. 1213599	. 8124229	. 5244986
. 3477893	. 7045936	. 1312899	. 7950687	. 5308682
. 3554373	. 7147712	. 1418674	. 7776459	. 5375069
. 3632723	. 7250504	. 1530108	. 7603317	. 5443536
. 3713701	. 7355393	. 1648252	. 7429987	. 5514639
. 3798019	. 7463374	. 1774150	. 7255489	. 5588887
. 3884616	. 7573169	. 1906087	. 7082596	. 5665166
. 3974856	. 7686622	. 2046043	. 6909056	. 5744522
. 4068921	. 7804073	. 2194157	. 6735169	. 5826916
. 4167025	. 7925924	. 2350568	. 6561219	. 5912301

TABLE II.—EXPANSIVE FLOW FIELD OBTAINED BY CHARACTERISTIC CALCULATIONS FOR JET FLOW FROM NEAR-SONIC EXIT (M_i=1.0038; μ_i=85°)—Continued

x/r_i	y/r_i	θ, radians	μ, radians	V/V_t
0. 1359276	0. 0000000	0. 0000000	1. 424893	0. 4118920
. 1468782	$.7452140\times10^{-1}$	$.1906271\times10^{-3}$	1. 405021	. 4129607
. 1564600	. 1318588	$.1411773\times10^{-2}$	1. 354225	. 4163369
. 1649605	. 1707552	$.1808748\times10^{-2}$	1. 334821	. 4178760
. 1739711	. 2085292	$.2422358\times10^{-2}$	1. 314519	. 4196373
. 1816614	. 2381696	$.3093383\times10^{-2}$	1. 297206	. 4212632
. 1895540	. 2666323	$.3947162\times10^{-2}$	1. 278987	. 4230093
. 1974399	. 2932662	$.4983637\times10^{-2}$	1. 260338	. 4251140
. 2046169	. 3160257	$.6093961\times10^{-2}$	1. 243126	. 4270970
. 2123265	. 3391683	$.7501300\times10^{-2}$	1. 224139	. 4294246
. 2194065	. 3592373	$.8989216\times10^{-2}$	1. 206515	. 4317196
. 2264186	. 3781363	$.1067089\times10^{-1}$	1. 188814	. 4341573
. 2333468	. 3959293	$.1255063\times10^{-1}$	1. 171125	. 4367292
. 2401848	. 4127019	$.1463214\times10^{-1}$	1. 153512	. 4394280
. 2472088	. 4291934	$.1702506\times10^{-1}$	1. 135243	. 4423760
. 2538511	. 4441262	$.1952326\times10^{-1}$	1. 117949	. 4453097
. 2606482	. 4588175	$.2234166\times10^{-1}$	1. 100165	. 4484748
. 2673459	. 4727438	$.2538041\times10^{-1}$	1. 082639	. 4517448
. 2741485	. 4863785	$.2874769\times10^{-1}$	1. 064836	. 4552240
. 2808573	. 4993530	$.3234617\times10^{-1}$	1. 047344	. 4588008
. 2876509	. 5120558	$.3628307\times10^{-1}$	1. 029697	. 4625729
. 2945145	. 5244770	$.4056324\times10^{-1}$	1. 011974	. 4665311
. 3013016	. 5363792	$.4509258\times10^{-1}$	. 9946041	. 4705804
. 3082911	. 5482784	$.5007684\times10^{-1}$	. 9768637	. 4748944
. 3152154	. 5597296	$.5532335\times10^{-1}$	. 9595018	. 4792962
. 3222105	. 5709876	$.6093845\times10^{-1}$	. 9421818	. 4838696
. 3293861	. 5822401	$.6702722\times10^{-1}$	. 9246555	. 4886882
. 3366282	. 5933152	$.7349830\times10^{-1}$	. 9072512	. 4936690
. 3440409	. 6043851	$.8045583\times10^{-1}$	. 8897409	. 4988828
. 3515276	. 6153143	$.8781199\times10^{-1}$	. 8723959	. 5042538
. 3591879	. 6262609	$.9567126\times10^{-1}$	. 8550108	. 5098499
. 3669383	. 6371146	. 1039465	. 8378118	. 5156017
. 3749557	. 6481332	. 1128377	. 8204325	. 5216384
. 3831586	. 6592078	. 1222585	. 8031029	. 5278896
. 3915563	. 6703600	. 1322196	. 7858393	. 5343541
. 4002343	. 6817109	. 1428252	. 7685067	. 5410895
. 4091281	. 6931834	. 1539926	. 7512817	. 5480336
. 4183245	. 7048987	. 1658269	. 7340381	. 5552427
. 4279050	. 7169685	. 1784318	. 7166780	. 5627683
. 4377493	. 7292502	. 1916356	. 6994775	. 5704971
. 4480131	. 7419510	. 2056355	. 6822119	. 5785351
. 4587184	. 7551097	. 2204450	. 6649119	. 5868780
. 4698901	. 7687723	. 2360769	. 6476040	. 5955211

TABLE II.—EXPANSIVE FLOW FIELD OBTAINED BY CHARACTERISTIC CALCULATIONS FOR JET FLOW FROM NEAR-SONIC EXIT (M_i=1.0038; μ_i=85°)—Continued

x/r_i	y/r_i	θ, radians	μ, radians	V/V_i
0. 1593610	0. 0000000	0. 0000000	1. 389366	0. 4139017
. 1712780	$.6496121\times10^{-1}$	$.2958171\times10^{-3}$	1. 369307	. 4152366
. 1801082	. 1082568	$.1891990\times10^{-2}$	1. 323004	. 4188823
. 1900372	. 1478175	$.2380173\times10^{-2}$	1. 301648	. 4208350
. 1985121	. 1788292	$.3006475\times10^{-2}$	1. 284288	. 4225516
. 2072104	. 2086840	$.3837739\times10^{-2}$	1. 266224	. 4244632
. 2158995	. 2367004	$.4865631\times10^{-2}$	1. 247804	. 4265461
. 2238017	. 2606960	$.5976022\times10^{-2}$	1. 230821	. 4285885
. 2322933	. 2851672	$.7390206\times10^{-2}$	1. 212084	. 4309803
. 2400871	. 3064308	$.8888718\times10^{-2}$	1. 194679	. 4333347
. 2478057	. 3264966	$.1058471\times10^{-1}$	1. 177188	. 4358322
. 2554317	. 3454236	$.1248187\times10^{-1}$	1. 159697	. 4384645
. 2629584	. 3632953	$.1458323\times10^{-1}$	1. 142268	. 4412243
. 2706918	. 3808982	$.1699955\times10^{-1}$	1. 124182	. 4442361
. 2780034	. 3968569	$.1952182\times10^{-1}$	1. 107051	. 4472312
. 2854871	. 4125809	$.2236693\times10^{-1}$	1. 089426	. 4504603
. 2928620	. 4275034	$.2543364\times10^{-1}$	1. 072051	. 4537944
. 3003540	. 4421318	$.2883053\times10^{-1}$	1. 054394	. 4573400
. 3077432	. 4560663	$.3245919\times10^{-1}$	1. 037040	. 4609831
. 3152274	. 4697238	$.3642788\times10^{-1}$	1. 019528	. 4648229
. 3227902	. 4830920	$.4074068\times10^{-1}$	1. 001937	. 4688502
. 3302695	. 4959128	$.4530229\times10^{-1}$	. 9846905	. 4729686
. 3379742	. 5087428	$.5031998\times10^{-1}$	. 9670745	. 4773541
. 3456081	. 5210996	$.5559921\times10^{-1}$	. 9498311	. 4818269
. 3533218	. 5332579	$.6124692\times10^{-1}$	. 9326279	. 4864722
. 3612369	. 5454206	$.6736827\times10^{-1}$	. 9152172	. 4913647
. 3692272	. 5574007	$.7387141\times10^{-1}$	. 8979266	. 4964197
. 3774081	. 5693845	$.8086053\times10^{-1}$	. 8805296	. 5017091
. 3856729	. 5812246	$.8824655\times10^{-1}$	. 8632956	. 5071561
. 3941319	. 5930922	$.9613430\times10^{-1}$	. 8460200	. 5128295
. 4026928	. 6048675	. 1044363	. 8289288	. 5186586
. 4115520	. 6168304	. 1133522	. 8116574	. 5247745
. 4206191	. 6288626	. 1227952	. 7944338	. 5311058
. 4299050	. 6409875	. 1327756	. 7772752	. 5376509
. 4395046	. 6533373	. 1433976	. 7600473	. 5444681
. 4493467	. 6658281	. 1545779	. 7429257	. 5514944
. 4595279	. 6785925	. 1664208	. 7257847	. 5587866
. 4701393	. 6917526	. 1790300	. 7085266	. 5663967
. 4810478	. 7051533	. 1922325	. 6914257	. 5742102
. 4924271	. 7190215	. 2062254	. 6742593	. 5823339
. 5043020	. 7334006	. 2210215	. 6570568	. 5907634
. 5167016	. 7483415	. 2366330	. 6398455	. 5994935

TABLE II.—EXPANSIVE FLOW FIELD OBTAINED BY CHARACTERISTIC CALCULATIONS FOR JET FLOW FROM NEAR-SONIC EXIT (M_i=1.0038; μ_i=85°)—Continued

x/r_i	y/r_i	θ, radians	μ, radians	V/V_i
0. 1845671	0. 0000000	0. 0000000	1. 352877	0. 4164393
. 1953253	$.4858321\times10^{-1}$	$.4086221\times10^{-3}$	1. 333616	. 4179762
. 2056973	$.9156796\times10^{-1}$	$.2443964\times10^{-2}$	1. 288541	. 4221204
. 2149323	. 1237064	$.2901022\times10^{-2}$	1. 270182	. 4240332
. 2244255	. 1546463	$.3654033\times10^{-2}$	1. 252043	. 4260547
. 2339109	. 1837465	$.4643372\times10^{-2}$	1. 233824	. 4282188
. 2425331	. 2087289	$.5736389\times10^{-2}$	1. 217102	. 4303254
. 2518018	. 2342824	$.7144294\times10^{-2}$	1. 198673	. 4327830
. 2603054	. 2565373	$.8644308\times10^{-2}$	1. 181552	. 4351966
. 2687271	. 2775857	$.1034697\times10^{-1}$	1. 164335	. 4377532
. 2770478	. 2974810	$.1225510\times10^{-1}$	1. 147105	. 4404446
. 2852605	. 3163026	$.1437066\times10^{-1}$	1. 129921	. 4432638
. 2937005	. 3348769	$.1680490\times10^{-1}$	1. 112077	. 4463378
. 3016790	. 3517408	$.1934601\times10^{-1}$	1. 095161	. 4493928
. 3098475	. 3683829	$.2221238\times10^{-1}$	1. 077748	. 4526847
. 3178978	. 3841982	$.2530155\times10^{-1}$	1. 060570	. 4560816
. 3260775	. 3997233	$.2872307\times10^{-1}$	1. 043105	. 4596917
. 3341461	. 4145289	$.3237689\times10^{-1}$	1. 025932	. 4633993
. 3423203	. 4290574	$.3637188\times10^{-1}$	1. 008597	. 4673052
. 3505822	. 4432938	$.4071180\times10^{-1}$	. 9911754	. 4713999
. 3587541	. 4569607	$.4530066\times10^{-1}$	. 9740920	. 4755851
. 3671748	. 4706519	$.5034636\times10^{-1}$	. 9566370	. 4800399
. 3755194	. 4838499	$.5565310\times10^{-1}$	. 9395479	. 4845814
. 3839534	. 4968476	$.6132788\times10^{-1}$	. 9224937	. 4892962
. 3926103	. 5098618	$.6747627\times10^{-1}$	. 9052311	. 4942600
. 4013516	. 5226914	$.7400515\times10^{-1}$	. 8880837	. 4993869
. 4103042	. 5355358	$.8101896\times10^{-1}$	. 8708282	. 5047496
. 4193511	. 5482364	$.8842834\times10^{-1}$	. 8537317	. 5102700
. 4286136	. 5609765	$.9633752\times10^{-1}$	. 8365916	. 5160181
. 4379906	. 5736273	. 1046588	. 8196320	. 5219219
. 4476979	. 5864897	. 1135922	. 8024934	. 5281138
. 4576366	. 5994365	. 1230496	. 7853990	. 5345220
. 4678190	. 6124928	. 1330417	. 7683685	. 5411442
. 4783497	. 6258014	. 1436715	. 7512663	. 5480399
. 4891509	. 6392721	. 1548557	. 7342678	. 5551449
. 5003292	. 6530483	. 1666984	. 7172493	. 5625163
. 5119855	. 6672625	. 1793024	. 7001127	. 5702067
. 5239740	. 6817476	. 1924953	. 6831314	. 5780999
. 5364865	. 6967497	. 2064725	. 6660830	. 5863040
. 5495517	. 7123167	. 2212469	. 6489973	. 5948142
. 5632023	. 7285050	. 2368299	. 6319015	. 6036249

TABLE II.—EXPANSIVE FLOW FIELD OBTAINED BY CHARACTERISTIC CALCULATIONS FOR JET FLOW FROM NEAR-SONIC EXIT ($M_i=1.0038$; $\mu_i=85°$)—Continued

x/r_i	y/r_i	θ, radians	μ, radians	V/V_i
0. 2070903	0. 0000000	0. 0000000	1. 317271	0. 4193894
. 2190201	$.4604310\times10^{-1}$	$.5277630\times10^{-3}$	1. 298912	. 4210979
. 2285396	$.8025925\times10^{-1}$	$.2954295\times10^{-2}$	1. 258188	. 4253552
. 2386838	. 1119649	$.3480637\times10^{-2}$	1. 239067	. 4275822
. 2488352	. 1417719	$.4376756\times10^{-2}$	1. 220848	. 4298433
. 2580621	. 1674012	$.5427922\times10^{-2}$	1. 204343	. 4320115
. 2679844	. 1936801	$.6812723\times10^{-2}$	1. 186209	. 4345274
. 2770853	. 2166143	$.8303044\times10^{-2}$	1. 169376	. 4369911
. 2860990	. 2383493	$.1000360\times10^{-1}$	1. 152442	. 4395965
. 2950050	. 2589328	$.1191467\times10^{-1}$	1. 135481	. 4423366
. 3037960	. 2784397	$.1403705\times10^{-1}$	1. 118554	. 4452044
. 3128321	. 2977235	$.1648157\times10^{-1}$	1. 100963	. 4483293
. 3213737	. 3152559	$.1903439\times10^{-1}$	1. 084274	. 4514333
. 3301204	. 3325831	$.2191512\times10^{-1}$	1. 067082	. 4547761
. 3387416	. 3490701	$.2501995\times10^{-1}$	1. 050114	. 4582238
. 3475032	. 3652749	$.2845844\times10^{-1}$	1. 032851	. 4618866
. 3561466	. 3807460	$.3212999\times10^{-1}$	1. 015868	. 4656467
. 3649049	. 3959441	$.3614369\times10^{-1}$	. 9987163	. 4696063
. 3737589	. 4108521	$.4050278\times10^{-1}$	. 9814729	. 4737559
. 3825181	. 4251764	$.4511056\times10^{-1}$	. 9645571	. 4779958
. 3915460	. 4395404	$.5017555\times10^{-1}$	. 9472682	. 4825073
. 4004942	. 4533980	$.5550123\times10^{-1}$	. 9303367	. 4871049
. 4095404	. 4670567	$.6119462\times10^{-1}$	. 9134356	. 4918764
. 4188278	. 4807445	$.6736103\times10^{-1}$	. 8963240	. 4968984
. 4282082	. 4942484	$.7390690\times10^{-1}$	. 8793224	. 5020839
. 4378180	. 5077782	$.8093681\times10^{-1}$	. 8622103	. 5075062
. 4475313	. 5211666	$.8836078\times10^{-1}$	. 8452536	. 5130862
. 4574791	. 5346063	$.9628302\times10^{-1}$	. 8282497	. 5188947
. 4675530	. 5479608	. 1046156	. 8114238	. 5248588
. 4779847	. 5615488	. 1135582	. 7944167	. 5311122
. 4886685	. 5752355	. 1230225	. 7774521	. 5375821
. 4996181	. 5890472	. 1330183	. 7605480	. 5442665
. 5109463	. 6031355	. 1436492	. 7435710	. 5512249
. 5225699	. 6174051	. 1548309	. 7266951	. 5583926
. 5346041	. 6320082	. 1666674	. 7097973	. 5658270
. 5471583	. 6470860	. 1792609	. 6927807	. 5735811
. 5600761	. 6624617	. 1924388	. 6759158	. 5815376
. 5735648	. 6783973	. 2063959	. 6589823	. 5898052
. 5876564	. 6949447	. 2211451	. 6420108	. 5983787
. 6023871	. 7121651	. 2366964	. 6250267	. 6072526

TABLE II.—EXPANSIVE FLOW FIELD OBTAINED BY CHARACTERISTIC CALCULATIONS FOR JET FLOW FROM NEAR-SONIC EXIT (M_i=1.0038; μ_i=85°)—Continued

x/r_i	y/r_i	θ, radians	μ, radians	V/V_i
0.2318825	0.0000000	0.0000000	1.282917	0.4226923
.2427547	$.3671761\times10^{-1}$	$.6490770\times10^{-3}$	1.265473	.4245454
.2532597	$.7012302\times10^{-1}$	$.3497615\times10^{-2}$	1.226097	.4291777
.2640742	.1005785	$.4082347\times10^{-2}$	1.206734	.4316902
.2739210	.1267404	$.5021827\times10^{-2}$	1.190241	.4339558
.2845175	.1536186	$.6346171\times10^{-2}$	1.172359	.4365454
.2942365	.1771229	$.7807542\times10^{-2}$	1.155828	.4390652
.3038636	.1994461	$.9493340\times10^{-2}$	1.139211	.4417227
.3133767	.2206300	$.1139874\times10^{-1}$	1.122563	.4445131
.3227681	.2407438	$.1352129\times10^{-1}$	1.105937	.4474306
.3324239	.2606644	$.1597074\times10^{-1}$	1.088644	.4506072
.3415511	.2788043	$.1853093\times10^{-1}$	1.072223	.4537607
.3508999	.2967601	$.2142203\times10^{-1}$	1.055296	.4571549
.3601157	.3138695	$.2453859\times10^{-1}$	1.038576	.4606542
.3694837	.3307093	$.2799074\times10^{-1}$	1.021554	.4643700
.3787267	.3468064	$.3167662\times10^{-1}$	1.004799	.4681831
.3880949	.3626384	$.3570563\times10^{-1}$	.9878679	.4721969
.3975678	.3781857	$.4008097\times10^{-1}$	.9708384	.4764016
.4069407	.3931399	$.4470445\times10^{-1}$	.9541242	.4806965
.4166040	.4081512	$.4978579\times10^{-1}$	.9370344	.4852647
.4261839	.4226469	$.5512686\times10^{-1}$	.9202905	.4899189
.4358710	.4369479	$.6083533\times10^{-1}$	.9035724	.4947473
.4458196	.4512922	$.6701635\times10^{-1}$	.8866402	.4998276
.4558702	.4654562	$.7357571\times10^{-1}$	.8698127	.5050717
.4661697	.4796594	$.8061807\times10^{-1}$	.8528715	.5105534
.4765835	.4937252	$.8805279\times10^{-1}$	.8360800	.5161930
.4872518	.5078566	$.9598421\times10^{-1}$	.8192384	.5220617
.4980588	.5219090	.1043237	.8025693	.5280859
.5092542	.5362179	.1132709	.7857174	.5344006
.5207239	.5506420	.1227371	.7689047	.5409320
.5324832	.5652089	.1327319	.7521488	.5476780
.5446542	.5800786	.1433585	.7353180	.5546986
.5571475	.5951509	.1545324	.7185851	.5619282
.5700880	.6105868	.1663570	.7018275	.5694248
.5835938	.6265368	.1789344	.6849503	.5772413
.5974975	.6428140	.1920918	.6682208	.5852595
.6120234	.6596968	.2060230	.6514216	.5935888
.6272064	.6772417	.2207399	.6345813	.6022240
.6430871	.6955146	.2362534	.6177268	.6111587

TABLE II.—EXPANSIVE FLOW FIELD OBTAINED BY CHARACTERISTIC CALCULATIONS FOR JET FLOW FROM NEAR-SONIC EXIT ($M_i=1.0038$; $\mu_i=85°$)—Continued

x/r_i	y/r_i	θ, radians	μ, radians	V/V_i
0. 2543535	0. 0000000	0. 0000000	1. 249970	0. 4262942
. 2659960	$.3503552\times10^{-1}$	$.7663570\times10^{-3}$	1. 233484	. 4282604
. 2771064	$.6679266\times10^{-1}$	$.4120058\times10^{-2}$	1. 195624	. 4332035
. 2874561	$.9339402\times10^{-1}$	$.4744754\times10^{-2}$	1. 178142	. 4356925
. 2986175	. 1207087	$.5927367\times10^{-2}$	1. 160157	. 4383934
. 3088600	. 1446194	$.7324464\times10^{-2}$	1. 143779	. 4409795
. 3190091	. 1673649	$.8974450\times10^{-2}$	1. 127386	. 4436915
. 3290408	. 1889848	$.1085975\times10^{-1}$	1. 110984	. 4465310
. 3389463	. 2095451	$.1297177\times10^{-1}$	1. 094609	. 4494949
. 3491333	. 2299412	$.1541684\times10^{-1}$	1. 077572	. 4527187
. 3587638	. 2485388	$.1797689\times10^{-1}$	1. 061388	. 4559163
. 3686306	. 2669733	$.2087098\times10^{-1}$	1. 044697	. 4593560
. 3783587	. 2845608	$.2399265\times10^{-1}$	1. 028201	. 4629003
. 3882500	. 3018922	$.2745190\times10^{-1}$	1. 011401	. 4666621
. 3980110	. 3184774	$.3114582\times10^{-1}$	. 9948546	. 4705208
. 4079063	. 3348075	$.3518379\times10^{-1}$	. 9781269	. 4745812
. 4179143	. 3508605	$.3956881\times10^{-1}$	. 9612954	. 4788331
. 4278188	. 3663151	$.4420233\times10^{-1}$	. 9447695	. 4831745
. 4380328	. 3818435	$.4929375\times10^{-1}$	. 9278657	. 4877909
. 4481605	. 3968517	$.5464469\times10^{-1}$	. 9112996	. 4924926
. 4584043	. 4116702	$.6036206\times10^{-1}$	. 8947532	. 4973692
. 4689275	. 4265458	$.6655171\times10^{-1}$	. 8779906	. 5024985
. 4795613	. 4412459	$.7311894\times10^{-1}$	. 8613272	. 5077916
. 4904614	. 4559981	$.8016804\times10^{-1}$	. 8445474	. 5133231
. 5014857	. 4706180	$.8760796\times10^{-1}$	. 8279114	. 5190125
. 5127829	. 4853167	$.9554294\times10^{-1}$	. 8112228	. 5249314
. 5242299	. 4999438	. 1038840	. 7947008	. 5310057
. 5360921	. 5148484	. 1128307	. 7779957	. 5373712
. 5482492	. 5298831	. 1222943	. 7613263	. 5439534
. 5607172	. 5450772	. 1322839	. 7447102	. 5507501
. 5736265	. 5605977	. 1429023	. 7280179	. 5578217
. 5868829	. 5763400	. 1540654	. 7114201	. 5651018
. 6006192	. 5924730	. 1658753	. 6947949	. 5726490
. 6149614	. 6091548	. 1784338	. 6780483	. 5805163
. 6297322	. 6261906	. 1915687	. 6614469	. 5885844
. 6451707	. 6438725	. 2054724	. 6447731	. 5969635
. 6613161	. 6622605	. 2201573	. 6280563	. 6056478
. 6782127	. 6814249	. 2356332	. 6113236	. 6146311

TABLE II.—EXPANSIVE FLOW FIELD OBTAINED BY CHARACTERISTIC CALCULATIONS FOR JET FLOW FROM NEAR-SONIC EXIT (M_i=1.0038; μ_i=85°)—Continued

x/r_i	y/r_i	θ, radians	μ, radians	V/V_t
0. 2783136	0. 0000000	0. 0000000	1. 218597	0. 4301322
. 2905062	$.3317486\times10^{-1}$	$.9090577\times10^{-3}$	1. 202505	. 4322601
. 3011374	$.6079862\times10^{-1}$	$.4760397\times10^{-2}$	1. 166519	. 4374215
. 3128506	$.8854062\times10^{-1}$	$.5512074\times10^{-2}$	1. 147344	. 4404062
. 3236224	. 1127961	$.6758233\times10^{-2}$	1. 130924	. 4430955
. 3343033	. 1358953	$.8331294\times10^{-2}$	1. 114705	. 4458755
. 3448648	. 1578849	$.1017342\times10^{-1}$	1. 098547	. 4487701
. 3552963	. 1788299	$.1226032\times10^{-1}$	1. 082437	. 4517833
. 3660279	. 1996411	$.1469067\times10^{-1}$	1. 065678	. 4550557
. 3761744	. 2186447	$.1724329\times10^{-1}$	1. 049756	. 4582980
. 3865730	. 2375085	$.2013483\times10^{-1}$	1. 033328	. 4617831
. 3968273	. 2555297	$.2325702\times10^{-1}$	1. 017084	. 4653722
. 4072564	. 2733111	$.2671938\times10^{-1}$	1. 000531	. 4691796
. 4175503	. 2903468	$.3041801\times10^{-1}$	. 9842202	. 4730833
. 4279887	. 3071394	$.3446174\times10^{-1}$	. 9677220	. 4771897
. 4385486	. 3236649	$.3885331\times10^{-1}$	. 9511130	. 4814882
. 4490016	. 3395903	$.4349335\times10^{-1}$	. 9347981	. 4858759
. 4597842	. 3556080	$.4859175\times10^{-1}$	. 9181040	. 4905399
. 4704782	. 3711032	$.5394936\times10^{-1}$	. 9017369	. 4952886
. 4812974	. 3864164	$.5967315\times10^{-1}$	. 8853843	. 5002123
. 4924150	. 4018020	$.6586822\times10^{-1}$	. 8688115	. 5053899
. 5036528	. 4170186	$.7244002\times10^{-1}$	. 8523319	. 5107314
. 5151757	. 4323015	$.7949240\times10^{-1}$	. 8357324	. 5163119
. 5268327	. 4474598	$.8693465\times10^{-1}$	. 8192719	. 5220499
. 5387822	. 4627115	$.9487026\times10^{-1}$	. 8027546	. 5280177
. 5508941	. 4779002	. 1032101	. 7863990	. 5341406
. 5634496	. 4933888	. 1121533	. 7698576	. 5405555
. 5763219	. 5090240	. 1216111	. 7533485	. 5471870
. 5895282	. 5248364	. 1315923	. 7368889	. 5540328
. 6032072	. 5410003	. 1421993	. 7203502	. 5611536
. 6172593	. 5574073	. 1533474	. 7039021	. 5684826
. 6318259	. 5742337	. 1651389	. 6874244	. 5760785
. 6470426	. 5916448	. 1776747	. 6708227	. 5839946
. 6627209	. 6094385	. 1907825	. 6543617	. 5921107
. 6791166	. 6279204	. 2046553	. 6378272	. 6005370
. 6962712	. 6471552	. 2193036	. 6212473	. 6092680
. 7142343	. 6672171	. 2347382	. 6046487	. 6182968

TABLE II.—EXPANSIVE FLOW FIELD OBTAINED BY CHARACTERISTIC CALCULATIONS FOR JET FLOW FROM NEAR-SONIC EXIT (M_i=1.0038; μ_i=85°)—Continued

x/r_i	y/r_i	θ, radians	μ, radians	V/V_i
0. 3033430	0. 0000000	0. 0000000	1. 187828	0. 4342970
. 3149758	$.2887517\times10^{-1}$	$.1055983\times10^{-2}$	1. 172168	. 4365738
. 3270209	$.5755836\times10^{-1}$	$.5519920\times10^{-2}$	1. 135775	. 4422879
. 3382915	$.8216565\times10^{-1}$	$.6294589\times10^{-2}$	1. 118202	. 4452655
. 3494929	. 1055748	$.7675911\times10^{-2}$	1. 101854	. 4481675
. 3605786	. 1278792	$.9420302\times10^{-2}$	1. 085823	. 4511394
. 3715333	. 1491520	$.1145104\times10^{-1}$	1. 069925	. 4542131
. 3828085	. 1703202	$.1384641\times10^{-1}$	1. 053418	. 4575407
. 3934716	. 1896759	$.1637810\times10^{-1}$	1. 037746	. 4608316
. 4044034	. 2089165	$.1925638\times10^{-1}$	1. 021577	. 4643649
. 4151862	. 2273219	$.2237090\times10^{-1}$	1. 005586	. 4680004
. 4261563	. 2455057	$.2582938\times10^{-1}$	. 9892860	. 4718544
. 4369869	. 2629474	$.2952644\times10^{-1}$	. 9732174	. 4758040
. 4479726	. 2801604	$.3357069\times10^{-1}$	. 9569575	. 4799565
. 4590895	. 2971181	$.3796391\times10^{-1}$	. 9405814	. 4843016
. 4700963	. 3134772	$.4260653\times10^{-1}$	. 9244891	. 4887349
. 4814539	. 3299478	$.4770778\times10^{-1}$	. 9080163	. 4934458
. 4927212	. 3458960	$.5306815\times10^{-1}$	. 8918604	. 4982406
. 5041235	. 3616715	$.5879414\times10^{-1}$	. 8757118	. 5032108
. 5158439	. 3775362	$.6499103\times10^{-1}$	. 8593418	. 5084355
. 5276946	. 3932401	$.7156402\times10^{-1}$	. 8430587	. 5138238
. 5398497	. 4090260	$.7861628\times10^{-1}$	. 8266519	. 5194517
. 5521505	. 4246957	$.8605688\times10^{-1}$	. 8103775	. 5252370
. 5647639	. 4404749	$.9398895\times10^{-1}$	. 7940424	. 5312524
. 5775532	. 4562010	. 1023238	. 7778643	. 5374222
. 5908156	. 4722504	. 1112597	. 7614970	. 5438847
. 6044179	. 4884639	. 1207079	. 7451589	. 5505634
. 6183785	. 5048737	. 1306768	. 7288663	. 5574562
. 6328441	. 5216614	. 1412685	. 7124923	. 5646239
. 6477111	. 5387139	. 1523978	. 6962039	. 5719094
. 6631290	. 5562156	. 1641669	. 6798826	. 5796414
. 6792425	. 5743393	. 1766767	. 6634363	. 5876032
. 6958530	. 5928753	. 1897545	. 6471263	. 5957639
. 7132321	. 6121432	. 2035925	. 6307400	. 6042343
. 7314265	. 6322112	. 2182013	. 6143061	. 6130083
. 7504885	. 6531592	. 2335903	. 5978499	. 6220793

502683 O—59——5

TABLE II.—EXPANSIVE FLOW FIELD OBTAINED BY CHARACTERISTIC CALCULATIONS FOR JET FLOW FROM NEAR-SONIC EXIT (M_i=1.0038; μ_i=85°)—Continued

x/r_i	y/r_i	θ, radians	μ, radians	V/V_i
0. 3271733	0. 0000000	0. 0000000	1. 157766	0. 4387635
. 3401723	. 2966202×10^{-1}	. 1221280×10^{-2}	1. 142362	. 4412090
. 3517103	. 5500565×10^{-1}	. 6326061×10^{-2}	1. 107516	. 4471478
. 3633643	. 7870891×10^{-1}	. 7177738×10^{-2}	1. 090053	. 4503428
. 3749241	. 1012664	. 8709378×10^{-2}	1. 073888	. 4534349
. 3863570	. 1227946	. 1063132×10^{-1}	1. 058098	. 4565829
. 3981312	. 1442418	. 1296168×10^{-1}	1. 041789	. 4599702
. 4092697	. 1638755	. 1545500×10^{-1}	1. 026339	. 4633097
. 4206932	. 1834167	. 1830773×10^{-1}	1. 010407	. 4668895
. 4319644	. 2021316	. 2140537×10^{-1}	. 9946528	. 4705688
. 4434349	. 2206432	. 2485244×10^{-1}	. 9785914	. 4744662
. 4547623	. 2384191	. 2854244×10^{-1}	. 9627553	. 4784575
. 4662556	. 2559805	. 3258208×10^{-1}	. 9467245	. 4826520
. 4778891	. 2732999	. 3697254×10^{-1}	. 9305745	. 4870390
. 4894106	. 2900236	. 4161316×10^{-1}	. 9146985	. 4915135
. 5013030	. 3068776	. 4671325×10^{-1}	. 8984411	. 4962665
. 5131039	. 3232116	. 5207249×10^{-1}	. 8824901	. 5011027
. 5250497	. 3393827	. 5779756×10^{-1}	. 8665417	. 5061141
. 5373326	. 3556593	. 6399322×10^{-1}	. 8503700	. 5113805
. 5497555	. 3717843	. 7056383×10^{-1}	. 8342778	. 5168106
. 5625013	. 3880068	. 7761273×10^{-1}	. 8180597	. 5224805
. 5754040	. 4041224	. 8504885×10^{-1}	. 8019676	. 5283074
. 5886389	. 4203631	. 9297483×10^{-1}	. 7858119	. 5343646
. 6020627	. 4365612	. 1013018	. 7698064	. 5405757
. 6159882	. 4531046	. 1102281	. 7536109	. 5470798
. 6302755	. 4698296	. 1196643	. 7374400	. 5537997
. 6449448	. 4867692	. 1296189	. 7213106	. 5607334
. 6601511	. 5041113	. 1401931	. 7050963	. 5679421
. 6757852	. 5217399	. 1513024	. 6889644	. 5753576
. 6920056	. 5398458	. 1630480	. 6727969	. 5830392
. 7089654	. 5586090	. 1755309	. 6565020	. 5910402
. 7264565	. 5778129	. 1885779	. 6403390	. 5992391
. 7447665	. 5977896	. 2023807	. 6240971	. 6077469
. 7639445	. 6186119	. 2169496	. 6078052	. 6165574
. 7840482	. 6403638	. 2322943	. 5914887	. 6256633

TABLE II.—EXPANSIVE FLOW FIELD OBTAINED BY CHARACTERISTIC CALCULATIONS FOR JET FLOW FROM NEAR-SONIC EXIT (M_i=1.0038; μ_i=85°) —Continued

x/r_i	y/r_i	θ, radians	μ, radians	V/V_t
0. 3537636	0. 0000000	0. 0000000	1. 128109	0. 4435692
. 3662539	$.2634665\times10^{-1}$	$.1409306\times10^{-2}$	1. 112822	. 4462065
. 3782223	$.5071303\times10^{-1}$	$.7148561\times10^{-2}$	1. 078285	. 4525808
. 3902680	$.7355075\times10^{-1}$	$.8016011\times10^{-2}$	1. 060889	. 4560172
. 4022118	$.9531618\times10^{-1}$	$.9677773\times10^{-2}$	1. 044974	. 4592977
. 4145247	. 1170150	$.1187141\times10^{-1}$	1. 028805	. 4627680
. 4261786	. 1369001	$.1429014\times10^{-1}$	1. 013576	. 4661662
. 4381364	. 1567169	$.1709468\times10^{-1}$	. 9979028	. 4697983
. 4499392	. 1757192	$.2016106\times10^{-1}$	. 9824147	. 4735249
. 4619551	. 1945392	$.2358661\times10^{-1}$	. 9666256	. 4774683
. 4738246	. 2126330	$.2726169\times10^{-1}$	. 9510547	. 4815036
. 4858719	. 2305298	$.3129081\times10^{-1}$	. 9352877	. 4857418
. 4980702	. 2482000	$.3567373\times10^{-1}$	. 9193967	. 4901723
. 5101546	. 2652807	$.4030849\times10^{-1}$	. 9037692	. 4946894
. 5226326	. 2825126	$.4540398\times10^{-1}$	. 8877590	. 4994858
. 5350180	. 2992299	$.5075898\times10^{-1}$	. 8720453	. 5043646
. 5475597	. 3157963	$.5648007\times10^{-1}$	. 8563274	. 5094184
. 5604597	. 3324869	$.6267138\times10^{-1}$	. 8403835	. 5147277
. 5735112	. 3490371	$.6923715\times10^{-1}$	. 8245131	. 5202004
. 5869067	. 3657025	$.7628019\times10^{-1}$	. 8085117	. 5259132
. 6004716	. 3822727	$.8370872\times10^{-1}$	. 7926297	. 5317828
. 6143911	. 3989858	$.9162608\times10^{-1}$	. 7766796	. 5378824
. 6285145	. 4156690	$.9994236\times10^{-1}$	. 7608730	. 5441356
. 6431715	. 4327222	. 1088561	. 7448746	. 5506818
. 6582153	. 4499768	. 1182770	. 7288956	. 5574436
. 6736675	. 4674673	. 1282138	. 7129538	. 5644185
. 6896929	. 4853877	. 1387675	. 6969238	. 5716681
. 7061764	. 5036190	. 1498530	. 6809710	. 5791238
. 7232869	. 5223586	. 1615716	. 6649795	. 5868449
. 7411856	. 5417950	. 1740232	. 6488578	. 5948849
. 7596555	. 5617038	. 1870349	. 6328625	. 6031216
. 7790000	. 5824313	. 2007980	. 6167862	. 6116661
. 7992739	. 6040542	. 2153227	. 6006565	. 6205119
. 8205395	. 6266619	. 2306177	. 5844988	. 6296517

TABLE II.—EXPANSIVE FLOW FIELD OBTAINED BY CHARACTERISTIC CALCULATIONS FOR JET FLOW FROM NEAR-SONIC EXIT ($M_j=1.0038$; $\mu_j=85°$)—Continued

x/r_j	y/r_j	θ, radians	μ, radians	V/V_l
0.3792871	0.0000000	0.0000000	1.098609	0.4487588
.3921533	$.2519185\times10^{-1}$	$.1587275\times10^{-2}$	1.083670	.4515482
.4044956	$.4858162\times10^{-1}$	$.7993560\times10^{-2}$	1.049918	.4582646
.4168861	$.7058406\times10^{-1}$	$.8928142\times10^{-2}$	1.032836	.4618897
.4296922	$.9248926\times10^{-1}$	$.1082943\times10^{-1}$	1.016540	.4654949
.4418241	.1125719	$.1310970\times10^{-1}$	1.001440	.4689665
.4542796	.1326060	$.1583111\times10^{-1}$	.9859765	.4726556
.4665789	.1518374	$.1884560\times10^{-1}$	.9707266	.4764299
.4791055	.1709058	$.2223612\times10^{-1}$	.9551895	.4804176
.4914836	.1892587	$.2588704\times10^{-1}$	.9398696	.4844942
.5040513	.2074319	$.2989846\times10^{-1}$	.9243540	.4887729
.5167810	.2253938	$.3426785\times10^{-1}$	.9087111	.4932435
.5293955	.2427743	$.3889214\times10^{-1}$	.8933233	.4977993
.5424250	.2603267	$.4397905\times10^{-1}$	.8775539	.5026348
.5553622	.2773704	$.4932644\times10^{-1}$	.8620688	.5075519
.5684667	.2942762	$.5504018\times10^{-1}$	.8465748	.5126438
.5819504	.3113240	$.6122420\times10^{-1}$	.8308525	.5179916
.5955968	.3282435	$.6778215\times10^{-1}$	.8151964	.5235024
.6096078	.3452955	$.7481684\times10^{-1}$	.7994074	.5292533
.6238013	.3622639	$.8223601\times10^{-1}$	.7837296	.5351605
.6383707	.3793932	$.9014249\times10^{-1}$	.7679810	.5412976
.6531592	.3965054	$.9844665\times10^{-1}$	.7523691	.5475876
.6685120	.4140114	.1073462	.7365632	.5541706
.6842770	.4317378	.1167505	.7207719	.5609690
.7004765	.4497207	.1266681	.7050125	.5679800
.7172837	.4681604	.1371999	.6891620	.5752652
.7345796	.4869344	.1482613	.6733846	.5827554
.7525408	.5062474	.1599525	.6575650	.5905102
.7713396	.5262939	.1723725	.6416122	.5985836
.7907472	.5468445	.1853495	.6257814	.6068521
.8110853	.5682570	.1990737	.6098662	.6154273
.8324127	.5906128	.2135549	.5938948	.6243026
.8547964	.6140063	.2288016	.5778919	.6334703

TABLE II.—EXPANSIVE FLOW FIELD OBTAINED BY CHARACTERISTIC CALCULATIONS FOR JET FLOW FROM NEAR-SONIC EXIT (M_i=1.0038; μ_i=85°)—Continued

x/r_i	y/r_i	θ, radians	μ, radians	V/V_i
0.4055487	0.0000000	0.0000000	1.069709	0.4542555
.4187748	$.2414776\times10^{-1}$	$.1777096\times10^{-2}$	1.055060	.4572032
.4314689	$.4663196\times10^{-1}$	$.8892727\times10^{-2}$	1.021980	.4642751
.4447341	$.6876598\times10^{-1}$	$.9945947\times10^{-2}$	1.004457	.4682625
.4573342	$.8902532\times10^{-1}$	$.1192228\times10^{-1}$	.9892515	.4718628
.4702838	.1092454	$.1448345\times10^{-1}$	.9739126	.4756299
.4830787	.1286724	$.1740603\times10^{-1}$	.9588666	.4794606
.4961162	.1479555	$.2073683\times10^{-1}$	.9435671	.4834969
.5090045	.1665342	$.2434784\times10^{-1}$	.9284929	.4876166
.5220954	.1849506	$.2833049\times10^{-1}$	.9132271	.4919365
.5353597	.2031724	$.3267846\times10^{-1}$	.8978362	.4964467
.5485085	.2208219	$.3728654\times10^{-1}$	.8826923	.5010403
.5620950	.2386639	$.4235948\times10^{-1}$	.8671671	.5059142
.5755893	.2560057	$.4769533\times10^{-1}$	.8519180	.5108682
.5892630	.2732231	$.5339870\times10^{-1}$	.8366549	.5159965
.6033375	.2906010	$.5957215\times10^{-1}$	.8211598	.5213812
.6175867	.3078637	$.6611954\times10^{-1}$	.8057258	.5269284
.6322219	.3252770	$.7314317\times10^{-1}$	.7901548	.5327155
.6470532	.3426197	$.8055086\times10^{-1}$	.7746897	.5386581
.6622834	.3601413	$.8844424\times10^{-1}$	.7591485	.5448307
.6777483	.3776600	$.9673382\times10^{-1}$	.7437375	.5511554
.6938107	.3955961	.1056169	.7281305	.5577732
.7103098	.4137737	.1150030	.7125338	.5646054
.7272714	.4322289	.1249000	.6969639	.5716497
.7448773	.4511680	.1354087	.6813000	.5789676
.7630032	.4704662	.1464433	.6657035	.5864899
.7818354	.4903344	.1581049	.6500610	.5942758
.8015557	.5109740	.1704923	.6342834	.6023792
.8219262	.5321496	.1834328	.6186221	.6106766
.8432848	.5542317	.1971160	.6028740	.6192795
.8656956	.5773061	.2115521	.5870658	.6281809
.8892308	.6014723	.2267494	.5712231	.6373729

TABLE II.—EXPANSIVE FLOW FIELD OBTAINED BY CHARACTERISTIC CALCULATIONS FOR JET FLOW FROM NEAR-SONIC EXIT (M_j=1.0038; μ_j=85°)—Concluded

x/r_j	y/r_j	θ, radians	μ, radians	V/V_j
0. 4325213	0. 0000000	0. 0000000	1. 041314	0. 4600710
. 4460920	$.2318861\times10^{-1}$	$.1978676\times10^{-2}$	1. 026918	. 4631821
. 4596826	$.4576376\times10^{-1}$	$.9925832\times10^{-2}$	. 9939206	. 4707432
. 4727123	$.6622906\times10^{-1}$	$.1101560\times10^{-1}$	. 9775566	. 4747224
. 4861397	$.8662500\times10^{-1}$	$.1321216\times10^{-1}$	. 9620467	. 4786396
. 4994218	. 1062261	$.1595126\times10^{-1}$	. 9470897	. 4825548
. 5129656	. 1256974	$.1917176\times10^{-1}$	. 9319692	. 4866537
. 5263613	. 1444747	$.2271253\times10^{-1}$	. 9171075	. 4908240
. 5399739	. 1631067	$.2664631\times10^{-1}$	. 9020738	. 4951892
. 5537730	. 1815599	$.3095787\times10^{-1}$	. 8869201	. 4997421
. 5674568	. 1994513	$.3553849\times10^{-1}$	. 8720113	. 5043753
. 5816018	. 2175557	$.4058909\times10^{-1}$	. 8567256	. 5092882
. 5956560	. 2351689	$.4590621\times10^{-1}$	. 8417080	. 5142795
. 6099024	. 2526719	$.5159314\times10^{-1}$	. 8266734	. 5194443
. 6245717	. 2703547	$.5775143\times10^{-1}$	. 8114062	. 5248650
. 6394292	. 2879353	$.6428410\times10^{-1}$	. 7961947	. 5304477
. 6546950	. 3056851	$.7129265\times10^{-1}$	. 7808433	. 5362700
. 6701711	. 3233783	$.7868470\times10^{-1}$	. 7655912	. 5422471
. 6860703	. 3412687	$.8656205\times10^{-1}$	. 7502597	. 5484536
. 7022206	. 3591715	$.9483405\times10^{-1}$	. 7350522	. 5548114
. 7190014	. 3775165	. 1036975	. 7196462	. 5614622
. 7362471	. 3961229	. 1130621	. 7042462	. 5683267
. 7539839	. 4150291	. 1229359	. 6888688	. 5754023
. 7724028	. 4344472	. 1334186	. 6733941	. 5827509
. 7913745	. 4542497	. 1444250	. 6579819	. 5903026
. 8110956	. 4746538	. 1560552	. 6425209	. 5981169
. 8317574	. 4958677	. 1684074	. 6269214	. 6062479
. 8531116	. 5176510	. 1813101	. 6114335	. 6145710
. 8755148	. 5403858	. 1949512	. 5958553	. 6231984
. 8990361	. 5641626	. 2093411	. 5802143	. 6321226
. 9237540	. 5890861	. 2244879	. 5645351	. 6413355
. 9365753	. 6020008	. 2073650	. 5737721	. 6358754

TABLE III.—VALUES OF INTEGRALS IN JOHANNESEN-MEYER METHOD OF CHARACTERISTICS, $\gamma=1.400$

[See appendix B]

z_n	$I_1(\phi)$		$I_2(\phi)$		$I_3(\phi)$		$I_4(\phi)$	
	$\int_{z_{n-1}}^{z_n}$	$\int_{z=0.03}^{z_n}$	$\int_{z_{n-1}}^{z_n}$	$\int_{z=0.03}^{z_n}$	$\int_{z_{n-1}}^{z_n}$	$\int_{z=0.03}^{z_n}$	$\int_{z_{n-1}}^{z_n}$	$\int_{z=0.03}^{z_n}$
0.04	0.5352399×10^{-1}	0.5352399×10^{-1}	0.4585197×10^{-2}	0.4585197×10^{-2}	0.1313719	0.1313719	1.544196	1.544196
.05	$.4711751\times10^{-1}$	.1006415	$.5205754\times10^{-2}$	$.9790952\times10^{-2}$	.1158030	.2471749	1.052538	2.596735
.06	$.4255425\times10^{-1}$	.1431957	$.5762908\times10^{-2}$	$.1555386\times10^{-1}$	.1047641	.3519390	.7757746	3.372510
.07	$.3908471\times10^{-1}$	.1822804	$.6274384\times10^{-2}$	$.2182824\times10^{-1}$	$.9641819\times10^{-1}$	.4483572	.6018302	3.974340
.08	$.3632673\times10^{-1}$	.2186072	$.6751271\times10^{-2}$	$.2857951\times10^{-1}$	$.8982827\times10^{-1}$	.5381855	.4840817	4.458422
.09	$.3406212\times10^{-1}$	.2526693	$.7201104\times10^{-2}$	$.3578062\times10^{-1}$	$.8445935\times10^{-1}$	.6226449	.3999835	4.858405
.10	$.3215590\times10^{-1}$	.2848252	$.7629288\times10^{-2}$	$.4340991\times10^{-1}$	$.7998045\times10^{-1}$	.7026253	.3374288	5.195834
.11	$.3051953\times10^{-1}$	.3153447	$.8039885\times10^{-2}$	$.5144979\times10^{-1}$	$.7617435\times10^{-1}$	.7787997	.2893914	5.485226
.12	$.2909210\times10^{-1}$	.3444368	$.8436044\times10^{-2}$	$.5988584\times10^{-1}$	$.7289173\times10^{-1}$	.8516914	.2515410	5.736767
.13	$.2783018\times10^{-1}$	.3722670	$.8820295\times10^{-2}$	$.6870613\times10^{-1}$	$.7002619\times10^{-1}$	.9217176	.2210781	5.957845
.14	$.2670182\times10^{-1}$	.3989688	$.9194703\times10^{-2}$	$.7790084\times10^{-1}$	$.6749949\times10^{-1}$	.9892171	.1961205	6.153965
.15	$.2568292\times10^{-1}$	.4246518	$.9560992\times10^{-2}$	$.8746183\times10^{-1}$	$.6525263\times10^{-1}$	1.054469	.1753608	6.329326
.16	$.2475490\times10^{-1}$	.4494067	$.9920643\times10^{-2}$	$.9738247\times10^{-1}$	$.6324029\times10^{-1}$	1.117710	.1578654	6.487192
.17	$.2390314\times10^{-1}$	.4733098	$.1027491\times10^{-1}$	.1076573	$.6142684\times10^{-1}$	1.179136	.1429516	6.630143
.18	$.2311597\times10^{-1}$	.4964258	$.1062493\times10^{-1}$	.1182823	$.5978392\times10^{-1}$	1.238920	.1301098	6.760253
.19	$.2238393\times10^{-1}$	.5188097	$.1097170\times10^{-1}$	.1292540	$.5828868\times10^{-1}$	1.297209	.1189527	6.879206
.20	$.2169923\times10^{-1}$	.5405090	$.1131612\times10^{-1}$	.1405701	$.5692242\times10^{-1}$	1.354131	.1091811	6.988387
.21	$.2105540\times10^{-1}$	.5615644	$.1165899\times10^{-1}$	.1522291	$.5566962\times10^{-1}$	1.409801	.1005609	7.088948
.22	$.2044699\times10^{-1}$	.5820114	$.1200110\times10^{-1}$	.1642302	$.5451743\times10^{-1}$	1.464318	$.9290630\times10^{-1}$	7.181854
.23	$.1986935\times10^{-1}$	.6018807	$.1234313\times10^{-1}$	.1765734	$.5345499\times10^{-1}$	1.517773	$.8606796\times10^{-1}$	7.267922
.24	$.1931851\times10^{-1}$	.6211992	$.1268577\times10^{-1}$	.1892591	$.5247307\times10^{-1}$	1.570247	$.7992504\times10^{-1}$	7.347847
.25	$.1879101\times10^{-1}$	.6399902	$.1302963\times10^{-1}$	.2022888	$.5156380\times10^{-1}$	1.621810	$.7437852\times01^{-1}$	7.422226
.26	$.1828381\times10^{-1}$	.6582741	$.1337534\times10^{-1}$	.2156641	$.5072044\times10^{-1}$	1.672531	$.6934663\times10^{-1}$	7.491572
.27	$.1779423\times10^{-1}$	.6760683	$.1372349\times10^{-1}$	.2293876	$.4993715\times10^{-1}$	1.722468	$.6476130\times10^{-1}$	7.556334
.28	$.1731989\times10^{-1}$	.6933882	$.1407465\times10^{-1}$	.2434623	$.4920884\times10^{-1}$	1.771677	$.6056543\times10^{-1}$	7.616899
.29	$.1685863\times10^{-1}$	.7102468	$.1442939\times10^{-1}$	.2578917	$.4853107\times10^{-1}$	1.820208	$.5671081\times10^{-1}$	7.673610
.30	$.1640848\times10^{-1}$	.7266553	$.1478827\times10^{-1}$	.2726799	$.4789999\times10^{-1}$	1.868108	$.5315643\times10^{-1}$	7.726766
.31	$.1596765\times10^{-1}$	.7426230	$.1515186\times10^{-1}$	.2878318	$.4731217\times10^{-1}$	1.915420	$.4986723\times10^{-1}$	7.776633
.32	$.1553445\times10^{-1}$	.7581574	$.1552071\times10^{-1}$	.3033525	$.4676459\times10^{-1}$	1.962185	$.4681307\times10^{-1}$	7.823447

TABLE III.—VALUES OF INTEGRALS IN JOHANNESEN-MEYER METHOD OF CHARACTERISTICS, $\gamma = 1.400$—Continued

[See appendix B]

z_n	$I_1(\phi)$		$I_2(\phi)$		$I_3(\phi)$		$I_4(\phi)$	
	$\int_{z_{n-1}}^{z_n}$	$\int_{z=0.03}^{z_n}$	$\int_{z_{n-1}}^{z_n}$	$\int_{z=0.03}^{z_n}$	$\int_{z_{n-1}}^{z_n}$	$\int_{z=0.03}^{z_n}$	$\int_{z_{n-1}}^{z_n}$	$\int_{z=0.03}^{z_n}$
0.33	0.1510733×10^{-1}	0.7732648	0.1589541×10^{-1}	0.3192479	0.4625459×10^{-1}	2.008439	0.4396785×10^{-1}	7.867414
.34	$.1468479\times10^{-1}$	.7879496	$.1627653\times10^{-1}$	.3355245	$.4577979\times10^{-1}$	2.054219	$.4130889\times10^{-1}$	7.908723
.35	$.1426544\times10^{-1}$	.8022150	$.1666465\times10^{-1}$	.3521891	$.4533810\times10^{-1}$	2.099557	$.3881638\times10^{-1}$	7.947540
.36	$.1384789\times10^{-1}$	.8160629	$.1706040\times10^{-1}$	.3692495	$.4492764\times10^{-1}$	2.144485	$.3647290\times10^{-1}$	7.984013
.37	$.1343081\times10^{-1}$	.8294937	$.1746439\times10^{-1}$	.3867139	$.4454674\times10^{-1}$	2.189031	$.3426313\times10^{-1}$	8.018276
.38	$.1301288\times10^{-1}$	.8425066	$.1787726\times10^{-1}$	.4045912	$.4419392\times10^{-1}$	2.233225	$.3217343\times10^{-1}$	8.050449
.39	$.1259280\times10^{-1}$	.8550994	$.1829970\times10^{-1}$	.4228909	$.4386783\times10^{-1}$	2.277093	$.3019169\times10^{-1}$	8.080641
.40	$.1216925\times10^{-1}$	.8672687	$.1873240\times10^{-1}$	.4416233	$.4356731\times10^{-1}$	2.320660	$.2830706\times10^{-1}$	8.108948
.41	$.1174090\times10^{-1}$	.8790096	$.1917609\times10^{-1}$	.4607994	$.4329129\times10^{-1}$	2.363952	$.2650979\times10^{-1}$	8.135458
.42	$.1130639\times10^{-1}$	.8903160	$.1963154\times10^{-1}$	.4804310	$.4303884\times10^{-1}$	2.406991	$.2479110\times10^{-1}$	8.160249
.43	$.1086430\times10^{-1}$	.9011803	$.2009956\times10^{-1}$	.5005305	$.4280913\times10^{-1}$	2.449800	$.2314296\times10^{-1}$	8.183392
.44	$.1041319\times10^{-1}$	.9115935	$.2058100\times10^{-1}$	.5211115	$.4260141\times10^{-1}$	2.492401	$.2155811\times10^{-1}$	8.204950
.45	$.9951523\times10^{-2}$	.9215450	$.2107676\times10^{-1}$	.5421883	$.4241506\times10^{-1}$	2.534816	$.2002984\times10^{-1}$	8.224980
.46	$.9477678\times10^{-2}$	.9310227	$.2158779\times10^{-1}$	.5637761	$.4224951\times10^{-1}$	2.577066	$.1855198\times10^{-1}$	8.243532
.47	$.8989955\times10^{-2}$	.9400126	$.2211511\times10^{-1}$	.5858912	$.4210428\times10^{-1}$	2.619170	$.1711880\times10^{-1}$	8.260651
.48	$.8486536\times10^{-2}$	.9484992	$.2265979\times10^{-1}$	.6085510	$.4197896\times10^{-1}$	2.661149	$.1572496\times10^{-1}$	8.276376
.49	$.7965466\times10^{-2}$	.9564646	$.2322299\times10^{-1}$	.6317740	$.4187320\times10^{-1}$	2.703022	$.1436542\times10^{-1}$	8.290741
.50	$.7424635\times10^{-2}$	.9638893	$.2380593\times10^{-1}$	.6555799	$.4178675\times10^{-1}$	2.744809	$.1303540\times10^{-1}$	8.303776
.51	$.6861774\times10^{-2}$	.9707511	$.2440994\times10^{-1}$	.6799899	$.4171937\times10^{-1}$	2.786528	$.1173038\times10^{-1}$	8.315507
.52	$.6274398\times10^{-2}$	.9770255	$.2503642\times10^{-1}$	.7050263	$.4167092\times10^{-1}$	2.828199	$.1044597\times10^{-1}$	8.325953
.53	$.5659799\times10^{-2}$	.9826853	$.2568690\times10^{-1}$	.7307132	$.4164131\times10^{-1}$	2.869841	$.9177912\times10^{-2}$	8.335131
.54	$.5015011\times10^{-2}$	.9877003	$.2636302\times10^{-1}$	.7570762	$.4163049\times10^{-1}$	2.911471	$.7922054\times10^{-2}$	8.343053
.55	$.4336768\times10^{-2}$	.9920370	$.2706654\times10^{-1}$	.7841428	$.4163848\times10^{-1}$	2.953110	$.6674287\times10^{-2}$	8.349727
.56	$.3621465\times10^{-2}$	.9956585	$.2779937\times10^{-1}$	.8119422	$.4166536\times10^{-1}$	2.994775	$.5430515\times10^{-2}$	8.355158
.57	$.2865101\times10^{-2}$	.9985236	$.2856359\times10^{-1}$	.8405058	$.4171125\times10^{-1}$	3.036486	$.4186601\times10^{-2}$	8.359344
.58	$.2063230\times10^{-2}$	1.000586	$.2936144\times10^{-1}$	.8698672	$.4177635\times10^{-1}$	3.078263	$.2938347\times10^{-2}$	8.362282
.59	$.1210885\times10^{-2}$	1.001797	$.3019535\times10^{-1}$	.9000626	$.4186088\times10^{-1}$	3.120124	$.1681434\times10^{-2}$	8.363964
.60	$.3025175\times10^{-3}$	1.002100	$.3106800\times10^{-1}$	.9311306	$.4196513\times10^{-1}$	3.162089	$.4113994\times10^{-3}$	8.364375
.61	$-.6681245\times10^{-3}$	1.001432	$.3198228\times10^{-1}$	.9631128	$.4208948\times10^{-1}$	3.204178	$-.8764540\times10^{-3}$	8.363499

TABLE III.—VALUES OF INTEGRALS IN JOHANNESEN-MEYER METHOD OF CHARACTERISTICS, $\gamma=1.400$—Concluded

[See appendix B]

z_n	$I_1(\phi)$		$I_2(\phi)$		$I_3(\phi)$		$I_4(\phi)$	
	$\int_{z_{n-1}}^{z_n}$	$\int_{z=0.03}^{z_n}$	$\int_{z_{n-1}}^{z_n}$	$\int_{z=0.03}^{z_n}$	$\int_{z_{n-1}}^{z_n}$	$\int_{z=0.03}^{z_n}$	$\int_{z_{n-1}}^{z_n}$	$\int_{z=0.03}^{z_n}$
0.62	-0.1708075×10^{-2}	0.9997241	0.3294136×10^{-1}	0.9960542	0.4223432×10^{-1}	3.246412	-0.2187067×10^{-2}	8.361312
.63	$-.2825310\times10^{-2}$	.9968987	$.3394871\times10^{-1}$	1.030003	$.4240011\times10^{-1}$	3.288813	$-.3525729\times10^{-2}$	8.357786
.64	$-.4028873\times10^{-2}$	.9928699	$.3500815\times10^{-1}$	1.065011	$.4258739\times10^{-1}$	3.331400	$-.4898113\times10^{-2}$	8.352888
.65	$-.5329072\times10^{-2}$	.9875408	$.3612387\times10^{-1}$	1.101135	$.4279675\times10^{-1}$	3.374197	$-.6310369\times10^{-2}$	8.346578
.66	$-.6737714\times10^{-2}$	.9808031	$.3730048\times10^{-1}$	1.138435	$.4302883\times10^{-1}$	3.417226	$-.7769236\times10^{-2}$	8.338808
.67	$-.8268349\times10^{-2}$	.9725347	$.3854308\times10^{-1}$	1.176978	$.4328435\times10^{-1}$	3.460510	$-.9282118\times10^{-2}$	8.329526
.68	$-.9936617\times10^{-2}$	.9625981	$.3985732\times10^{-1}$	1.216836	$.4356407\times10^{-1}$	3.504074	$-.1085724\times10^{-1}$	8.318669
.69	$-.1176063\times10^{-1}$	.9508375	$.4124943\times10^{-1}$	1.258085	$.4386883\times10^{-1}$	3.547943	$-.1250380\times10^{-1}$	8.306165
.70	$-.1376151\times10^{-1}$	.9370760	$.4272634\times10^{-1}$	1.300811	$.4419951\times10^{-1}$	3.592142	$-.1423214\times10^{-1}$	8.291933
.71	$-.1596390\times10^{-1}$	.9211121	$.4429578\times10^{-1}$	1.345107	$.4455705\times10^{-1}$	3.636699	$-.1605397\times10^{-1}$	8.275879
.72	$-.1839683\times10^{-1}$	.9027152	$.4596633\times10^{-1}$	1.391073	$.4494241\times10^{-1}$	3.681642	$-.1798267\times10^{-1}$	8.257896
.73	$-.2109460\times10^{-1}$	.8816206	$.4774760\times10^{-1}$	1.438821	$.4535658\times10^{-1}$	3.726998	$-.2003360\times10^{-1}$	8.237863
.74	$-.2409803\times10^{-1}$	.8575226	$.4965030\times10^{-1}$	1.488471	$.4580056\times10^{-1}$	3.772799	$-.2222450\times10^{-1}$	8.215638
.75	$-.2745595\times10^{-1}$	.8300667	$.5168645\times10^{-1}$	1.540158	$.4627530\times10^{-1}$	3.819074	$-.2457605\times10^{-1}$	8.191062
.76	$-.3122721\times10^{-1}$	.7988394	$.5386948\times10^{-1}$	1.594027	$.4678165\times10^{-1}$	3.865856	$-.2711252\times10^{-1}$	8.163950
.77	$-.3548324\times10^{-1}$	.7633562	$.5621443\times10^{-1}$	1.650242	$.4732033\times10^{-1}$	3.913176	$-.2986256\times10^{-1}$	8.134087
.78	$-.4031146\times10^{-1}$	.7230447	$.5873818\times10^{-1}$	1.708980	$.4789176\times10^{-1}$	3.961068	$-.3286031\times10^{-1}$	8.101227
.79	$-.4581971\times10^{-1}$	.6772250	$.6145953\times10^{-1}$	1.770439	$.4849597\times10^{-1}$	4.009564	$-.3614678\times10^{-1}$	8.065080
.80	$-.5214234\times10^{-1}$	.6250827	$.6439940\times10^{-1}$	1.834839	$.4913233\times10^{-1}$	4.058696	$-.3977166\times10^{-1}$	8.025308
.81	$-.5944837\times10^{-1}$	.5656343	$.6758087\times10^{-1}$	1.902420	$.4979922\times10^{-1}$	4.108496	$-.4379578\times10^{-1}$	7.981513
.82	$-.6795293\times10^{-1}$	.4976814	$.7102914\times10^{-1}$	1.973449	$.5049361\times10^{-1}$	4.158989	$-.4829433\times10^{-1}$	7.933218
.83	$-.7793315\times10^{-1}$	.4197482	$.7477106\times10^{-1}$	2.048220	$.5121030\times10^{-1}$	4.210200	$-.5336135\times10^{-1}$	7.879857
.84	$-.8975104\times10^{-1}$	.3299972	$.7883422\times10^{-1}$	2.127054	$.5194083\times10^{-1}$	4.262140	$-.5911600\times10^{-1}$	7.820741
.85	$-.1038868$	.2261104	$.8324503\times10^{-1}$	2.210299	$.5267185\times10^{-1}$	4.314812	$-.6571129\times10^{-1}$	7.755030
.86	$-.1209884$	.1051220	$.8802483\times10^{-1}$	2.298324	$.5338258\times10^{-1}$	4.368195	$-.7334691\times10^{-1}$	7.681683
.87	$-.1419476$	$-.3682561\times10^{-1}$	$.9318267\times10^{-1}$	2.391507	$.5404066\times10^{-1}$	4.422236	$-.8228804\times10^{-1}$	7.599395
.88	$-.1680194$	$-.2048450$	$.9870152\times10^{-1}$	2.490208	$.5459551\times10^{-1}$	4.476831	$-.9289409\times10^{-1}$	7.506501
.89	$-.2010158$	$-.4058609$	.1045119	2.594720	$.5496715\times10^{-1}$	4.531798	$-.1056635$	7.400837
.90	$-.2436336$	$-.6494945$	.1104406	2.705161	$.5502670\times10^{-1}$	4.586825	$-.1213067$	7.279531

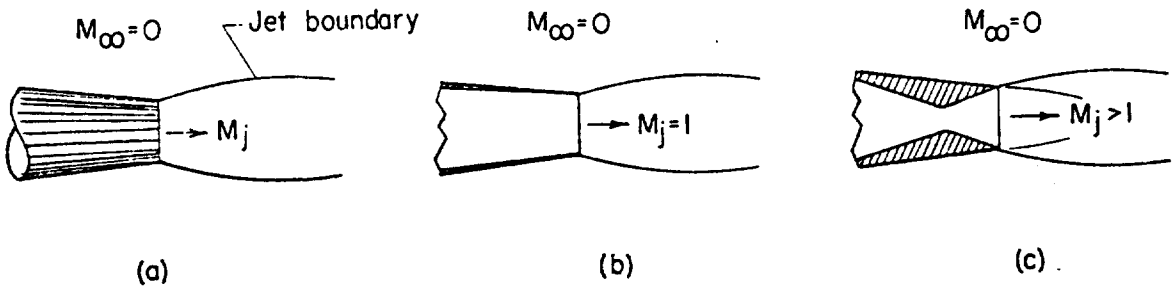

FIGURE 1.—Sketch of jets exhausting into still air.

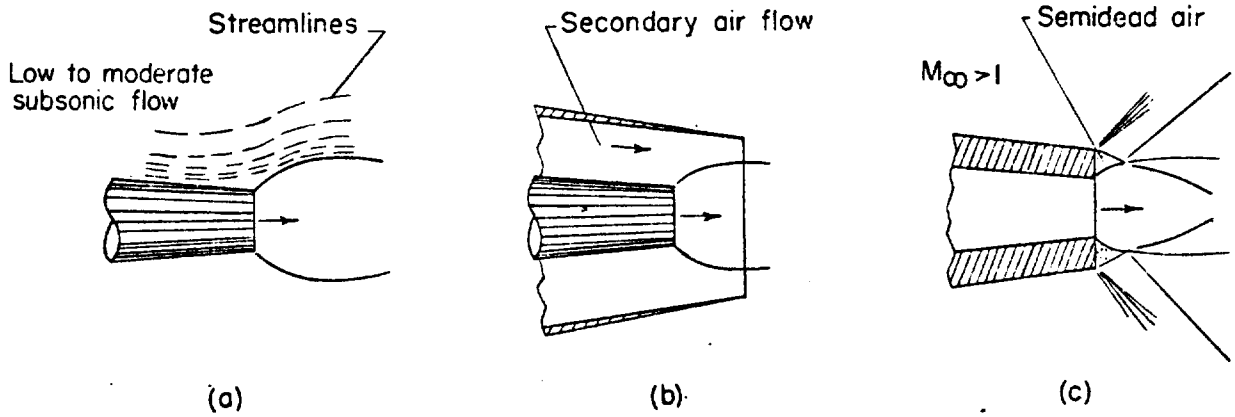

FIGURE 2.—Sketch of probable fields of application of free jet characteristics.

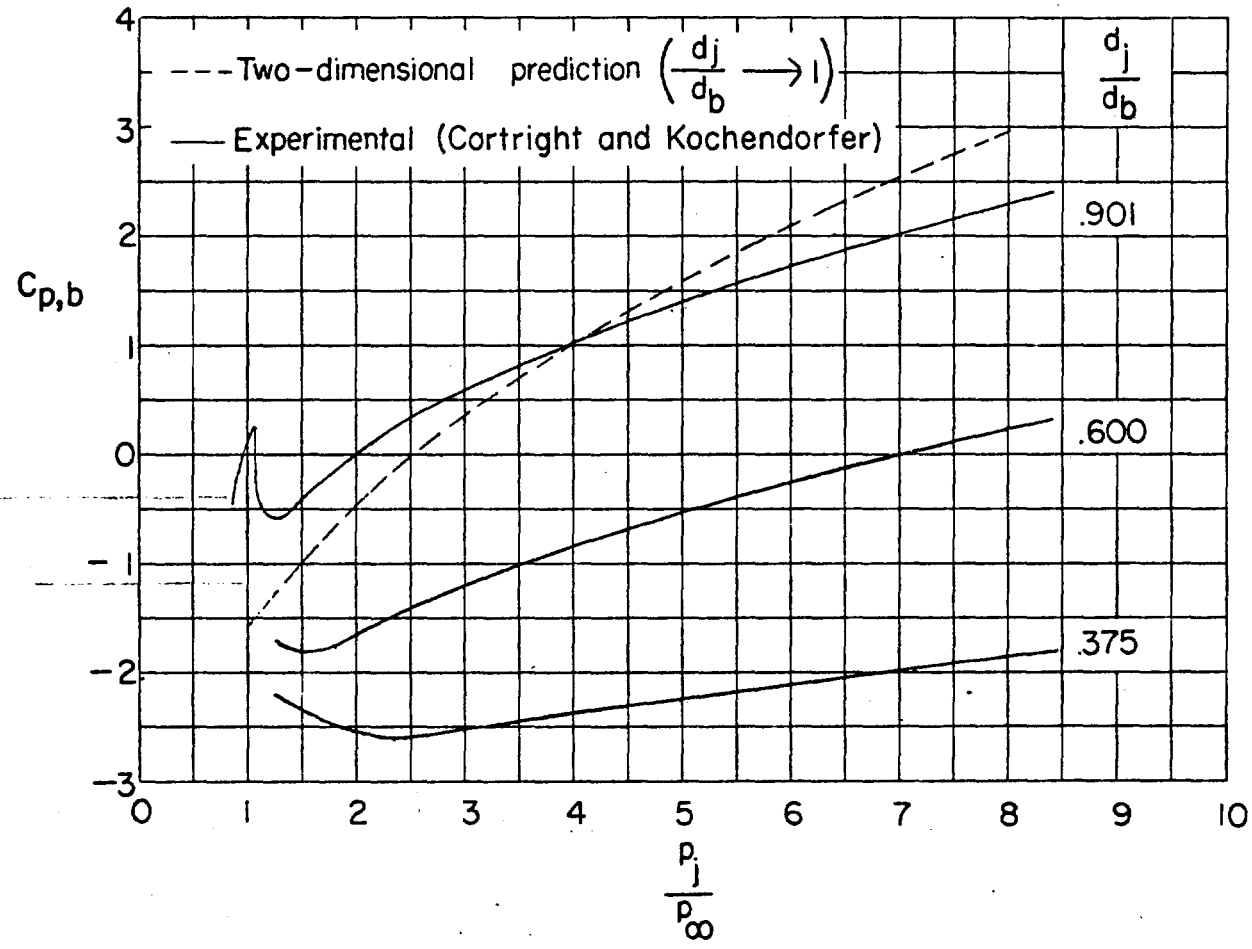

FIGURE 3.—Example of effects of jet pressure ratio and ratio of jet exit diameter to base diameter upon base pressure coefficient. $M_\infty = 1.91$; $M_j = 1.00$; $\beta = 5.6°$; ratio of jet exit diameter to maximum body diameter, 0.37.

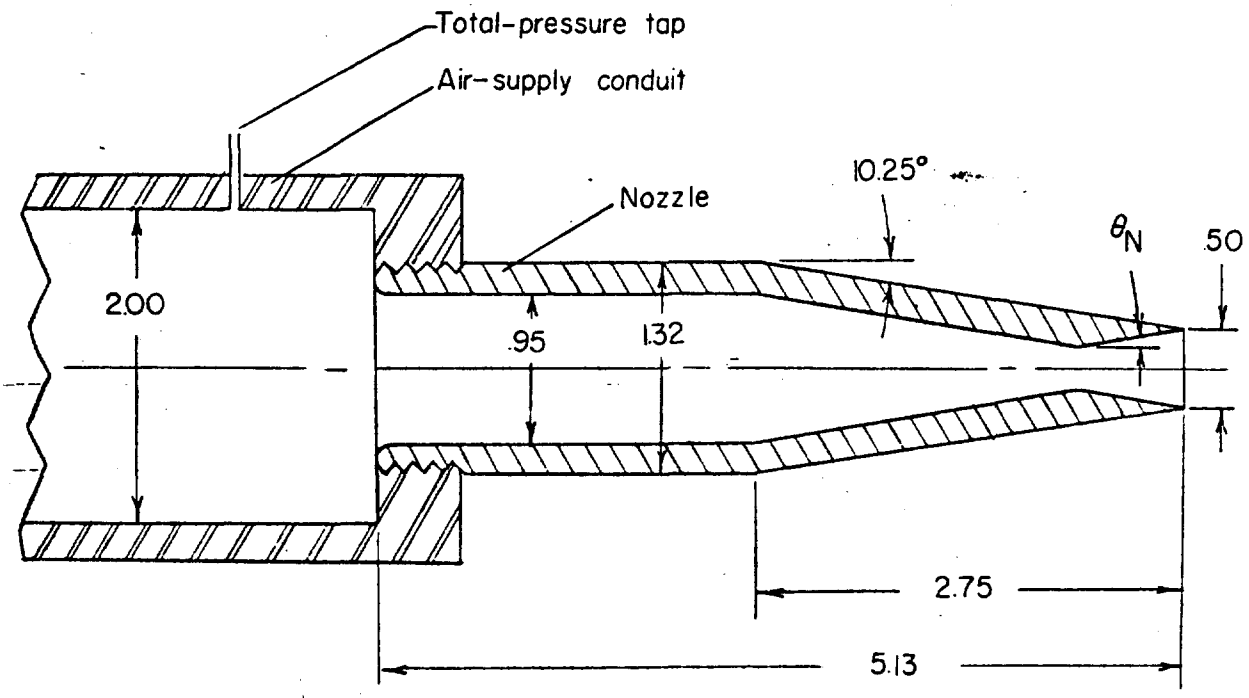

FIGURE 4.—Sketch of typical divergent nozzle employed in tests. All dimensions are in inches unless otherwise specified.

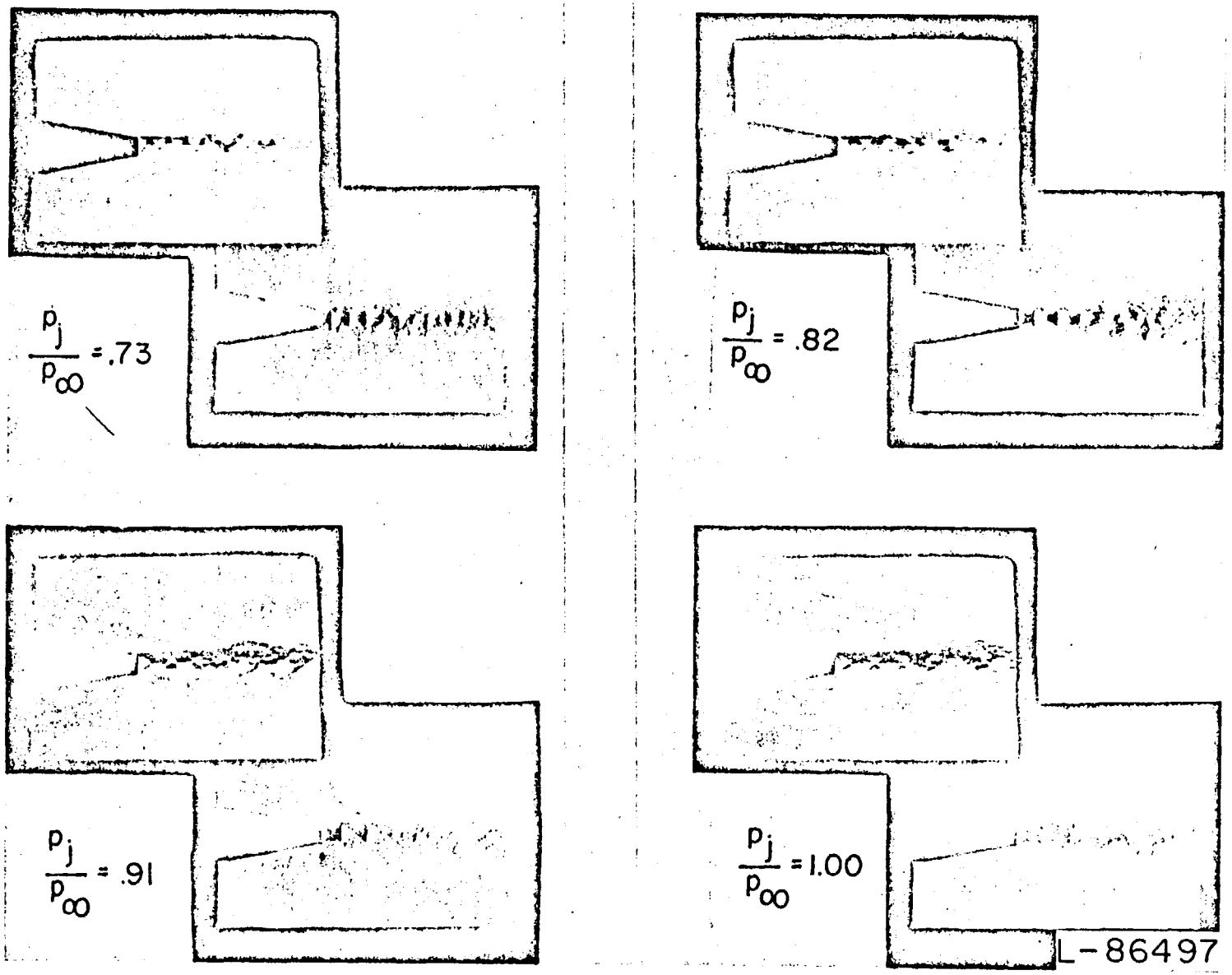

FIGURE 5.—Illustrative sequence of double-image schlieren photographs. $M_j = 1.50$; $\theta_N = 5°$.

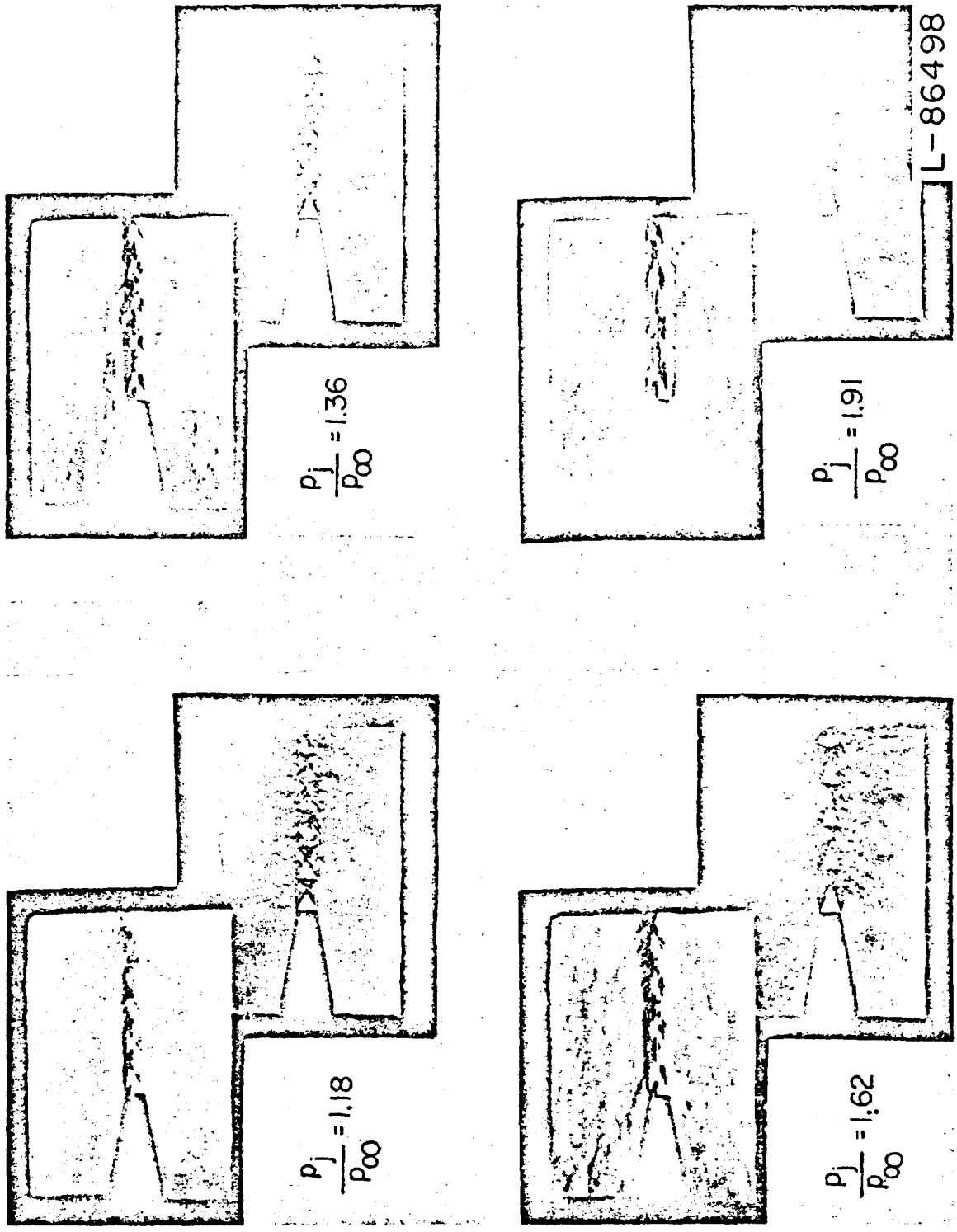

FIGURE 5.—Continued.

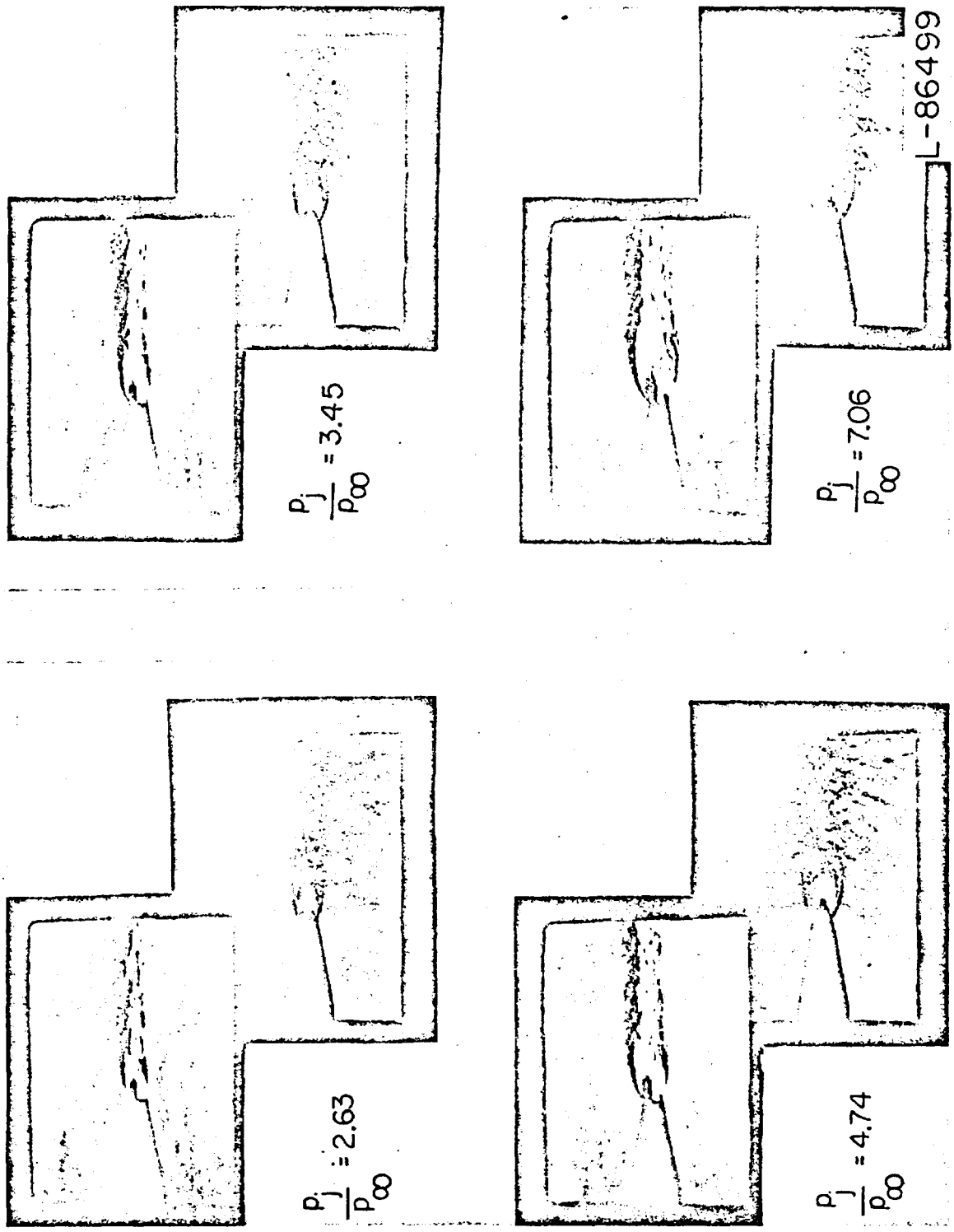

FIGURE 5.—Concluded.

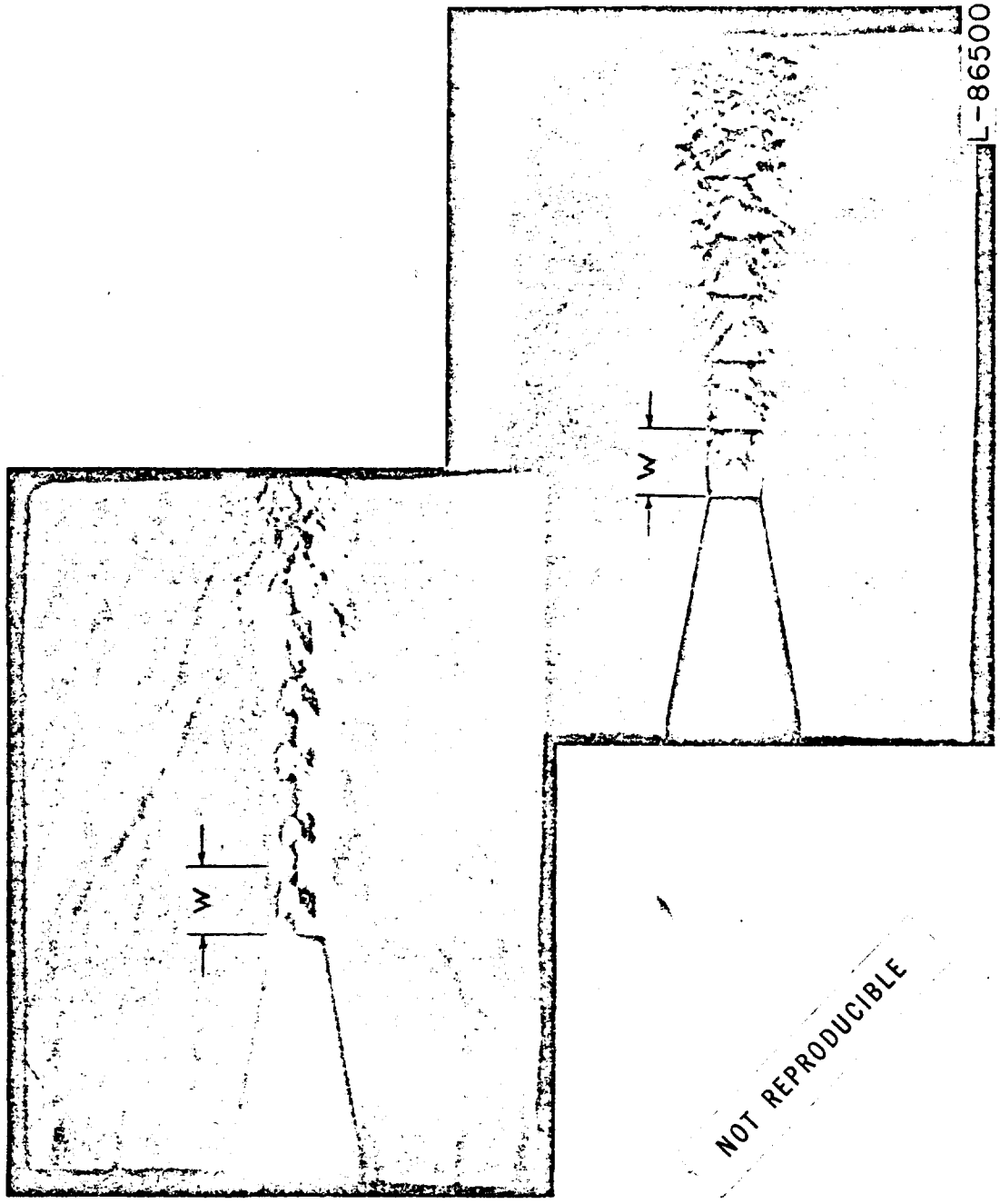

FIGURE 6.—Example of primary wavelength. $M_j = 1.00$; $\theta_N = 0°$; $p_j/p_\infty = 1.76$.

502683 O—60—6

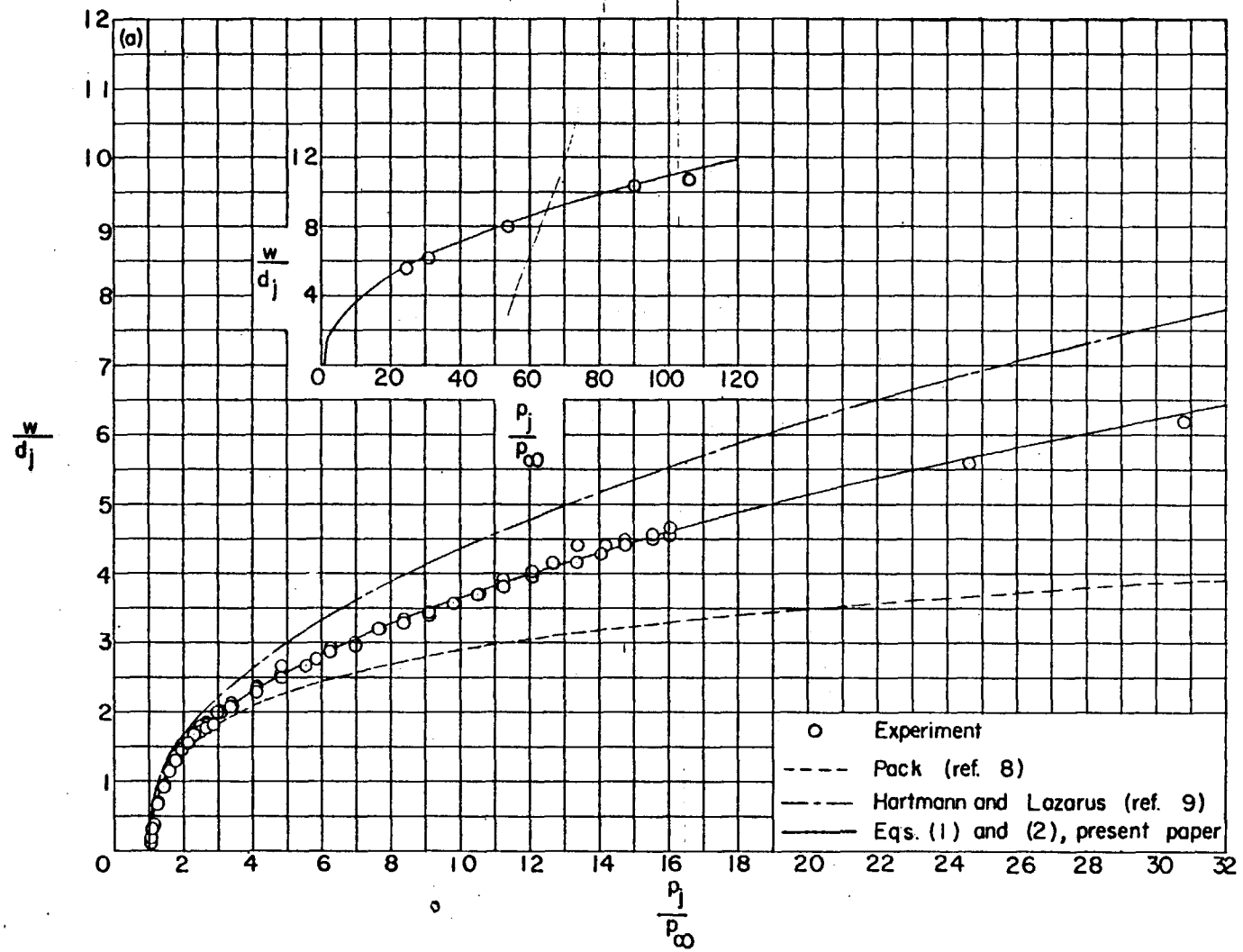

(a) $M_j = 1.00$.

FIGURE 7.—Effects of jet pressure ratio and nozzle divergence angle upon nondimensional primary wavelength.

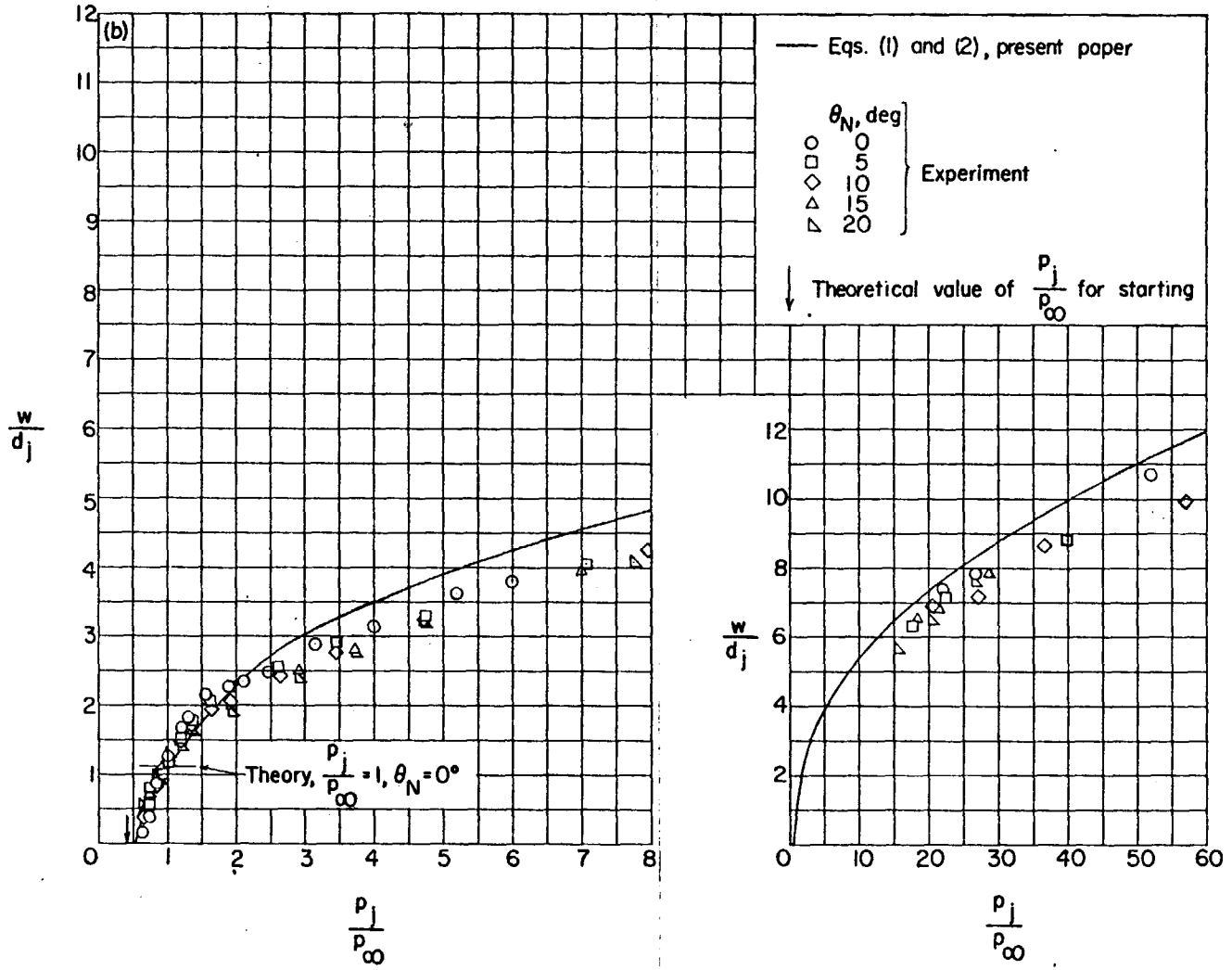

(b) $M_j = 1.50$.

FIGURE 7.—Continued.

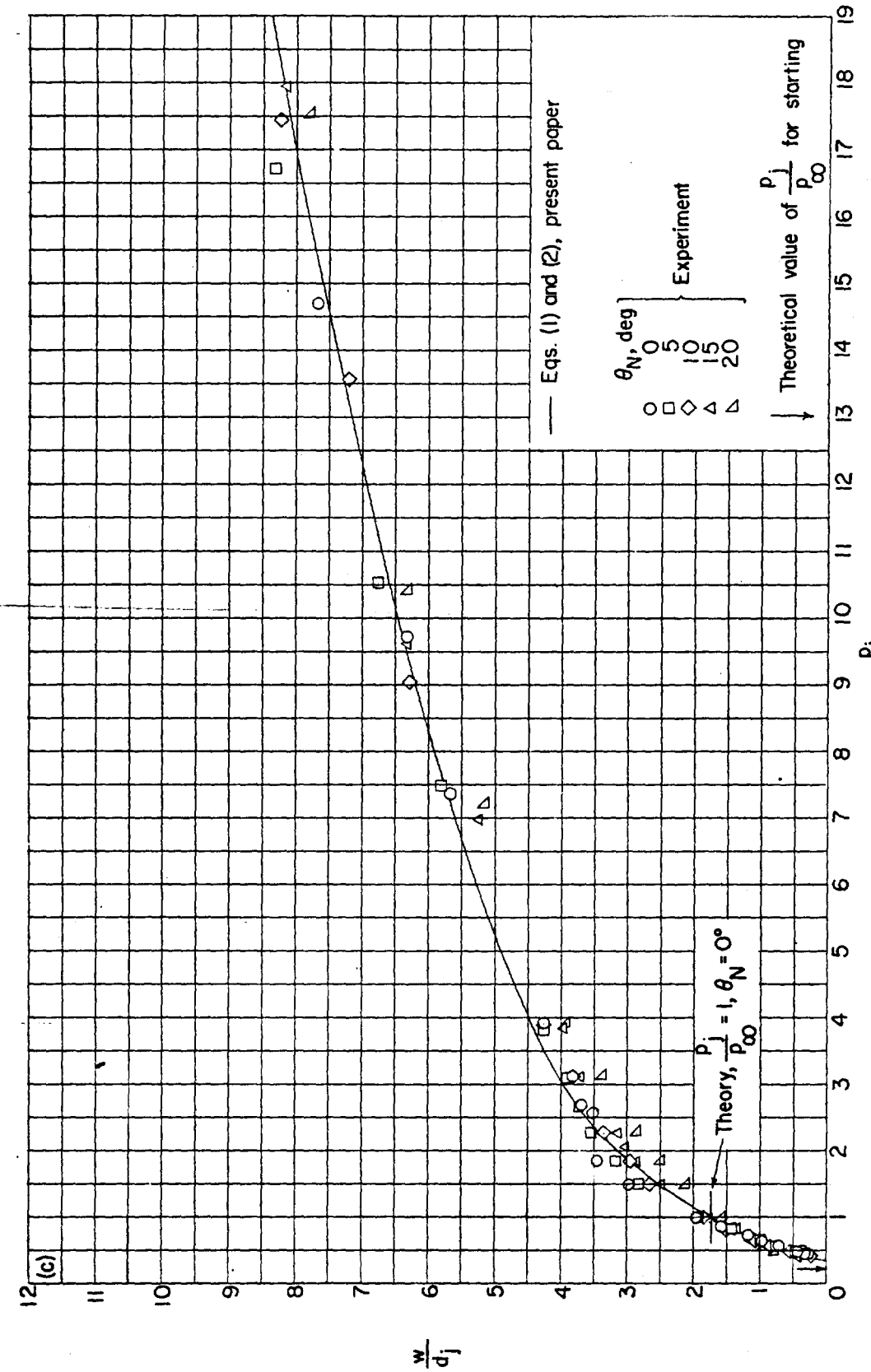

(c) $M_j = 2.00$.

FIGURE 7.—Continued.

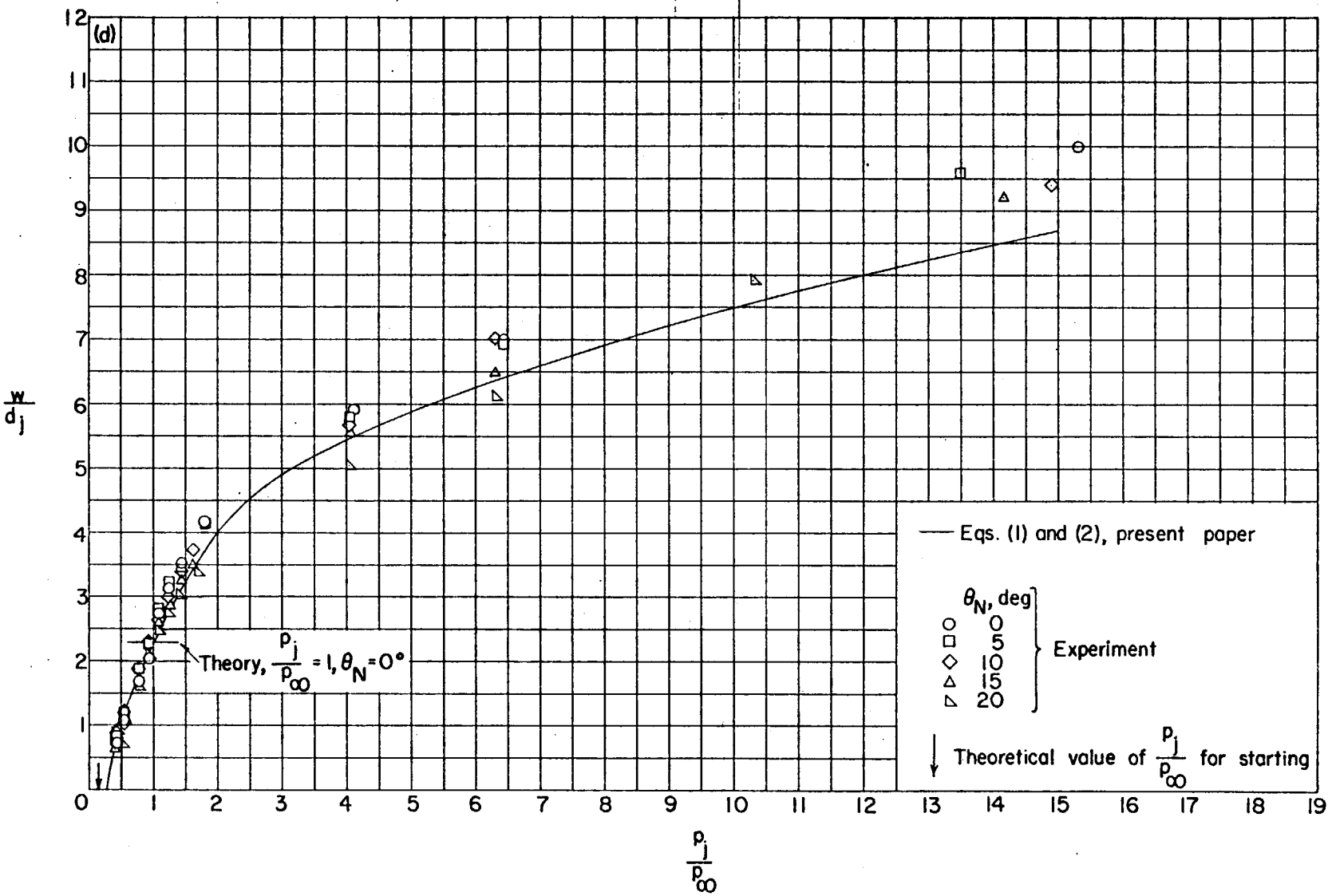

(d) $M_j = 2.50$.

FIGURE 7.—Continued.

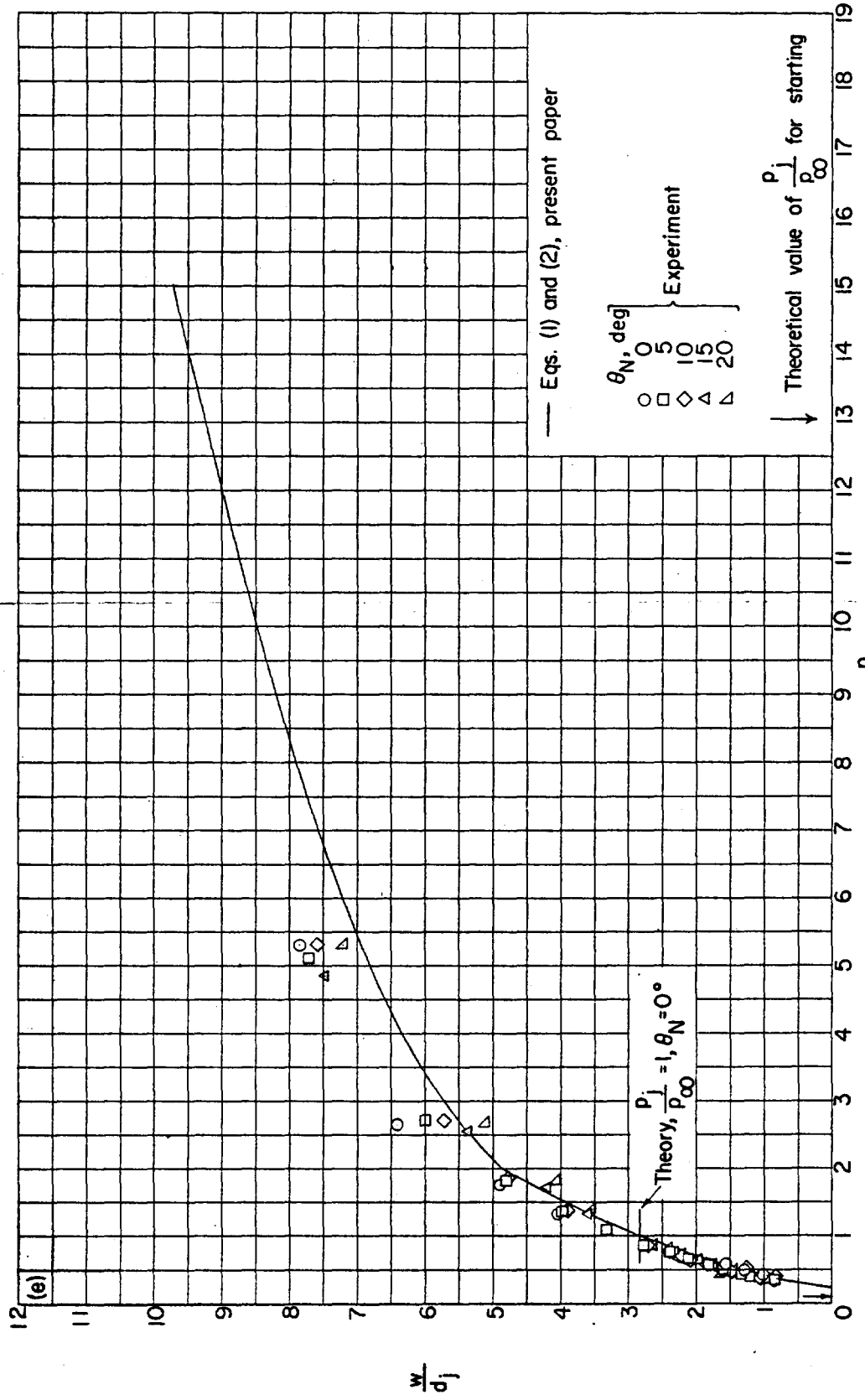

(e) $M_j=3.00$.

FIGURE 7.—Concluded.

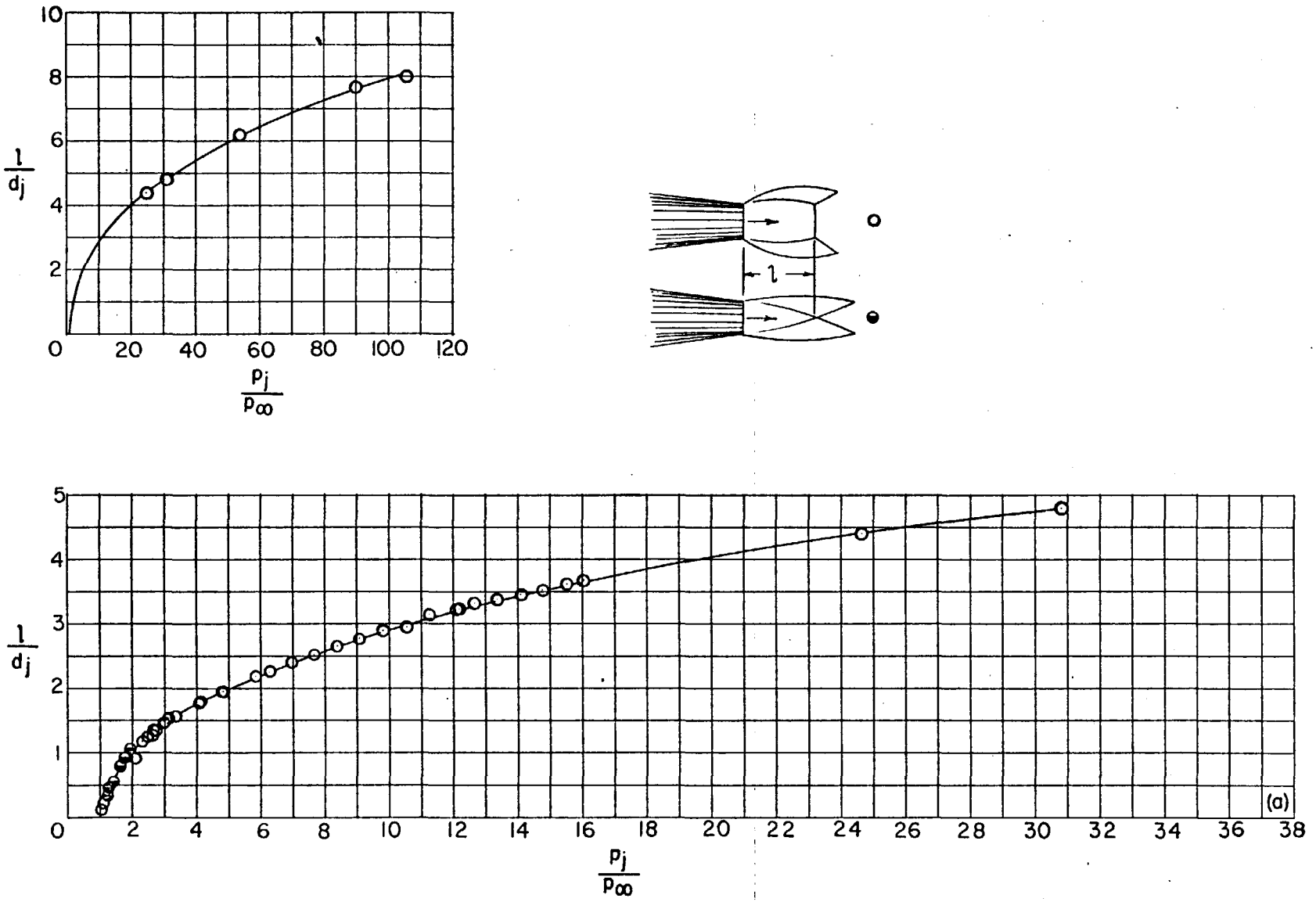

(a) $M_j = 1.00$.

FIGURE 8.—Effects of jet pressure ratio and nozzle divergence angle upon nondimensional distance along let axis from plane of jet exit to focal point of intersecting shock pattern or to Riemann wave.

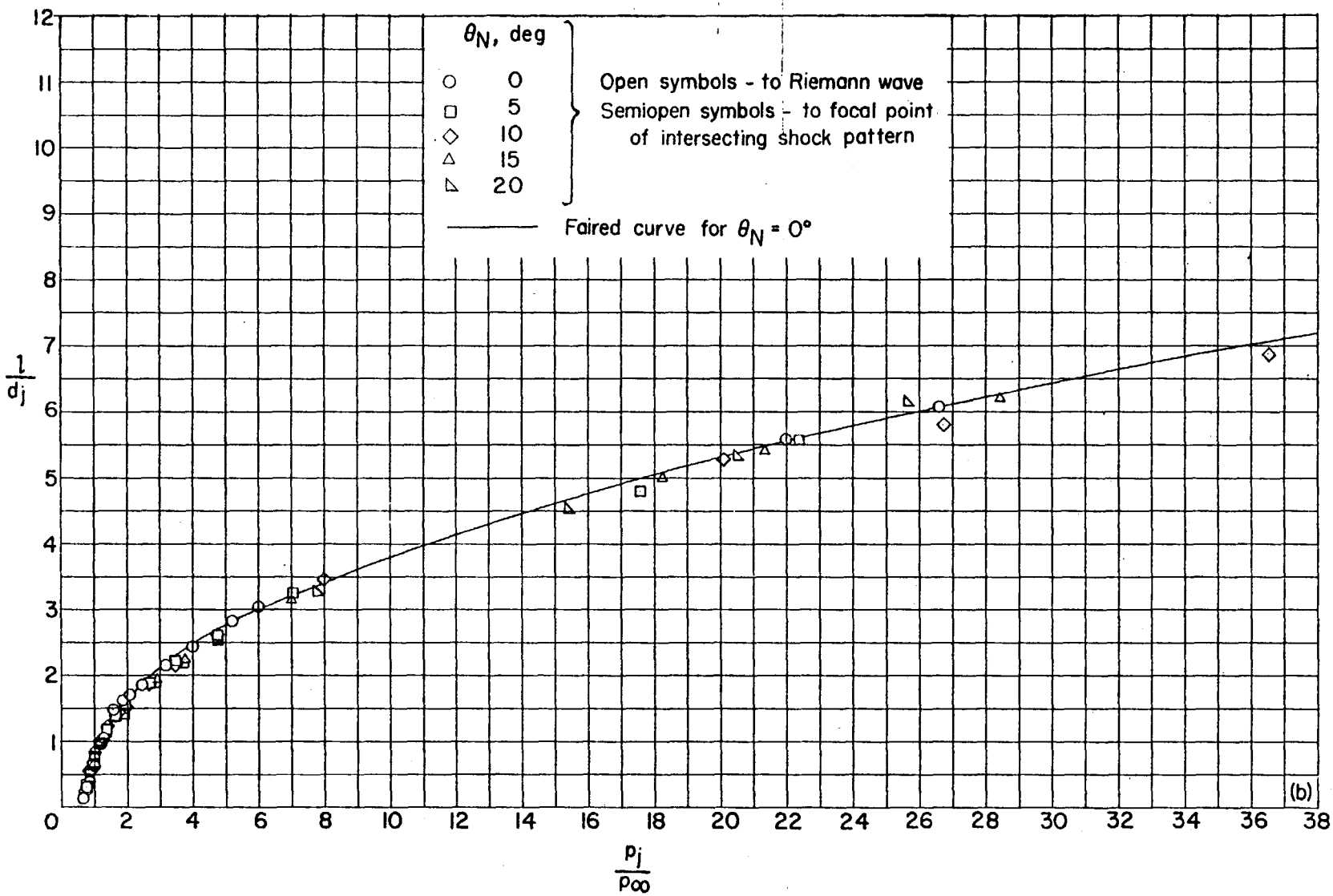

(b) $M_j = 1.50$.

FIGURE 8.—Continued.

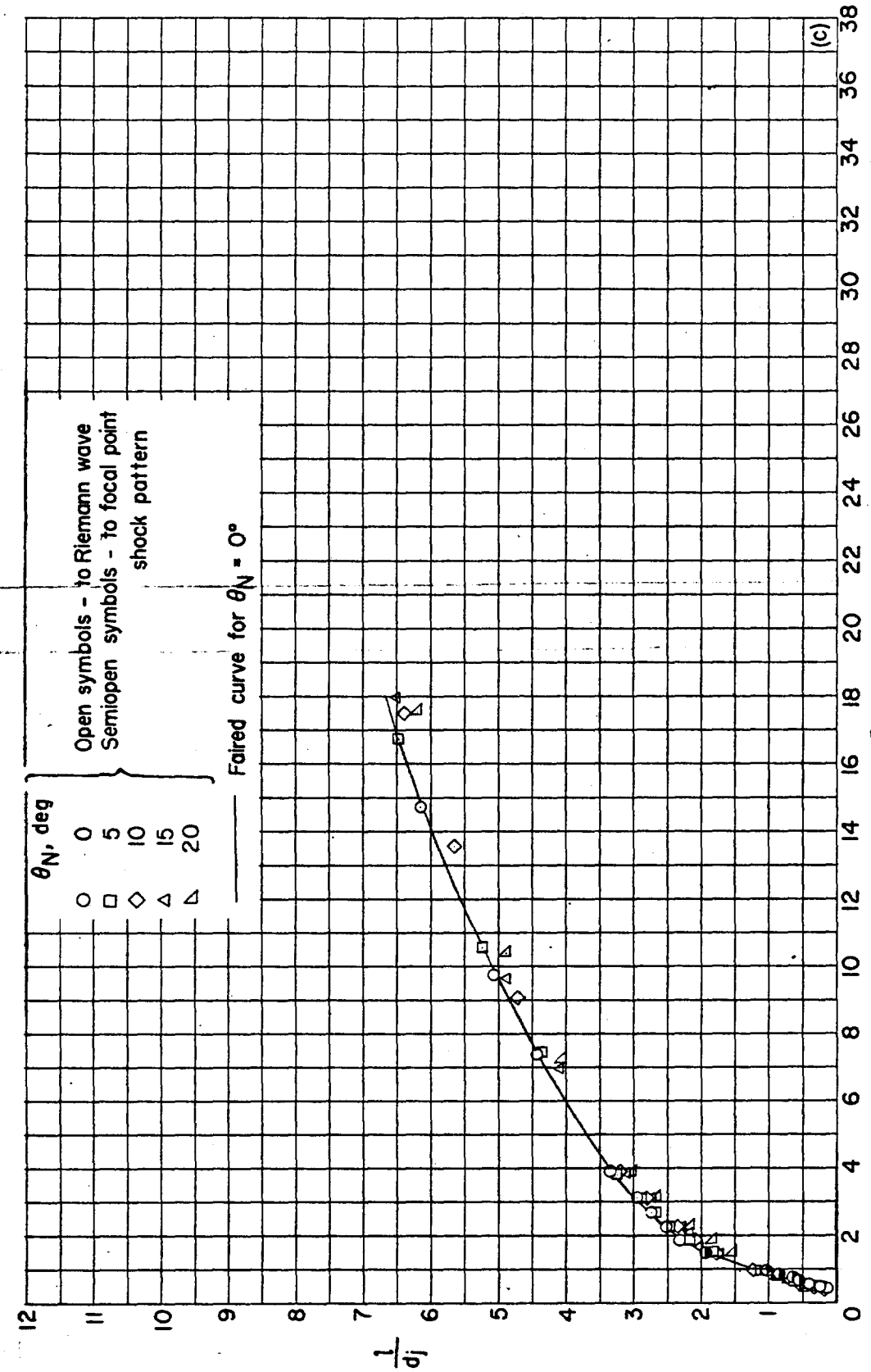

(c) $M_j = 2.00$.

FIGURE 8.—Continued.

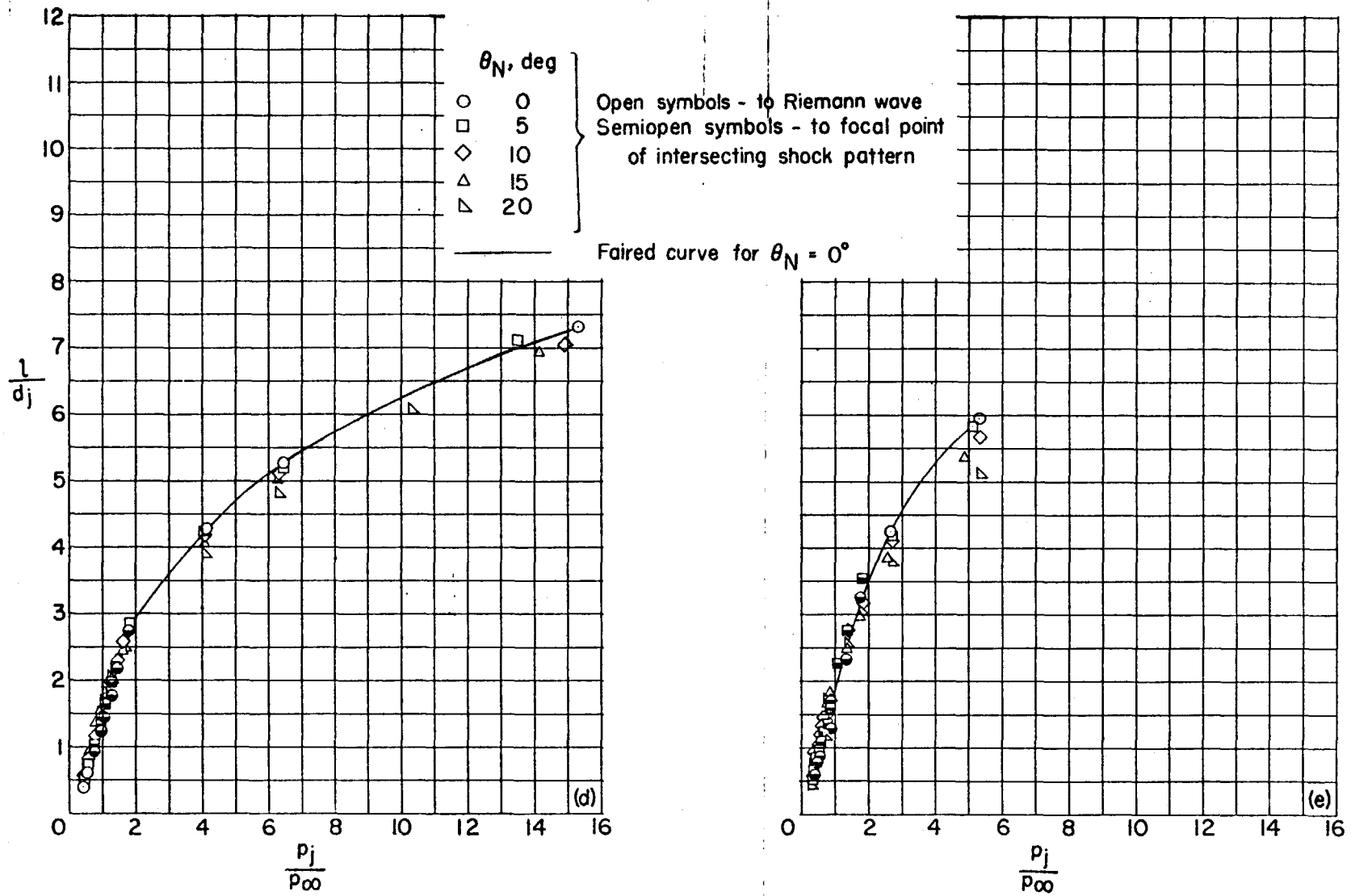

(d) $M_j = 2.50$.

(e) $M_j = 3.00$.

FIGURE 8.—Concluded.

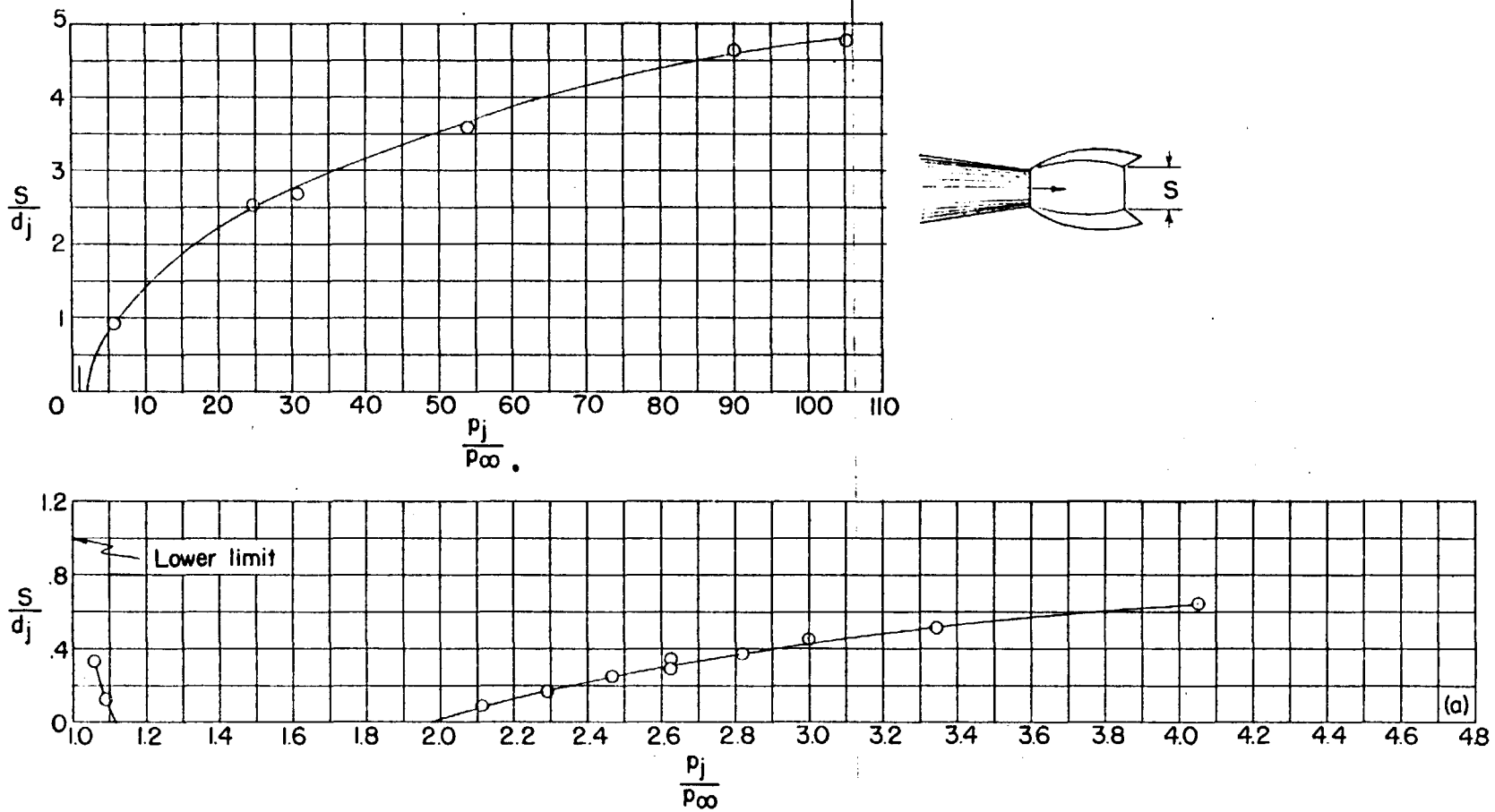

(a) $M_j = 1.00$.

FIGURE 9.—Effects of jet pressure ratio and nozzle divergence angle upon nondimensional diameter of Riemann wave.

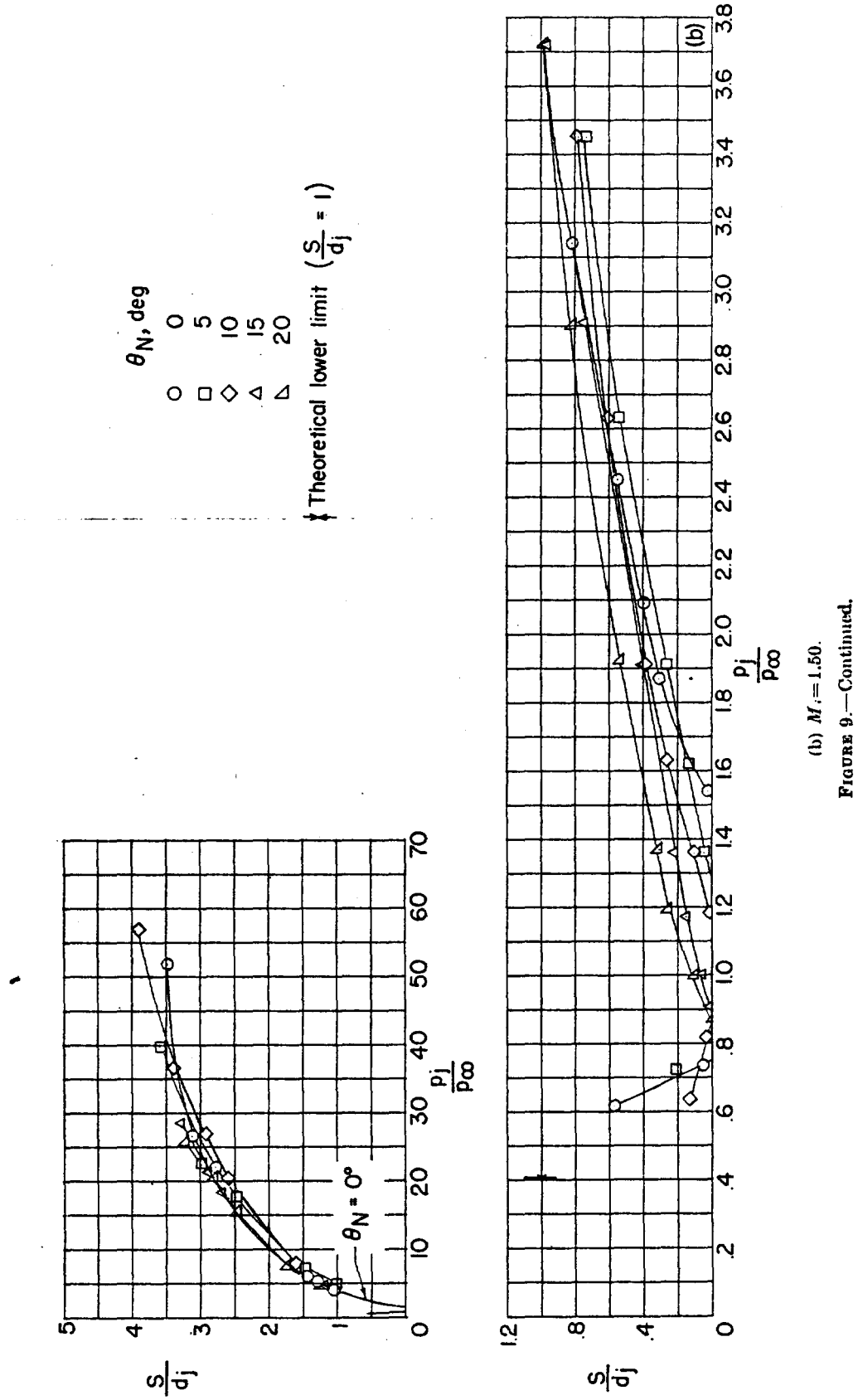

(b) $M_j = 1.50$.

FIGURE 9.—Continued.

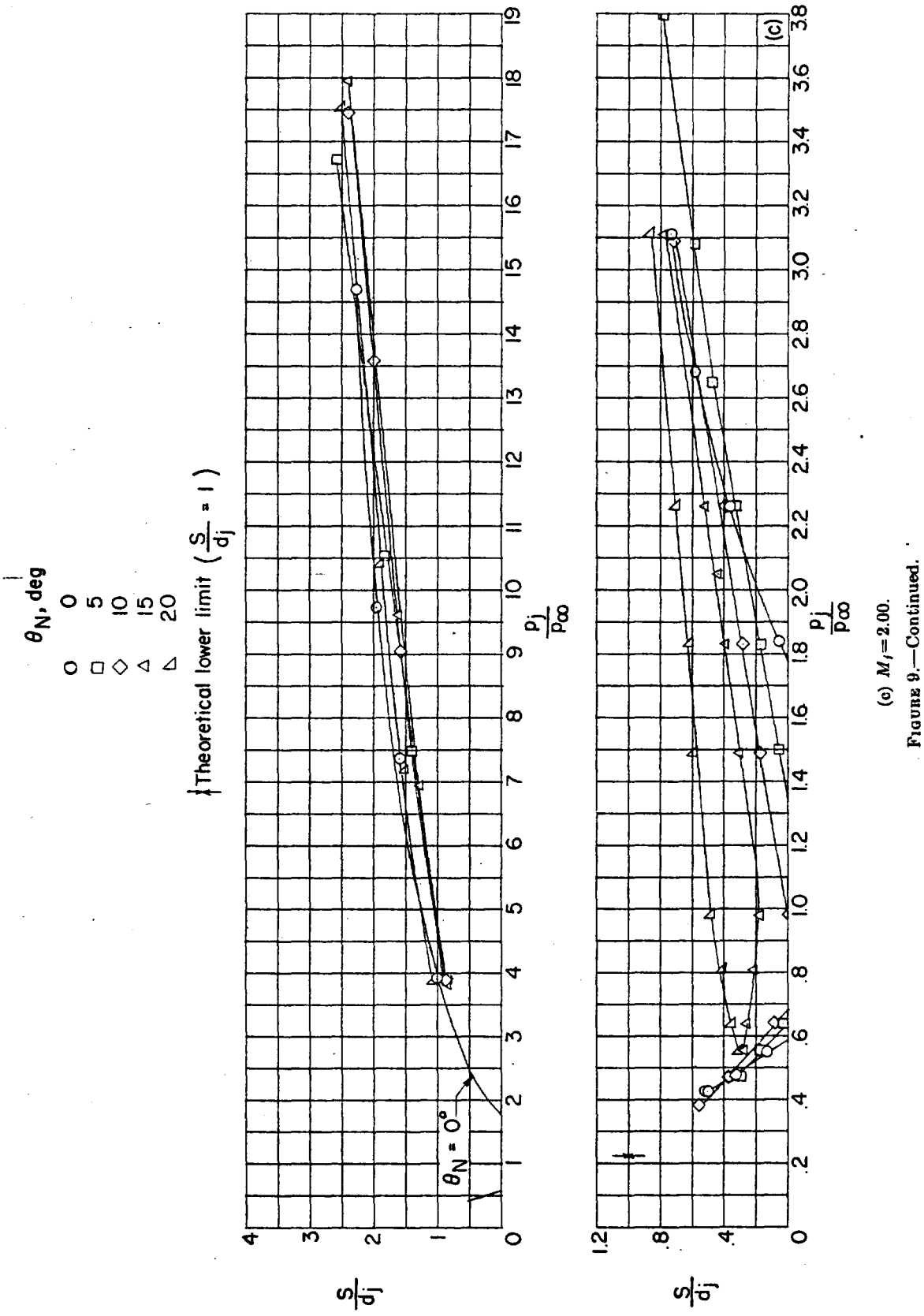

(c) $M_j = 2.00$.

FIGURE 9.—Continued.

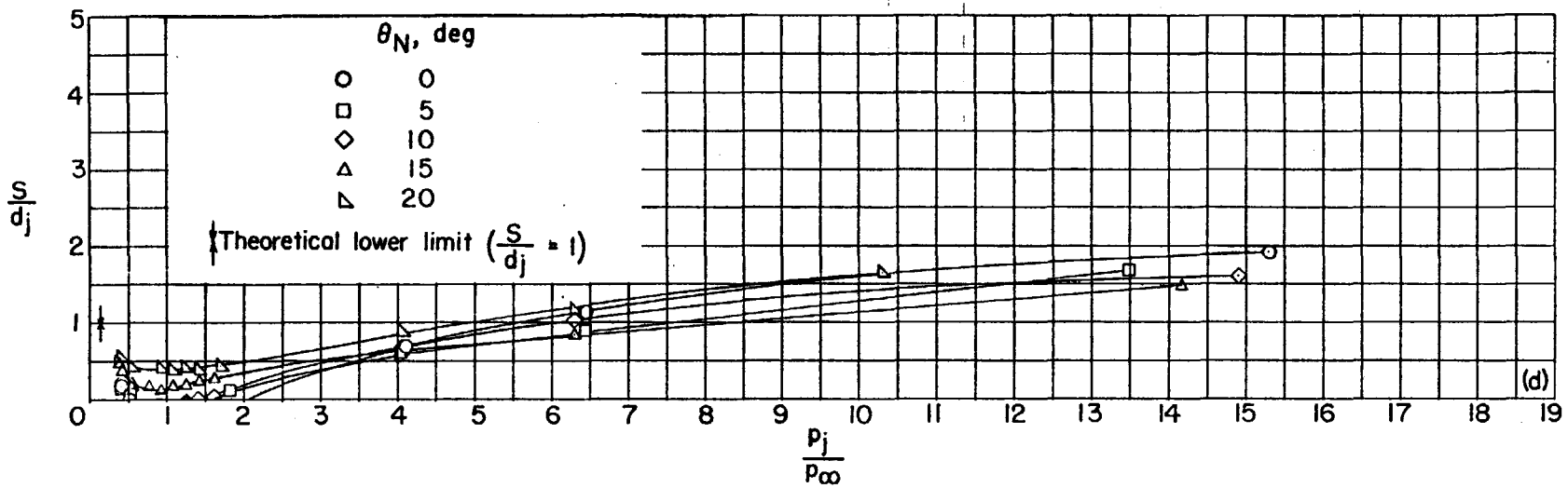

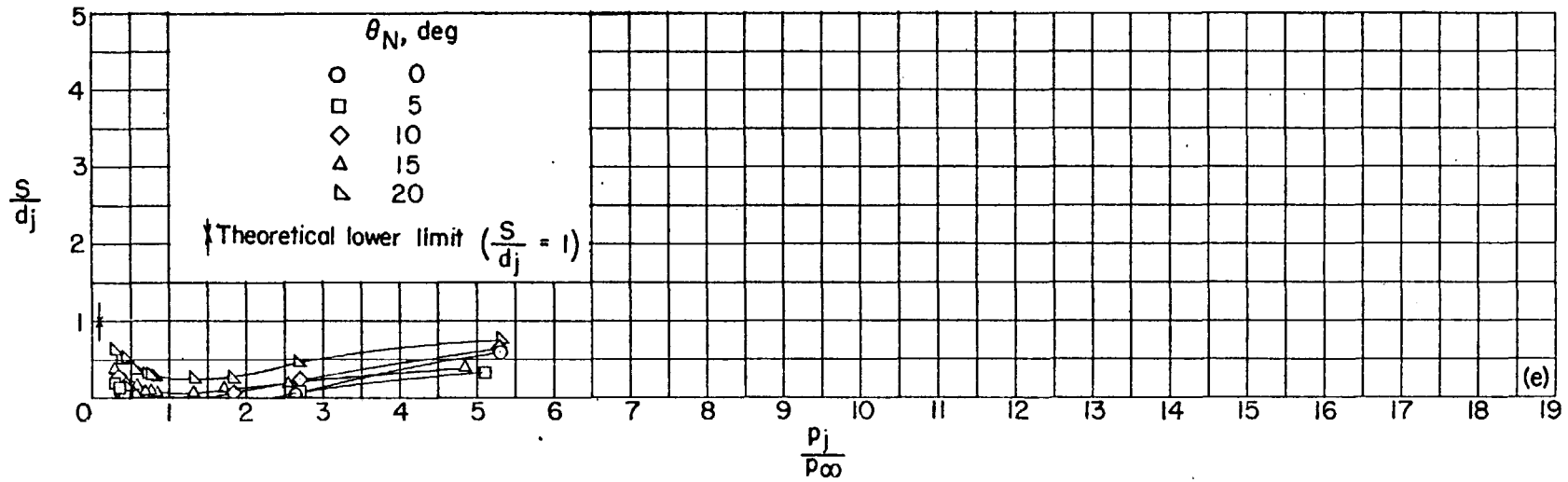

(d) $M_j = 2.50$.

(e) $M_j = 3.00$.

FIGURE 9.—Concluded.

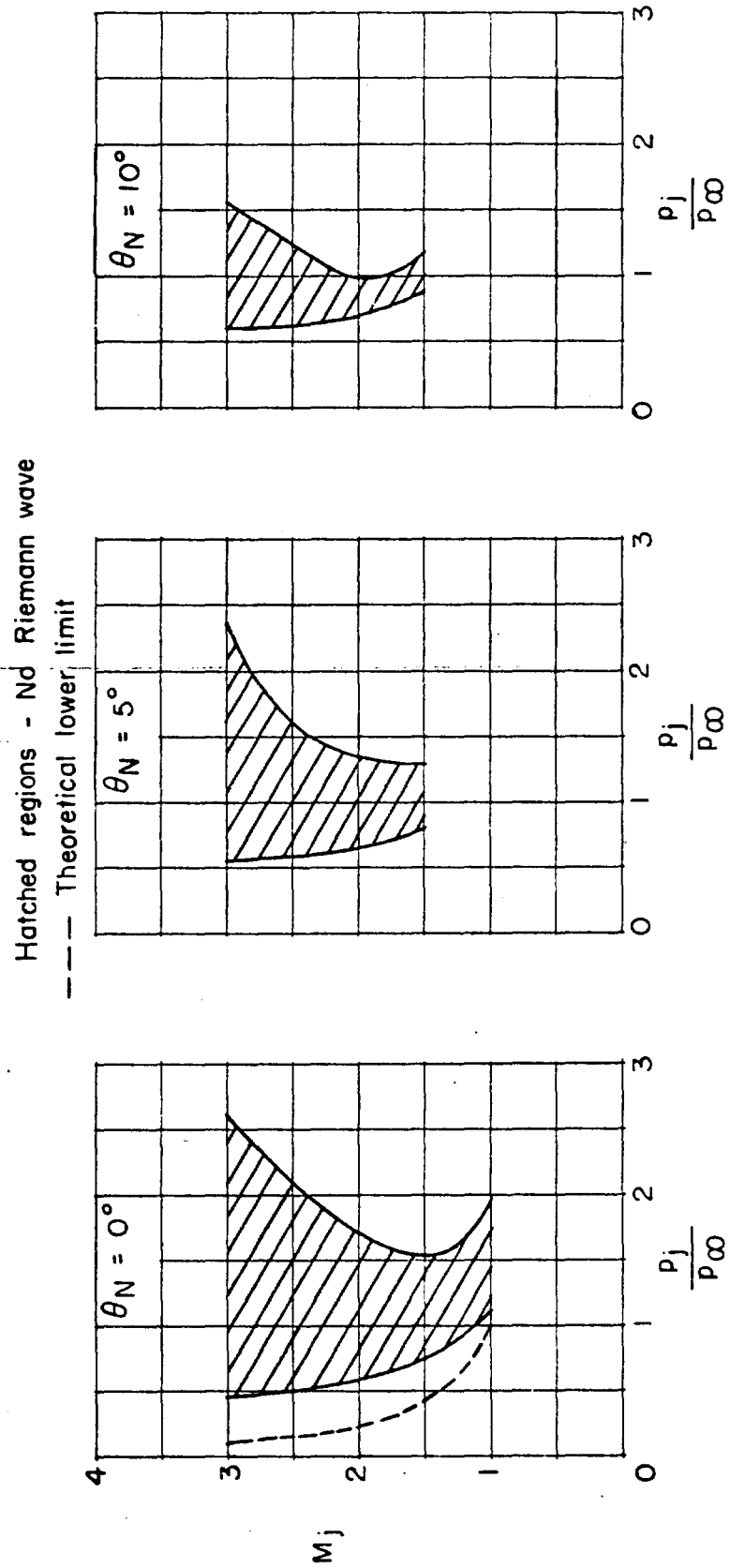

FIGURE 10.—Range of M_j and p_j/p_∞ in which no Riemann wave occurs.

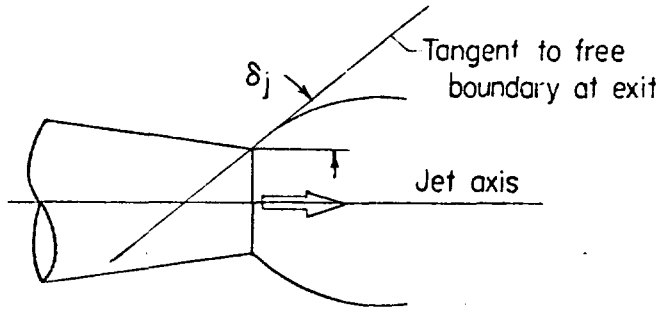

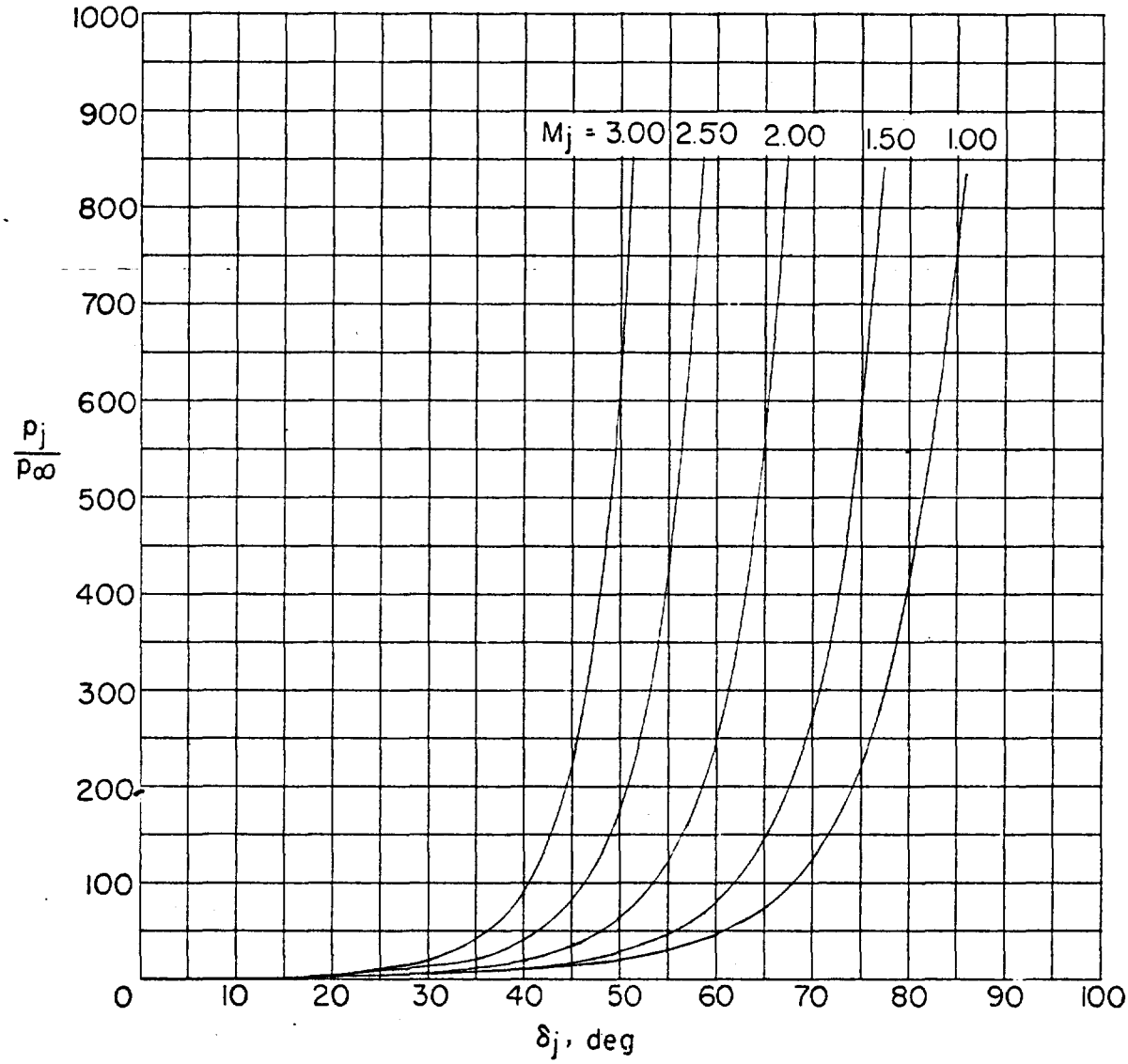

FIGURE 11.—Theoretical variation in initial inclination of jet boundary with jet pressure ratio and jet Mach number. $\theta_N = 0°; \gamma_j = 1.400$.

FIGURE 12.—Example of large initial inclination of jet boundary. $M_j = 1.00$; $\theta_N = 0°$; $p_j/p_\infty \approx 105$.

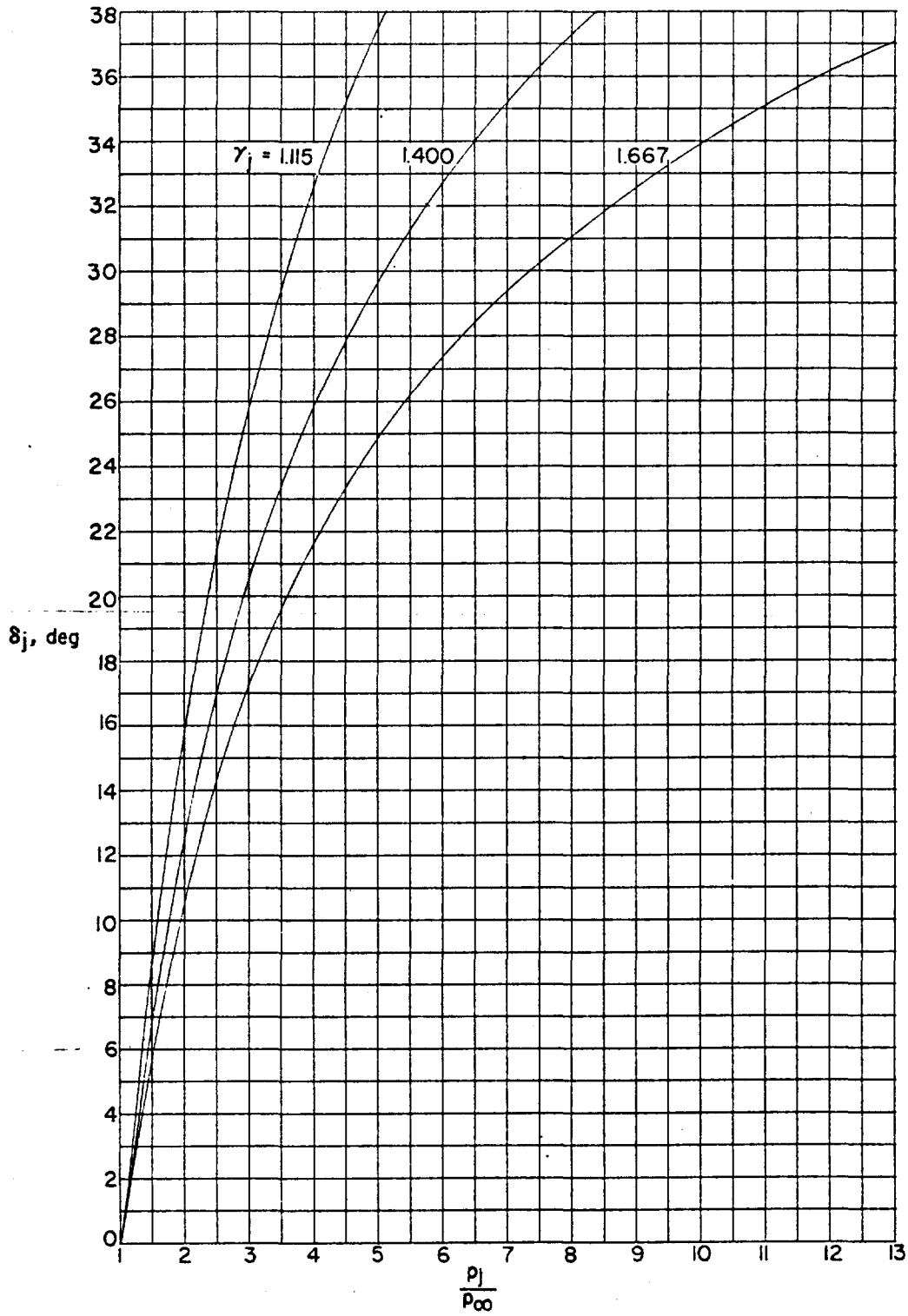

FIGURE 13.—Effect of the ratio of specific heats of the jet upon the initial inclination of the jet boundary. $M_j = 1.00$.

502683 O—59——7

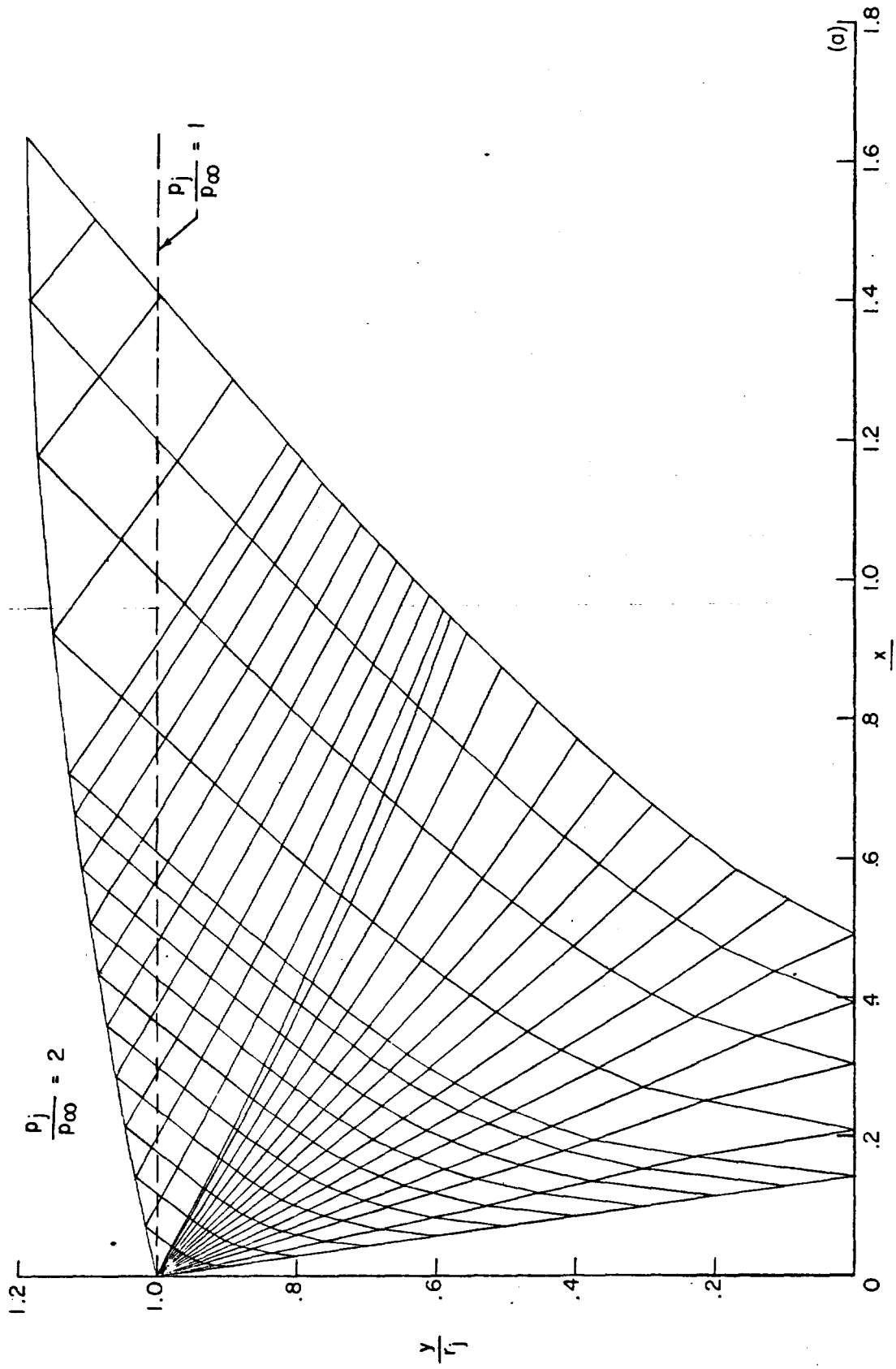

(a) $M_j = 1.01$; $\theta_W = 0°$; $\gamma_j = 1.400$.

FIGURE 14.—Characteristic nets.

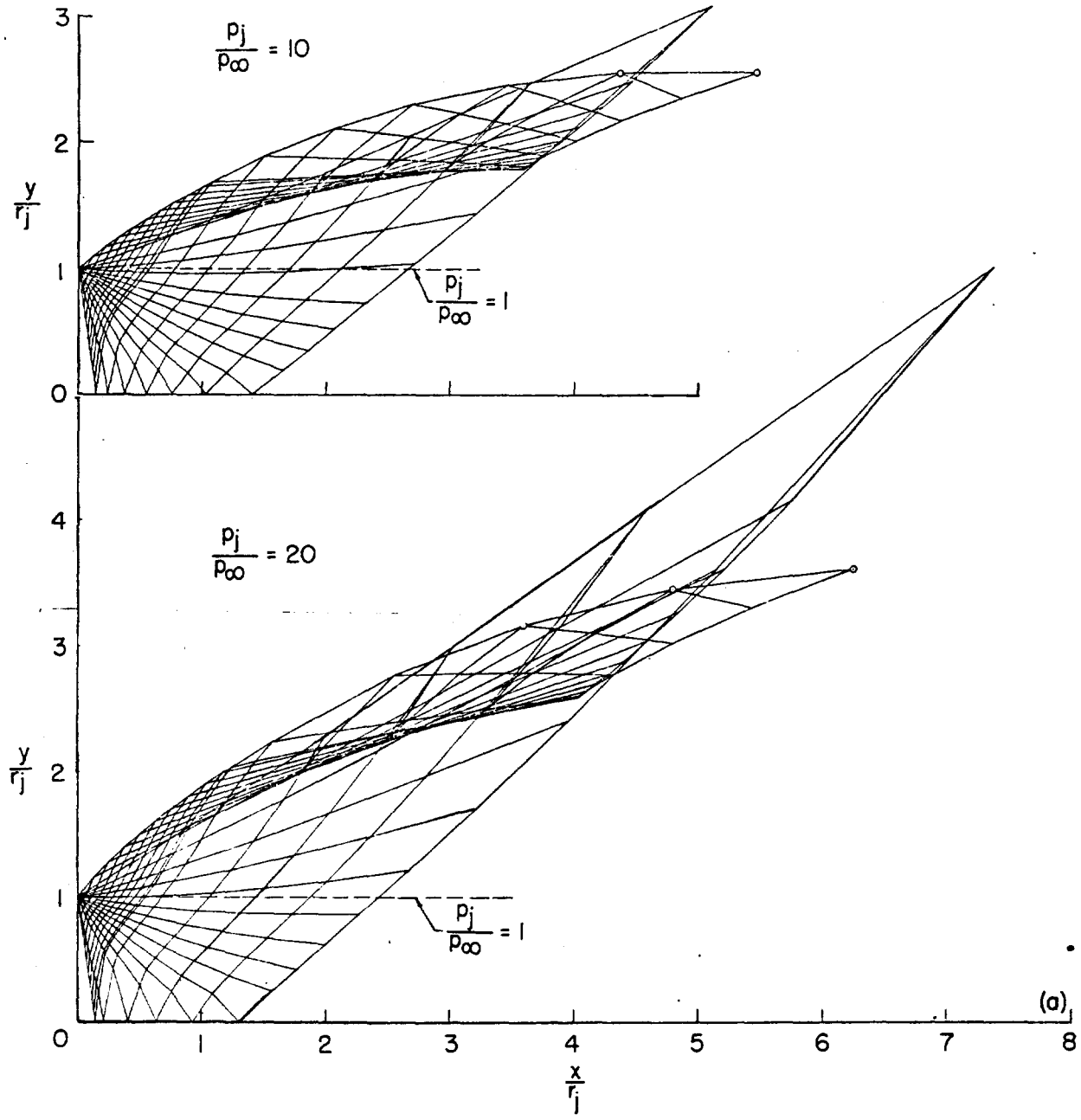

(a) Concluded.

FIGURE 14.—Continued.

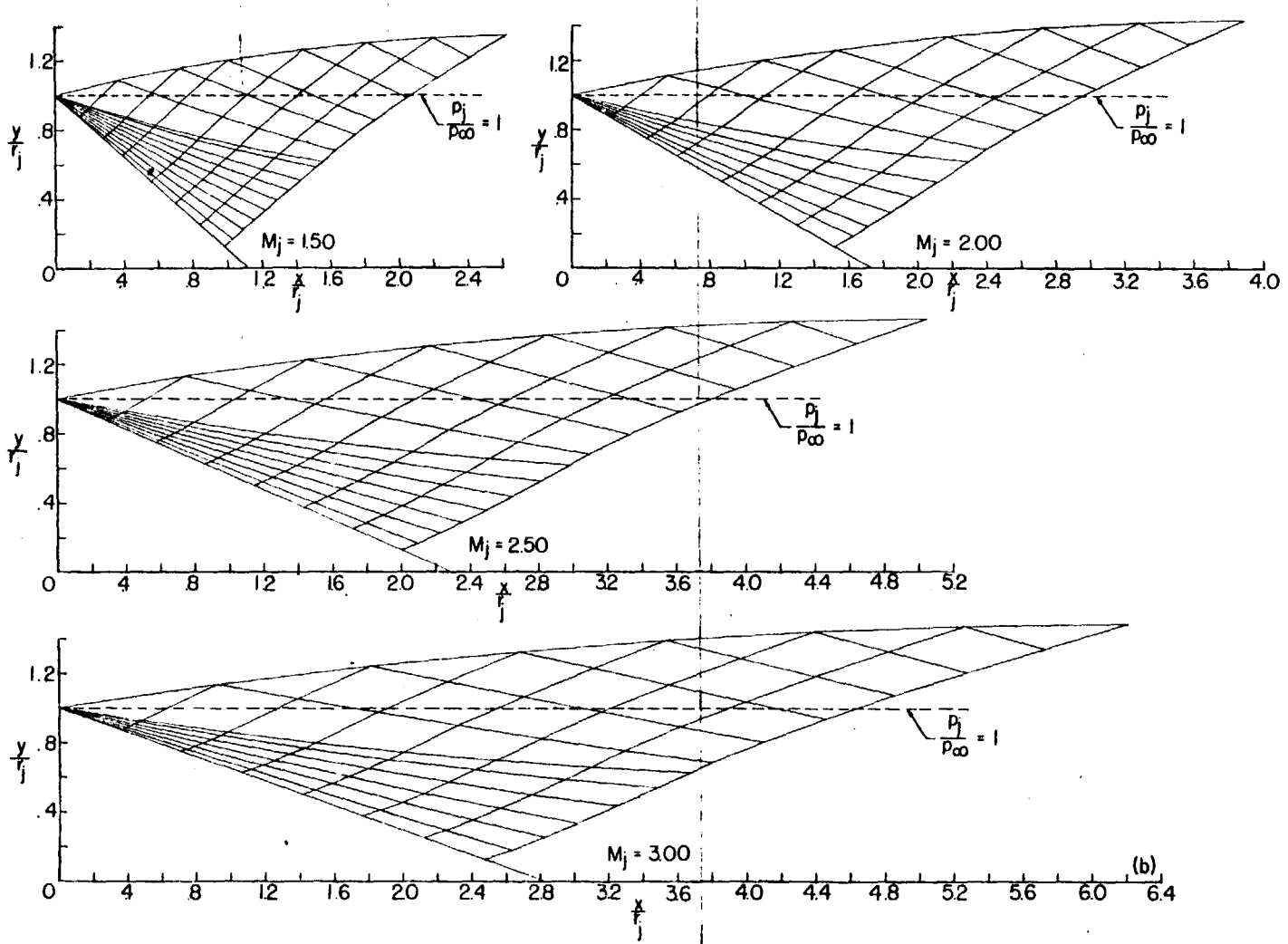

(b) $M_j = 1.50$ to 3.00; $p_j/p_\infty = 2$; $\theta_N = 0°$; $\gamma_j = 1.400$.

FIGURE 14.—Continued.

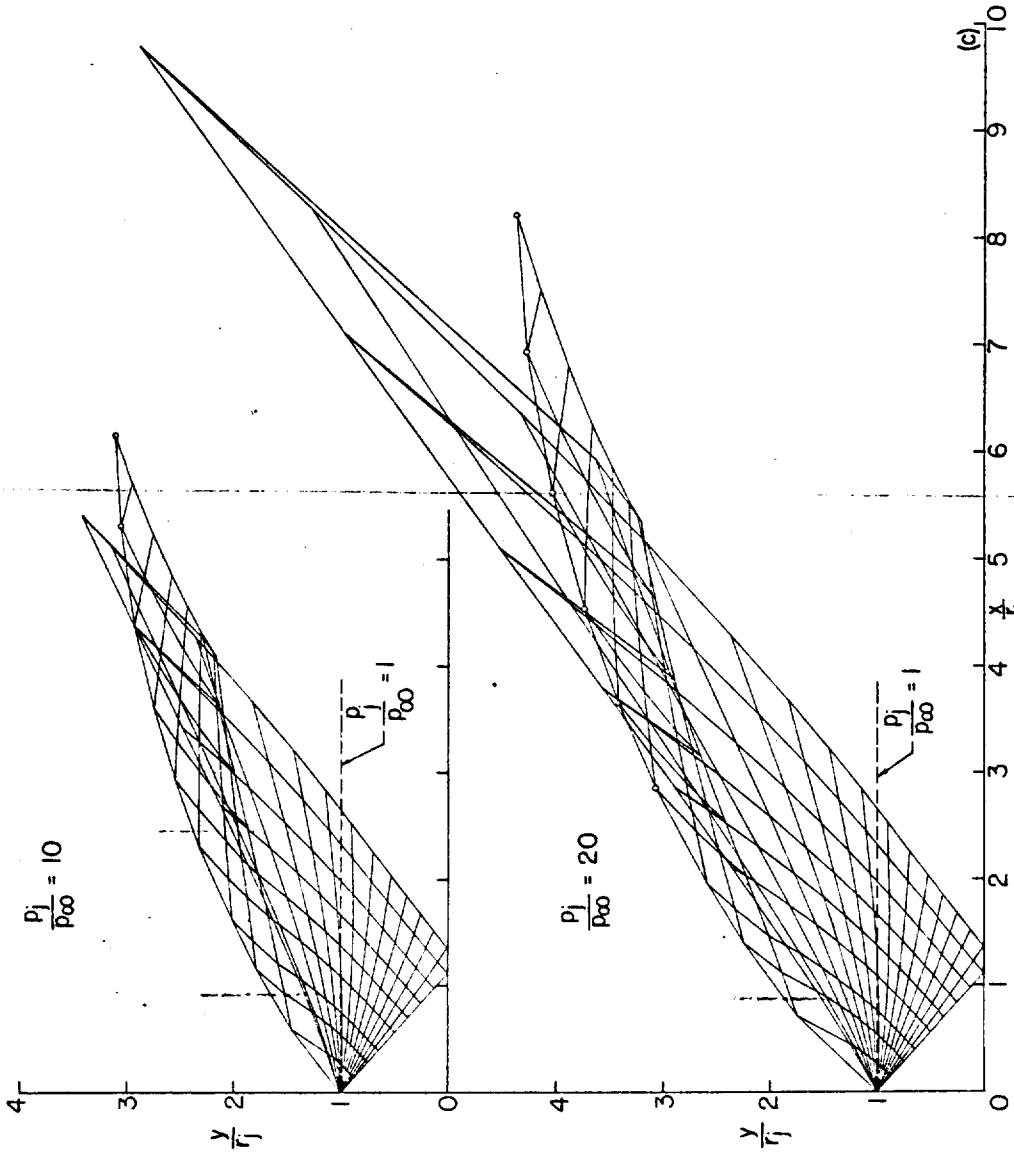

(c) $M_j = 1.50$; $p_j/p_\infty = 10$ and 20; $\theta_N = 0°$; $\gamma_j = 1.400$.

FIGURE 14.—Continued.

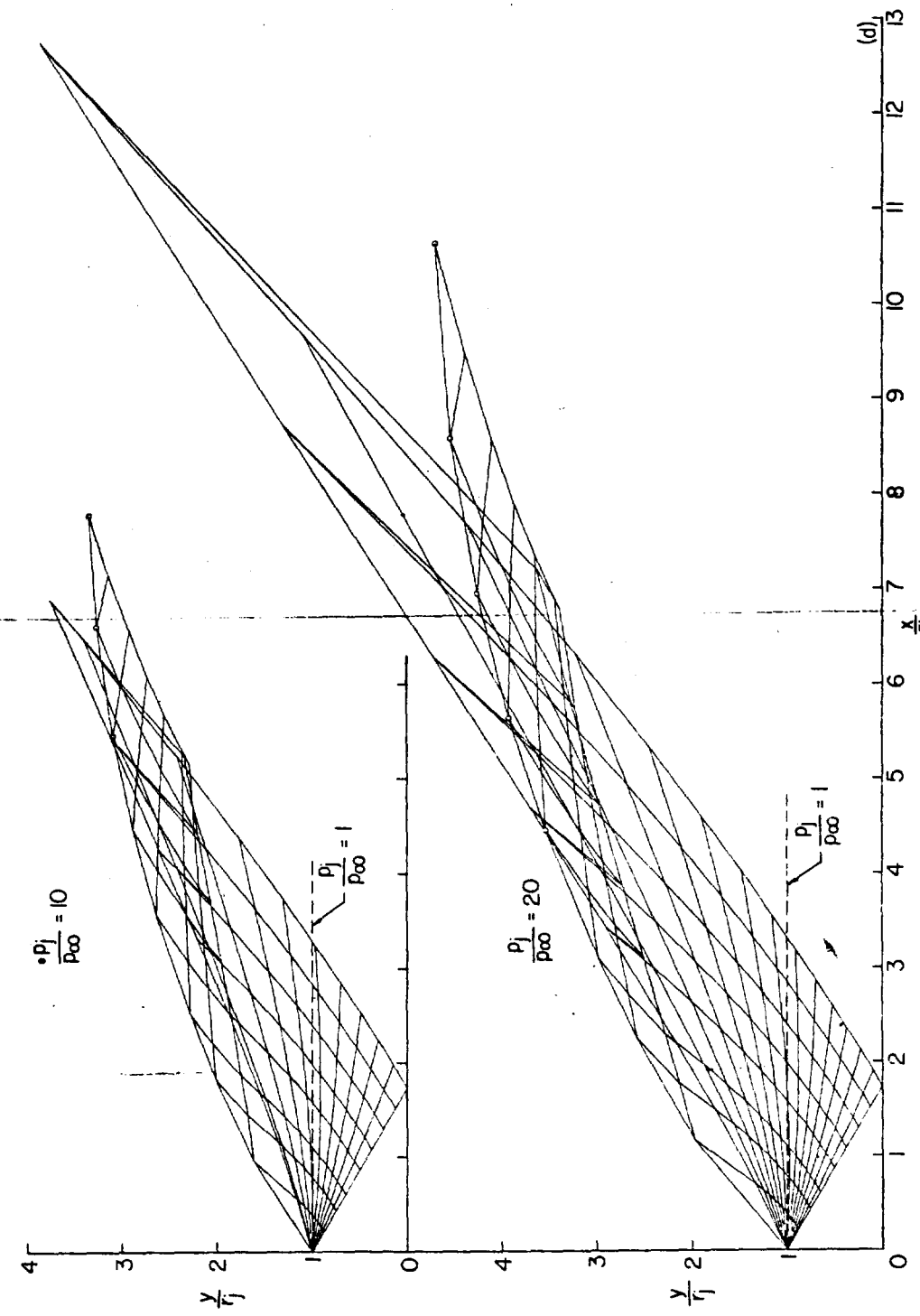

(d) $M_j = 2.00$; $p_j/p_\infty = 10$ and 20; $\theta_N = 0°$; $\gamma_j = 1.400$.

FIGURE 14.— Continued.

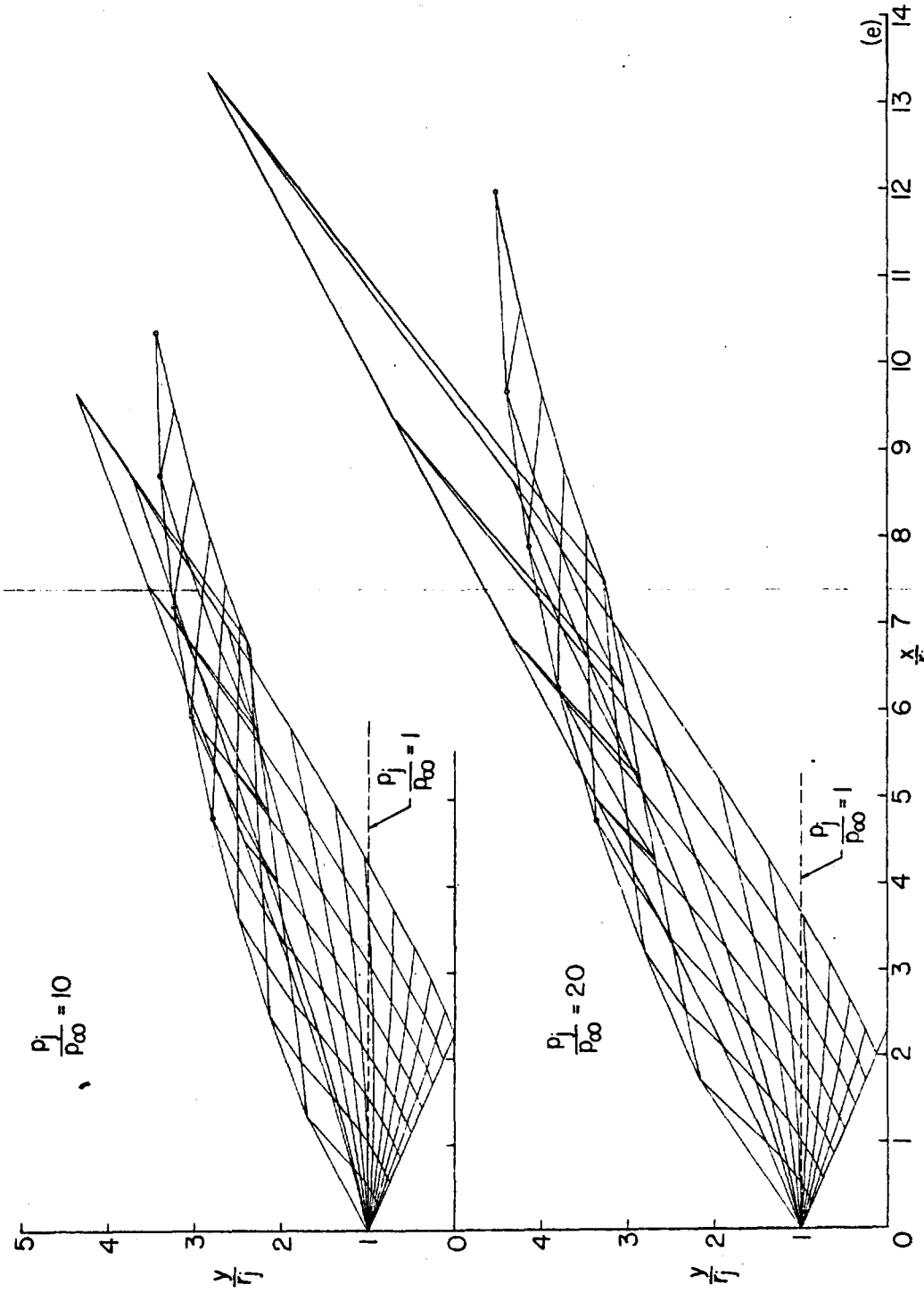

(e) $M_j = 2.50$; $p_{tj}/p_\infty = 10$ and 20; $\theta_N = 0°$; $\gamma_j = 1.400$.

FIGURE 14.—Continued.

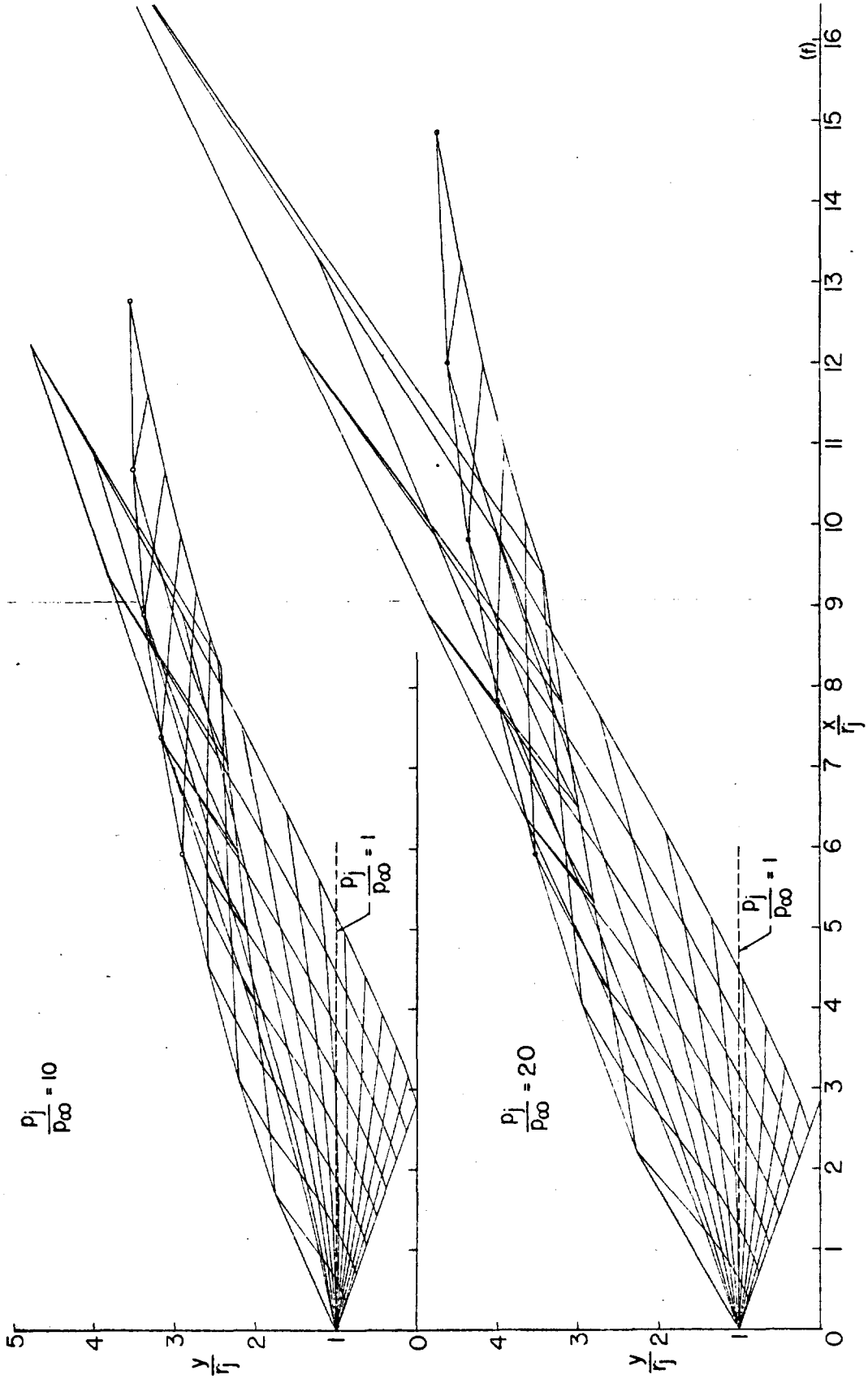

(f) $M_j = 3.00$; $p_j/p_\infty = 10$ and 20; $\theta_N = 0°$; $\gamma_j = 1.400$.

FIGURE 14.—Continued.

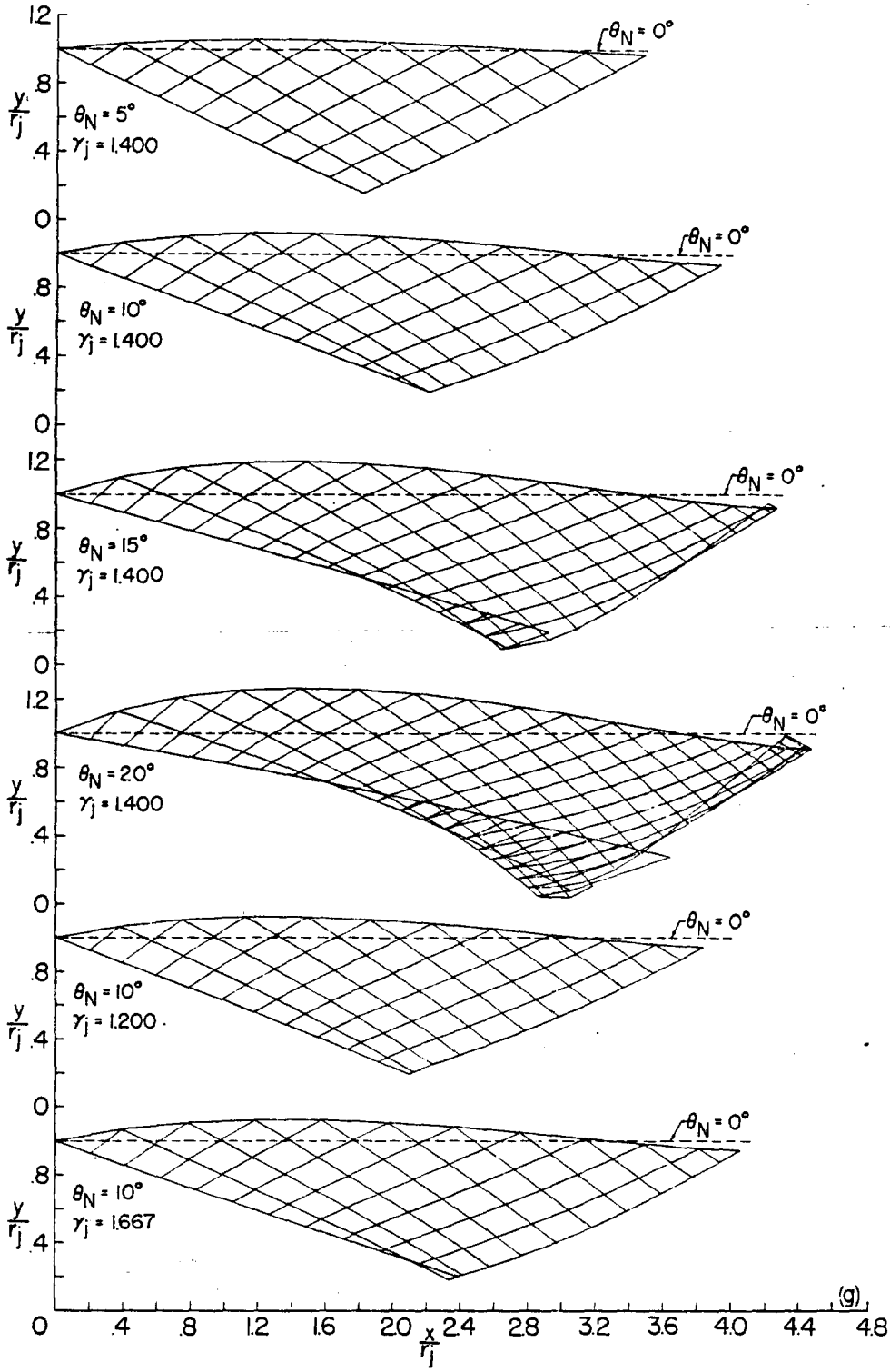

(g) $M_i=2.00$; $p_i/p_\infty=1$; varying θ_N and γ_i.

FIGURE 14.—Concluded.

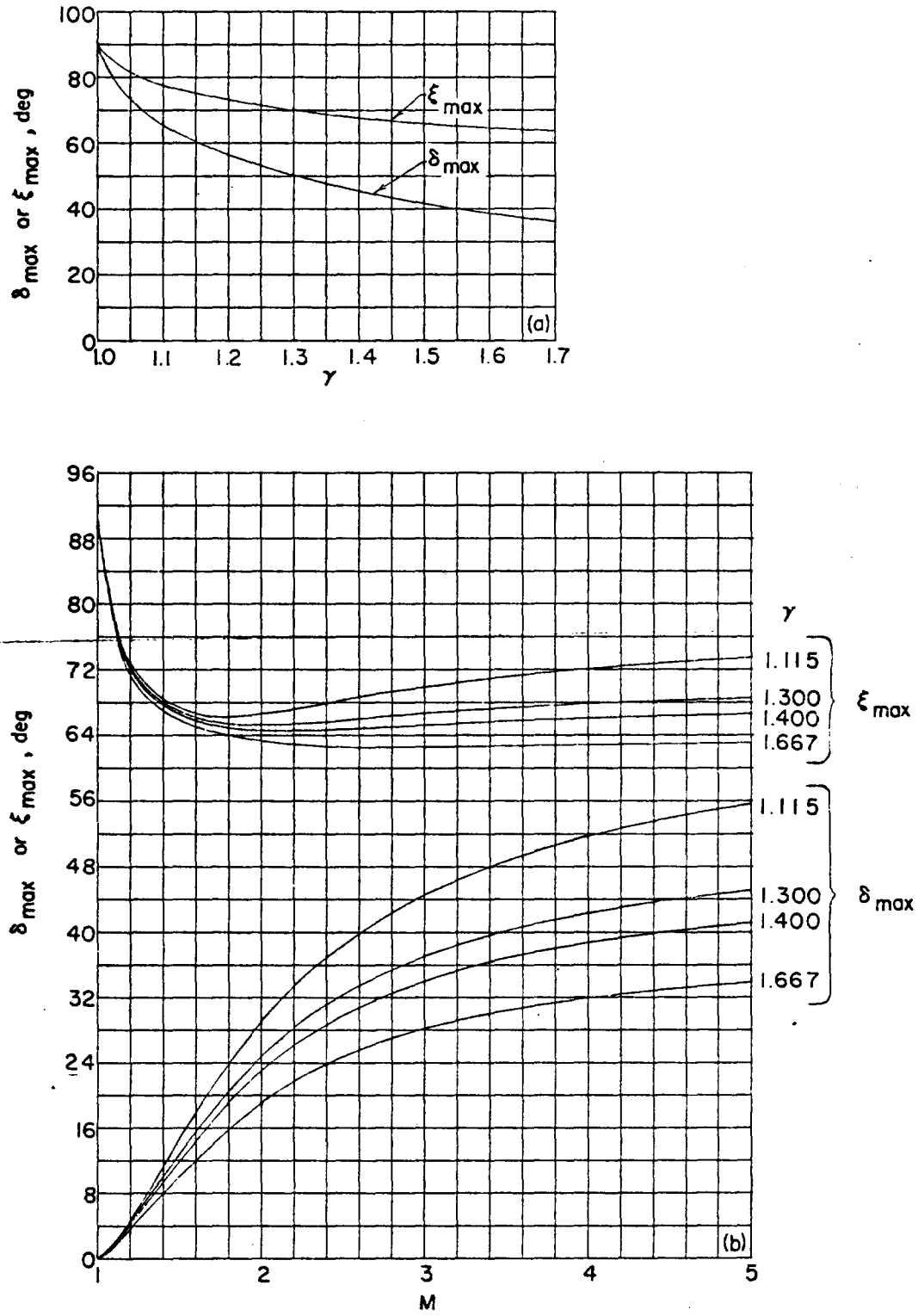

(a) $M=\infty$.

(b) $M=1$ to 5.

FIGURE 15.—Effect of the ratio of specific heats upon the maximum turning angle of two-dimensional flow through an attached shock and upon the inclination of the shock.

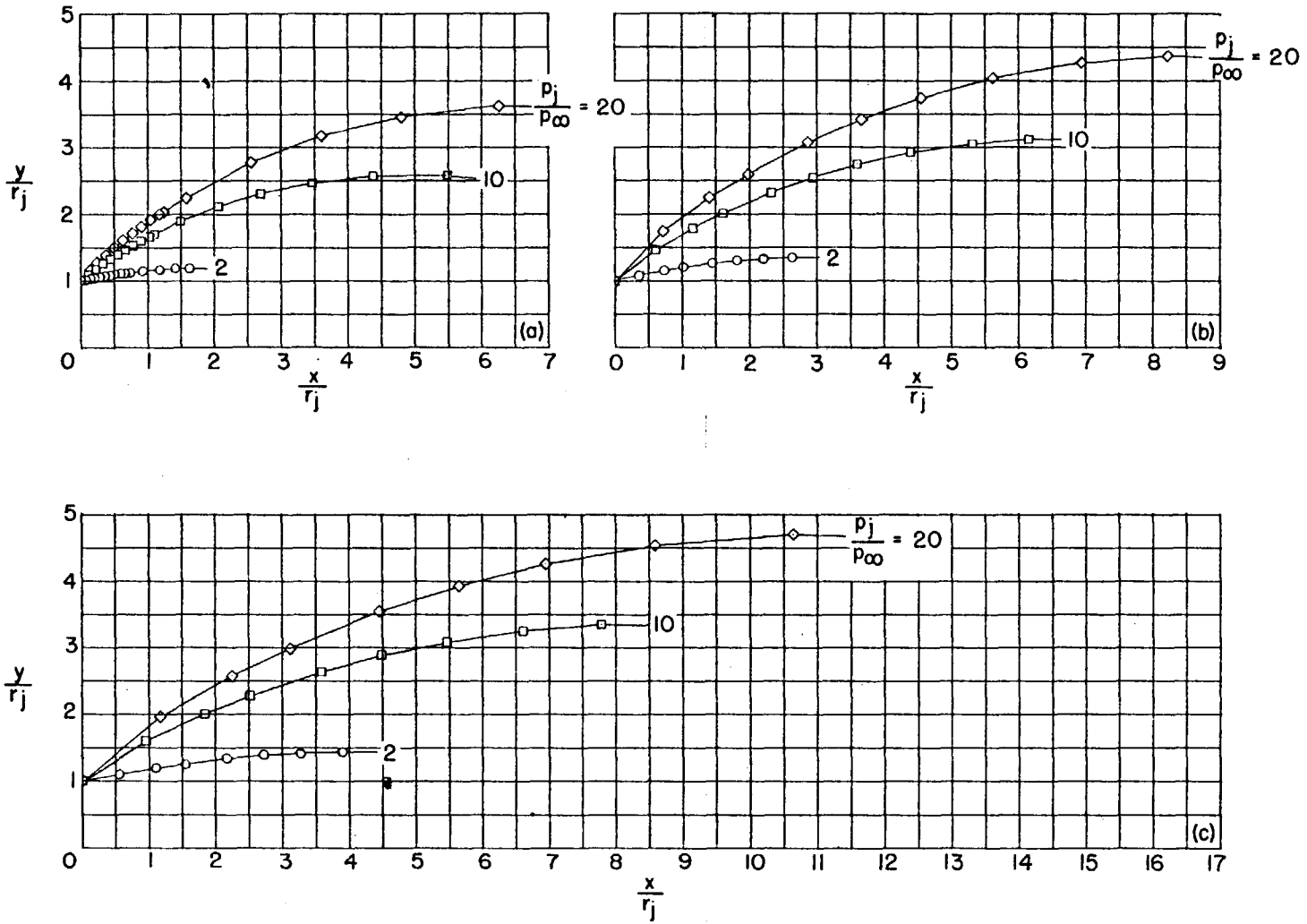

(a) $M_i = 1.01$. (b) $M_i = 1.50$.

(c) $M_i = 2.00$.

FIGURE 16.—Theoretical jet boundaries obtained from characteristic calculations. $\theta_N = 0°$; $\gamma_i = 1.400$.

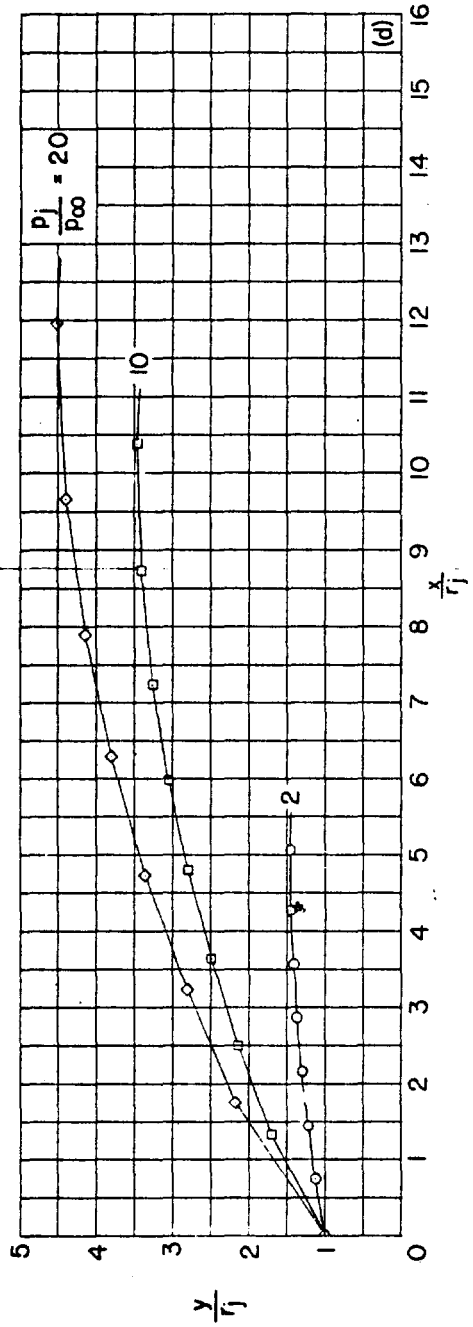

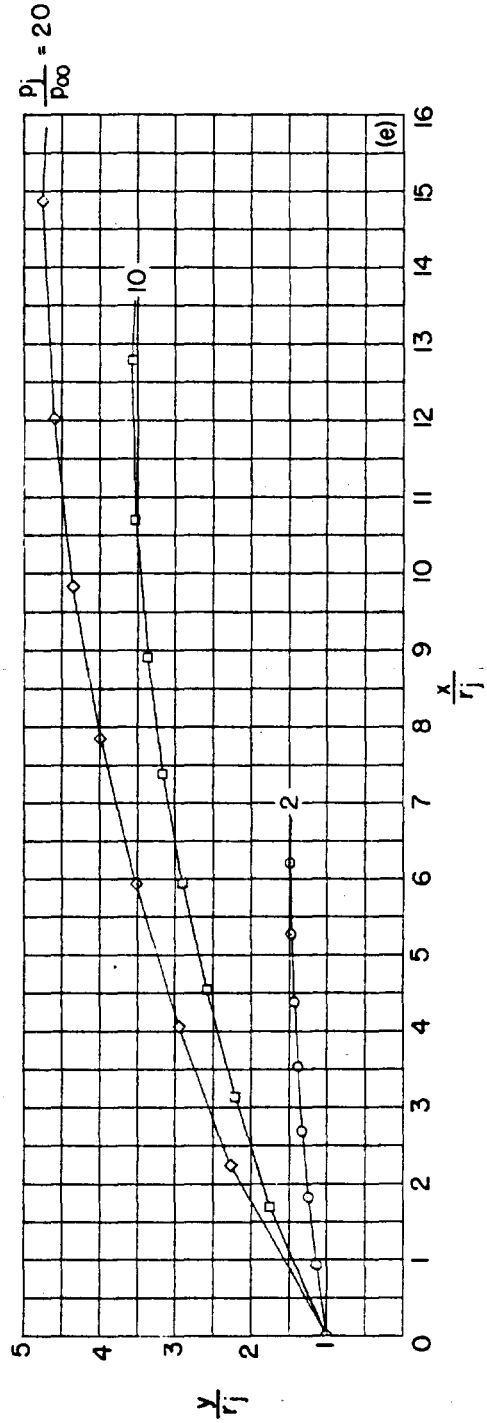

(d) $M_j = 2.50$.
(e) $M_j = 3.00$.

FIGURE 16.—Concluded.

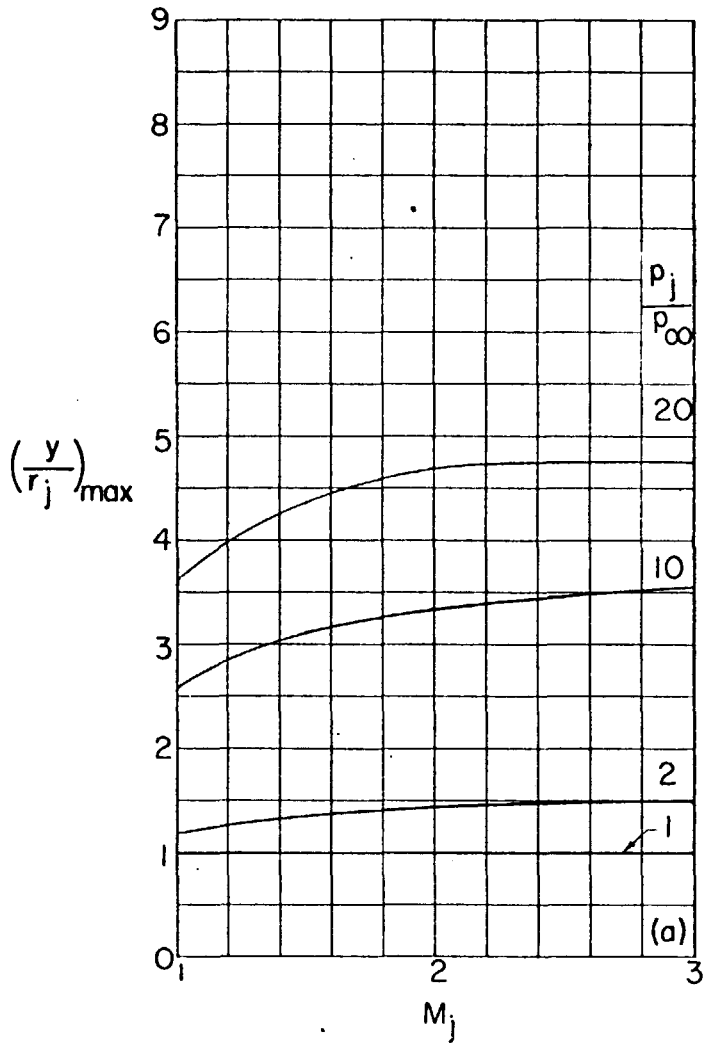

(a) Variation of $\left(\frac{y}{r_j}\right)_{max}$.

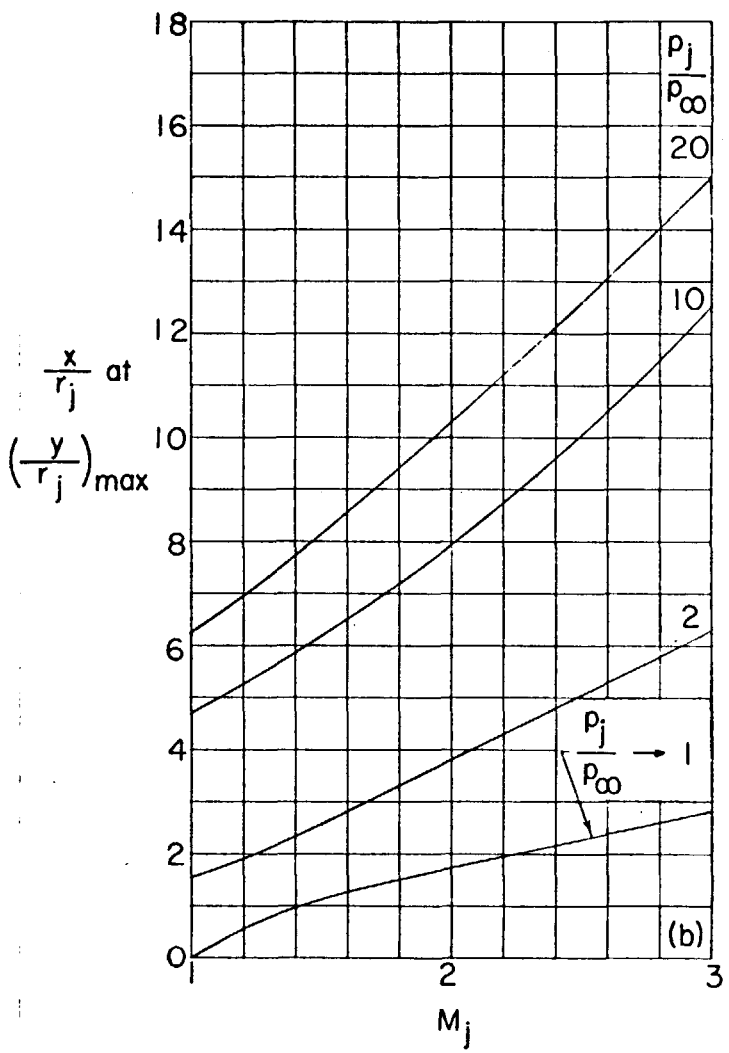

(b) Variation of $\frac{x}{r_j}$ at $\left(\frac{y}{r_j}\right)_{max}$.

FIGURE 17.—Maximum height of jet boundary and its location as obtained from characteristic calculations. $\theta_N = 0°$; $\gamma_j = 1.400$.

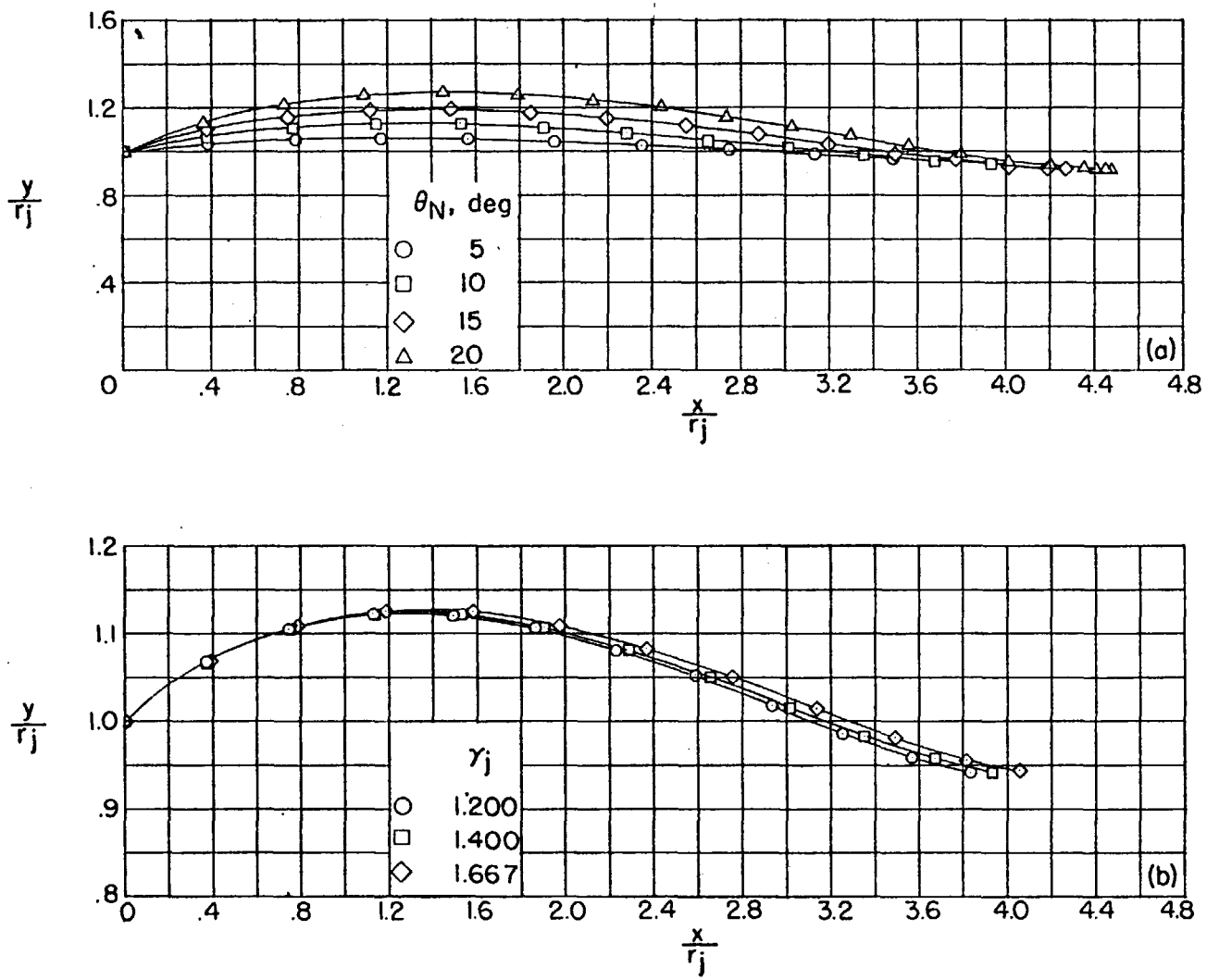

(a) $\gamma_j = 1.400$.

(b) $\theta_N = 10°$.

FIGURE 18.—Effect of nozzle divergence angle and ratio of specific heats of the jet upon the shape of the jet boundary as obtained from characteristic calculations. $M_j = 2.00$; $p_j/p_\infty = 1$.

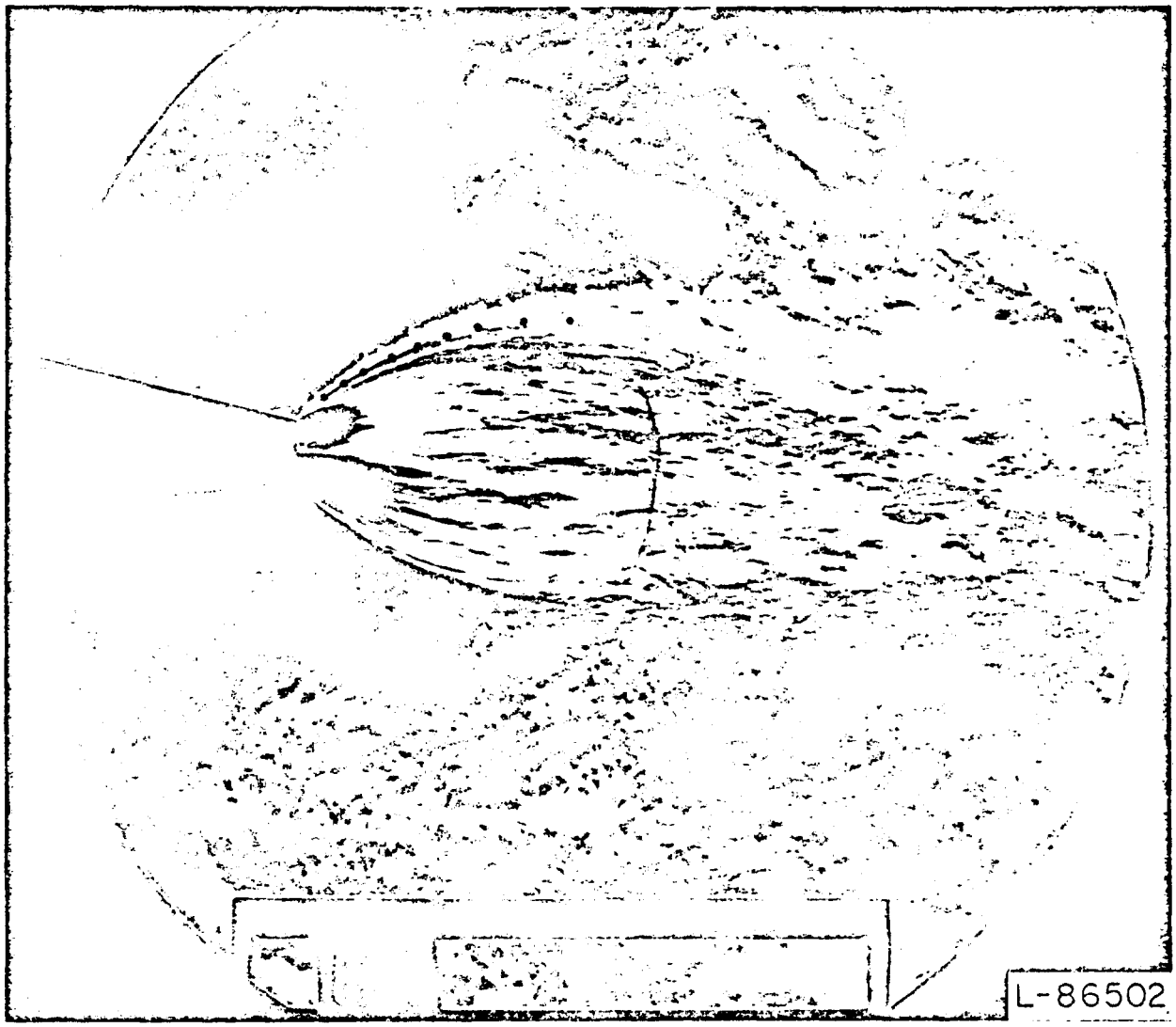

FIGURE 19.—Comparison of theoretical boundary (dots) and shock location (dashes) for $p_i/p_\infty=20$ with experimental observation for $p_i/p_\infty=21.9$. $M_i=1.50$; $\theta_N=0°$; $\gamma_i=1.400$.

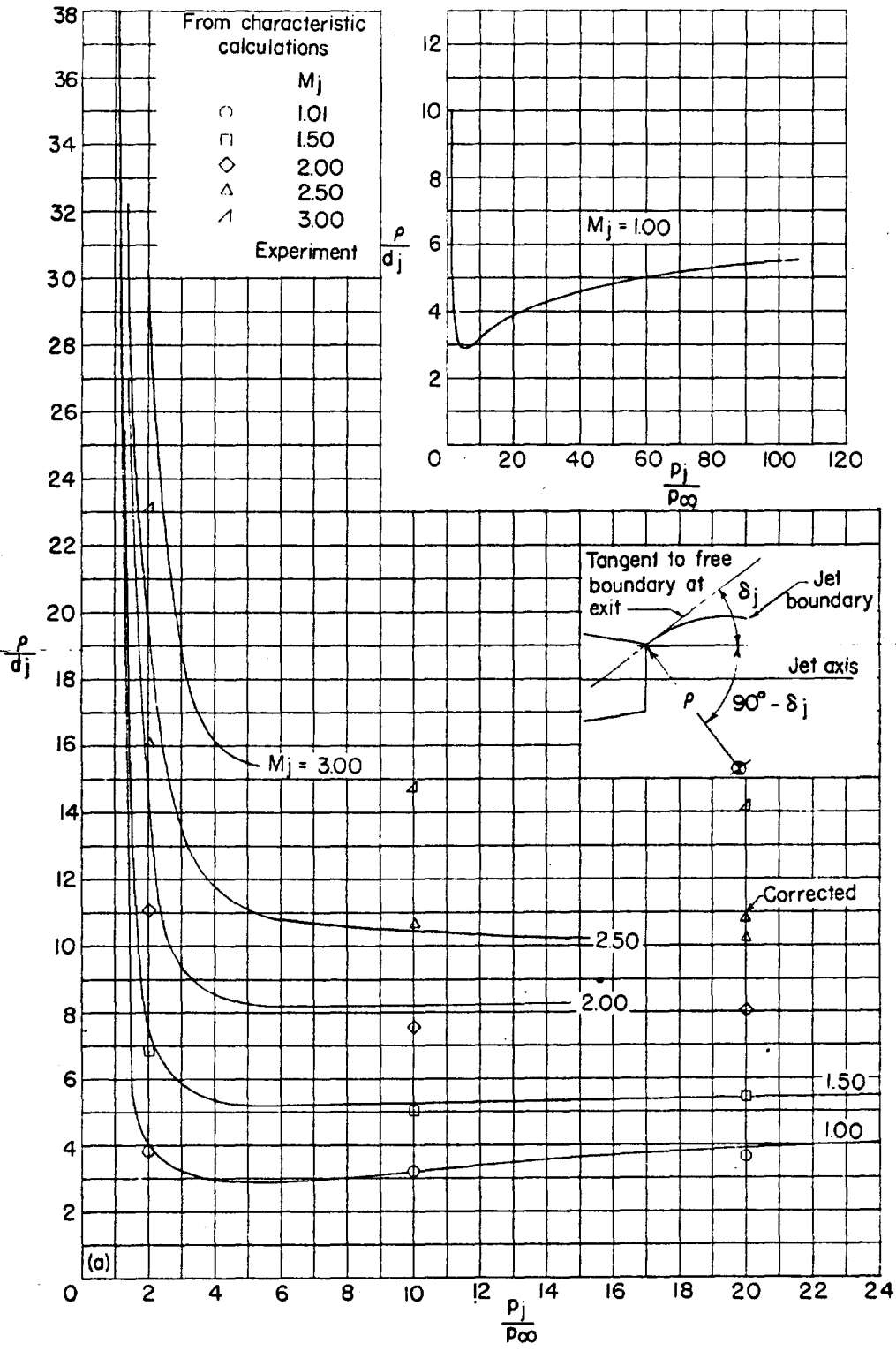

(a) $\theta_N = 0°$.

FIGURE 20.—Effects of jet pressure ratio and jet Mach number upon the nondimensional average radius of curvature of the jet boundary.

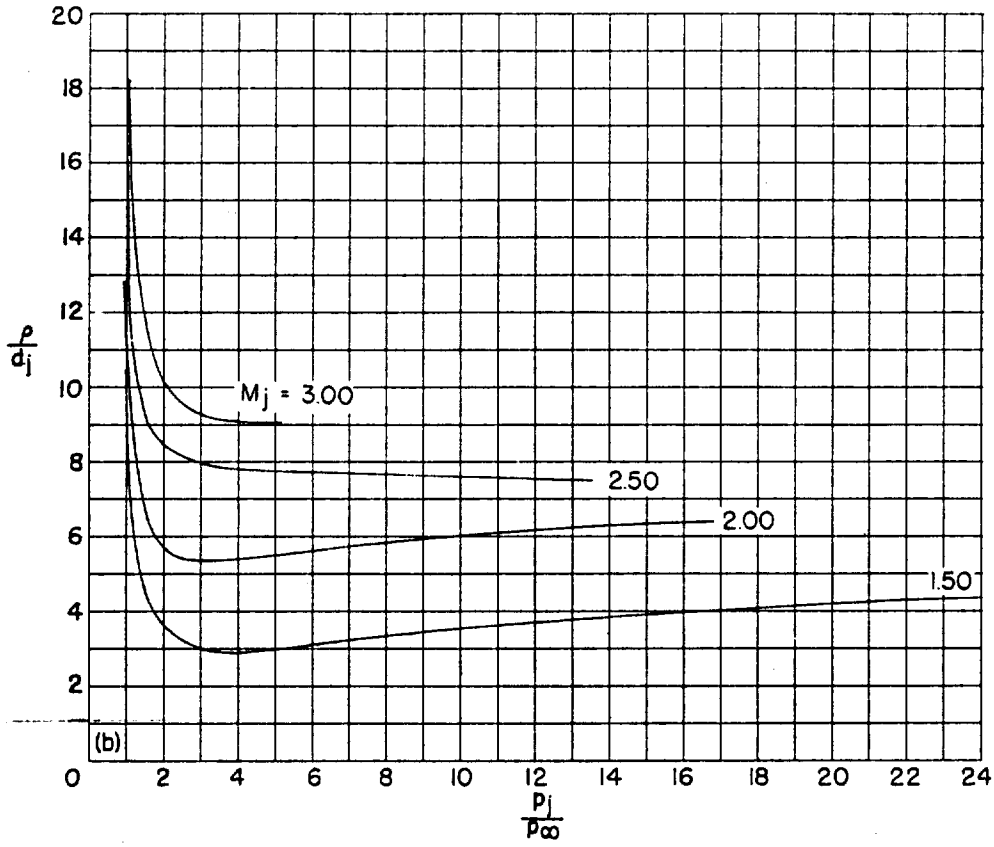

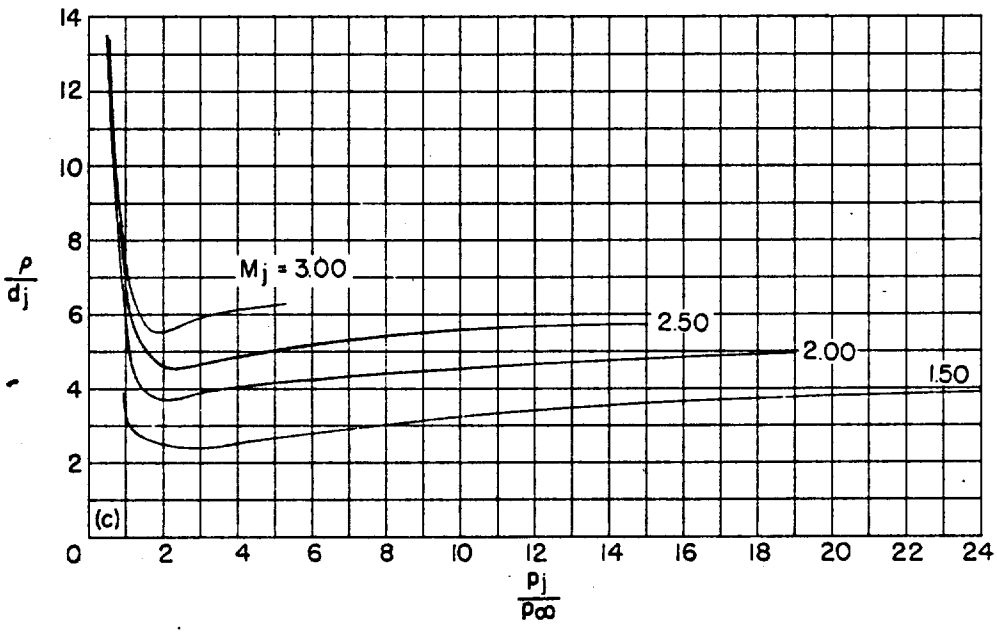

(b) $\theta_N = 5°$.

(c) $\theta_N = 10°$.

FIGURE 20.—Continued.

502683 O—59——8

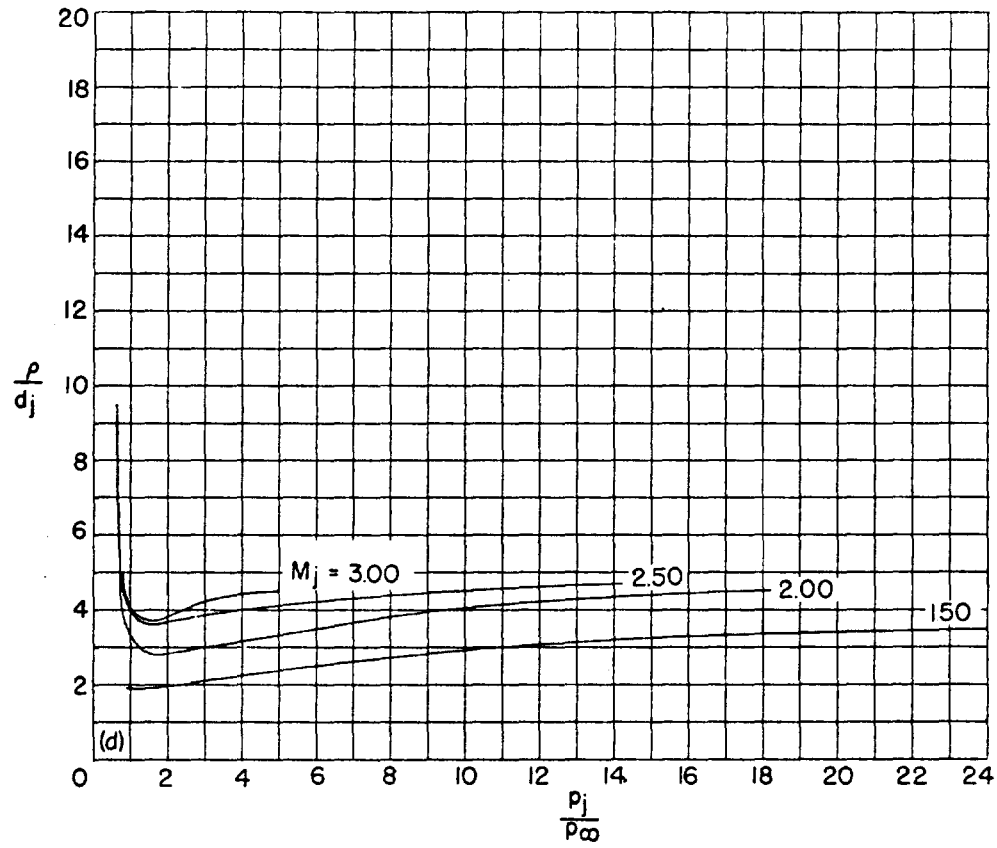

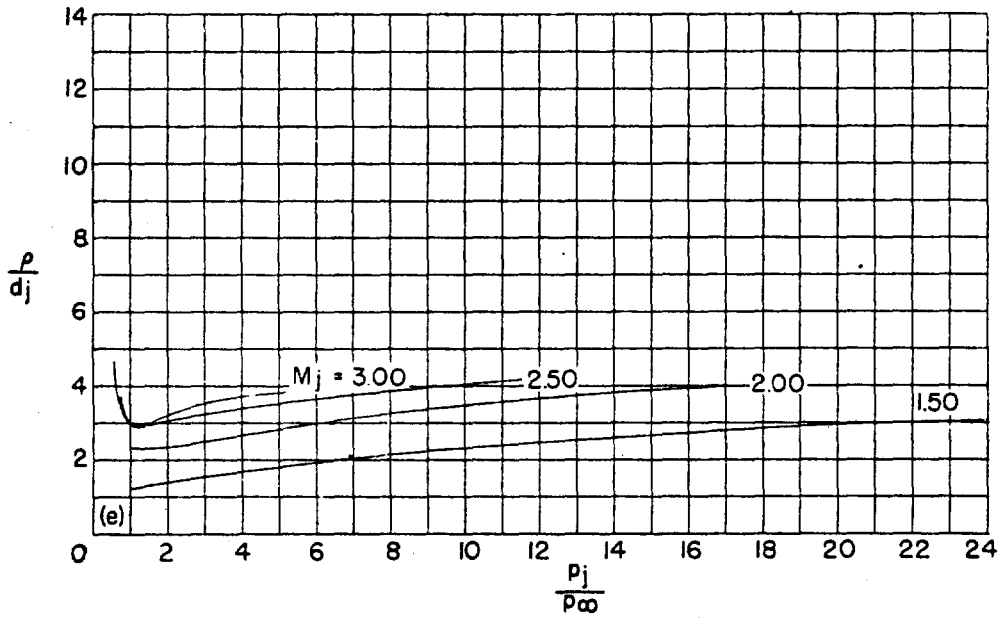

(d) $\theta_N = 15°$.

(e) $\theta_N = 20°$.

FIGURE 20.—Concluded.

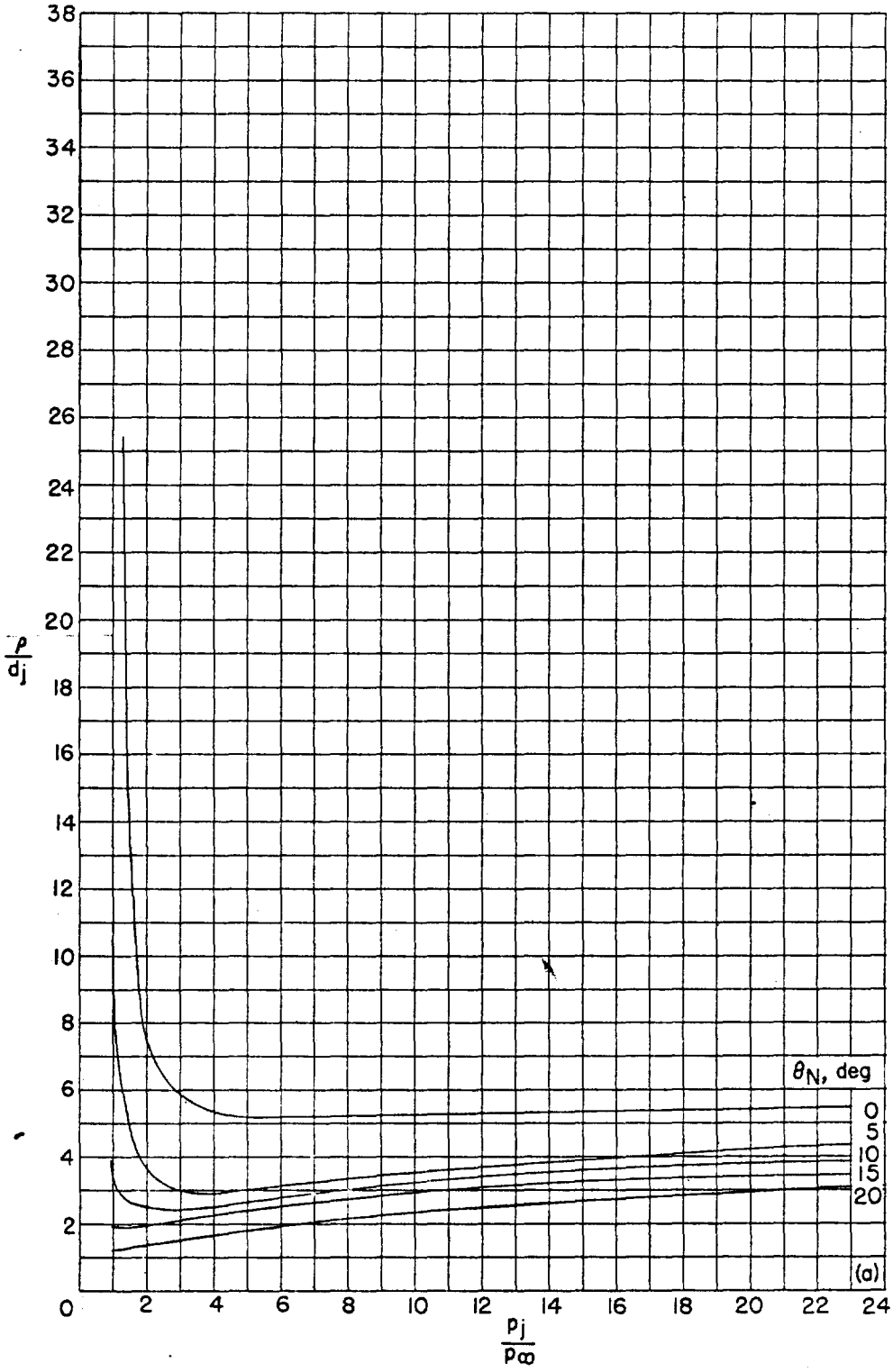

(a) $M_j=1.50$.

FIGURE 21.—Effects of jet pressure ratio and nozzle divergence angle upon the nondimensional average radius of curvature of the jet boundary.

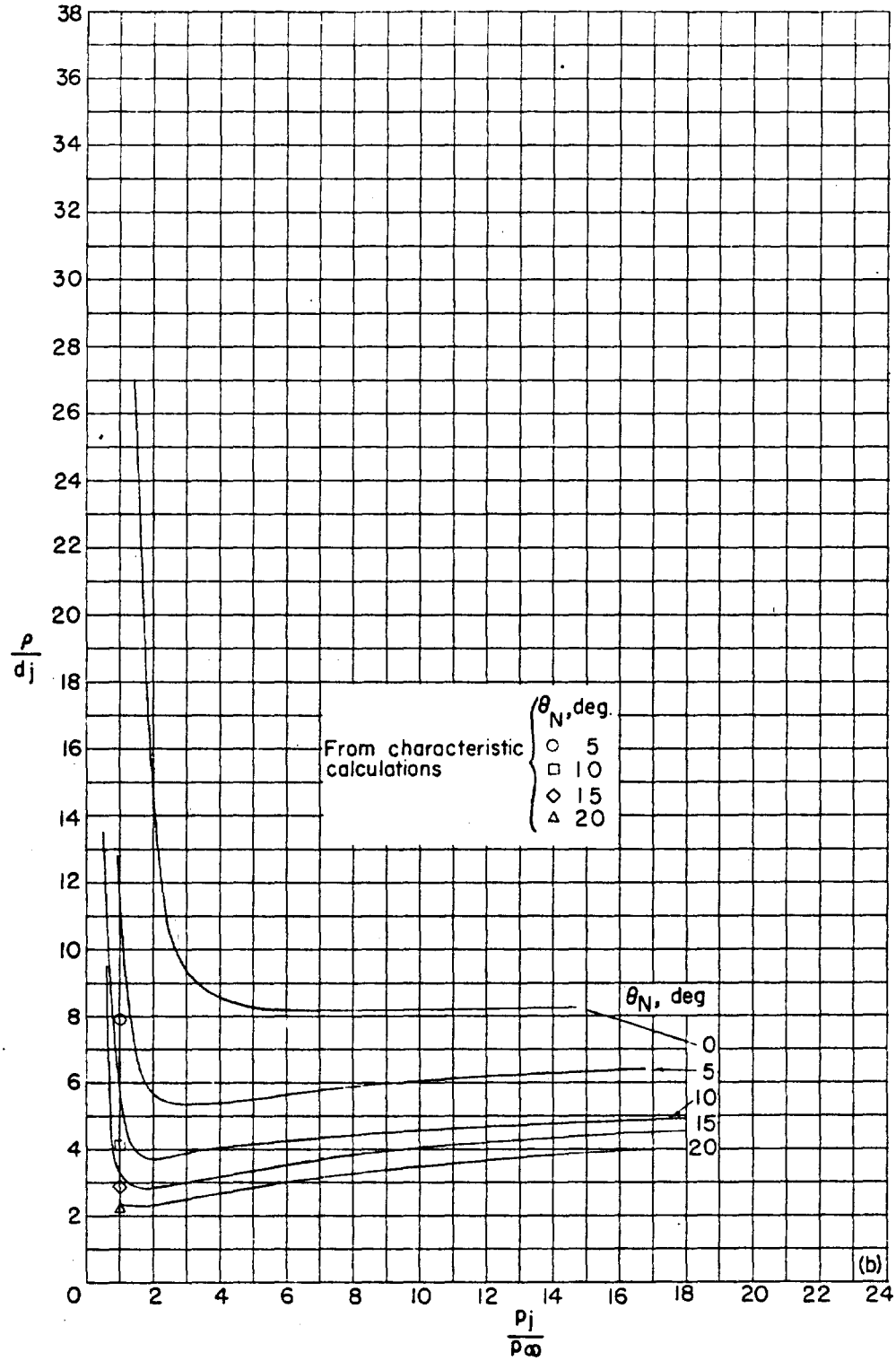

(b) $M_j=2.00$.

FIGURE 21.—Continued.

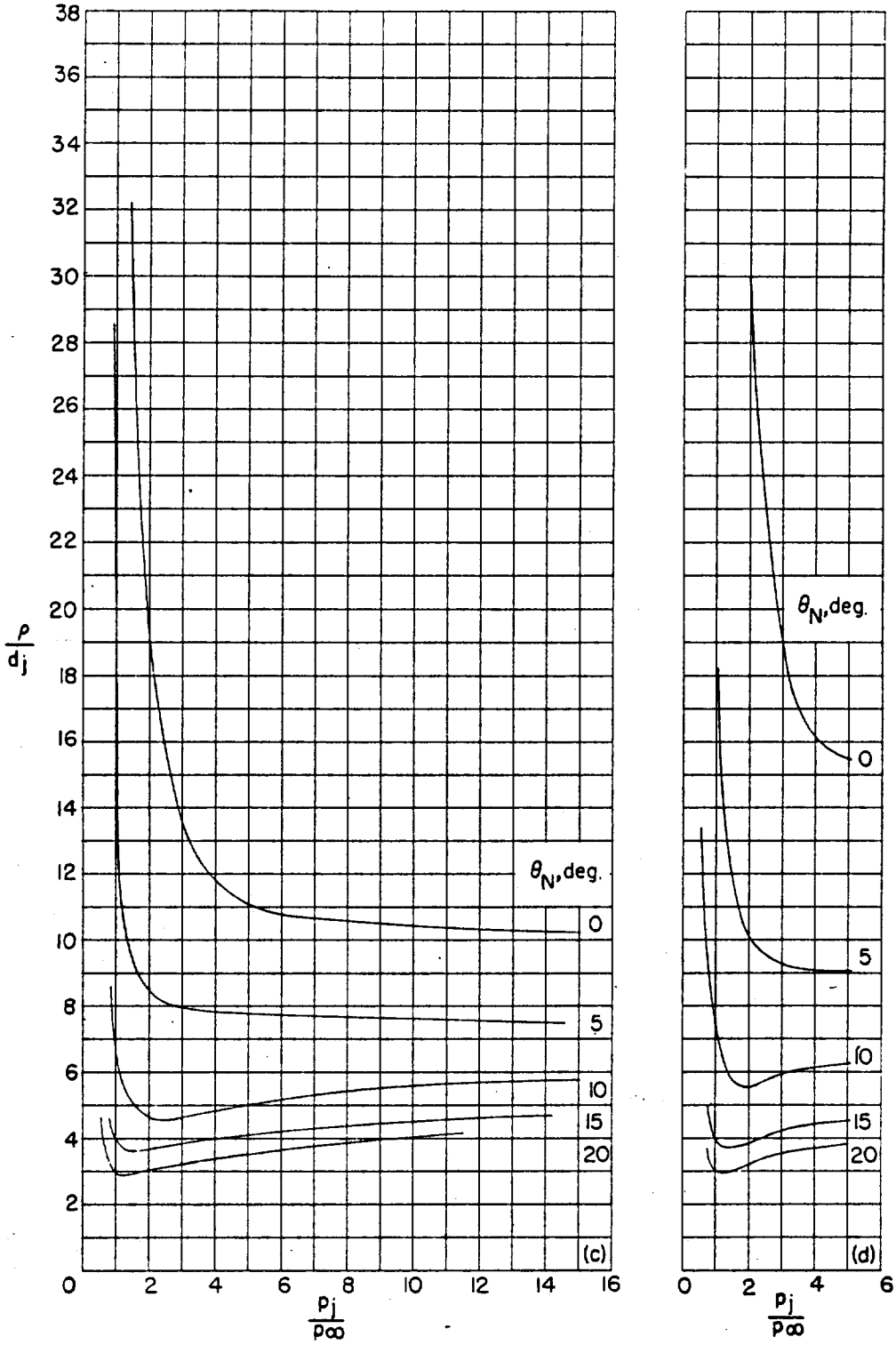

(c) $M_j = 2.50$. (d) $M_j = 3.00$.

FIGURE 21.—Concluded.

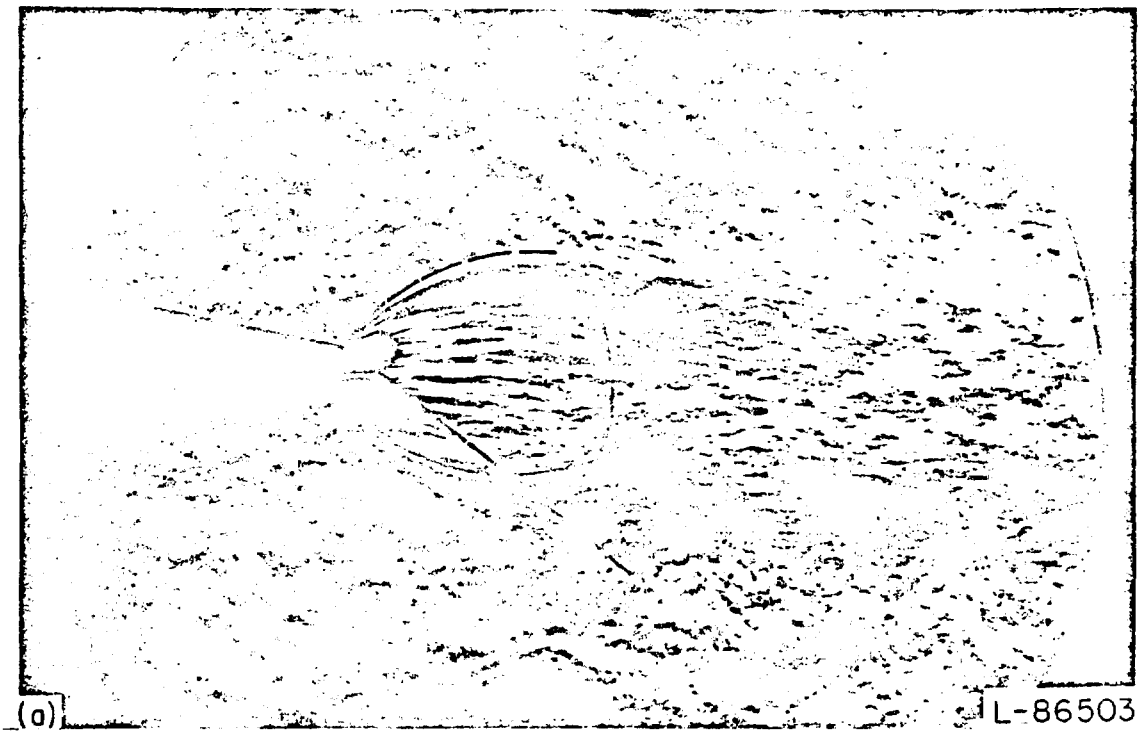

(a) $M_i = 1.0$; $\theta_N = 0°$; $p_i/p_\infty = 24.6$.

(b) $M_i = 2.0$; $\theta_N = 15°$; $p_i/p_\infty = 6.97$.

FIGURE 22.—Examples of circular-arc boundaries given by ρ/d_i superposed on schlieren photographs.

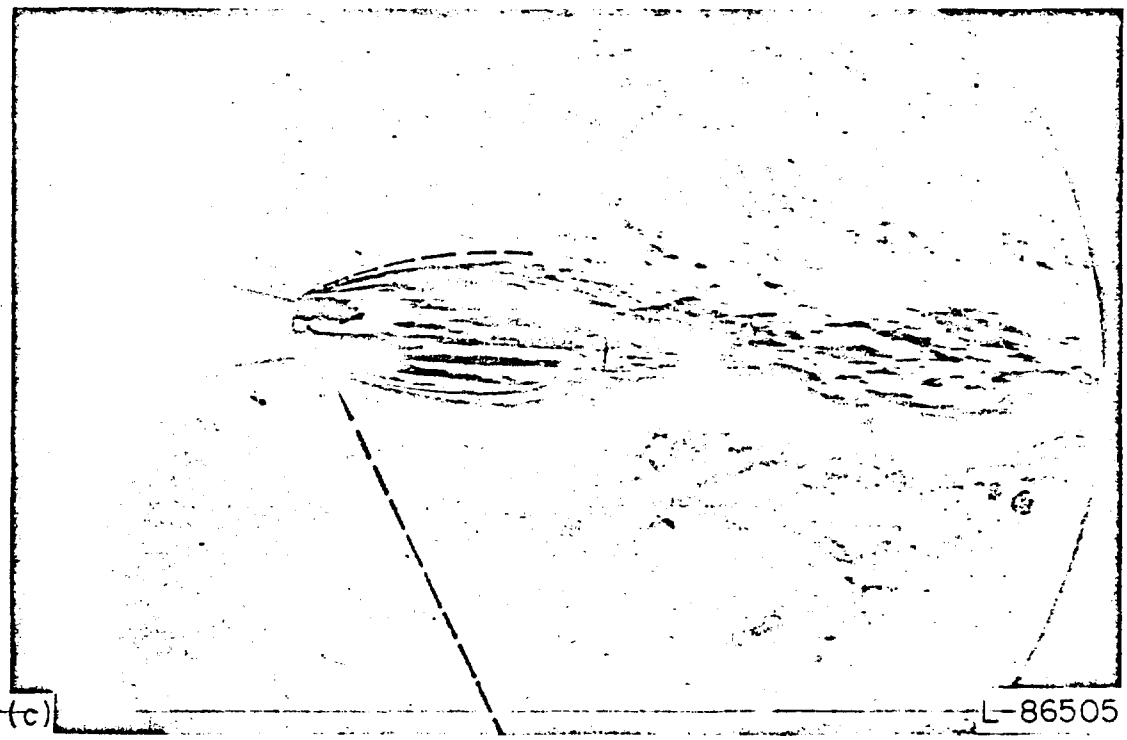

(c) $M_j=2.5$; $\theta_N=5°$; $p_j/p_\infty=6.43$.

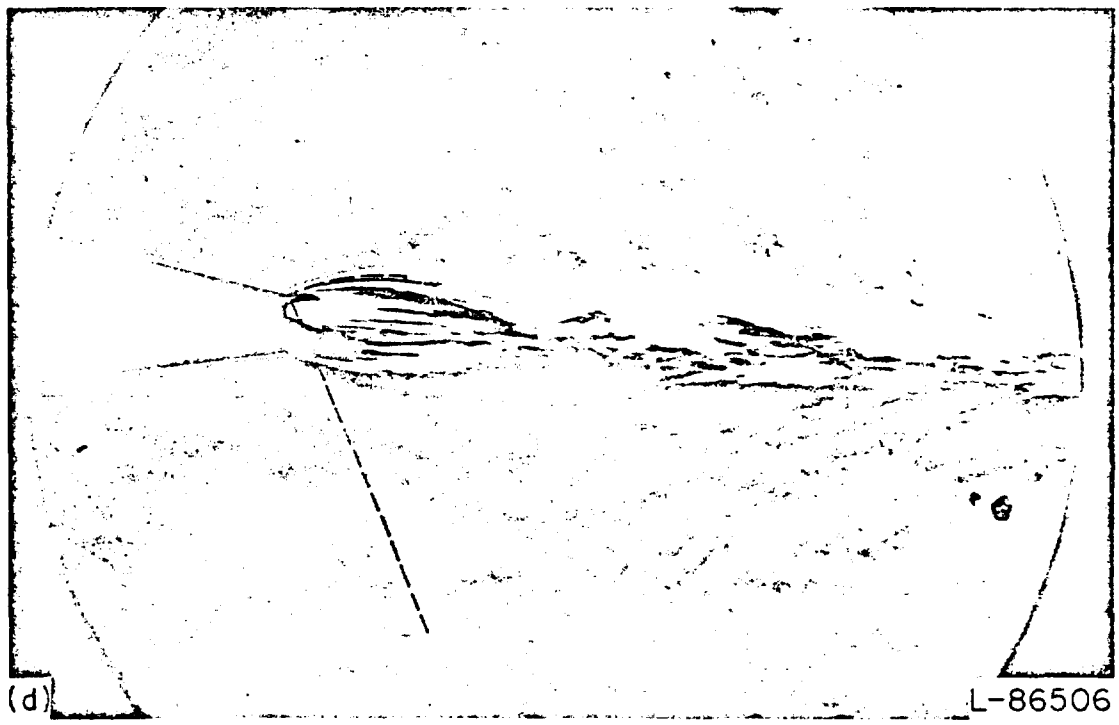

(d) $M_j=3.0$; $\theta_N=15°$; $p_j/p_\infty=2.54$.

FIGURE 22.—Concluded.

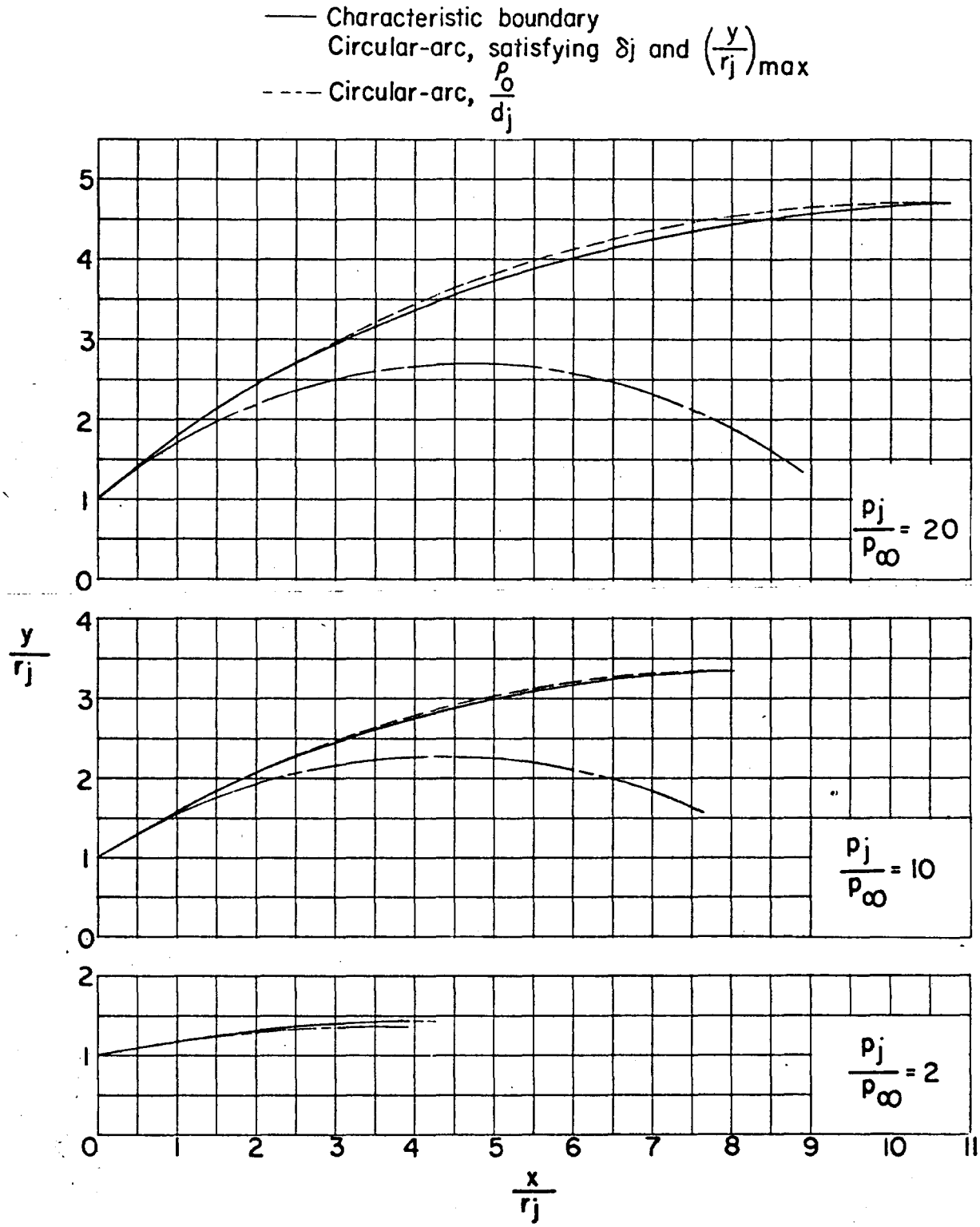

FIGURE 23.—Comparison of jet boundary given by characteristic calculations, circular-arc boundary passing through $\left(\frac{y}{r_j}\right)_{max}$, and the circular-arc defined by initial radius of curvature. $M_j = 2.00$.

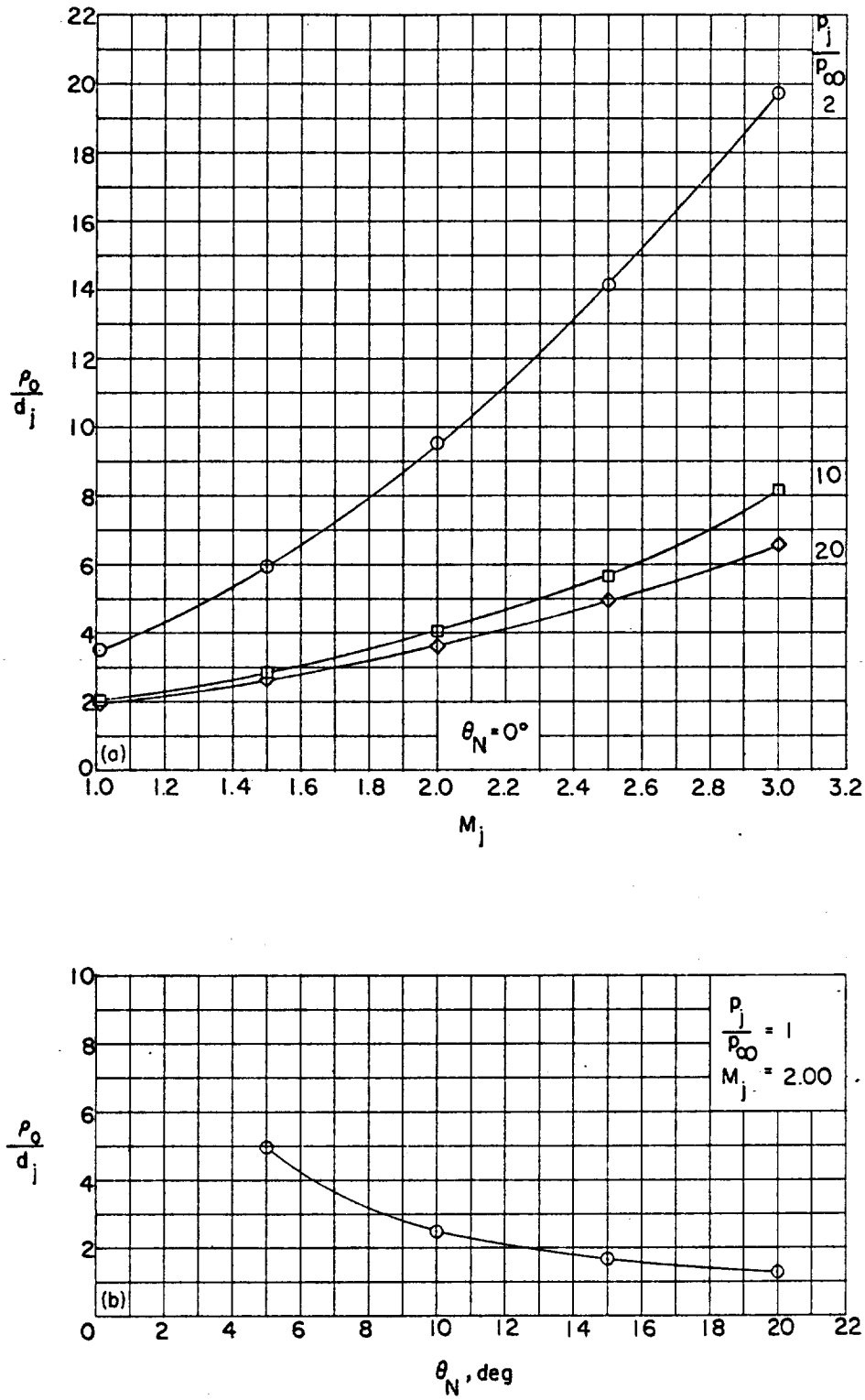

(a) Effects of jet Mach number and jet pressure ratio.

(b) Effects of nozzle divergence angle.

FIGURE 24.—Theoretical calculations of the nondimensional initial radius of curvature of the jet boundary. $\gamma_j = 1.400$.

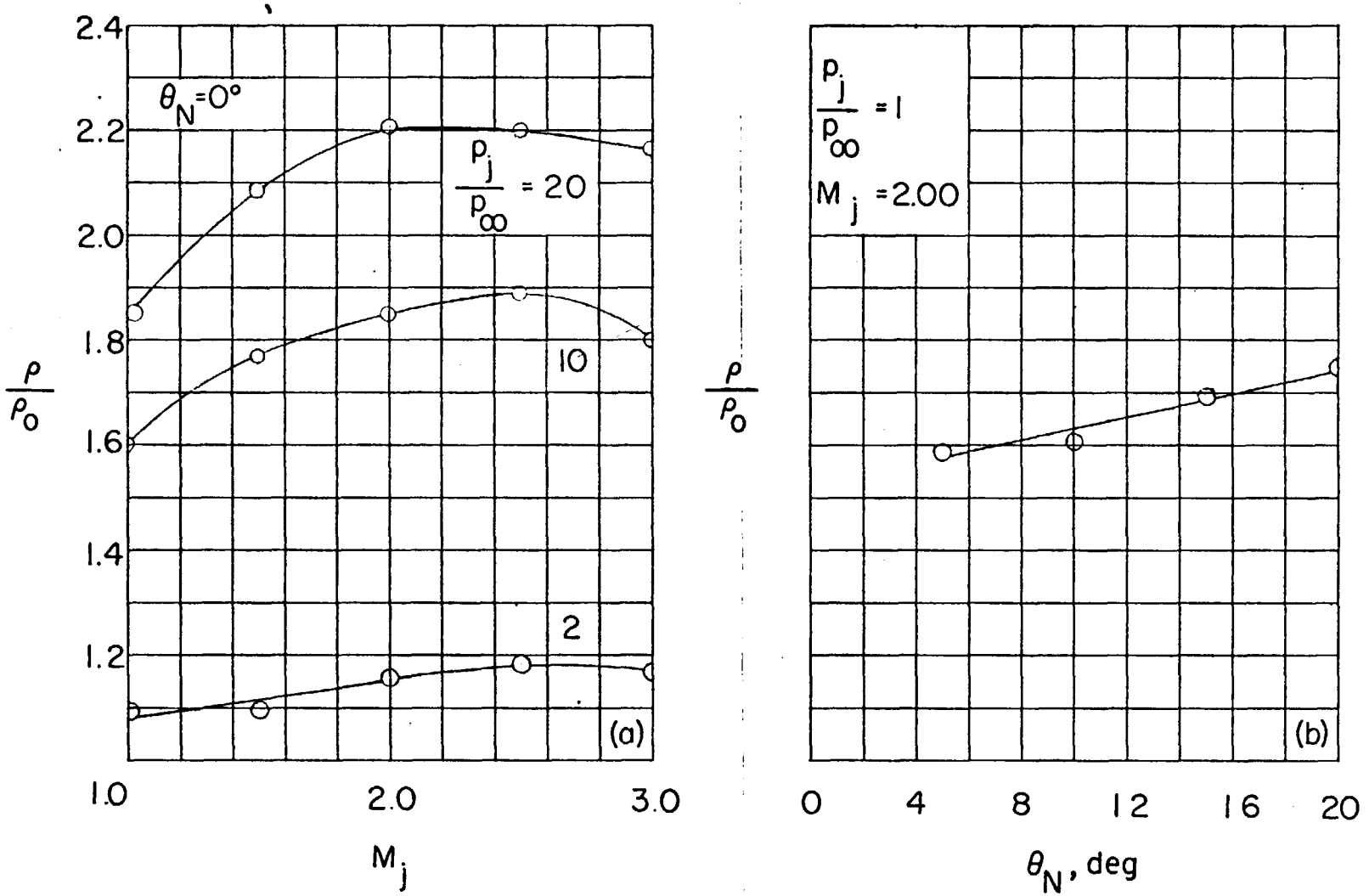

(a) Effects of jet Mach number and jet pressure ratio. (b) Effects of nozzle divergence angle.

FIGURE 25.—Ratio of average radius of curvature, as obtained from characteristic solution for $\left(\frac{y}{r_i}\right)_{max}$, to theoretical initial radius of curvature of jet boundary. γ_j=1.400.

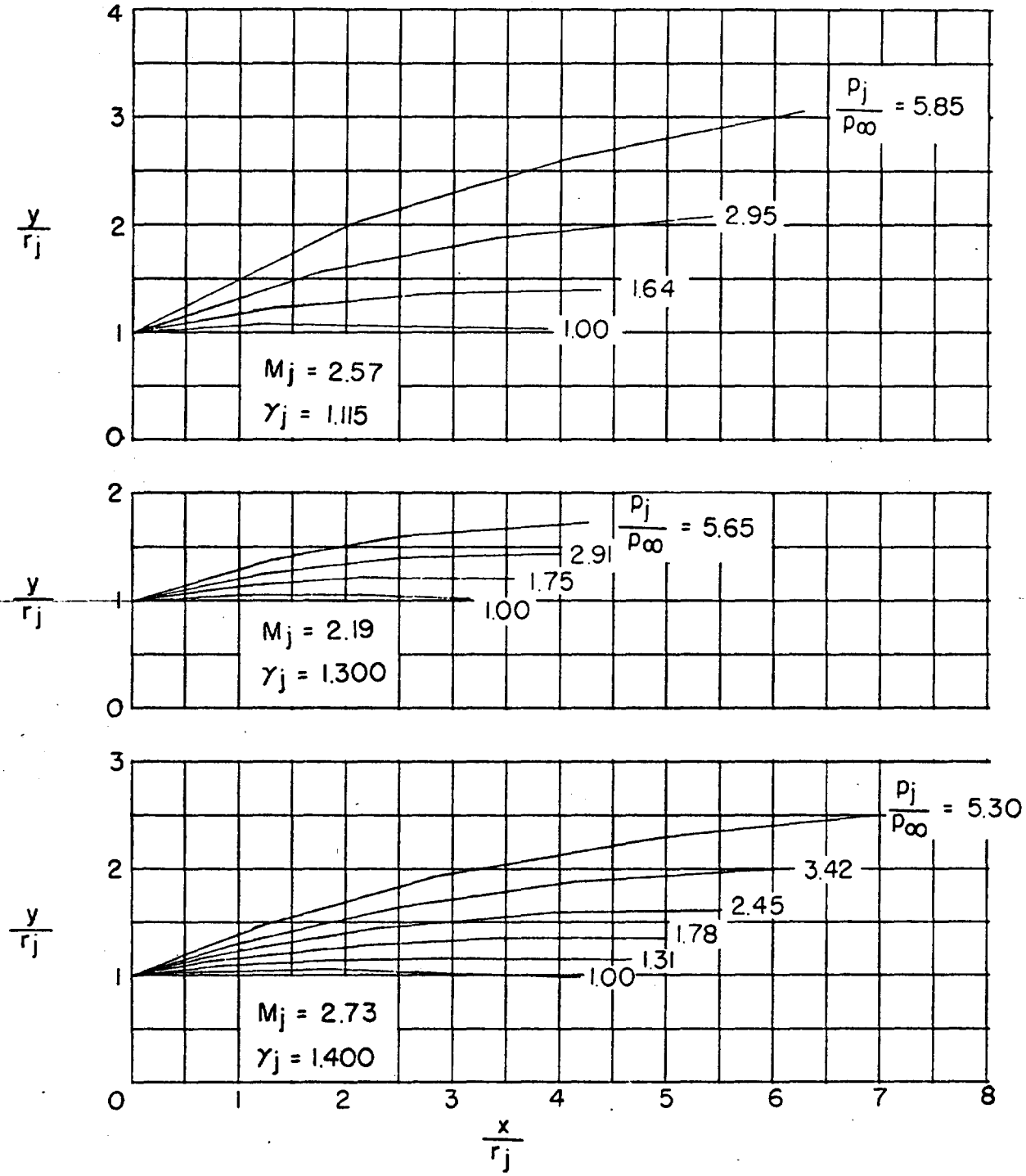

FIGURE 26.—Calculations of jet boundaries by Johannesen (ref. 2). $\theta_N = 4°$.

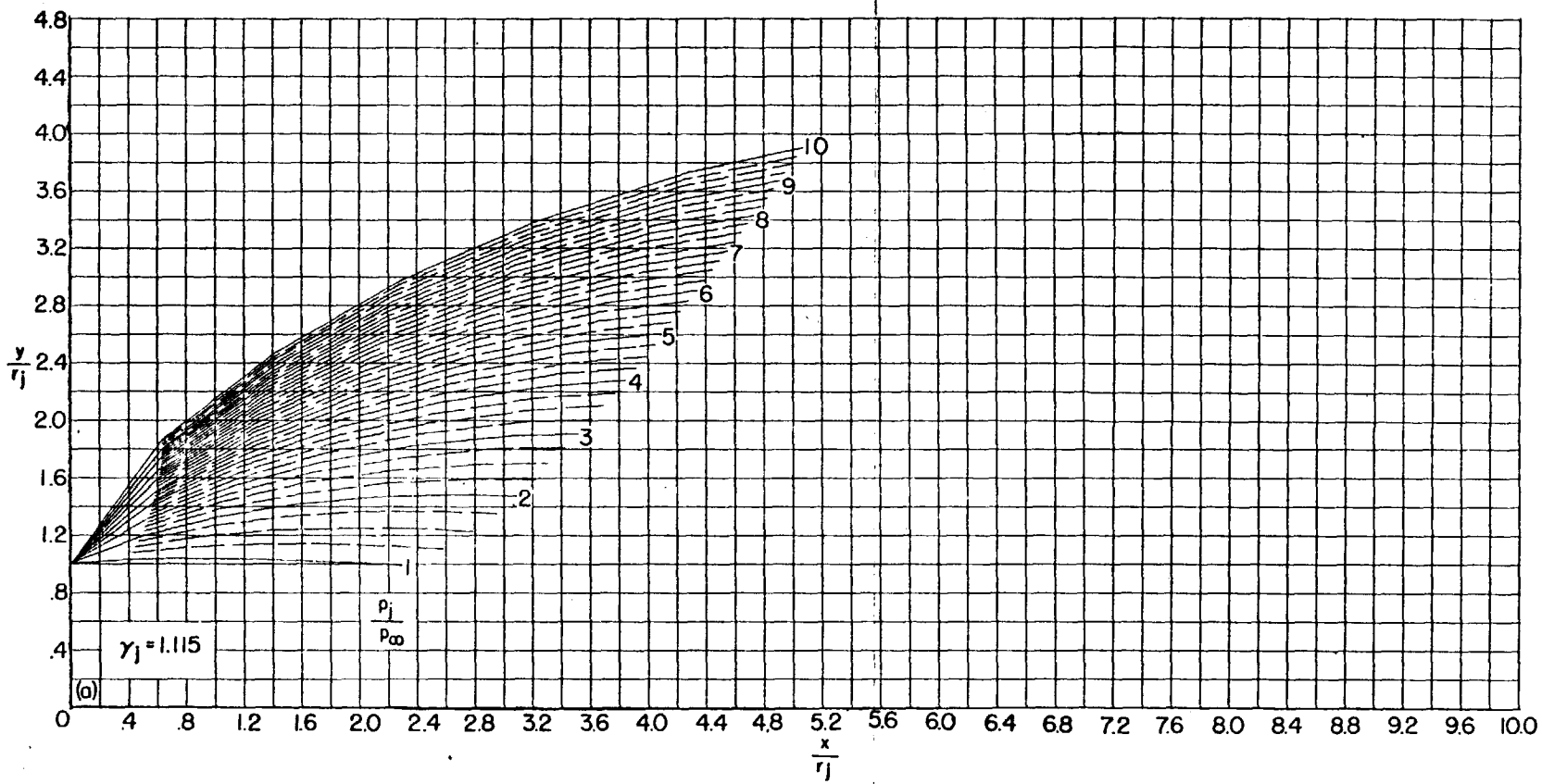

(a) $\theta_N = 5°$.

FIGURE 27.—Jet boundaries at $M_j = 1.5$ for jet pressure ratios from 1 to 10. (Dashed boundaries denote changes in p_j/p_∞ of 0.25.)

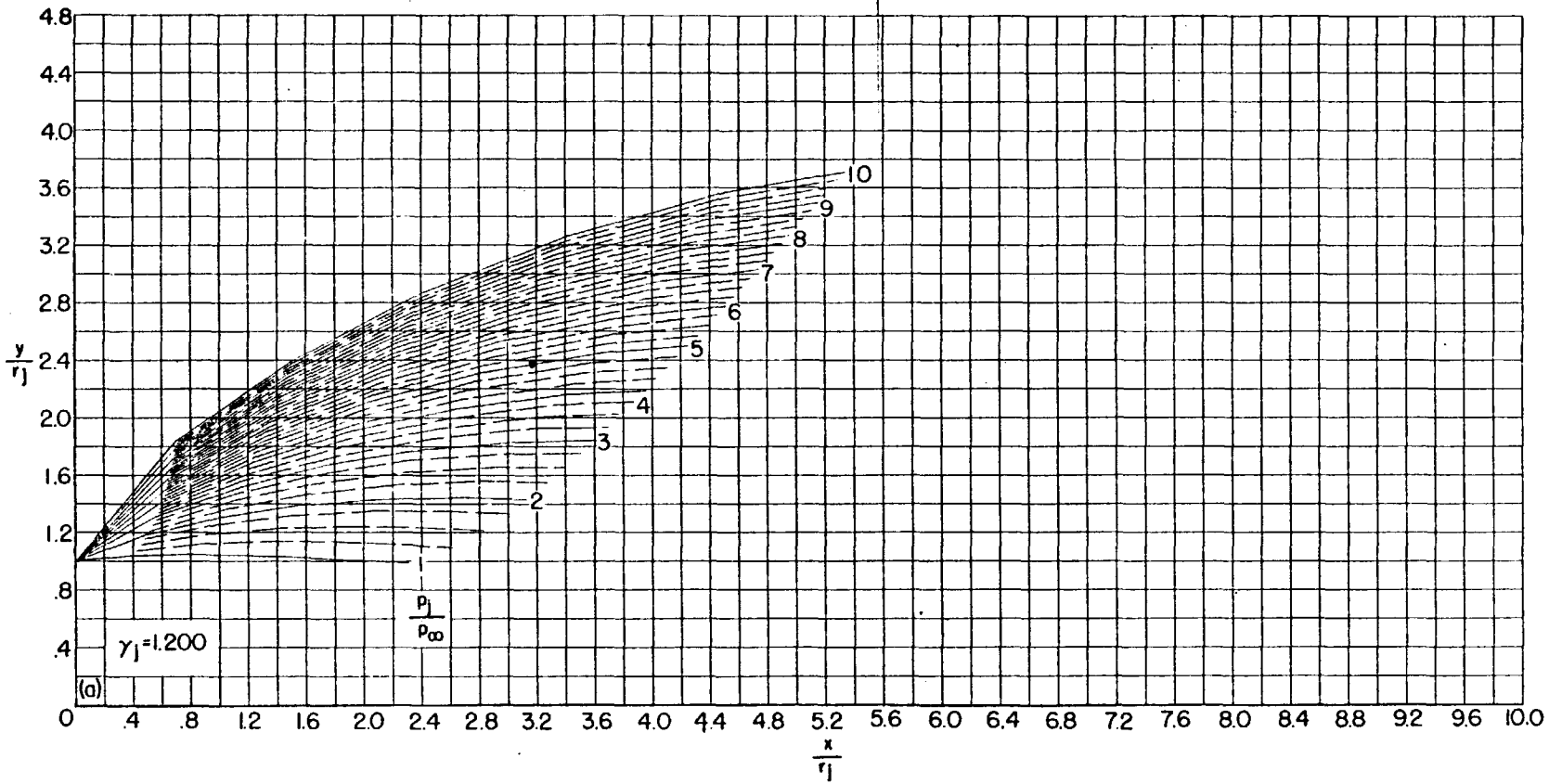

(a) $\theta_N = 5°$. Continued.

FIGURE 27.—Continued.

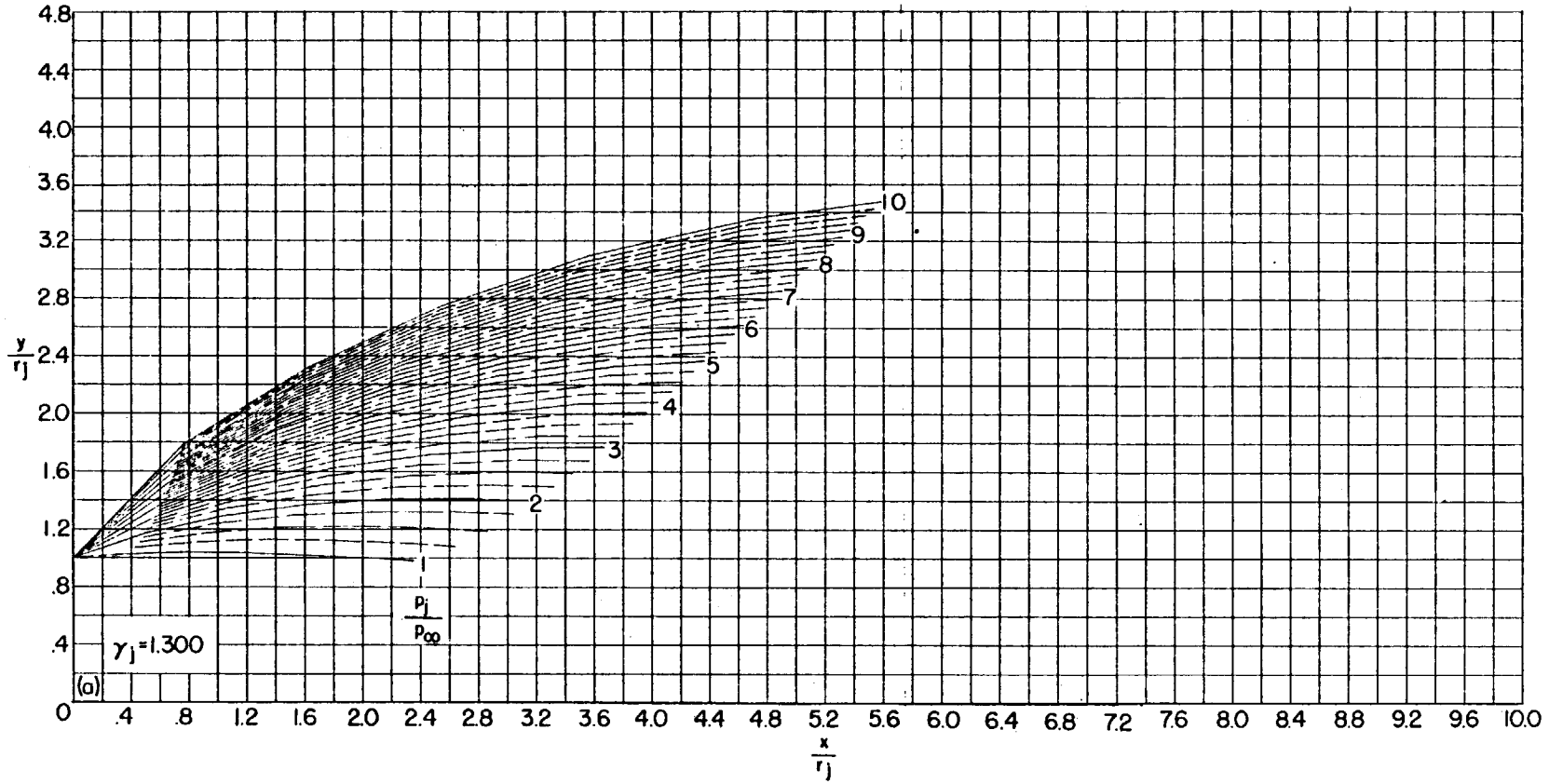

(a) $\theta_N = 5°$. Continued.

FIGURE 27.— Continued.

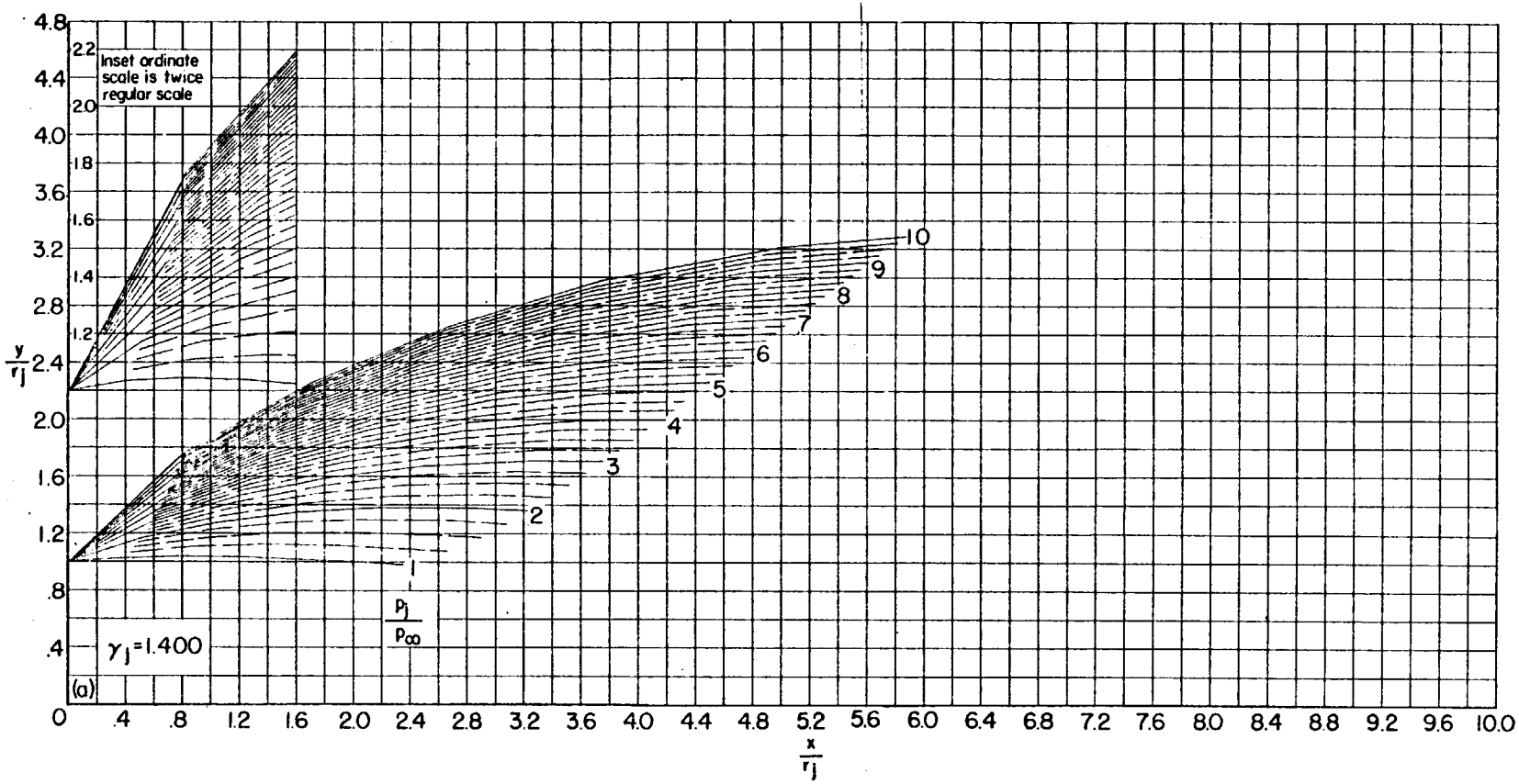

(a) θ_N=5°. Continued.

FIGURE 27.—Continued.

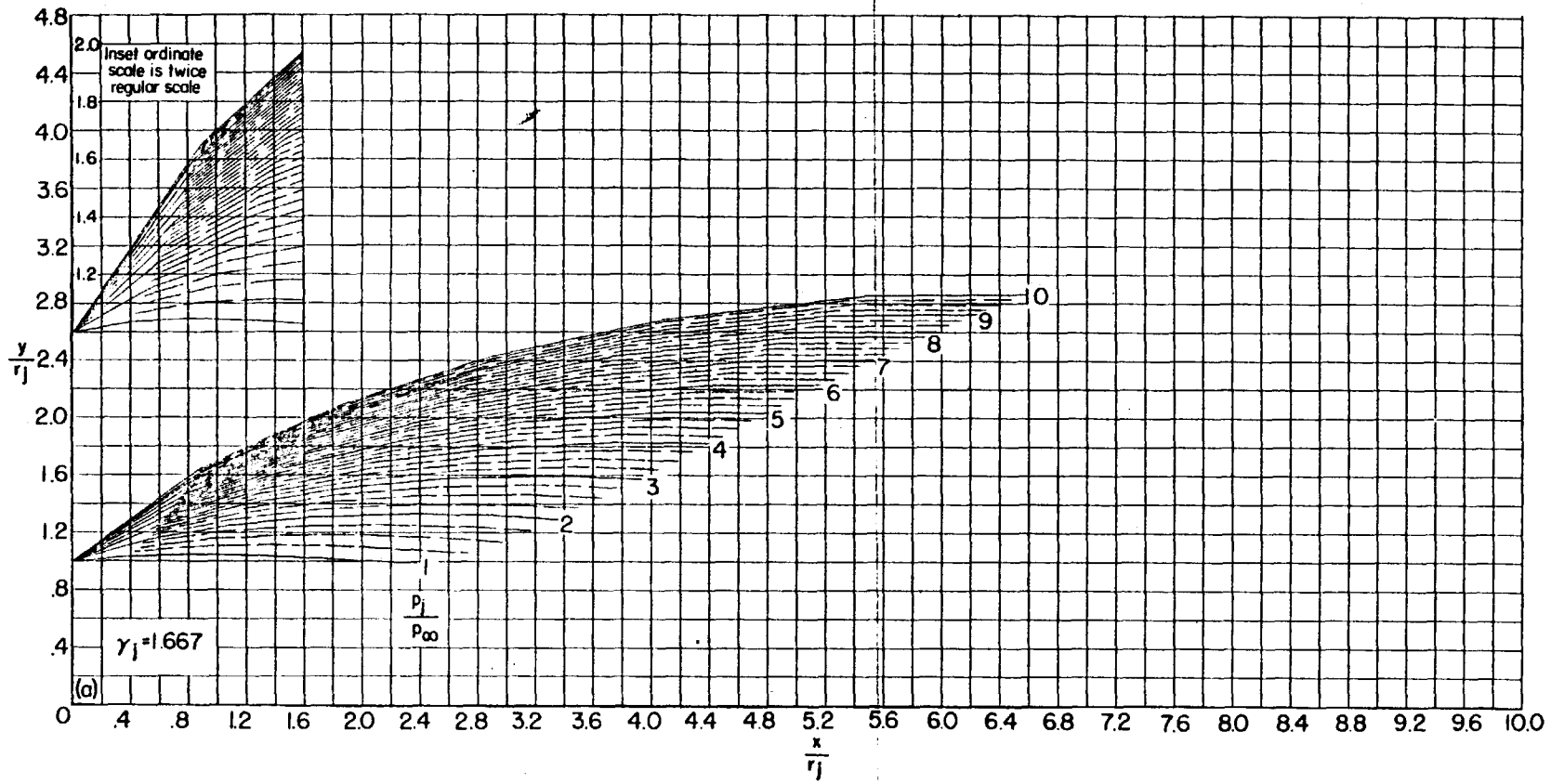

(a) $\theta_N = 5°$. Concluded.

FIGURE 27.—Continued.

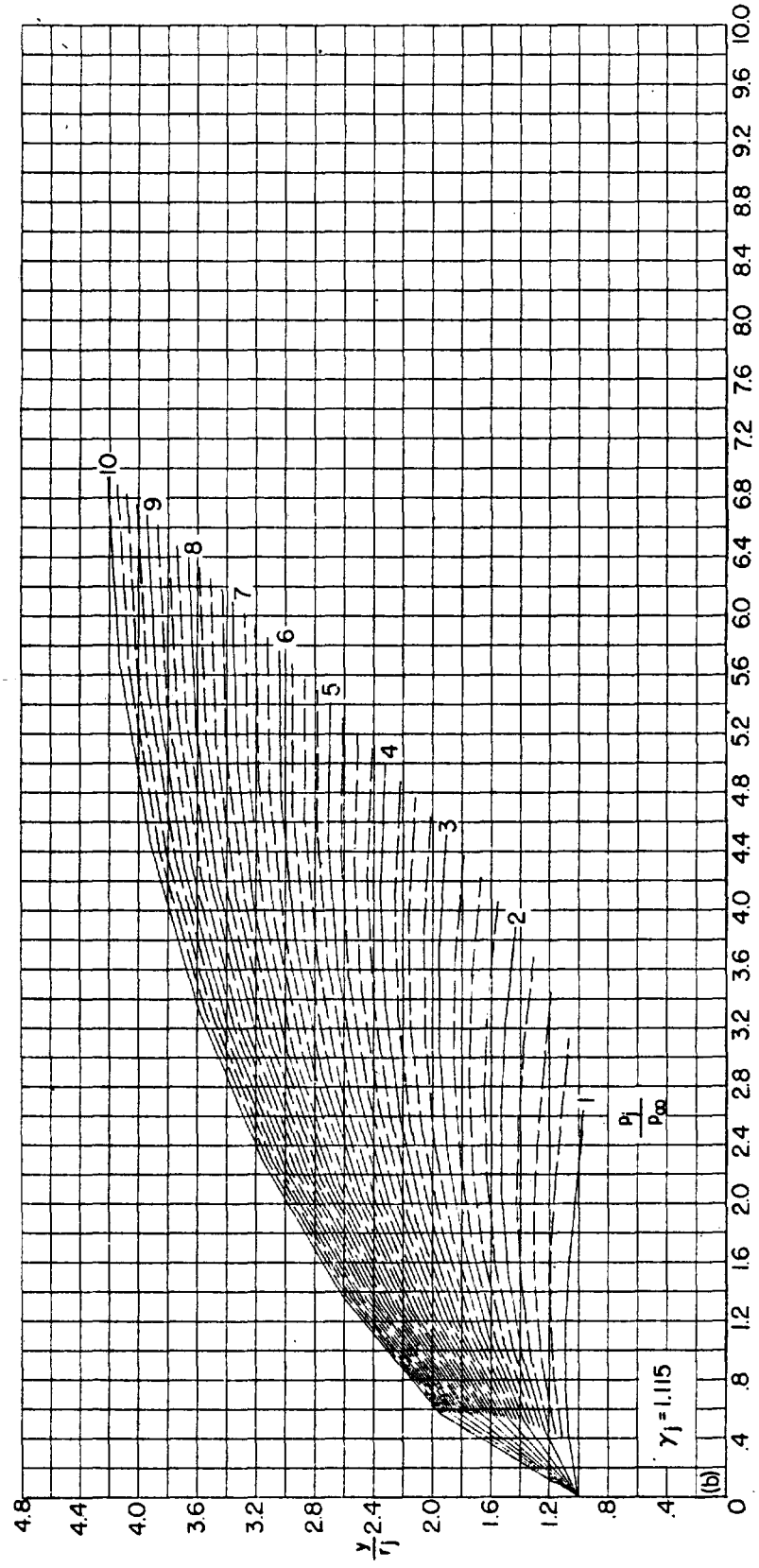

(b) $\theta_N = 10°$.

FIGURE 27.—Continued.

502683 O—59——9

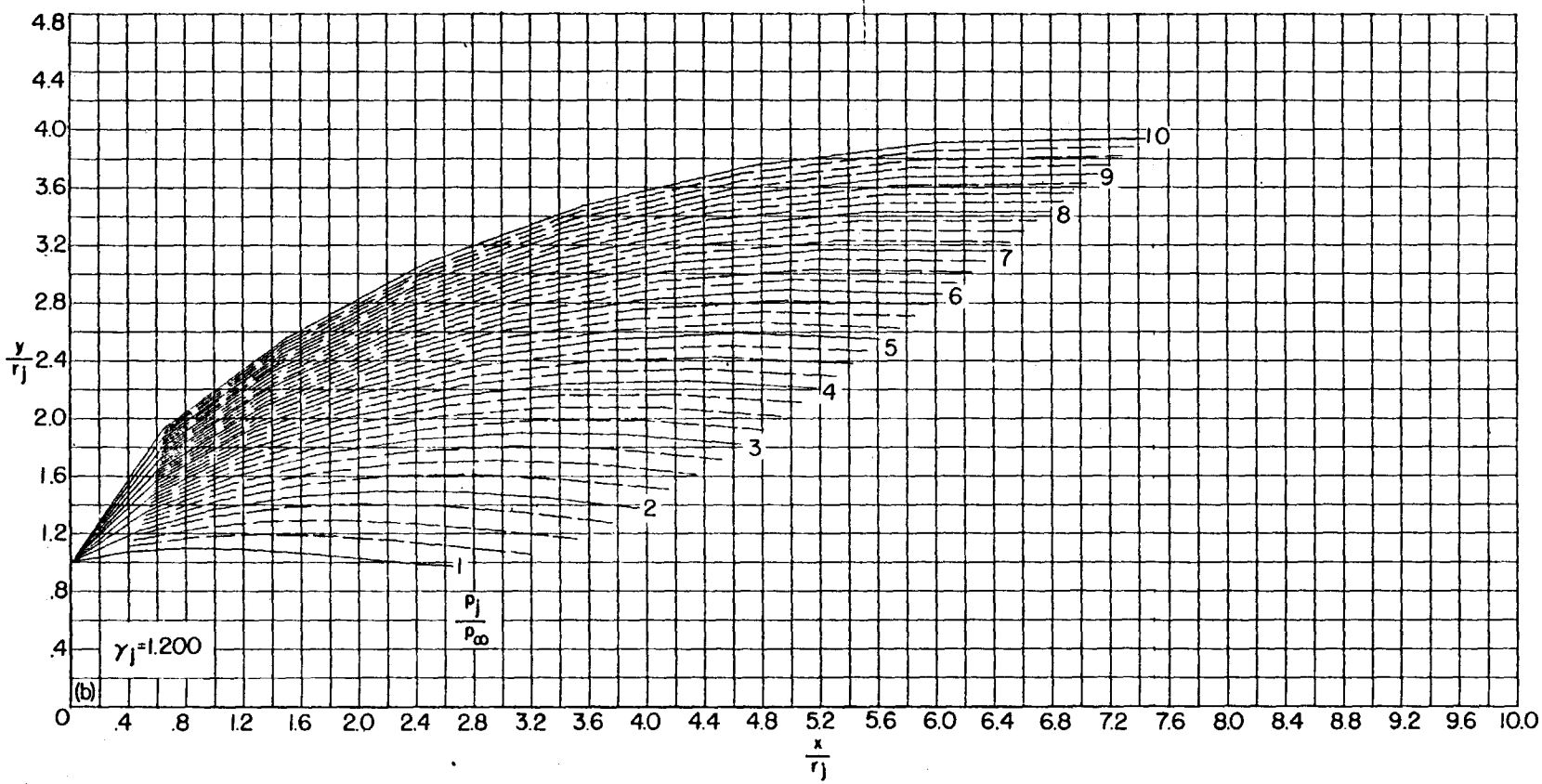

(b) $\theta_N = 10°$. Continued.

FIGURE 27.—Continued.

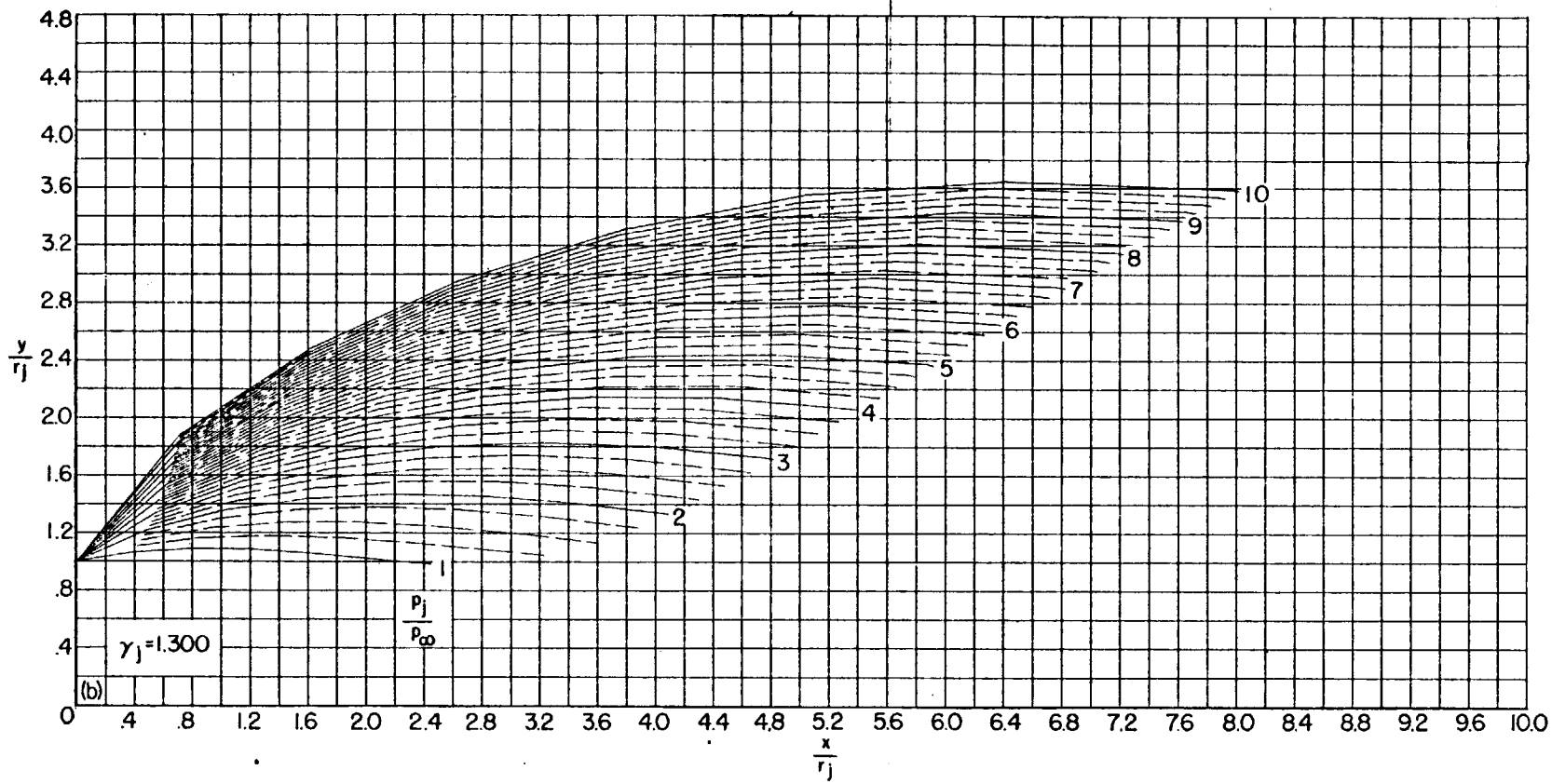

(b) $\theta_N = 10°$. Continued.

FIGURE 27.--Continued.

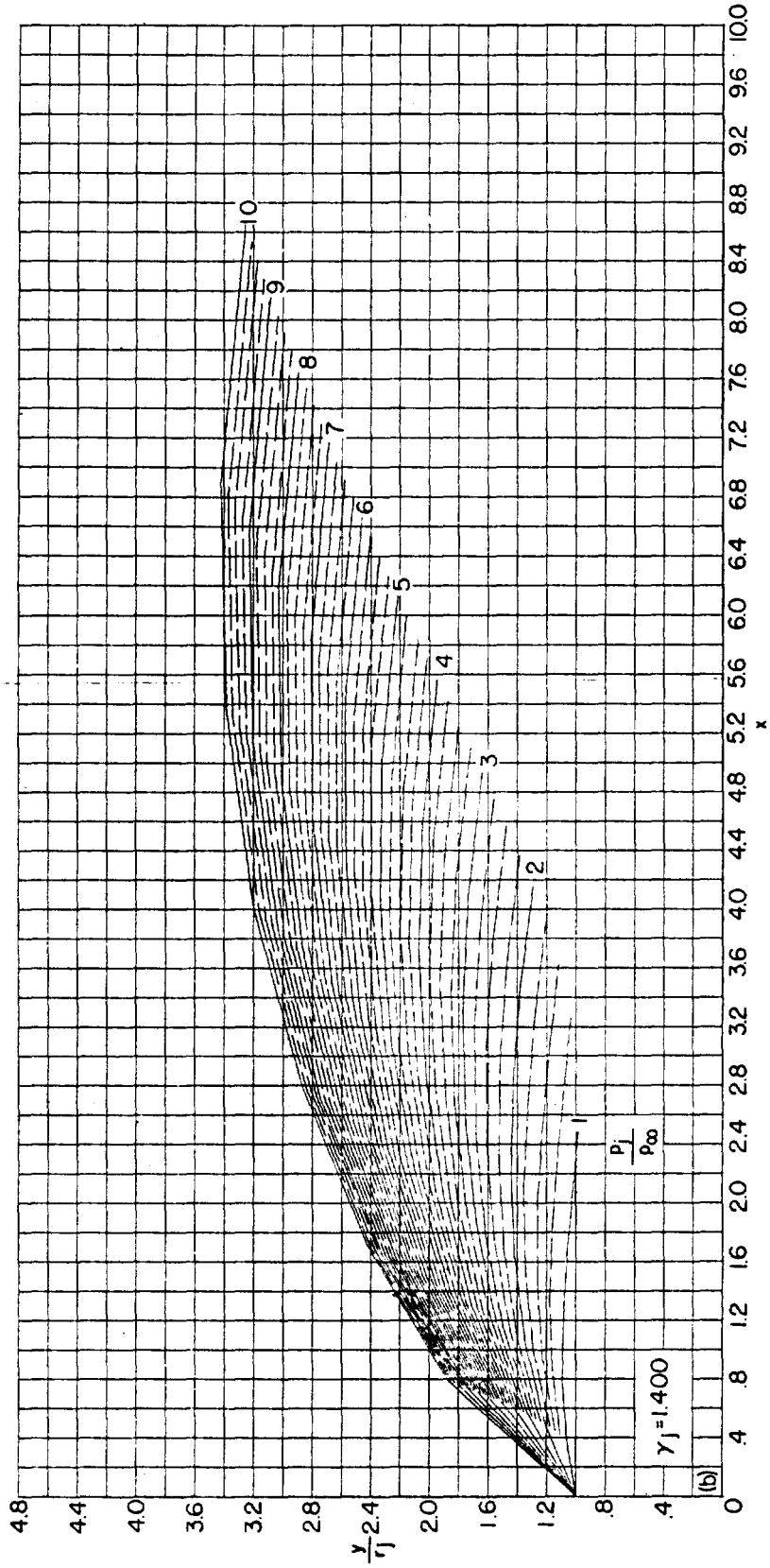

(b) $\theta_N = 10°$. Continued.

FIGURE 27.—Continued.

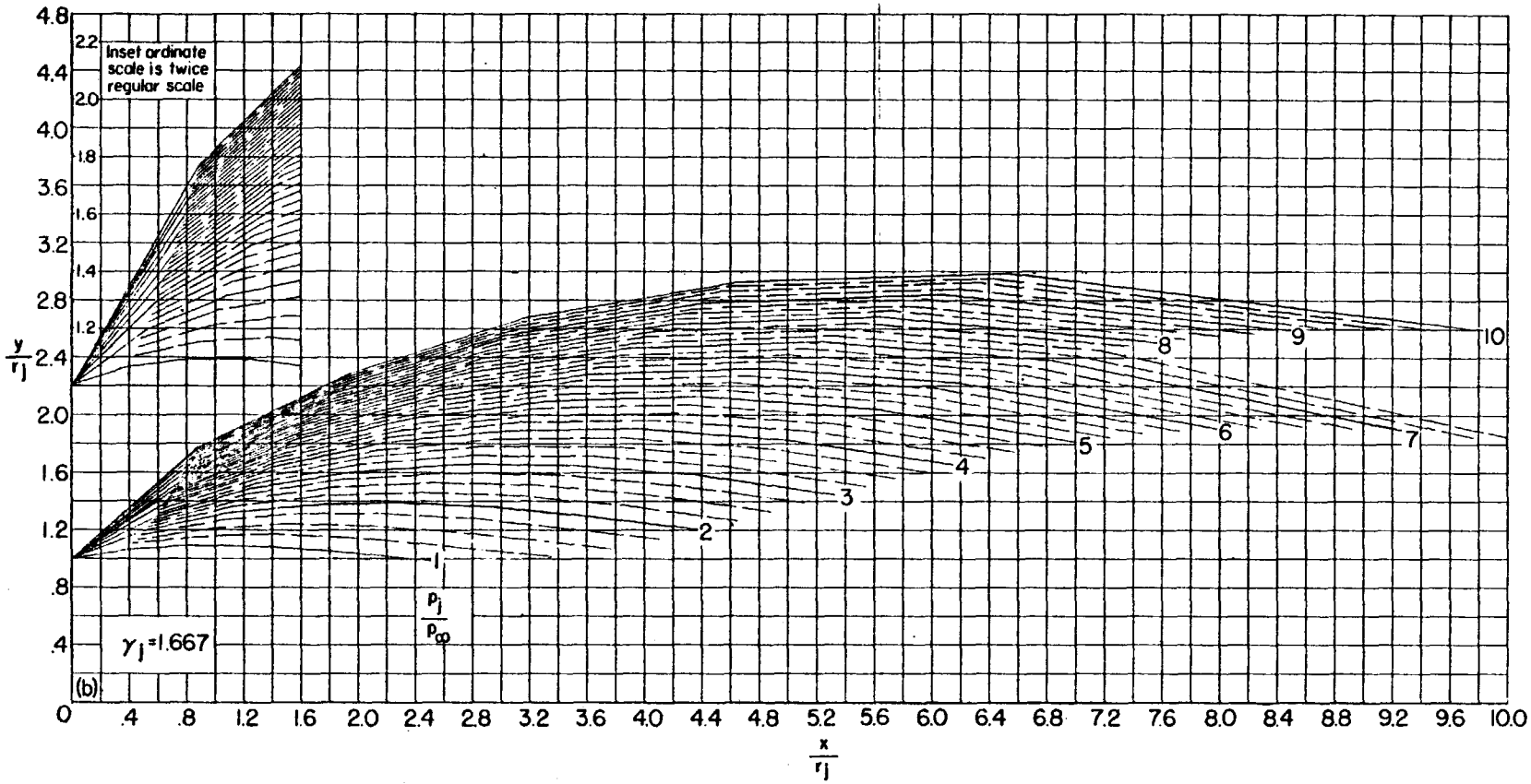

(b) $\theta_N = 10°$. Concluded.

FIGURE 27.—Continued.

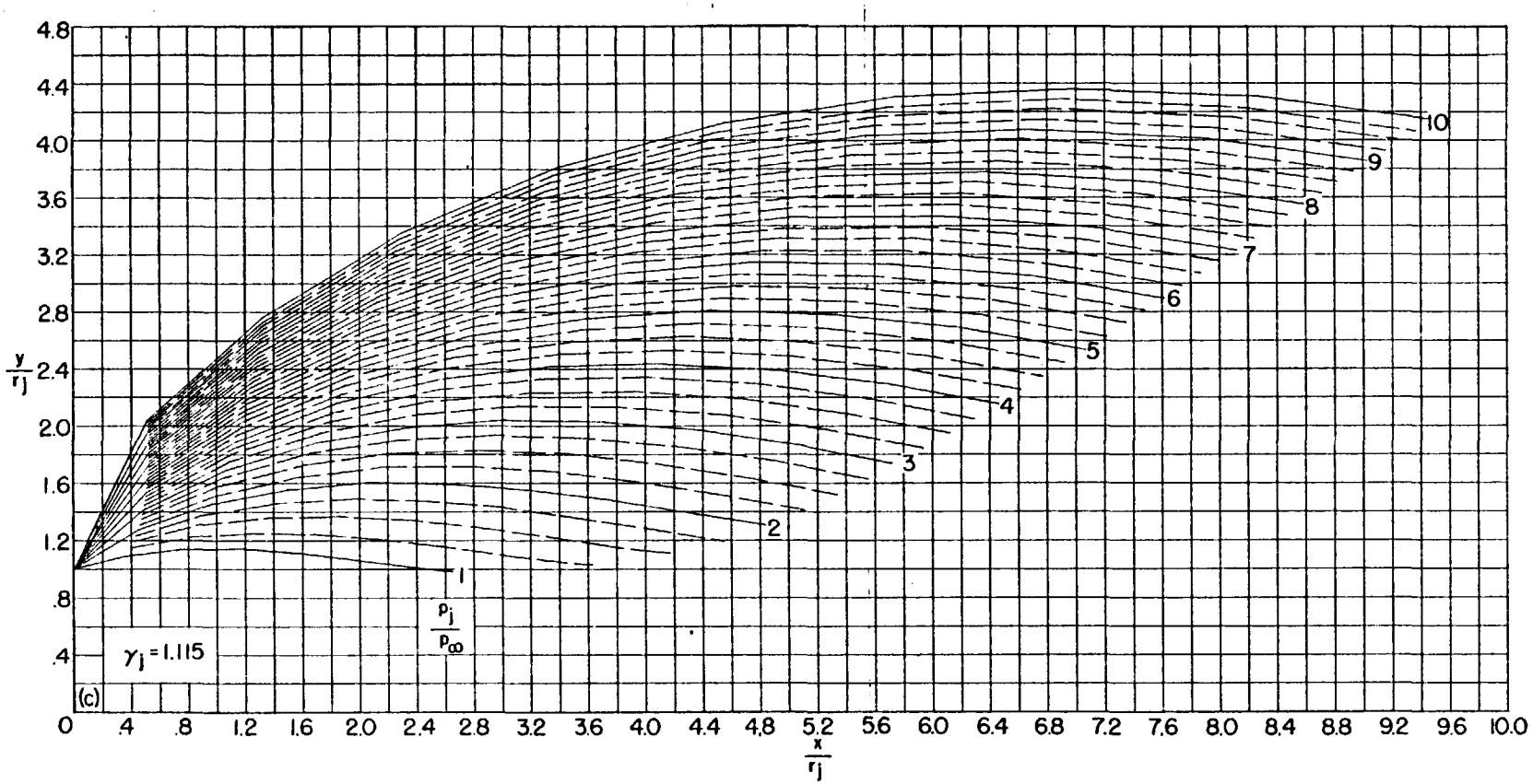

(c) $\theta_N = 15°$.

FIGURE 27.—Continued.

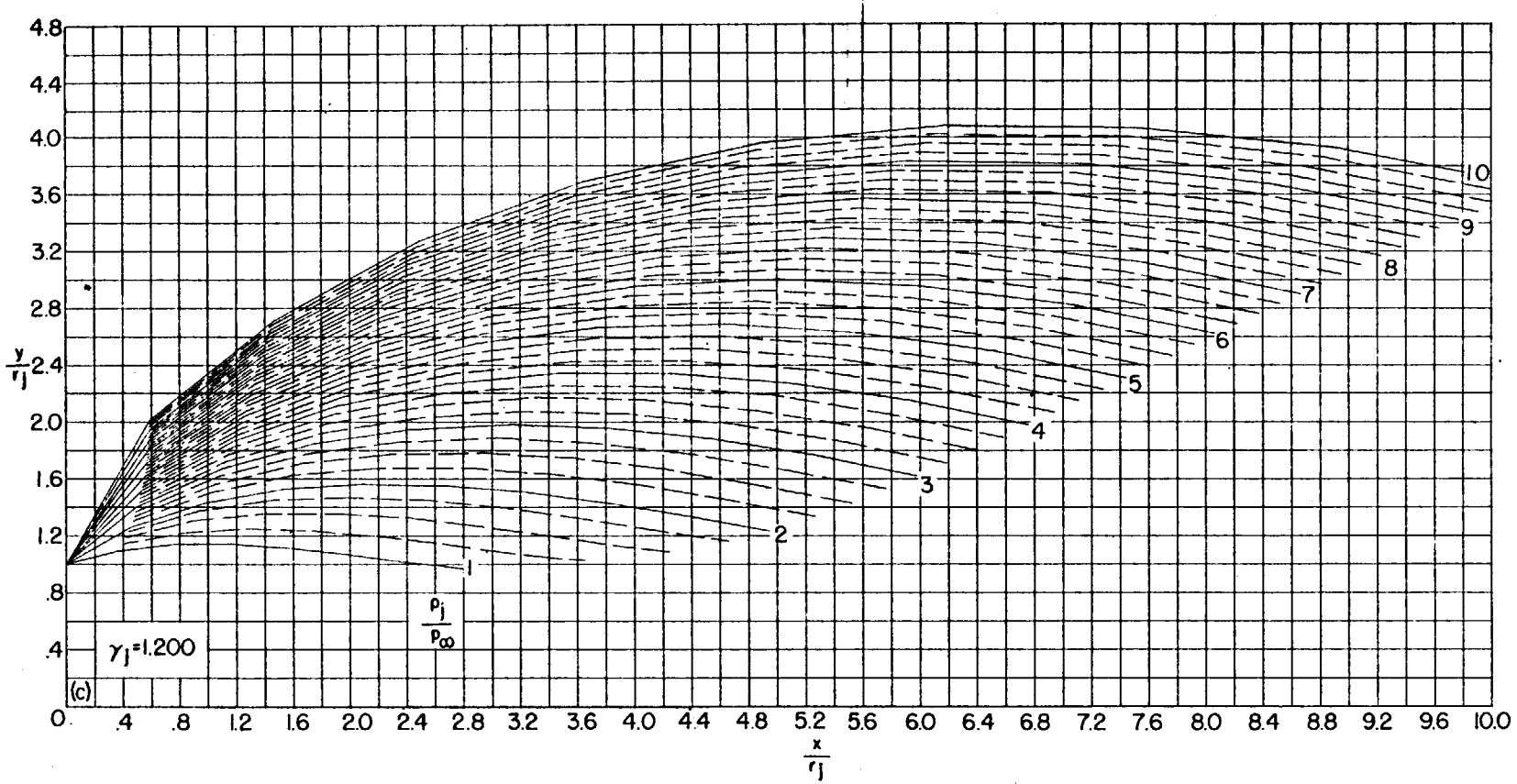

(c) $\theta_N = 15°$. Continued.

FIGURE 27.—Continued.

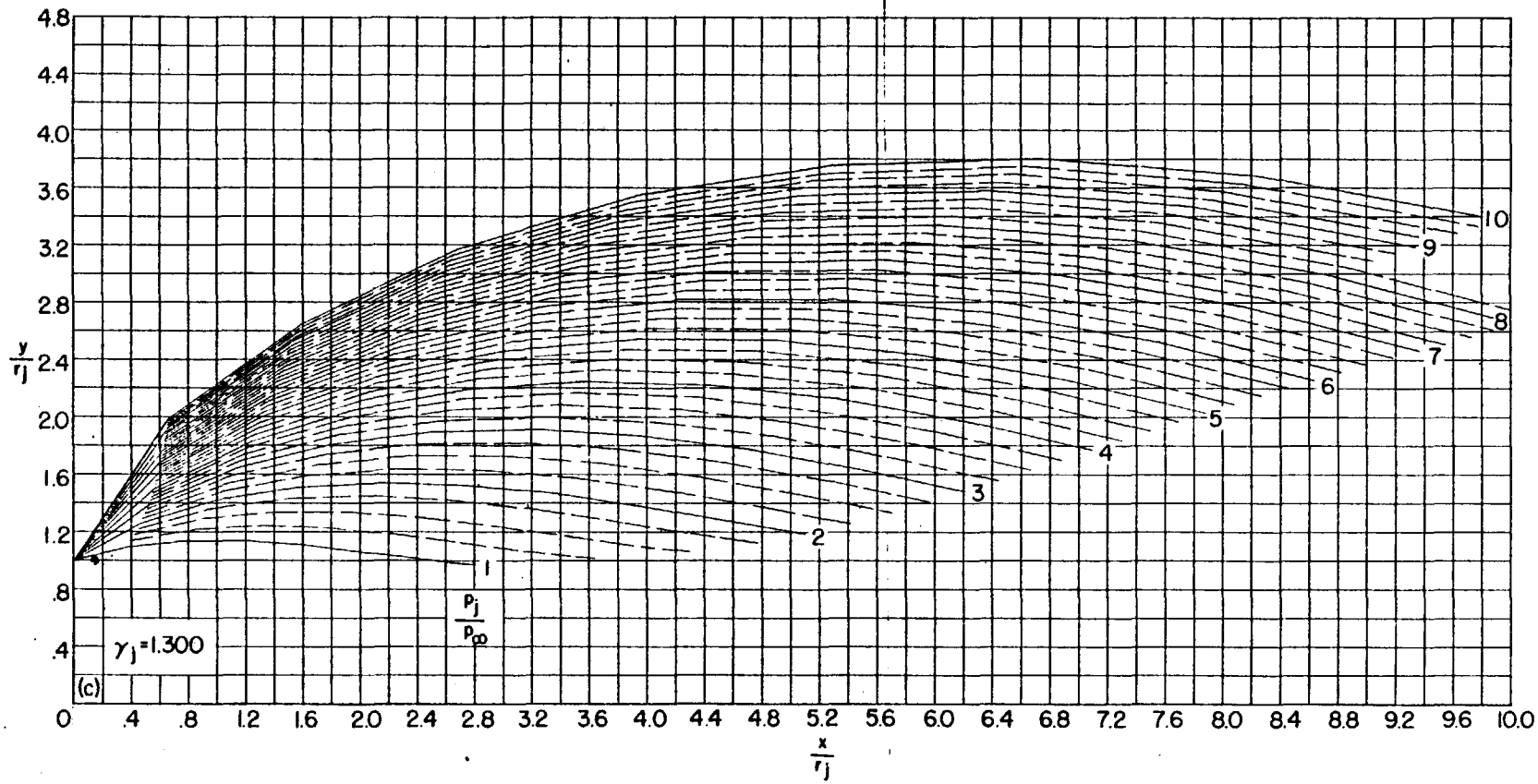

(c) $\theta_N = 15°$. Continued.

FIGURE 27.—Continued.

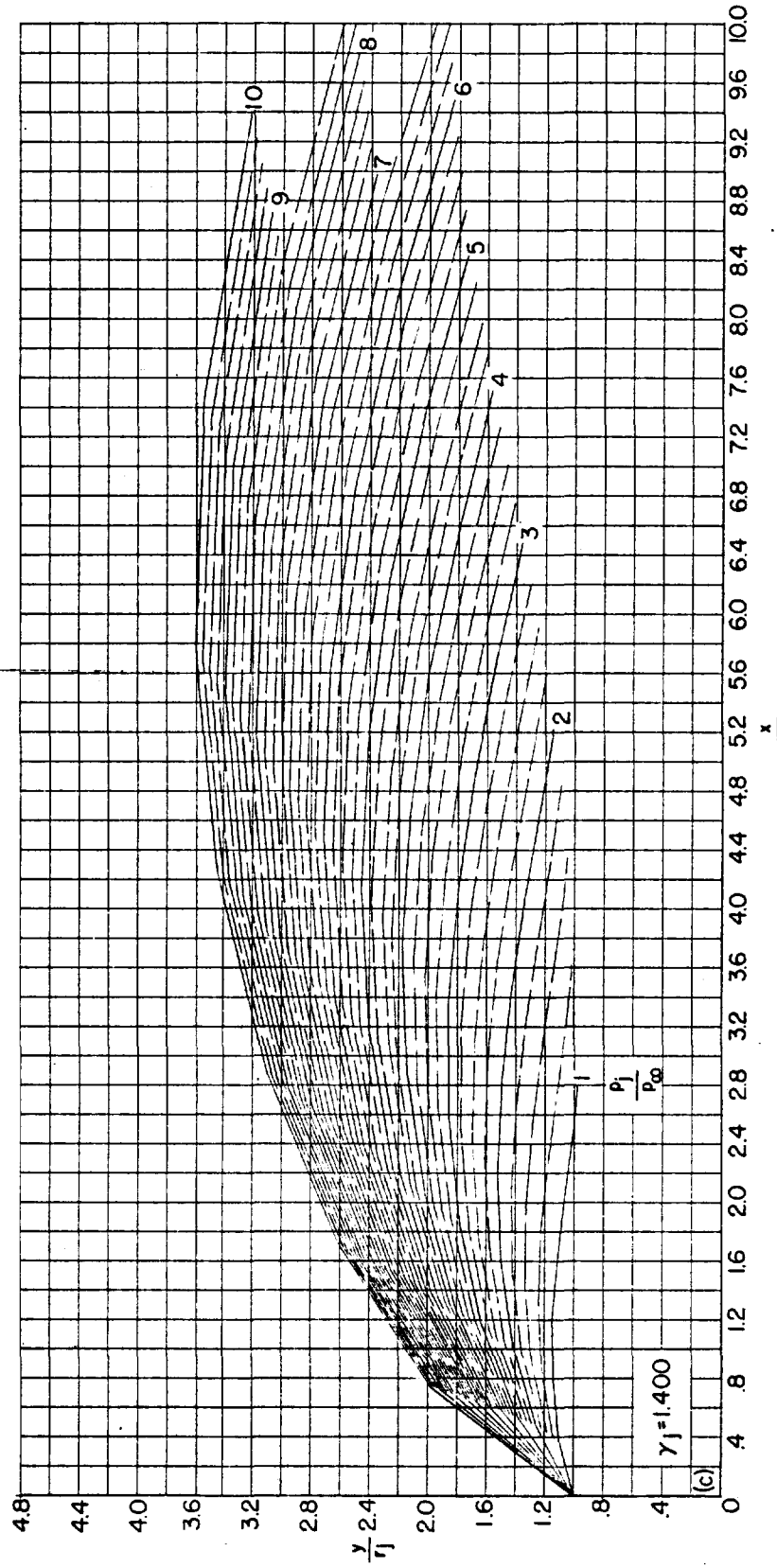

(c) $\theta_N = 15°$. Continued.

FIGURE 27.—Continued.

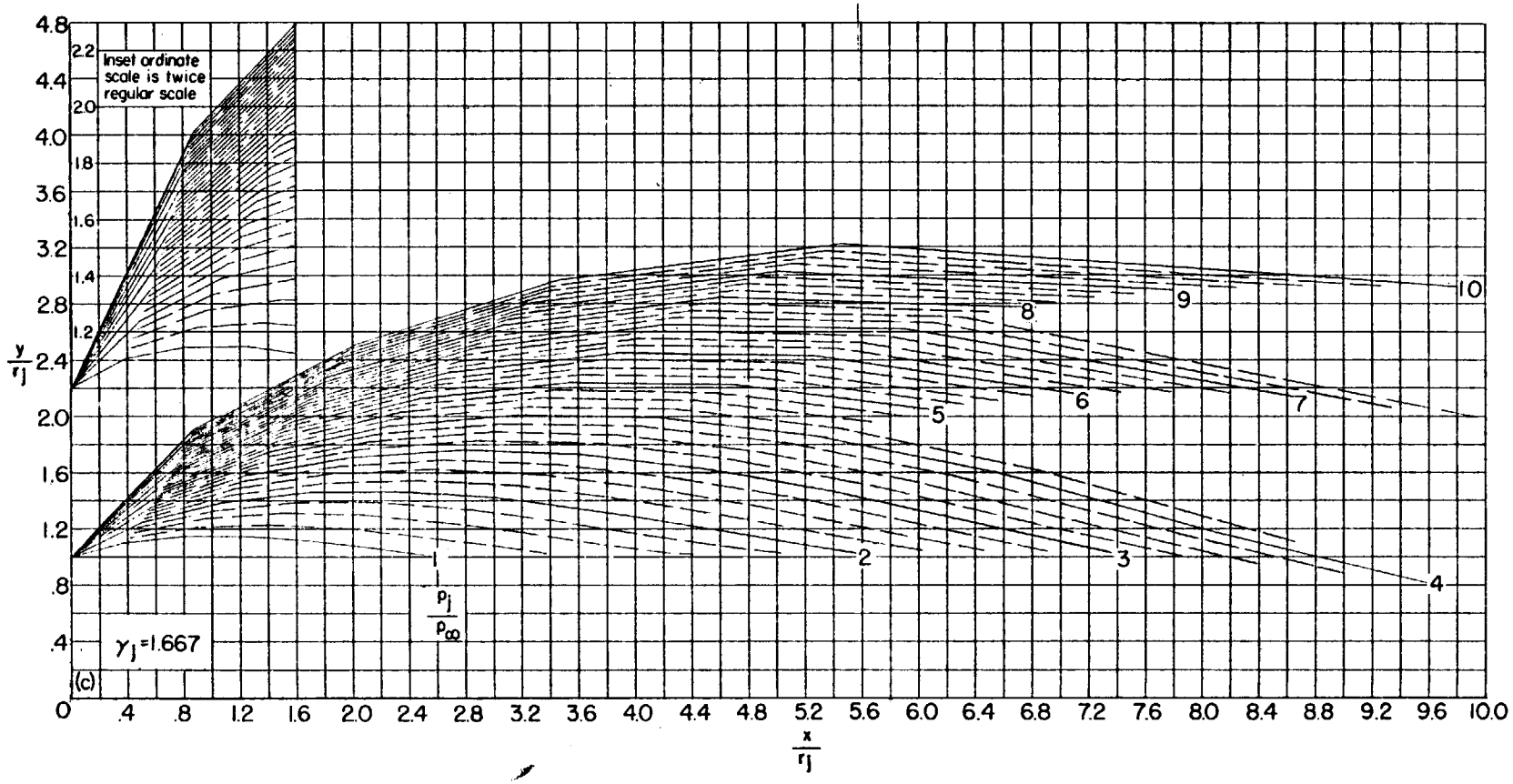

(c) $\theta_N = 15°$. Concluded.

FIGURE 27.—Continued.

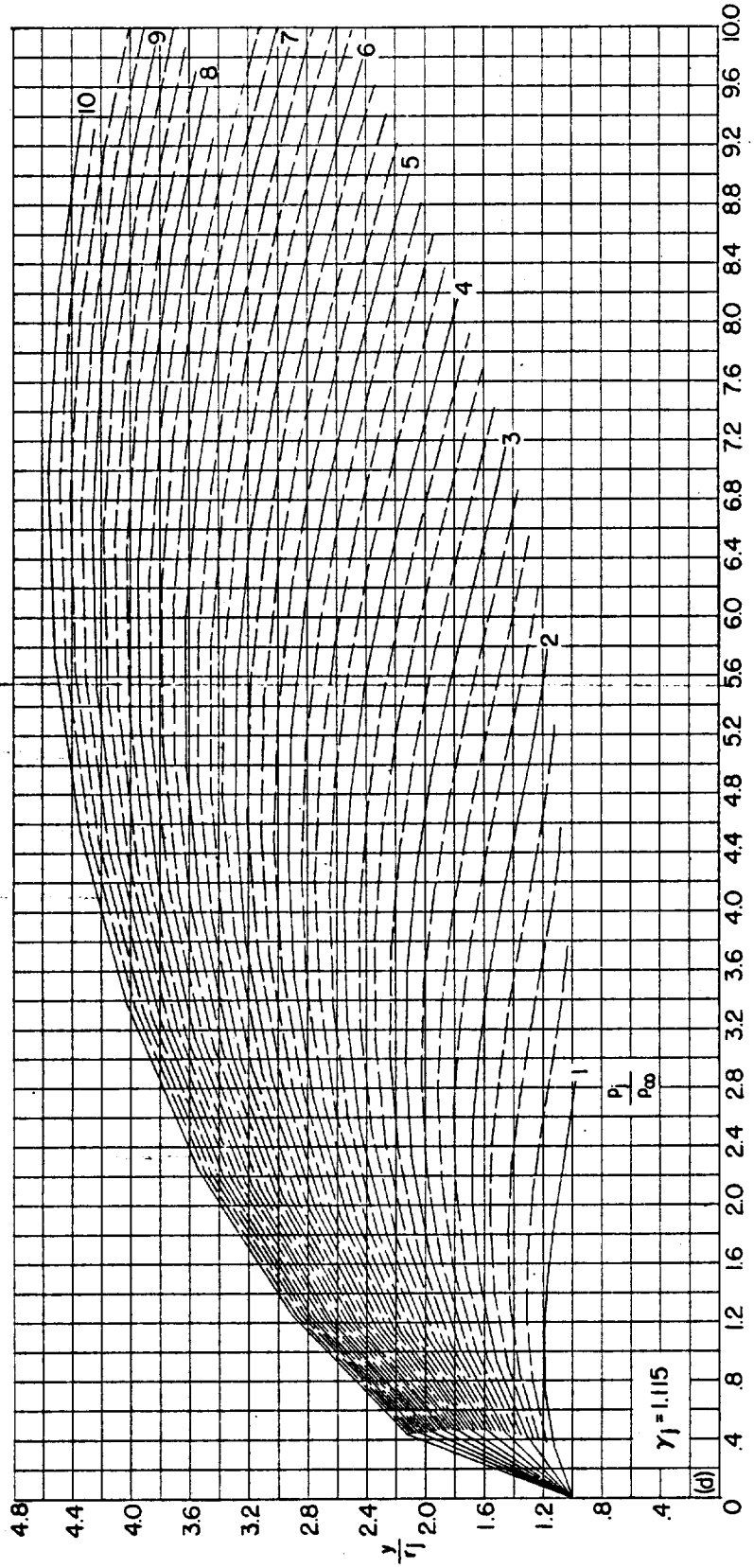

(d) $\theta_N = 20°$.

FIGURE 27.—Continued.

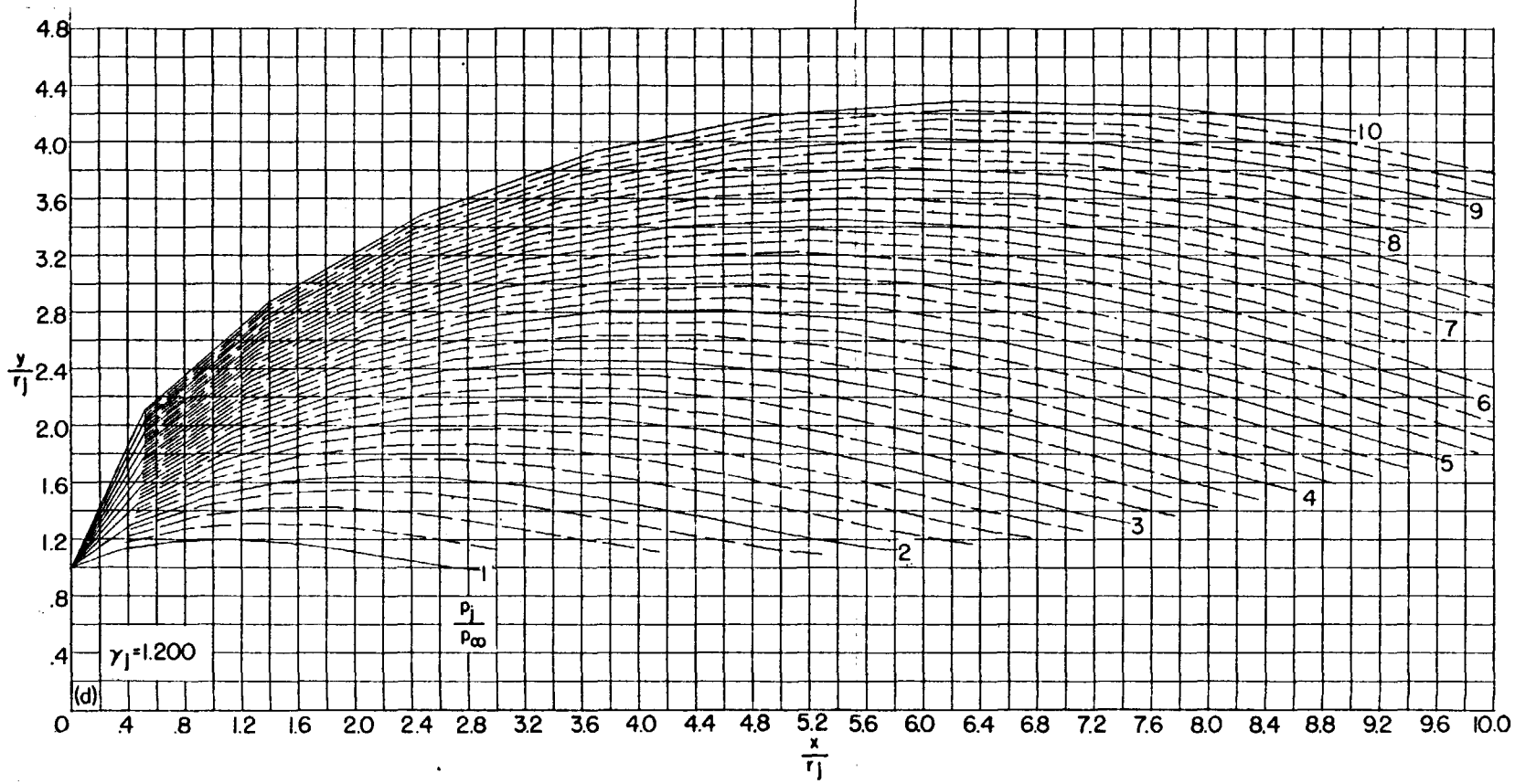

(d) $\theta_N = 20°$. Continued.

FIGURE 27.—Continued.

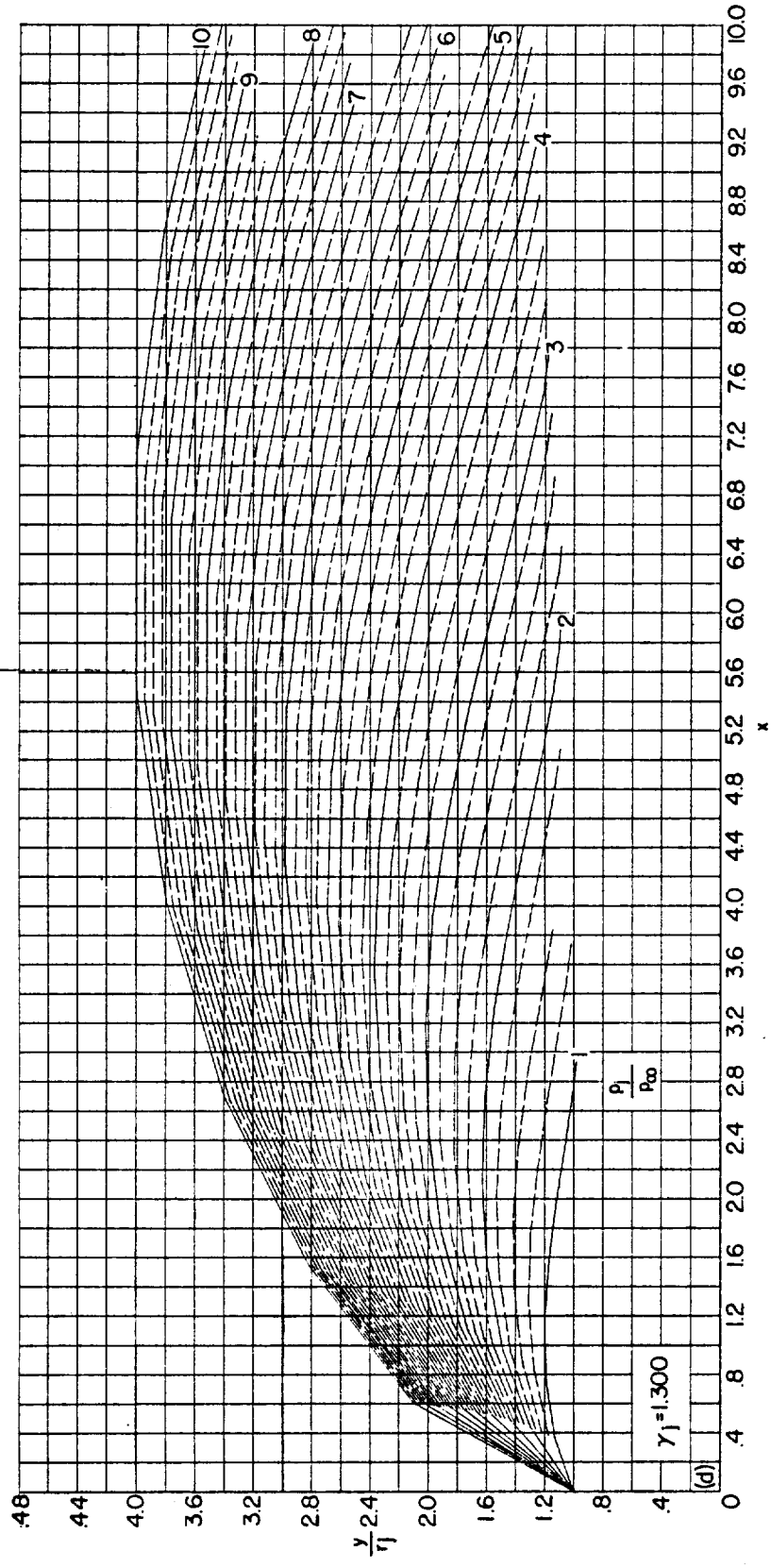

(d) $\theta_N = 20°$. Continued.

FIGURE 27.—Continued.

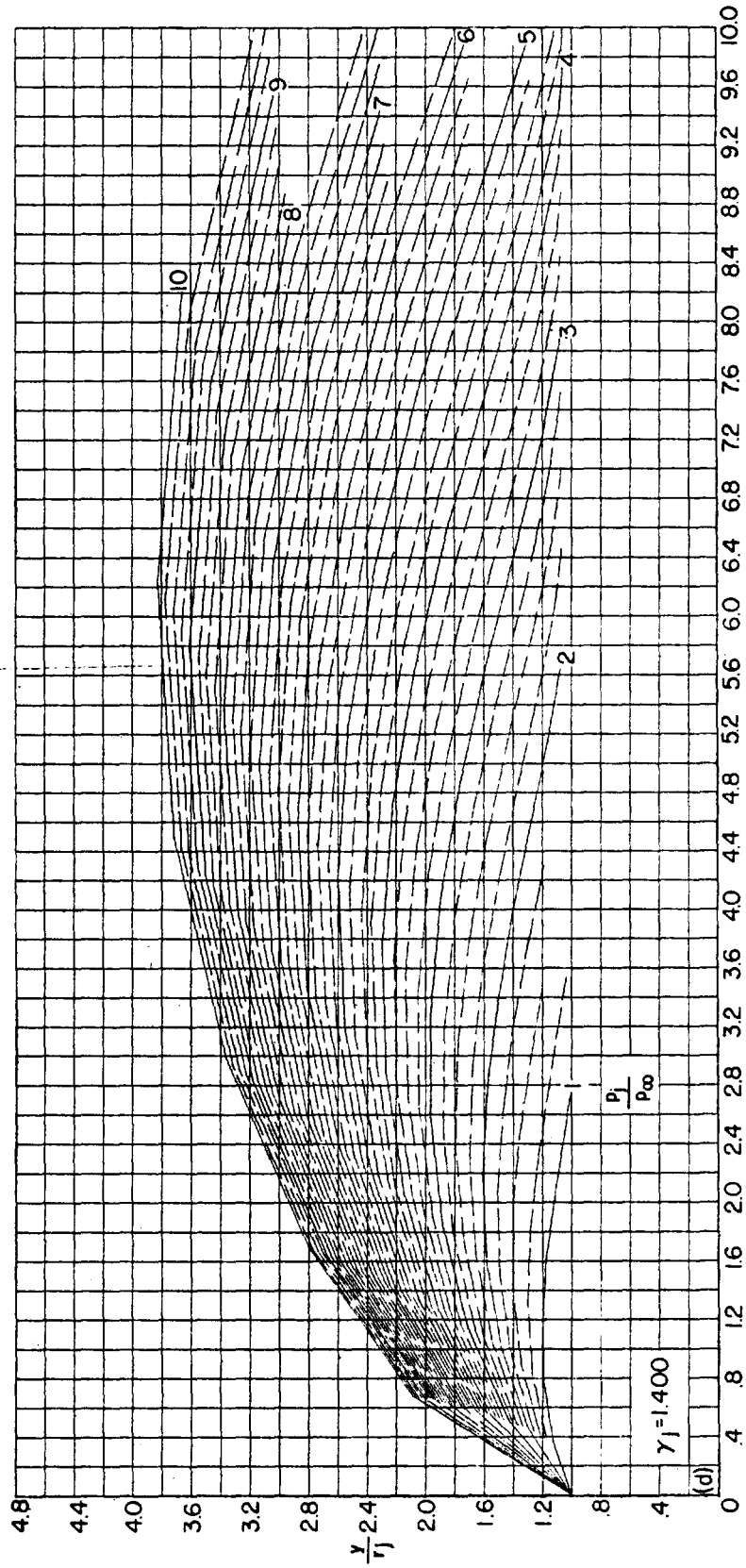

(d) $\theta_N = 20°$. Continued.

FIGURE 27.—Continued.

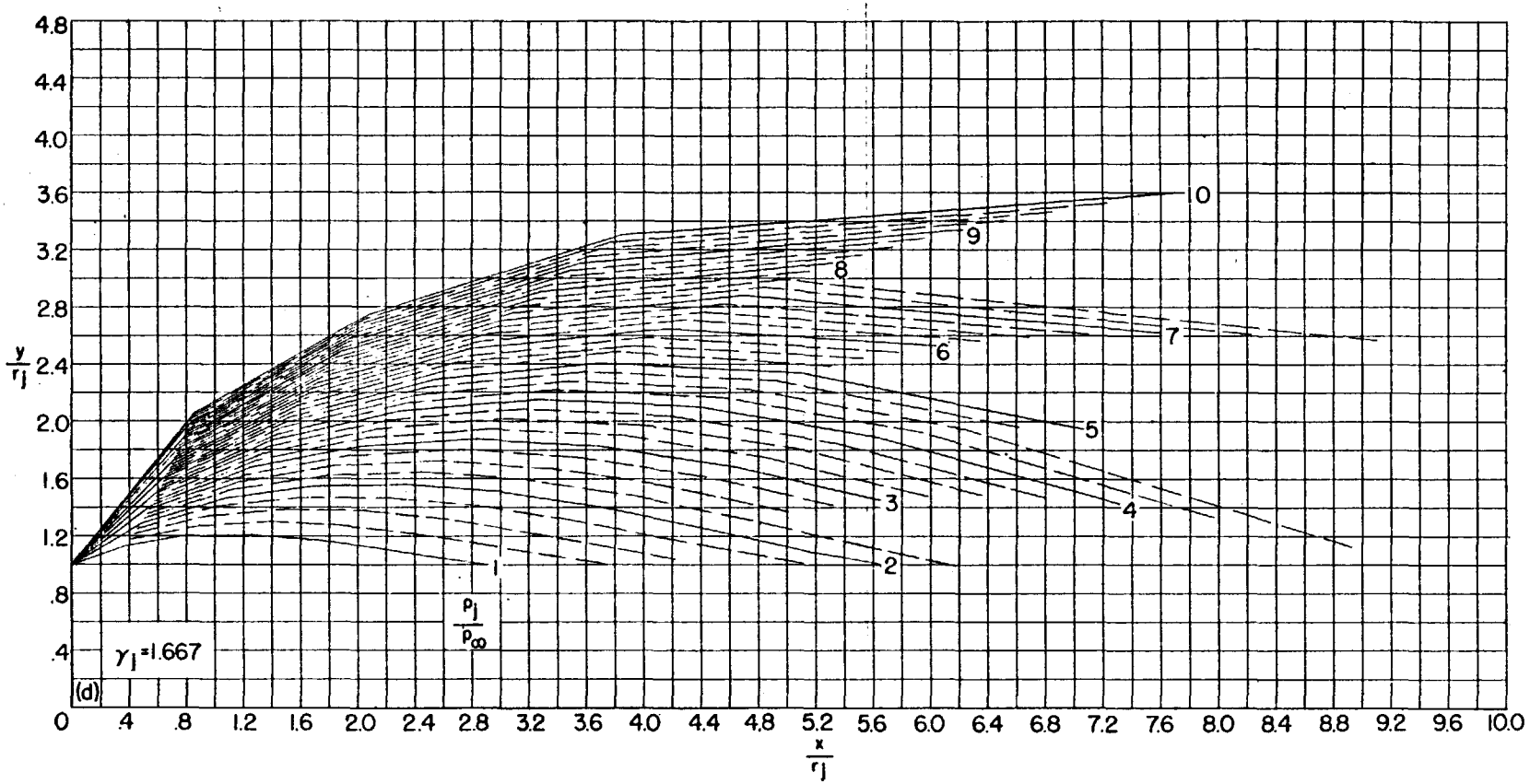

(d) $\theta_N = 20°$. Concluded.

FIGURE 27.—Concluded.

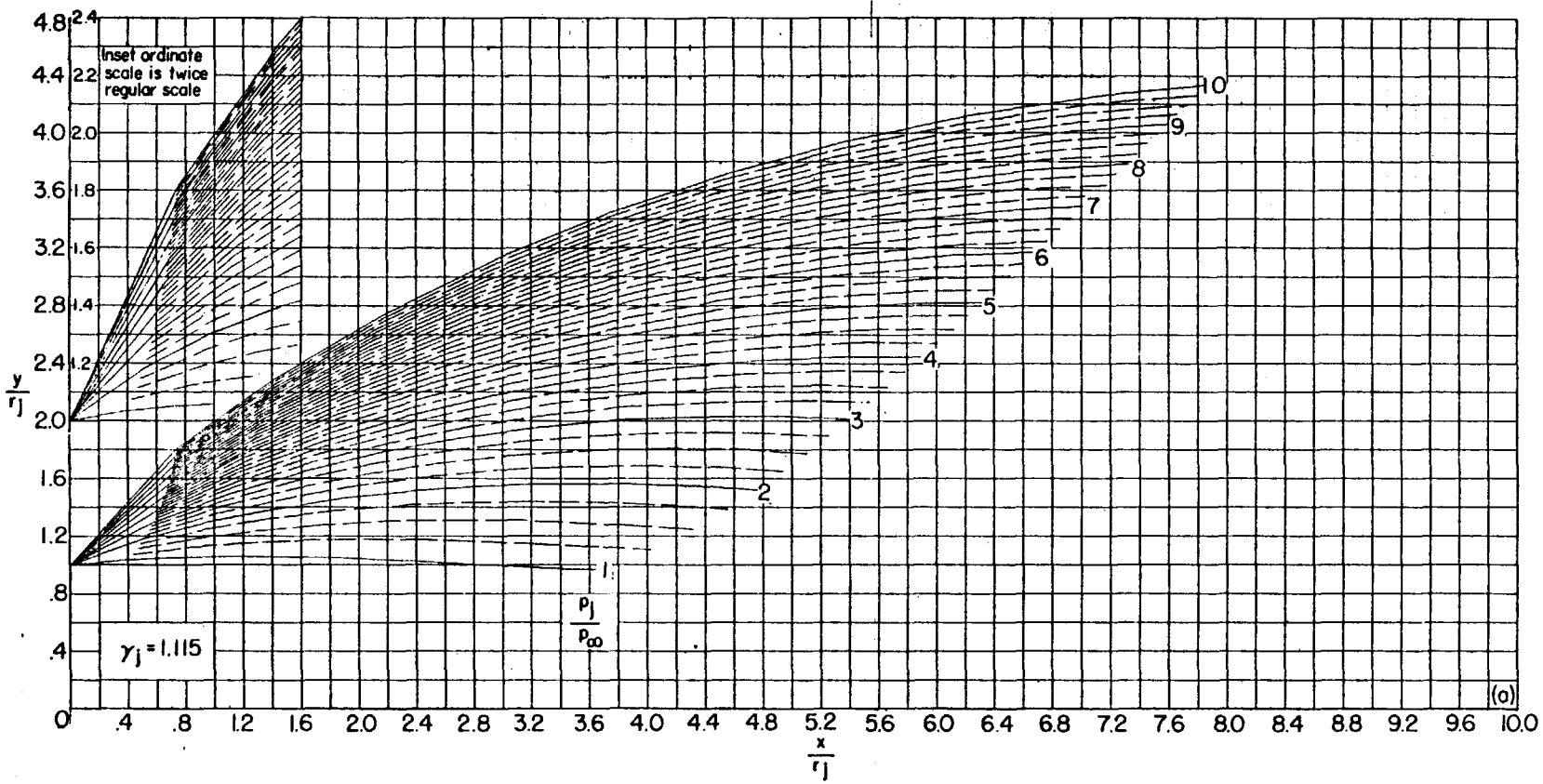

(a) $\theta_N = 5°$

FIGURE 28.—Jet boundaries at $M_i = 2.0$ for jet pressure ratios from 1 to 10. (Dashed boundaries denote changes in p_i/p_∞ of 0.25.)

502633 O—59——10

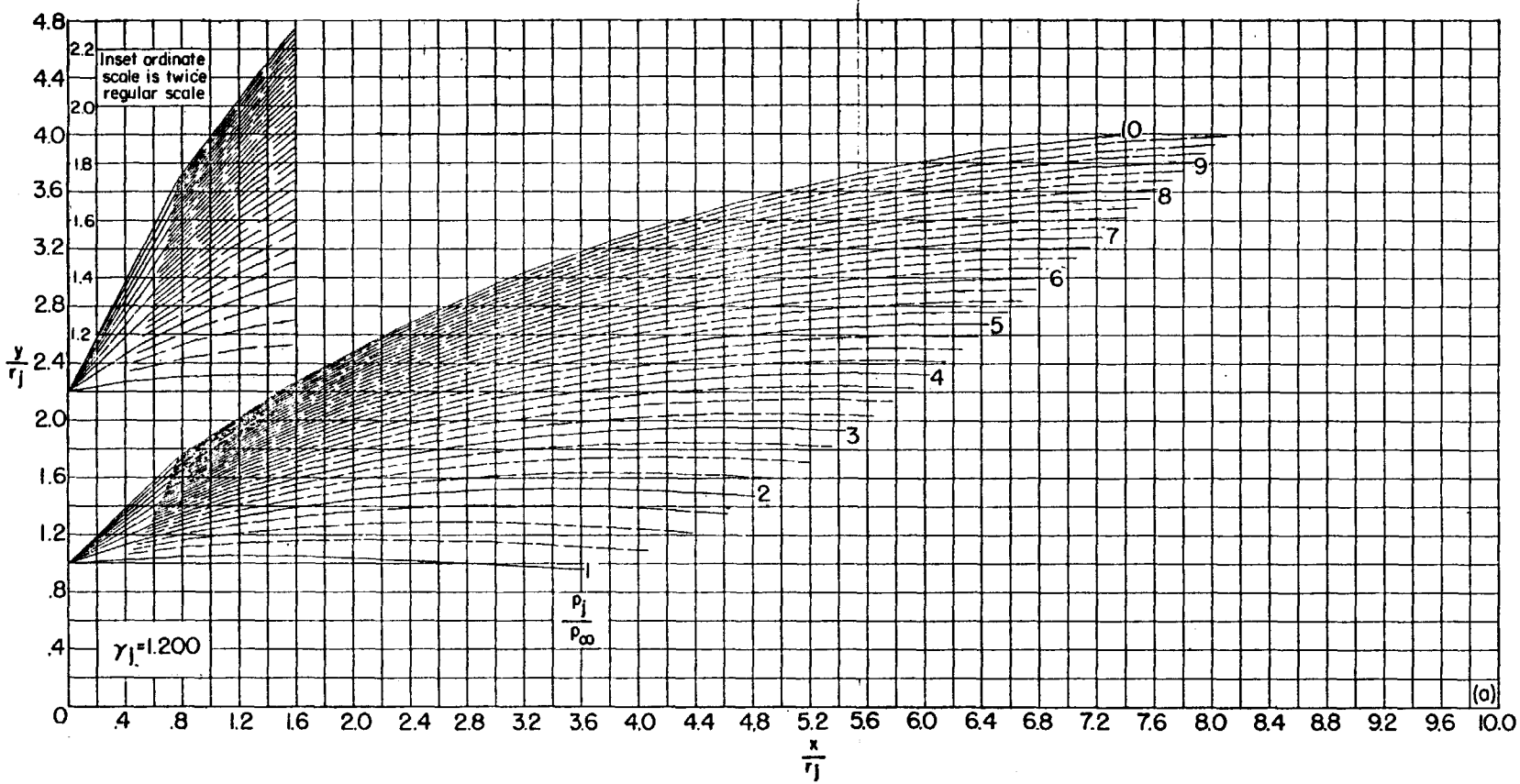

(a) $\theta_N = 5°$. Continued.

FIGURE 28.—Continued.

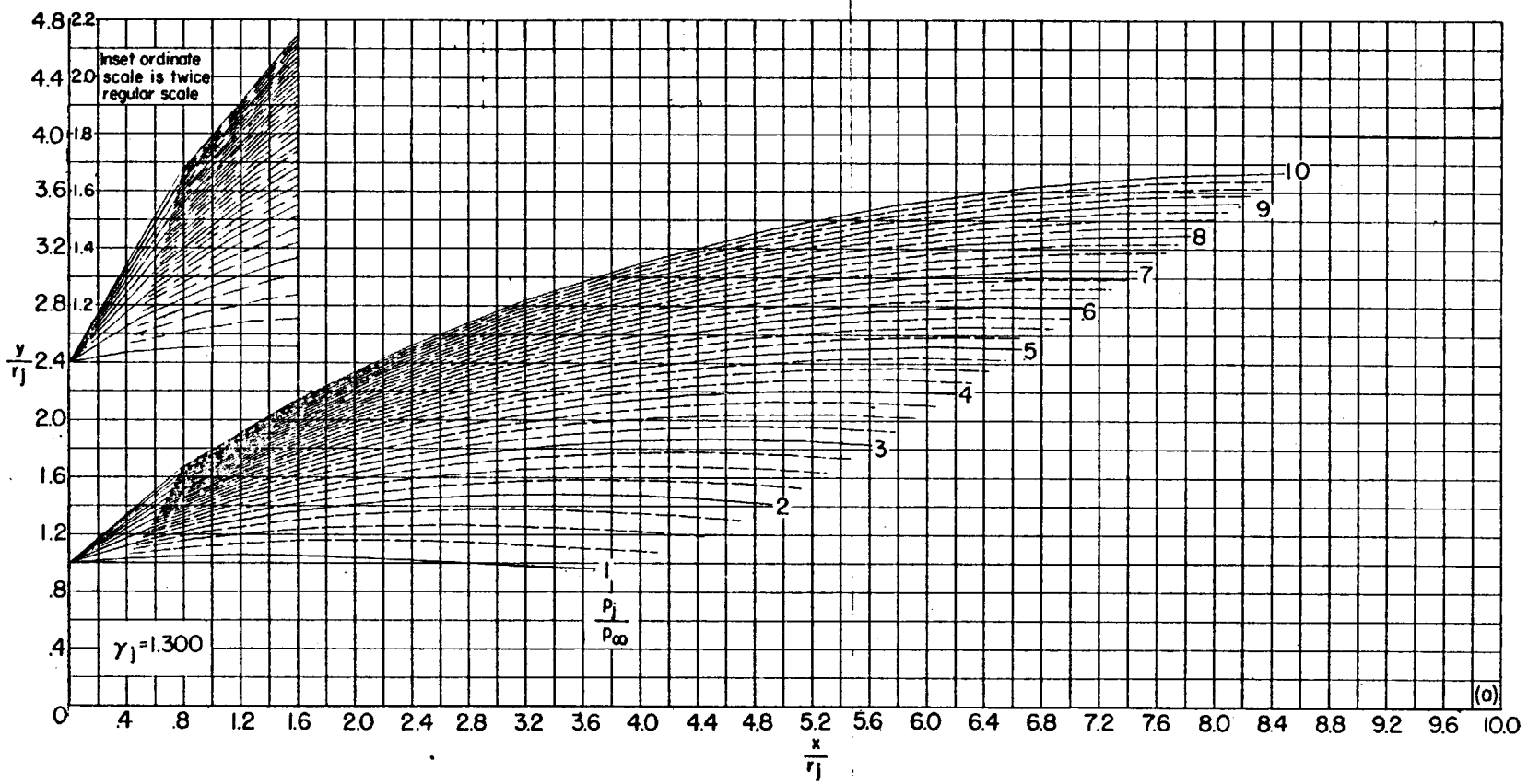

(a) $\theta_N = 5°$. Continued.

FIGURE 28.—Continued.

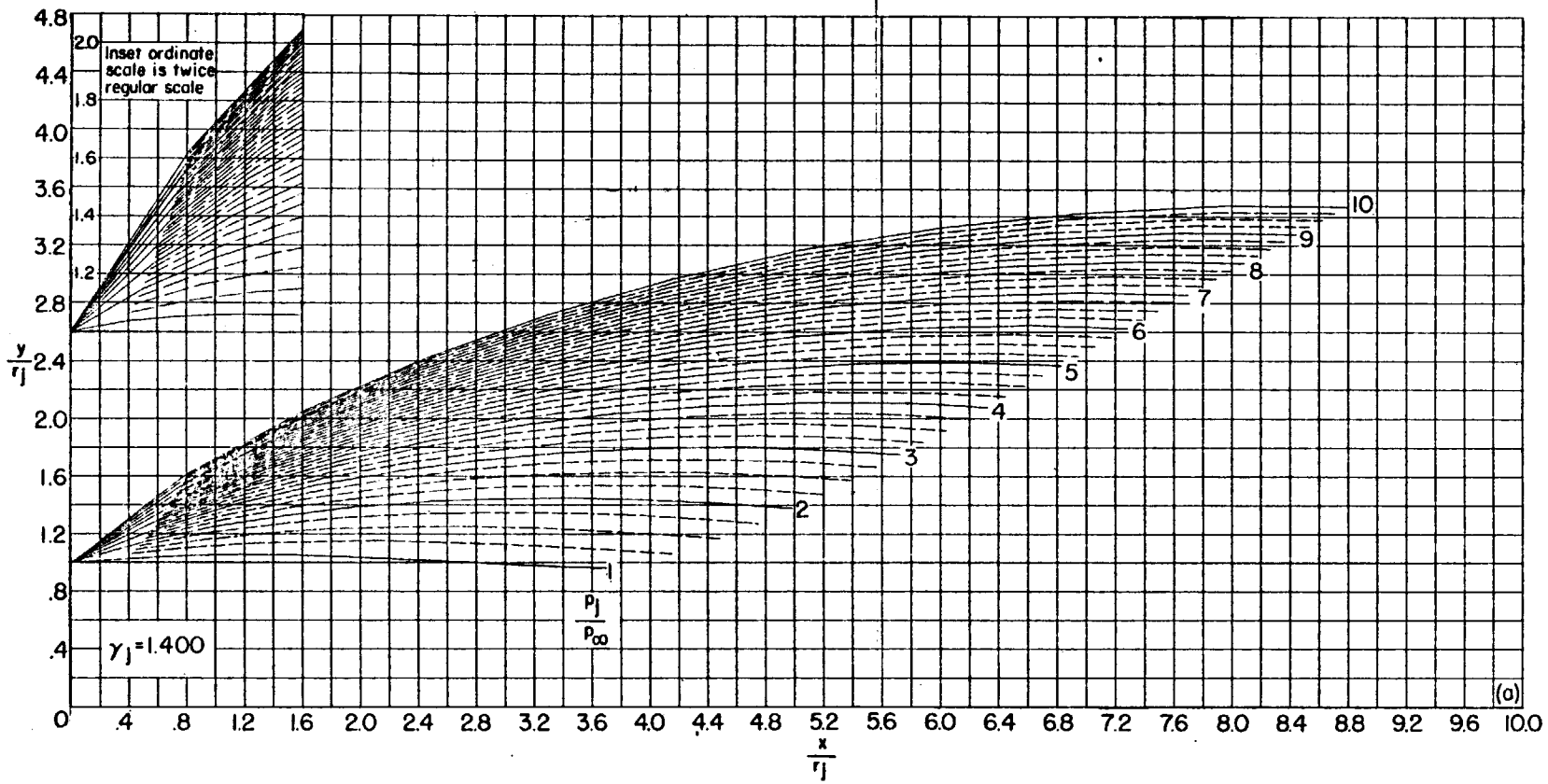

(a) $\theta_N = 5°$. Continued.

FIGURE 28.—Continued.

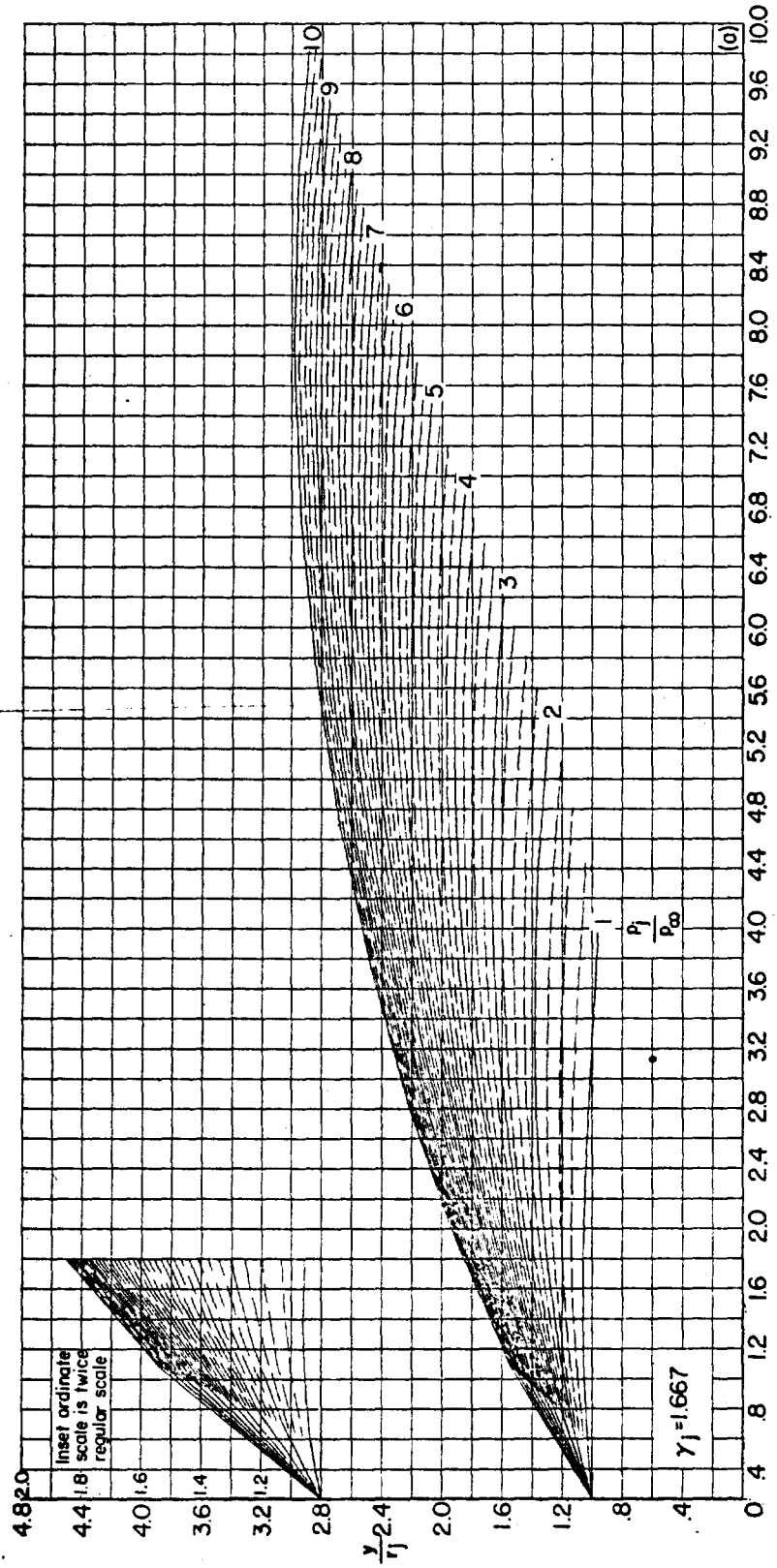

(a) $\theta_N = 5°$. Concluded.

FIGURE 28.—Continued.

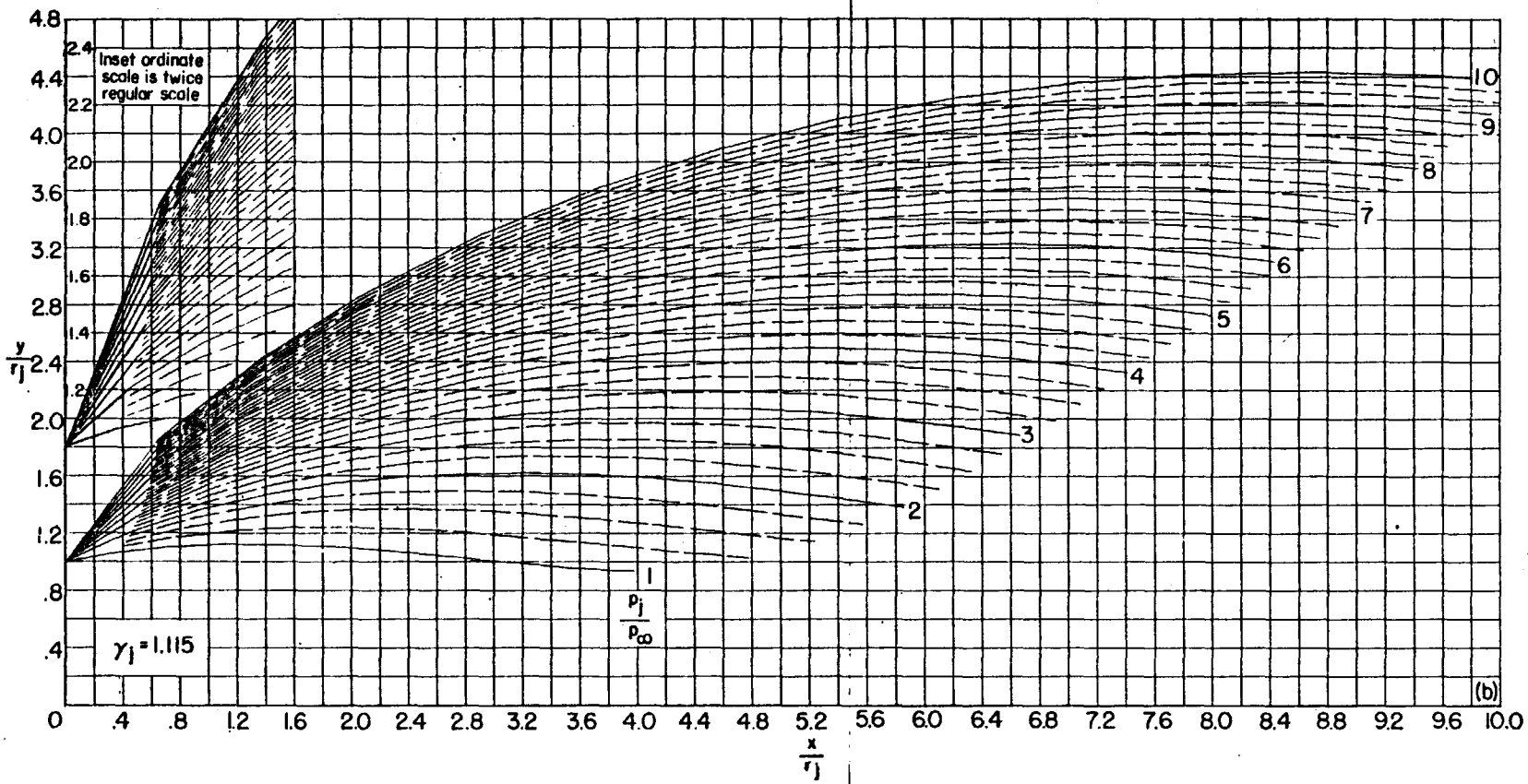

(b) $\theta_N = 10°$.

FIGURE 28.—Continued.

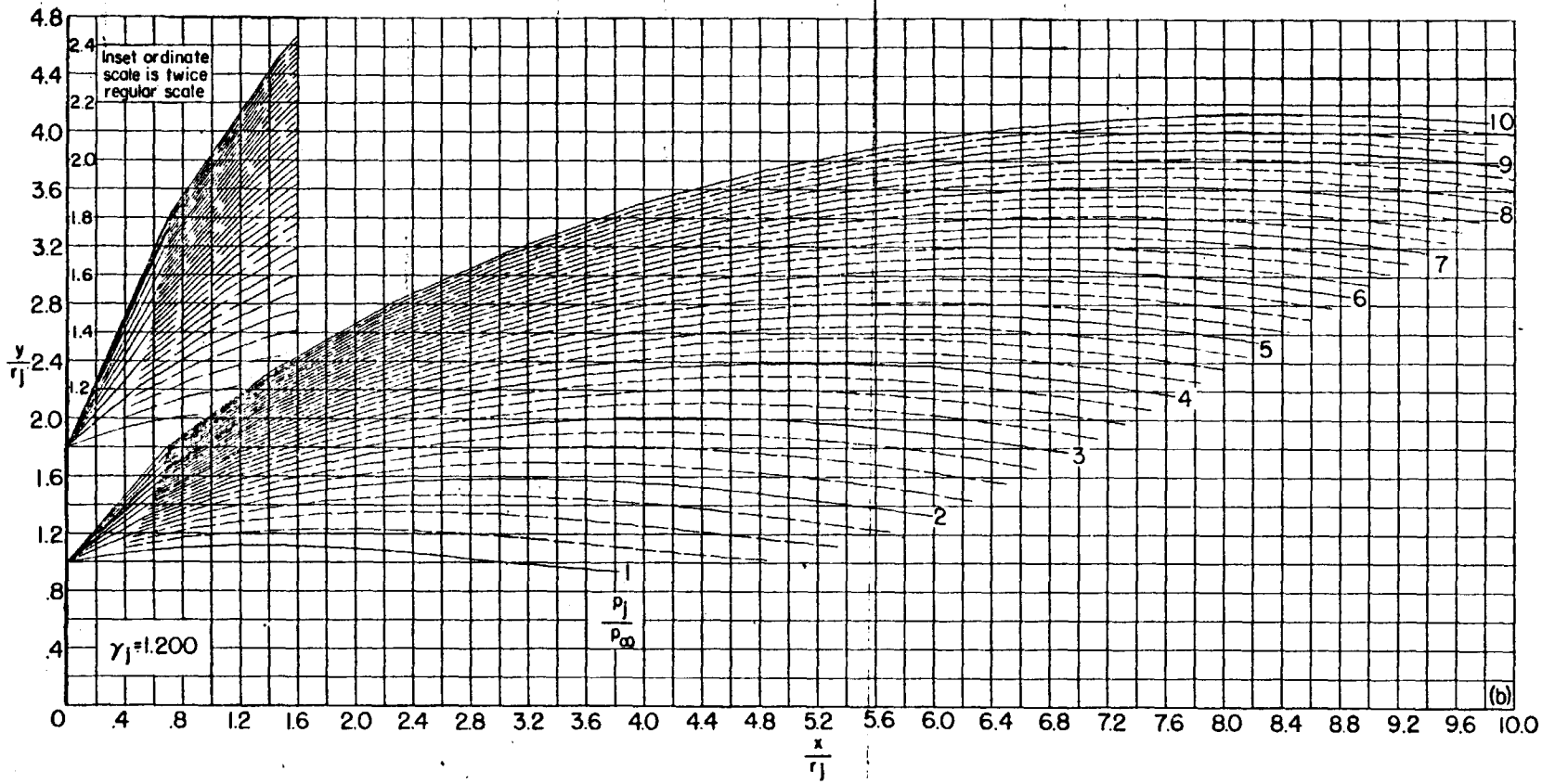

(b) $\theta_N = 10°$. Continued.

FIGURE 28.—Continued.

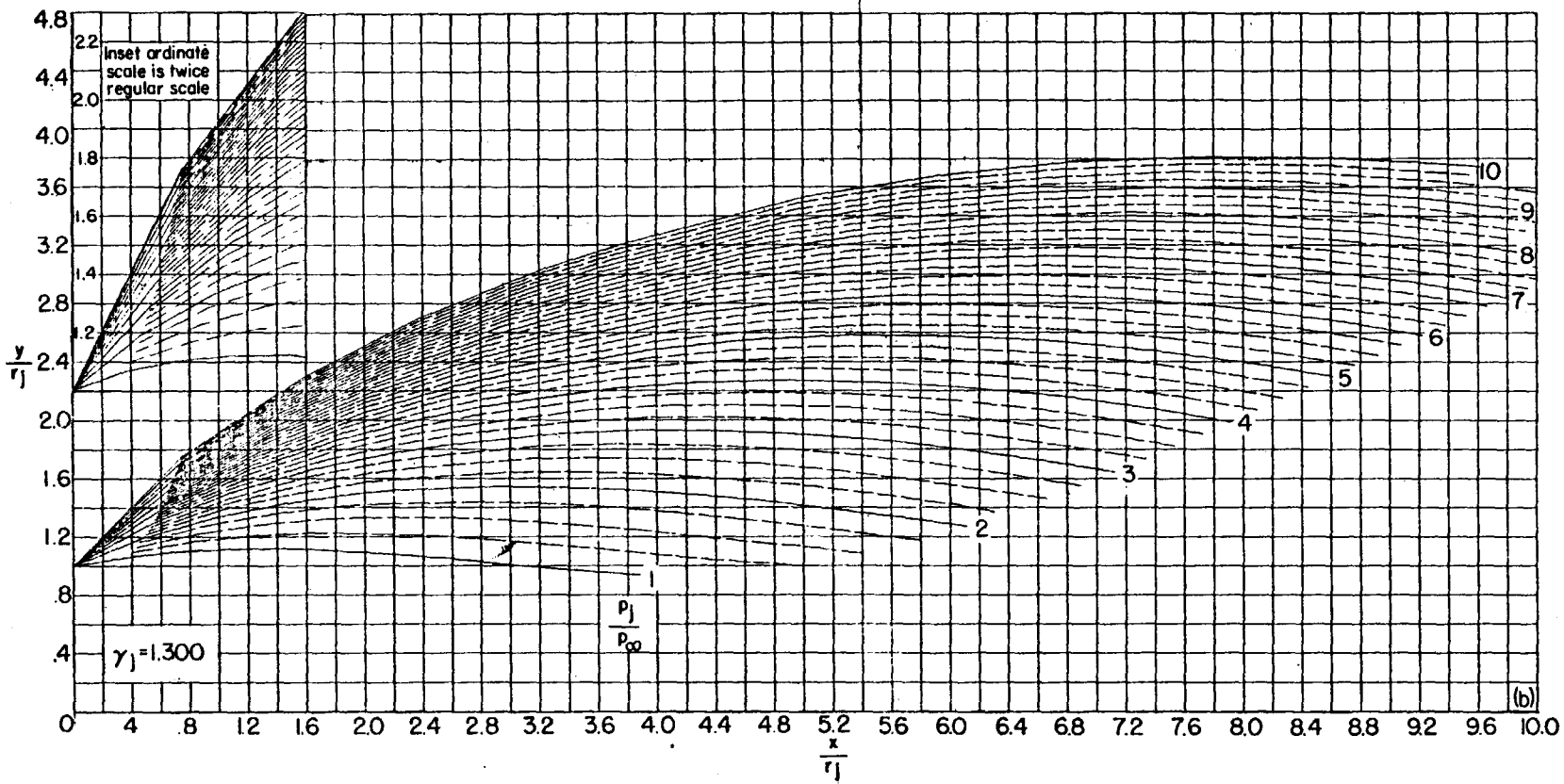

(b) $\theta_N = 10°$. Continued.

FIGURE 28.—Continued.

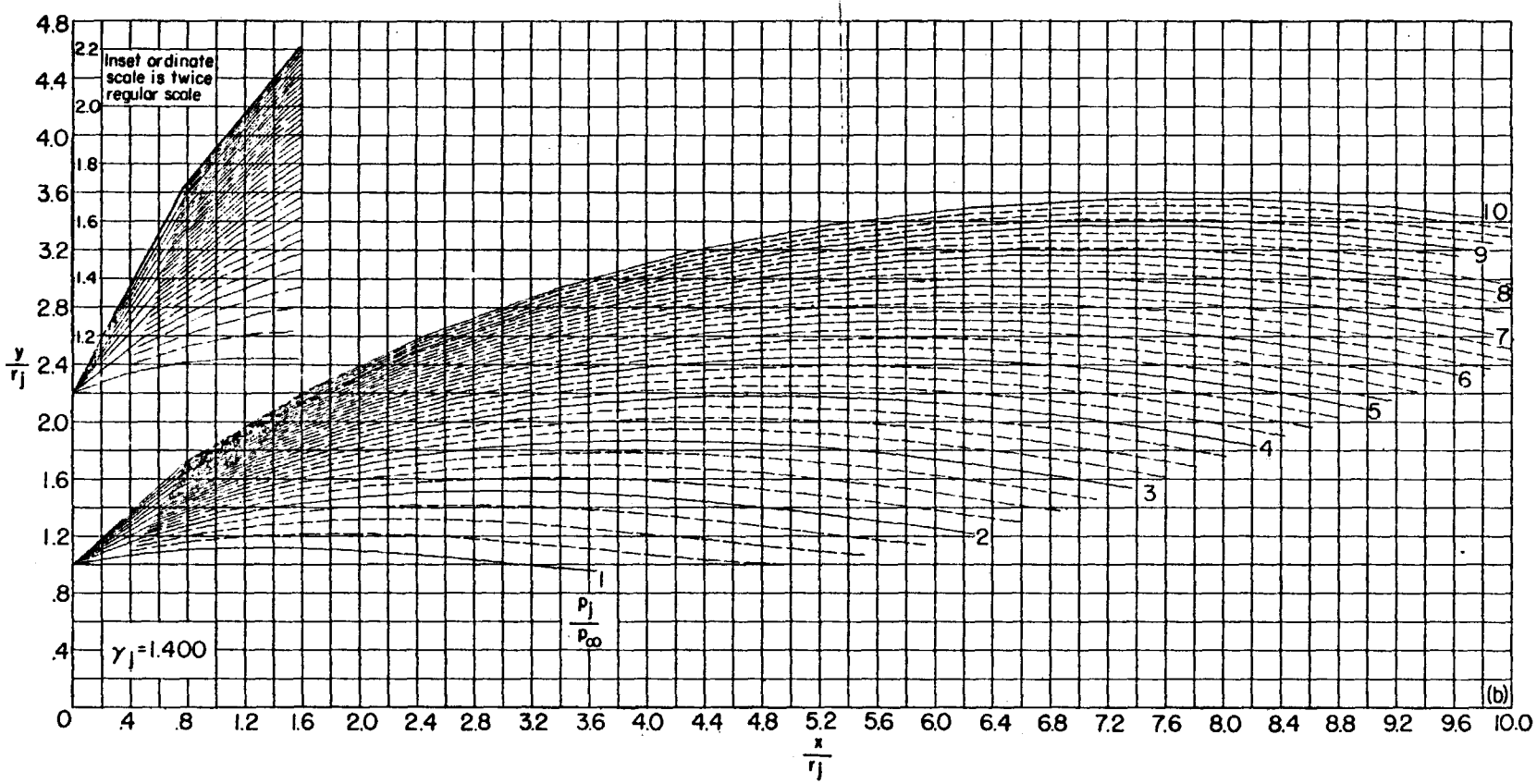

(b) $\theta_N = 10°$. Continued.

FIGURE 28.—Continued.

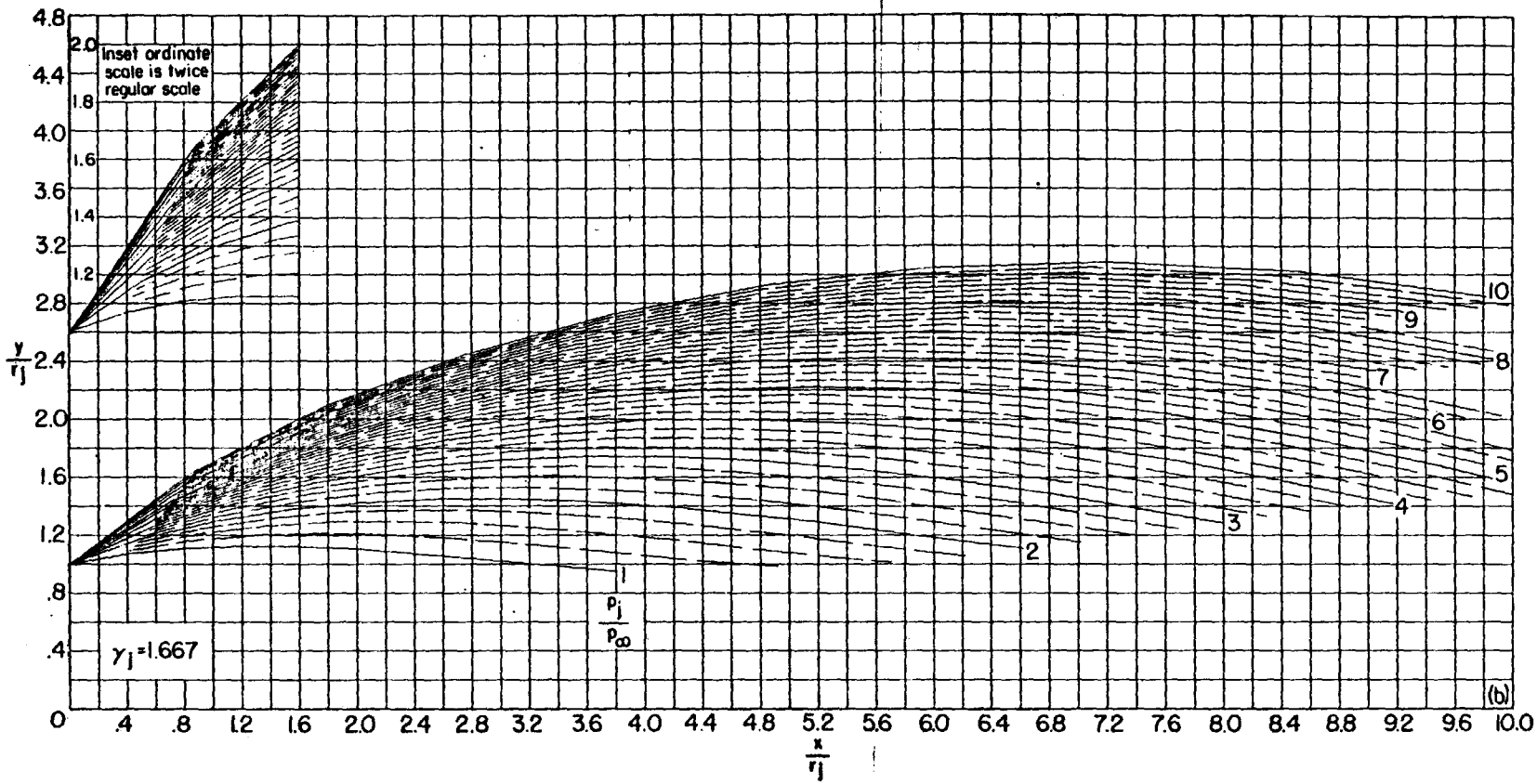

(b) $\theta_N = 10°$. Concluded.

FIGURE 28.—Continued.

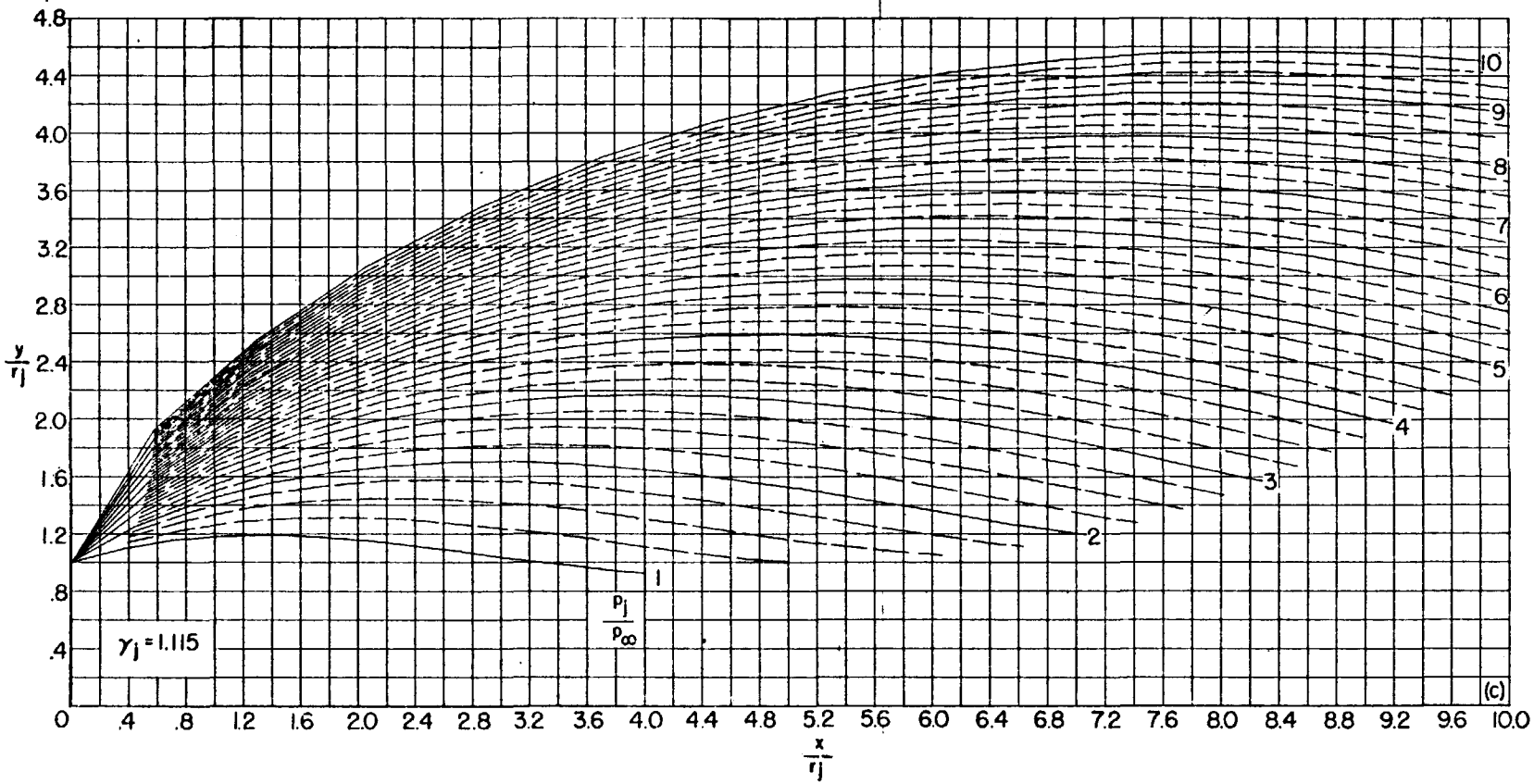

(c) $\theta_N = 15°$.

FIGURE 28.—Continued.

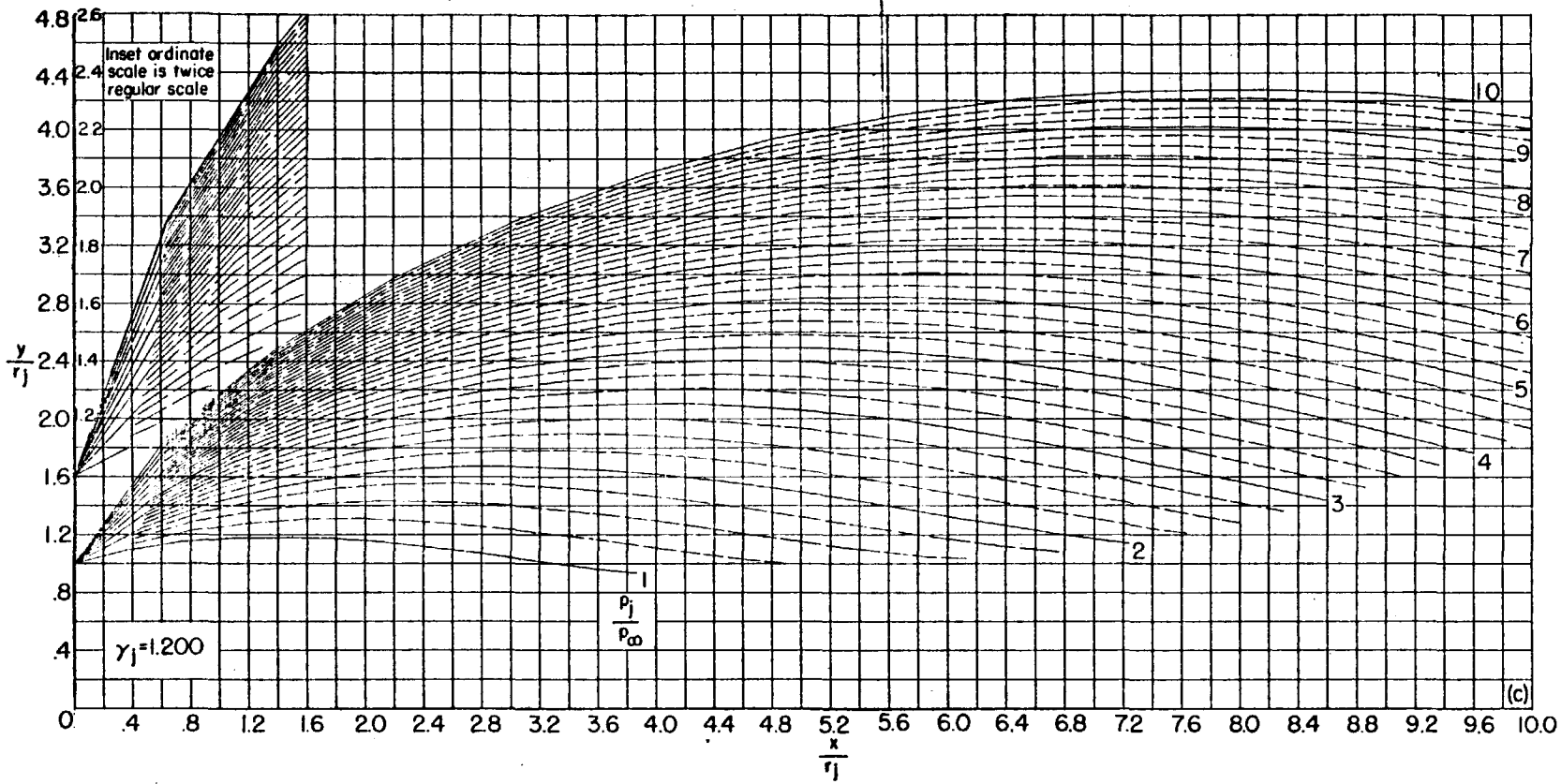

(c) $\vartheta_N = 15°$. Continued.

FIGURE 28.—Continued.

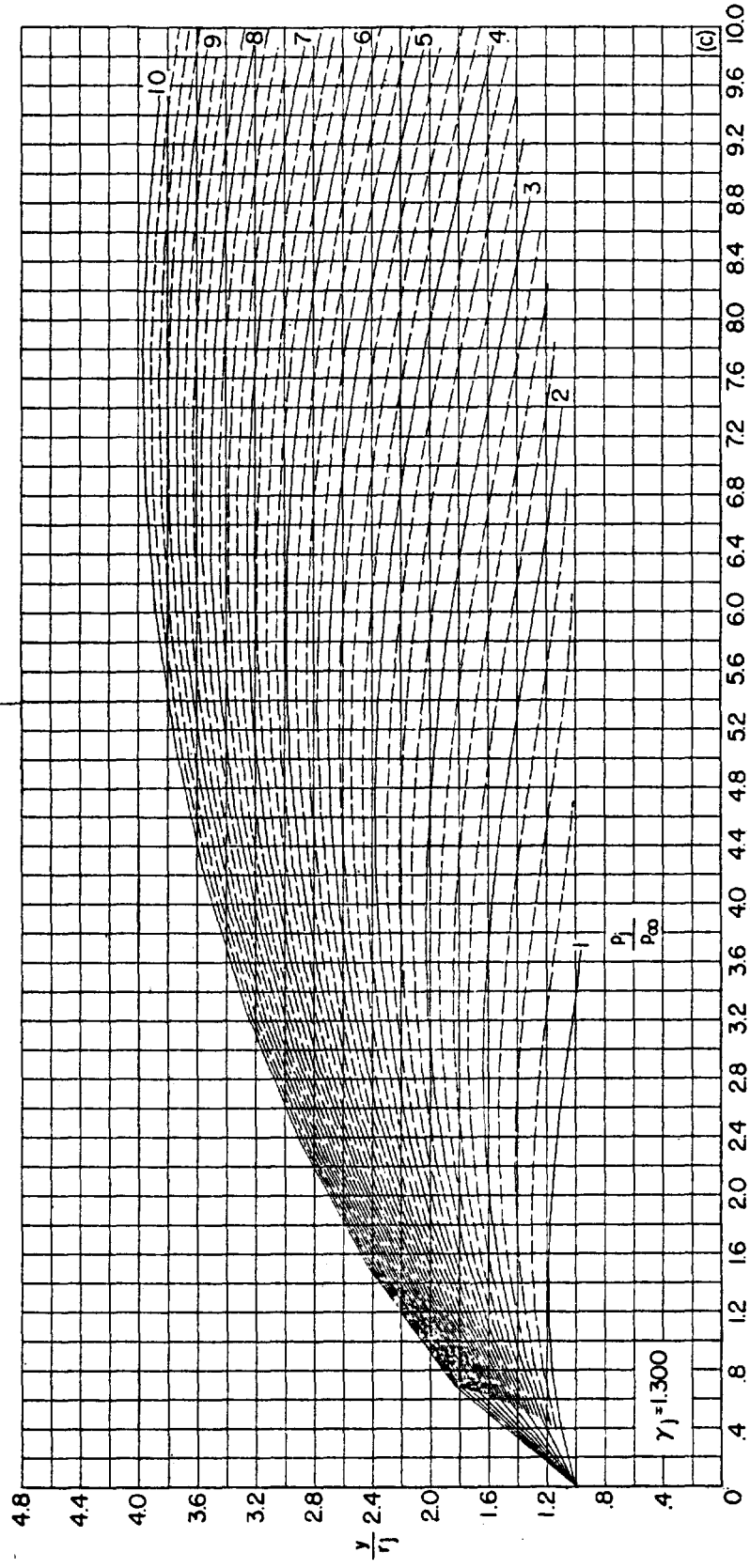

(c) $\theta_N = 15°$. Continued.

FIGURE 28.—Continued.

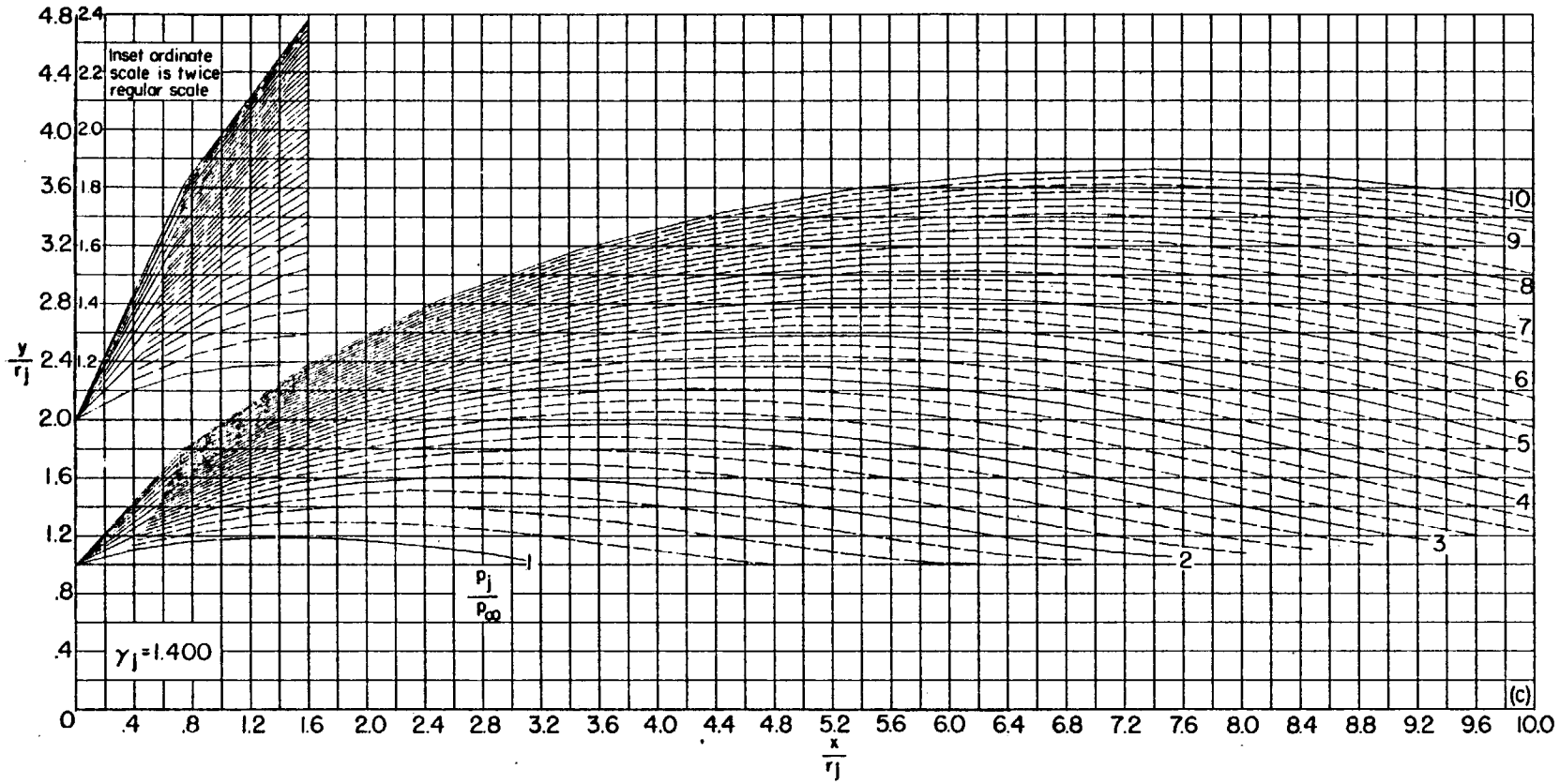

(c) $\theta_N = 15°$. Continued.

FIGURE 28.—Continued.

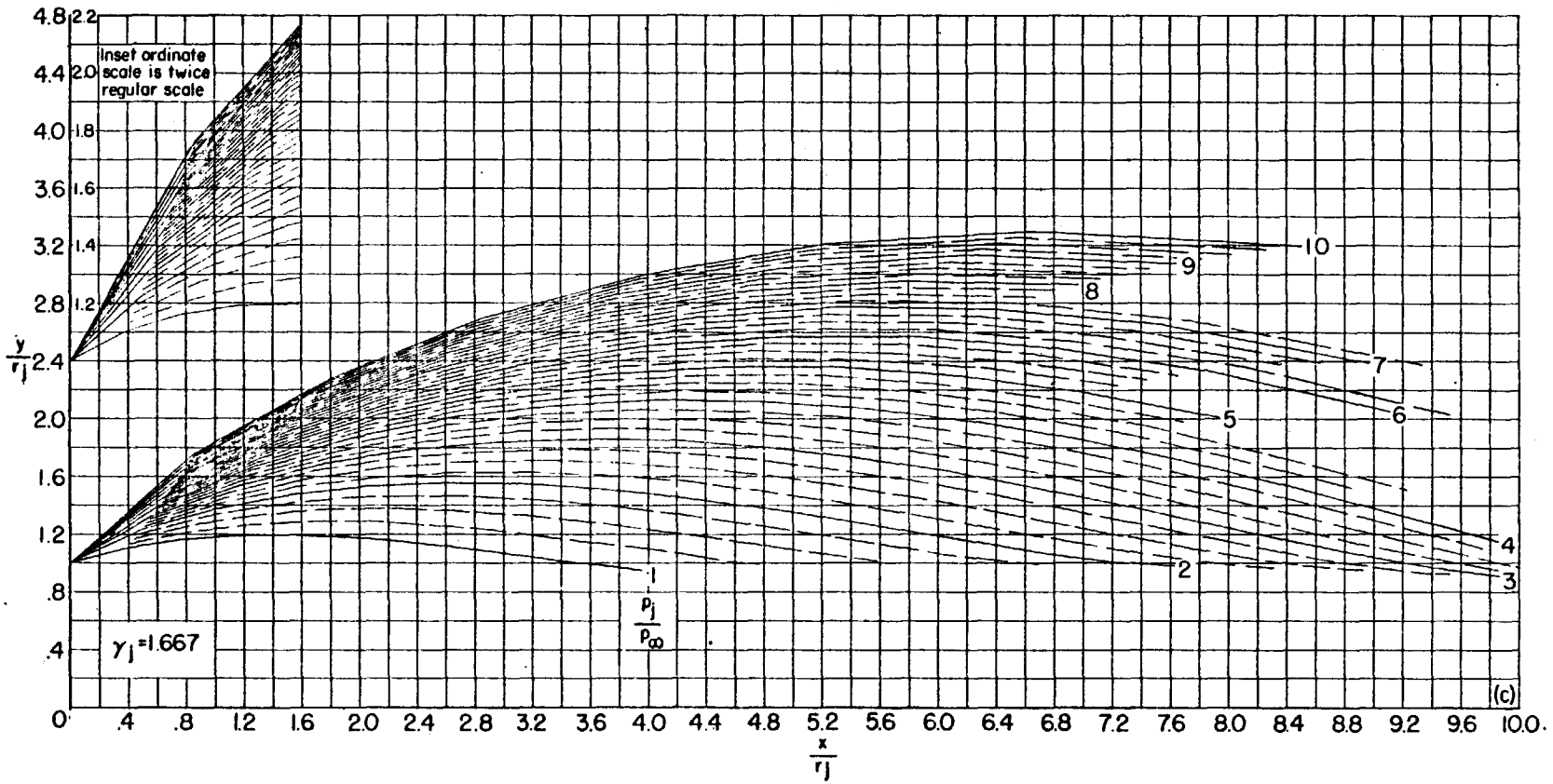

(c) $\theta_N = 15°$. Concluded.

FIGURE 28.—Continued.

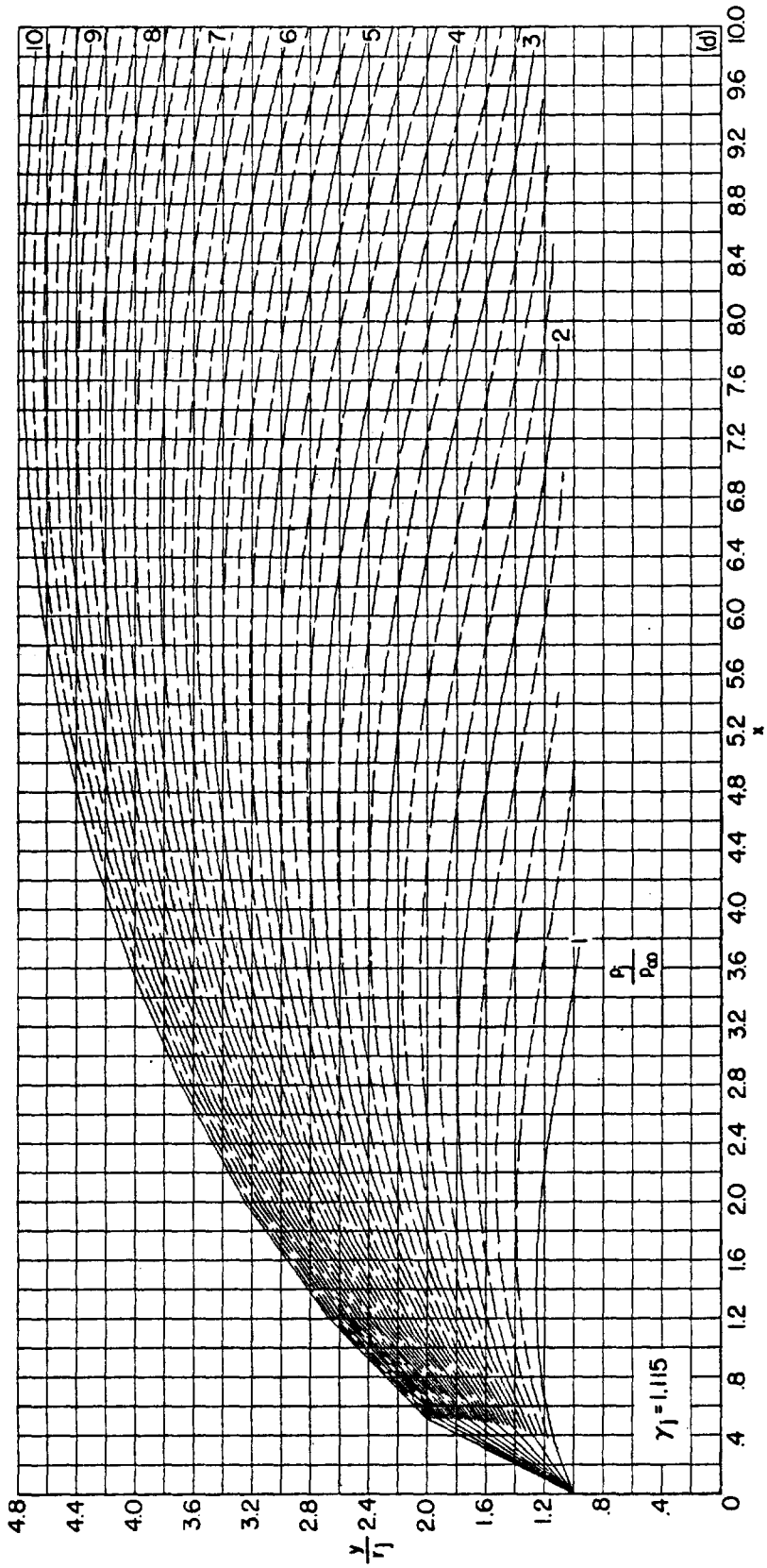

(d) $\theta_N = 20°$.

FIGURE 28.—Continued.

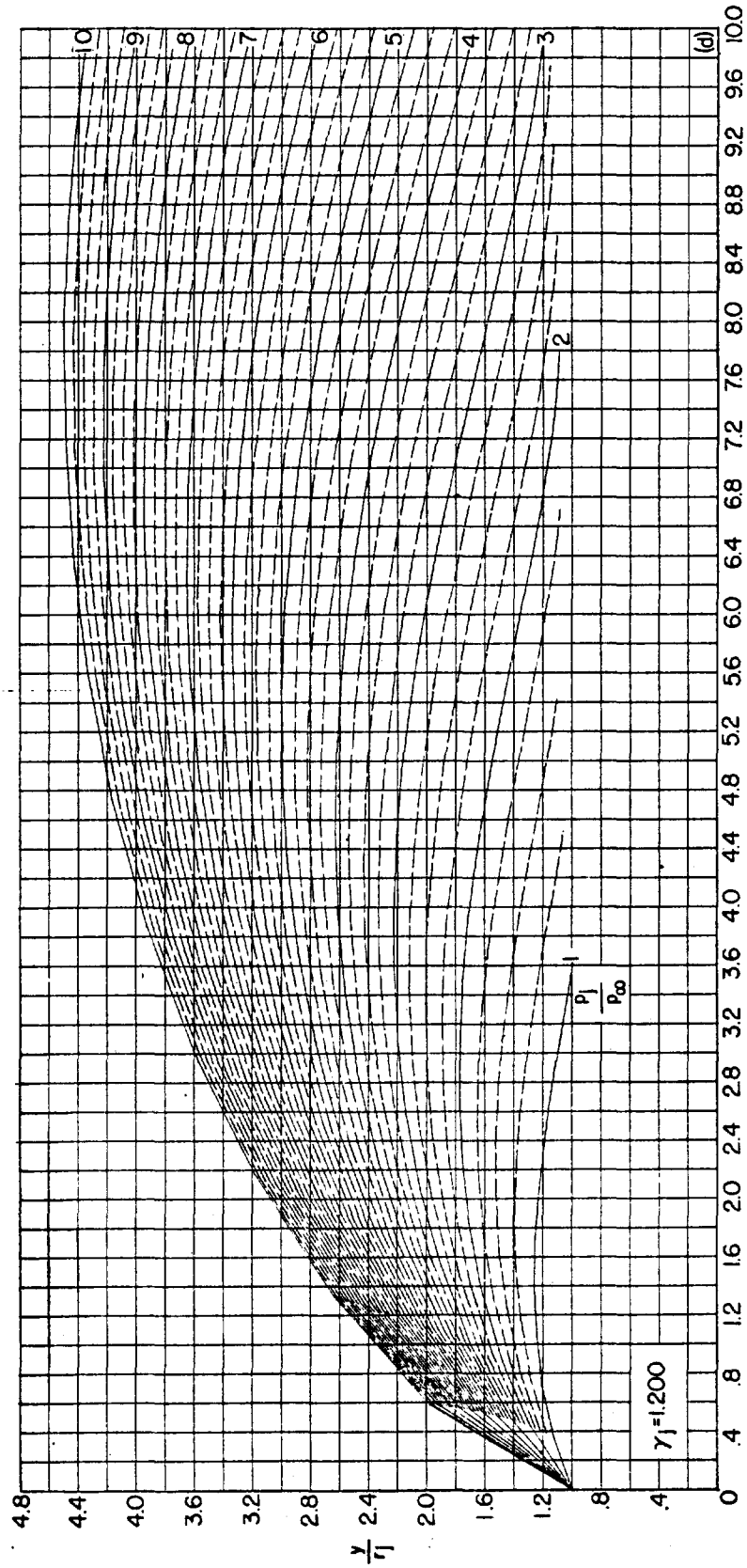

(d) $\theta_N = 20°$. Continued.

FIGURE 28.—Continued.

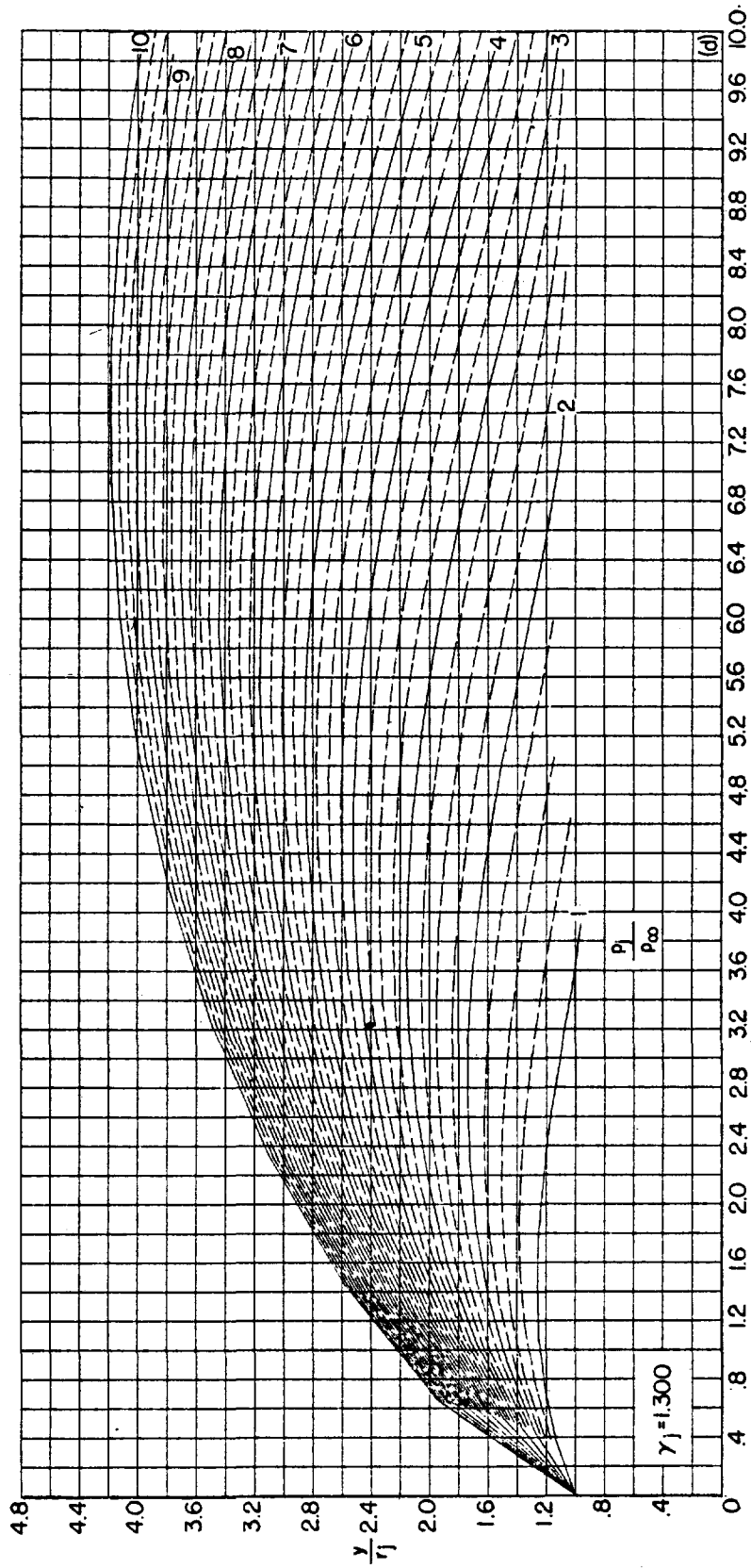

(d) $\theta_N = 20°$. Continued.

FIGURE 28.—Continued.

502683 O—59——11

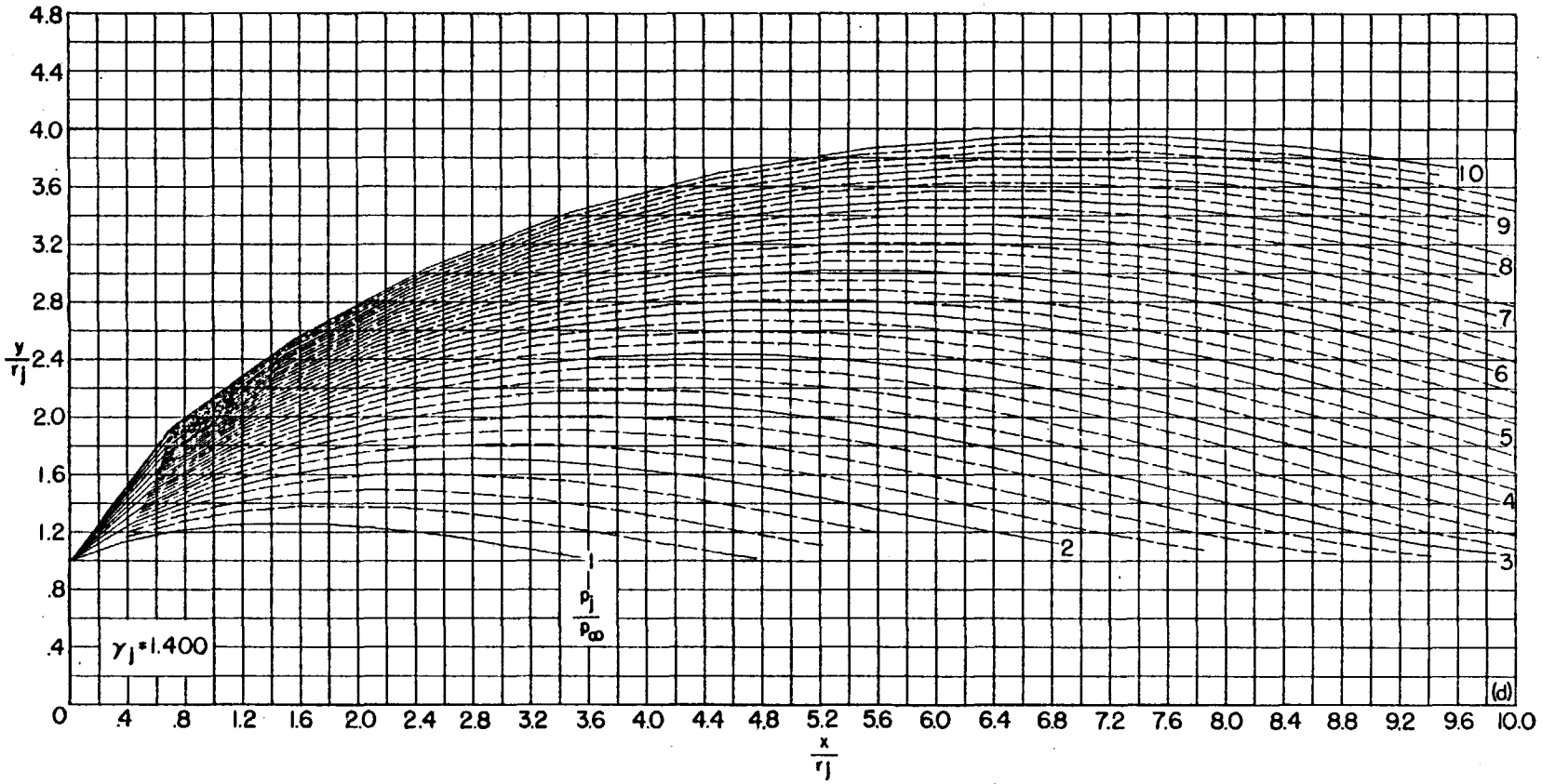

(d) $\theta_N = 20°$. Continued.

FIGURE 28.—Continued.

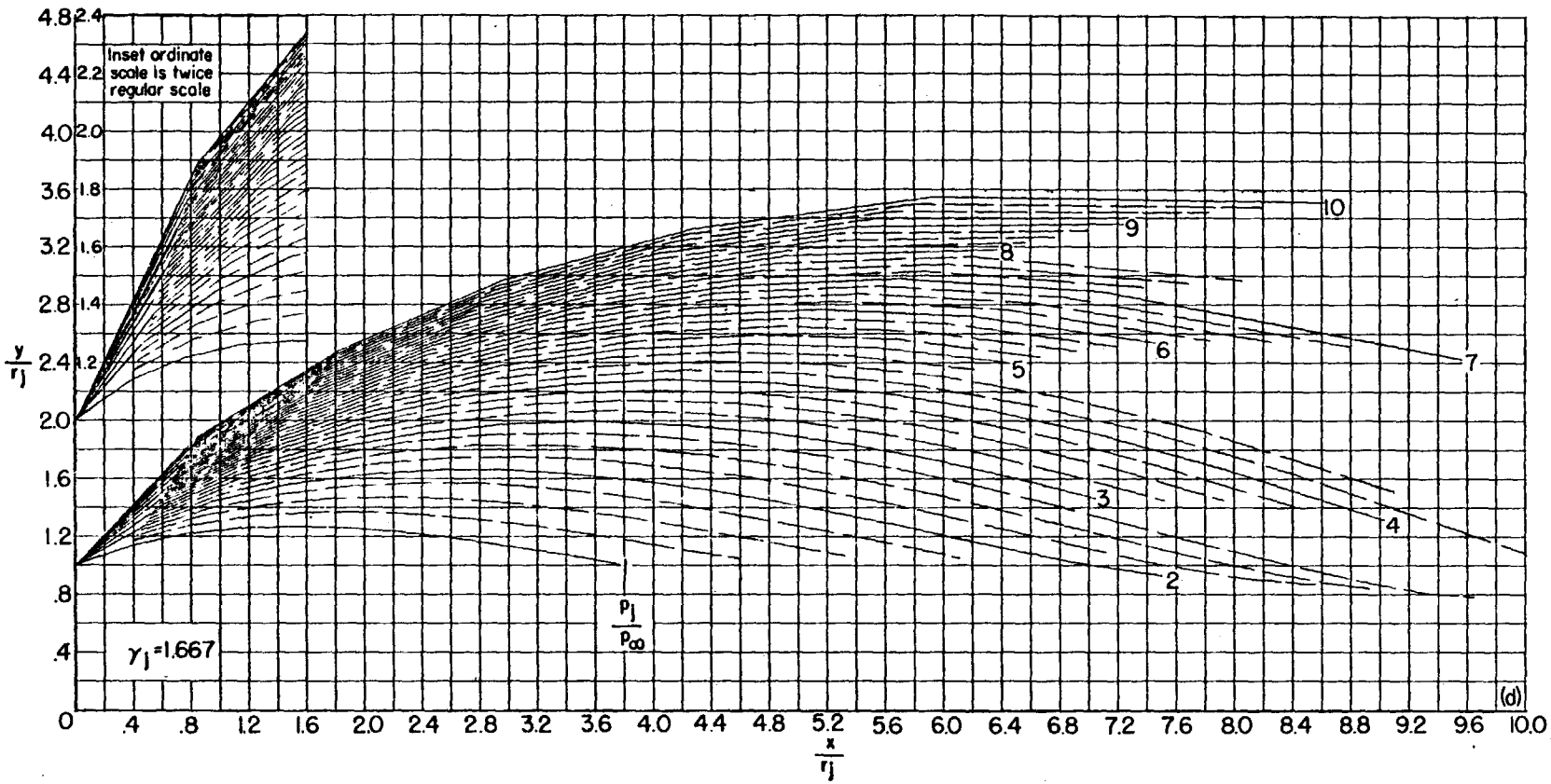

(d) θ_N=20°. Concluded.

FIGURE 28.—Concluded.

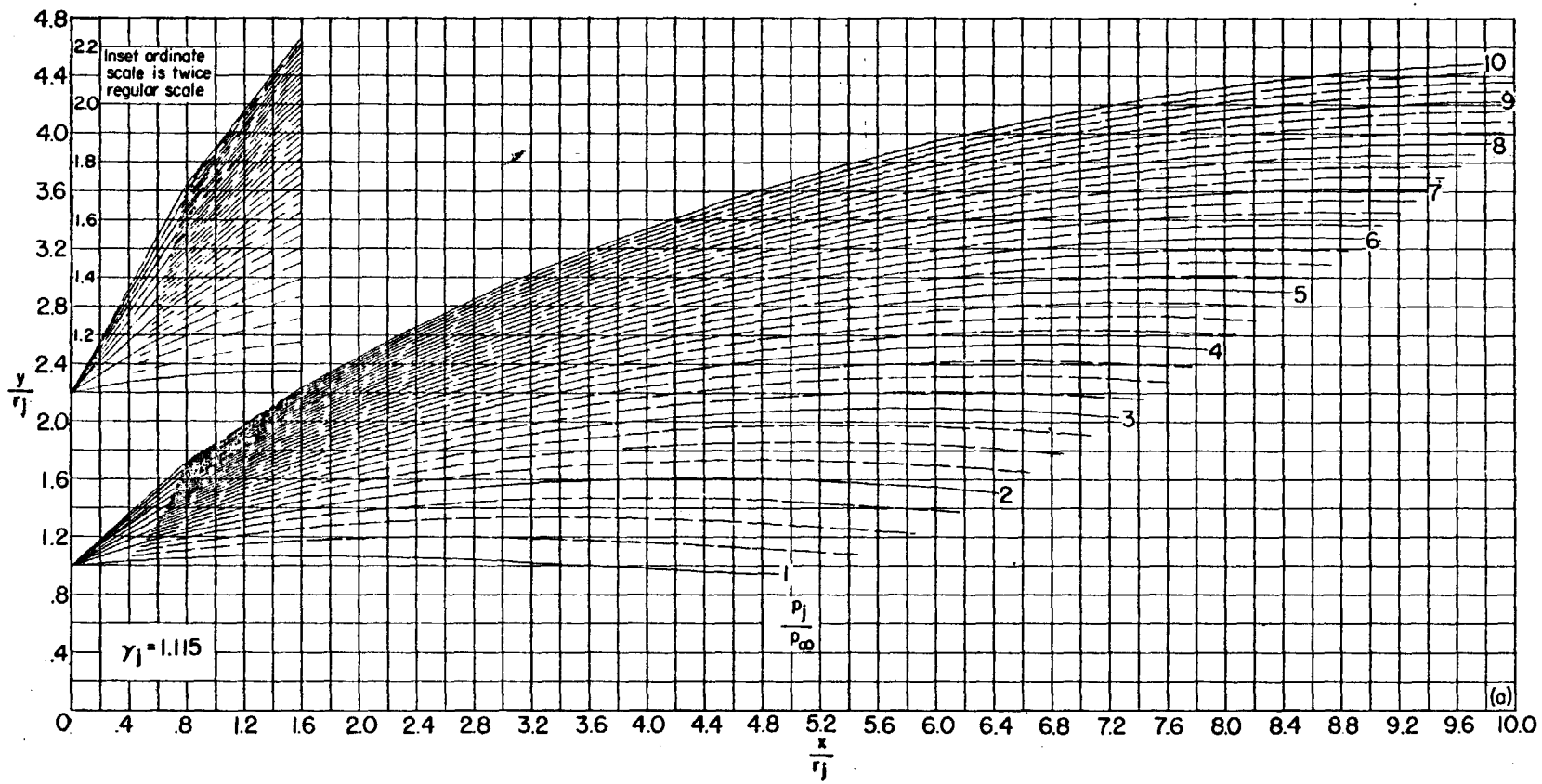

(a) $\theta_N = 5°$.

FIGURE 29.—Jet boundaries at $M_j = 2.5$ for jet pressure ratios from 1 to 10. (Dashed boundaries denote changes in p_j/p_∞ of 0.25.)

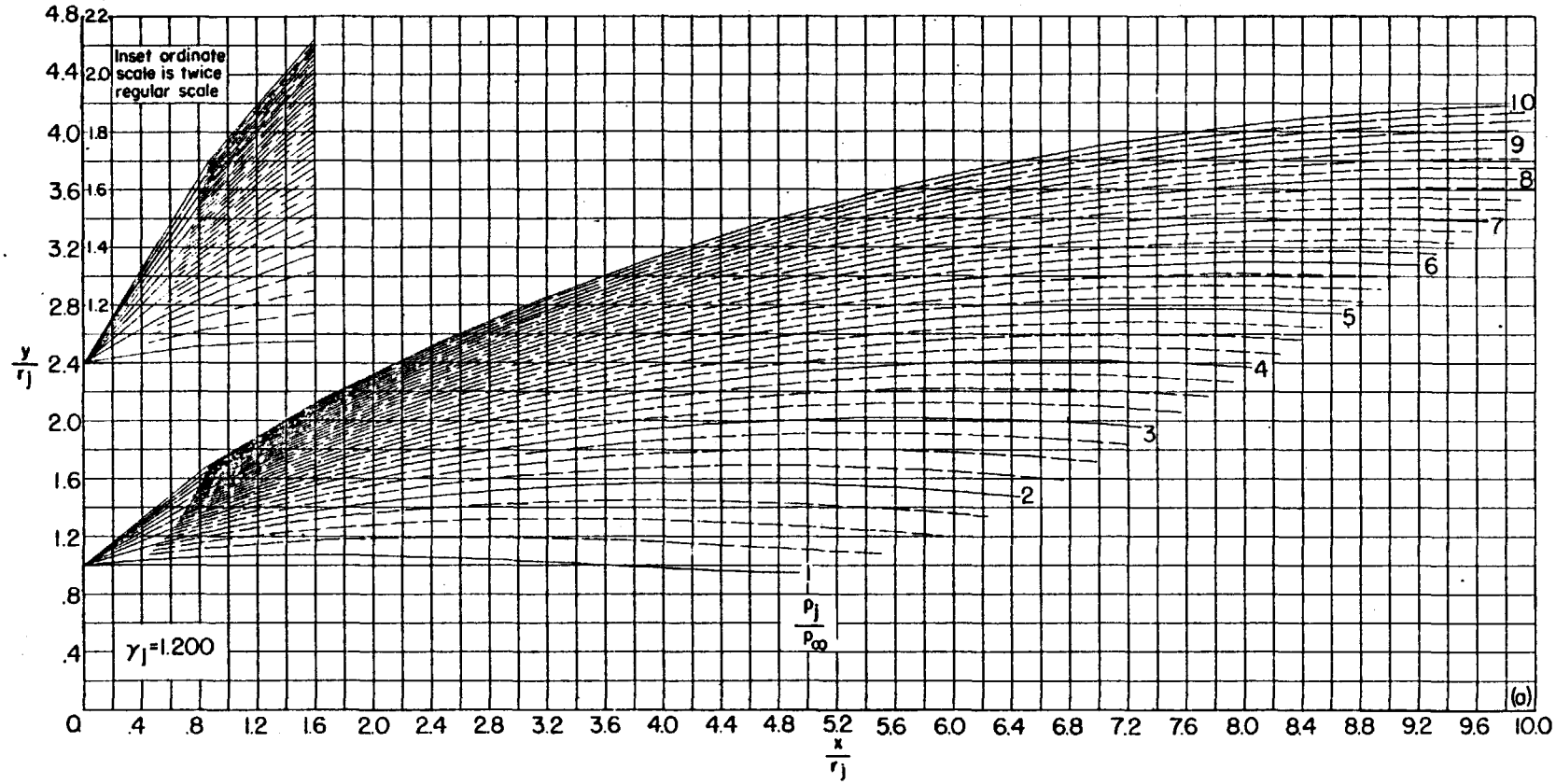

(a) $\theta_N = 5°$. Continued.

FIGURE 29.—Continued.

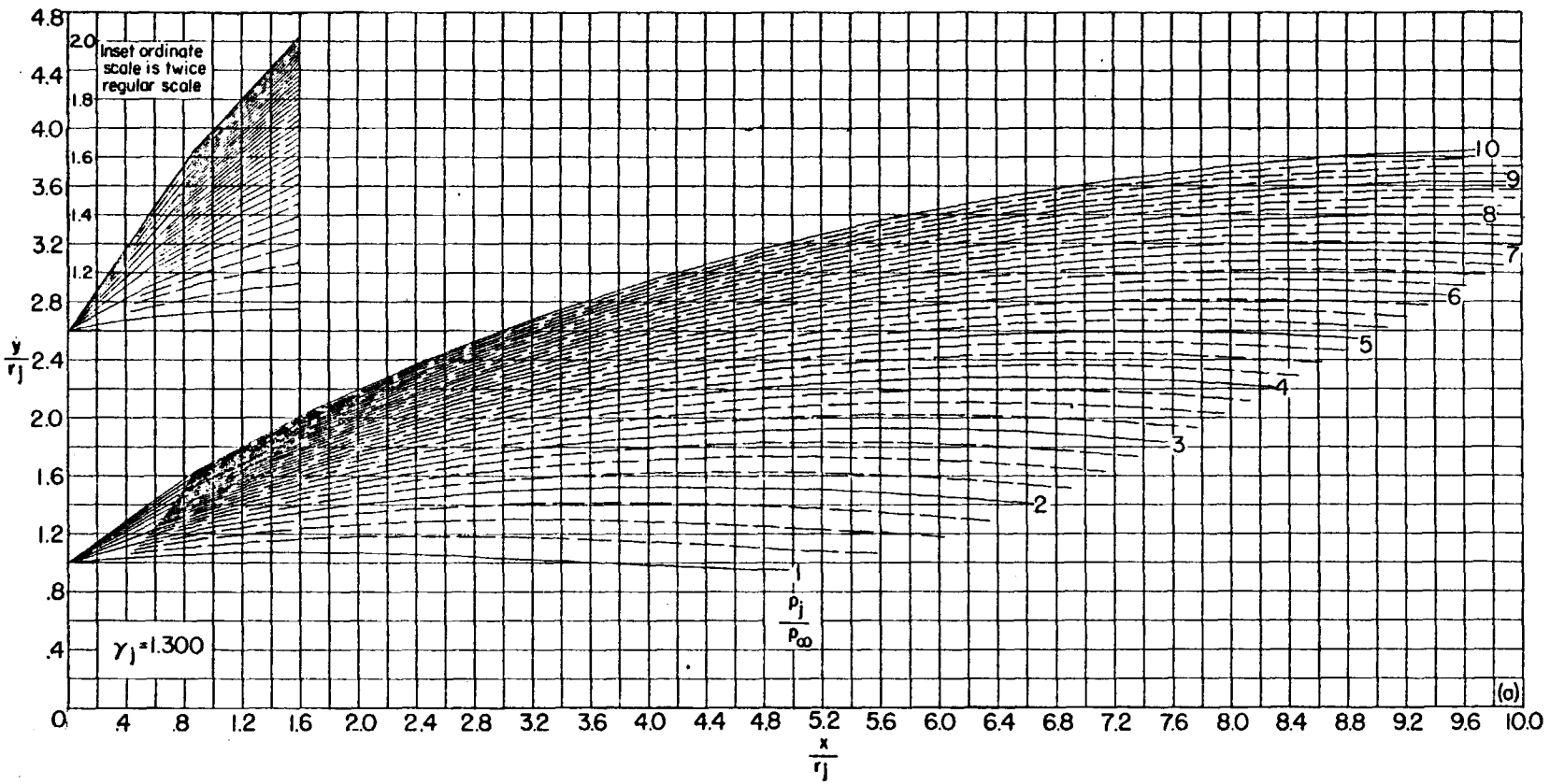

(a) θ_N=5°. Continued.

FIGURE 29.—Continued.

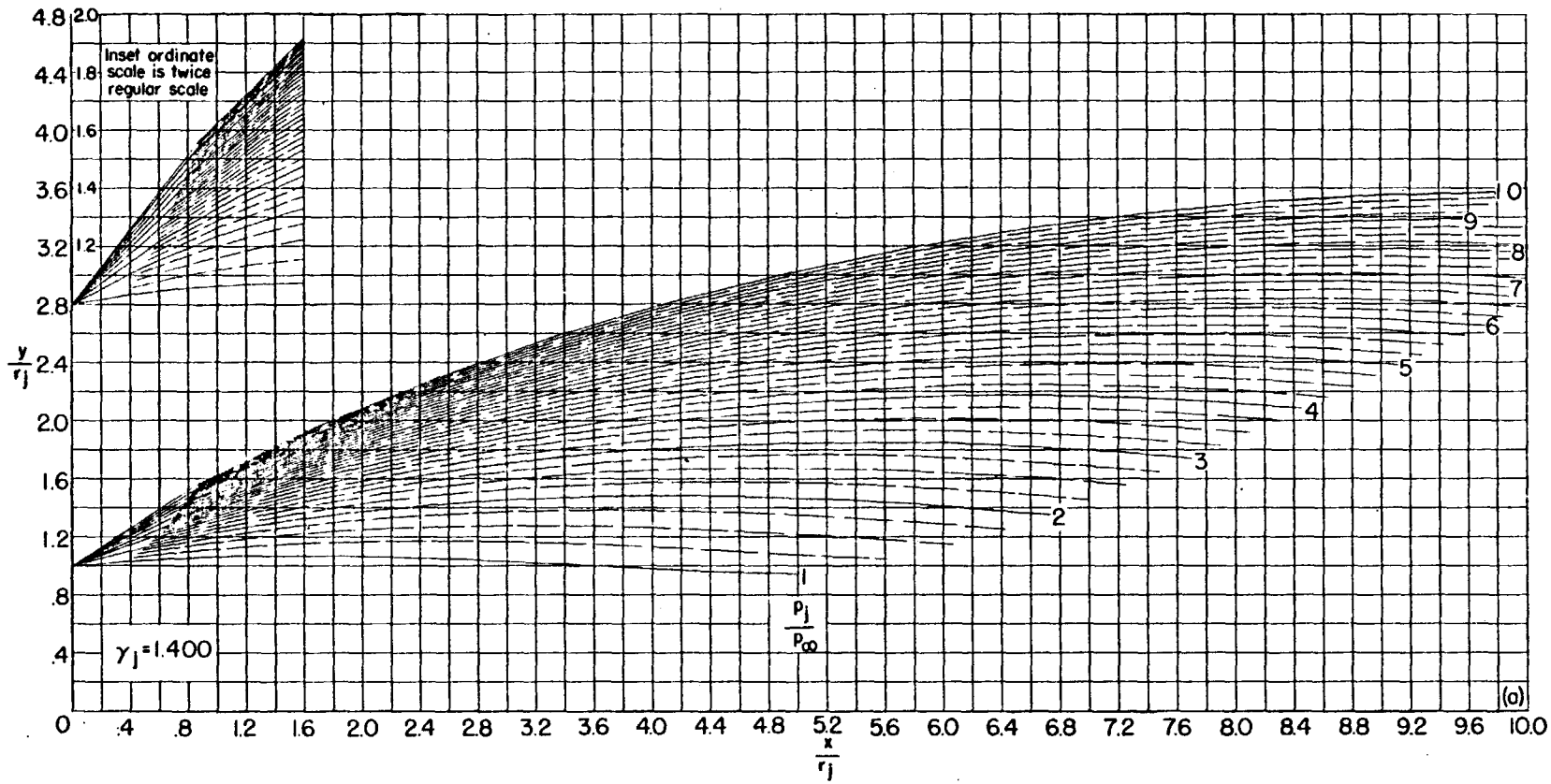

(a) $\theta_N = 5°$. Continued.

FIGURE 29.—Continued.

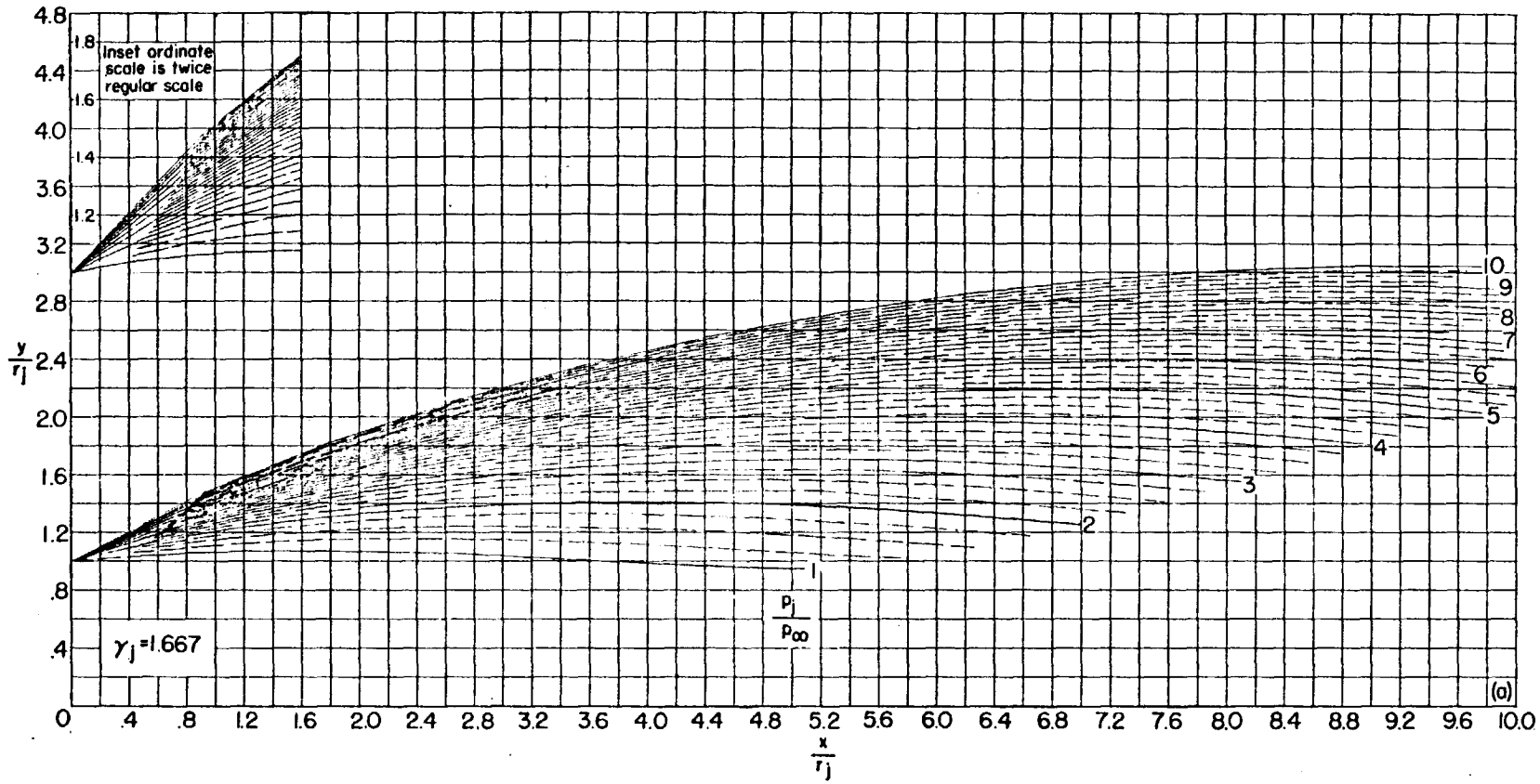

(a) θ_N=5°. Concluded.

FIGURE 29.—Continued.

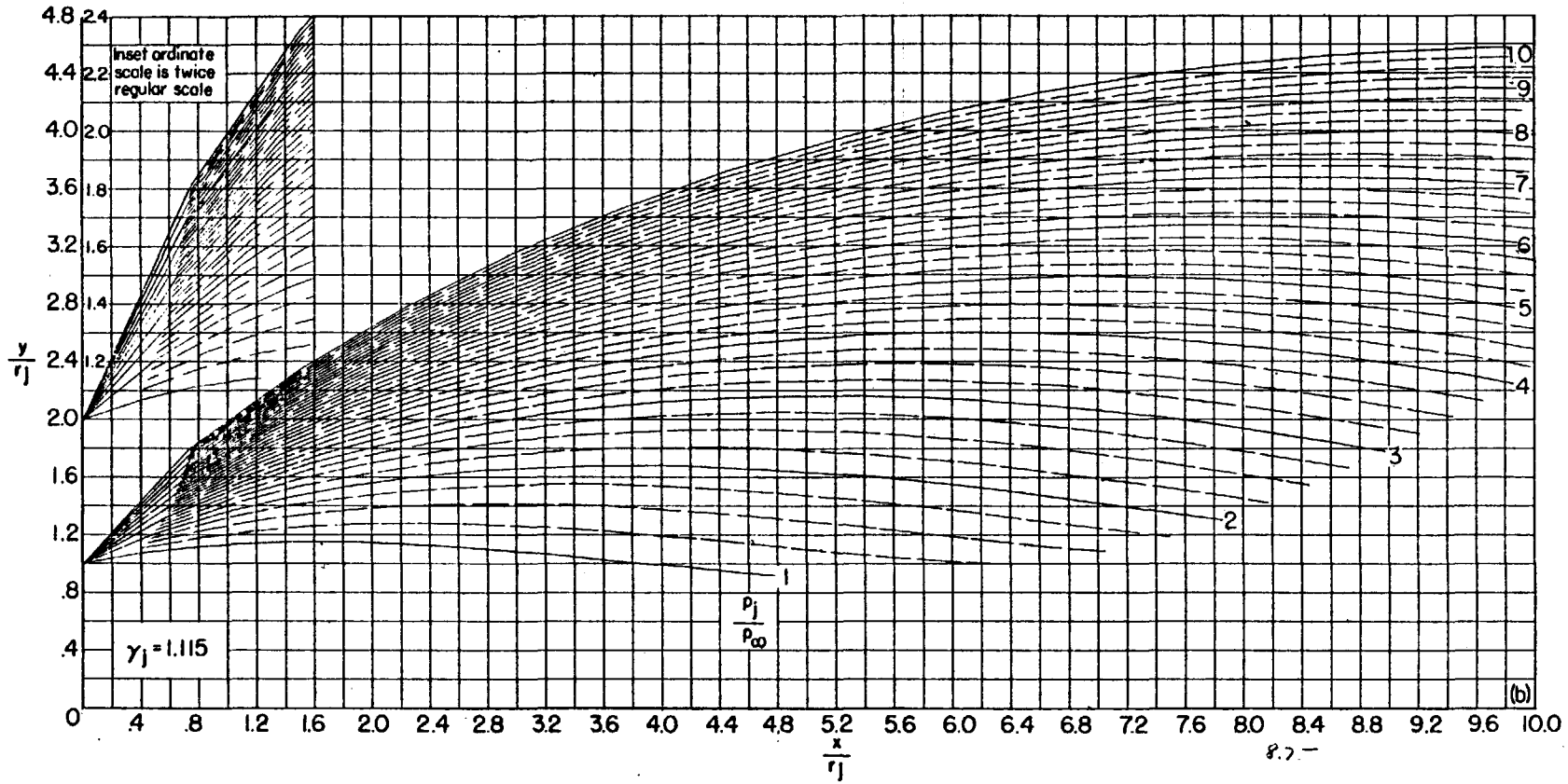

(b) $\theta_N = 10°$.

FIGURE 29.—Continued.

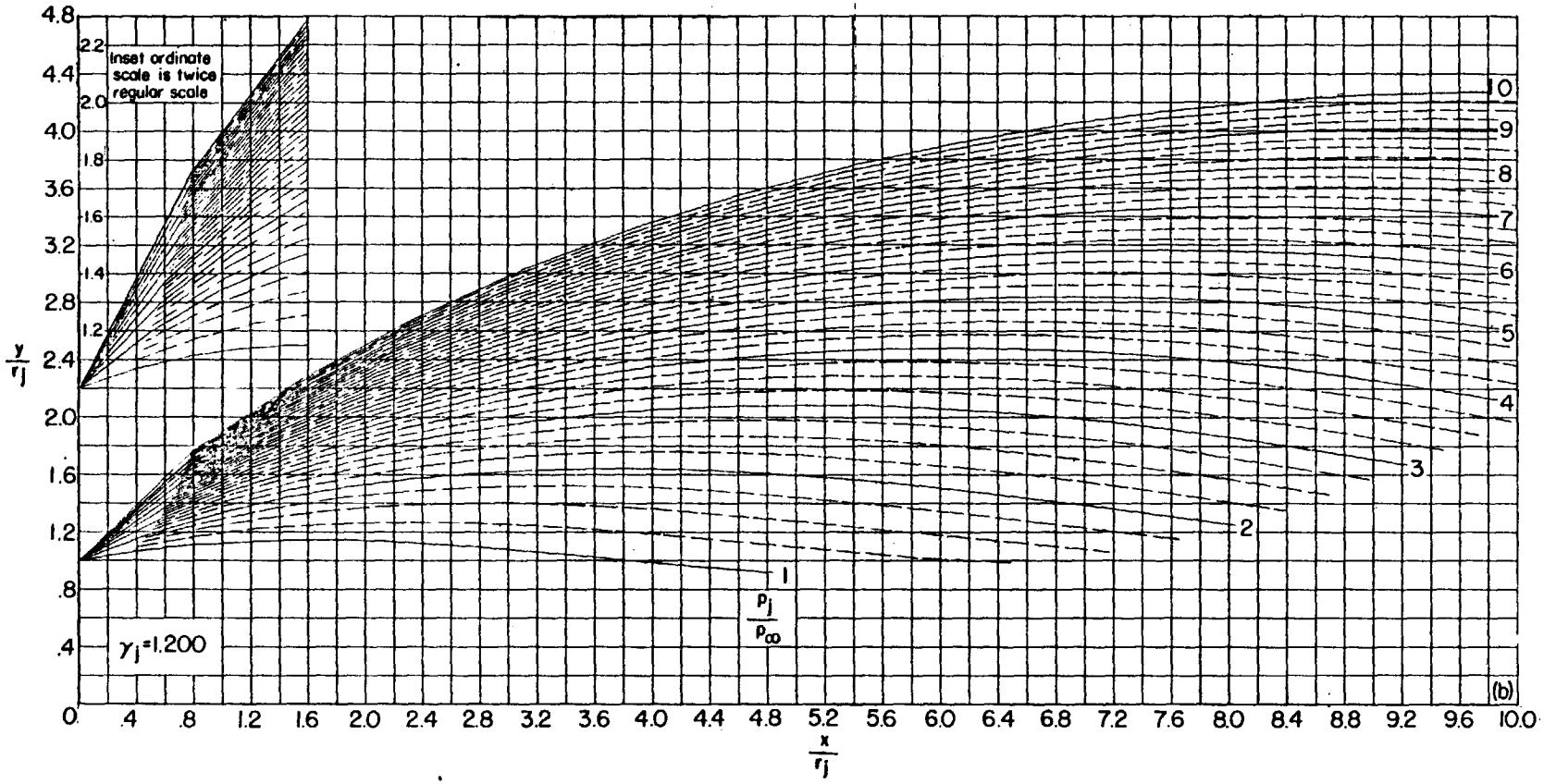

(b) $\theta_N = 10°$. Continued.

FIGURE 29.—Continued.

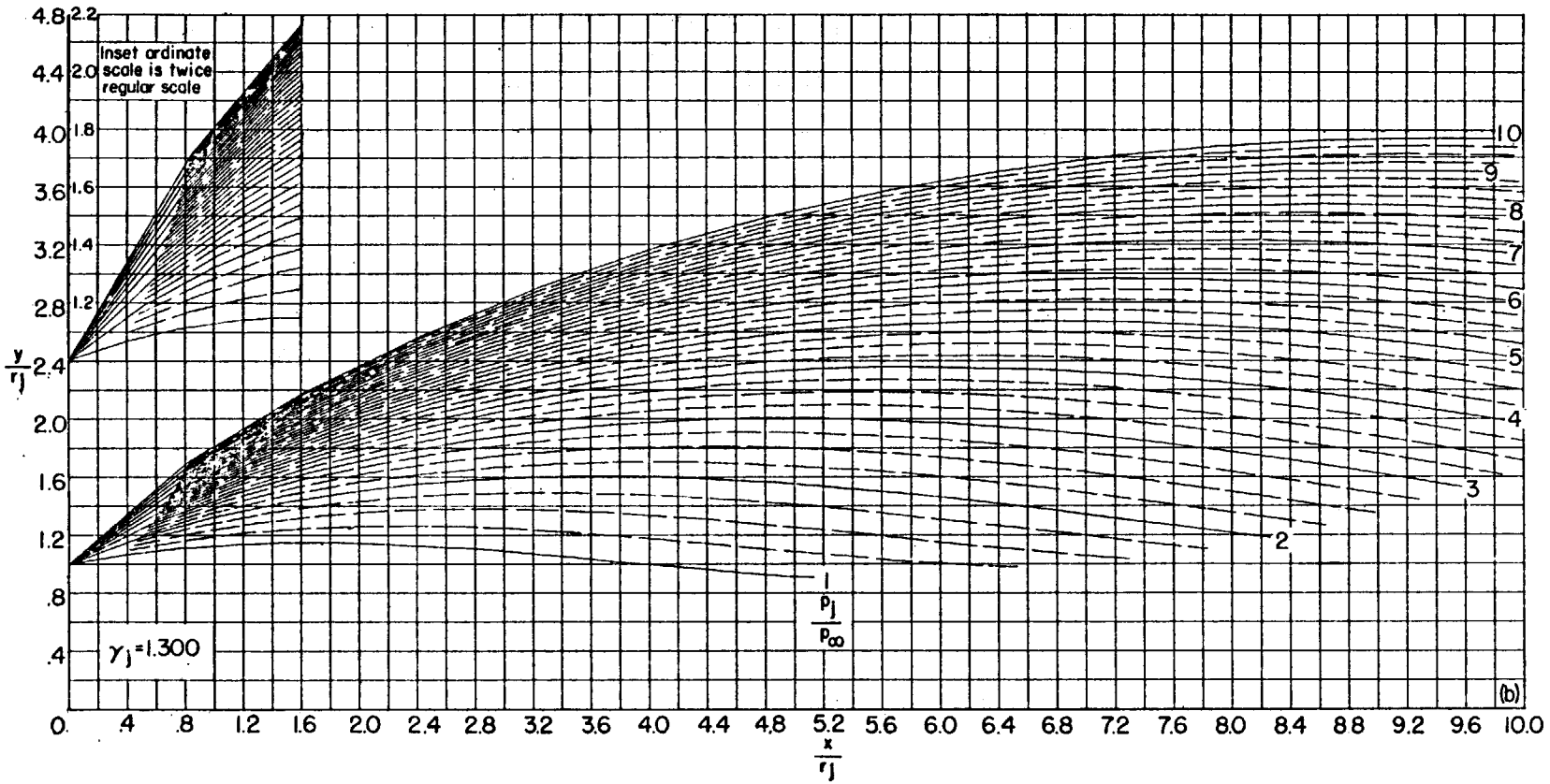

(b) $\theta_N = 10°$. Continued.

FIGURE 29.—Continued.

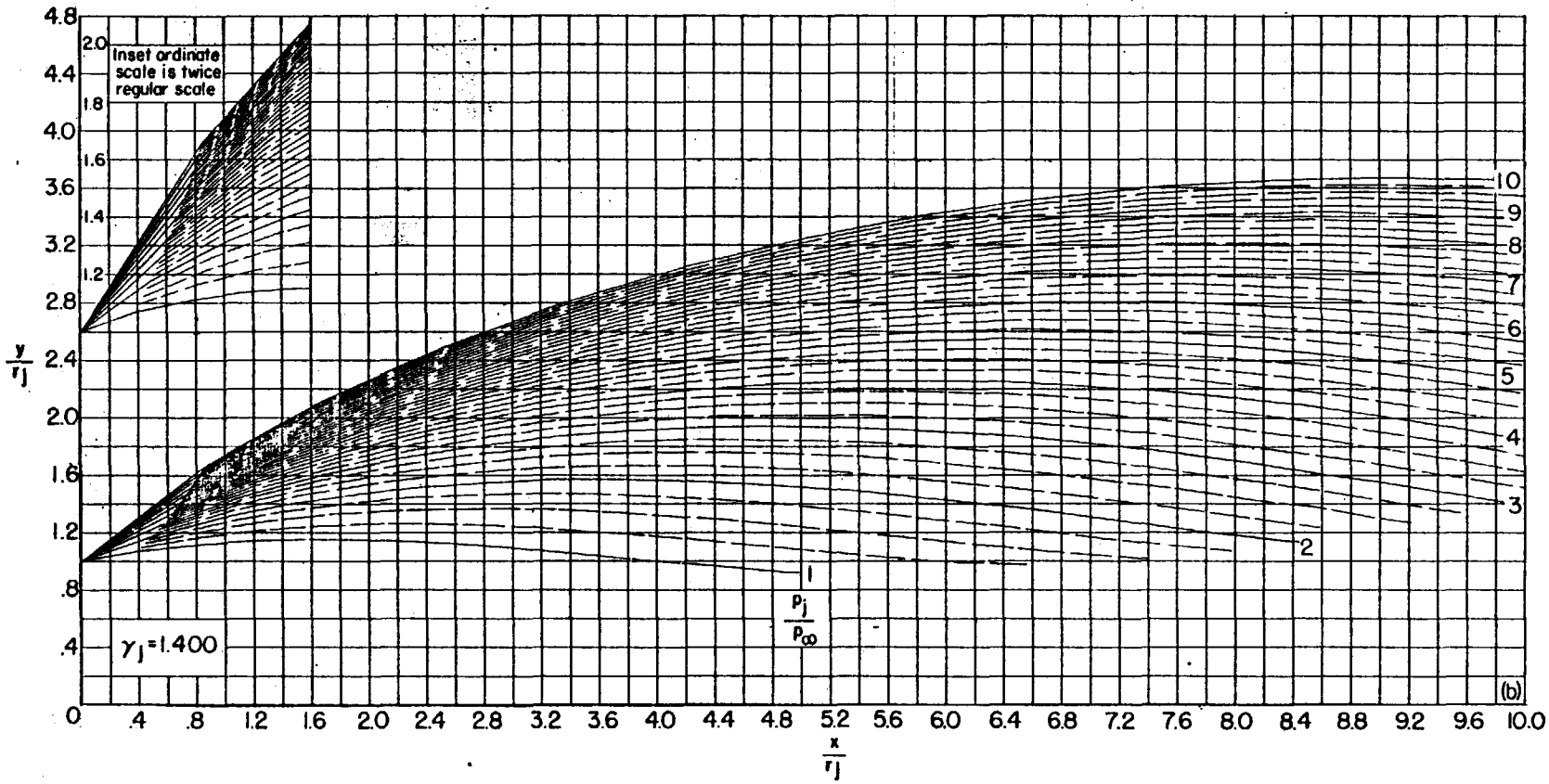

(b) $\theta_N = 10°$. Continued.

FIGURE 29.—Continued.

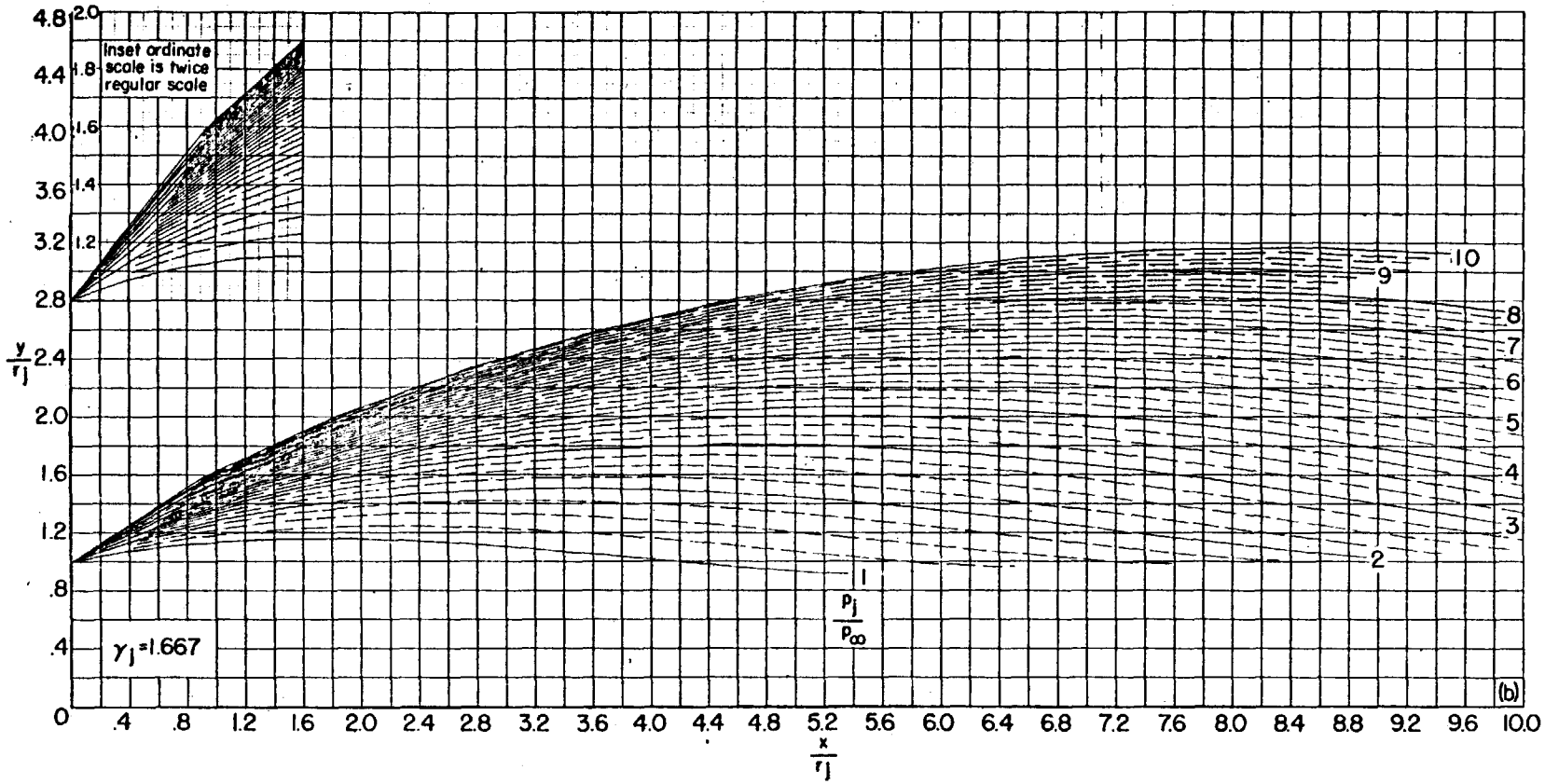

(b) $\theta_N = 10°$. Concluded.

FIGURE 29.—Continued.

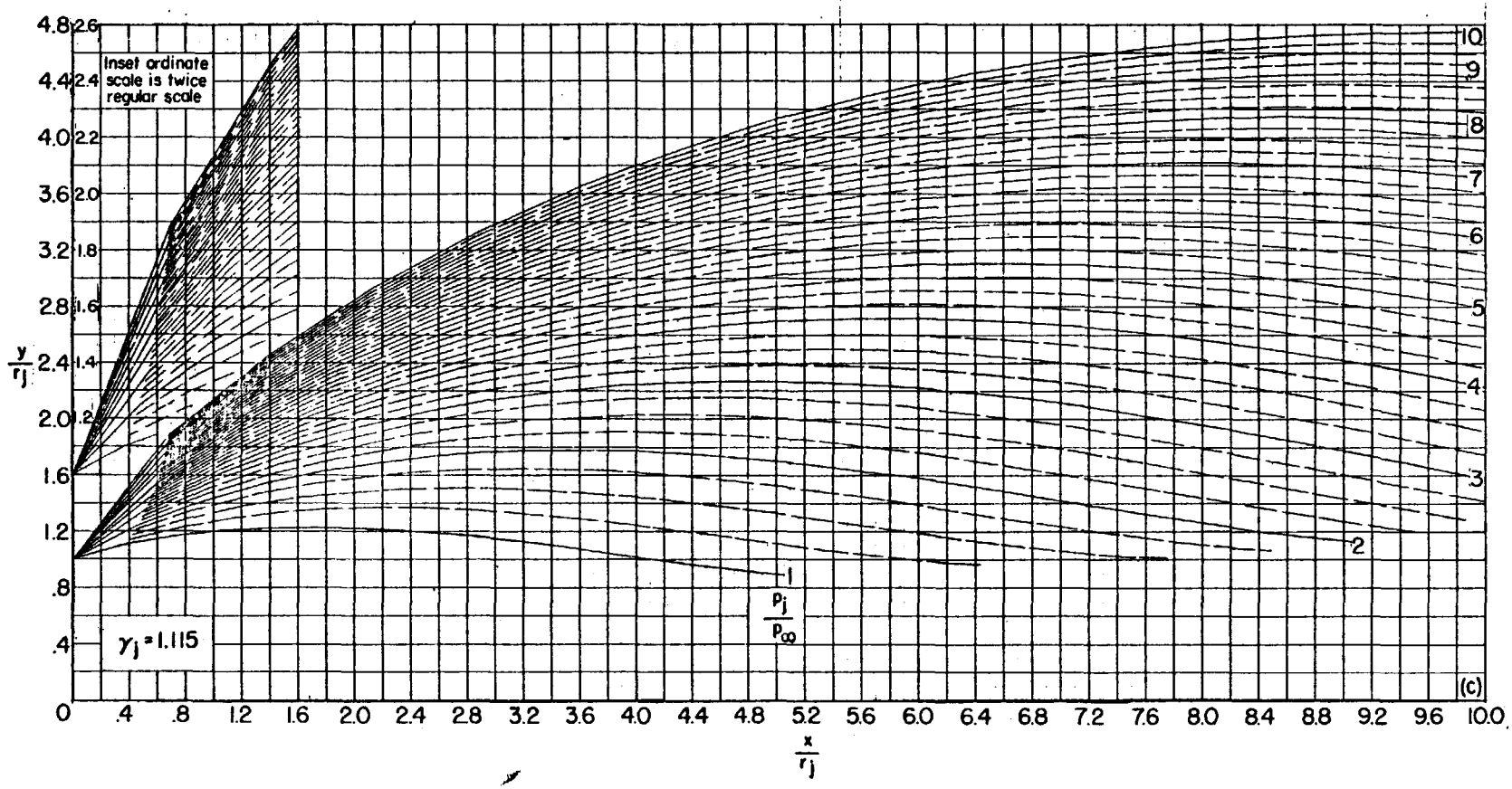

(c) $\theta_N = 15°$

FIGURE 29.—Continued.

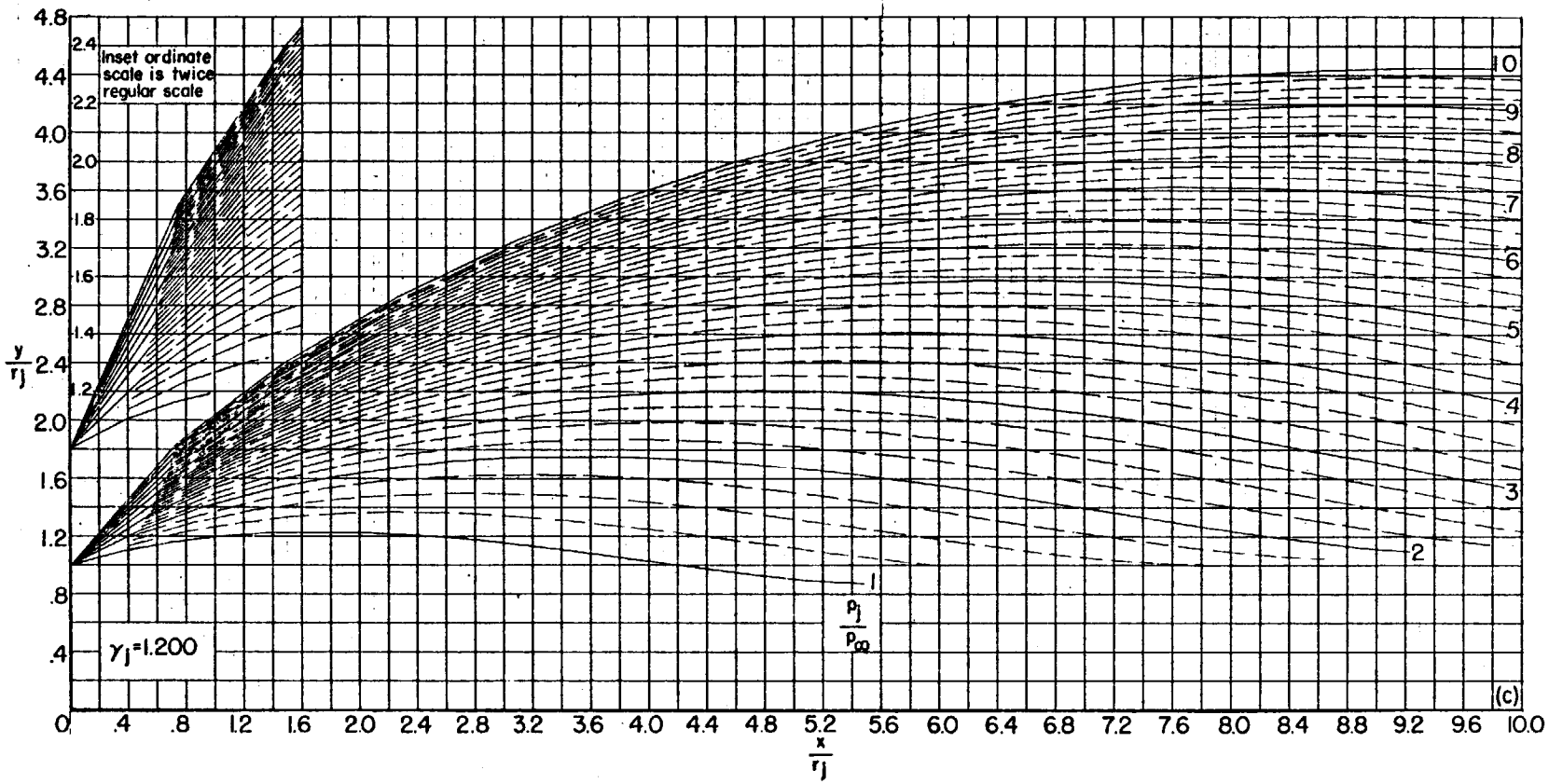

(c) $\theta_N = 15°$. Continued.

FIGURE 29.—Continued.

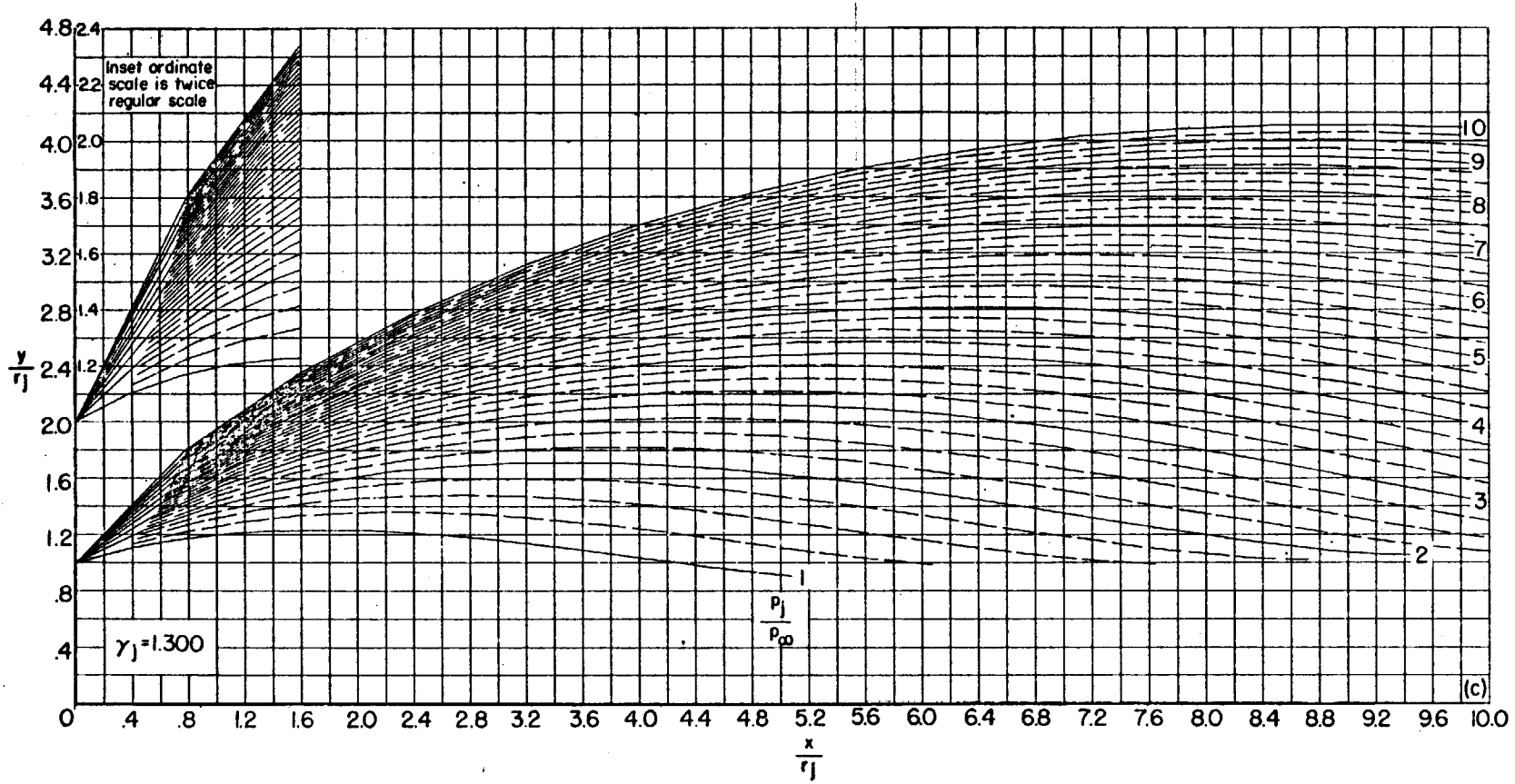

(c) $\theta_N = 15°$. Continued.

FIGURE 29.—Continued.

502683 O—59——12

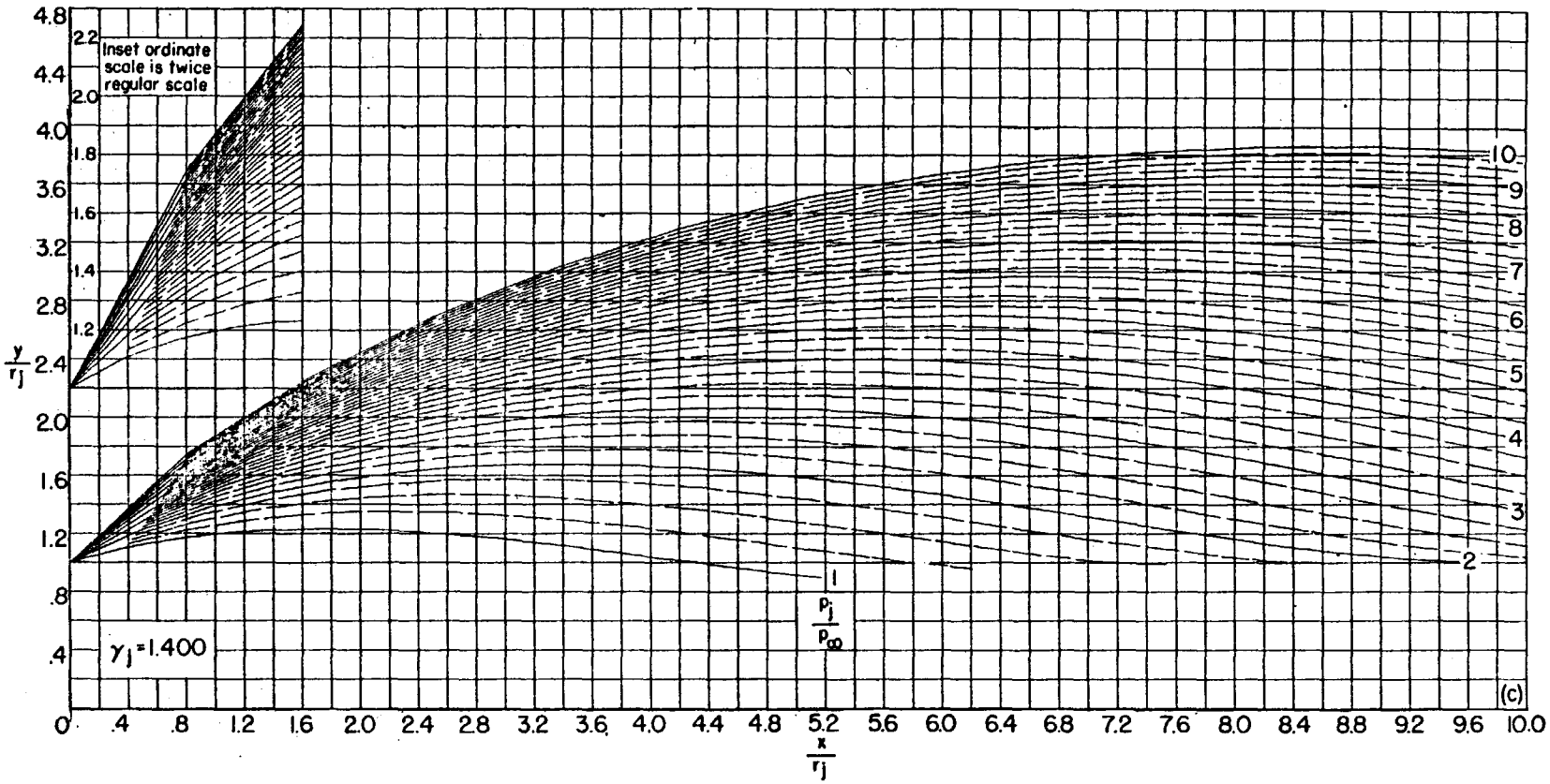

(c) $\theta_N = 15°$. Continued.

FIGURE 29.—Continued.

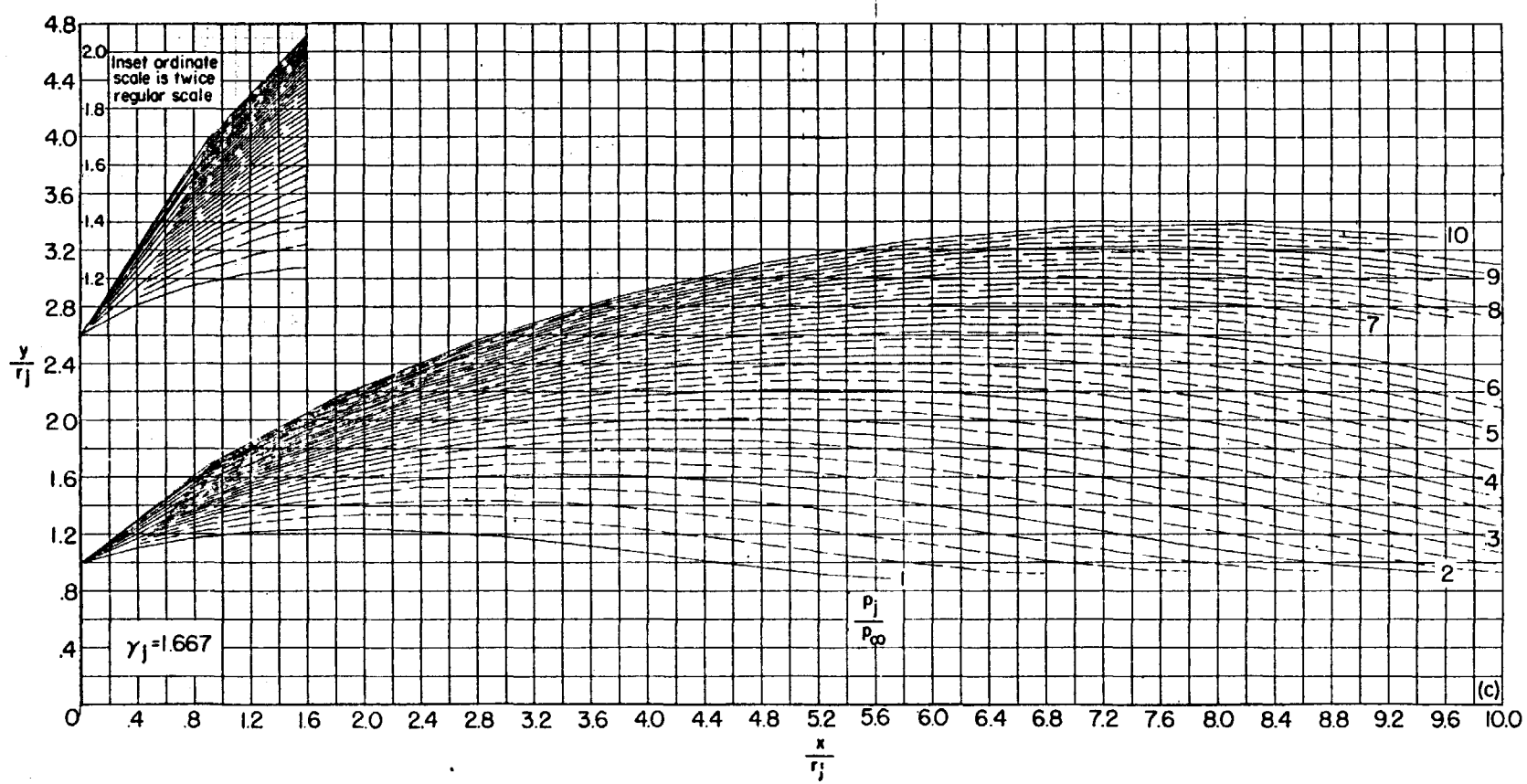

(c) $\theta_N = 15°$. Concluded.

FIGURE 29.—Continued.

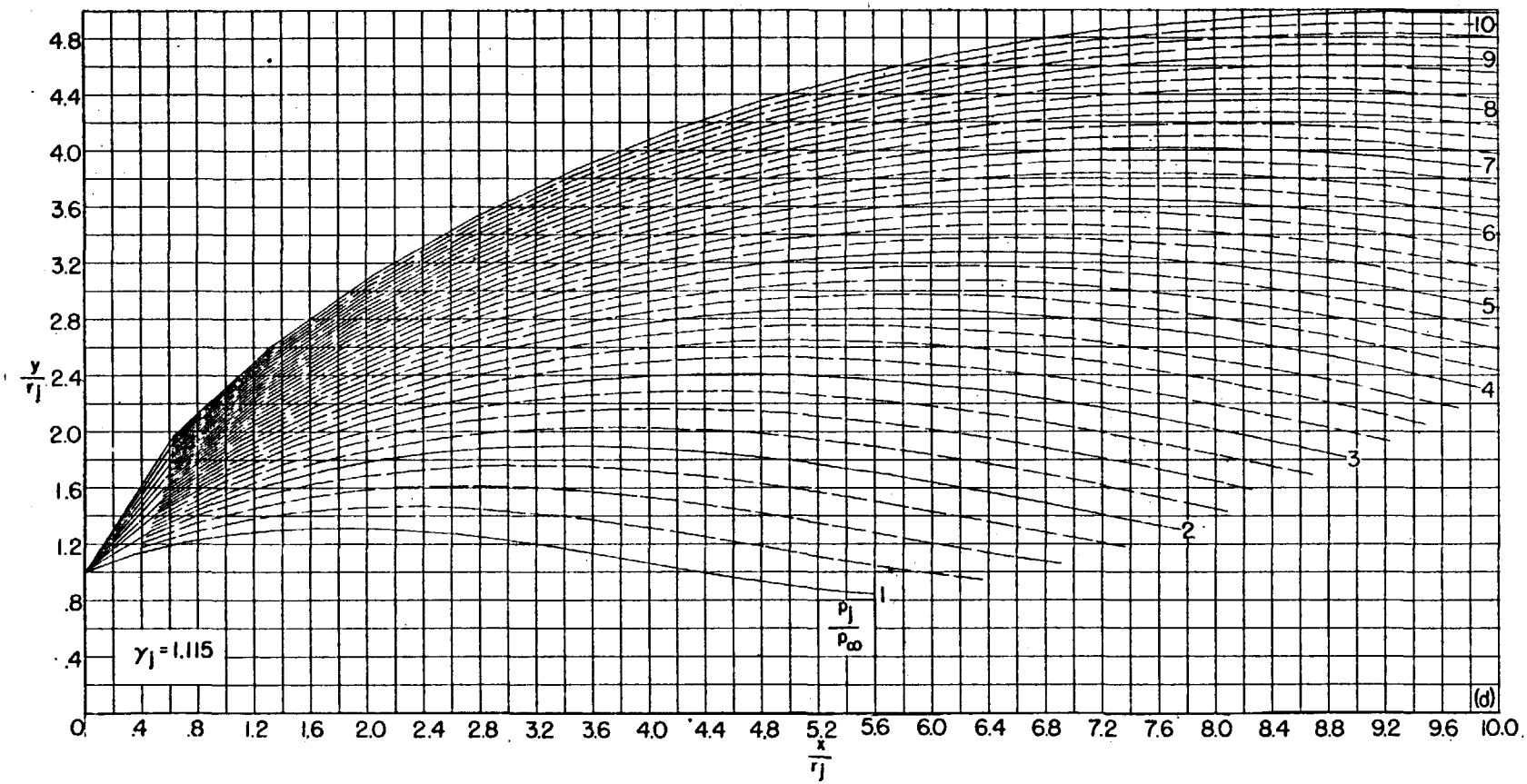

(d) $\theta_N = 20°$

FIGURE 29.—Continued.

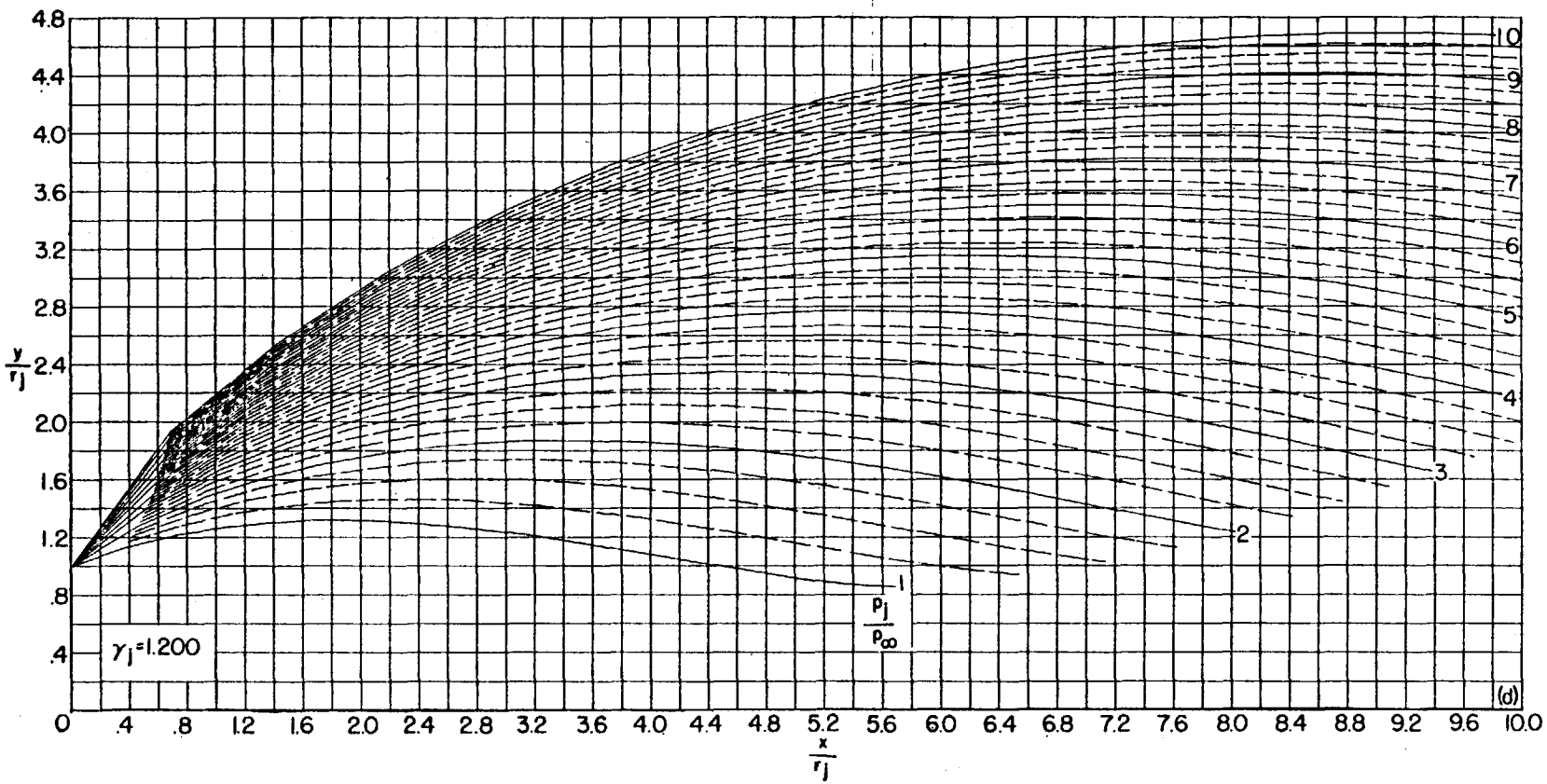

(d) $\theta_N = 20°$. Continued.

FIGURE 29.—Continued.

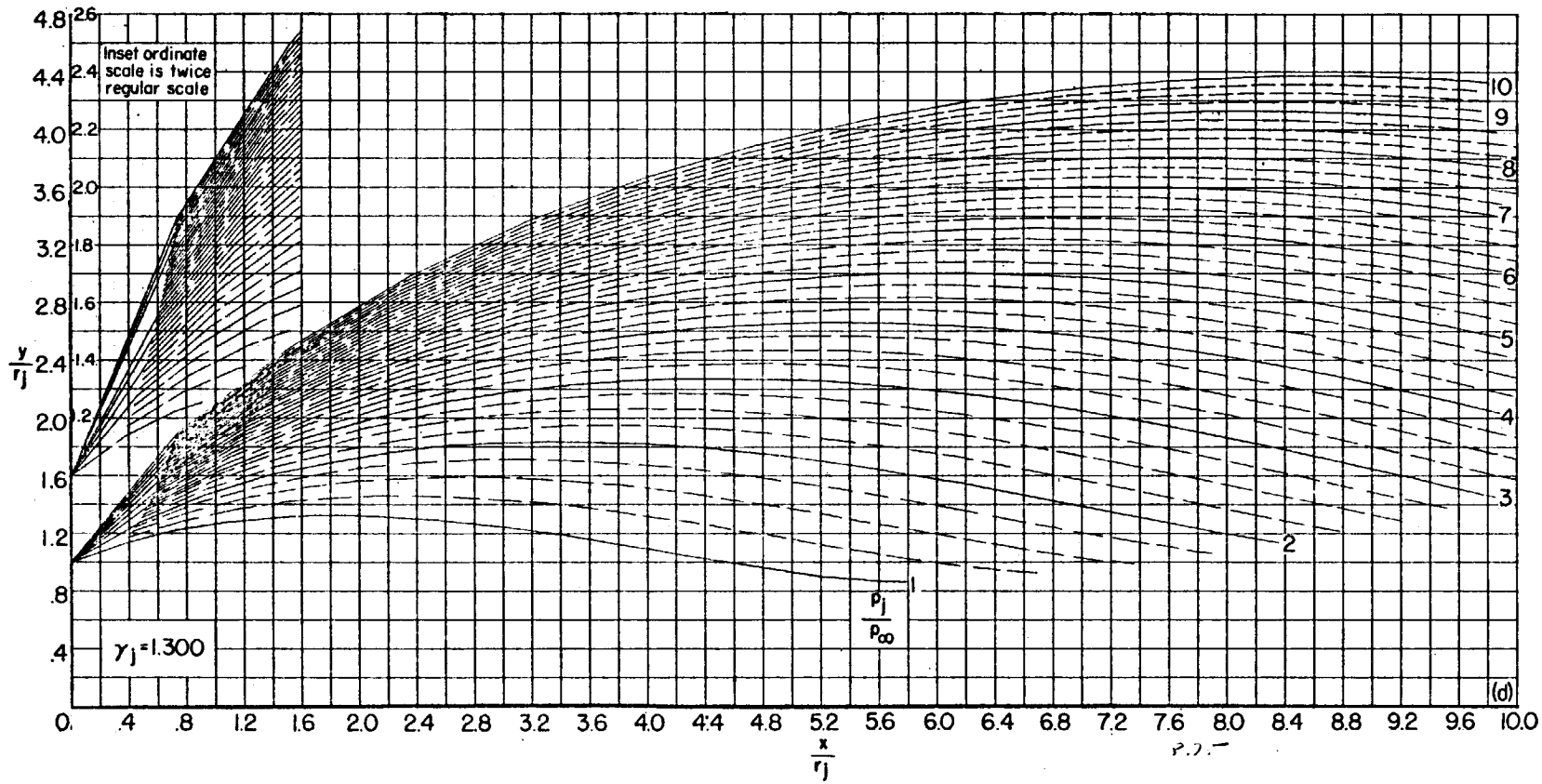

(d) $\theta_N = 20°$. Continued.

FIGURE 29.—Continued.

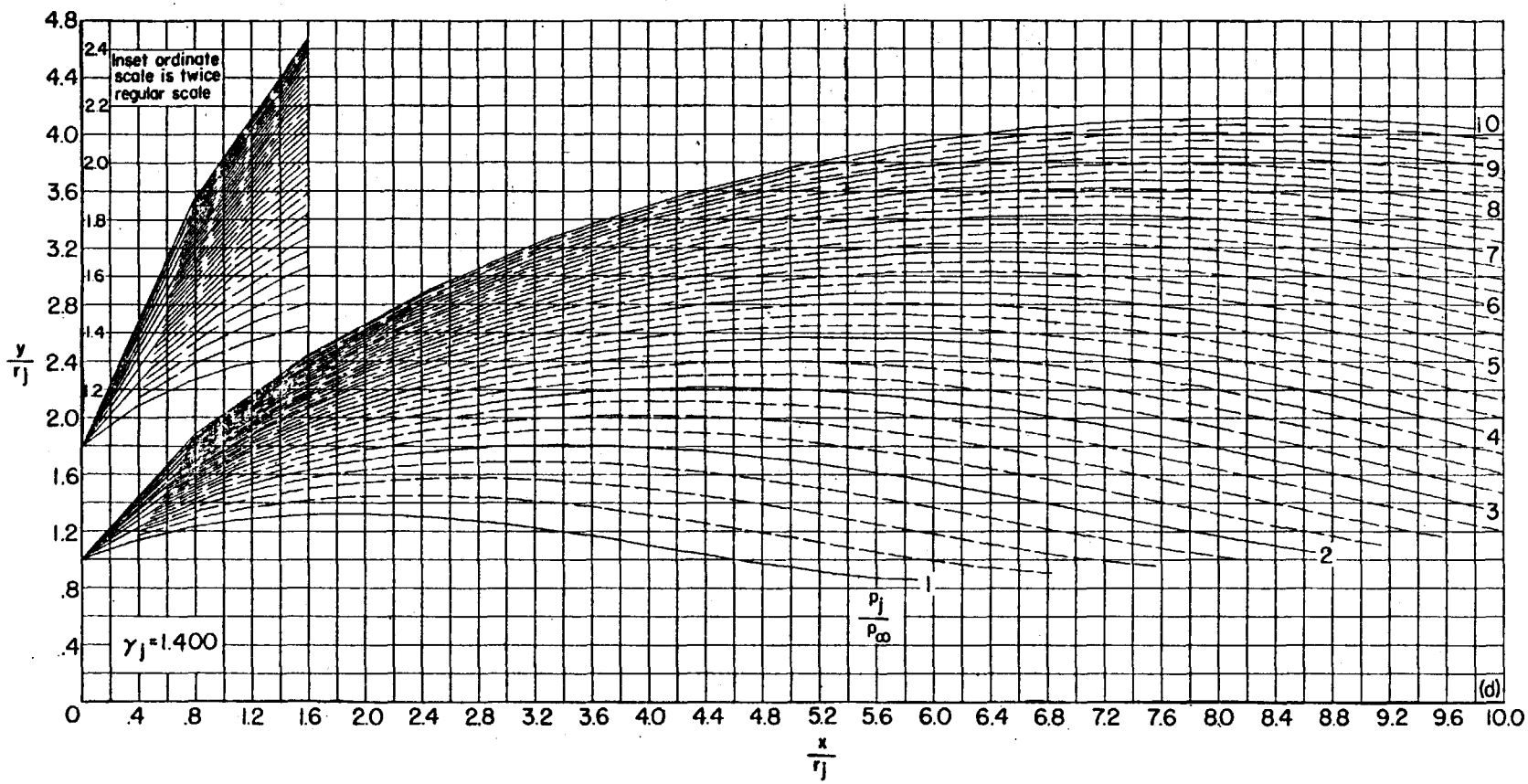

(d) $\theta_N = 20°$. Continued.

FIGURE 29.—Continued.

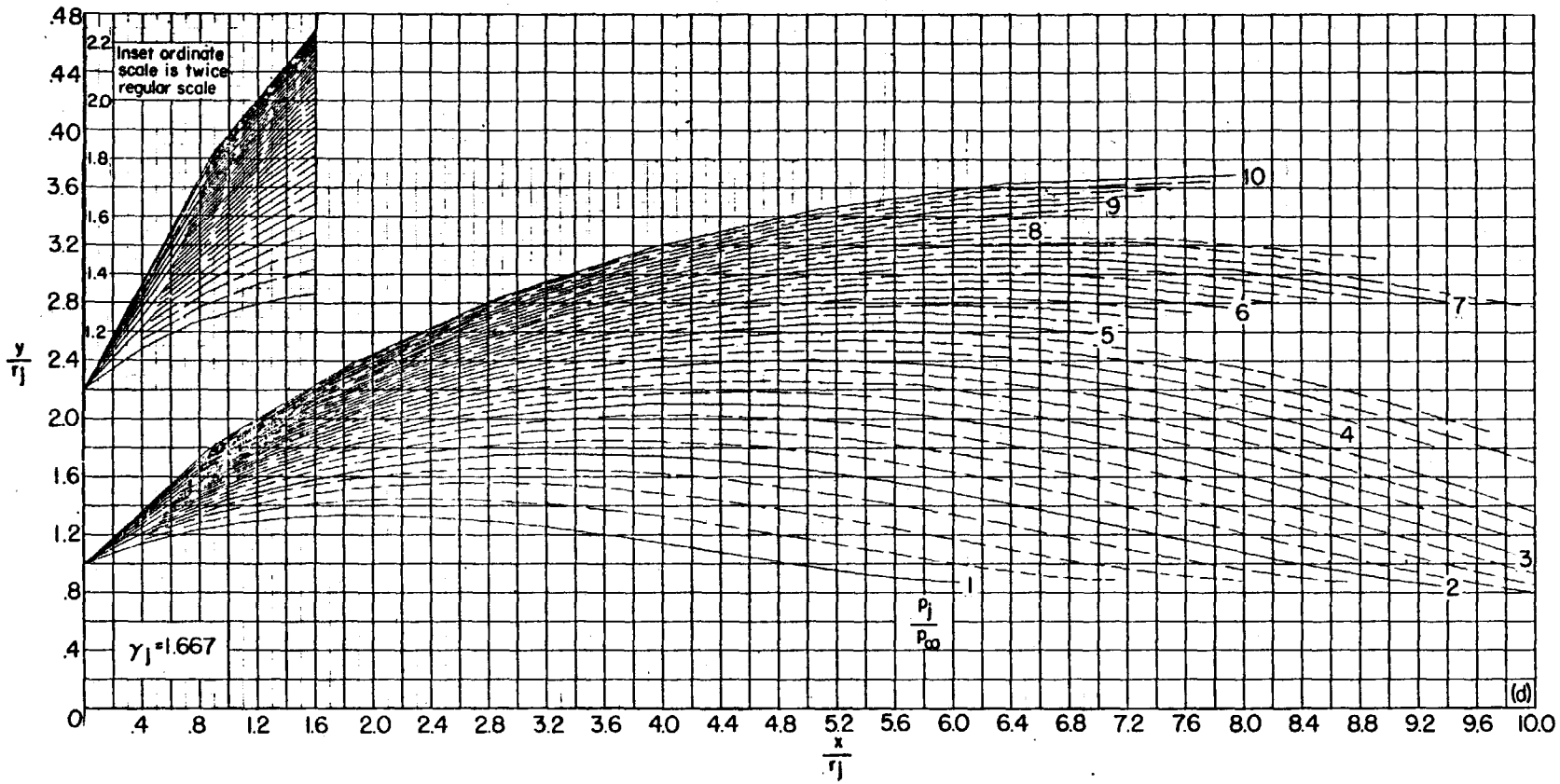

(d) $\theta_N = 20°$. Concluded.

FIGURE 29.—Concluded.

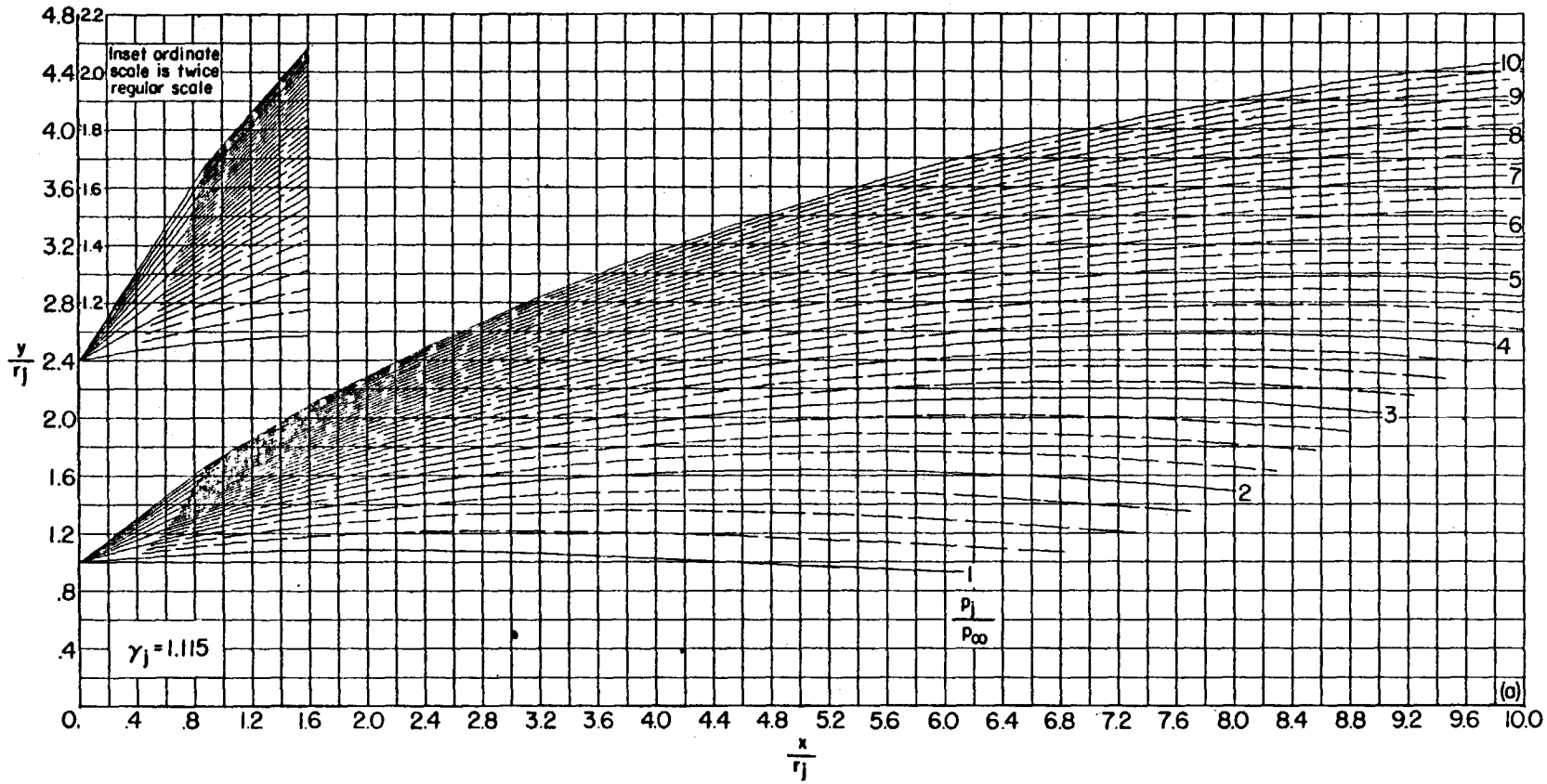

(a) $\theta_N = 5°$.

FIGURE 30.—Jet boundaries at $M_j = 3.0$ for jet pressure ratios from 1 to 10. (Dashed boundaries denote changes in p_j/p_∞ of 0.25.)

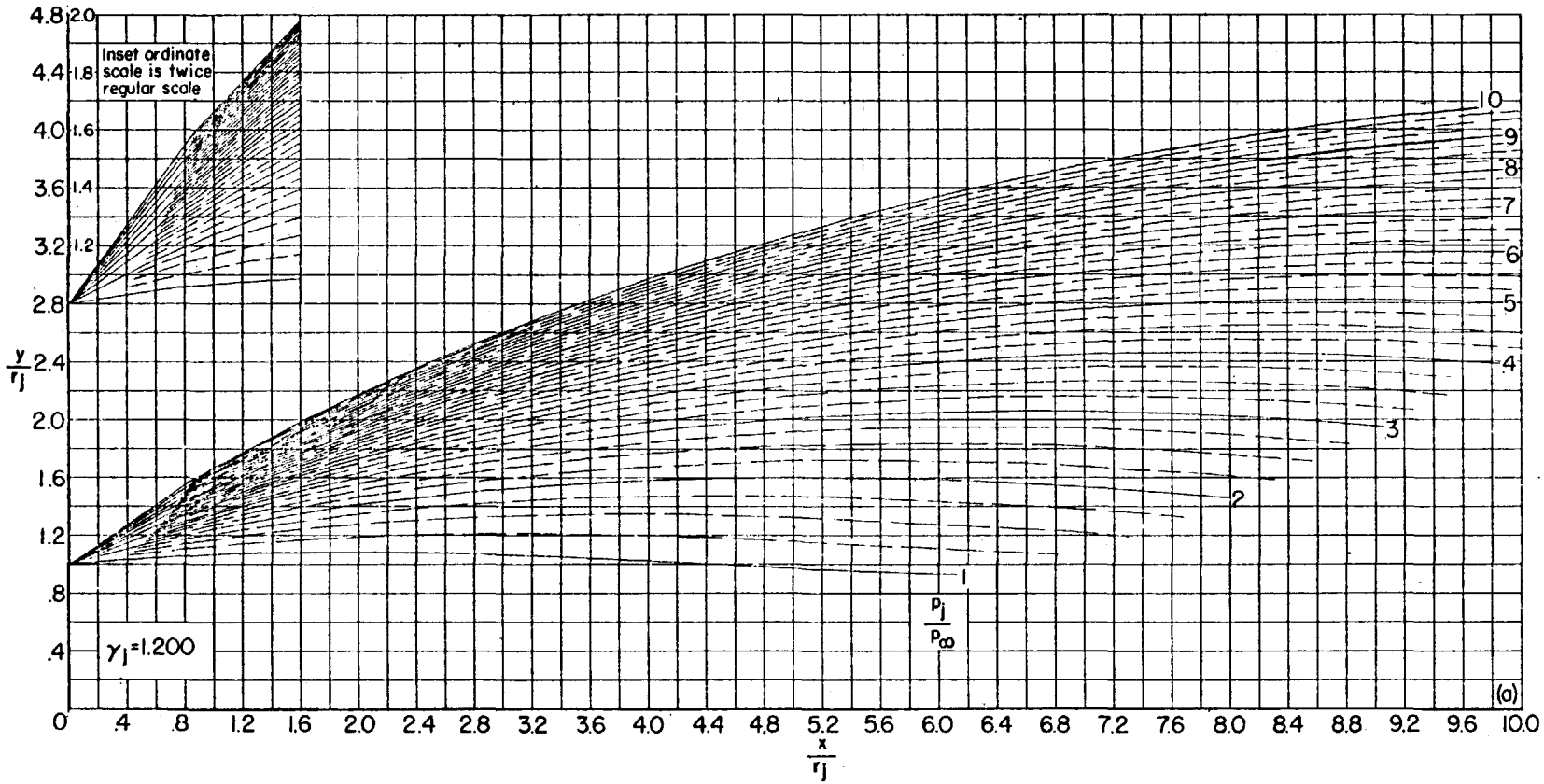

(a) $\theta_N = 5°$. Continued.

FIGURE 30.—Continued.

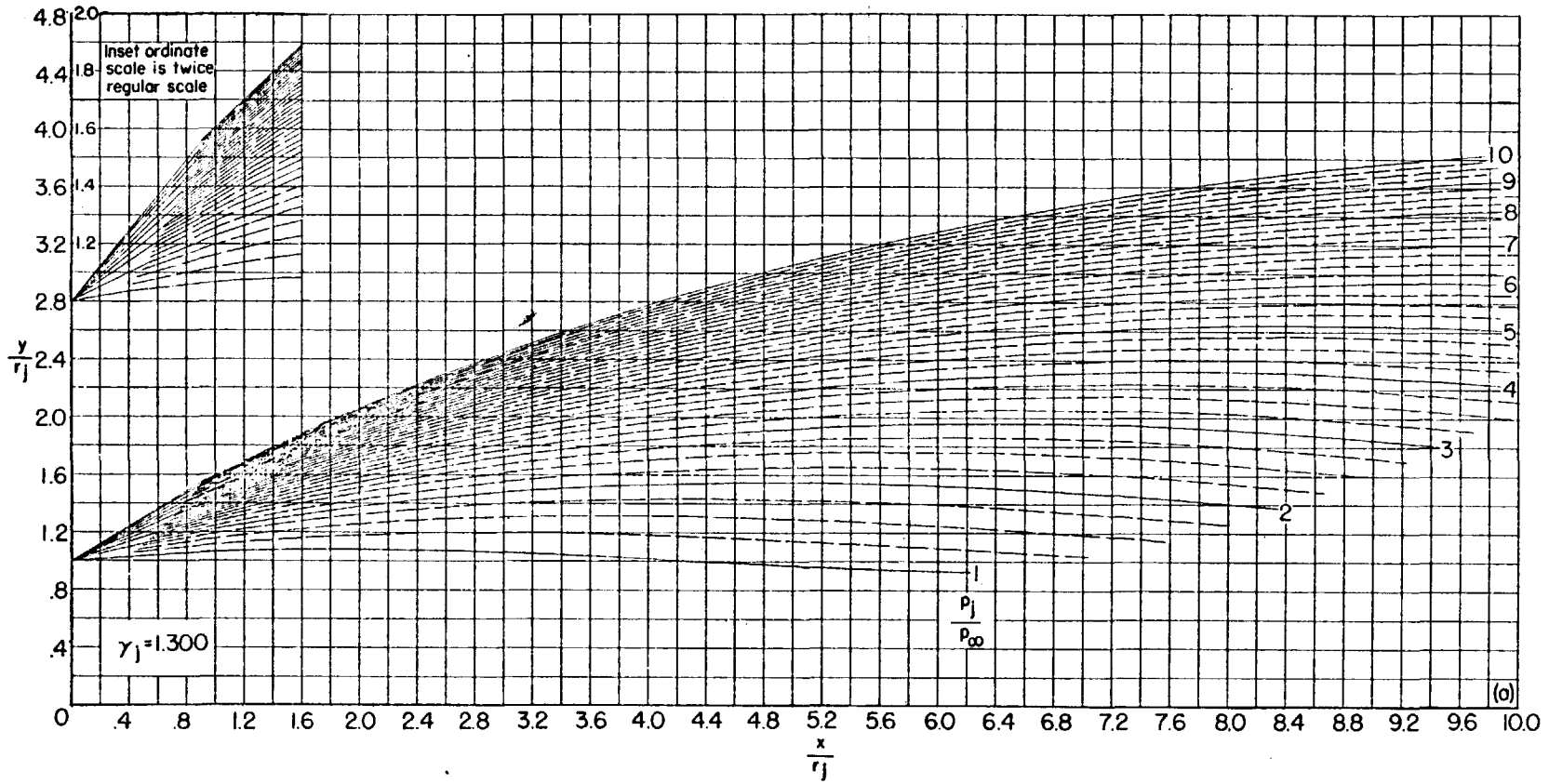

(a) $\theta_N = 5°$. Continued.

FIGURE 30.—Continued.

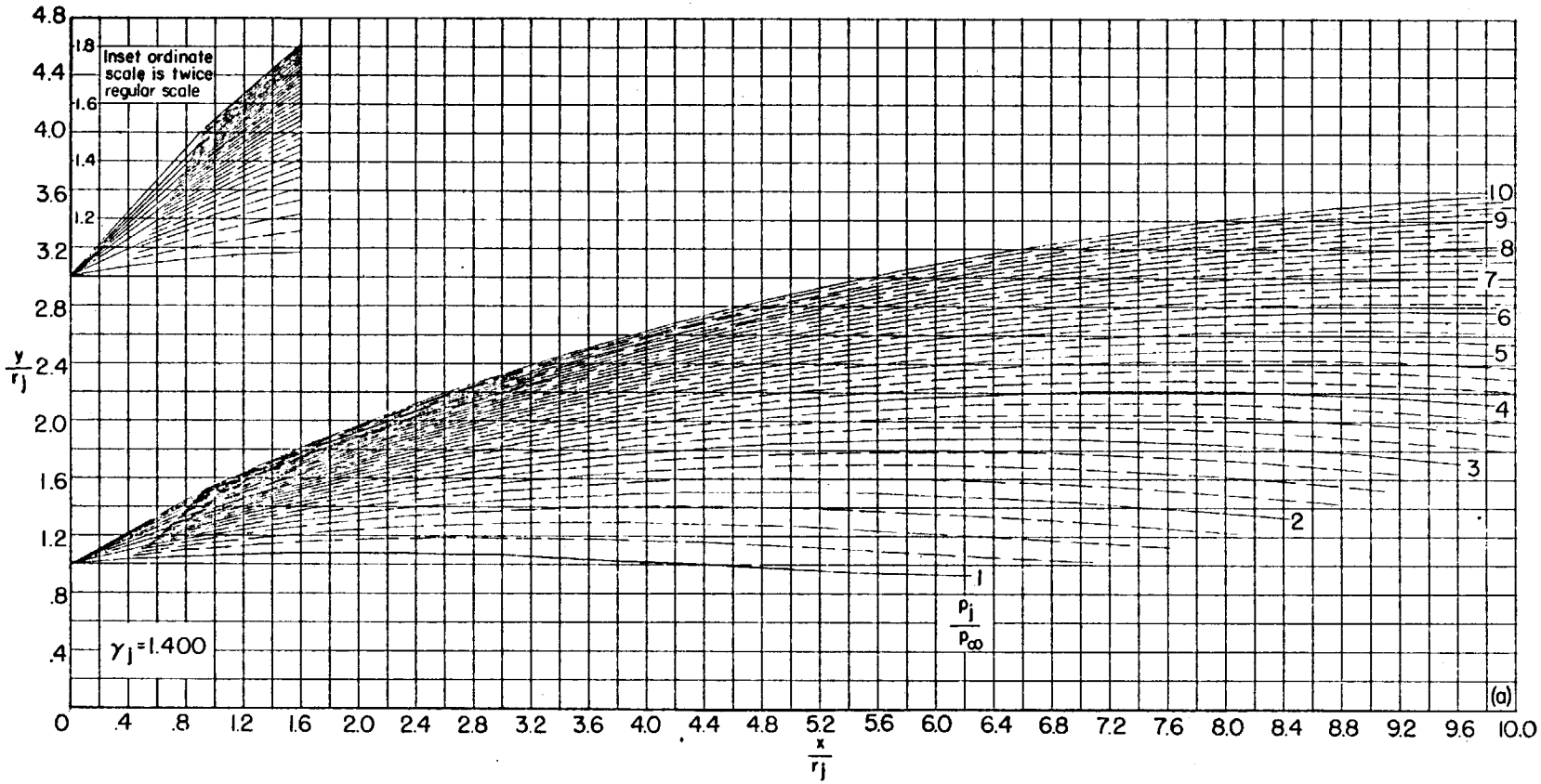

(a) $\theta_N = 5°$. Continued.

FIGURE 30.—Continued.

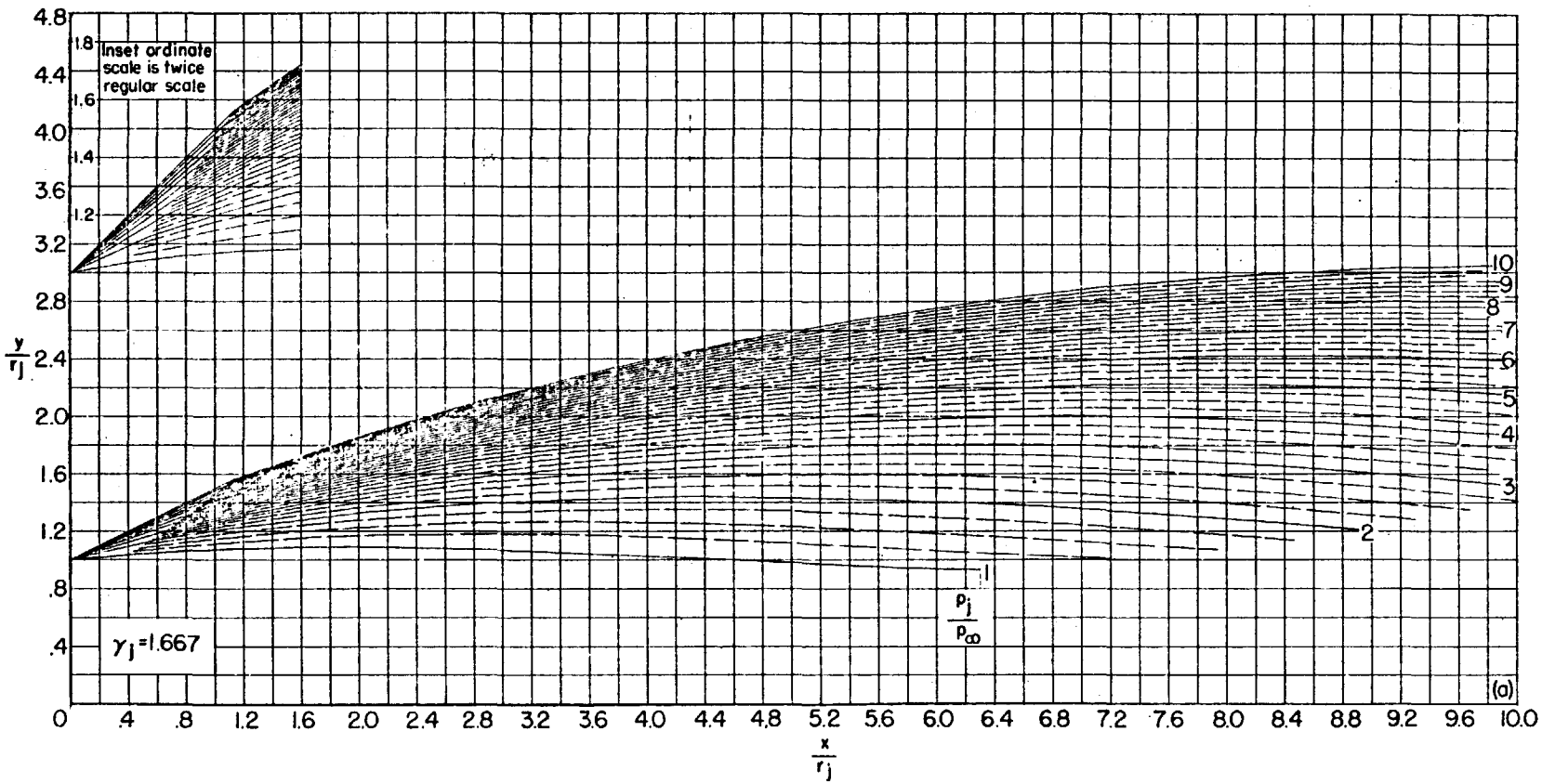

(a) θ_N=5°. Concluded.

FIGURE 30.—Continued.

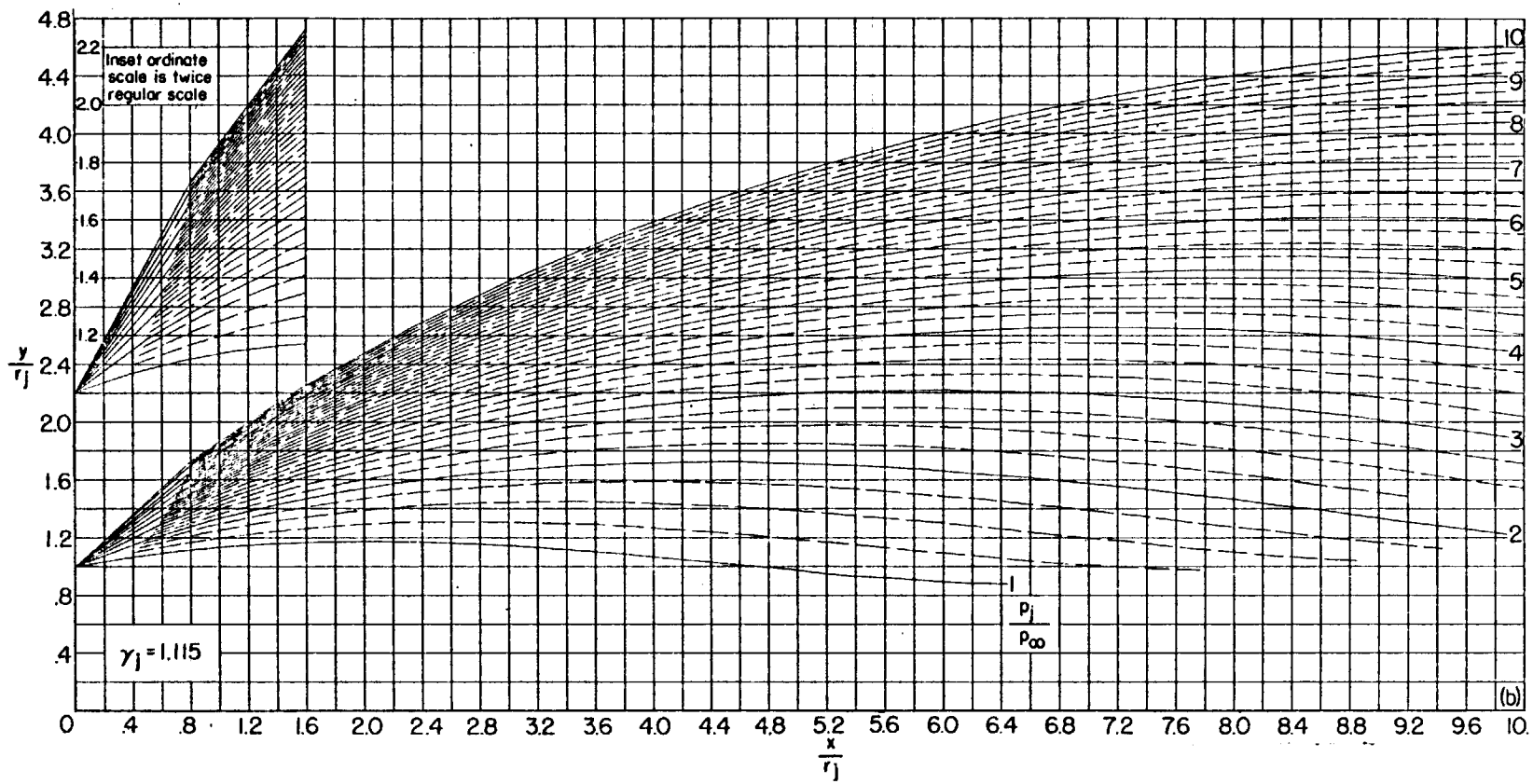

(b) $\theta_N = 10°$.

FIGURE 30.—Continued.

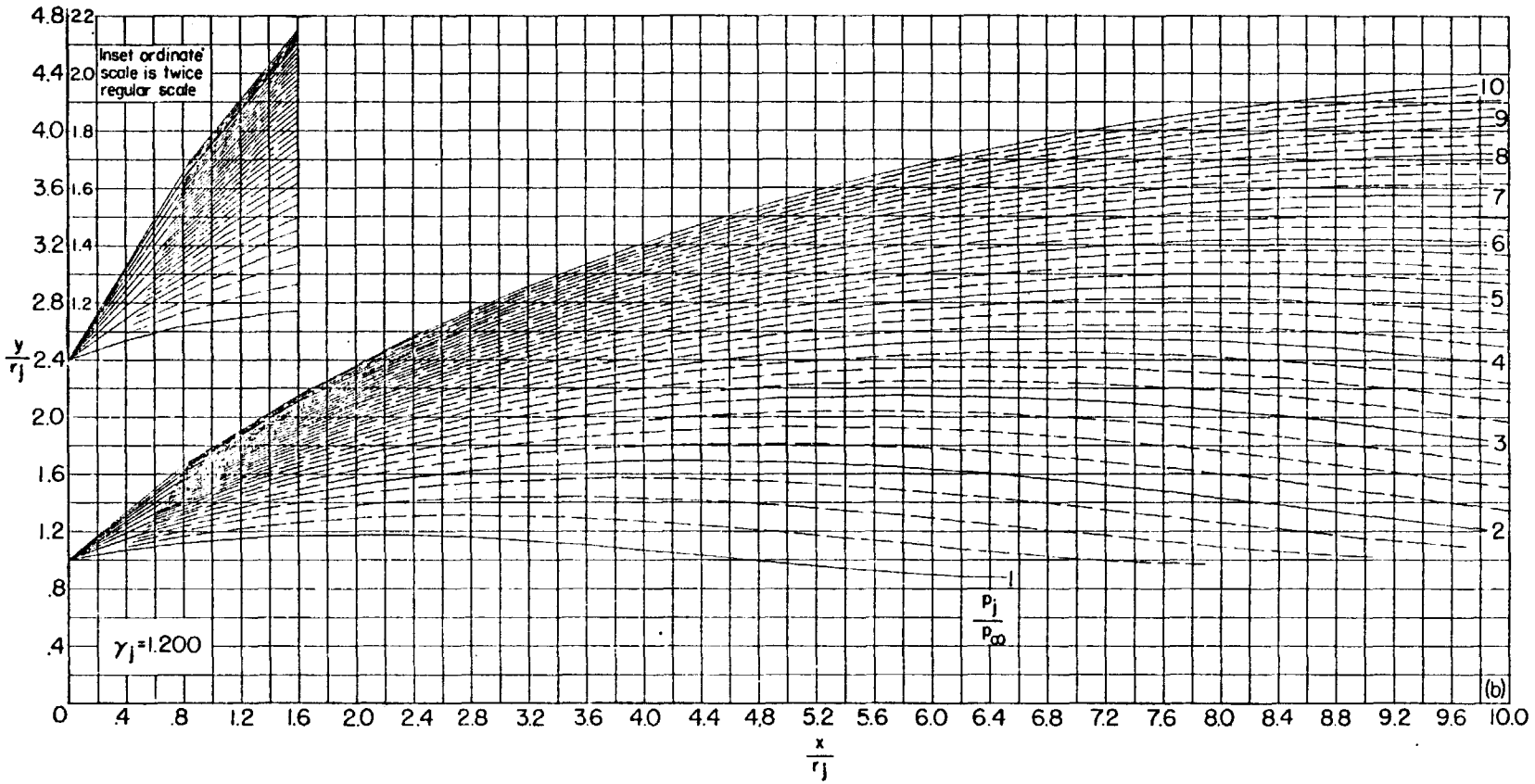

(b) $\theta_N = 10°$. Continued.

FIGURE 30.—Continued.

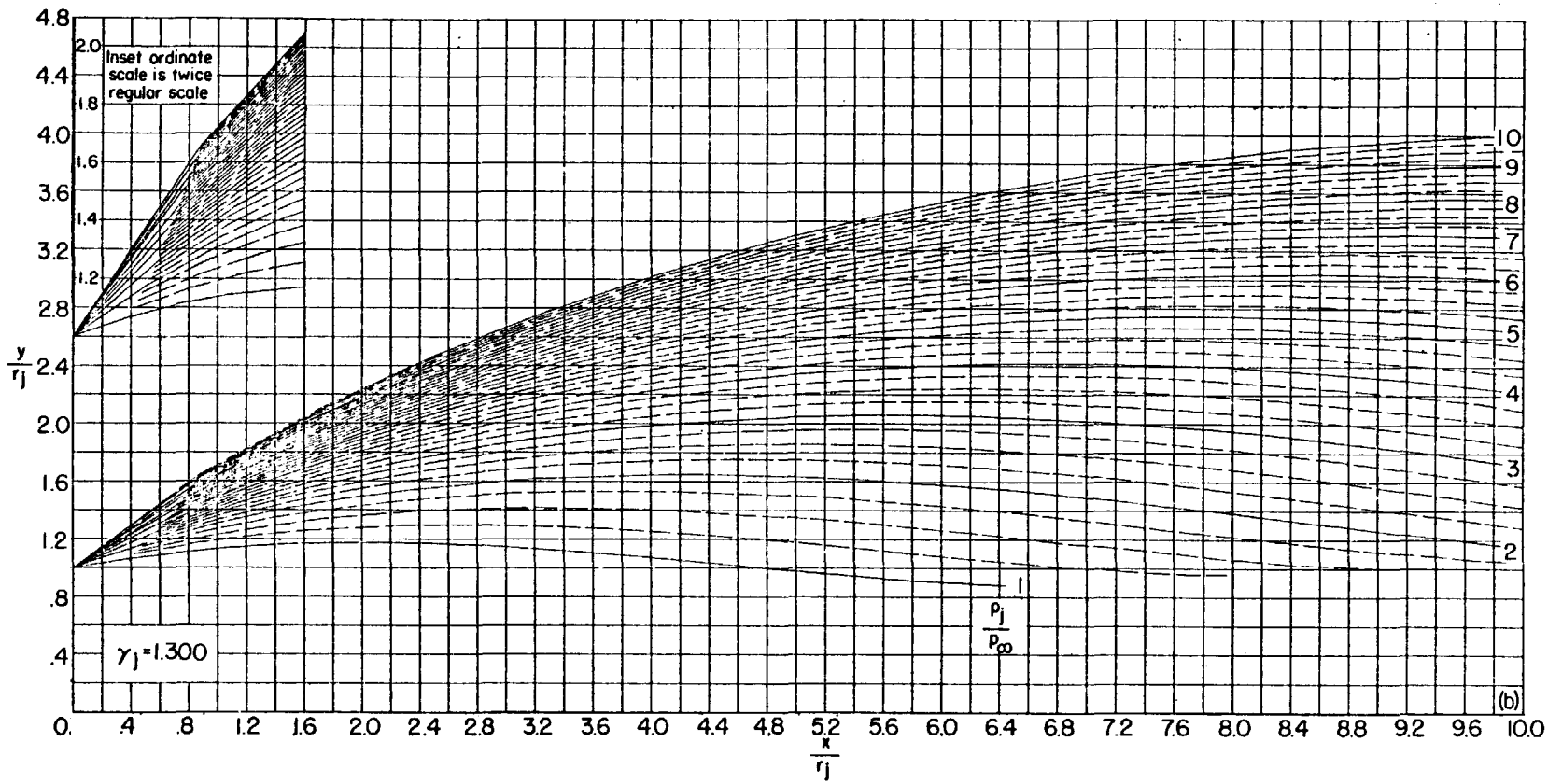

(b) $\theta_N = 10°$. Continued.

FIGURE 30.—Continued.

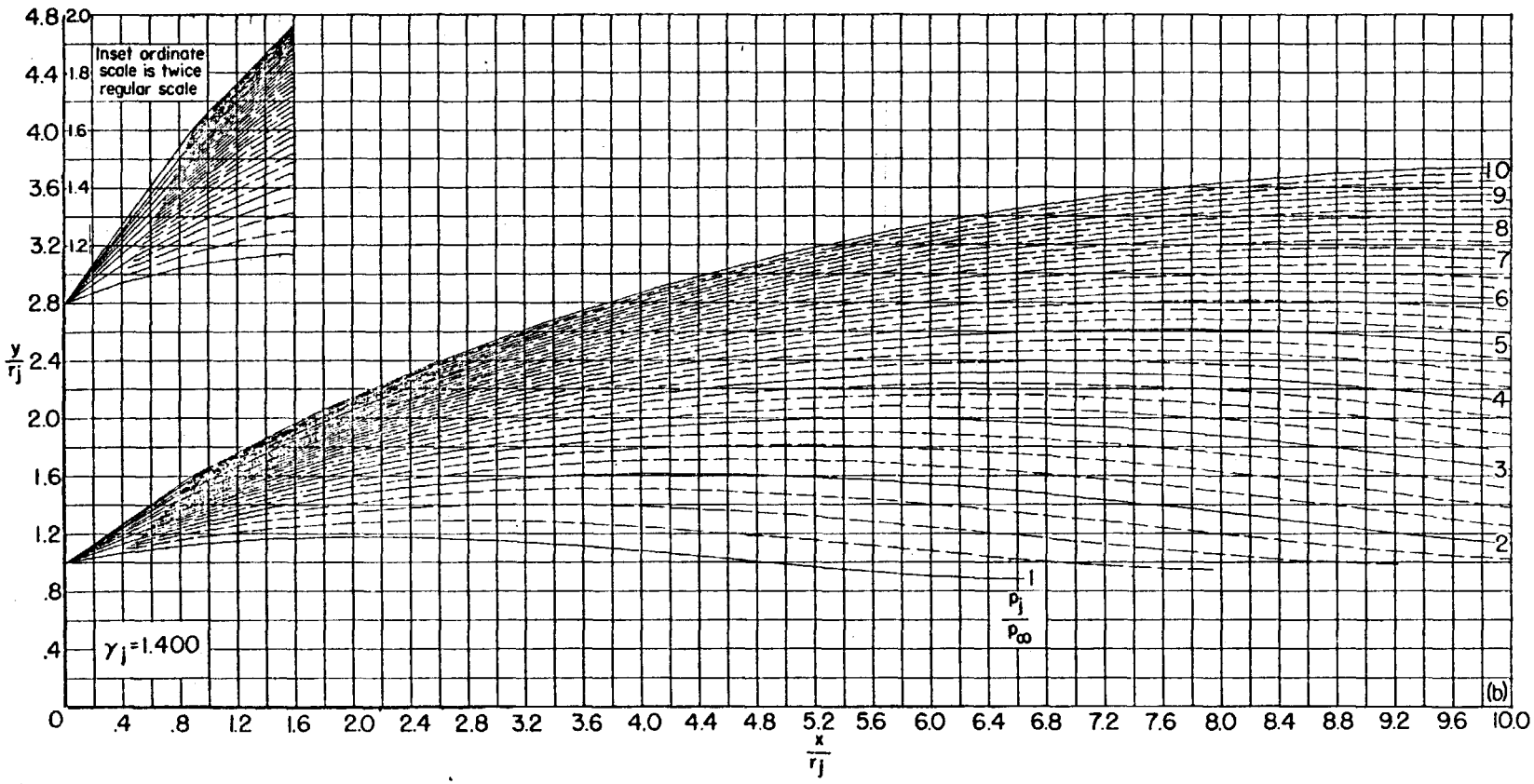

(b) $\theta_N = 10°$. Continued.

FIGURE 30.—Continued.

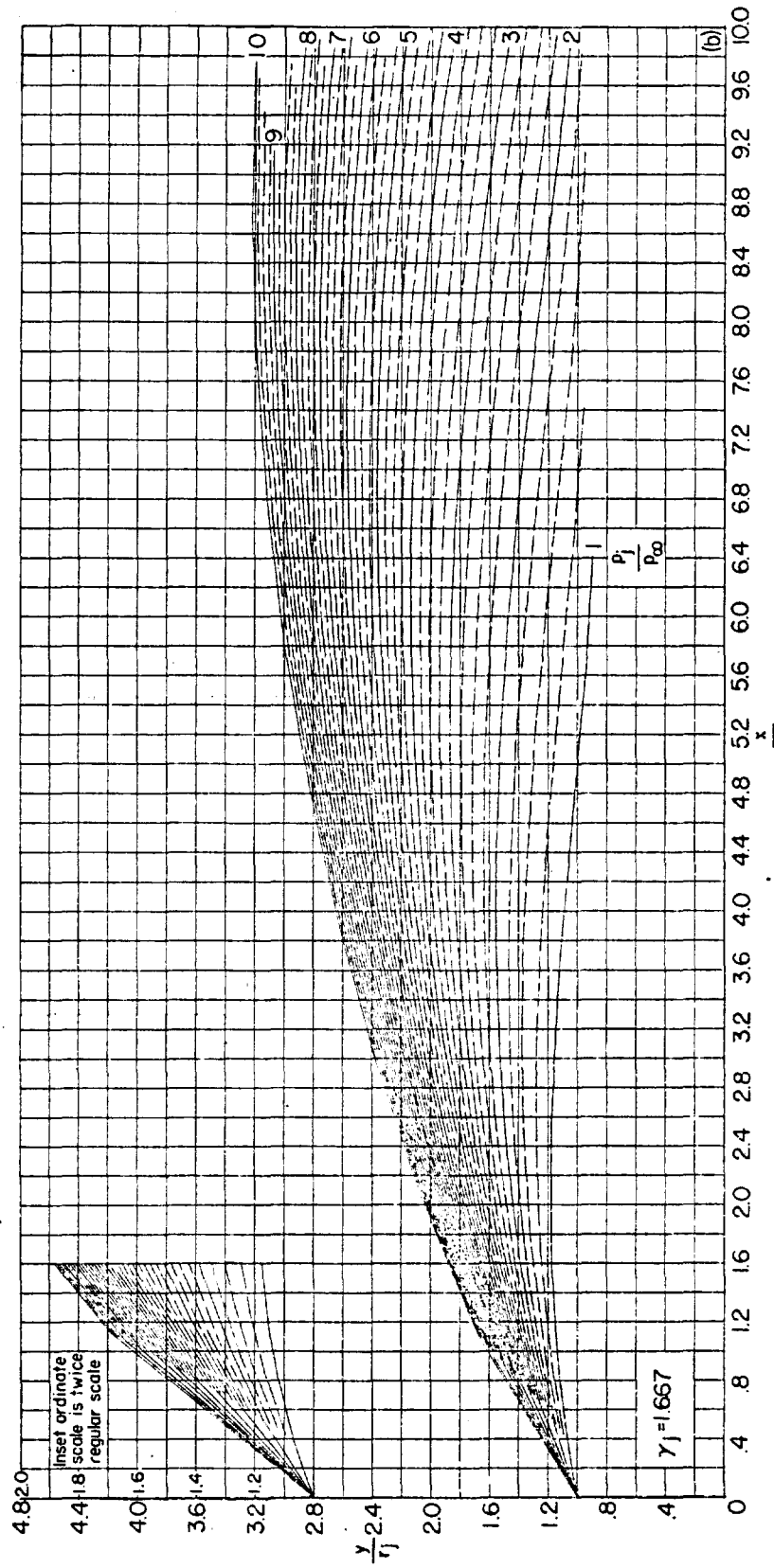

(b) $\theta_N = 10°$. Concluded.

FIGURE 30.—Continued.

502683 O—59——13

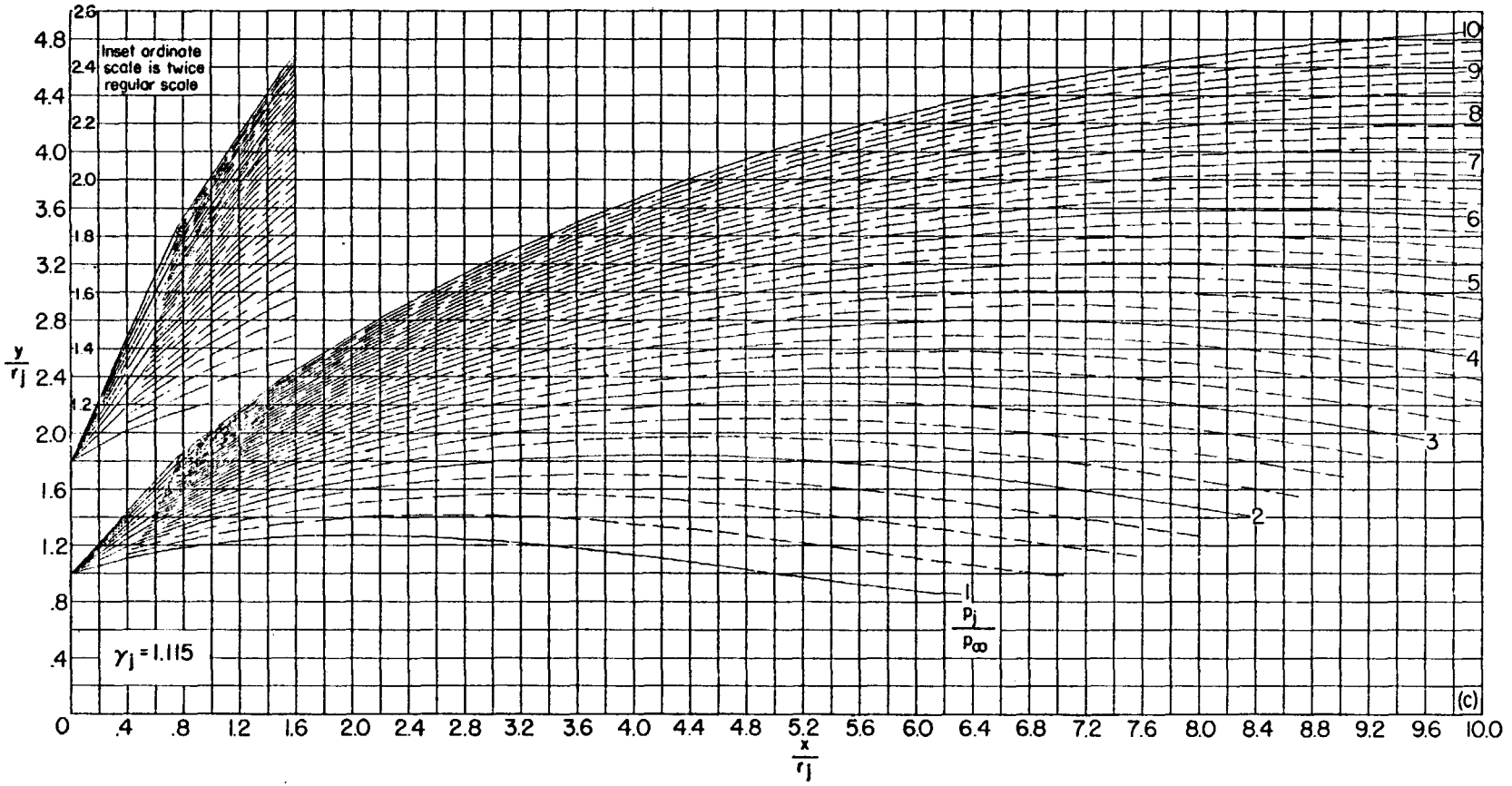

(c) $\theta_N = 15°$.

FIGURE 30.—Continued.

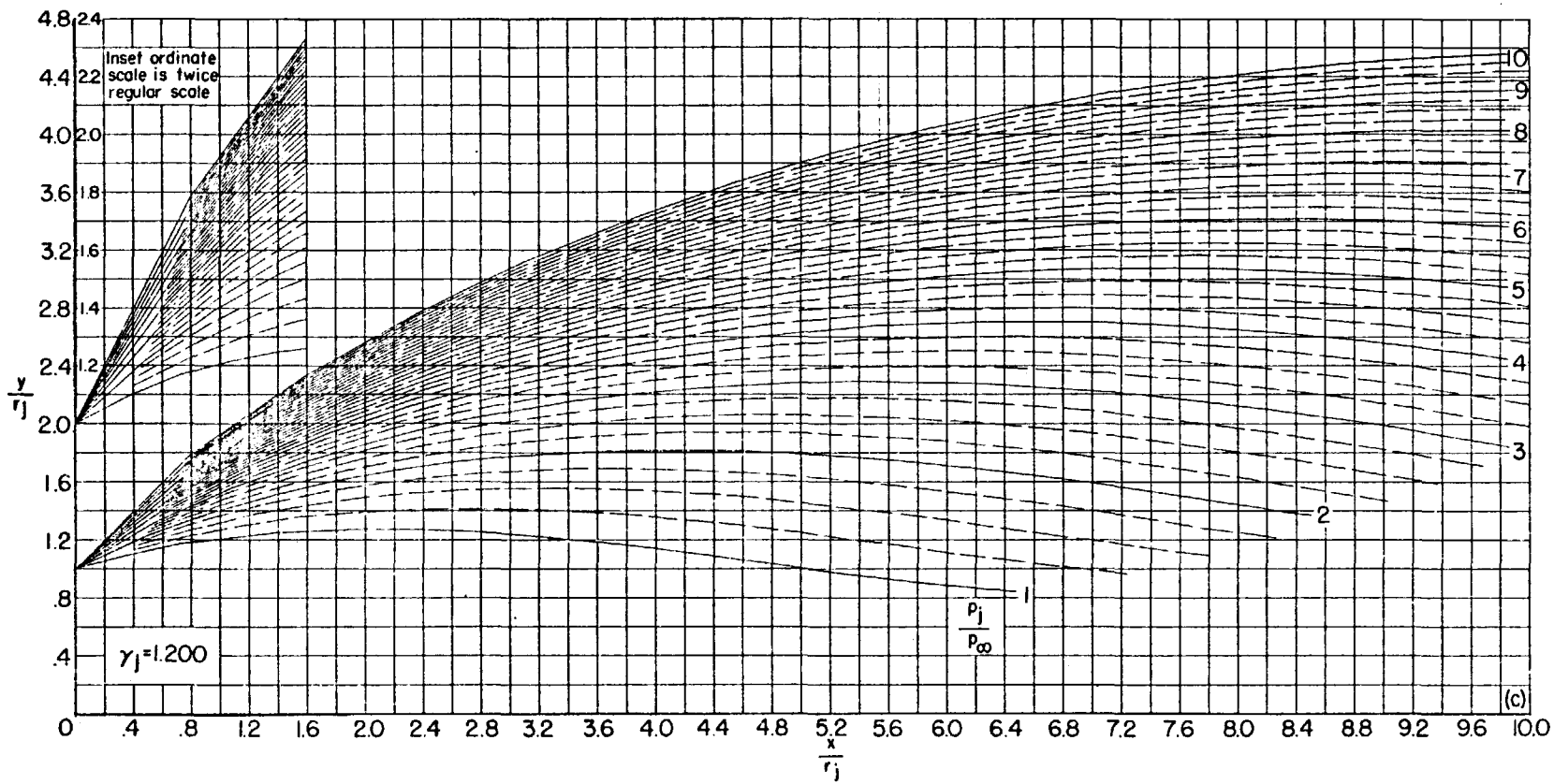

(c) $\theta_N = 15°$. Continued.

FIGURE 30.--Continued.

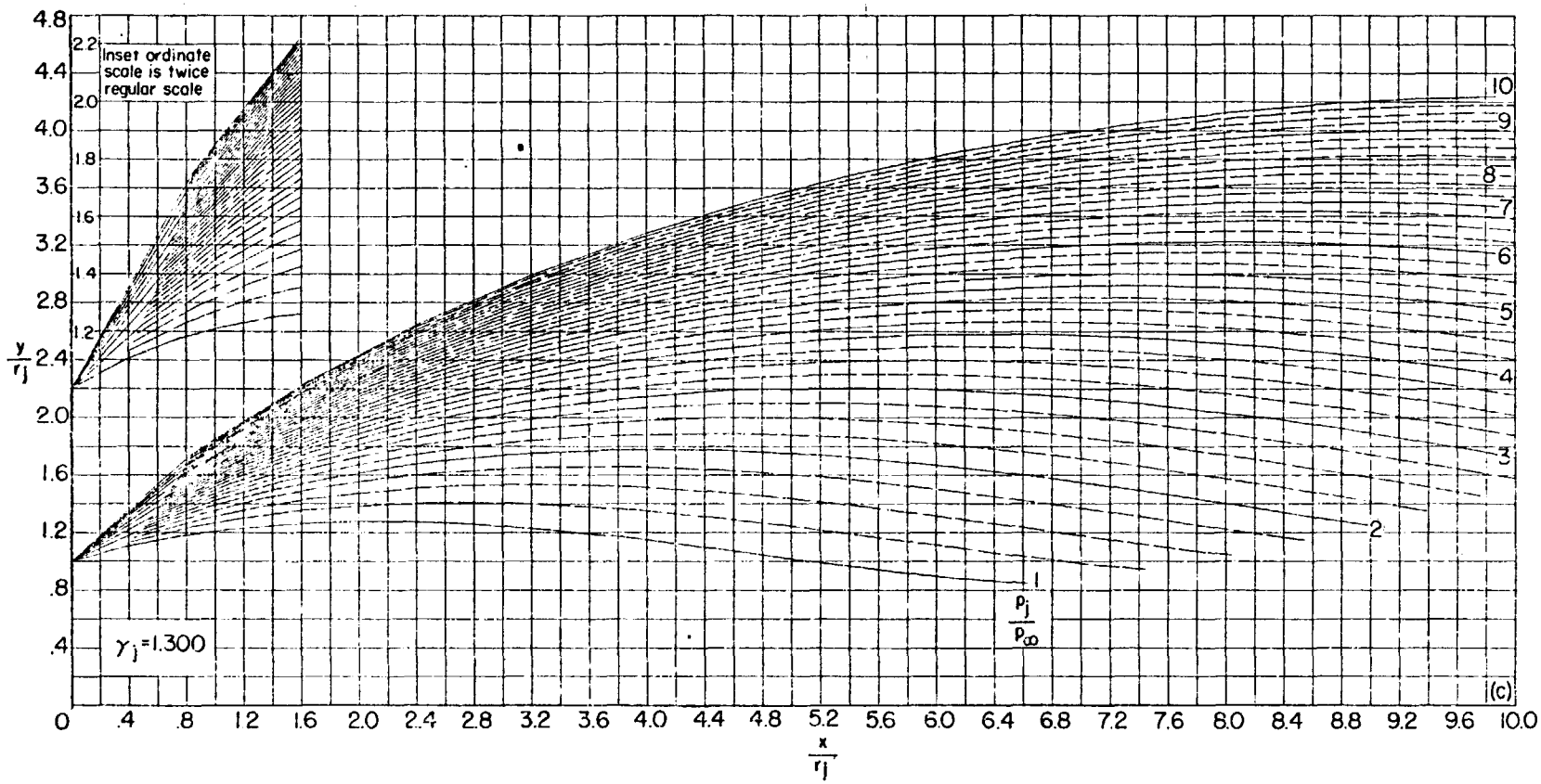

(c) $\theta_N = 15°$. Continued.

FIGURE 30.—Continued.

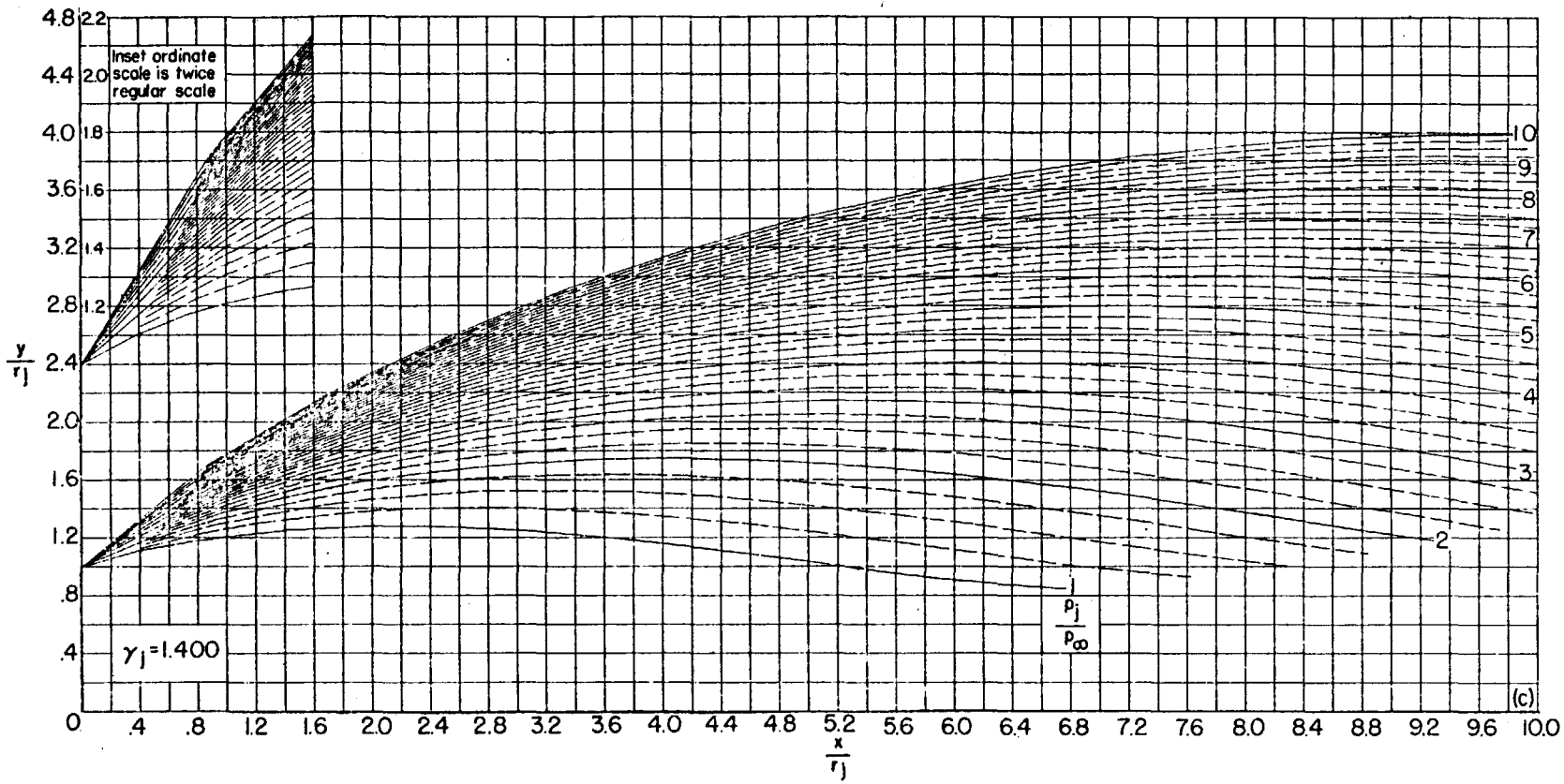

(c) $\theta_N = 15°$. Continued.

FIGURE 30.—Continued.

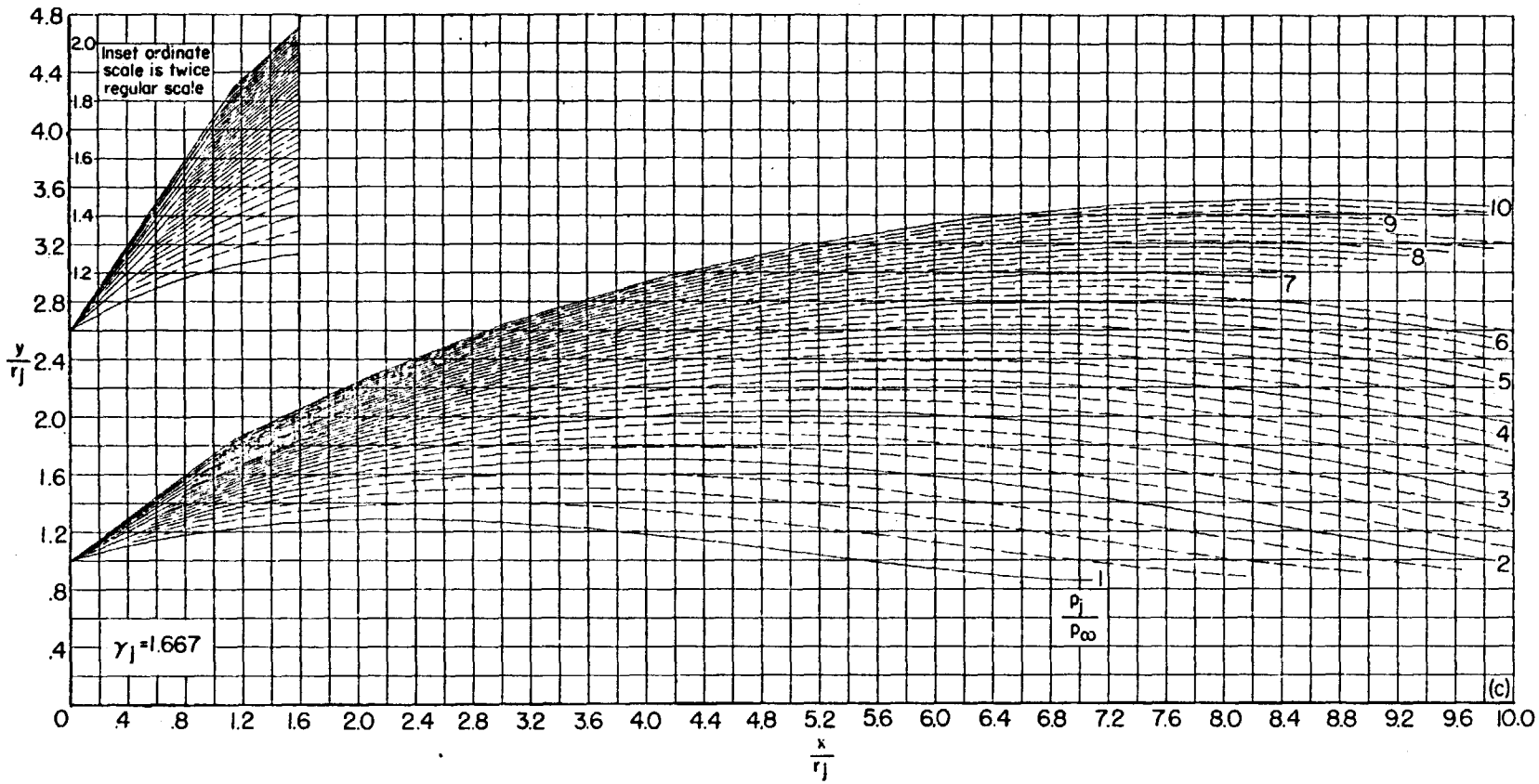

(c) $\theta_N = 15°$. Concluded.

FIGURE 30.—Continued.

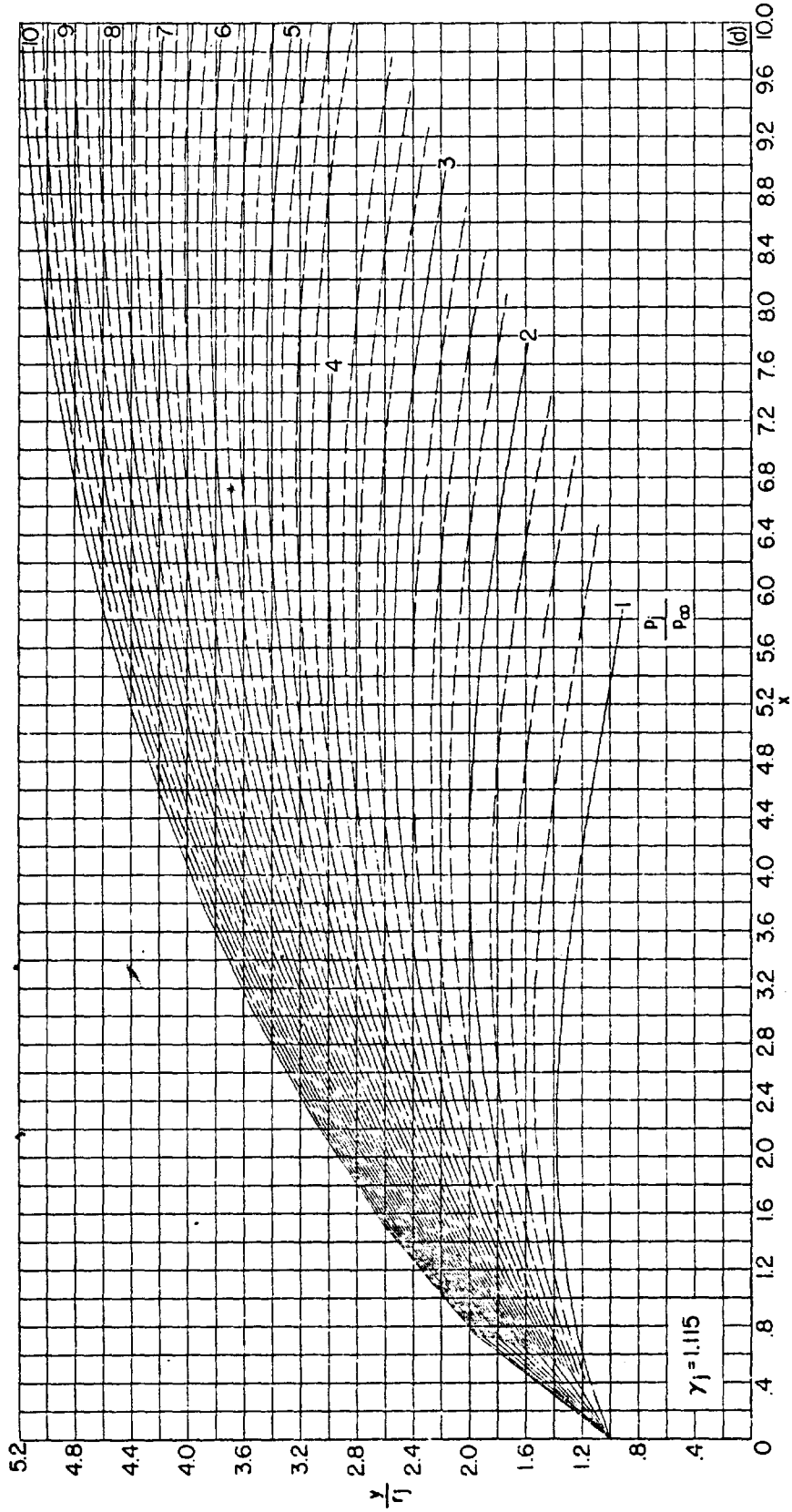

(d) $\theta_N = 20°$.

FIGURE 30.—Continued.

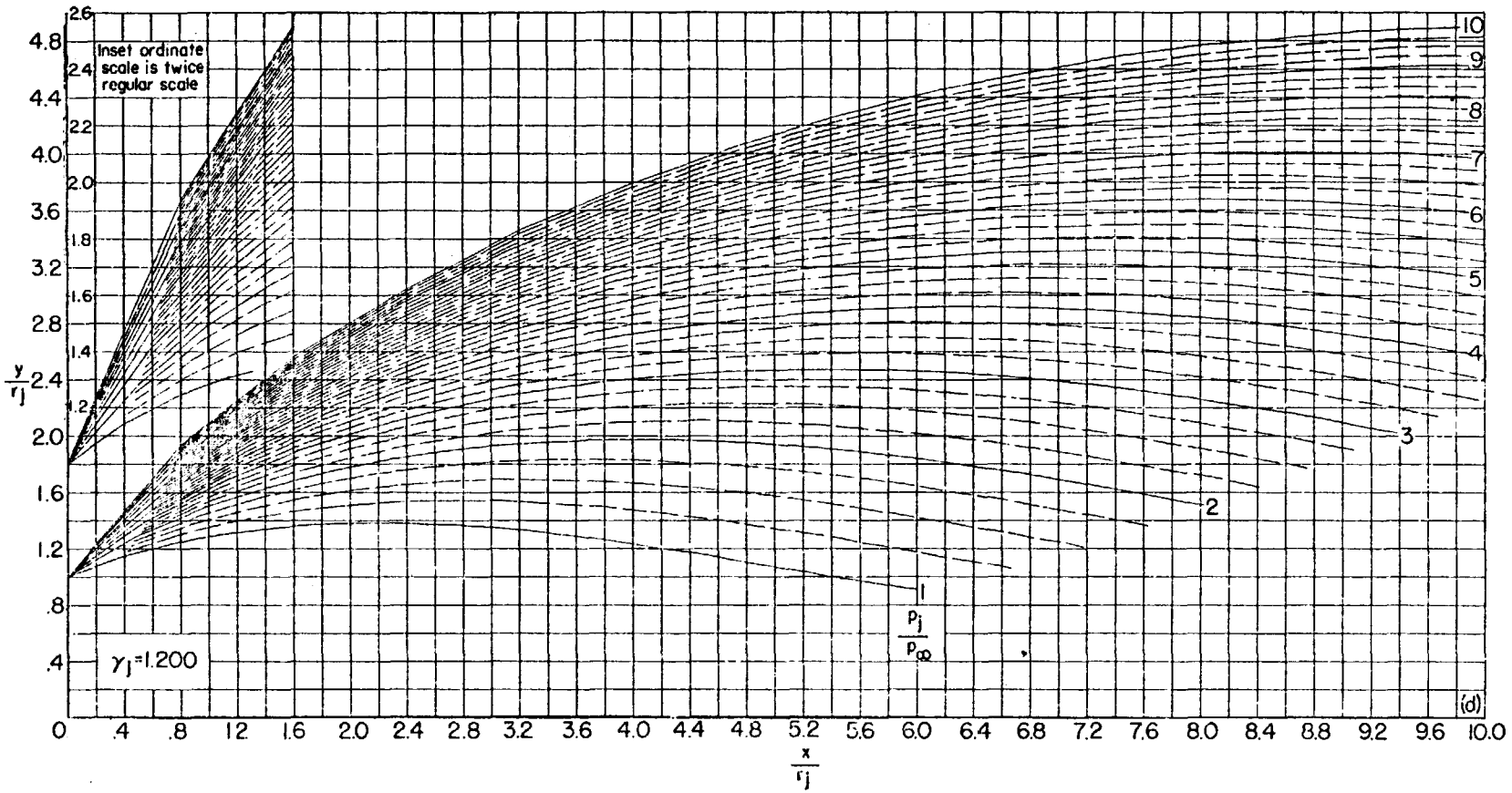

(d) $\theta_N = 20°$. Continued.

FIGURE 30.—Continued.

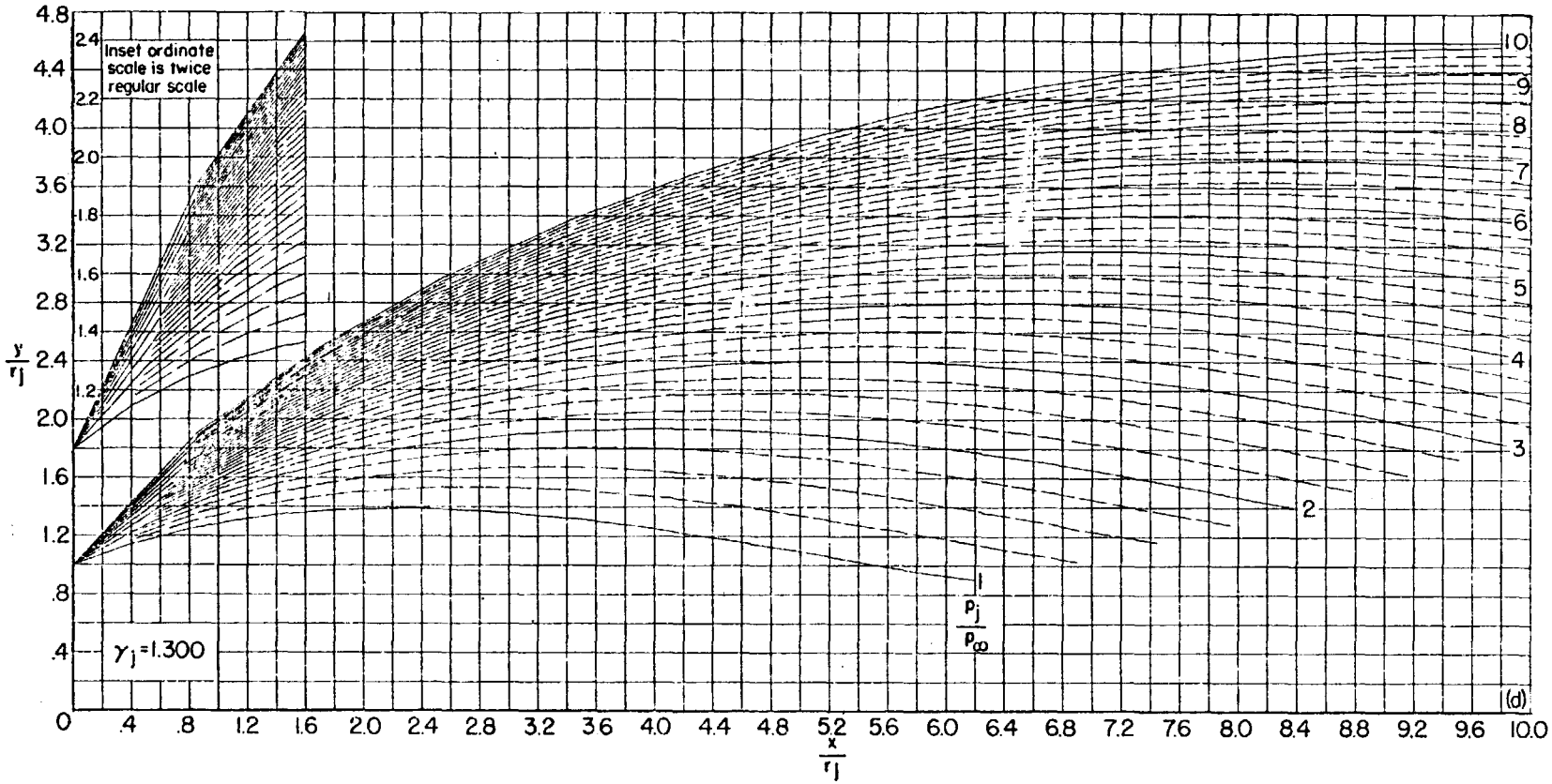

(d) $\theta_N = 20°$. Continued.

FIGURE 30.—Continued.

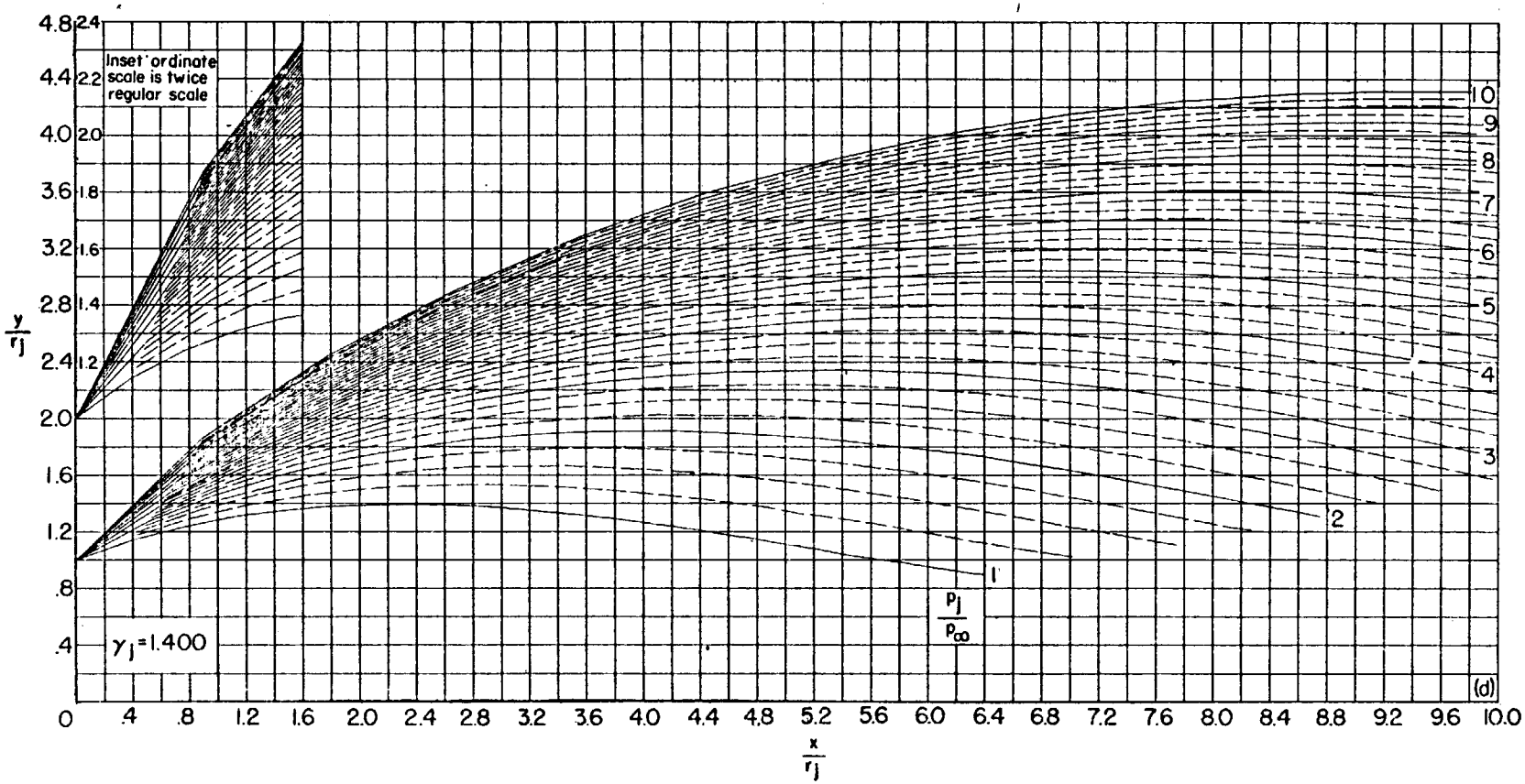

(d) $\theta_N = 20°$. Continued.

FIGURE 30.—Continued.

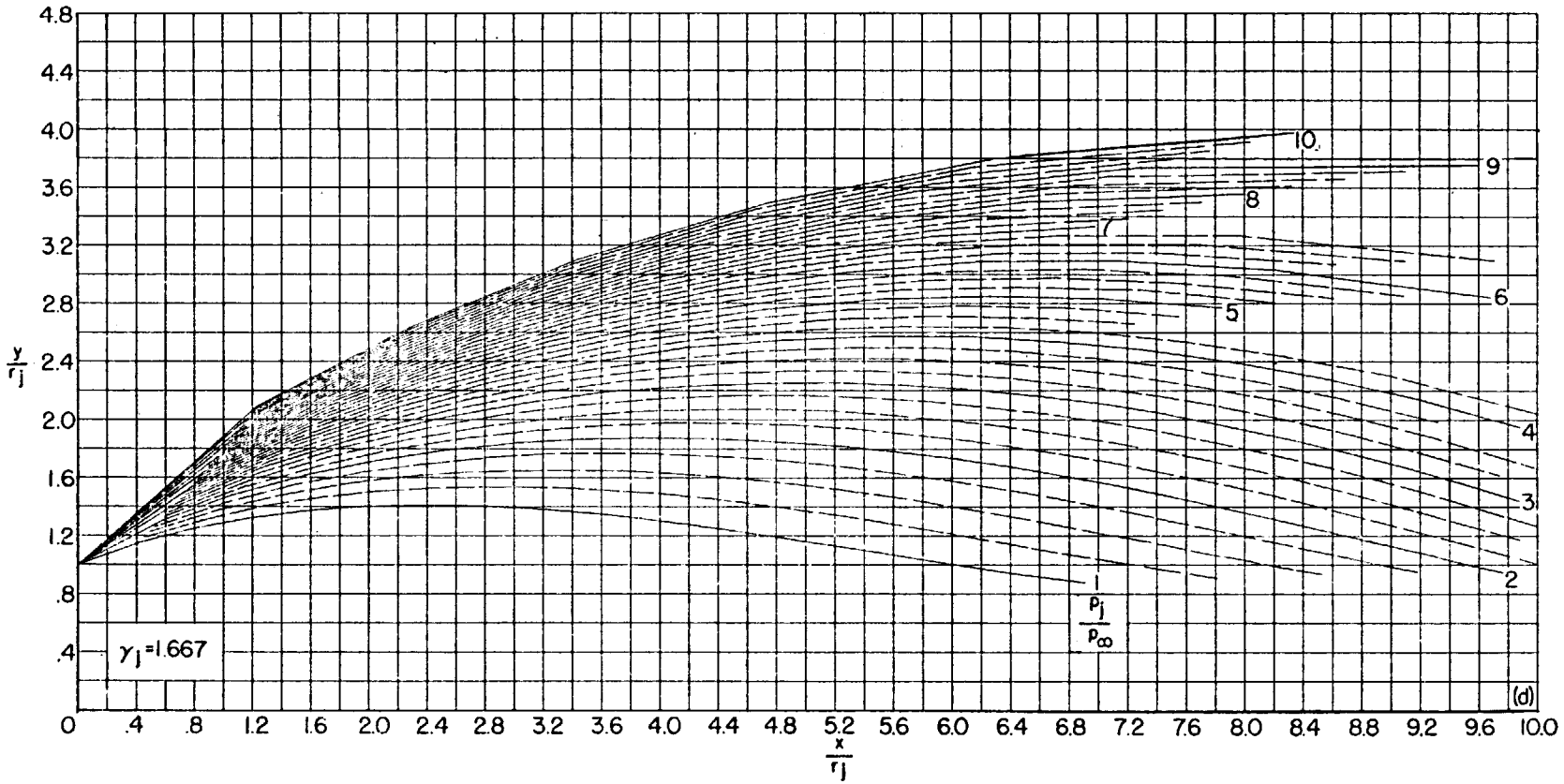

(d) $\theta_N = 20°$. Concluded.

FIGURE 30.—Concluded.

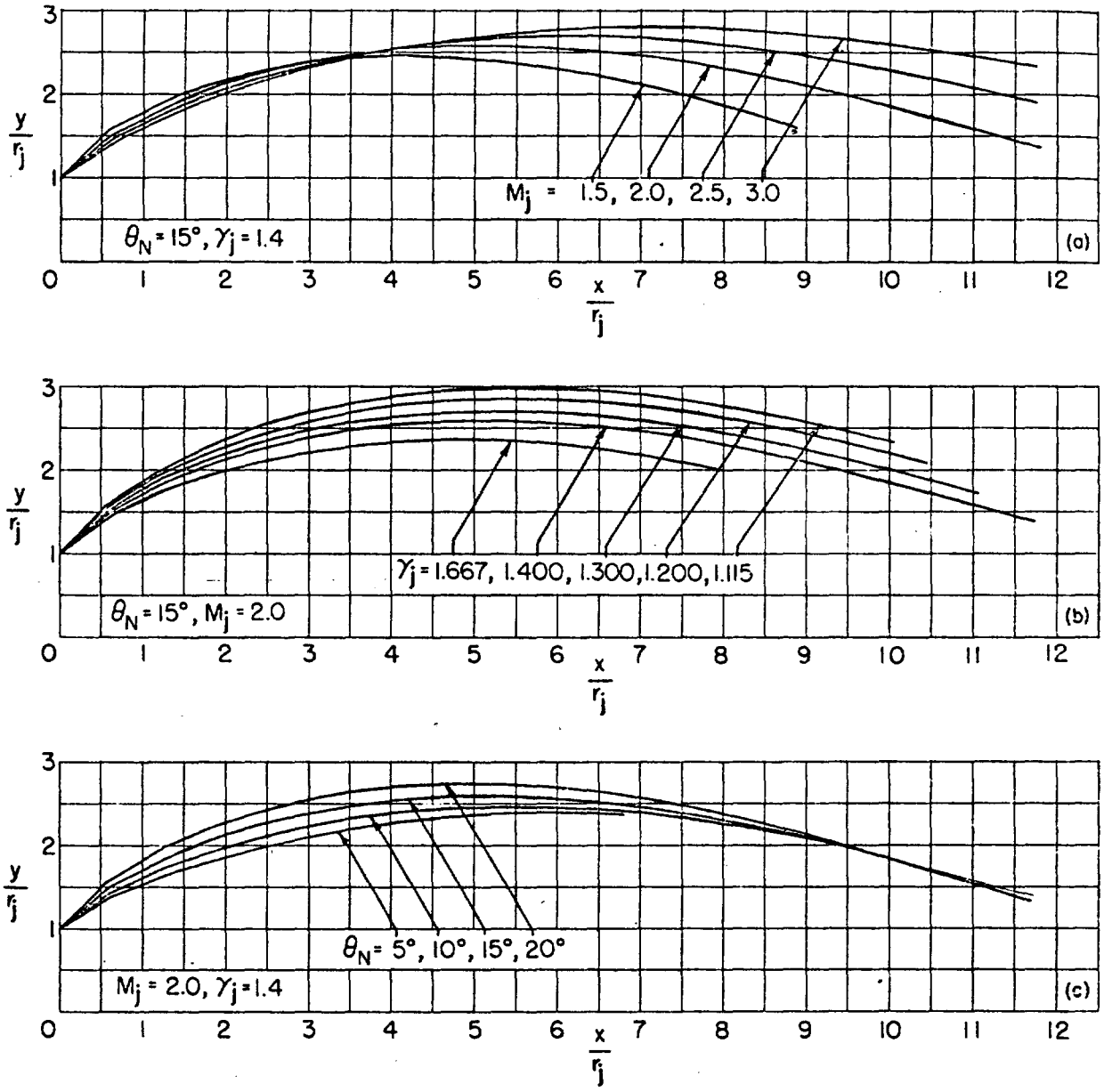

(a) Effect of M_j.
(b) Effect of γ_j.
(c) Effect of θ_N.

FIGURE 31.—Example of the effects of jet Mach number, ratio of specific heats of the jet, and nozzle divergence angle upon the shape of the jet boundary. $p_j/p_\infty = 5$.

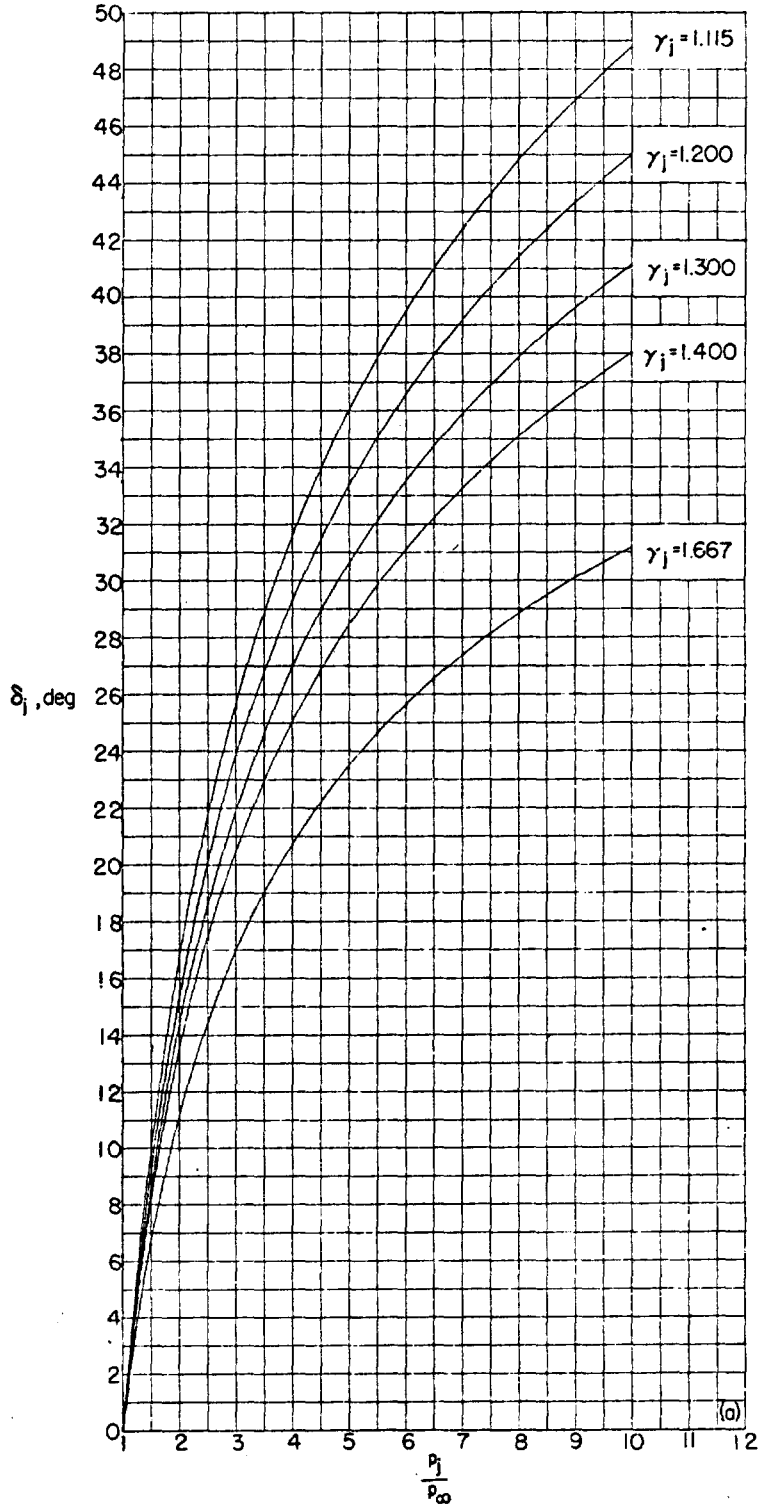

(a) $M_j = 1.5$.

FIGURE 32.—Effect of jet pressure ratio upon the initial inclination of the jet boundary for $\theta_N = 0°$.

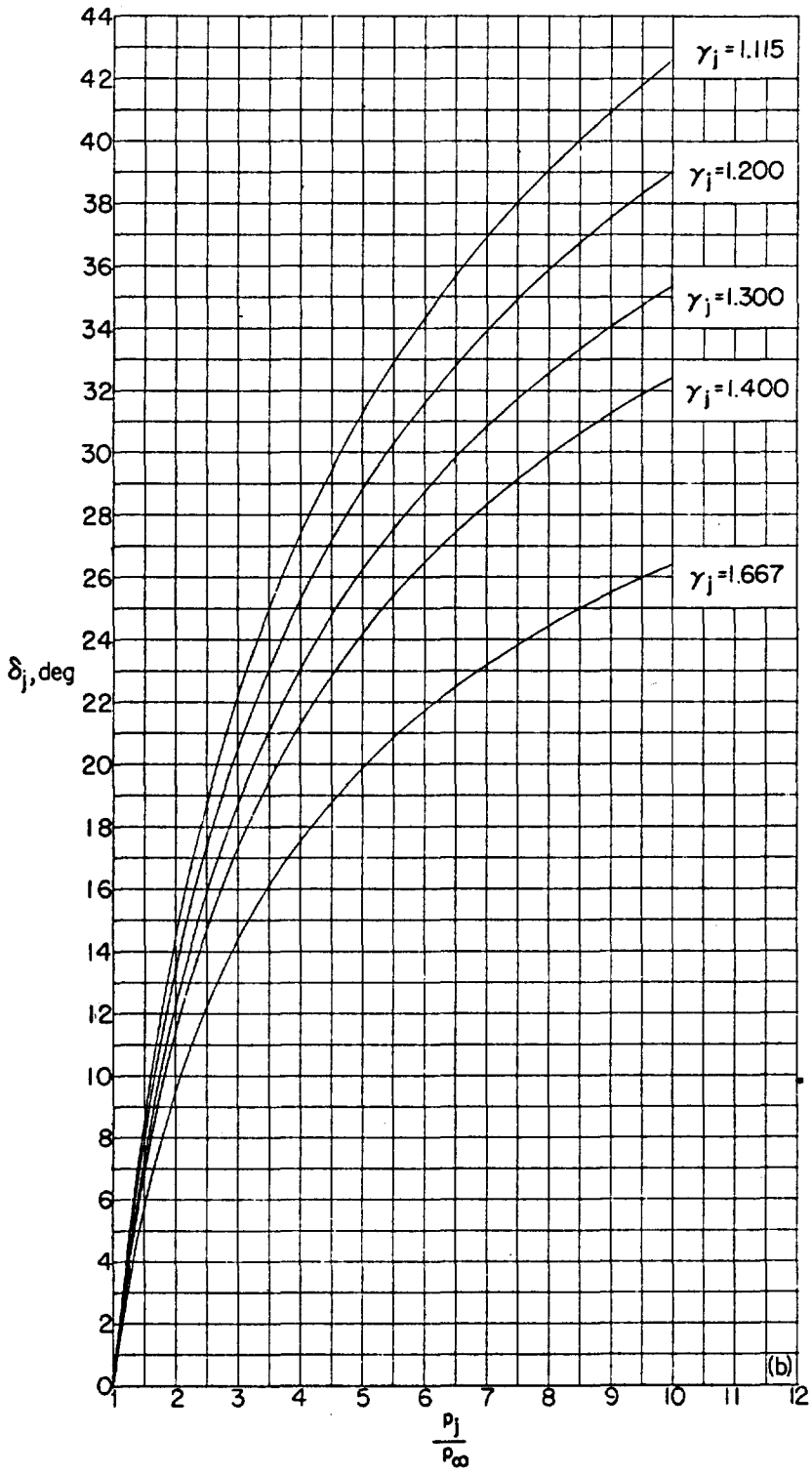

(b) $M_j = 2.0$.

FIGURE 32.—Continued.

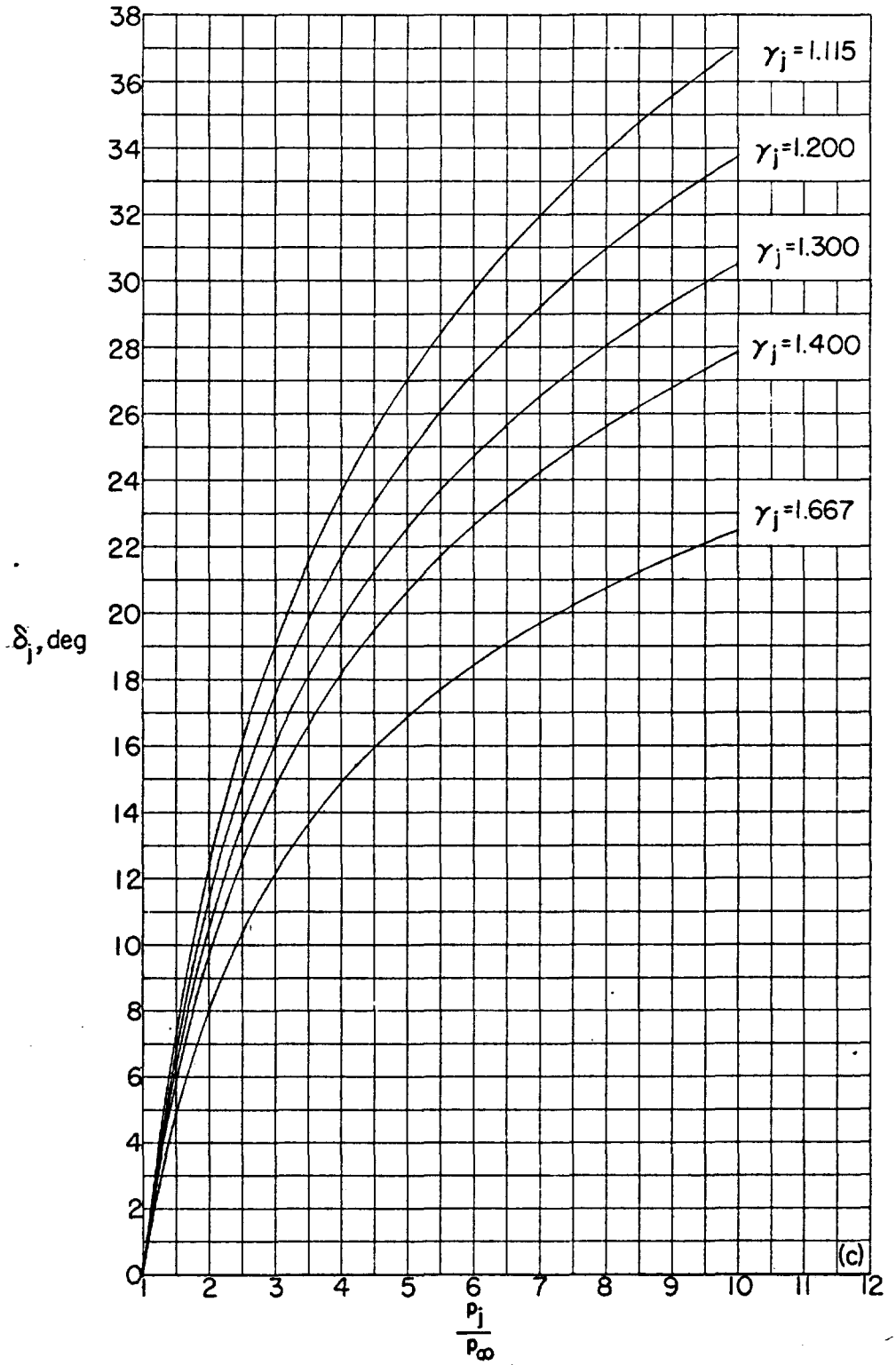

(c) $M_j=2.5$.

FIGURE 32.—Continued.

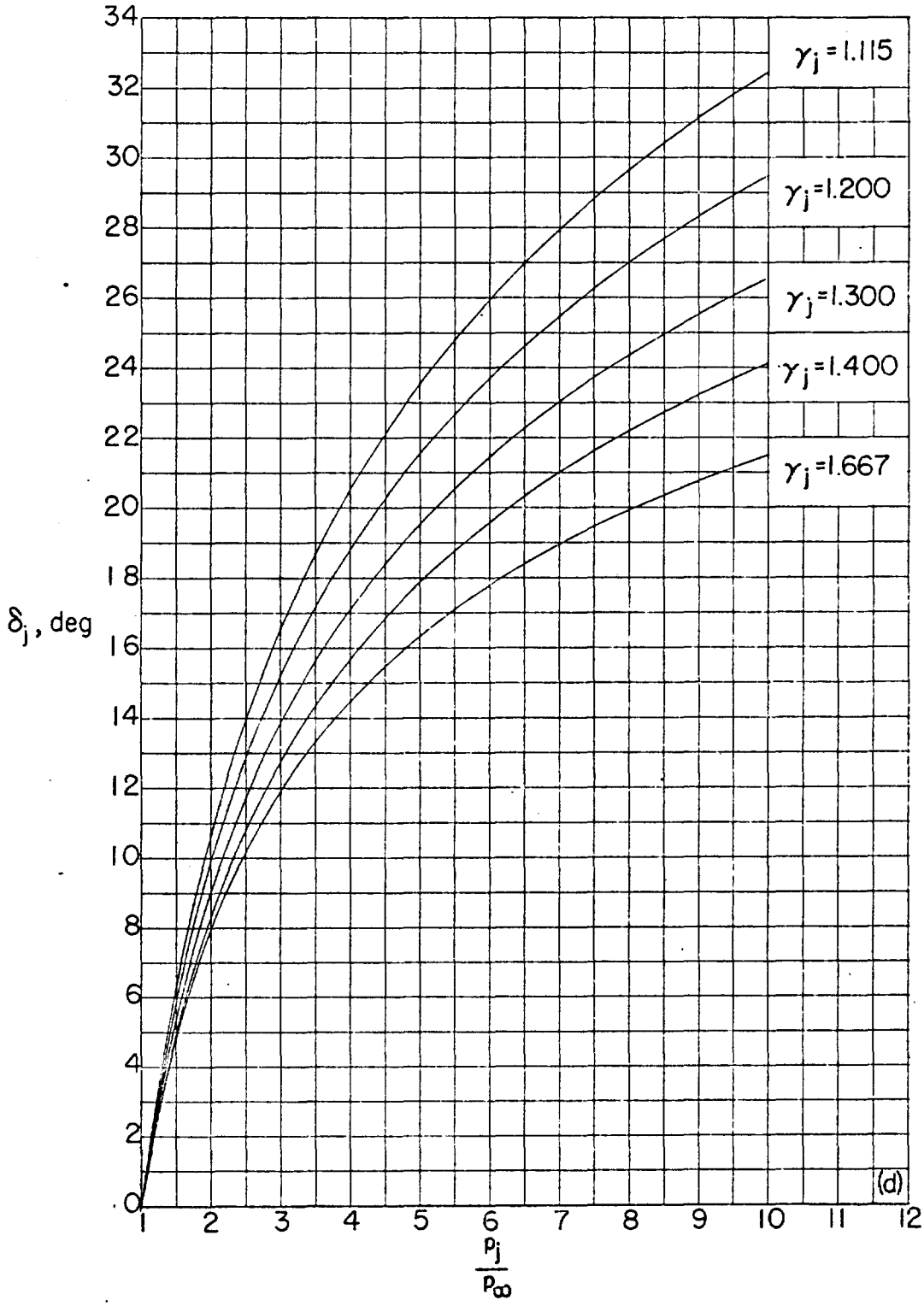

(d) M_j=3.0.

FIGURE 32.—Concluded.

502683 O—59——14

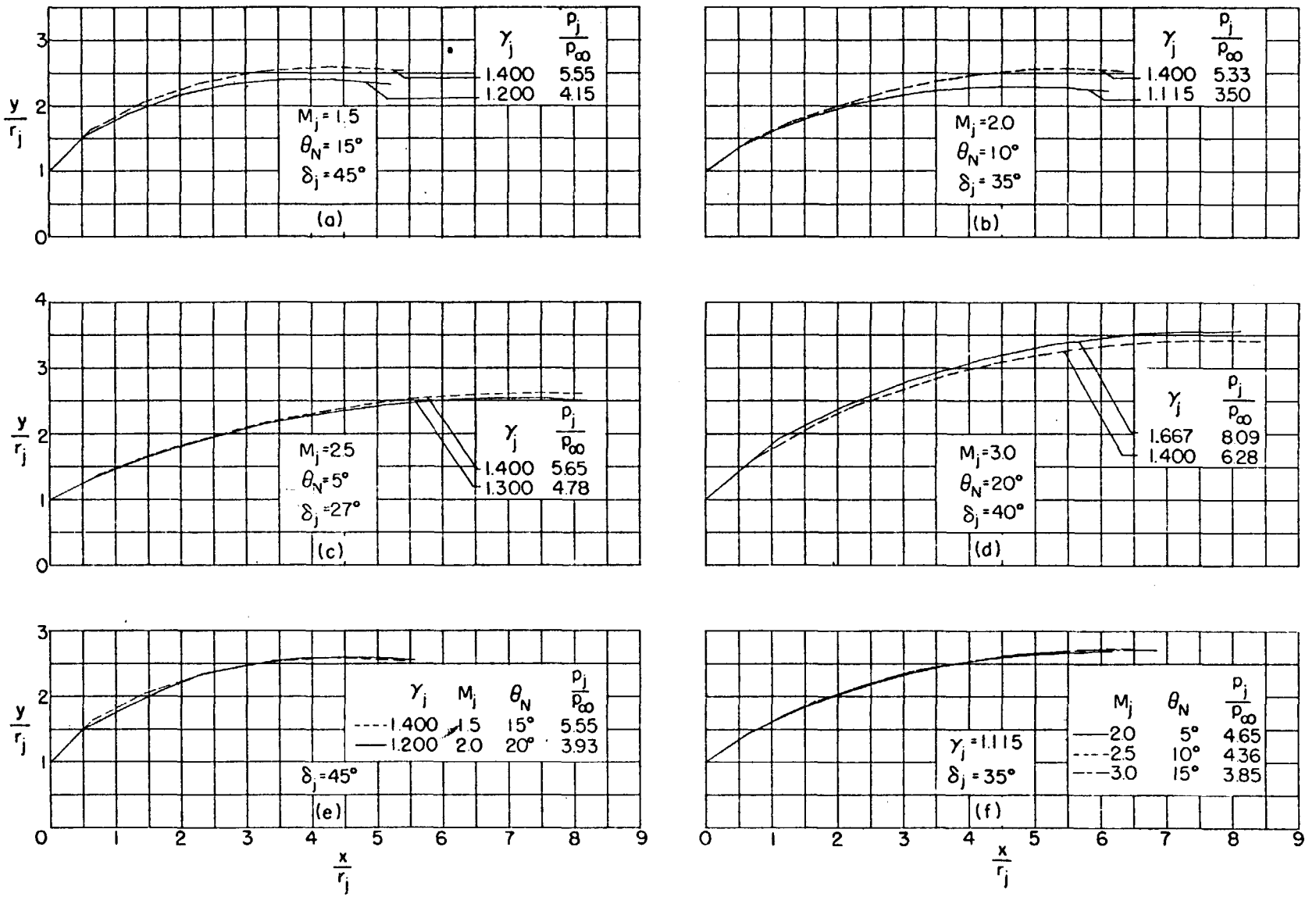

FIGURE 33.—Examples of jet boundary simulation.

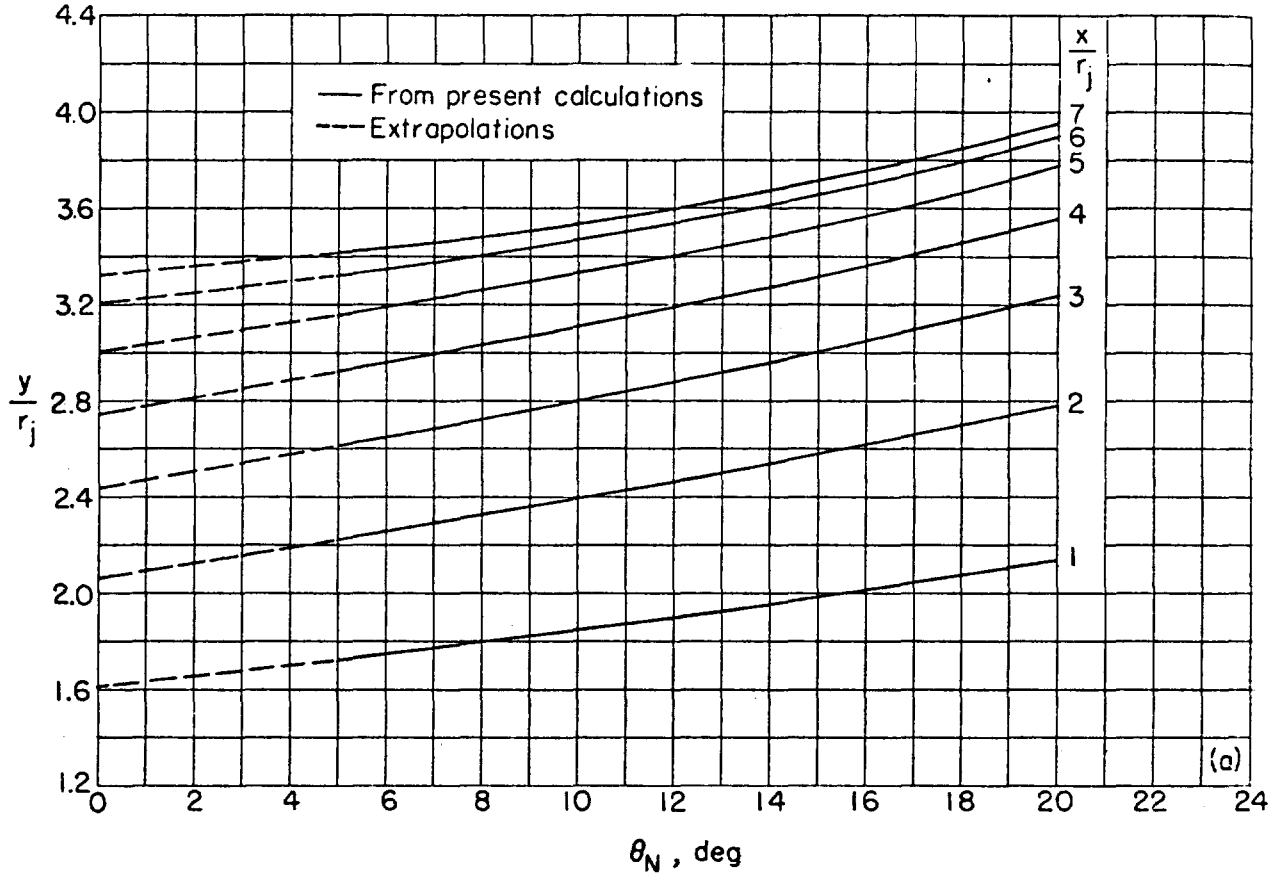

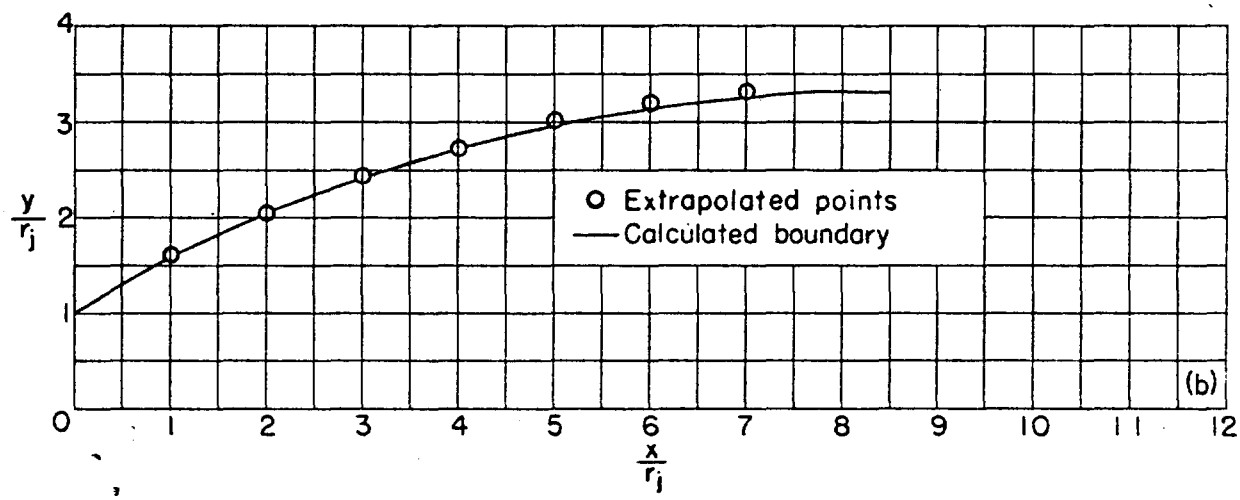

(a) Extrapolation to $\theta_N = 0°$.
(b) Comparison of extrapolated and calculated boundary.

FIGURE 34.—Example of extrapolation to $\theta_N = 0°$. $M_j = 2.0$; $\gamma_j = 1.400$; $p_j/p_\infty = 10$.

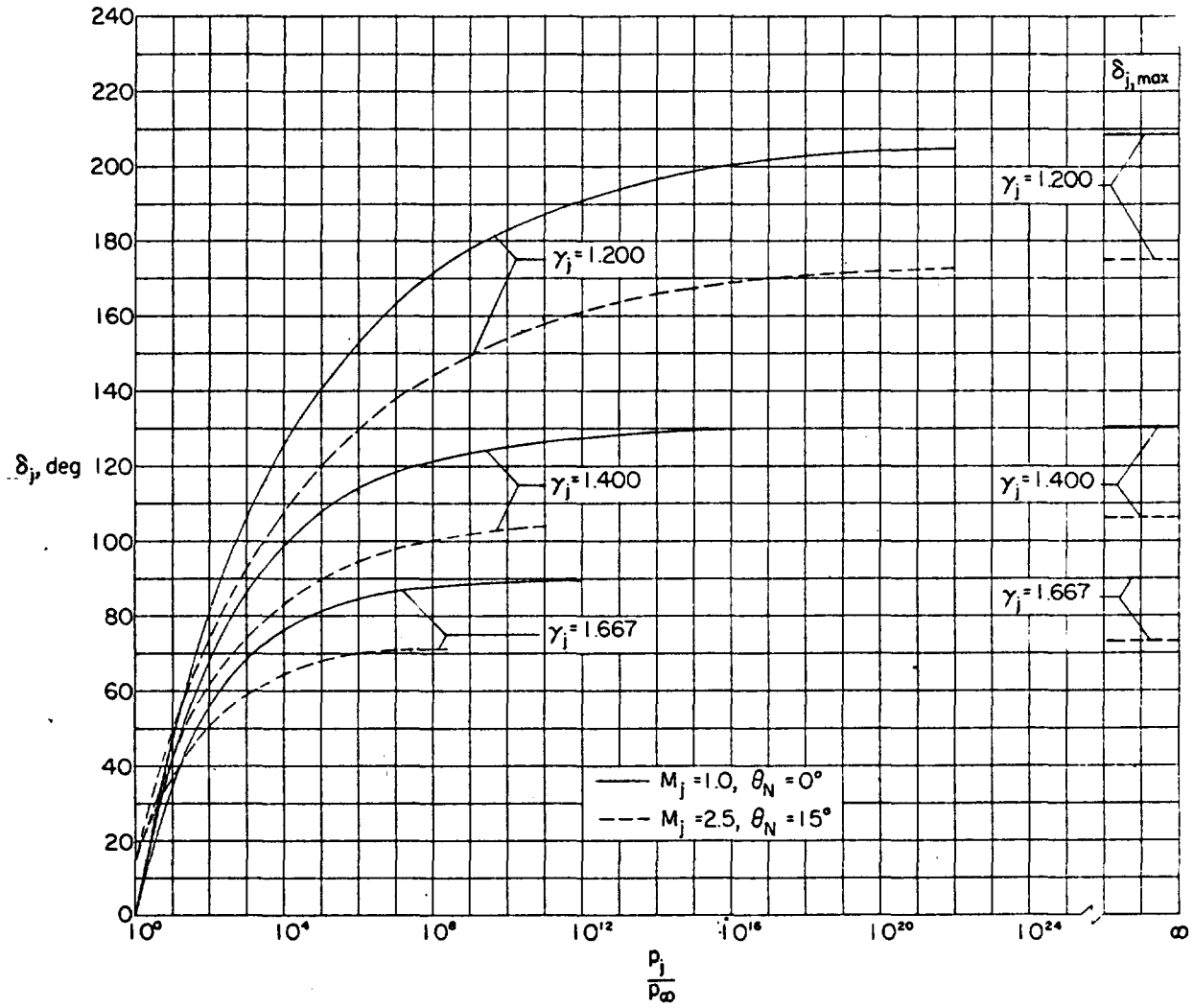

FIGURE 35.—Variation of the initial inclination of the free-jet boundary with jet pressure ratio for jets exhausting into still air.

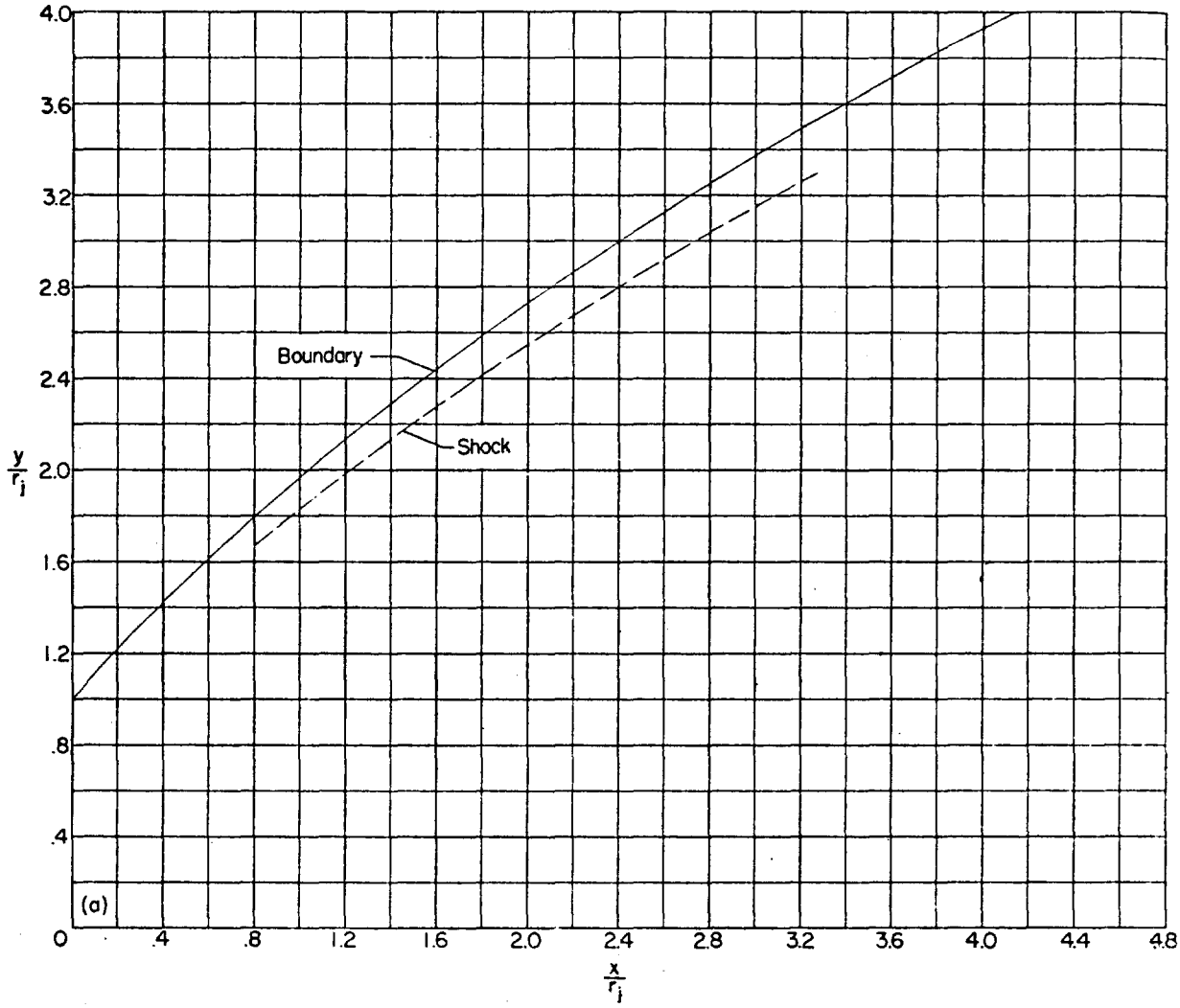

(a) $p_i/p_\infty = 59.92$; $\delta_i = 48.55°$.

FIGURE 36.—Calculated boundaries and jet shocks for jet exhausting into still air with $\gamma_i = 1.667$, $M_i = 2.5$, and $\theta_N = 15°$.

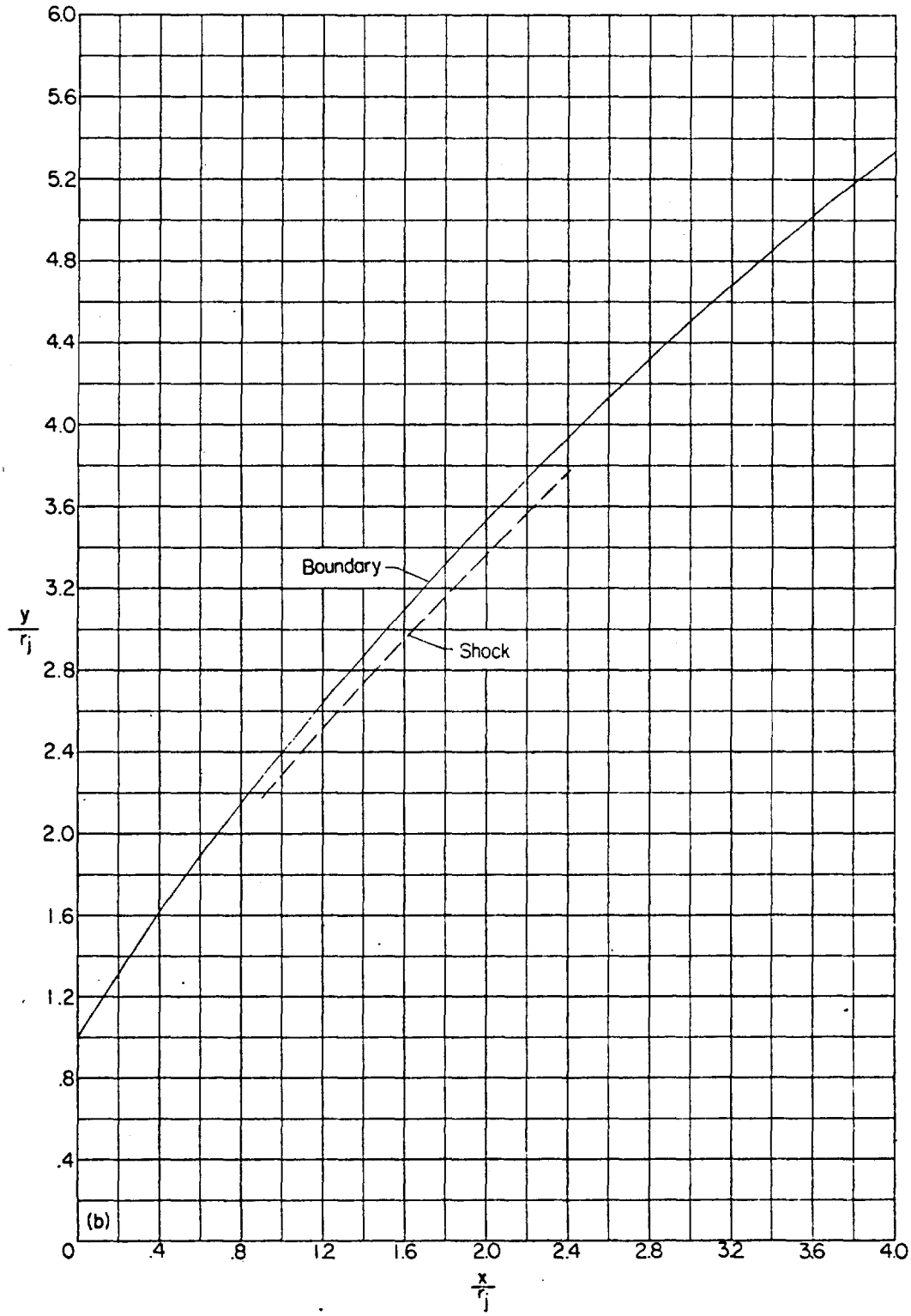

(b) $p_i/p_\infty = 569.2$; $\delta_i = 57.72°$.

FIGURE 36.—Continued.

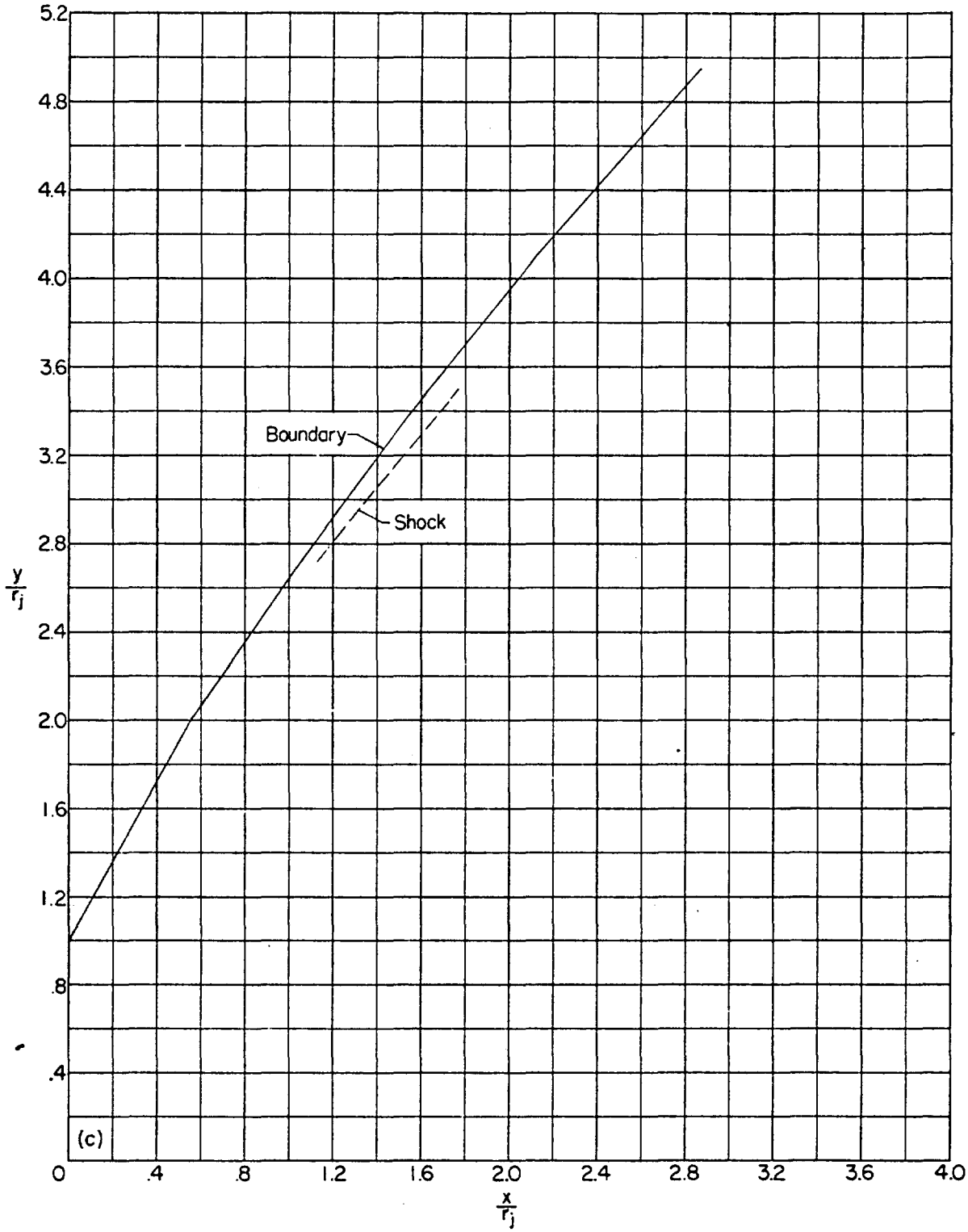

(c) $p_i/p_\infty = 1{,}618$; $\delta_i = 60.74°$.

FIGURE 36.—Concluded.

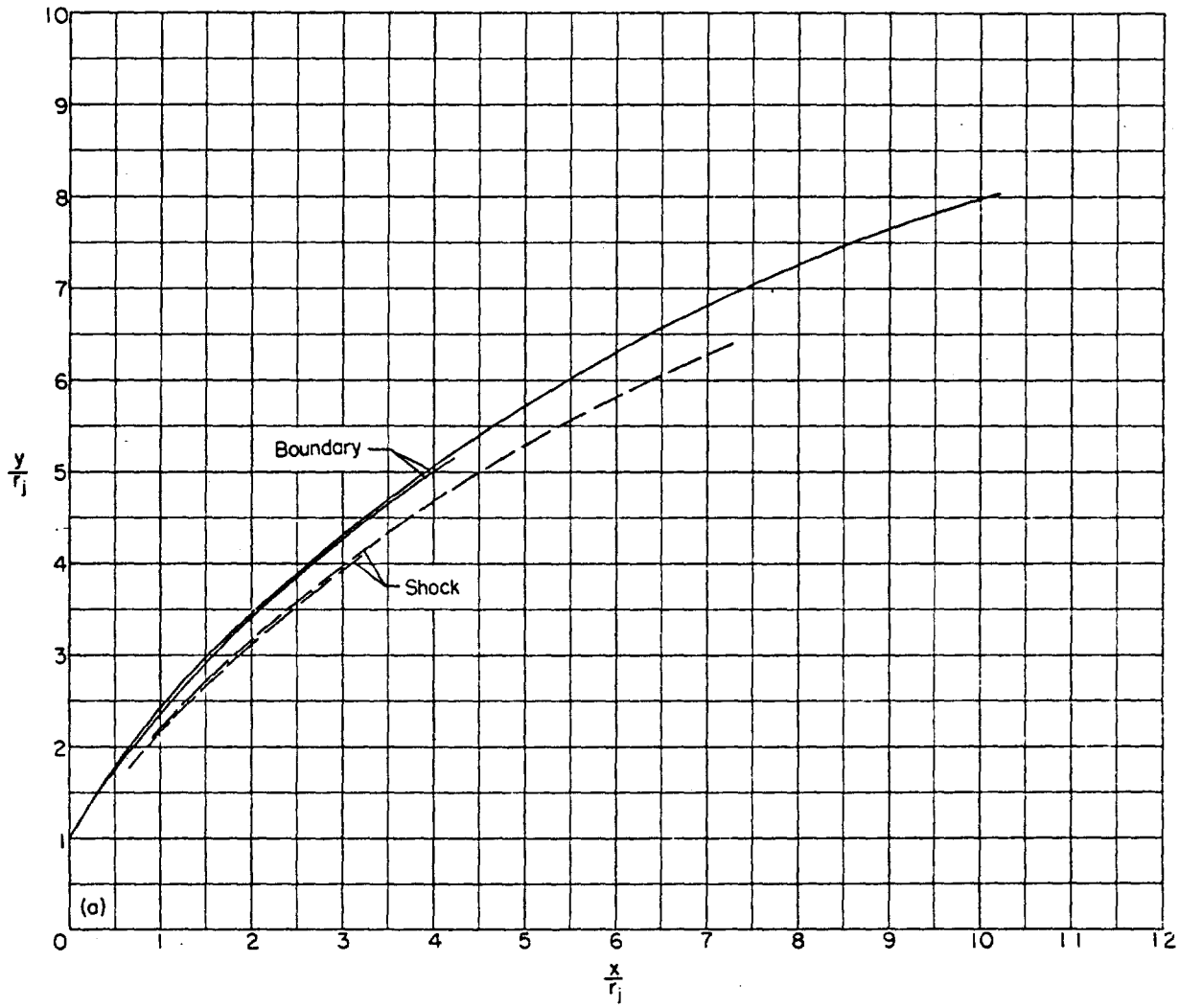

(a) $p_i/p_\infty = 81.94$; $\delta_i = 60.02°$.

FIGURE 37.—Calculated boundaries and jet shocks for jet exhausting into still air with $\gamma_i = 1.400$, $M_i = 2.5$, and $\theta_N = 15°$. Longer boundary and shock correspond to greater spacing between points on leading characteristic than for shorter boundary and shock (see appendix C).

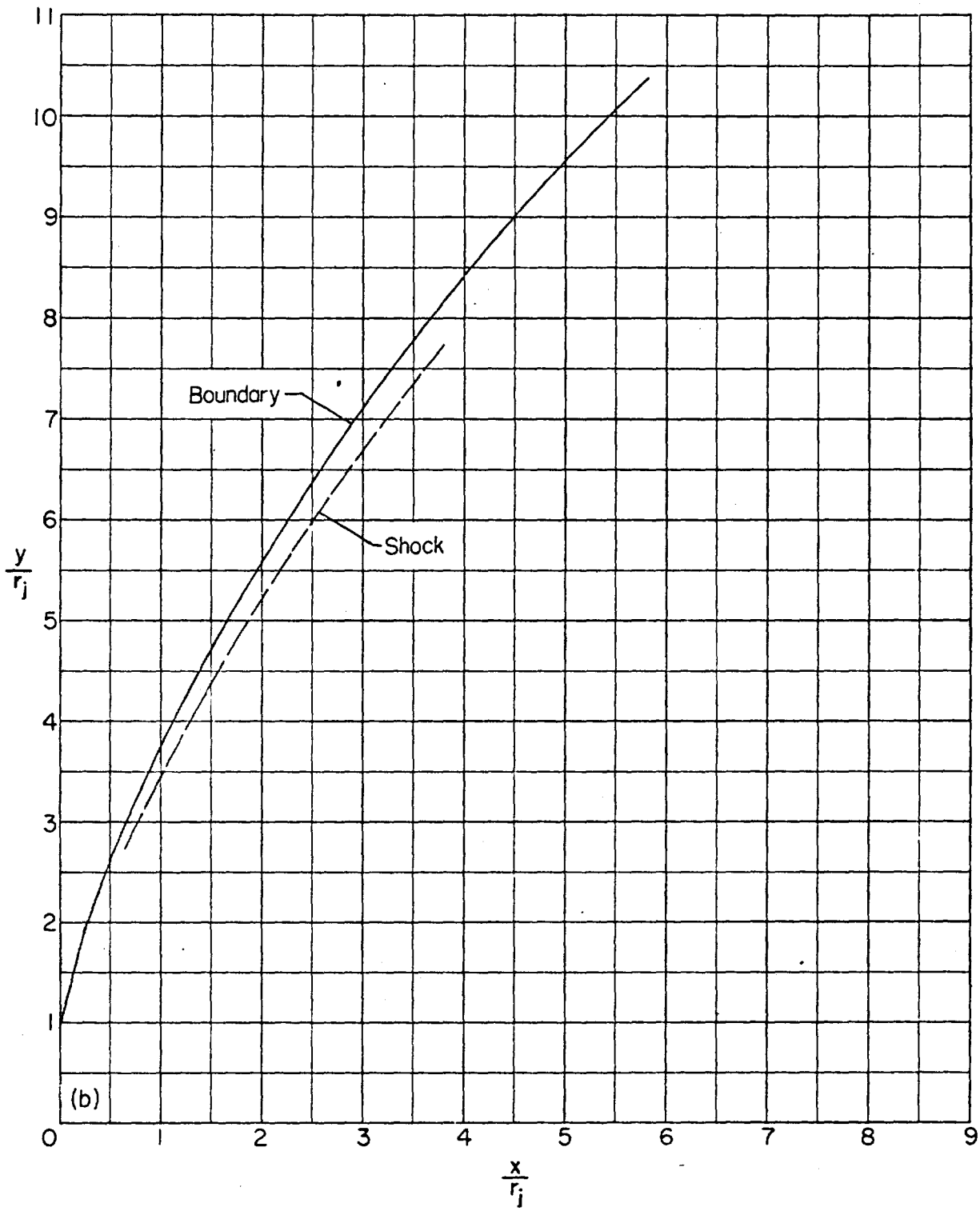

(b) $p_i/p_\infty = 1{,}346$; $\delta_i = 75.59°$.

FIGURE 37.—Continued.

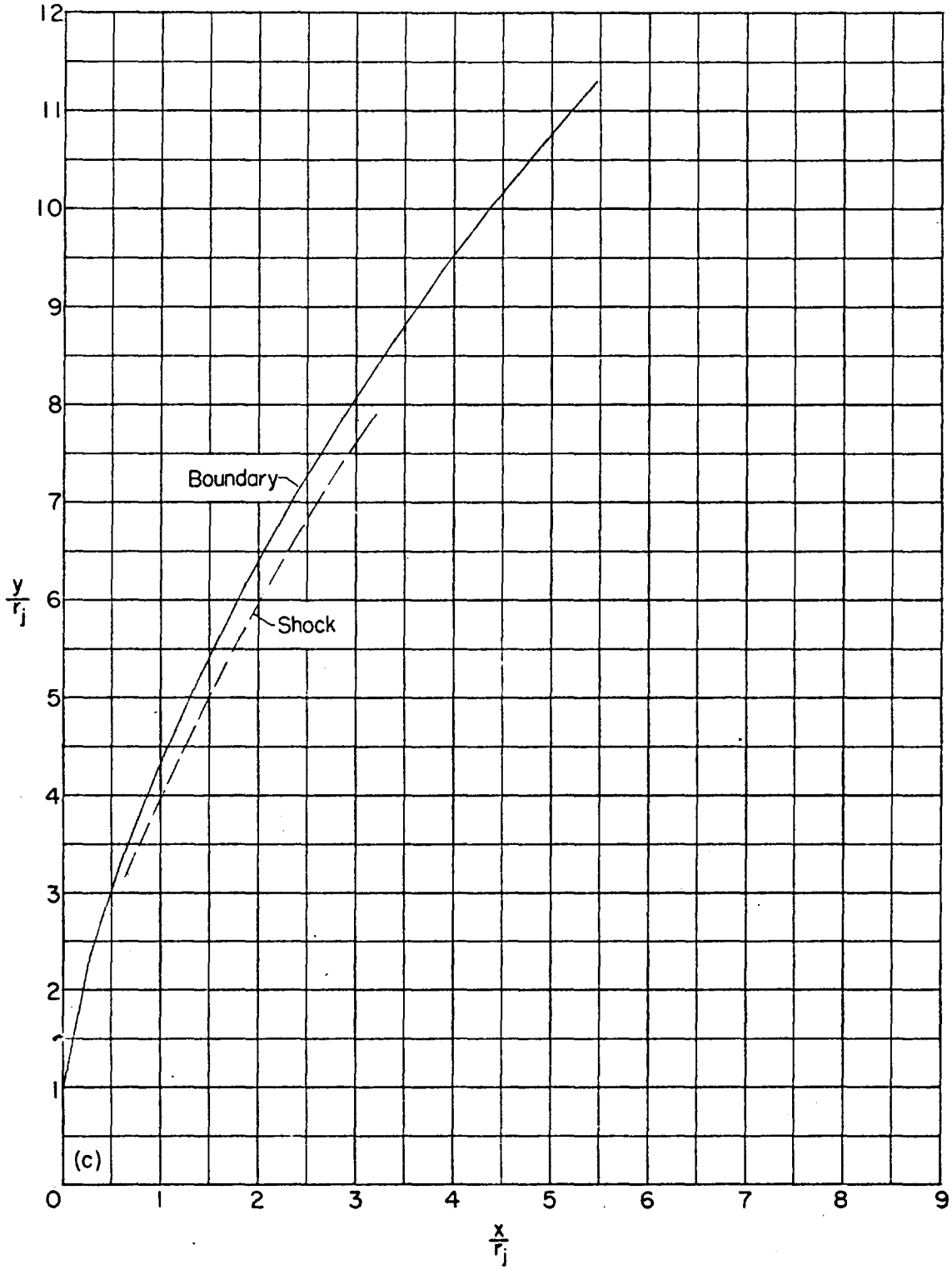

(c) $p_i/p_\infty = 2{,}692$; $\delta_i = 78.53°$.

FIGURE 37.—Concluded.

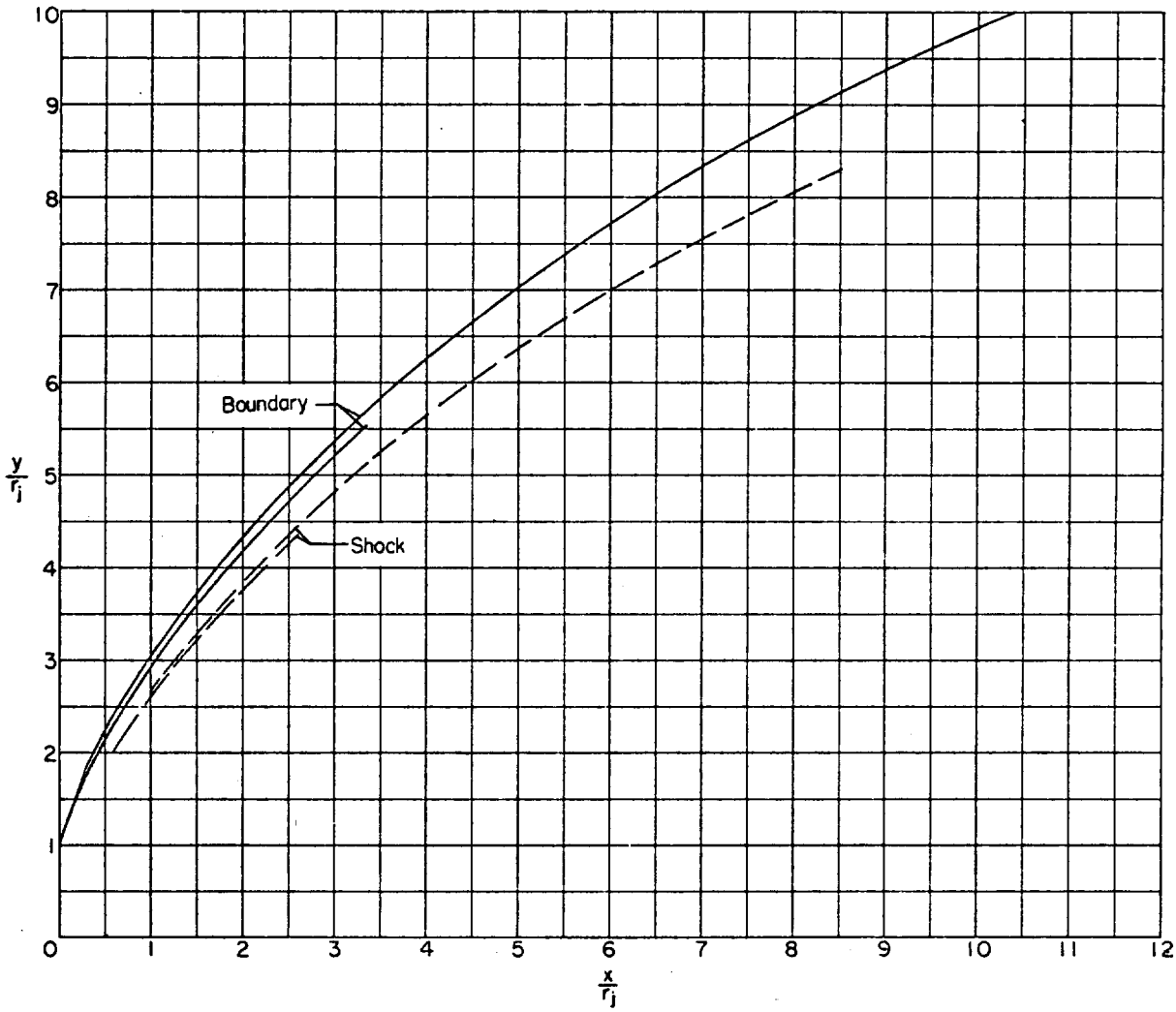

FIGURE 38.—Calculated boundary and jet shock for jet exhausting into still air at $p_j/p_\infty = 76.58$ with $\gamma_j = 1.200$, $M_j = 2.5$, and $\theta_N = 15°$. Longer boundary and shock correspond to greater spacing between points on leading characteristic than for shorter boundary and shock (see appendix C).

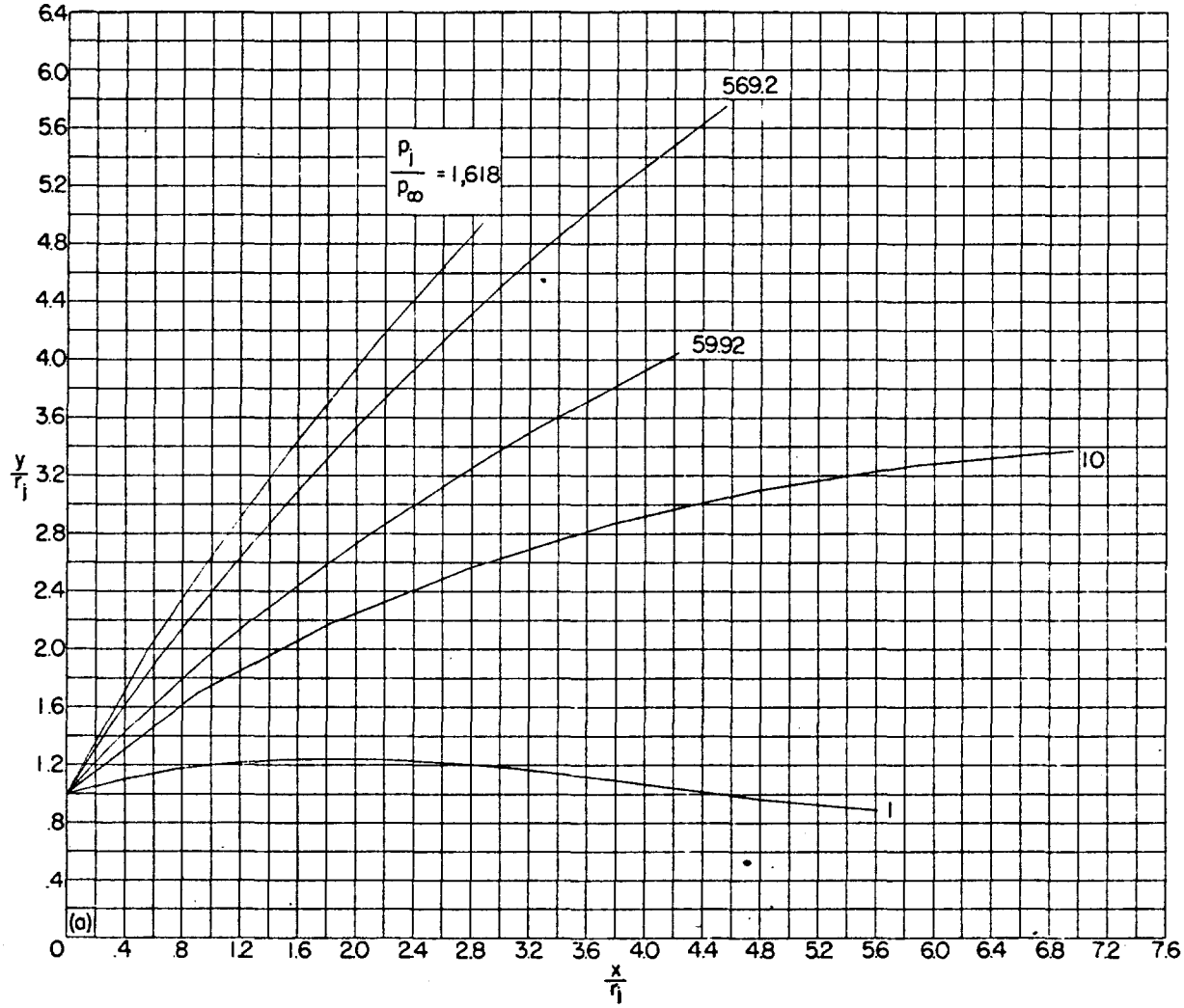

(a) $\gamma_j = 1.667$.

FIGURE 39.—Composite presentation of calculated boundaries for jet exhausting into still air with $M_j = 2.5$ and $\theta_N = 15°$.

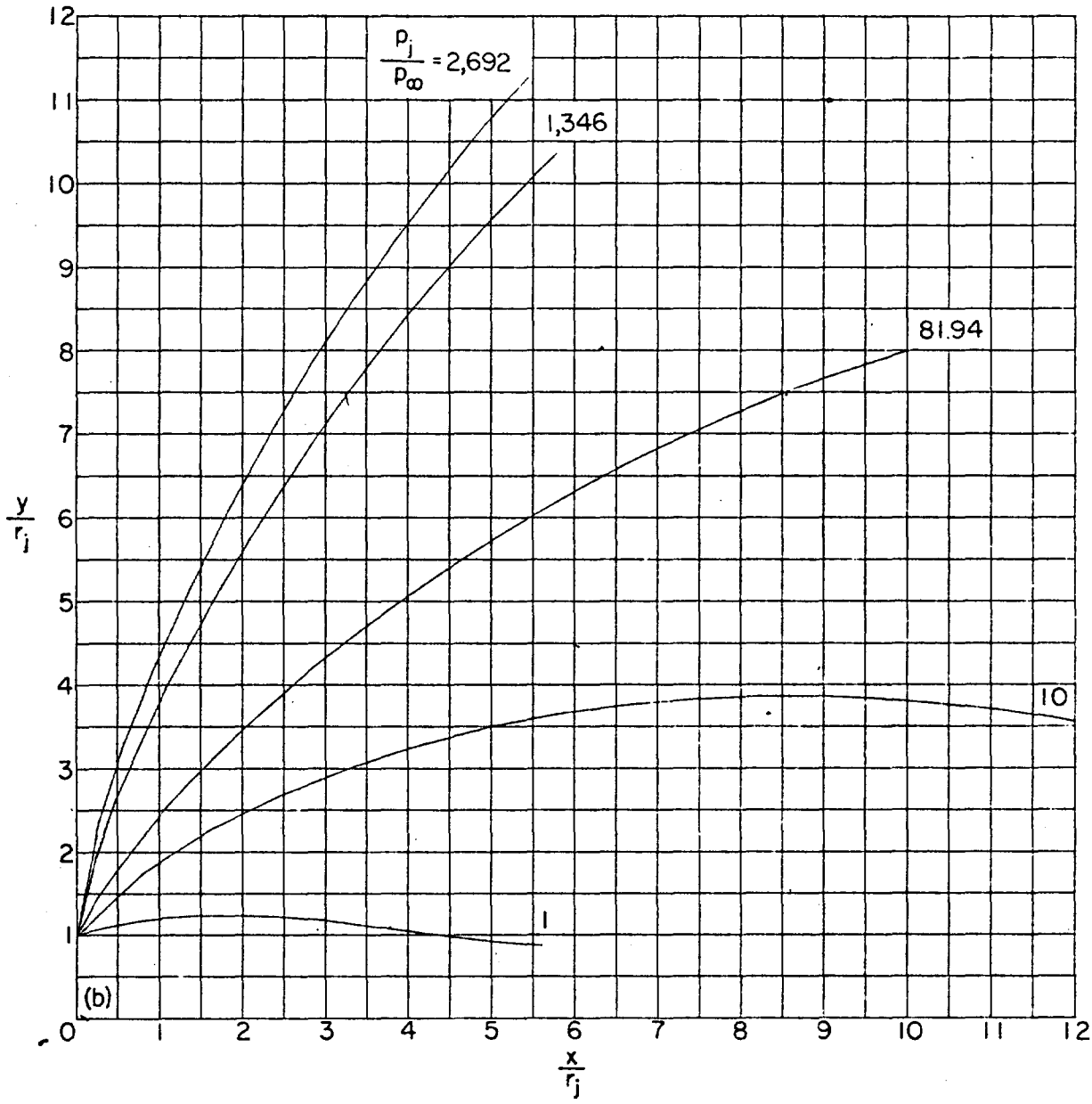

(b) $\gamma_j = 1.400$.

FIGURE 39.—Continued.

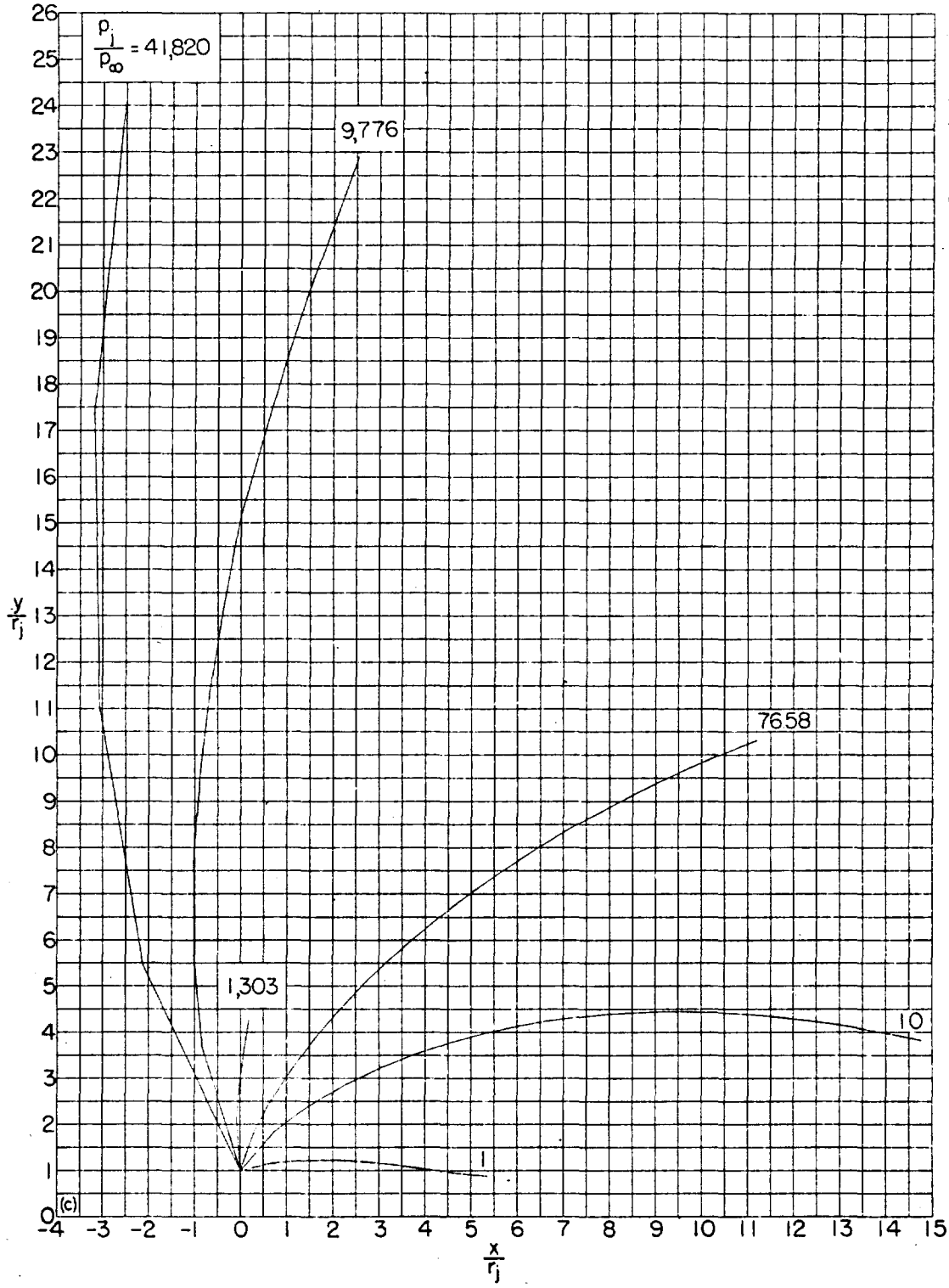

(c) $\gamma_j = 1.200$.

FIGURE 39.—Concluded.

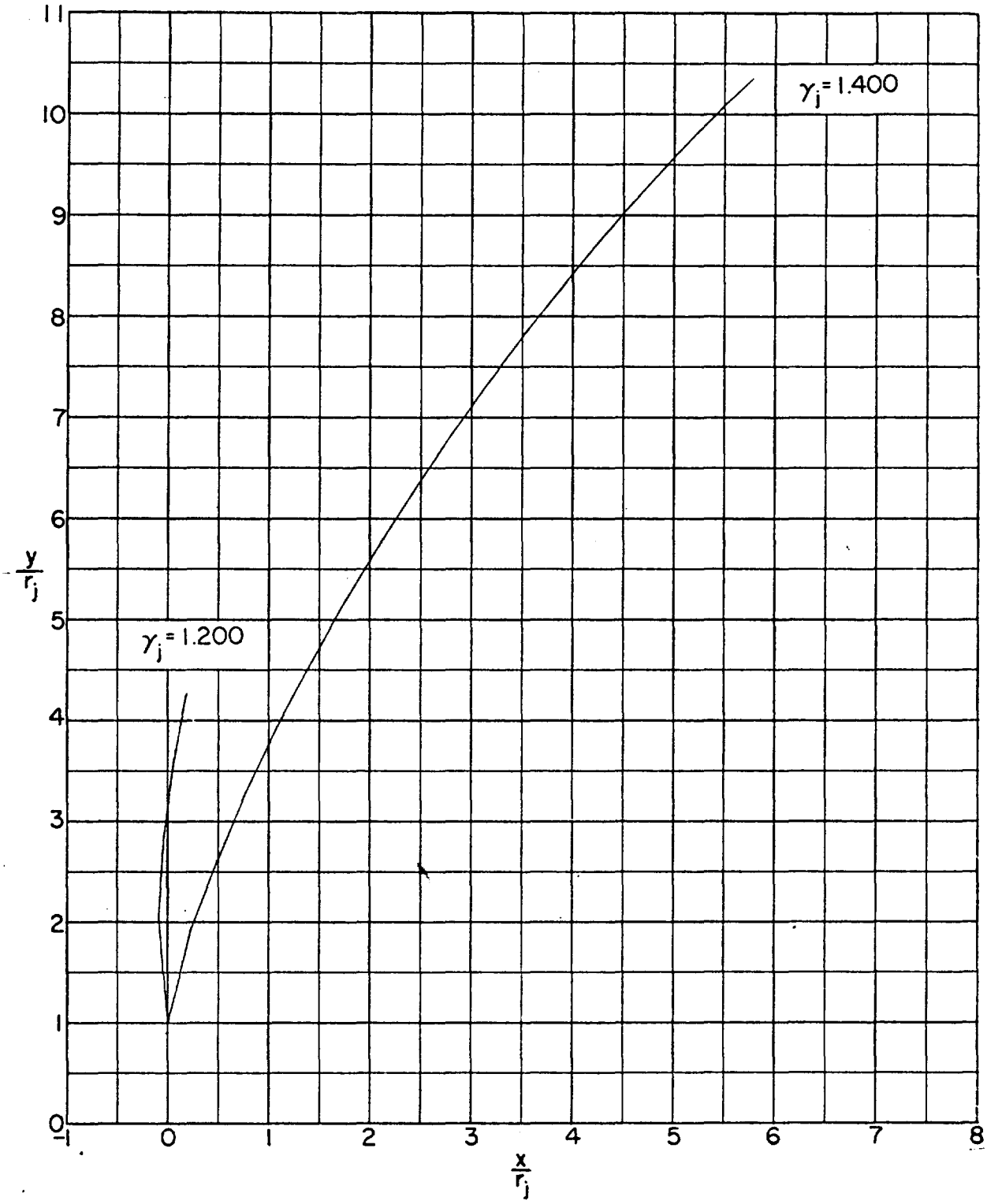

FIGURE 40.—Example of the effect of γ_j at large pressure ratios upon shape of boundary for similar pressure ratios. Jet exhausting into still air; $M_j = 2.5$; $\theta_N = 15°$; $p_j/p_\infty \approx 1{,}300$.

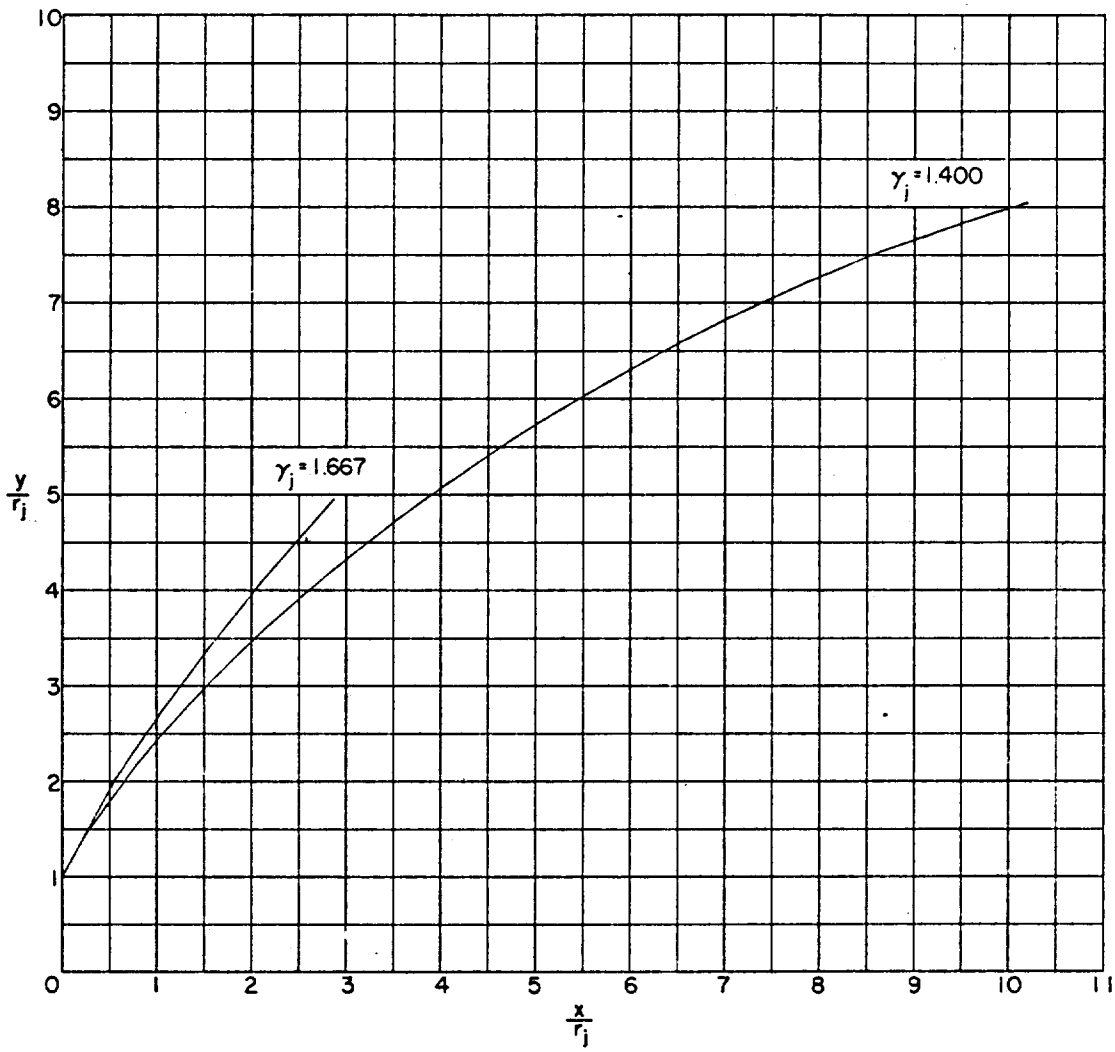

FIGURE 41.—Example of effect of γ_j at large pressure ratios upon shape of boundary for similar initial inclinations of boundary. Jet exhausting into still air; $M_j = 2.5$; $\theta_N = 15°$; $\delta_j \approx 60°$.

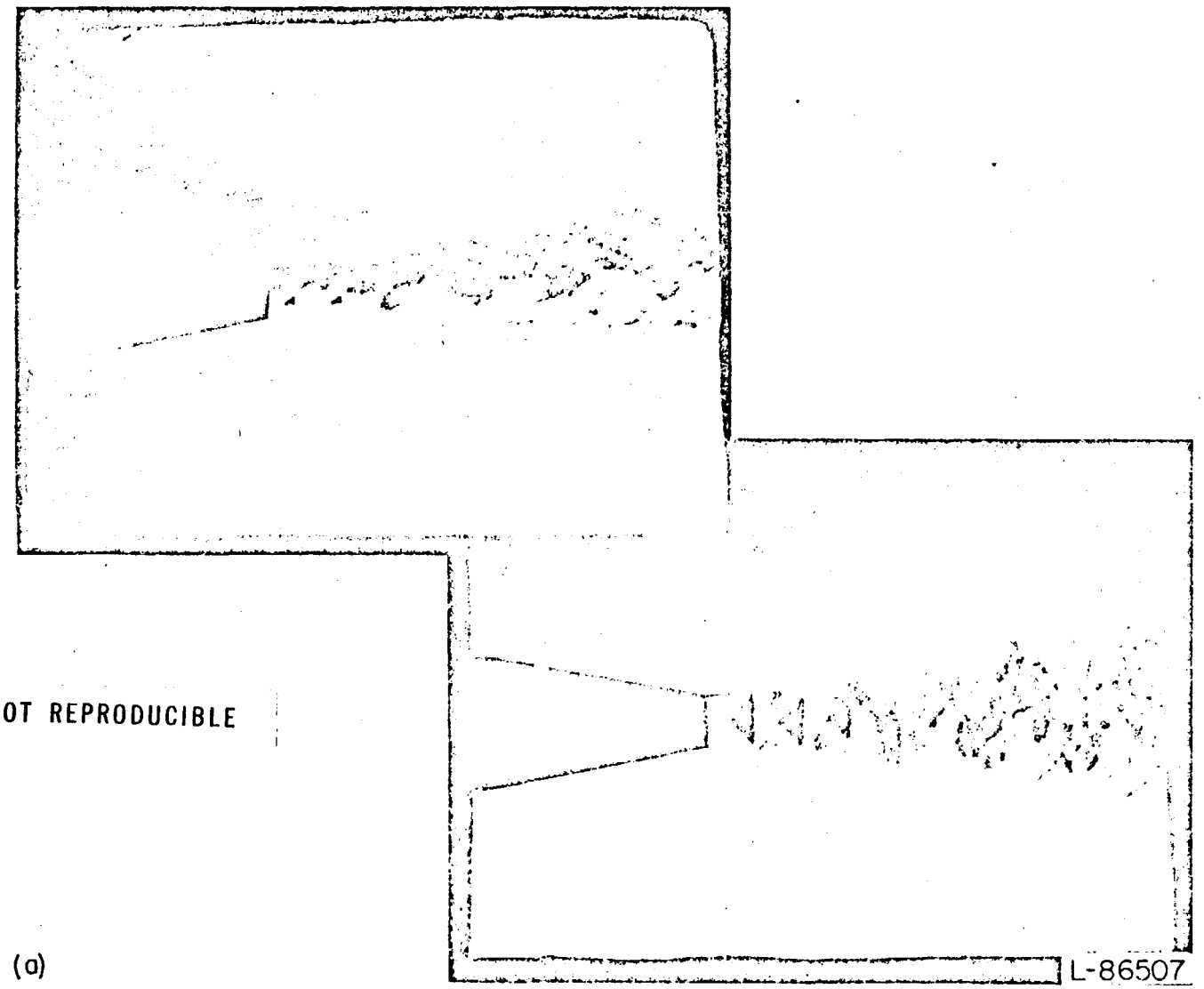

(a) $p_i/p_\infty = 1.41$.

FIGURE 42.—Examples of alternate deflection and degeneration of jet structure. $M_i = 1.00$; $\theta_N = 0°$.

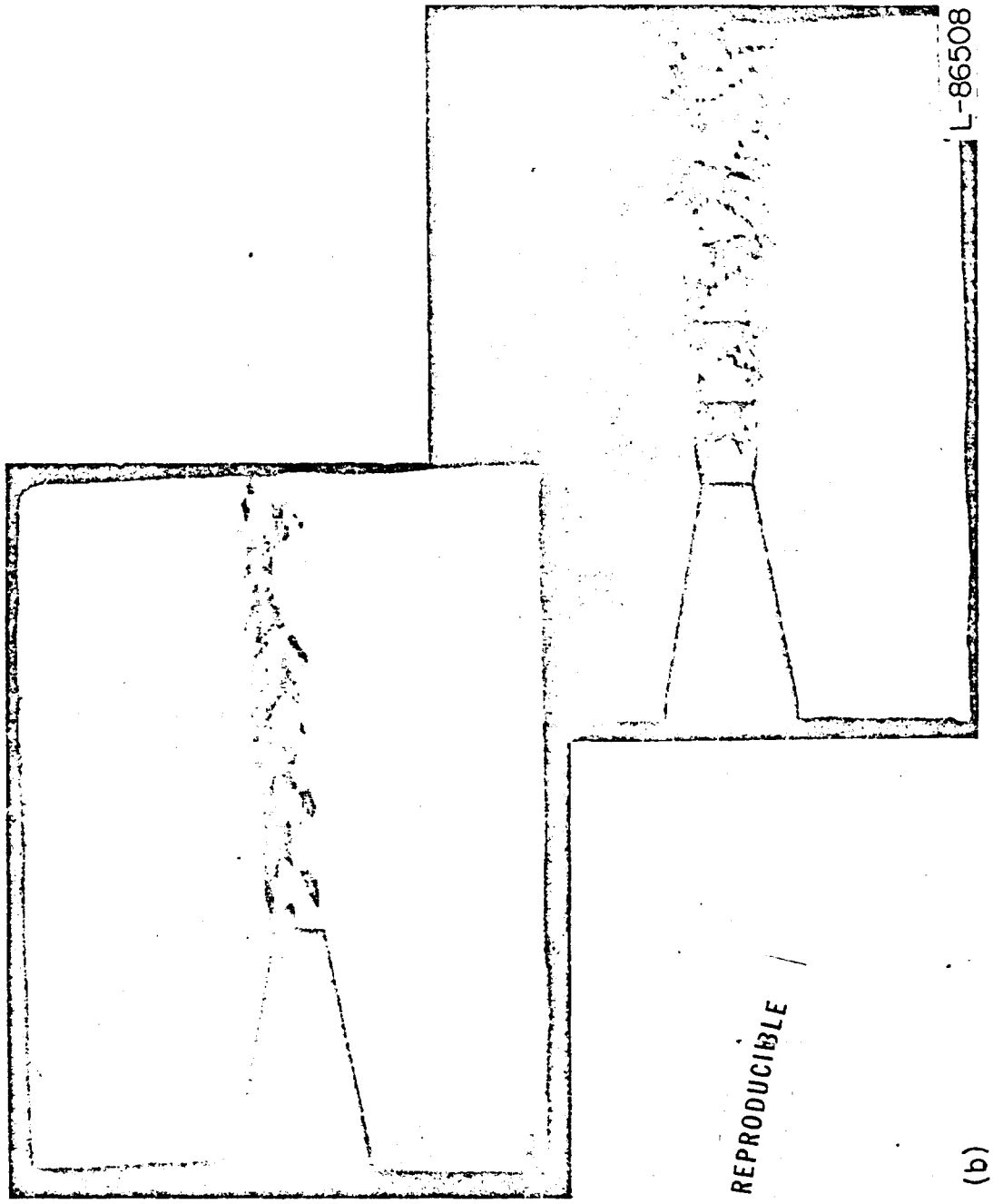

(b) $p_i/p_\infty = 2.11$.

FIGURE 42.—Concluded.

502683 O—59——15

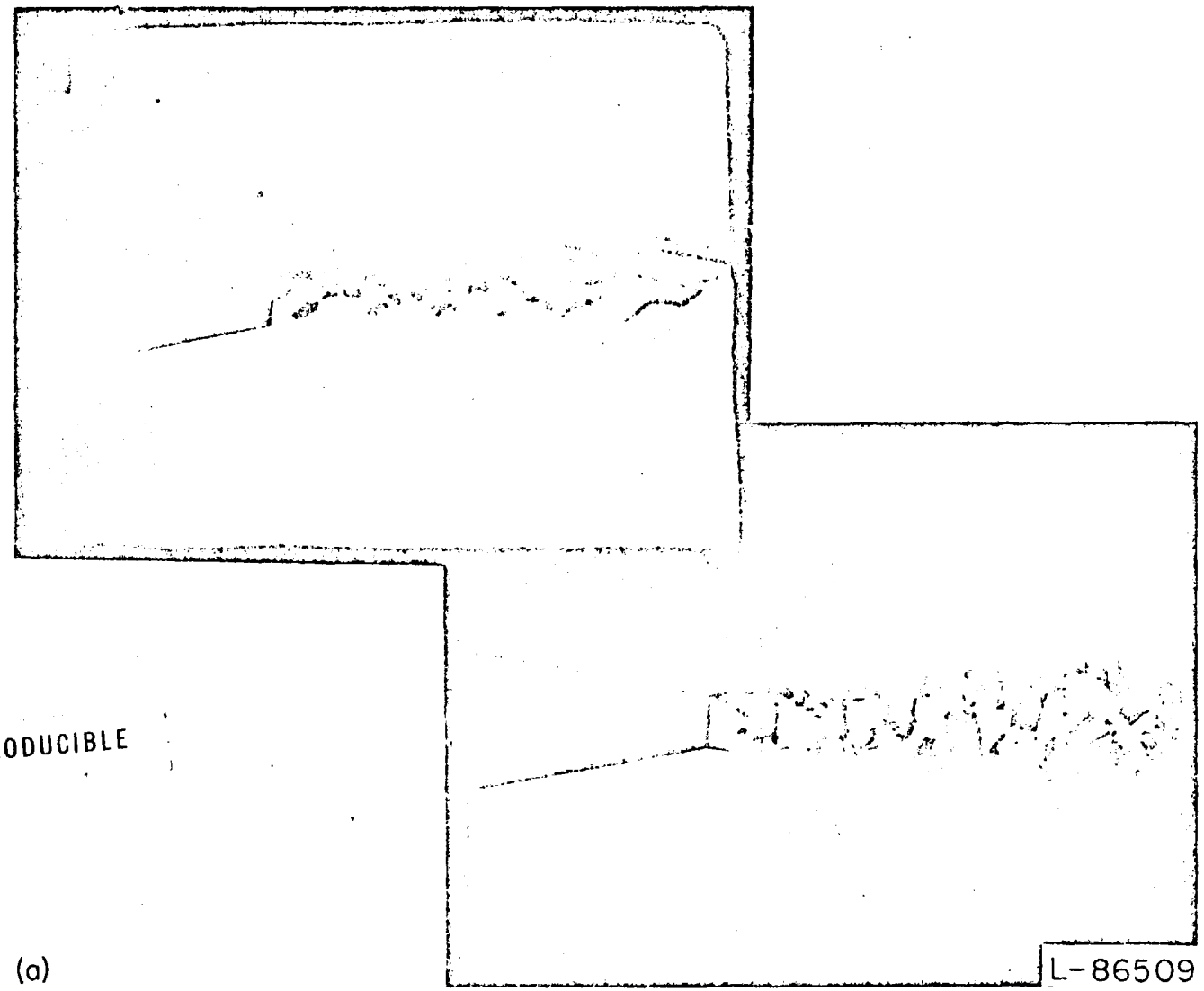

(a) $p_i/p_\infty = 1.76$.

FIGURE 43.—Examples of sound waves associated with the degeneration of jet structure. $M_i = 1.00$; $\theta_N = 0°$.

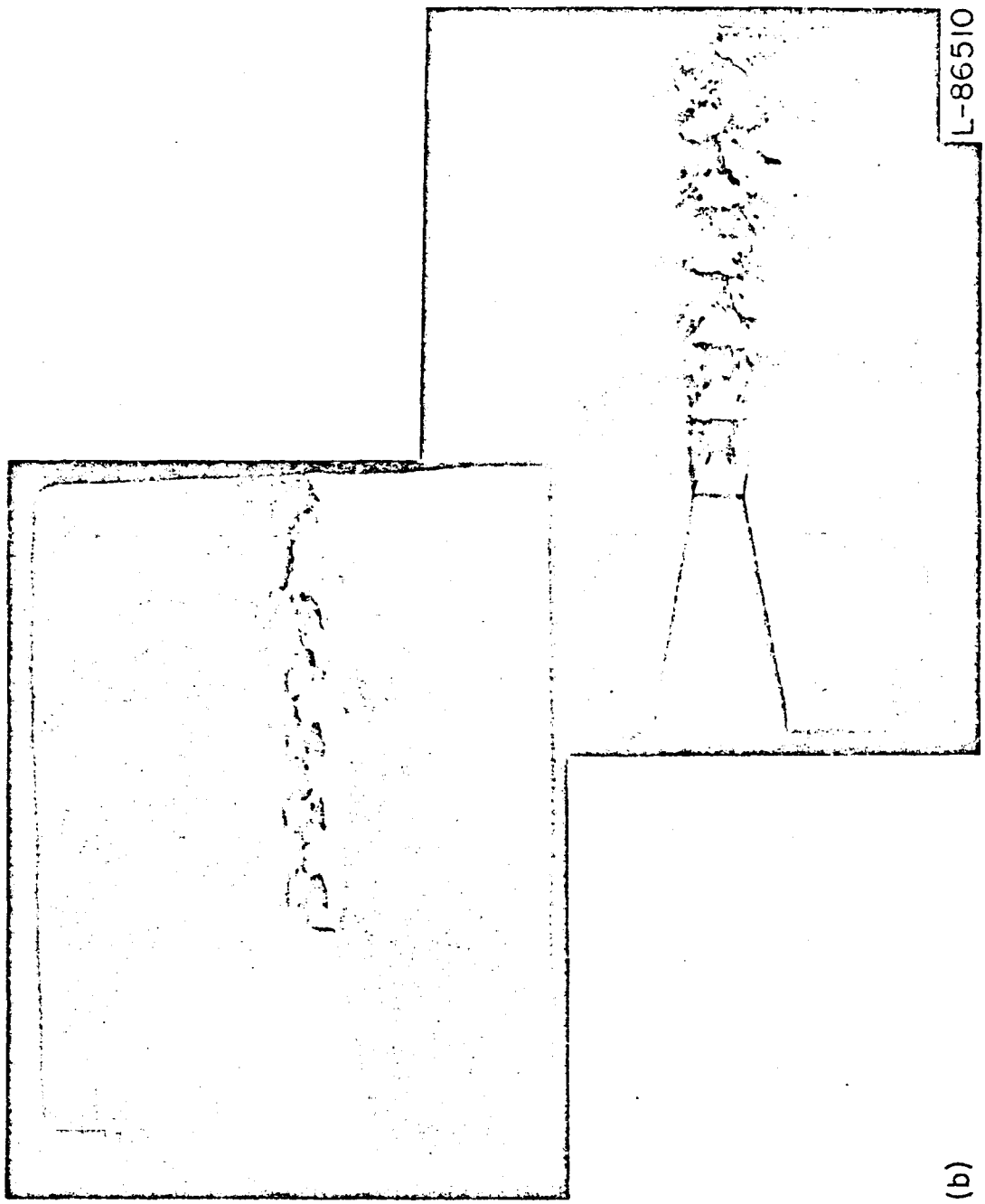

(b) $p_j/p_\infty = 1.94$.

FIGURE 43.—Concluded

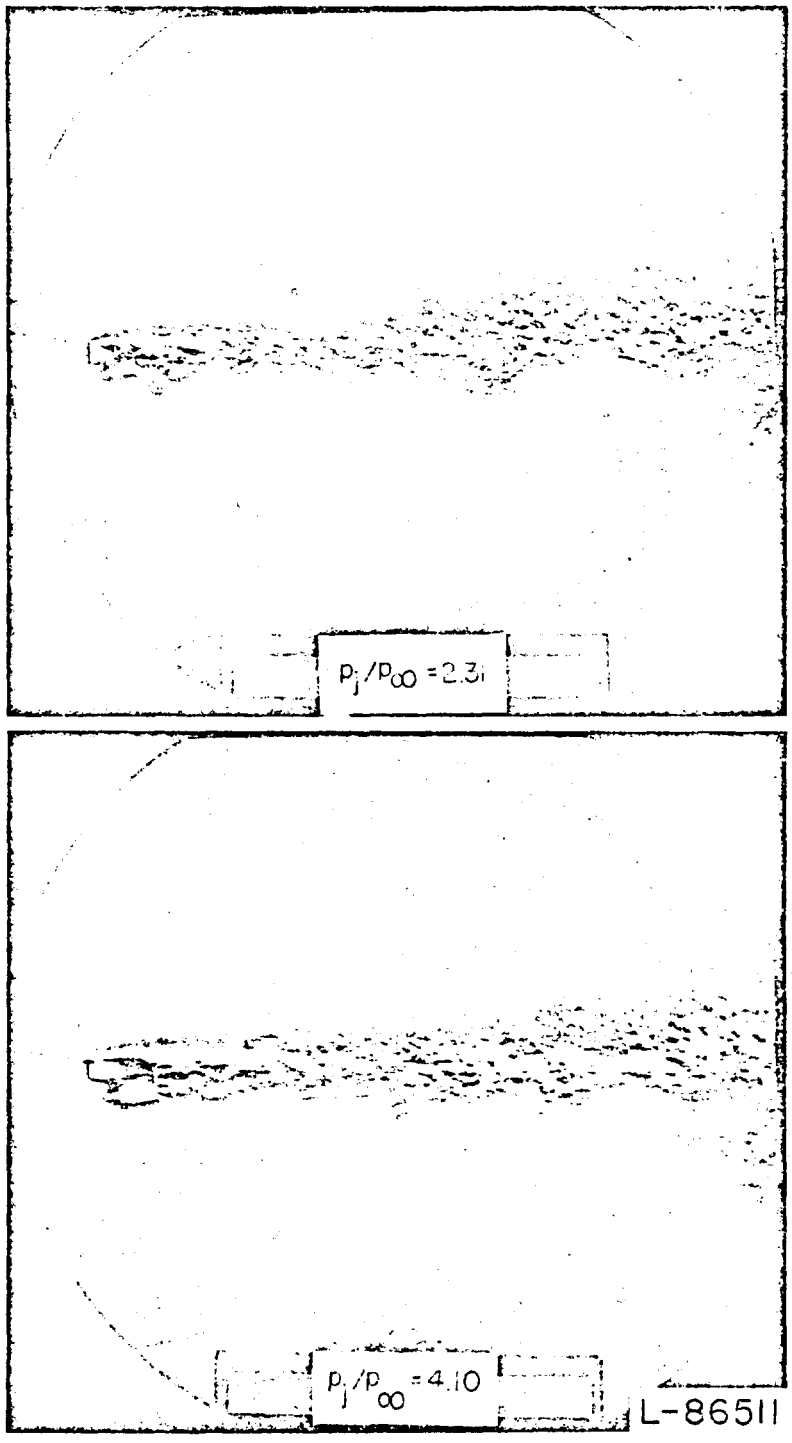

FIGURE 44.—Photographs of sound waves generated by jet beyond jet pressure ratio for reappearance of Riemann wave. $M_i = 1.00$; $\theta_N = 0°$.

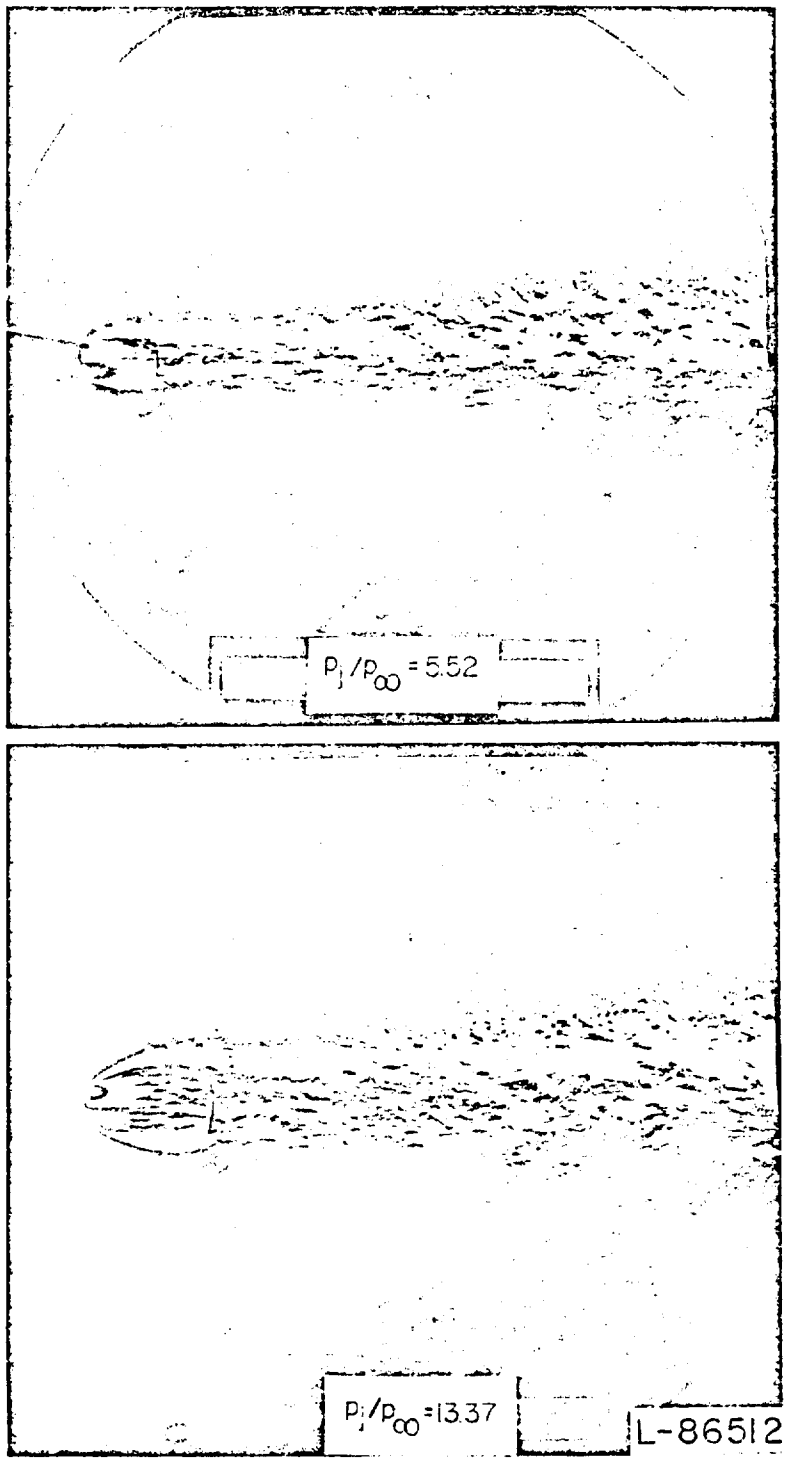

FIGURE 44.—Concluded.

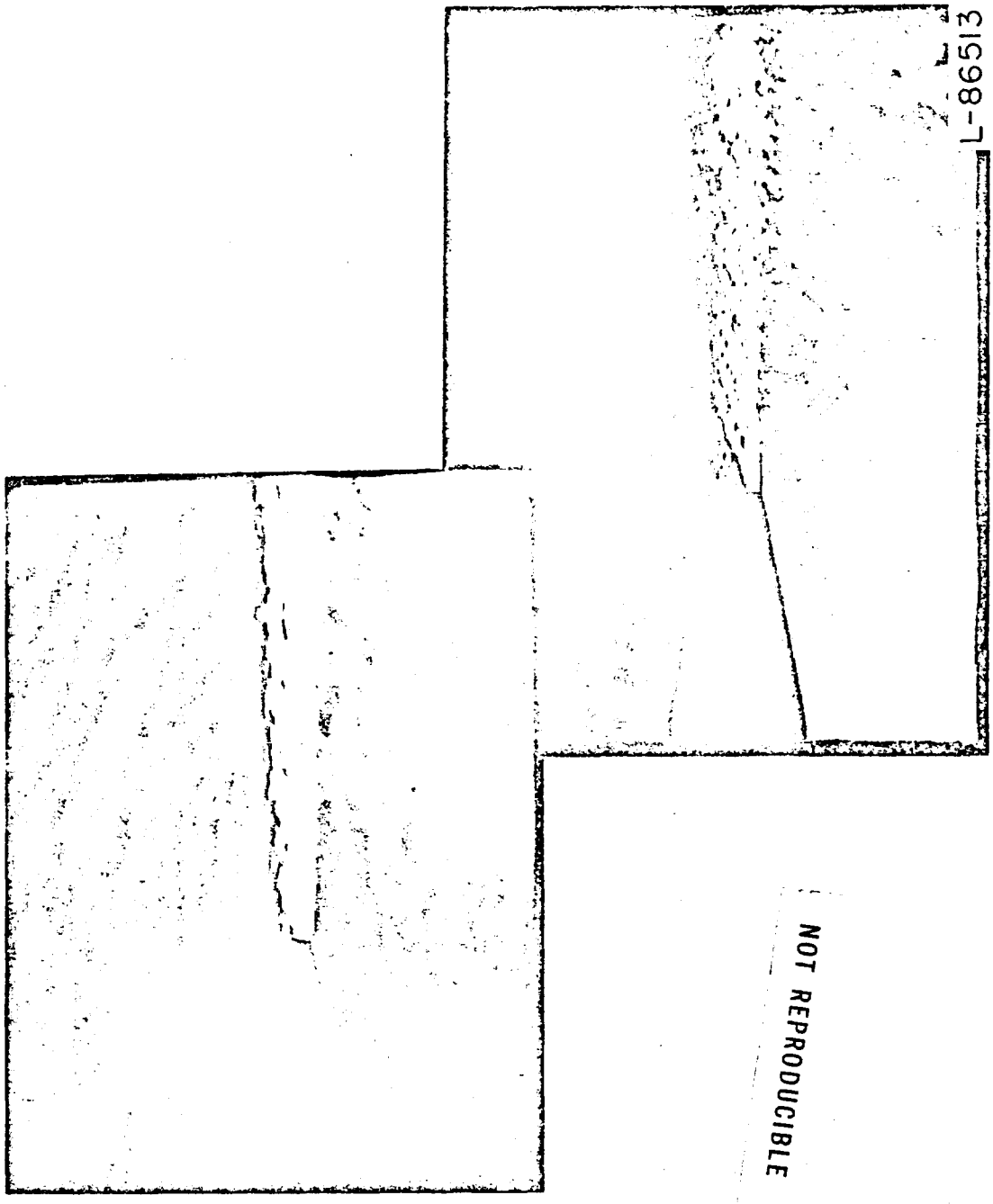

FIGURE 45.—Example of oblique compression waves generated in ambient air by supersonic eddy convection velocity. $M_j=3.00$; $\theta_N=0°$; $p_i/p_\infty=0.86$.

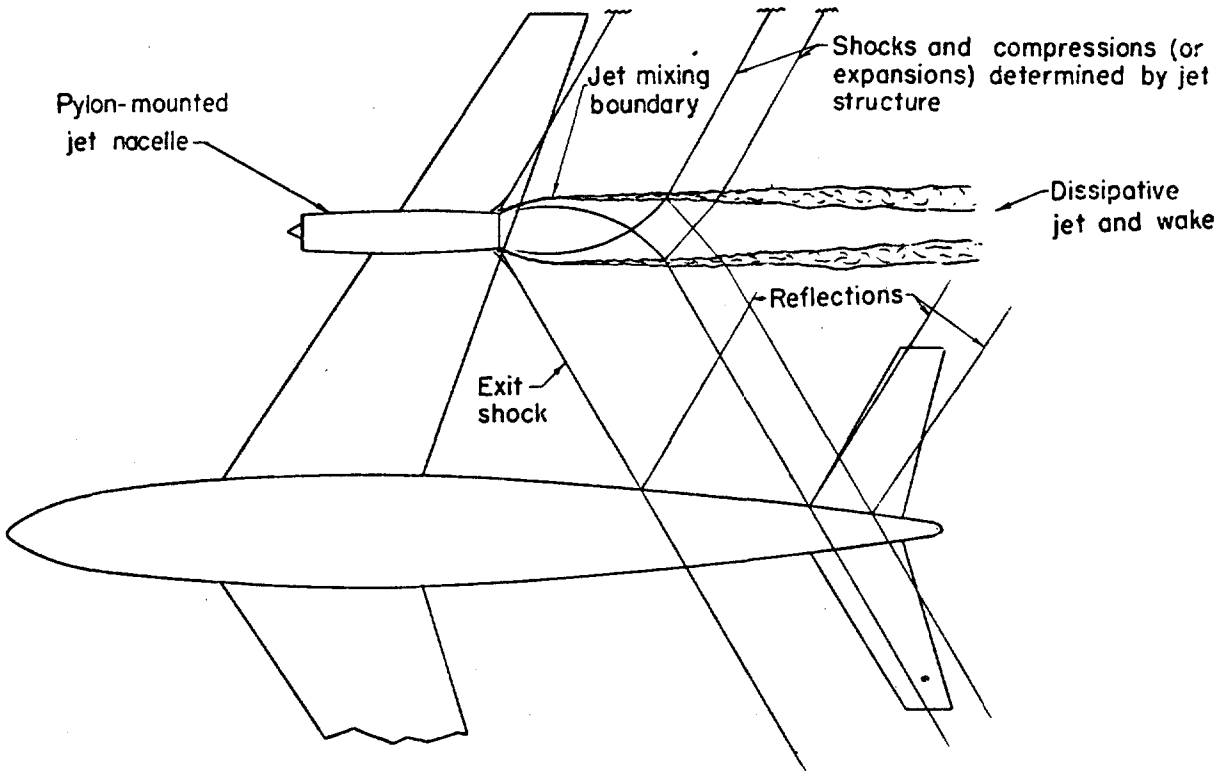

FIGURE 46.—Illustrative sketch of interference flow field created by jet. Mixing boundary assumed to be supersonic throughout.

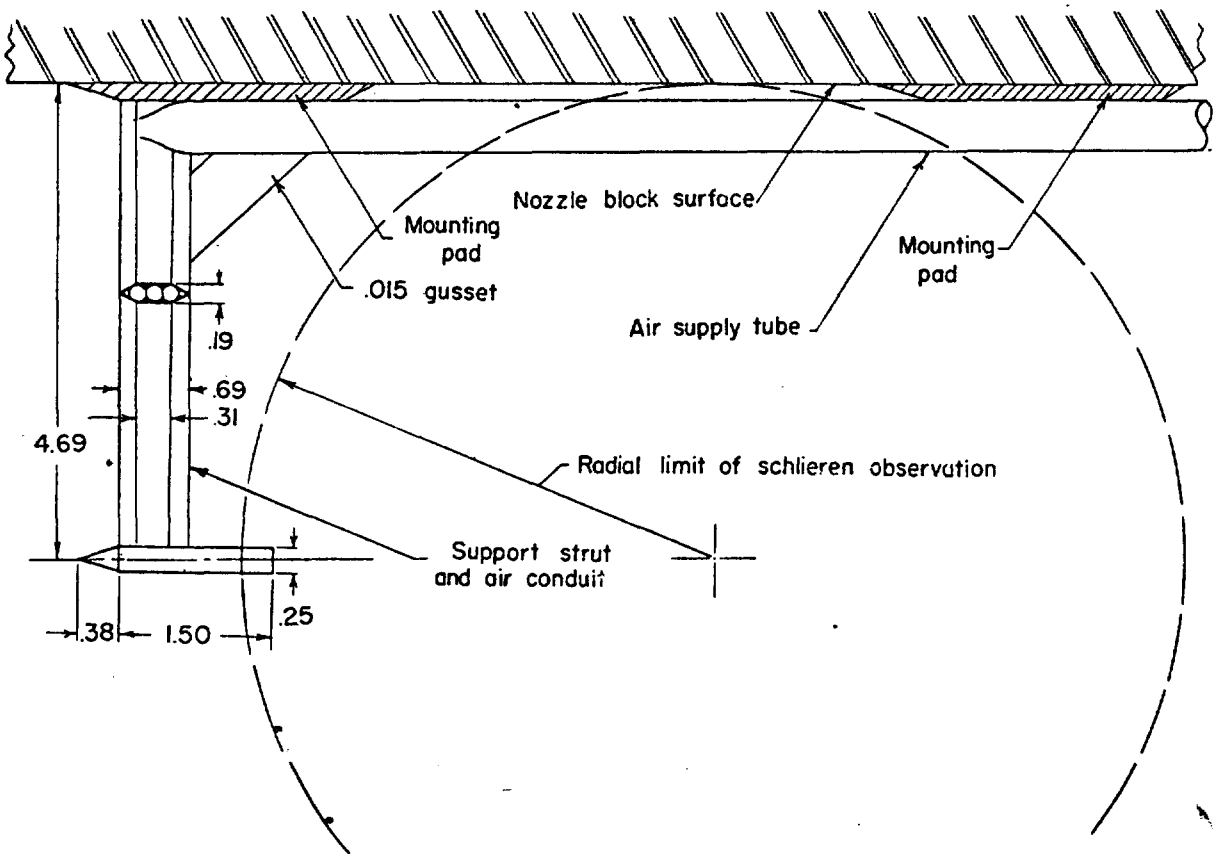

FIGURE 47.—Sketch of model employed in visual studies of jet exhausting into supersonic stream. All dimensions are in inches.

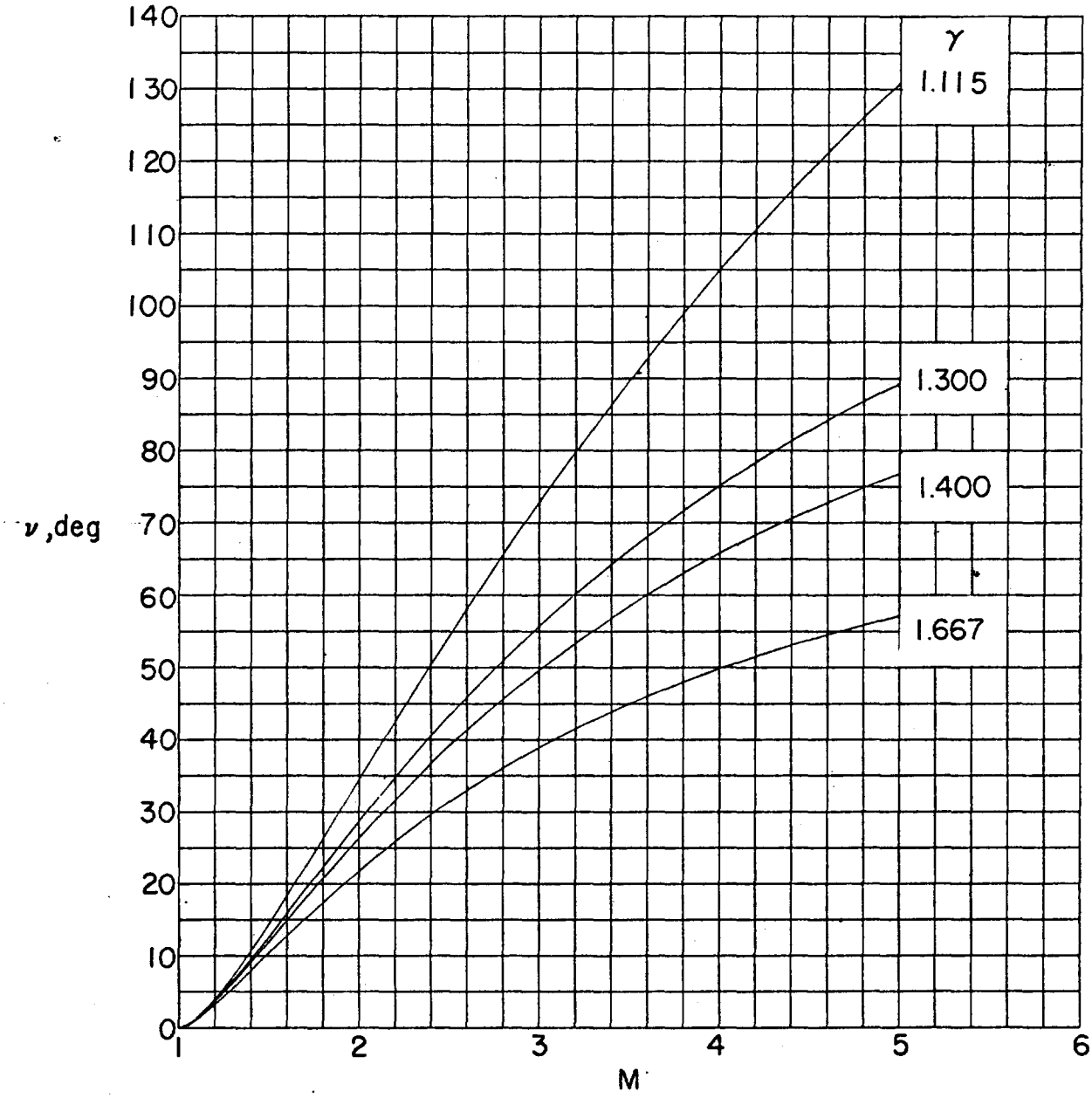

FIGURE 48.—Effect of the ratio of specific heats upon the variation in Prandtl-Meyer turning angle from sonic velocity with Mach number.

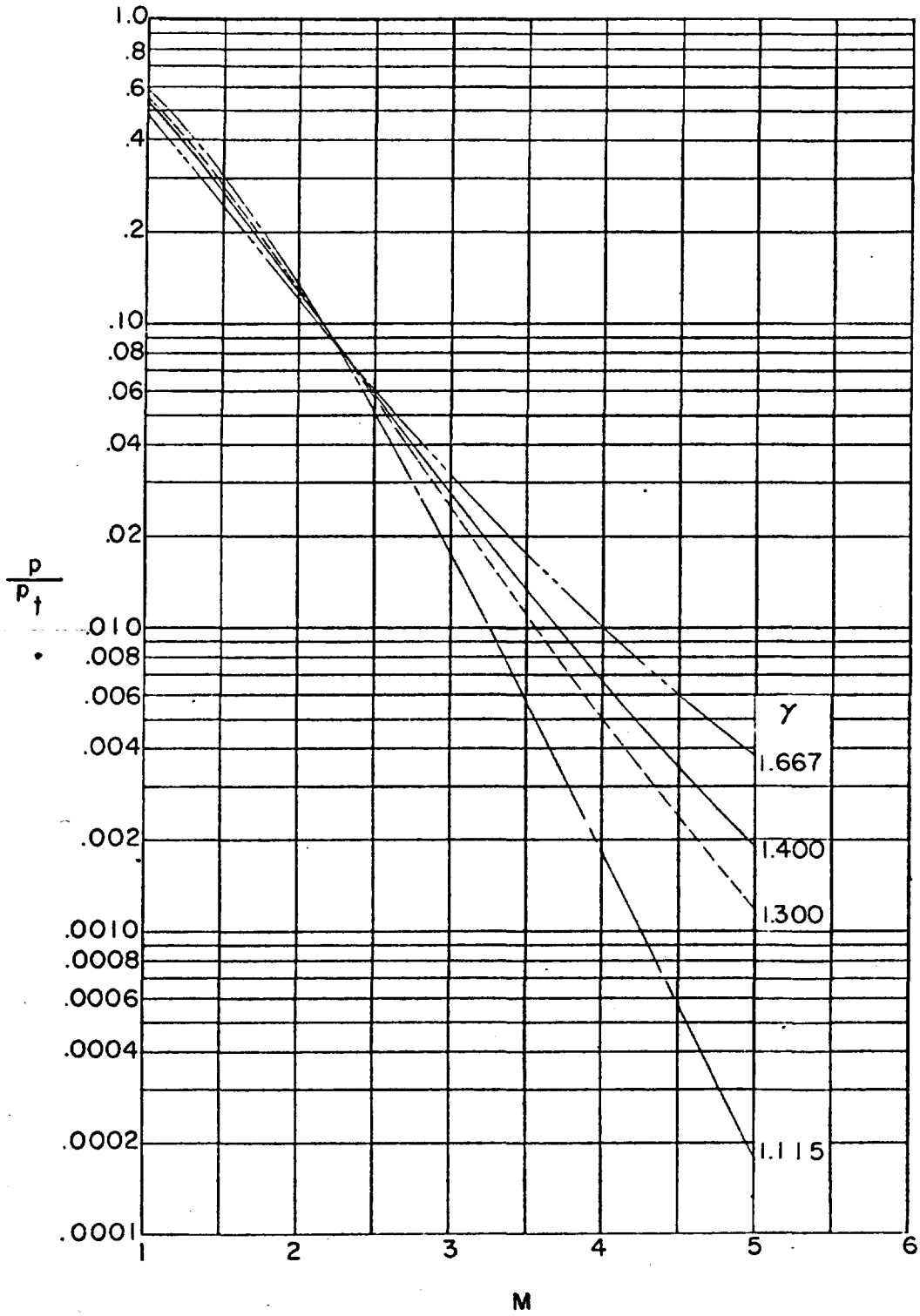

FIGURE 49.—Effect of the ratio of specific heats upon the variation in the ratio of static to stagnation pressure with Mach number.

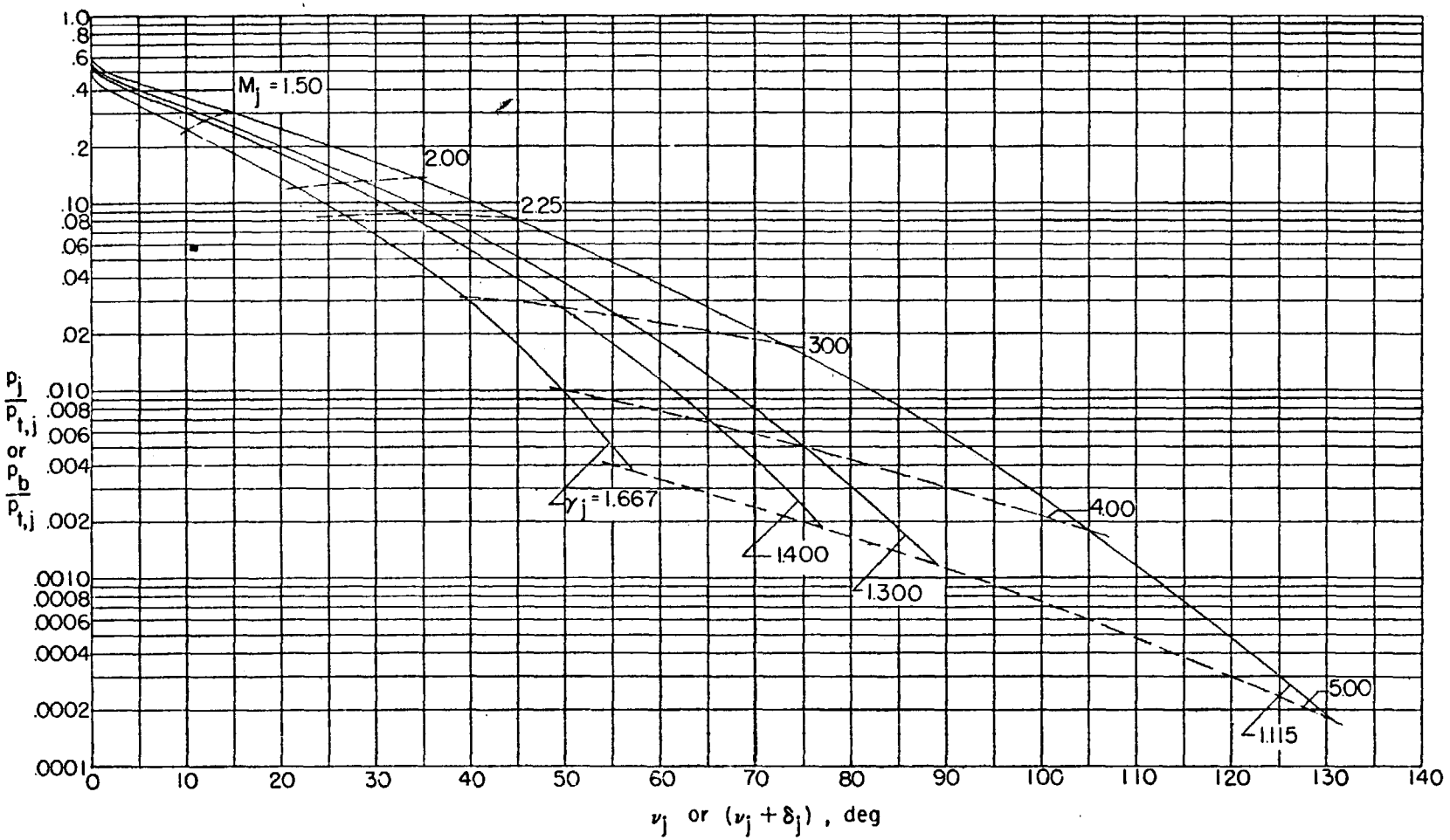

FIGURE 50.—Curves for correcting base-pressure data for a change in the ratio of specific heats of the jet.

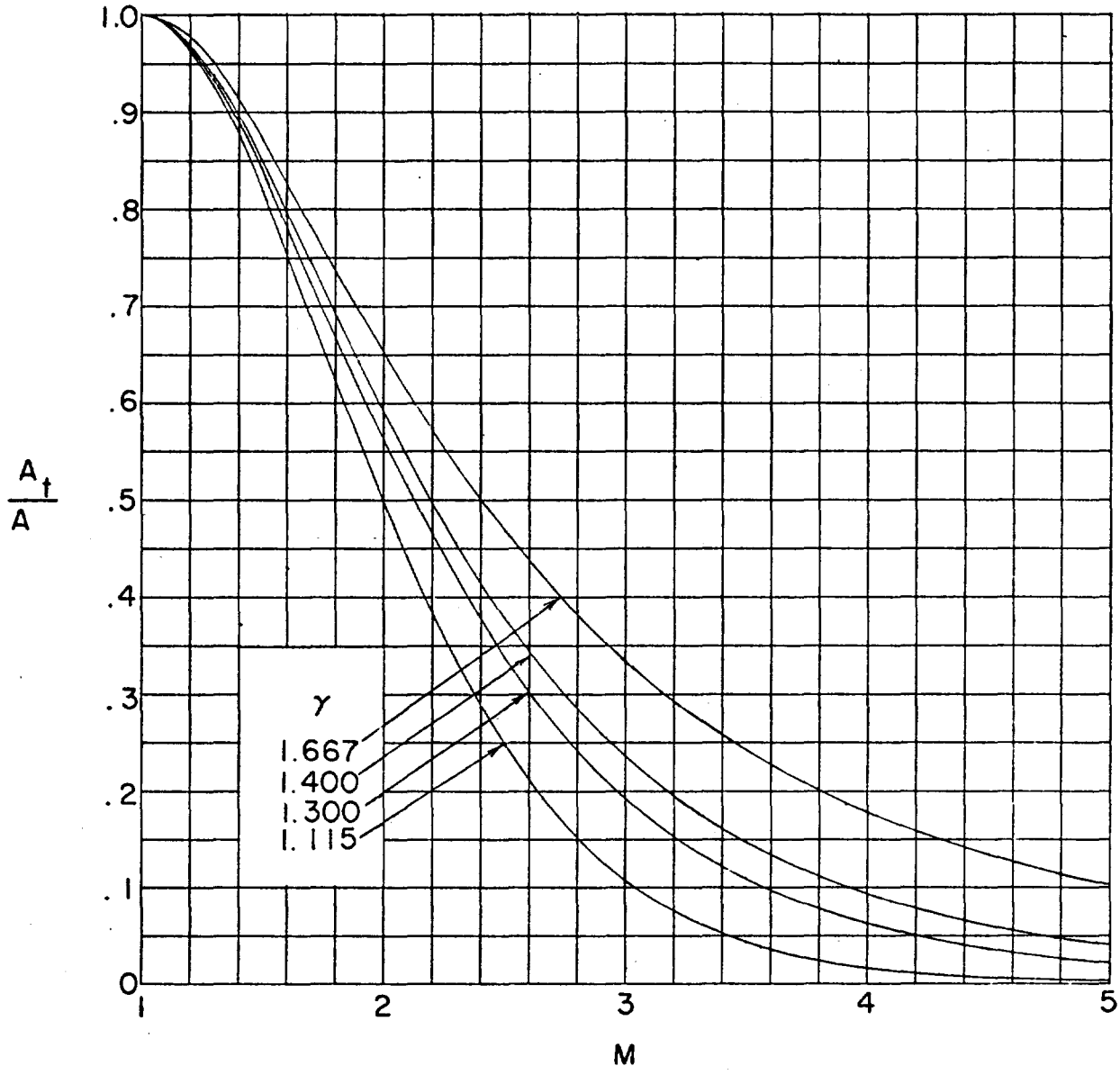

FIGURE 51.—Effect of the ratio of specific heats upon the variation in nozzle area ratio with Mach number.

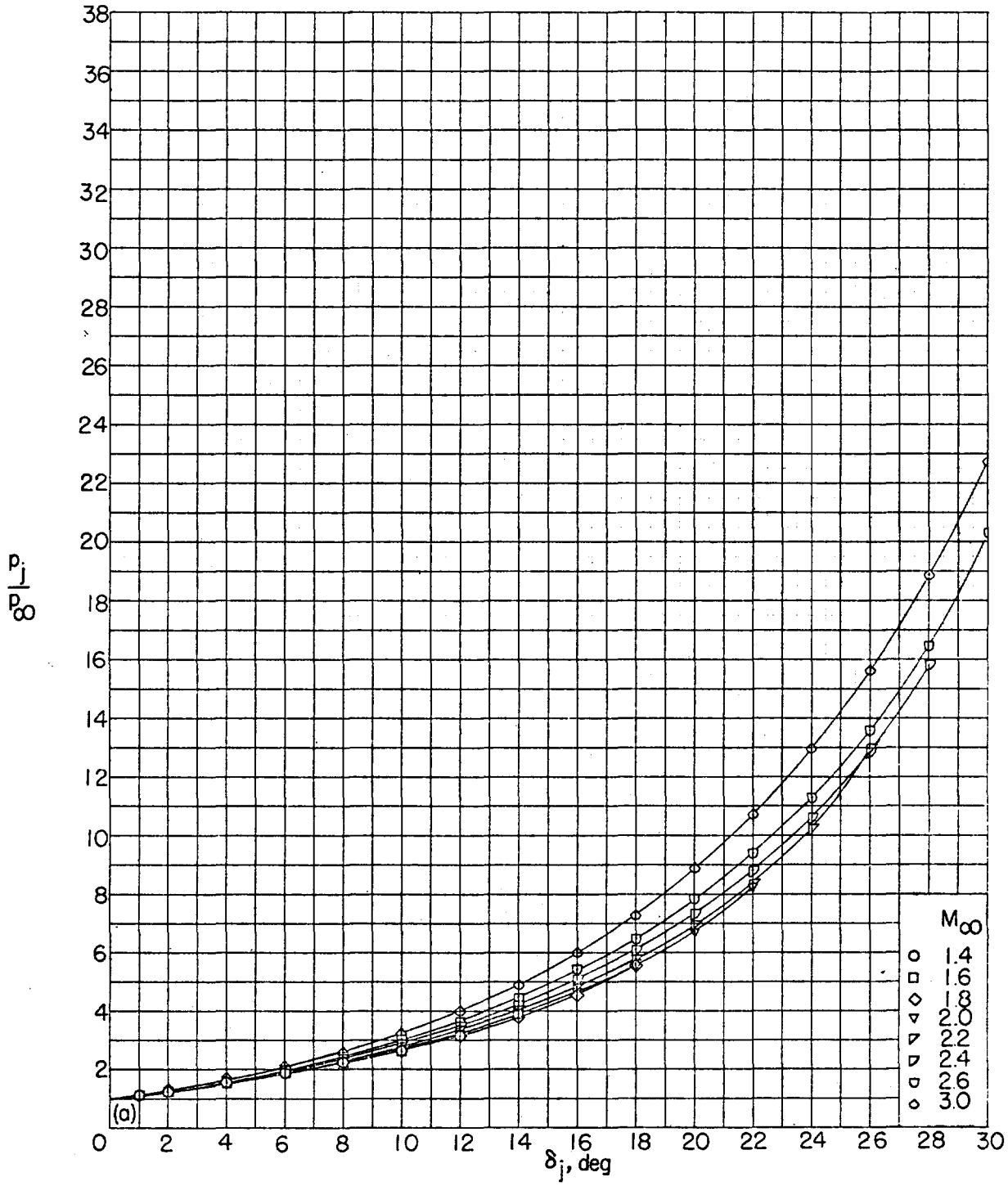

(a) $\gamma_f = 1.115$.

FIGURE 52.—Variation of initial inclination of jet boundary with jet pressure ratio for several free-stream Mach numbers and ratios of specific heats of the jet. $M_j = 1.00$; $\theta_N = 0°$; $\beta = 0°$.

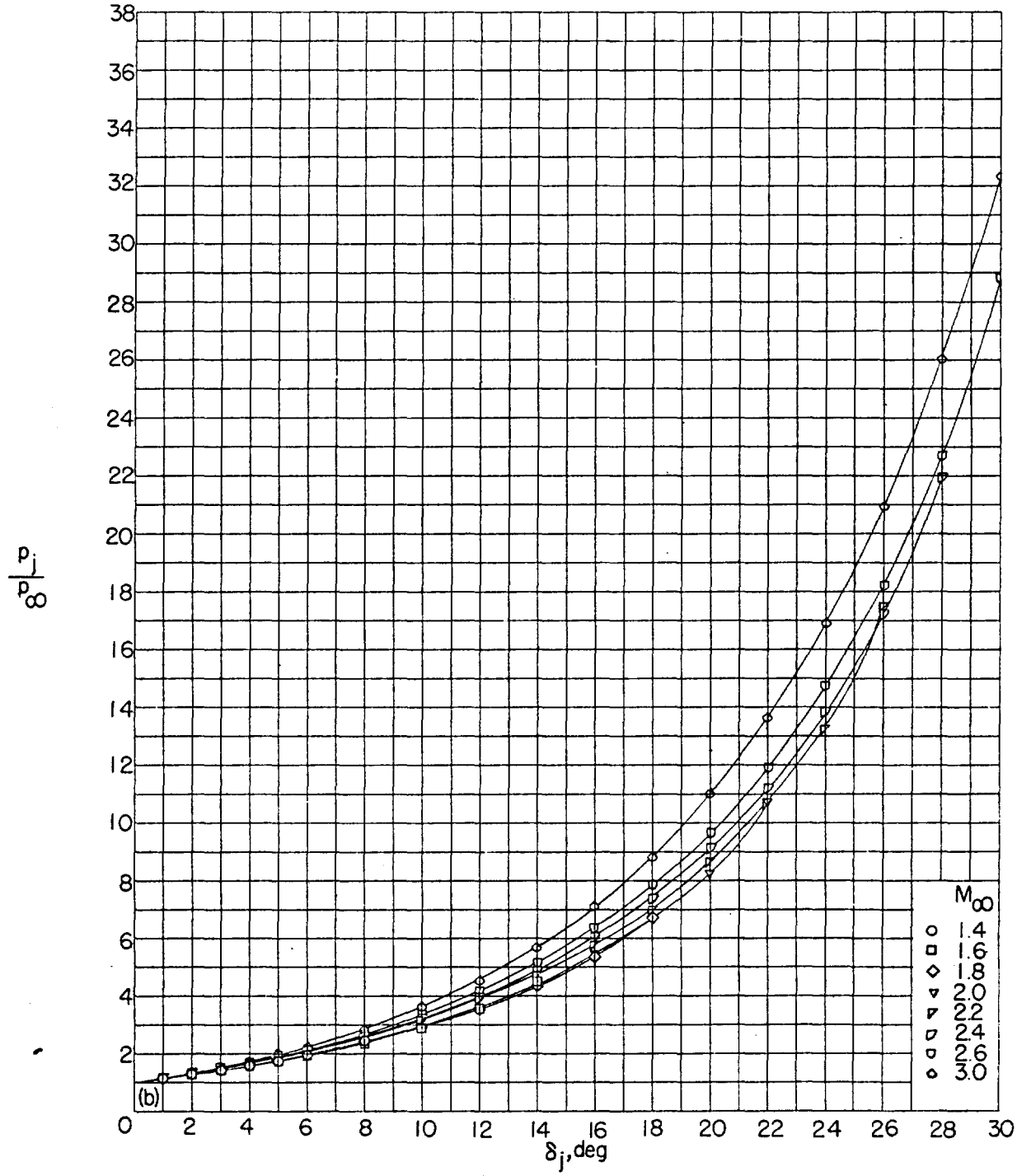

(b) $\gamma_j = 1.400$.

FIGURE 52.—Continued.

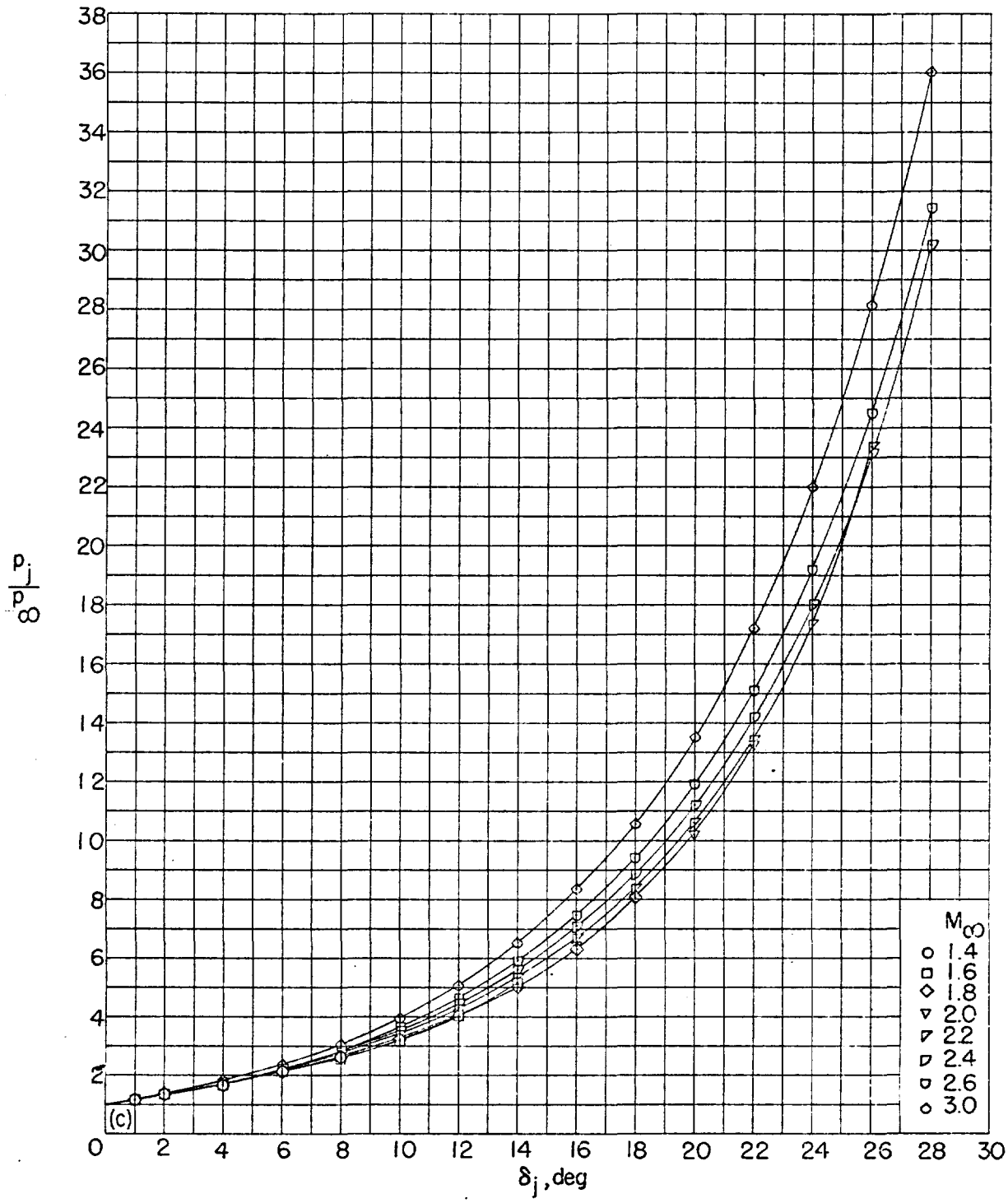

(c) $\gamma_j = 1.667$.

FIGURE 52.—Concluded.

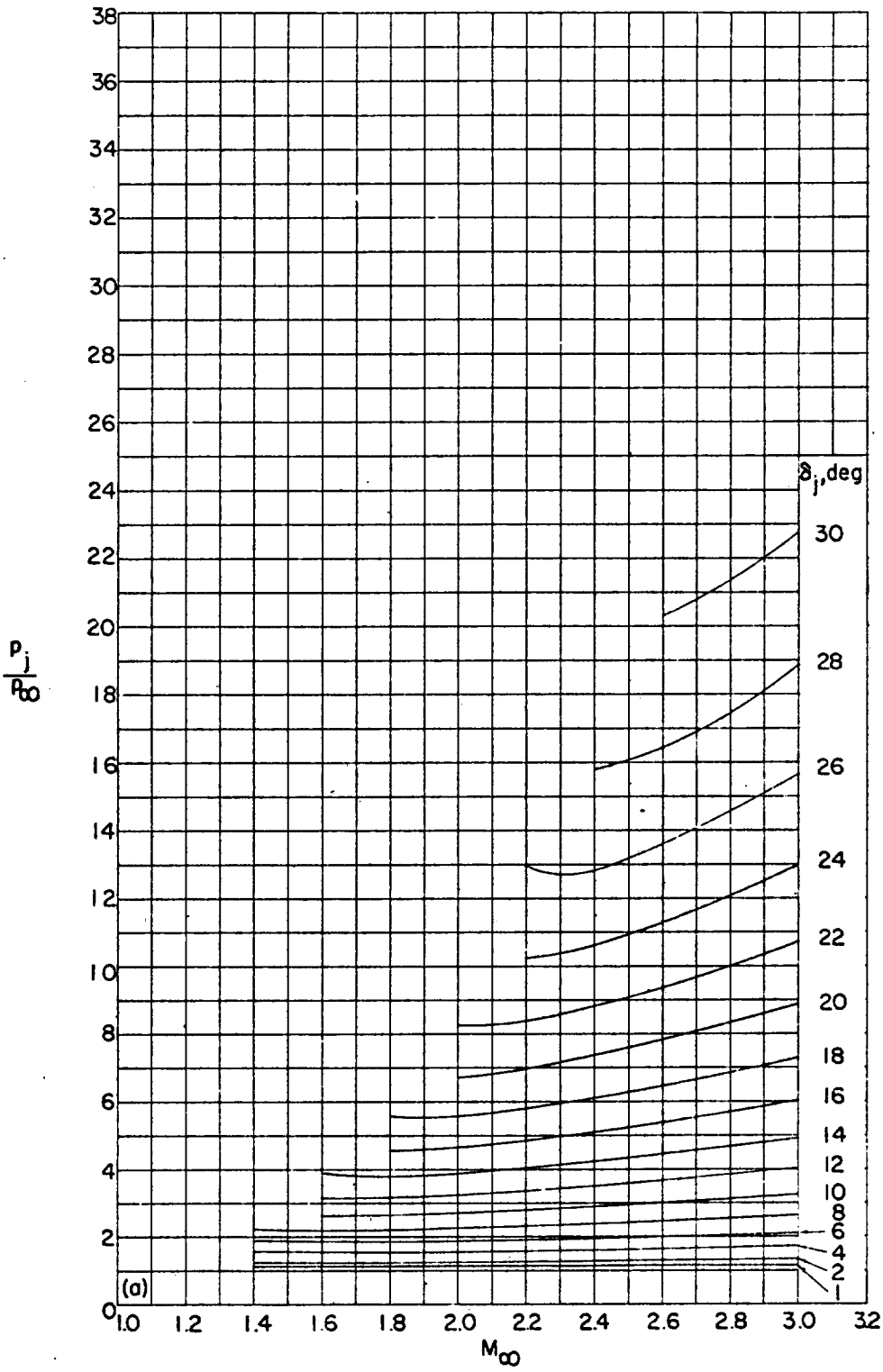

(a) $\gamma_i = 1.115$.

FIGURE 53.—Cross plots showing variation of jet pressure ratio with free-stream Mach number for several initial inclinations of the jet boundary and ratios of specific heats of the jet. $M_j = 1.00$; $\theta_N = 0°$; $\beta = 0°$.

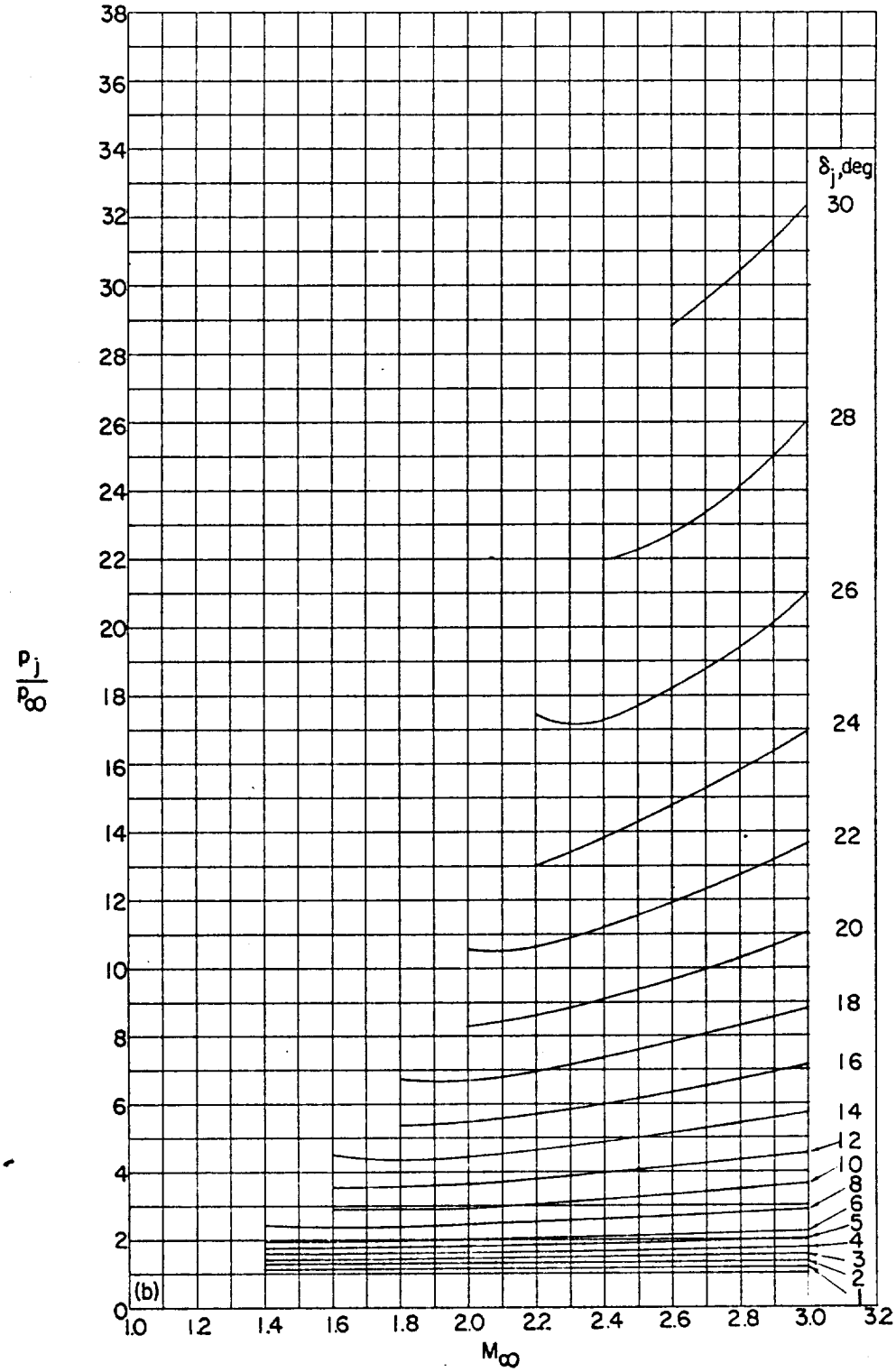

(b) $\gamma_i = 1.400$.

FIGURE 53.—Continued.

502683 O—59——16

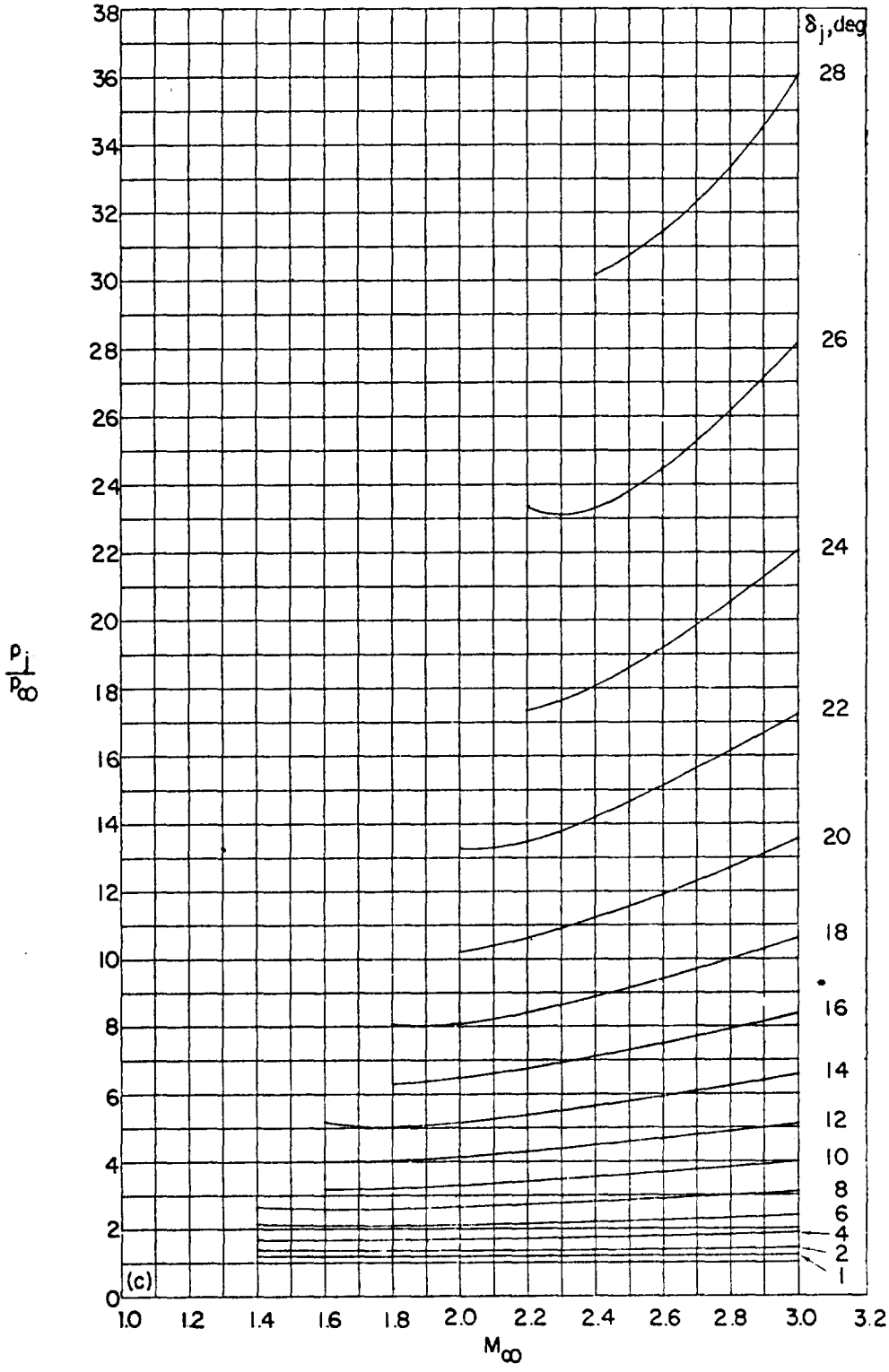

(c) $\gamma_j = 1.667$.

FIGURE 53.—Concluded.

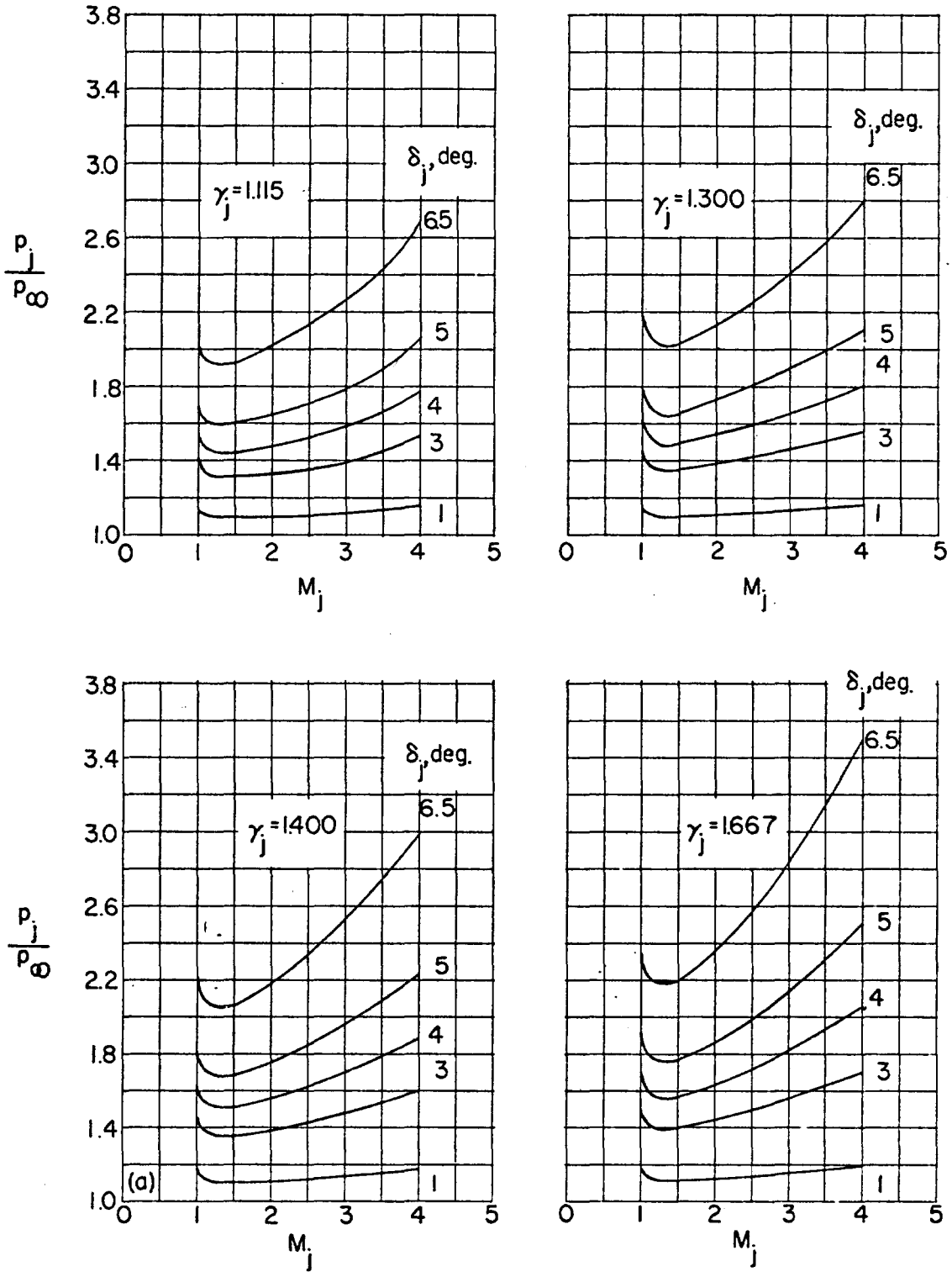

(a) $M_\infty = 1.30$.

FIGURE 54.—Variation of jet pressure ratio with jet Mach number for several initial inclinations of the jet boundary and ratios of specific heats of the jet. $\theta_N = 0°$; $\beta = 0°$.

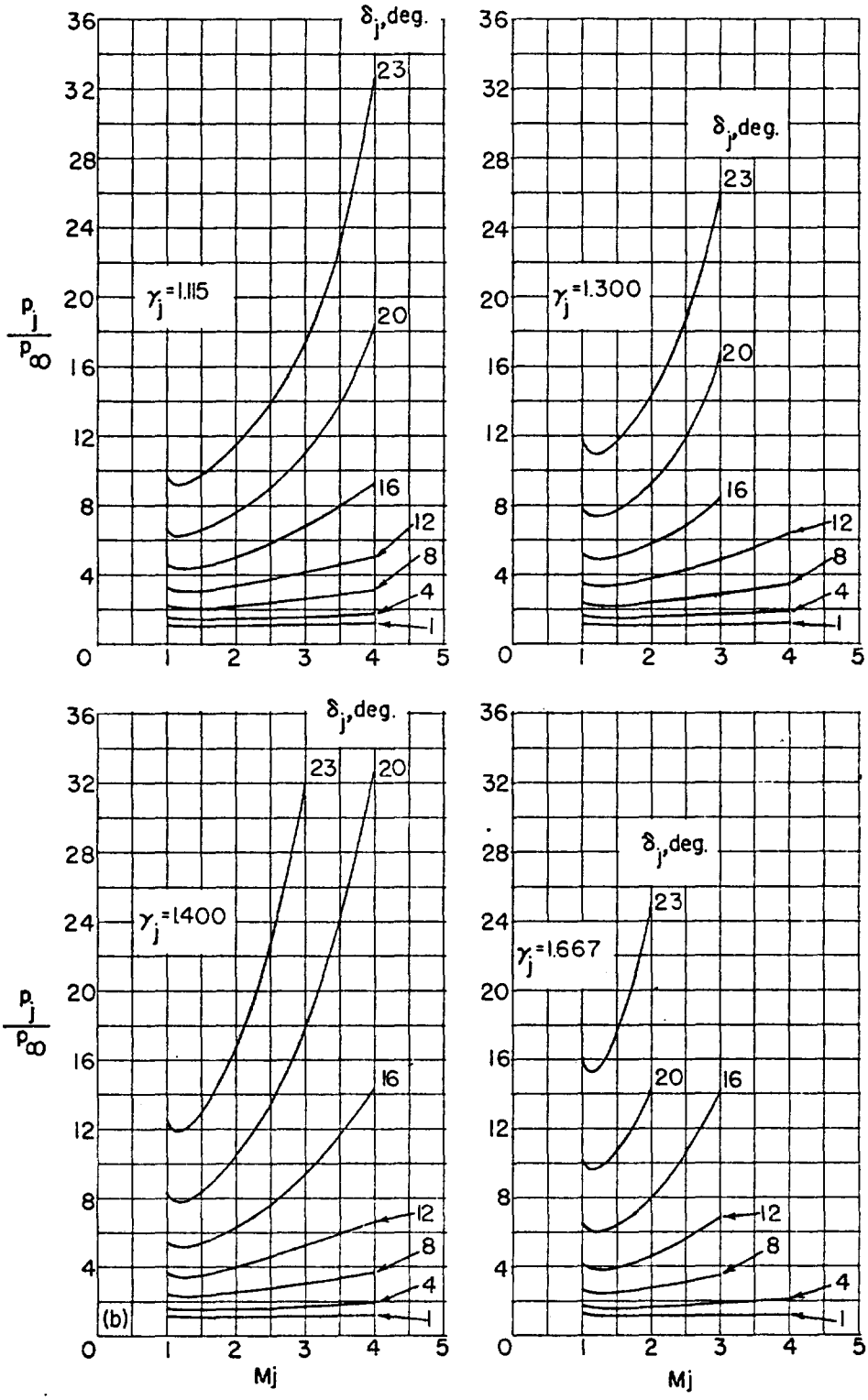

(b) $M_\infty = 2.00$.

FIGURE 54.—Concluded.

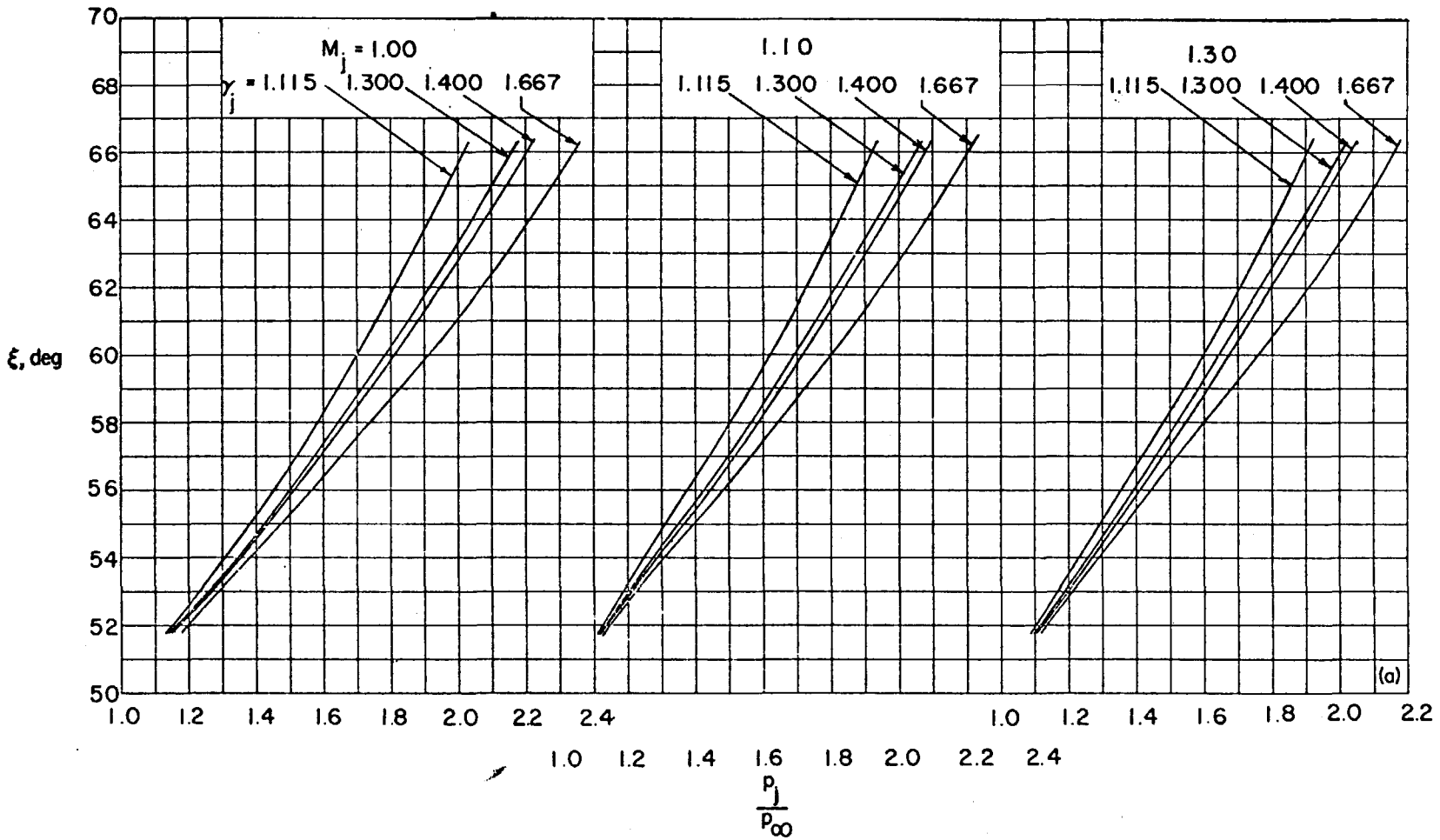

(a) $M_\infty = 1.30$.

FIGURE 55.—Variation of initial inclination of exit shock with jet pressure ratio for several jet Mach numbers and ratios of specific heats of the jet. $\theta_N = 0°$; $\beta = 0°$.

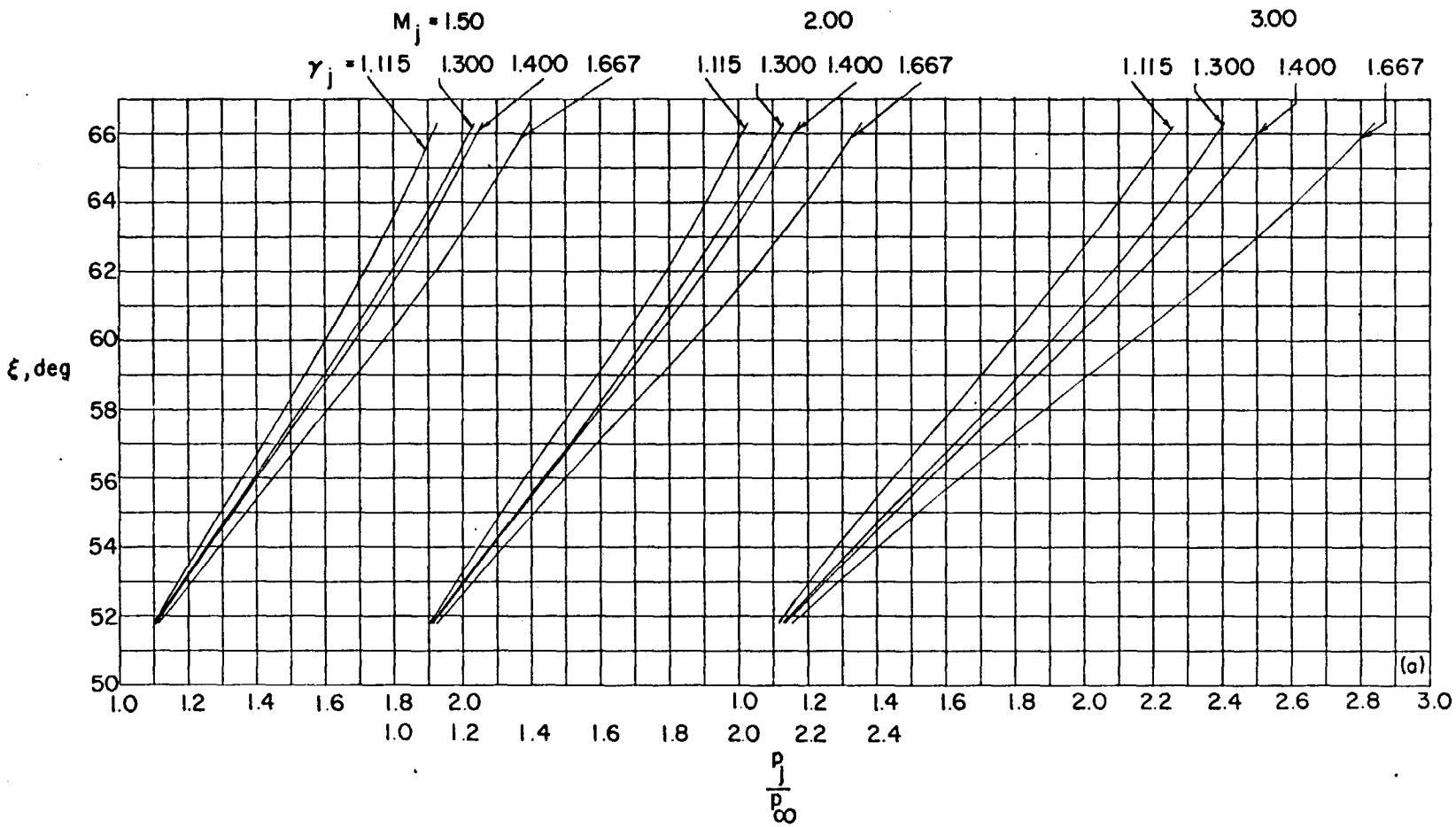

(a) $M_\infty = 1.30$. Continued.

FIGURE 55.—Continued.

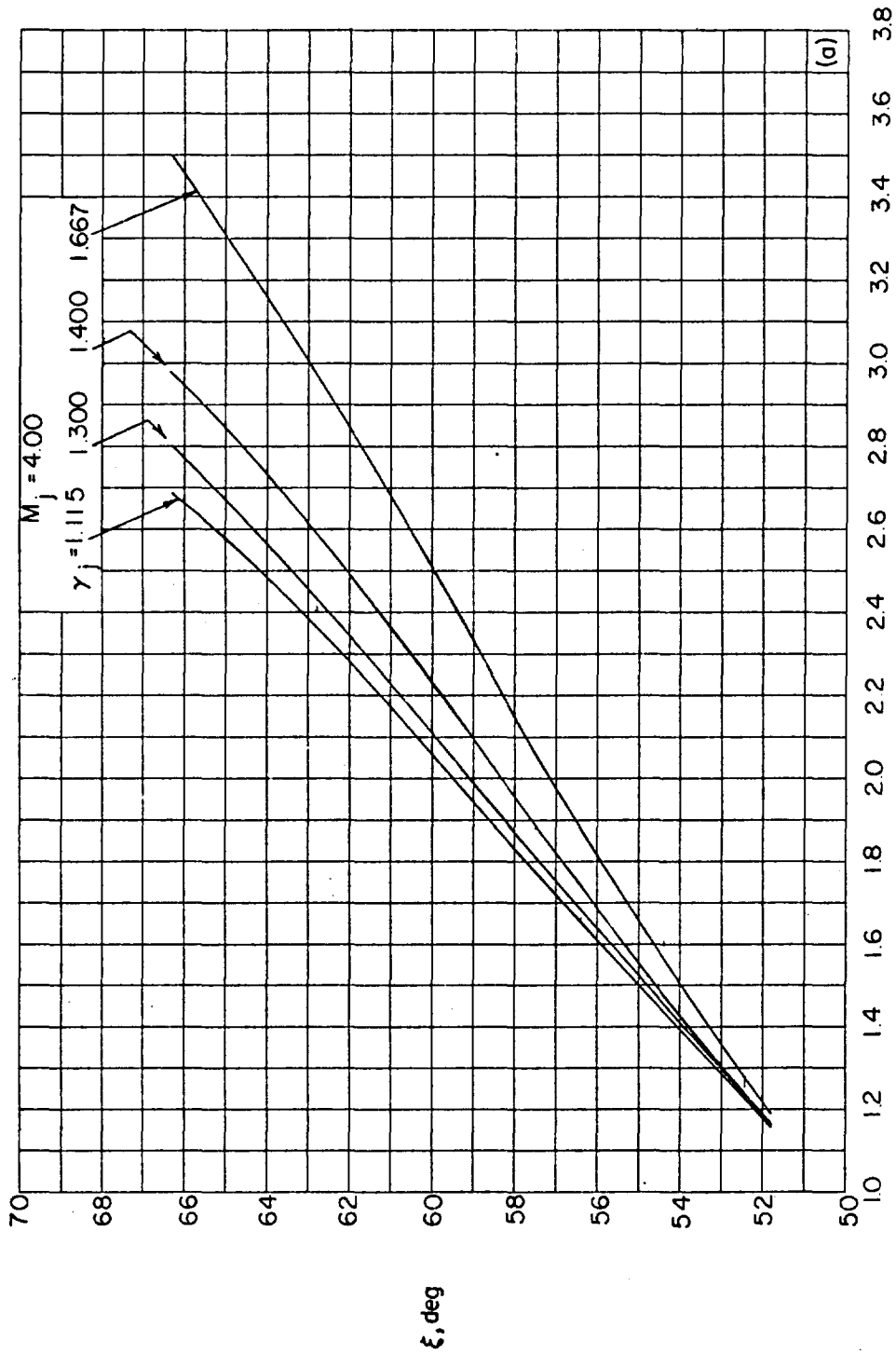

(a) $M_\infty = 1.30$. Concluded.

FIGURE 55.—Continued.

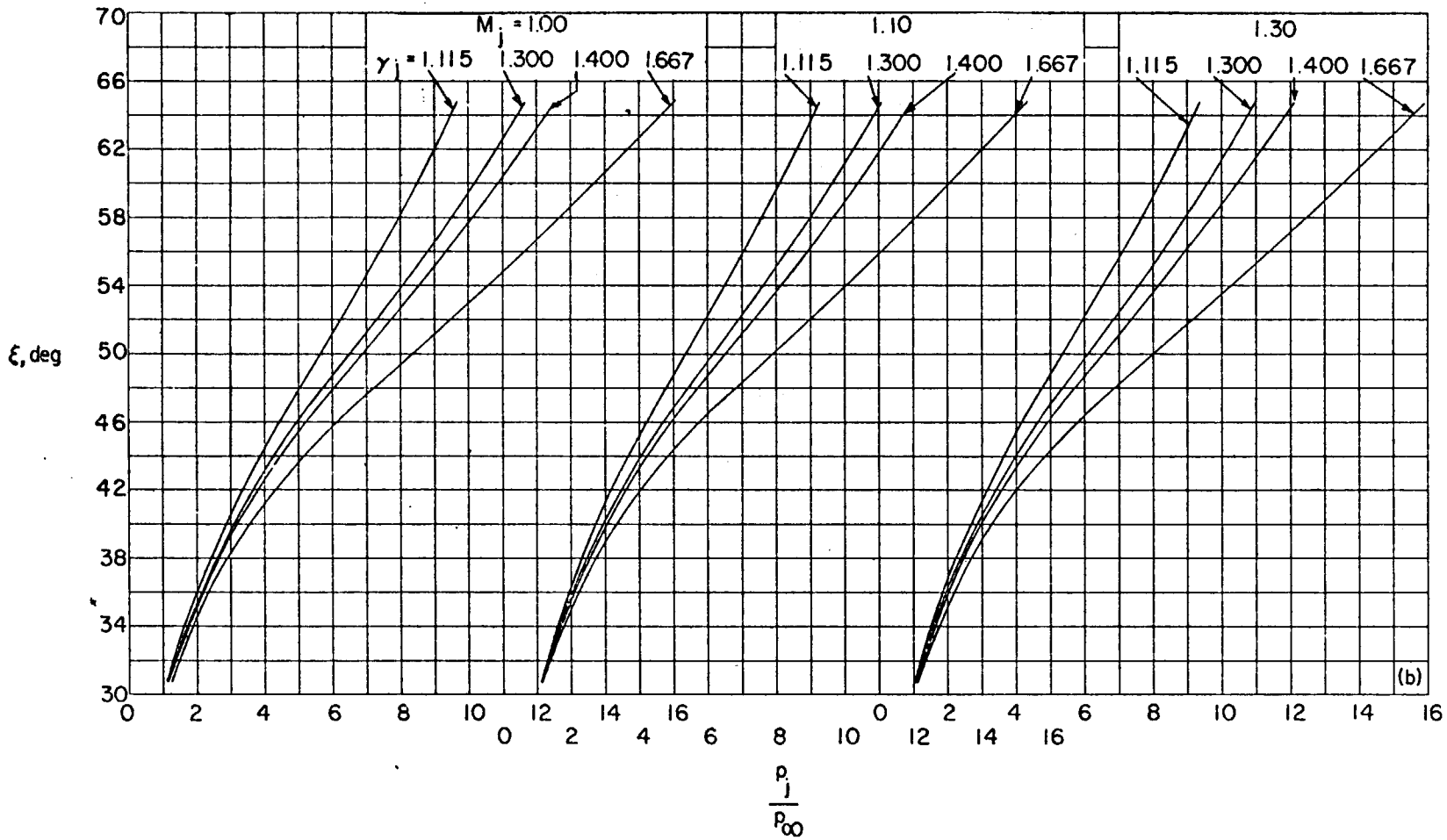

(b) $M_\infty = 2.00$.

FIGURE 55.—Continued.

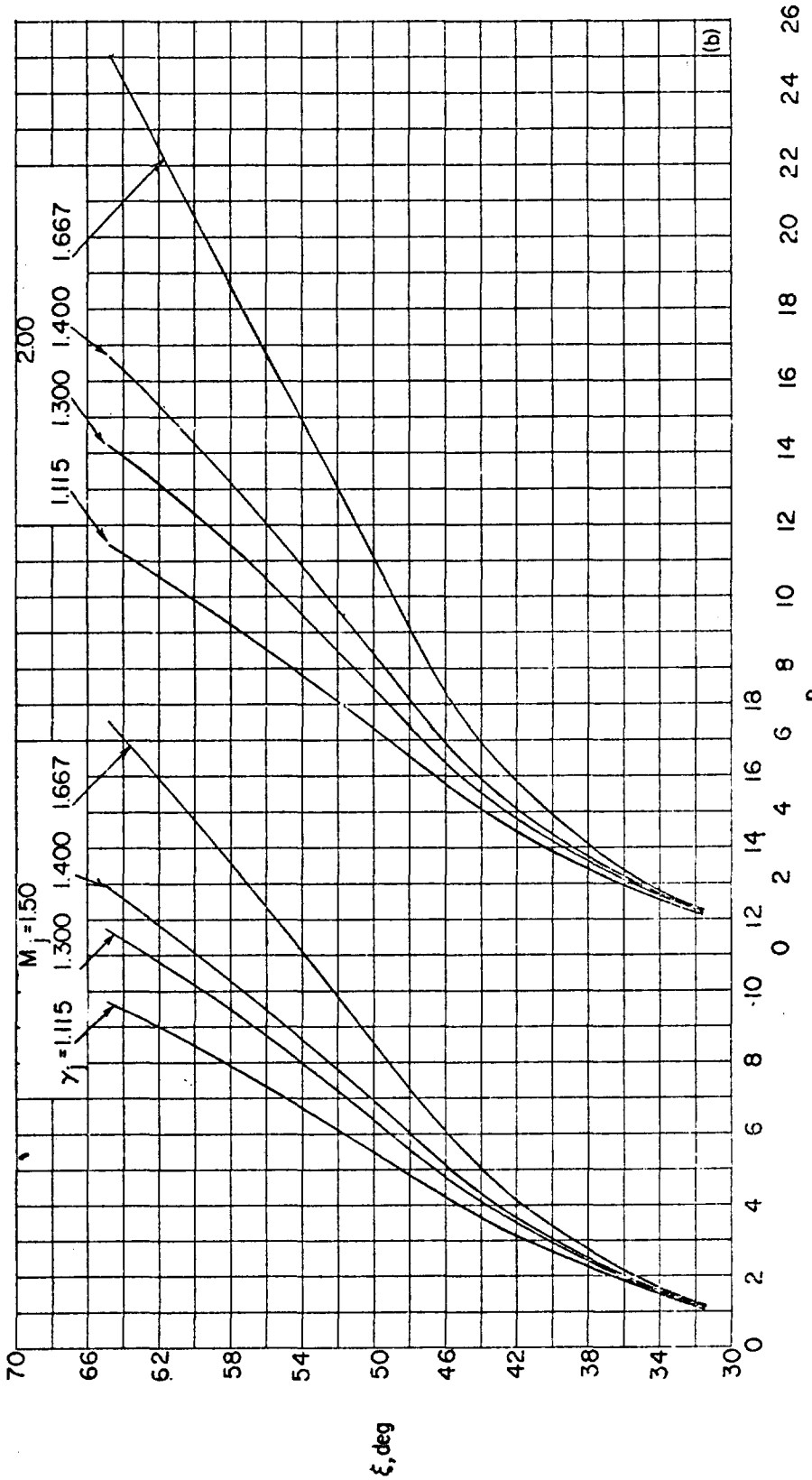

(b) $M_\infty = 2.00$. Continued.

FIGURE 55.—Continued.

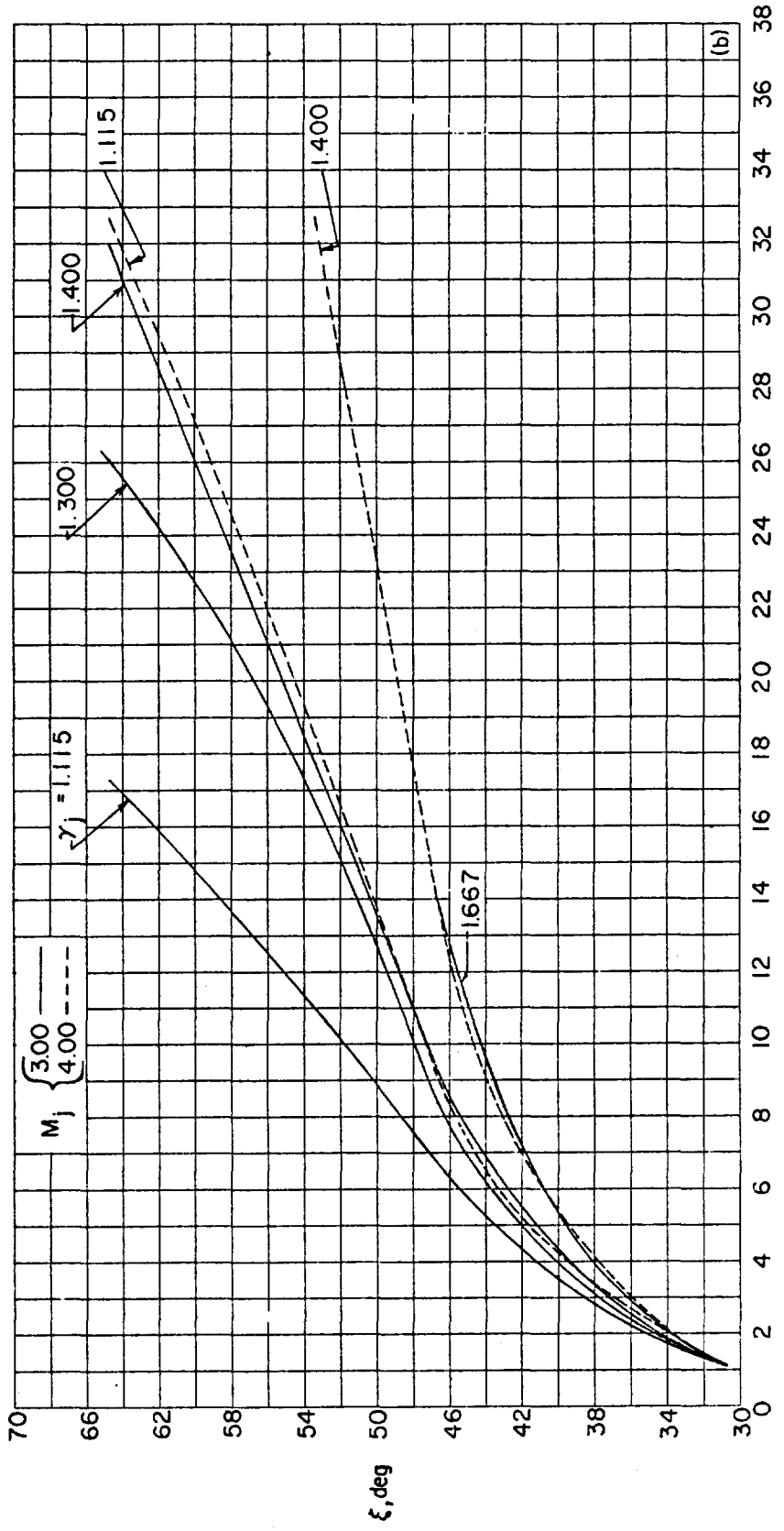

(b) $M_\infty = 2.00$. Concluded.

FIGURE 55.—Concluded.

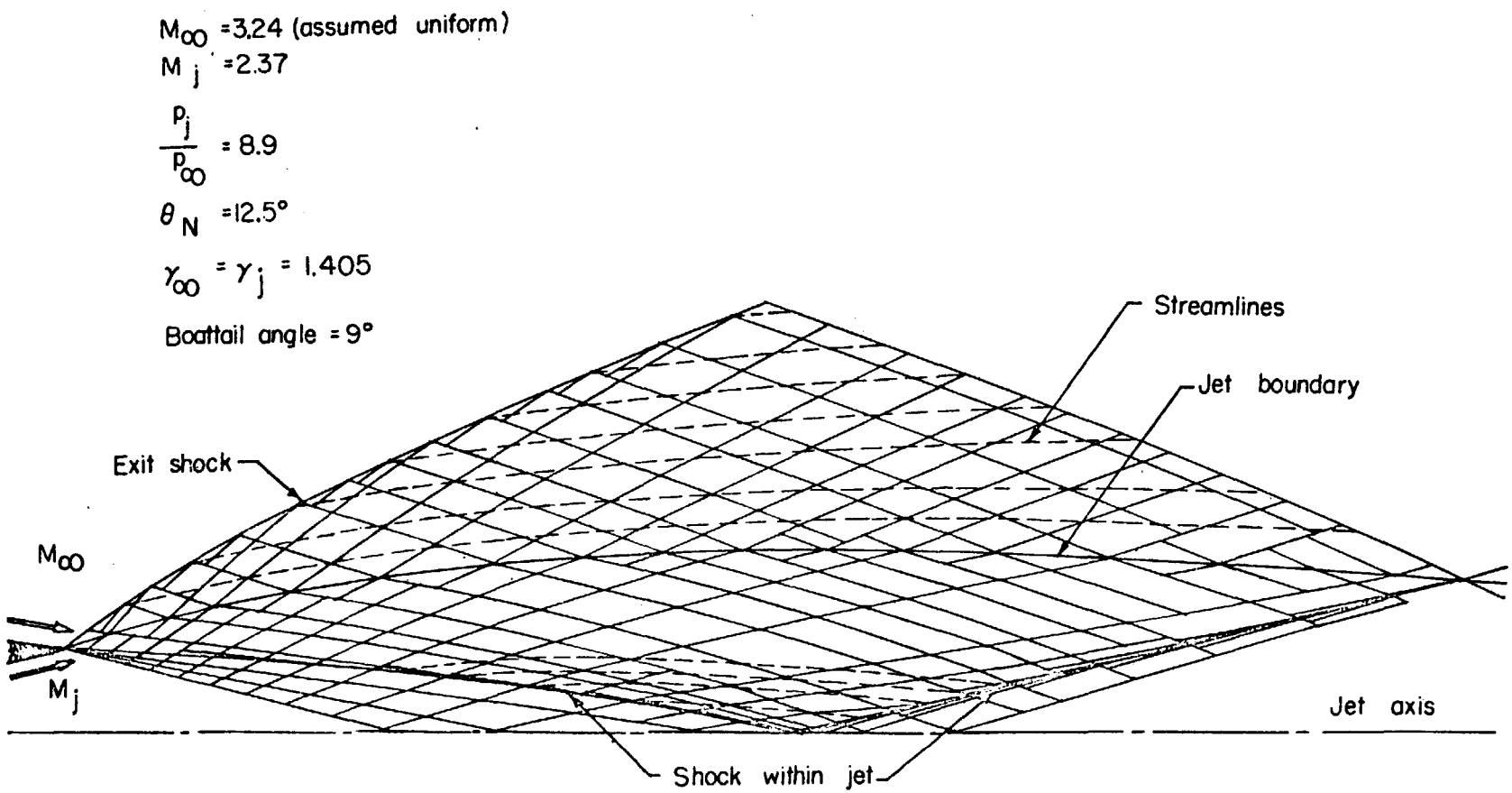

FIGURE 56.—Characteristic calculation by Schäfer (ref. 20) of a supersonic jet exhausting into a supersonic stream.

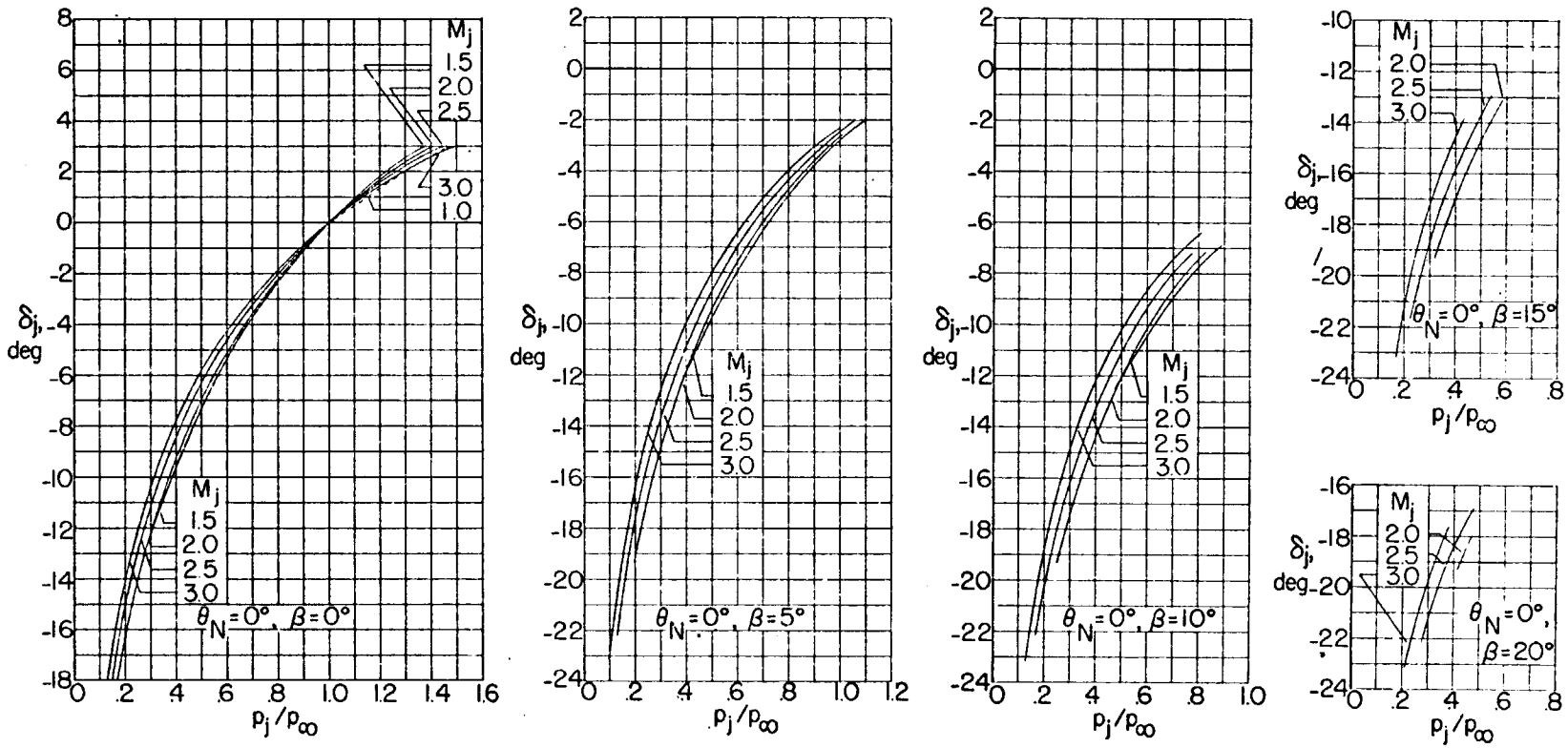

FIGURE 57.—The effects of jet pressure ratio upon the initial inclination of the mixing boundary at $M_\infty=1.2$, $\gamma_\infty=1.400$, $\gamma_j=1.286$.

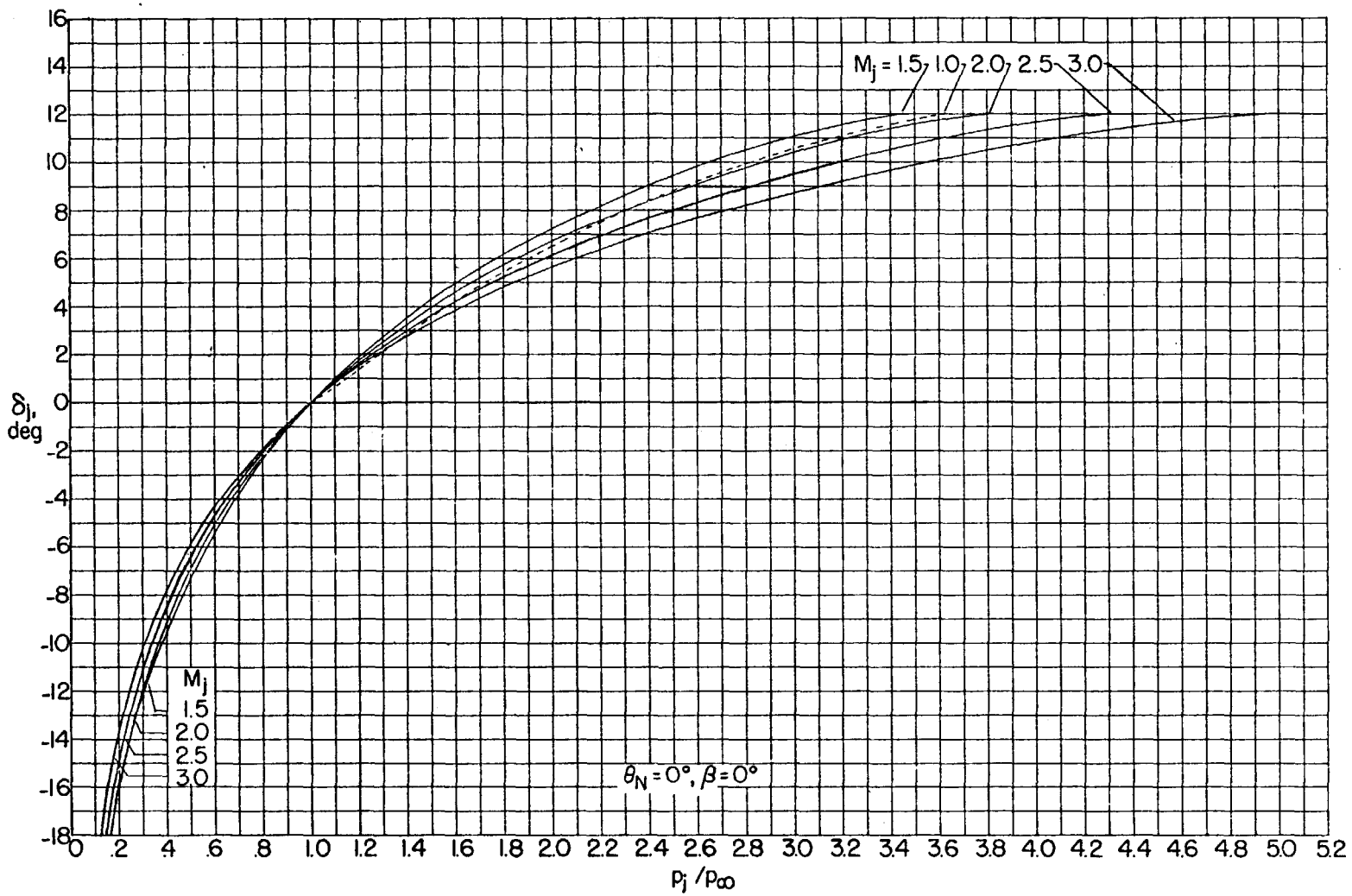

FIGURE 58.—The effects of jet pressure ratio upon the initial inclination of the mixing boundary at $M_\infty = 1.5$, $\gamma_\infty = 1.400$, $\gamma_j = 1.286$.

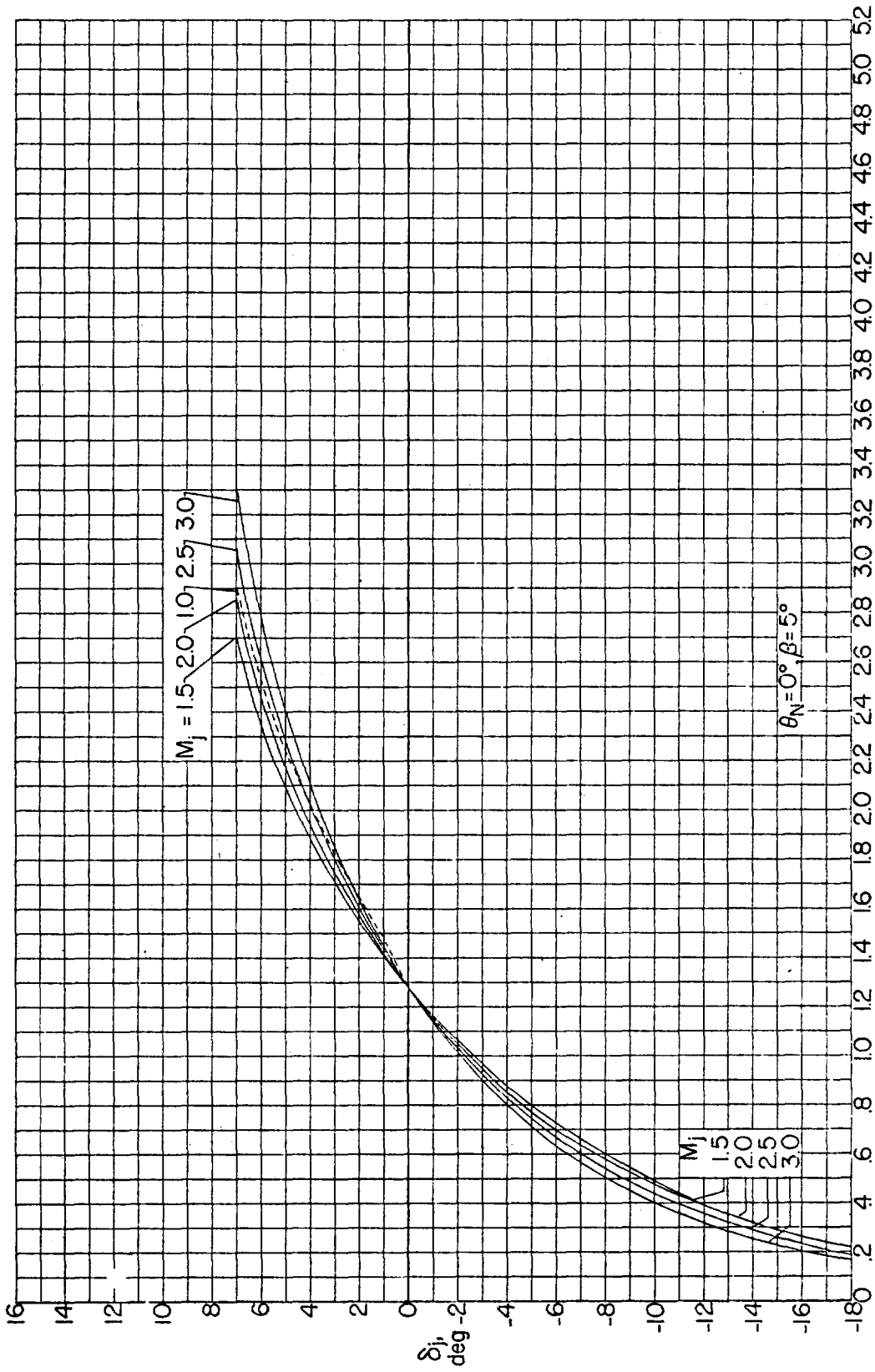

FIGURE 58.—Continued

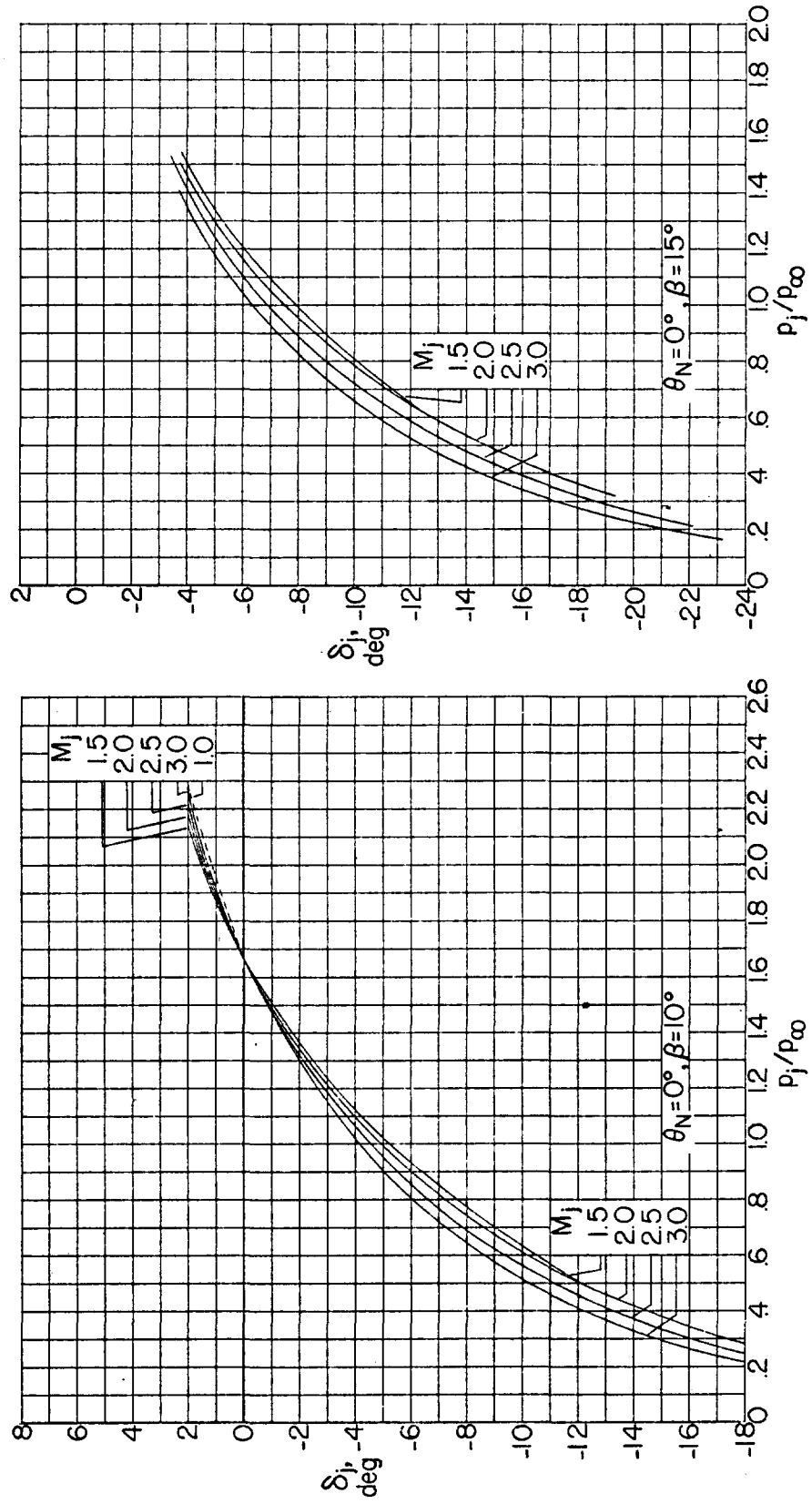

FIGURE 58.—Continued.

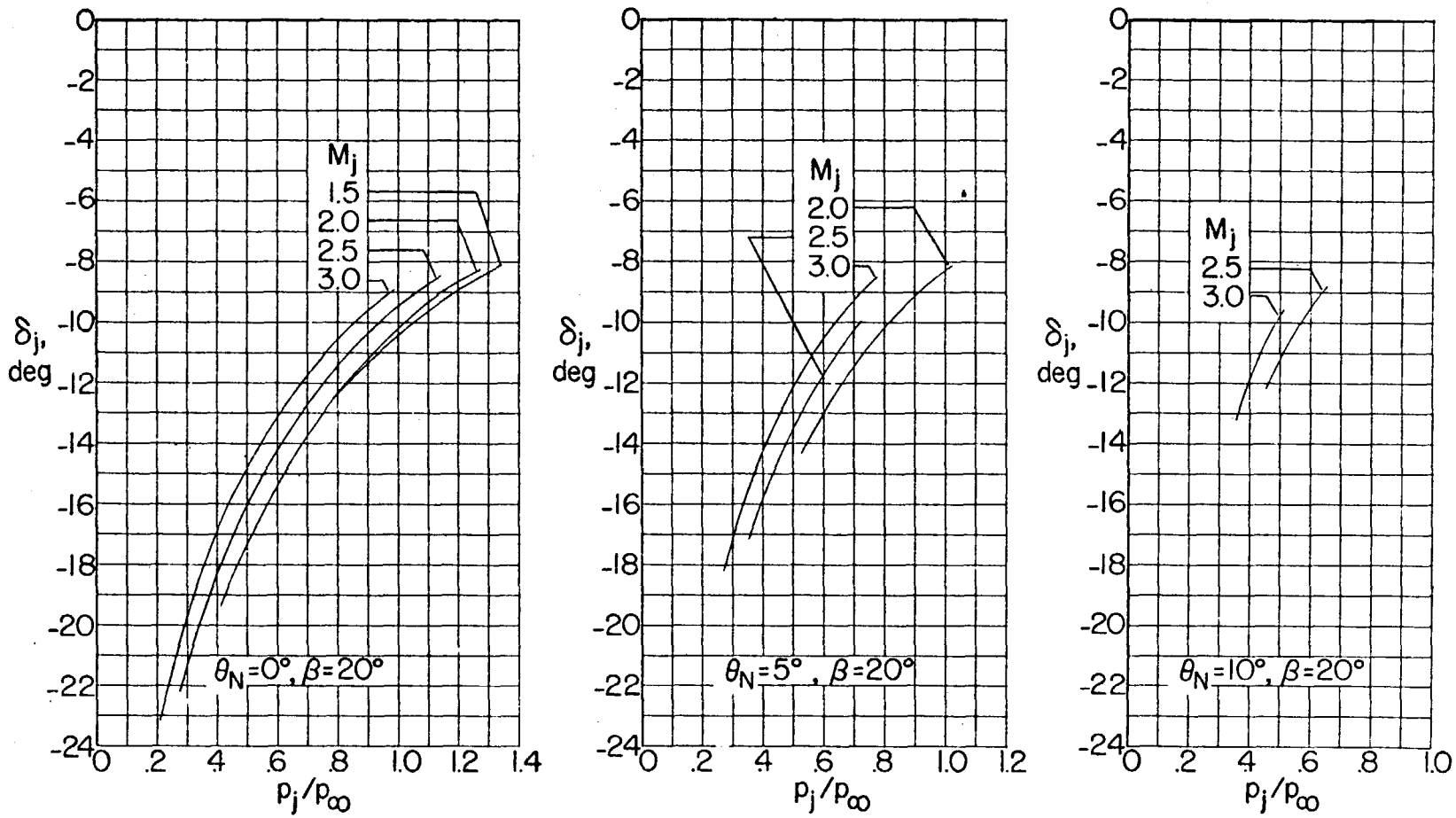

FIGURE 58.—Concluded.

502683 O—59——17

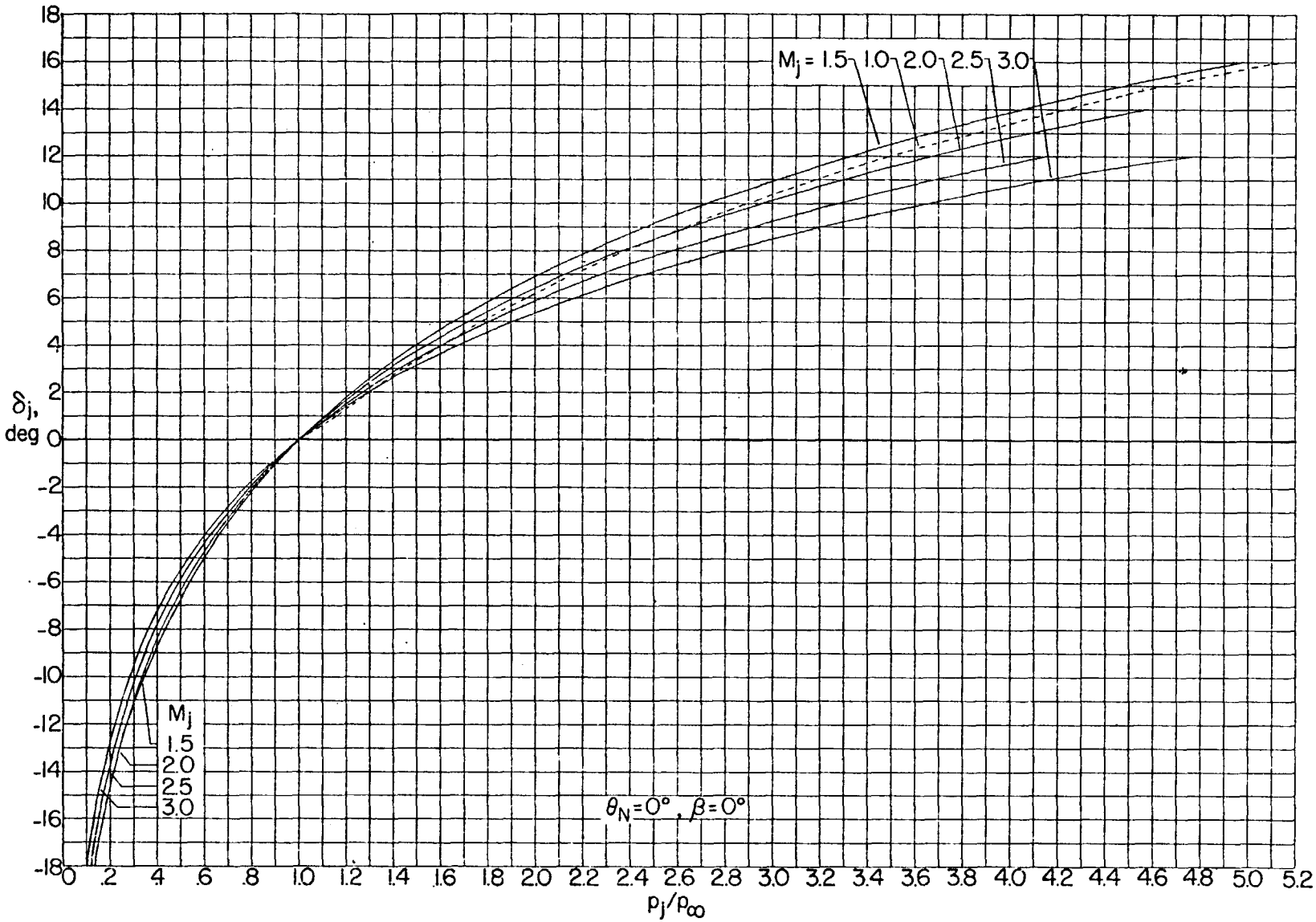

FIGURE 59.—The effects of jet pressure ratio upon the initial inclination of the mixing boundary at $M_\infty = 2.0$, $\gamma_\infty = 1.400$, $\gamma_j = 1.286$.

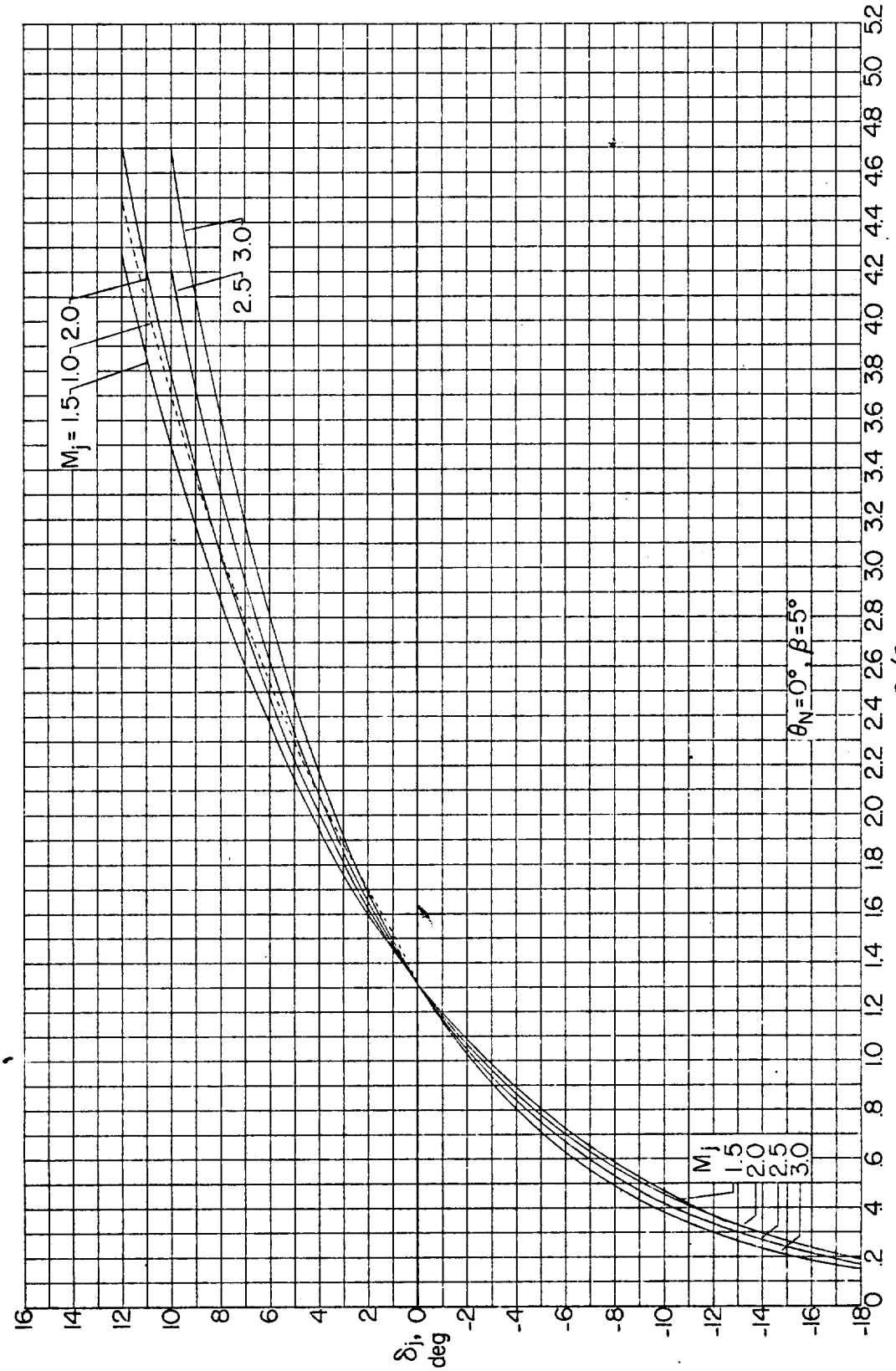

FIGURE 59.—Continued.

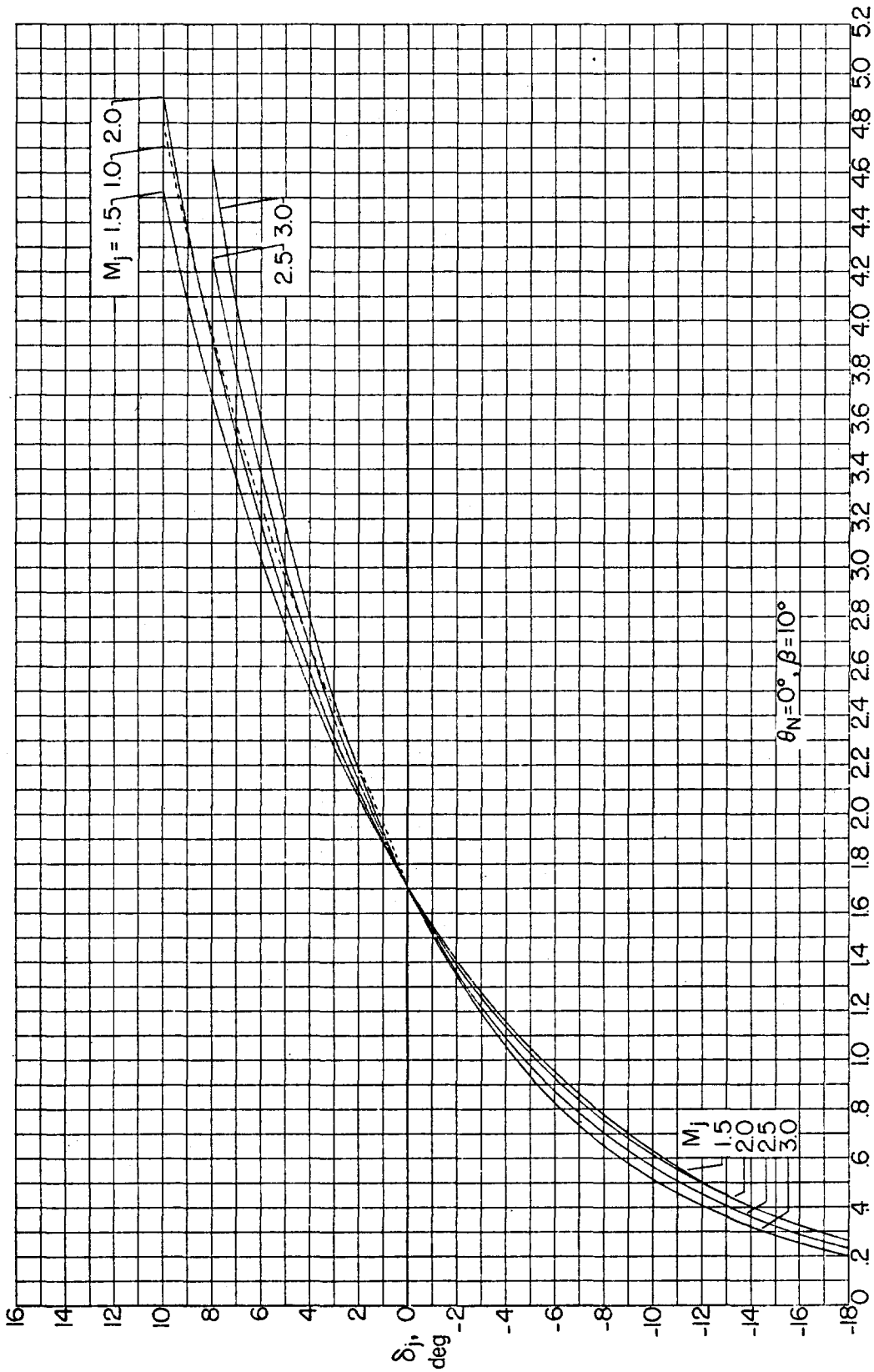

FIGURE 59.—Continued.

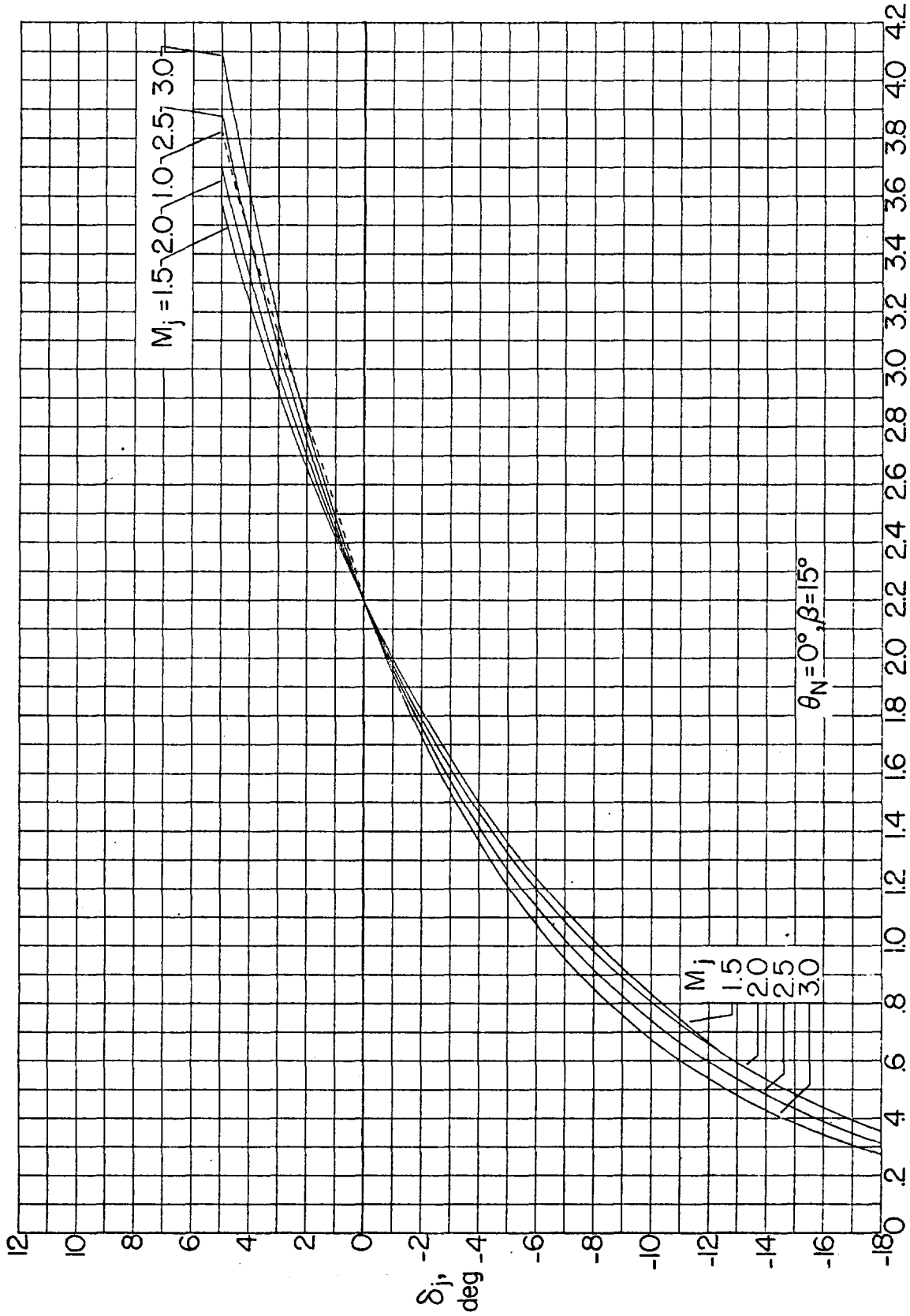

FIGURE 59.—Continued.

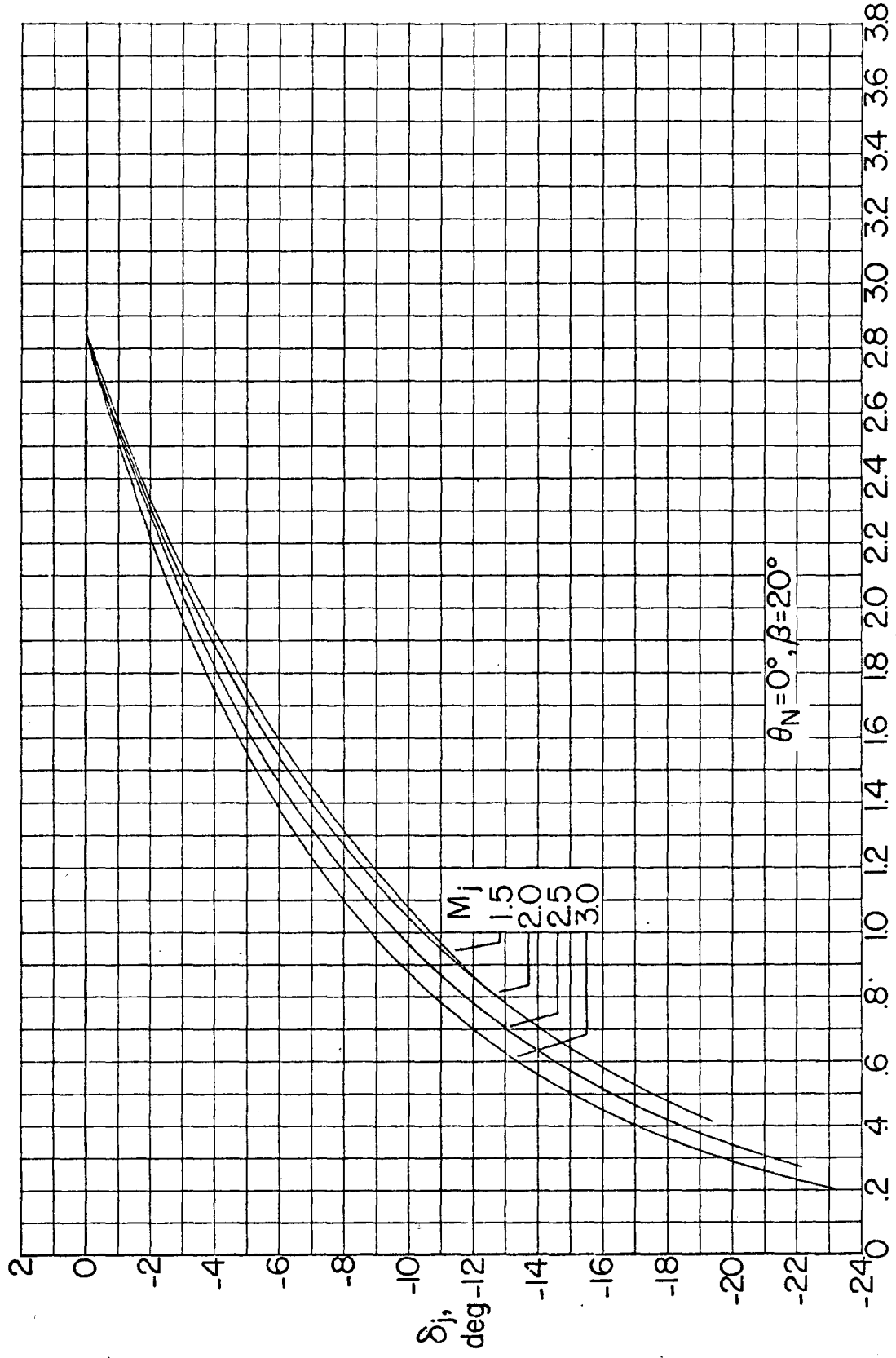

FIGURE 59.—Continued.

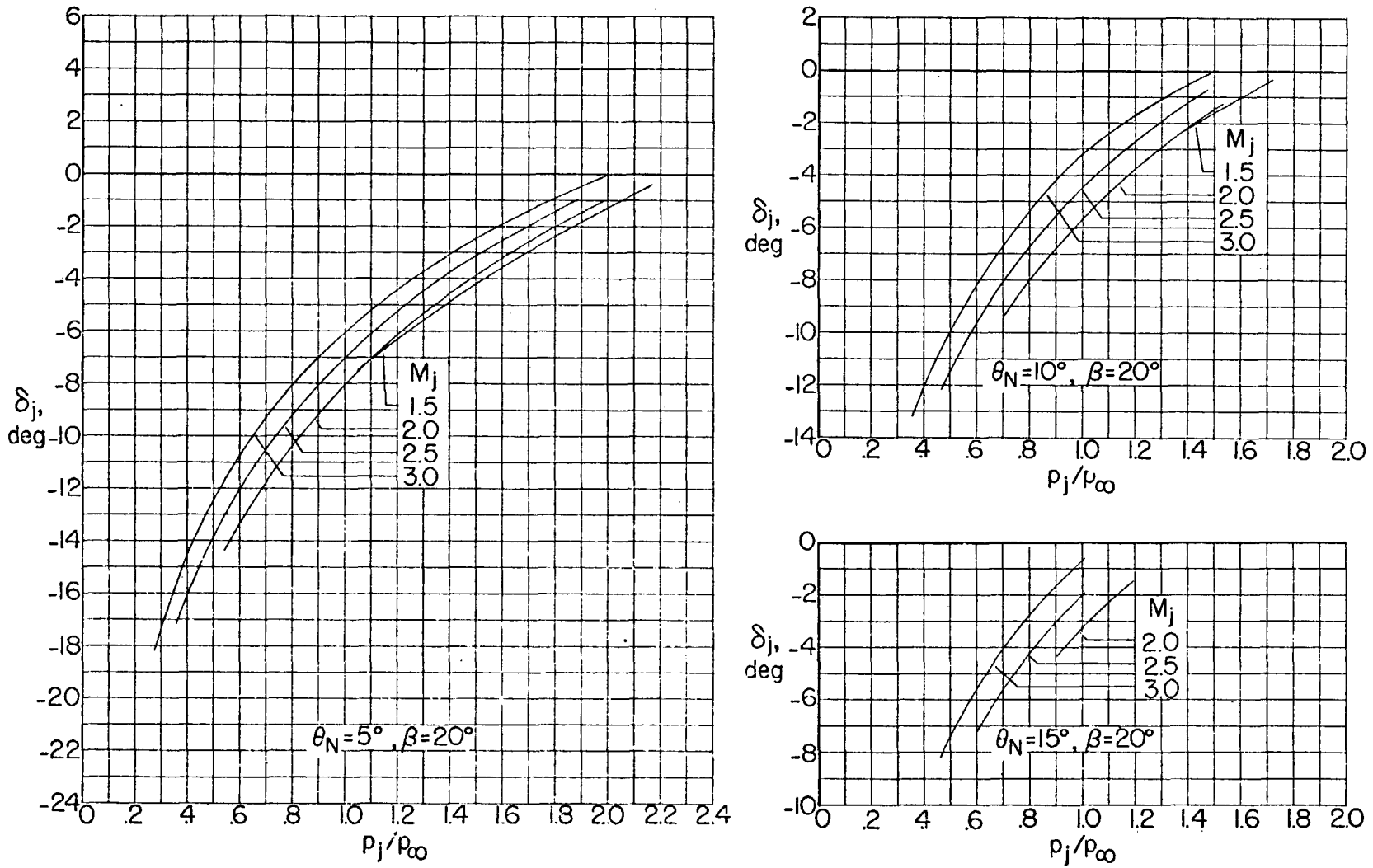

FIGURE 59.—Concluded.

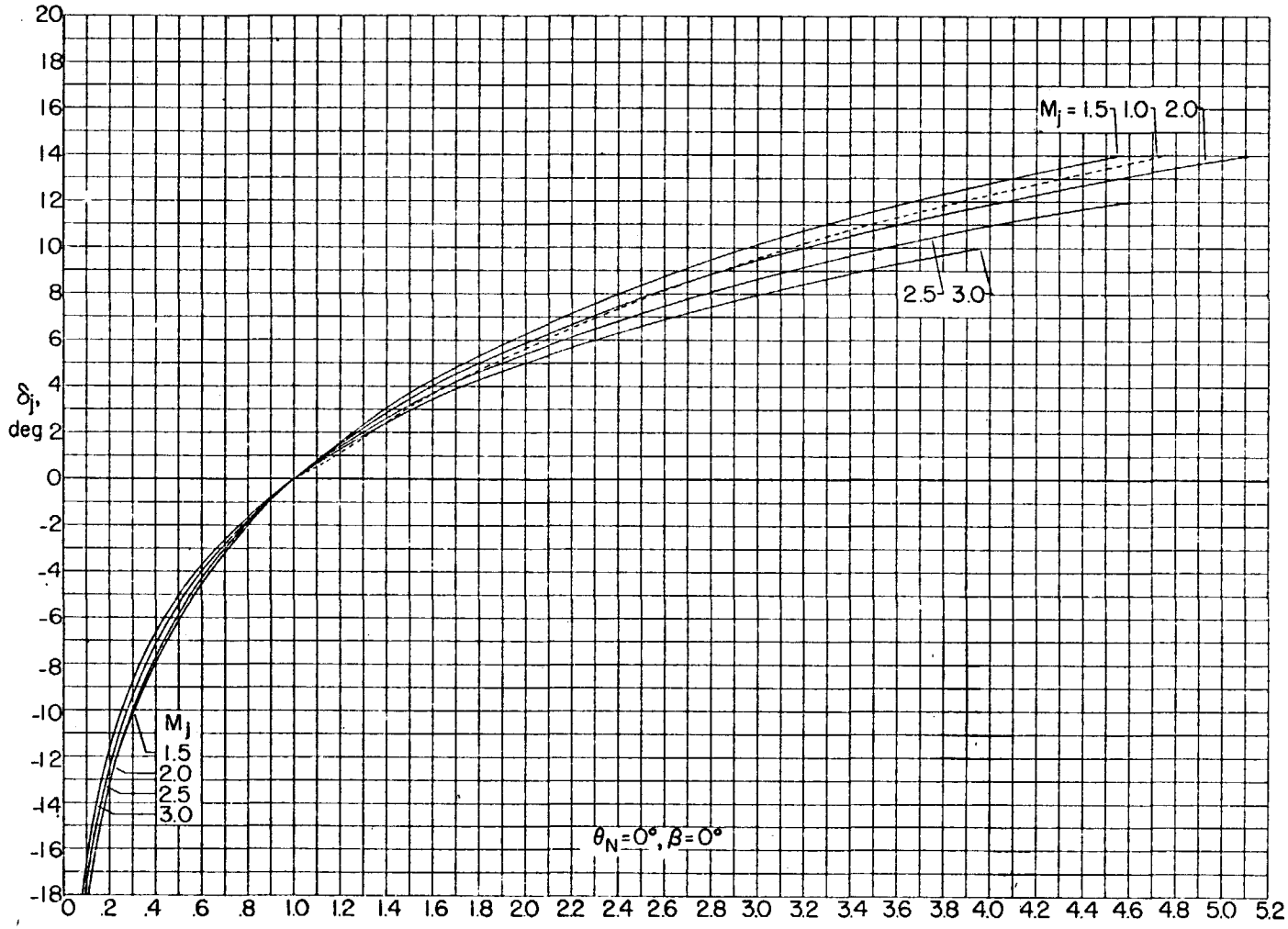

FIGURE 60.—The effects of jet pressure ratio upon the initial inclination of the mixing boundary at $M_\infty = 2.5$, $\gamma_\infty = 1.400$, $\gamma_j = 1.286$.

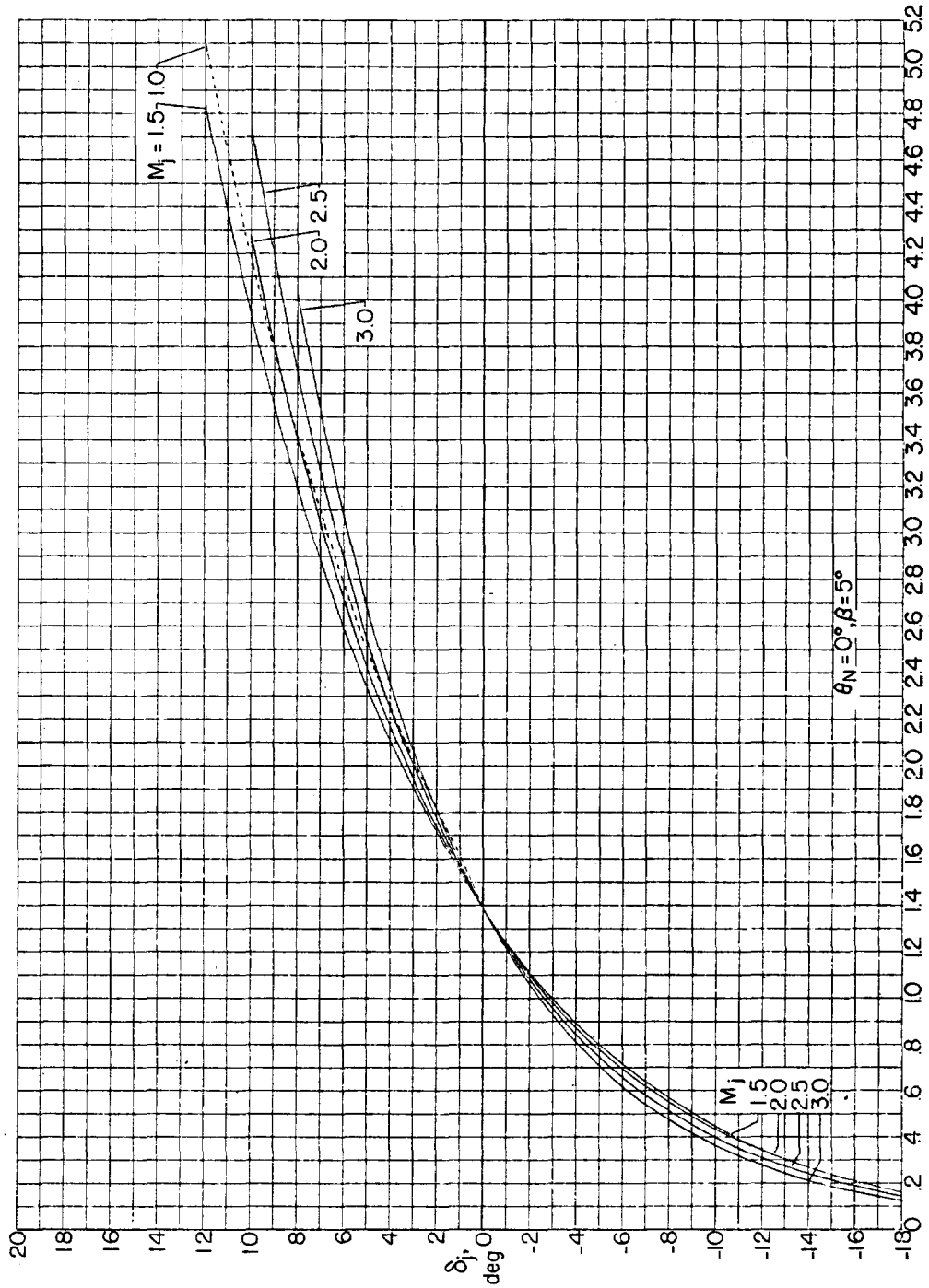

FIGURE 60.—Continued.

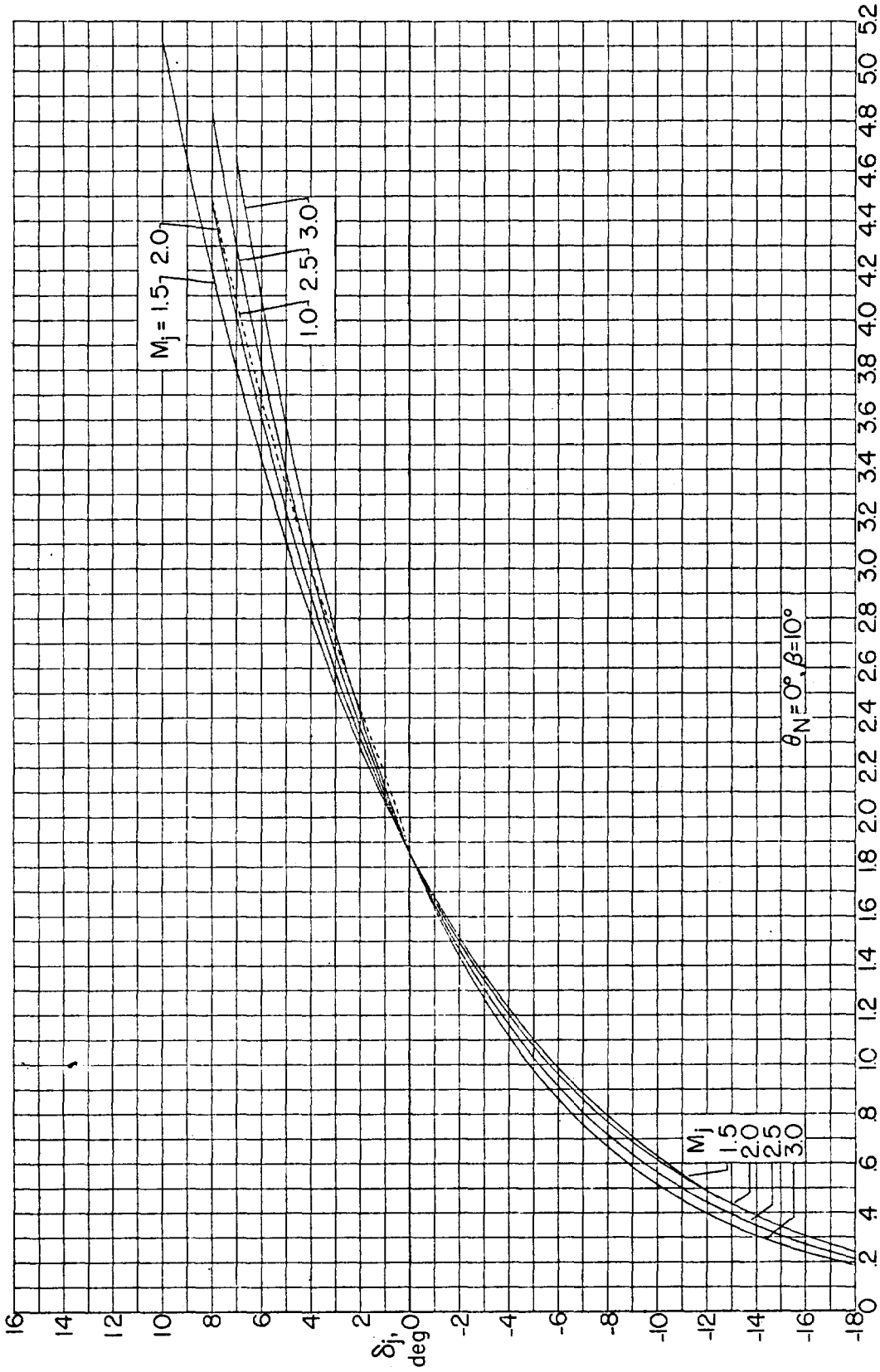

FIGURE 60.—Continued.

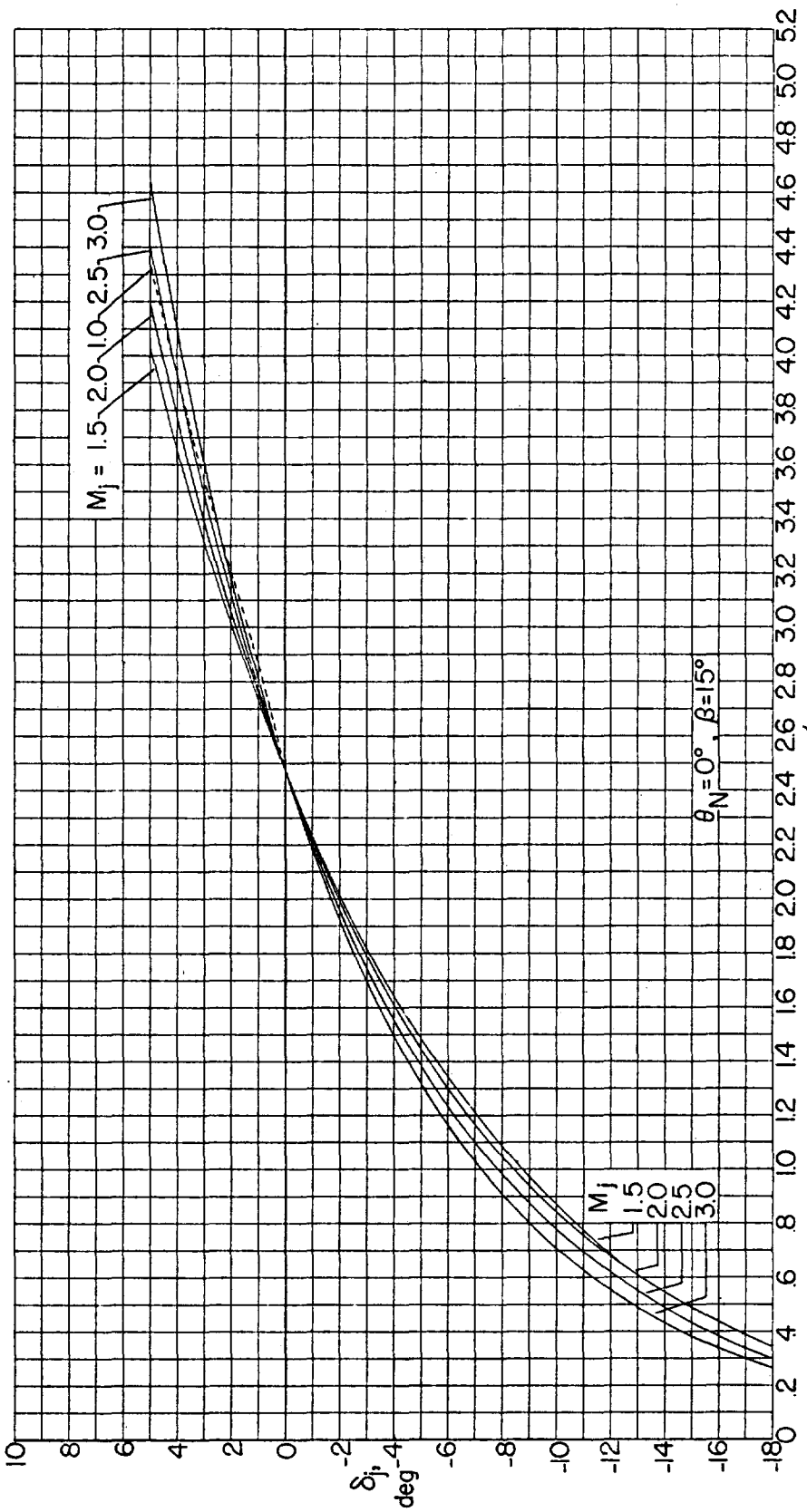

FIGURE 60.—Continued.

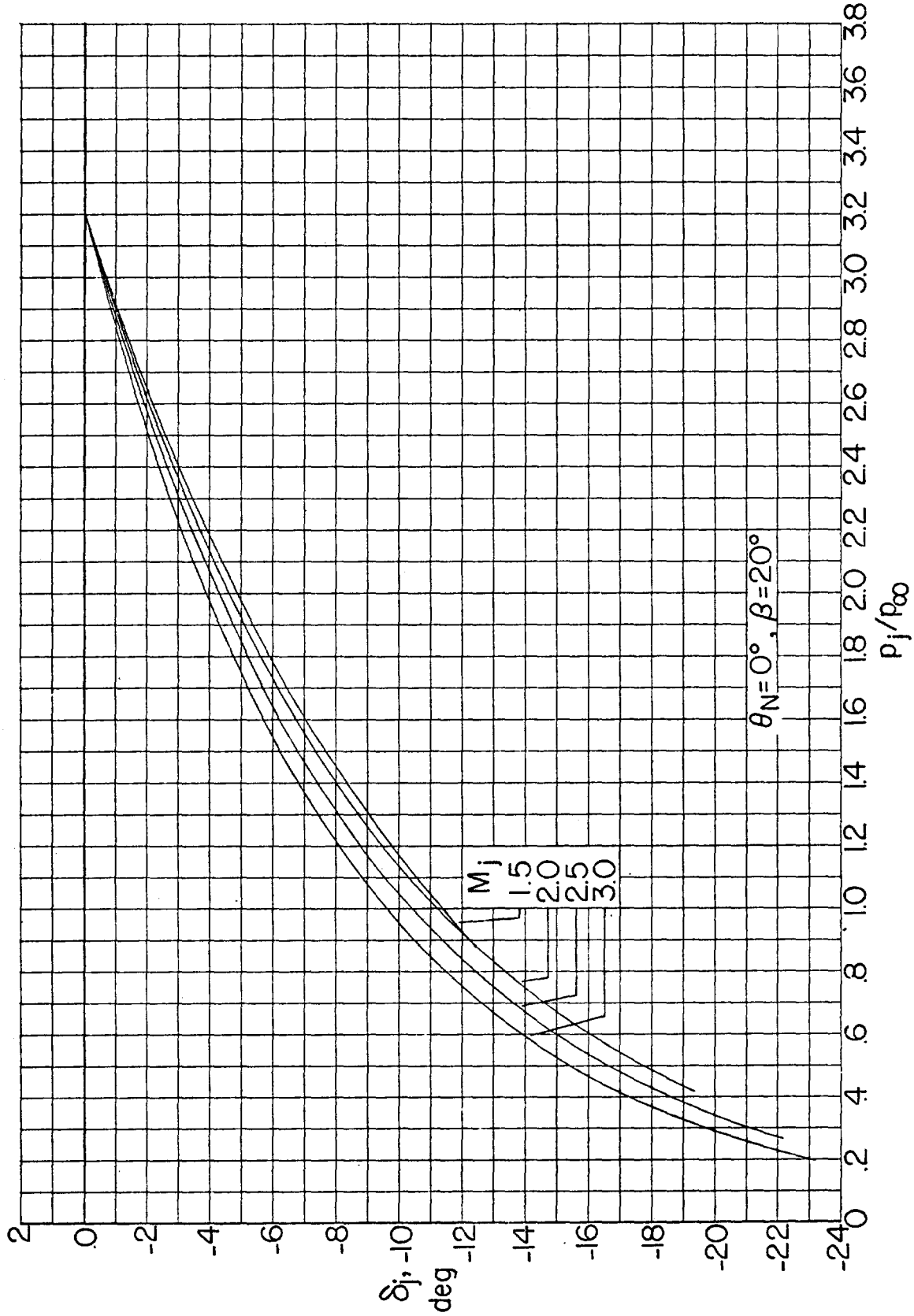

FIGURE 60.—Continued.

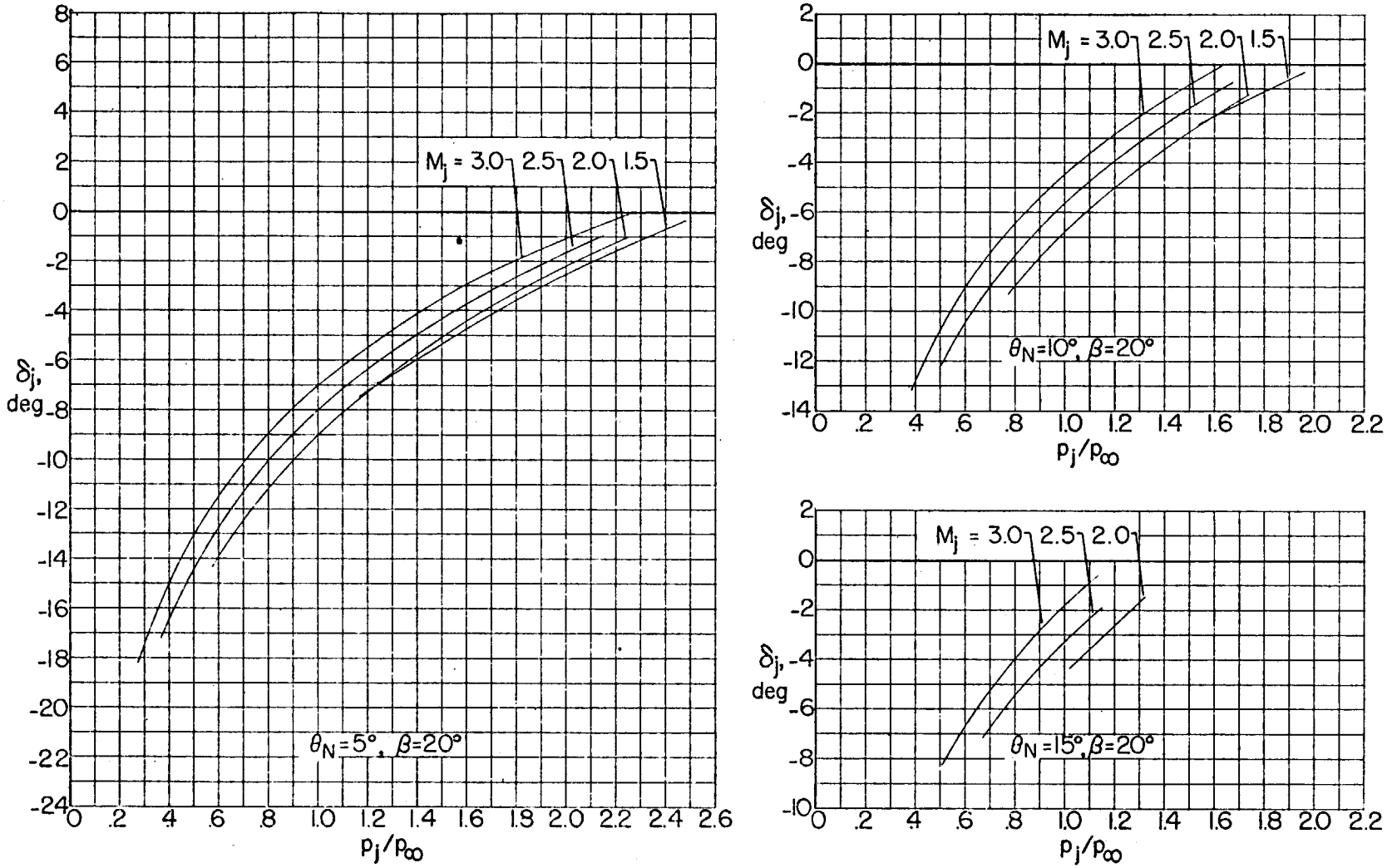

FIGURE 60.—Concluded.

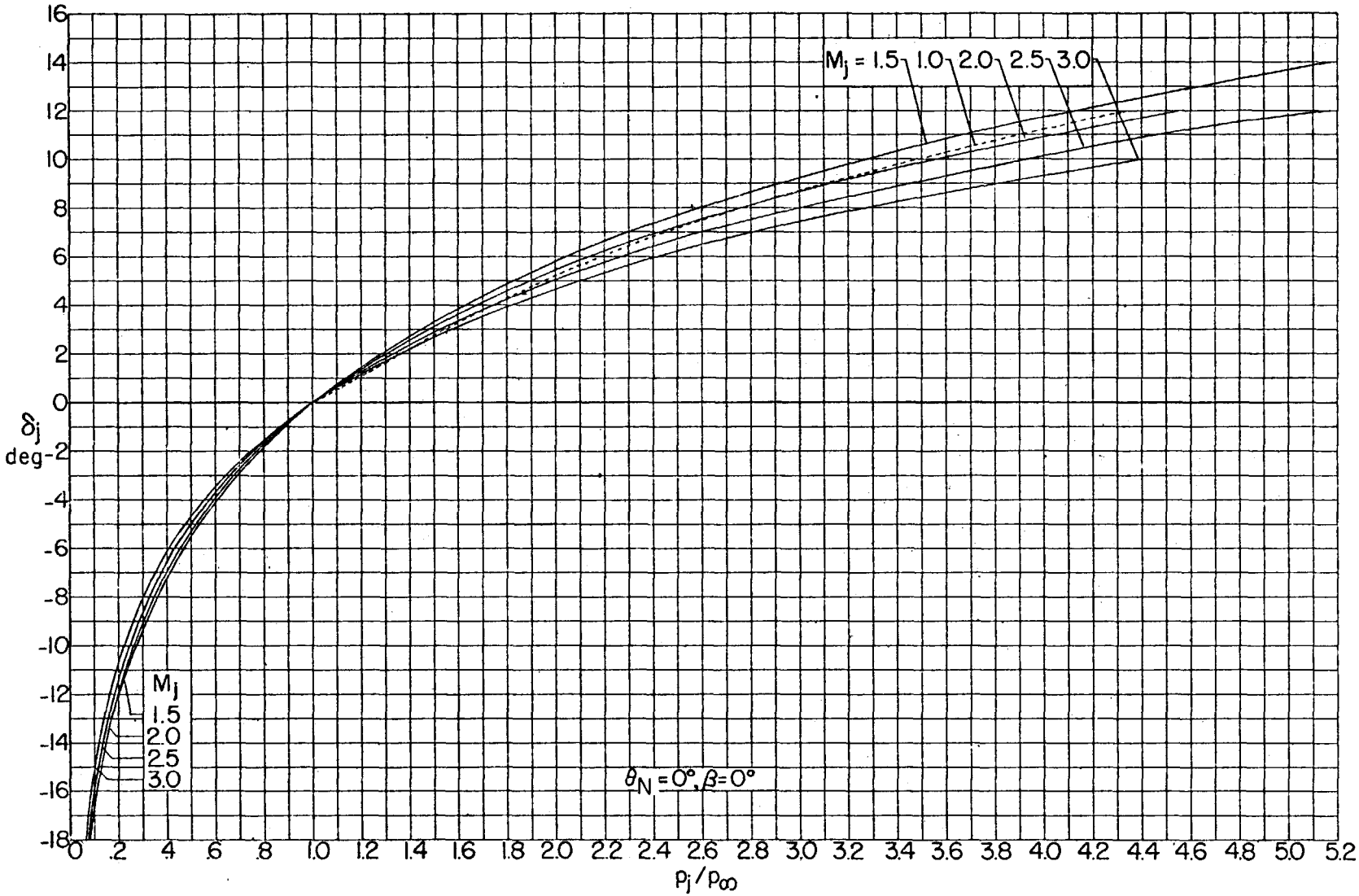

FIGURE 61.--The effects of jet pressure ratio upon the initial inclination of the mixing boundary at $M_\infty = 3.0$, $\gamma_\infty = 1.400$, $\gamma_j = 1.286$.

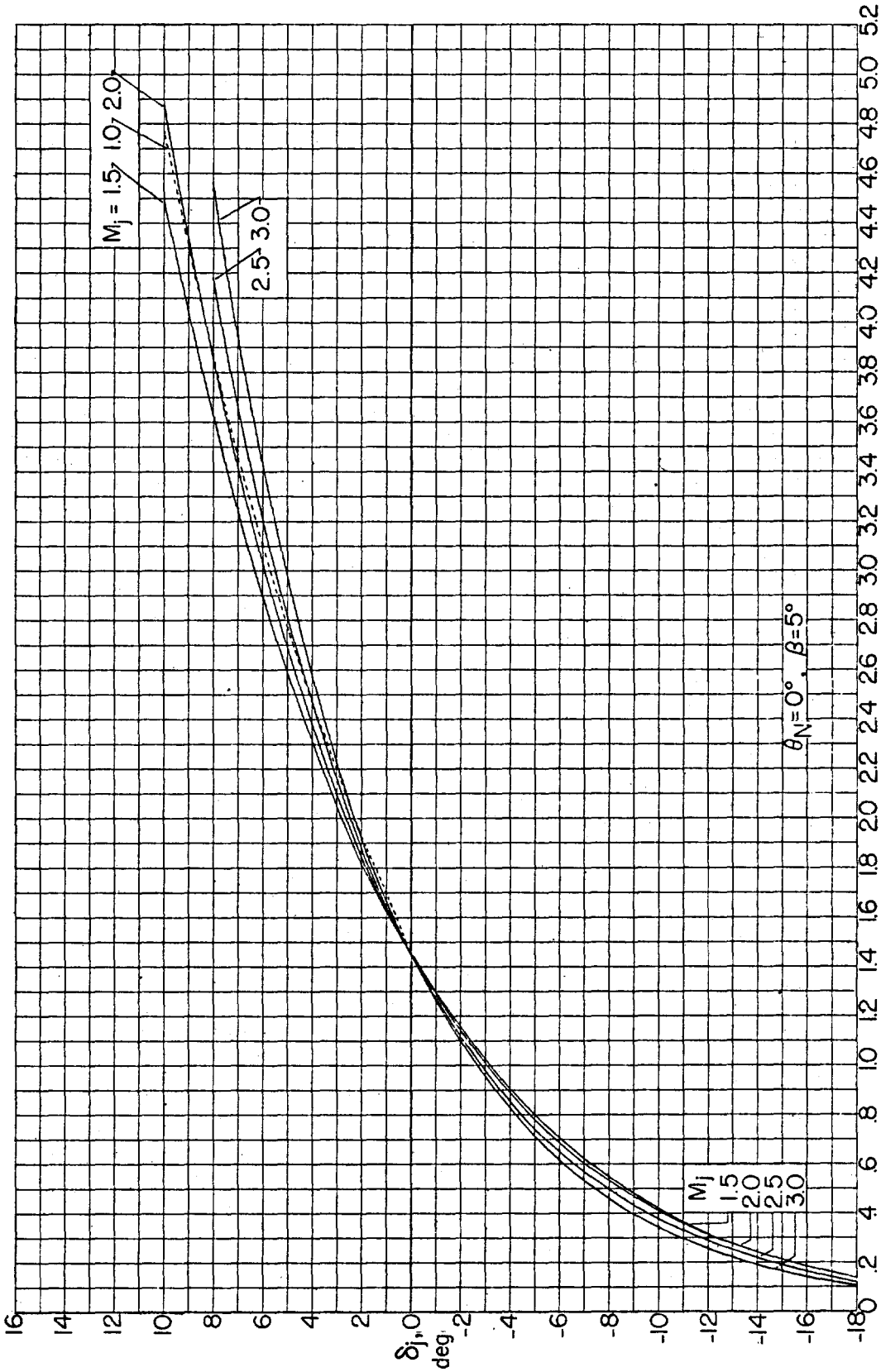

FIGURE 61.—Continued.

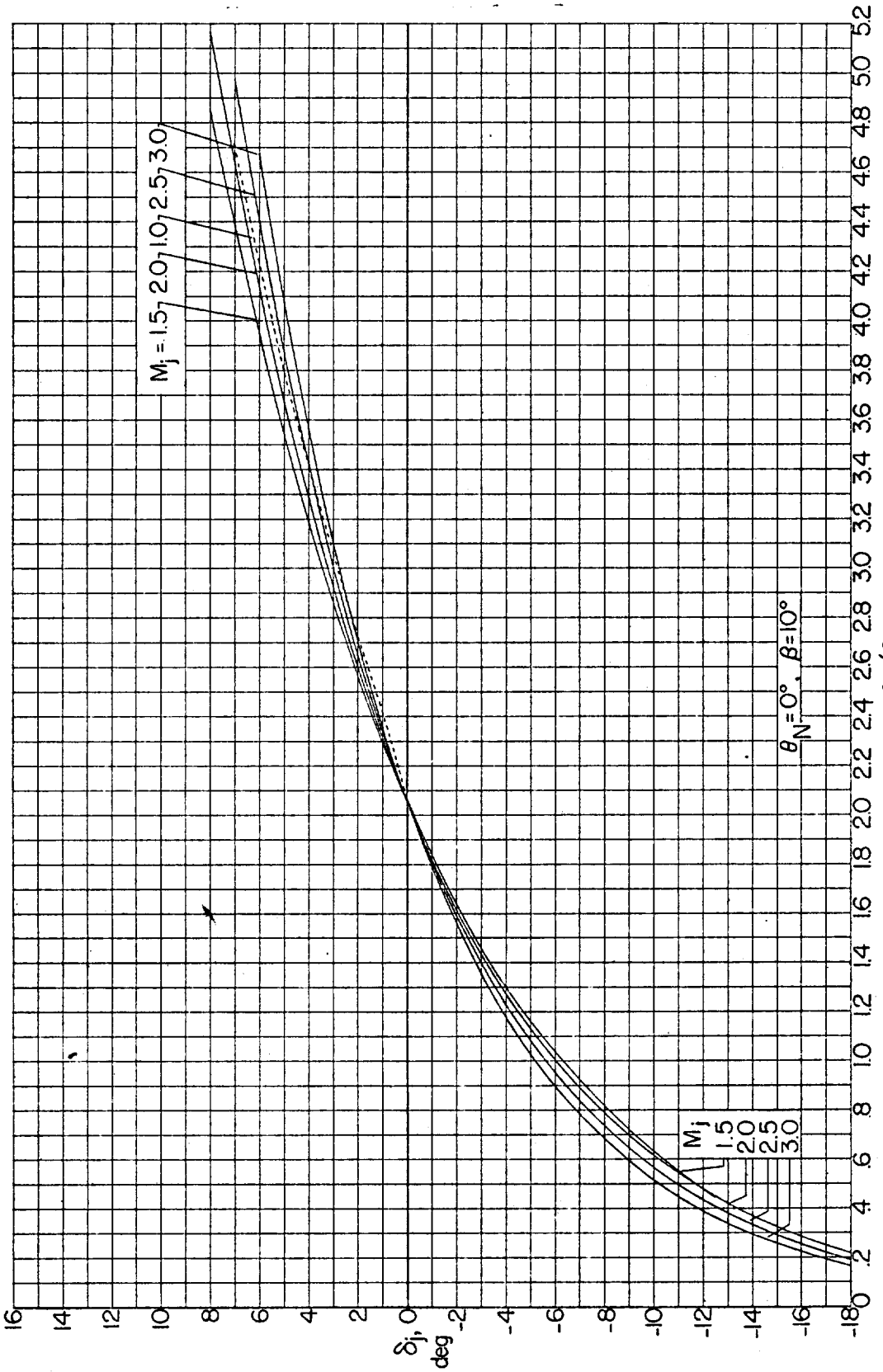

FIGURE 61.—Continued.

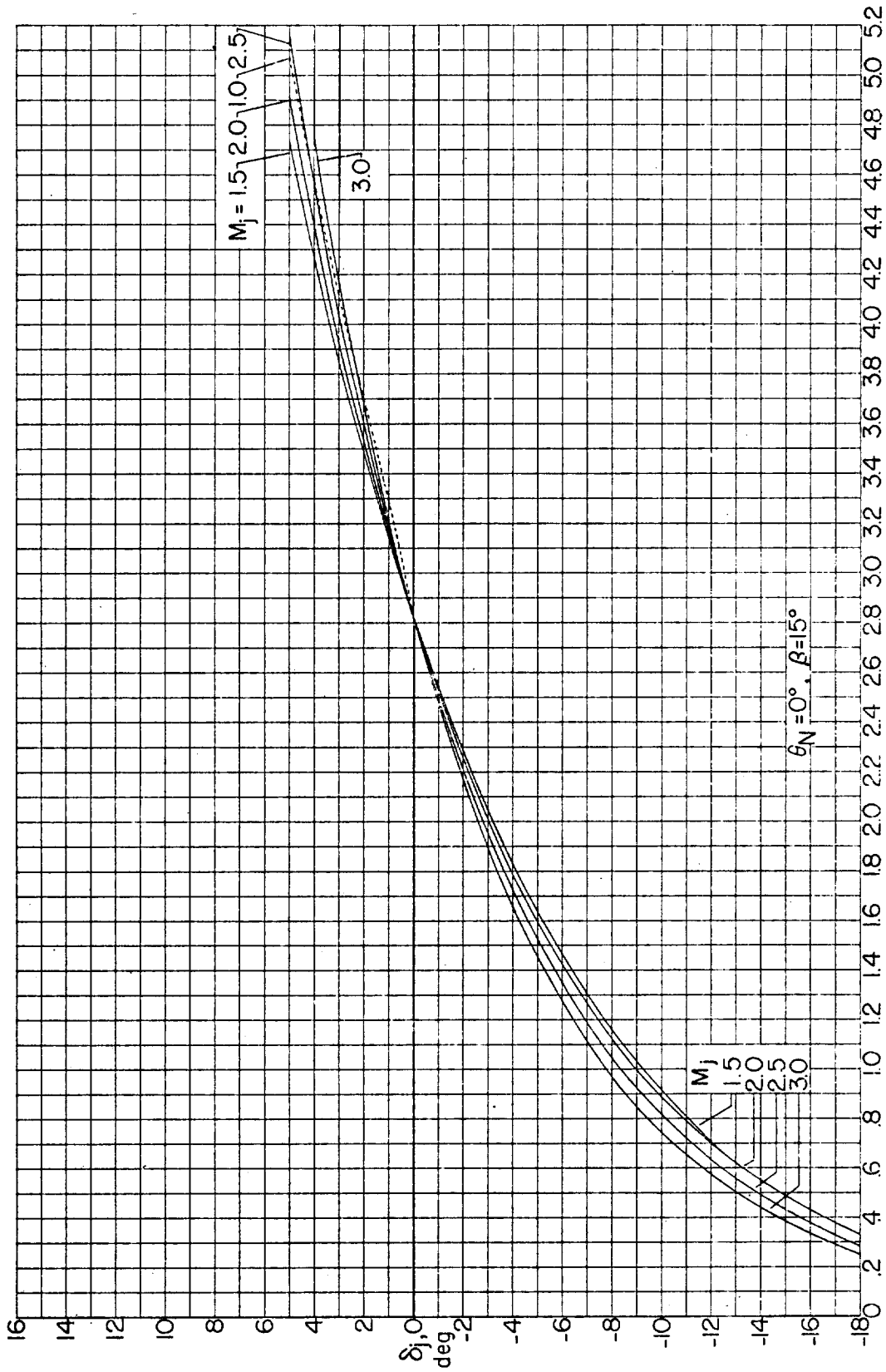

FIGURE 61.—Continued.

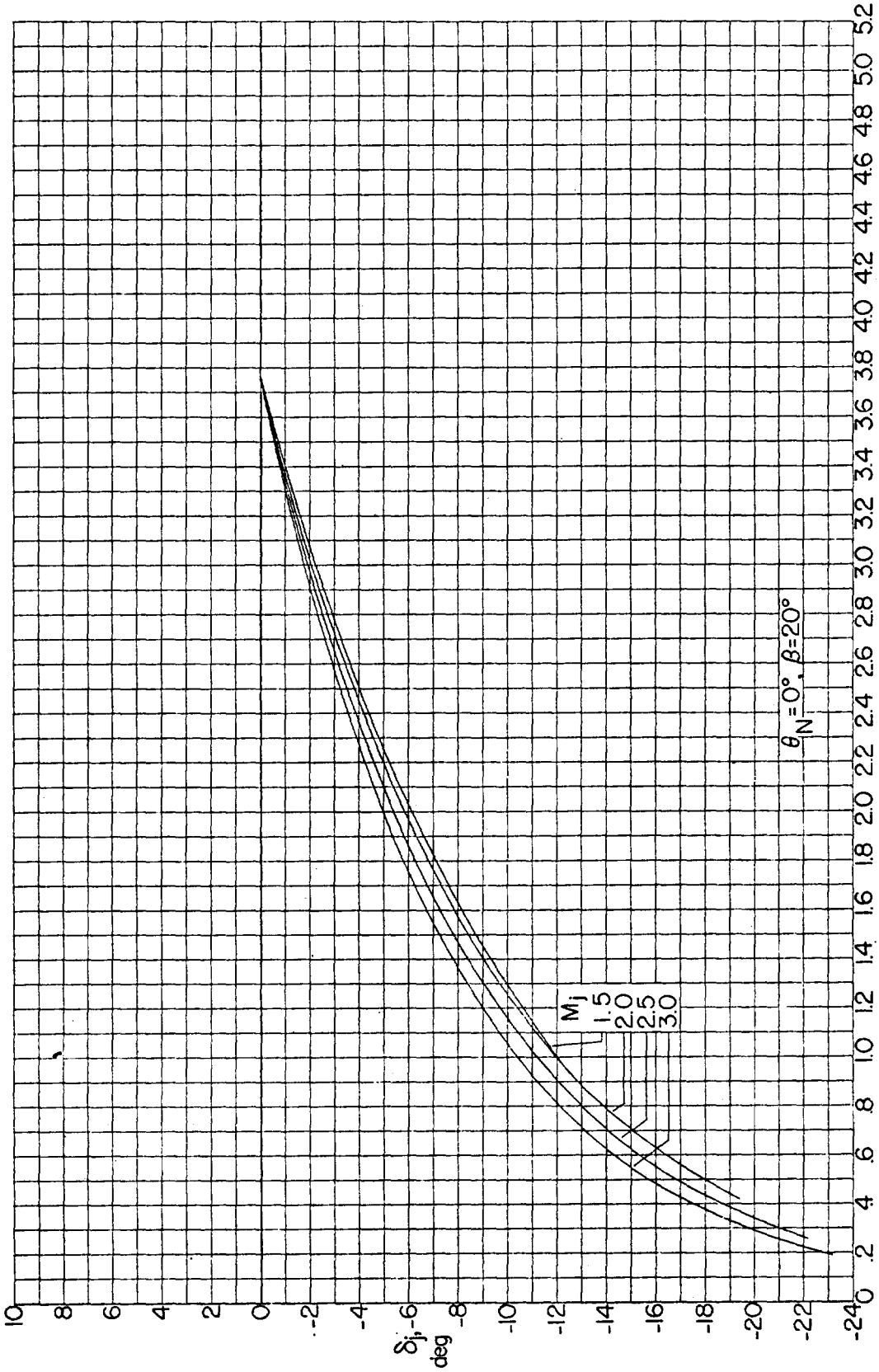

FIGURE 61.—Continued.

502683 O—59——18

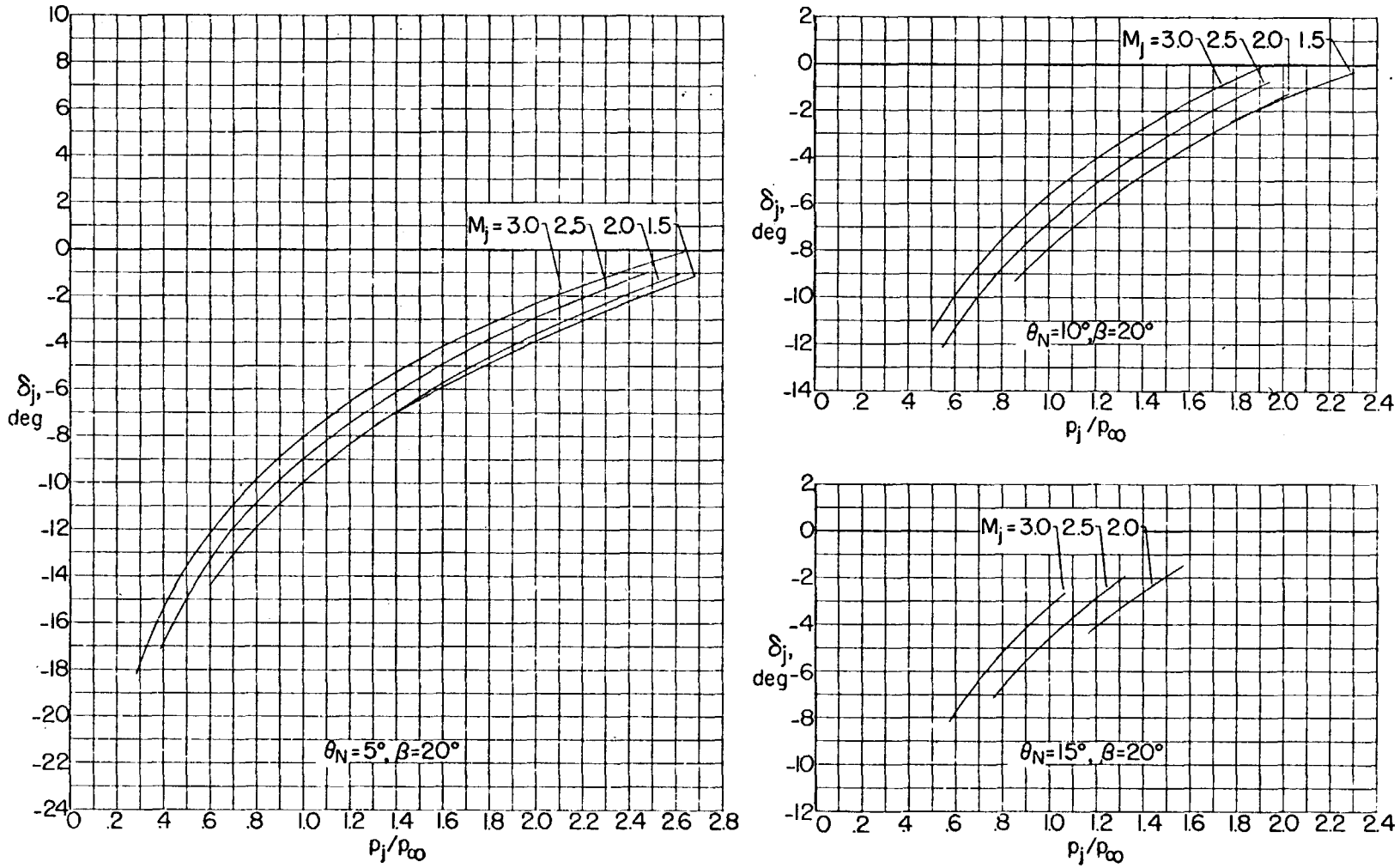

FIGURE 61.—Concluded.

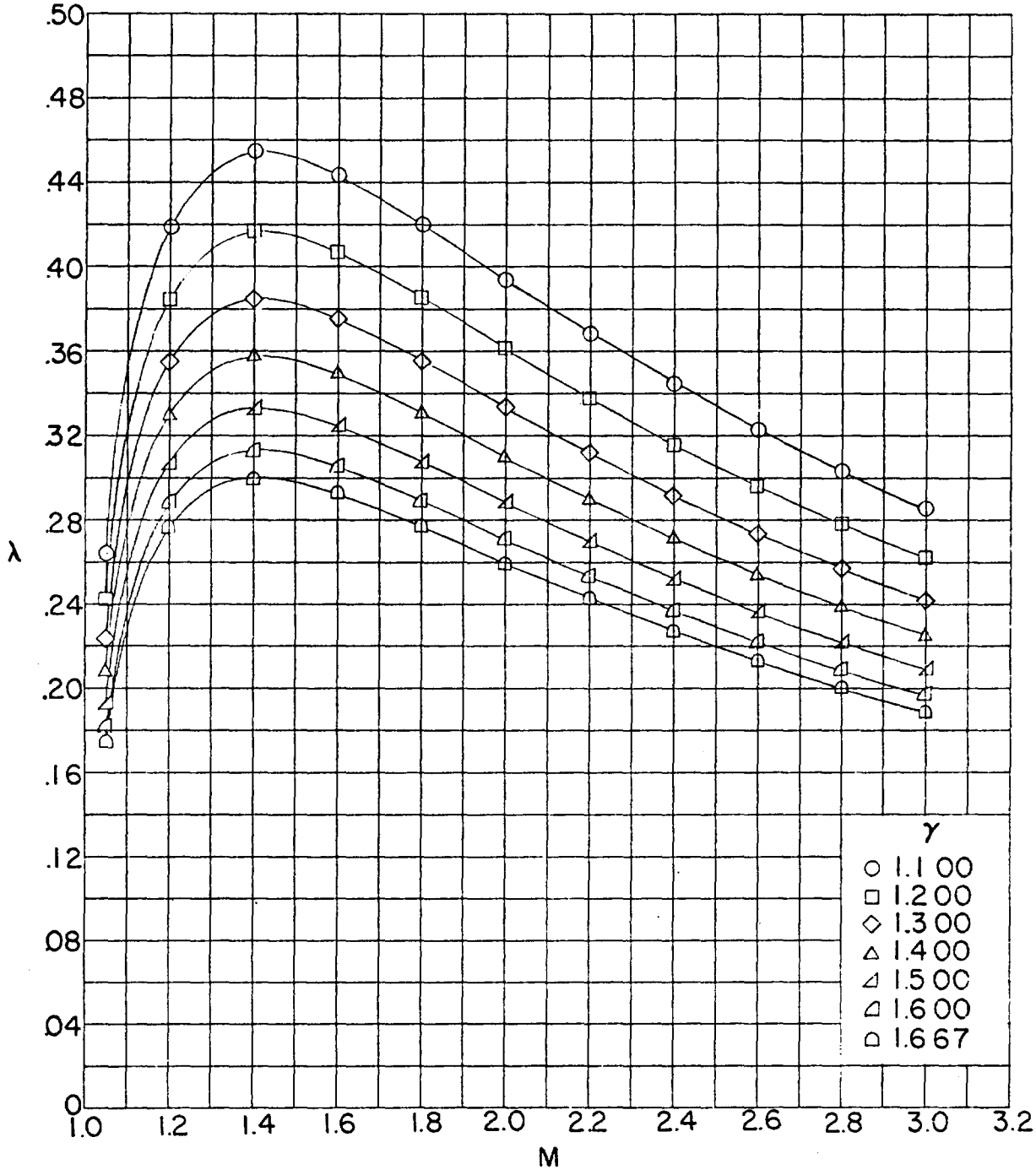

FIGURE 62.—Variation of basic Kawamura parameter with Mach number for several ratios of specific heats.

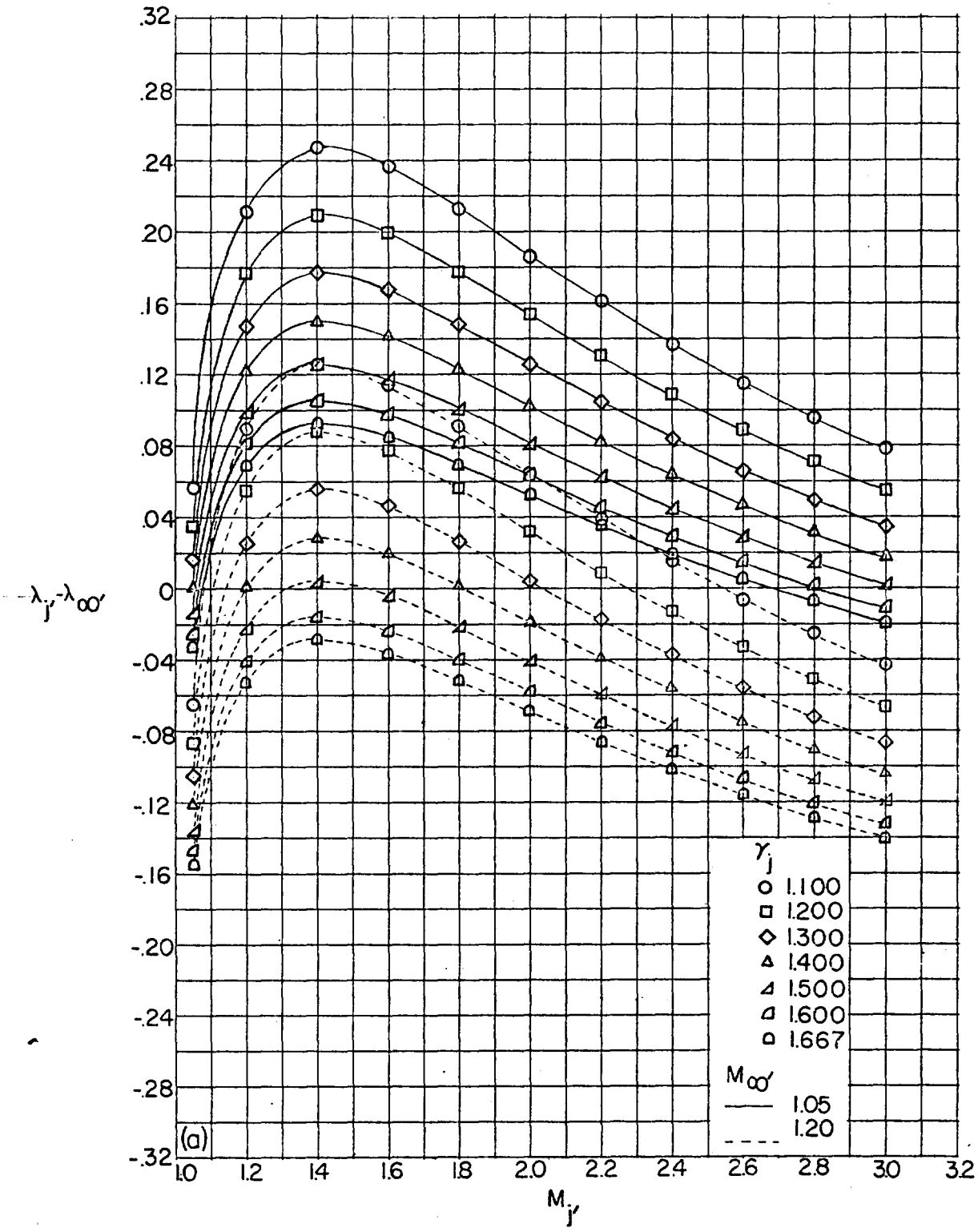

(a) $M_{\infty'}=1.05$ and 1.20.

FIGURE 63.—Variation of the Kawamura difference parameter with local Mach number at the boundary in the free jet and in the free stream for several ratios of specific heats of the jet.

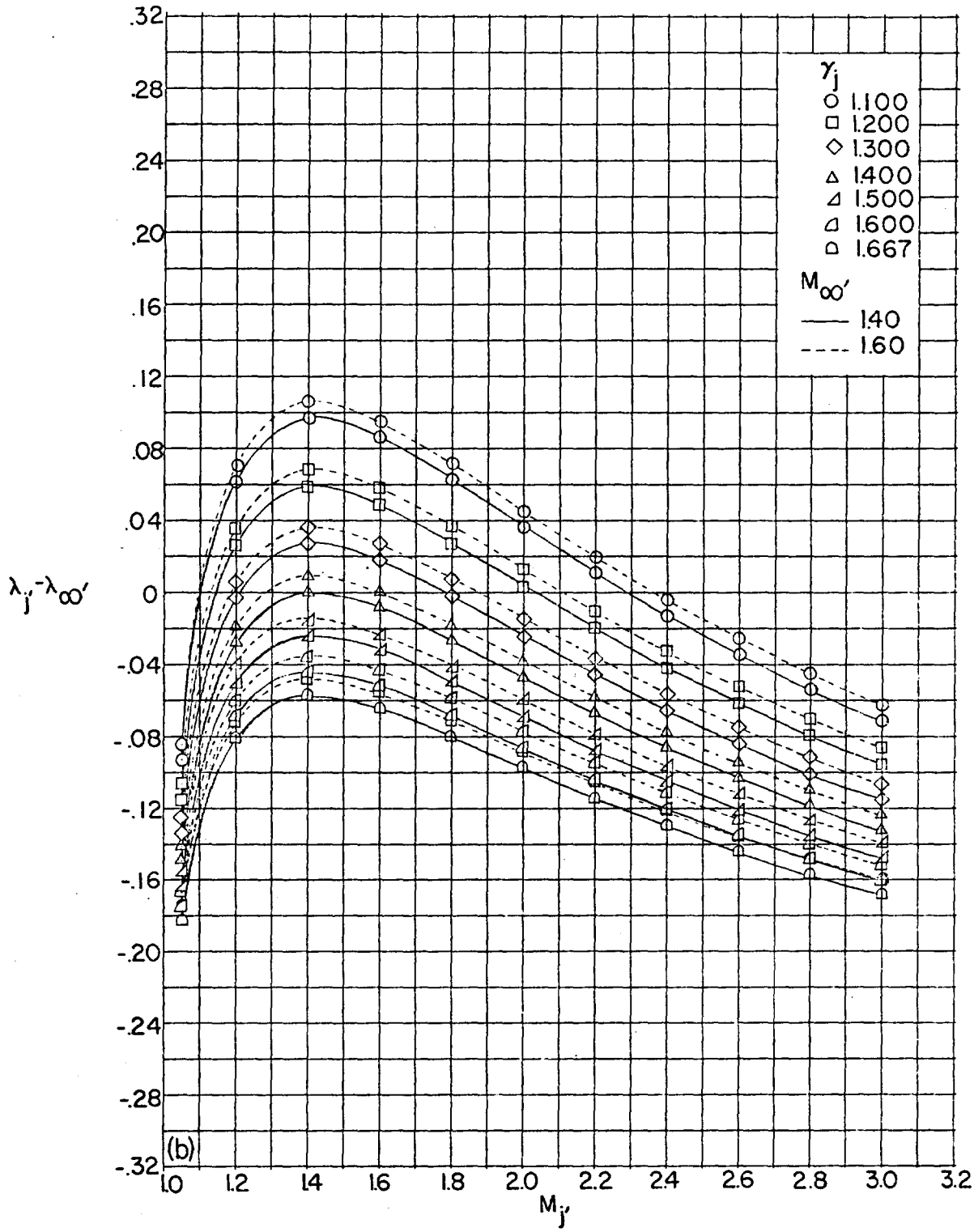

(b) $M_{\infty'}=1.40$ and 1.60.

FIGURE 63.—Continued.

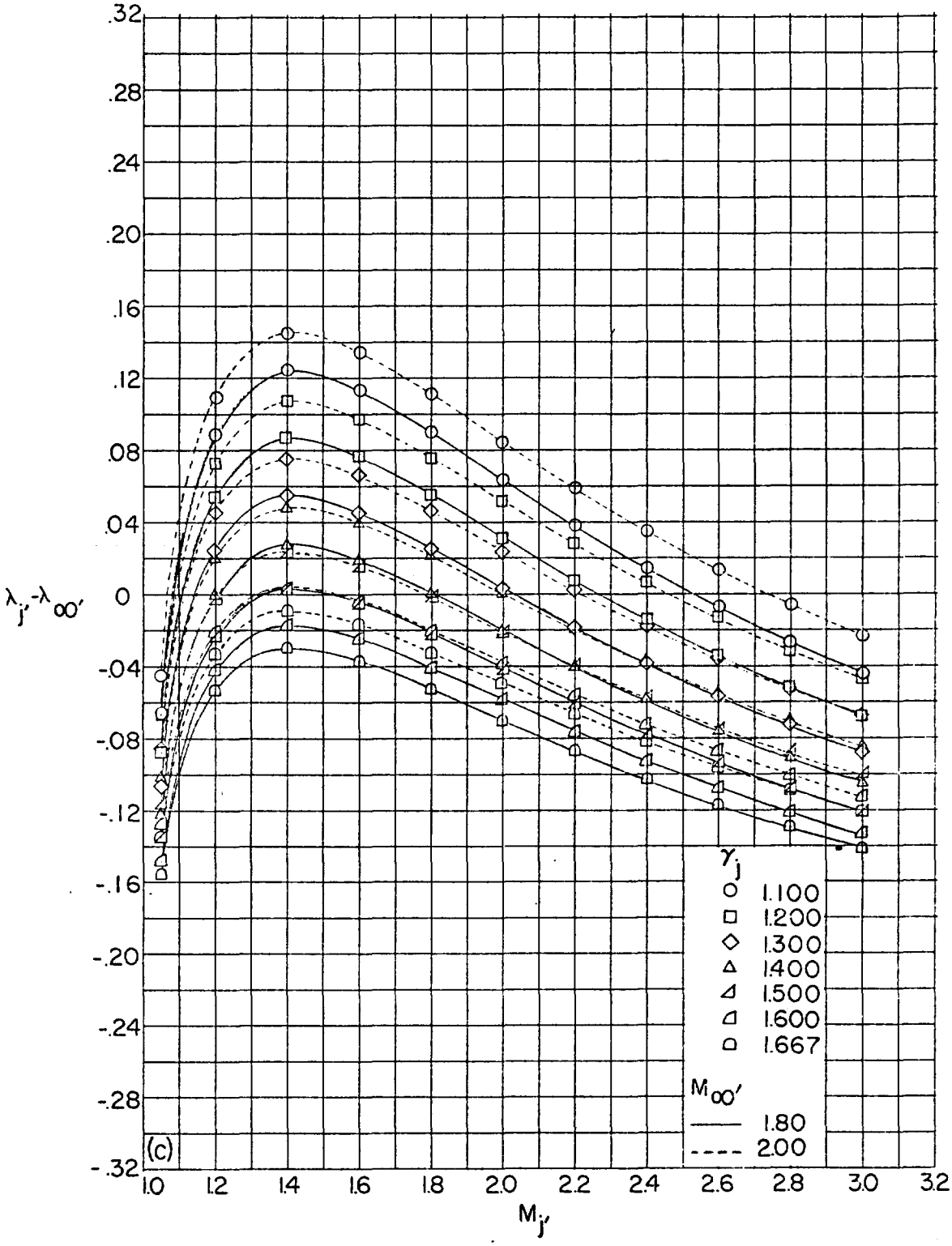

(c) $M_{\infty'} = 1.80$ and 2.00.

FIGURE 63.—Continued.

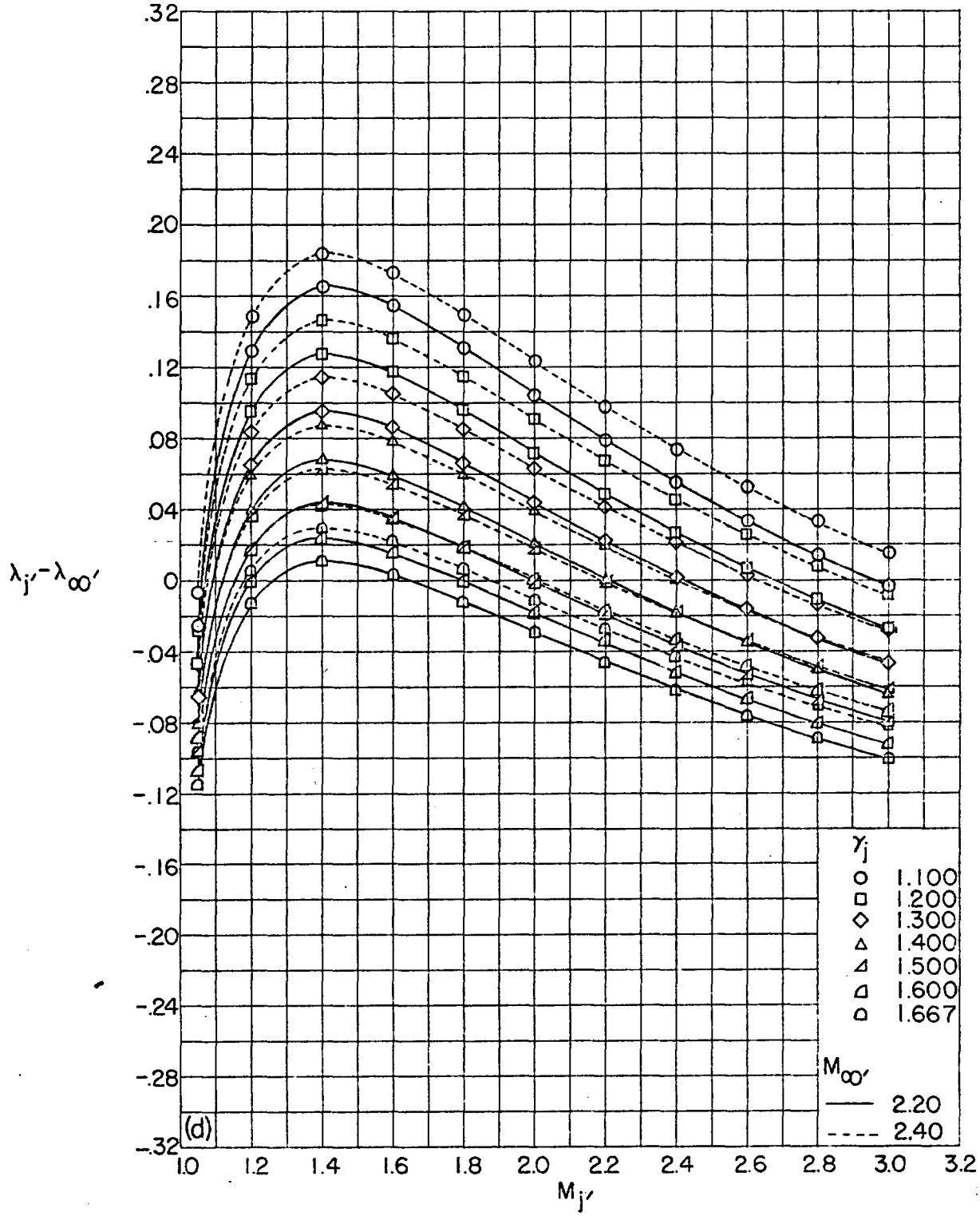

(d) $M_{\infty'}=2.20$ and 2.40.

FIGURE 63.—Continued.

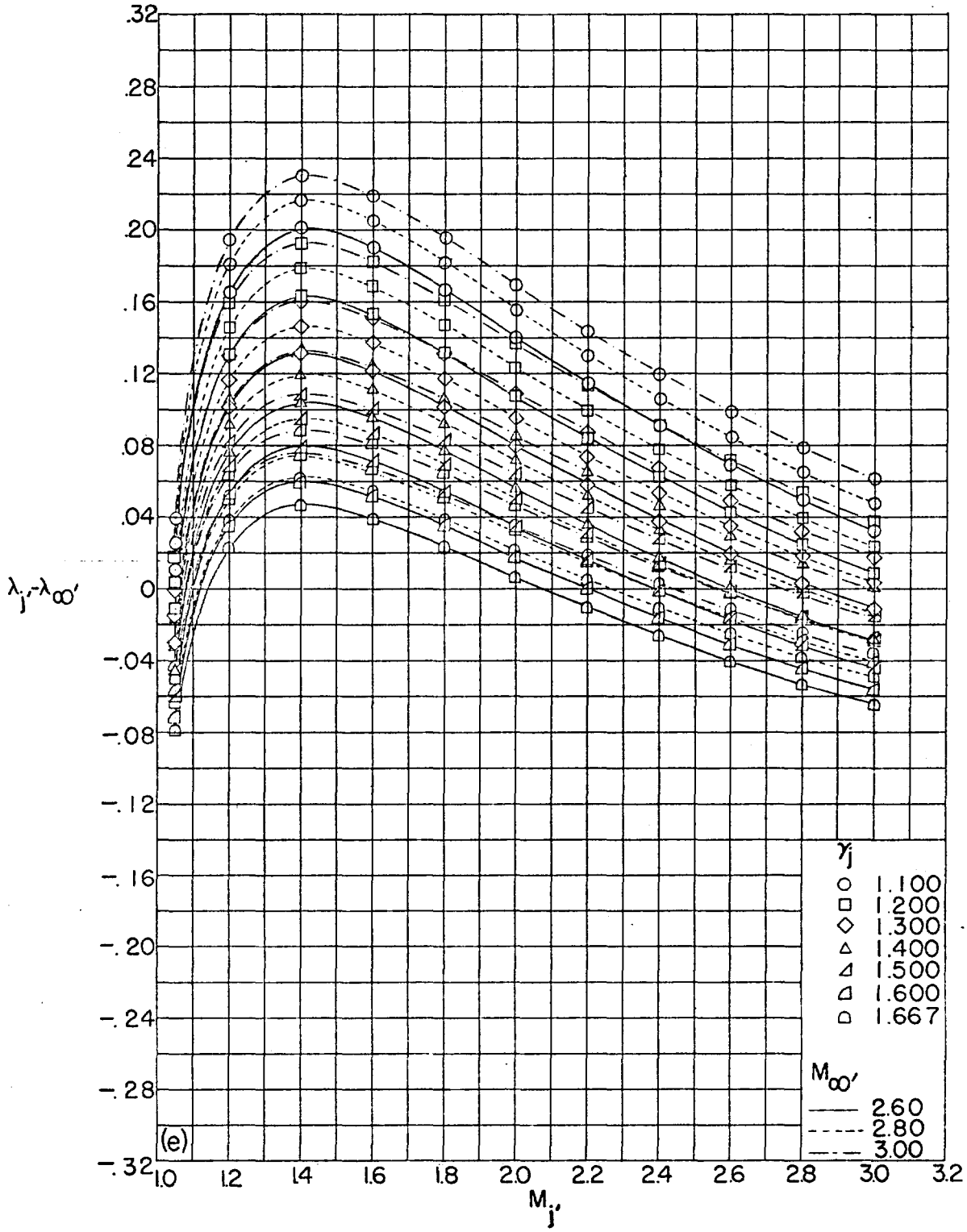

(c) $M_{\infty'}=2.60$, 2.80, and 3.00.

FIGURE 63.—Concluded.

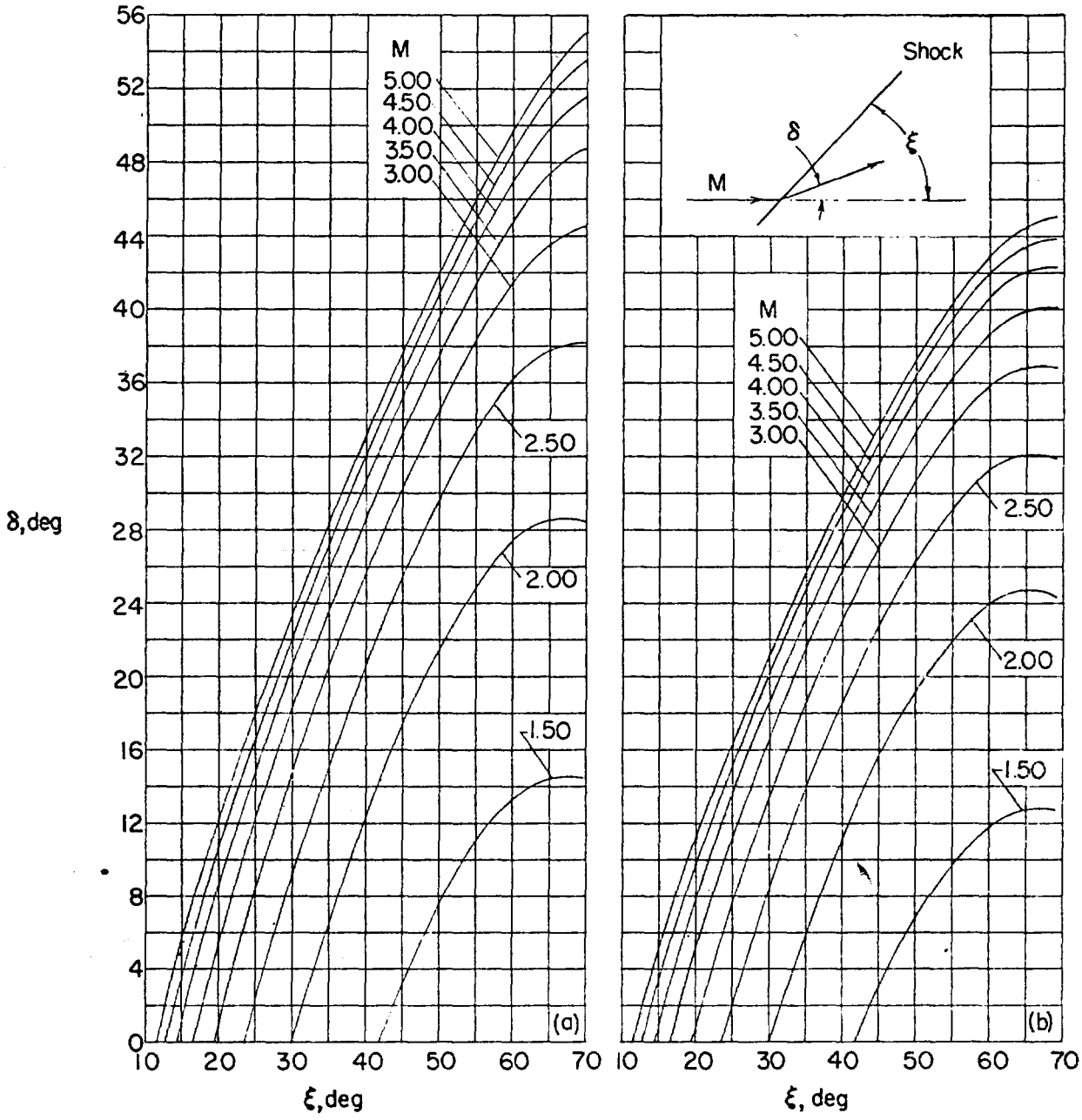

(a) $\gamma = 1.115$. (b) $\gamma = 1.300$.

FIGURE 64.—Variation of shock inclination with turning angle for several values of Mach number and ratio of specific heats.

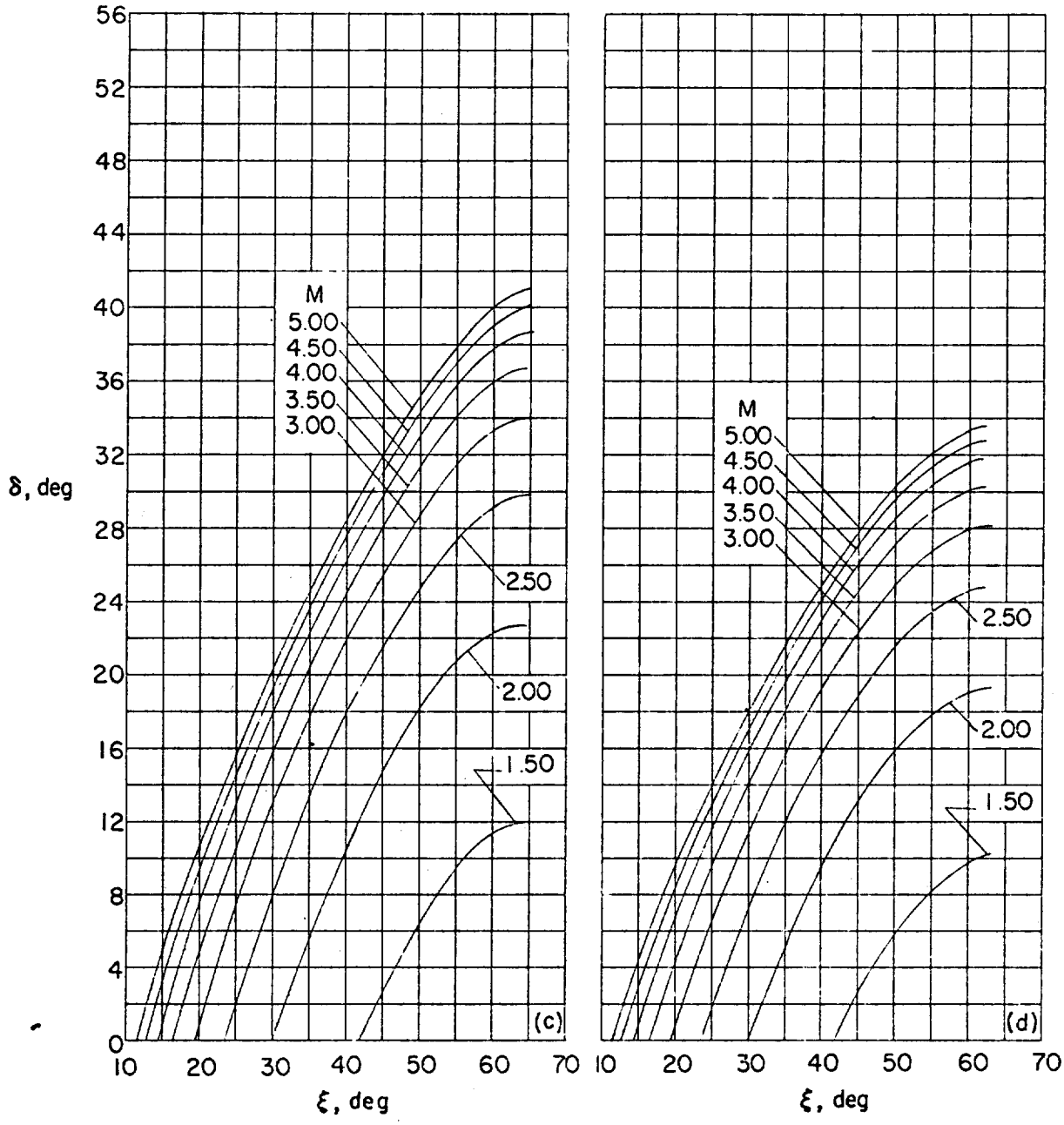

(c) $\gamma = 1.400$.

(d) $\gamma = 1.667$.

FIGURE 64.—Concluded.

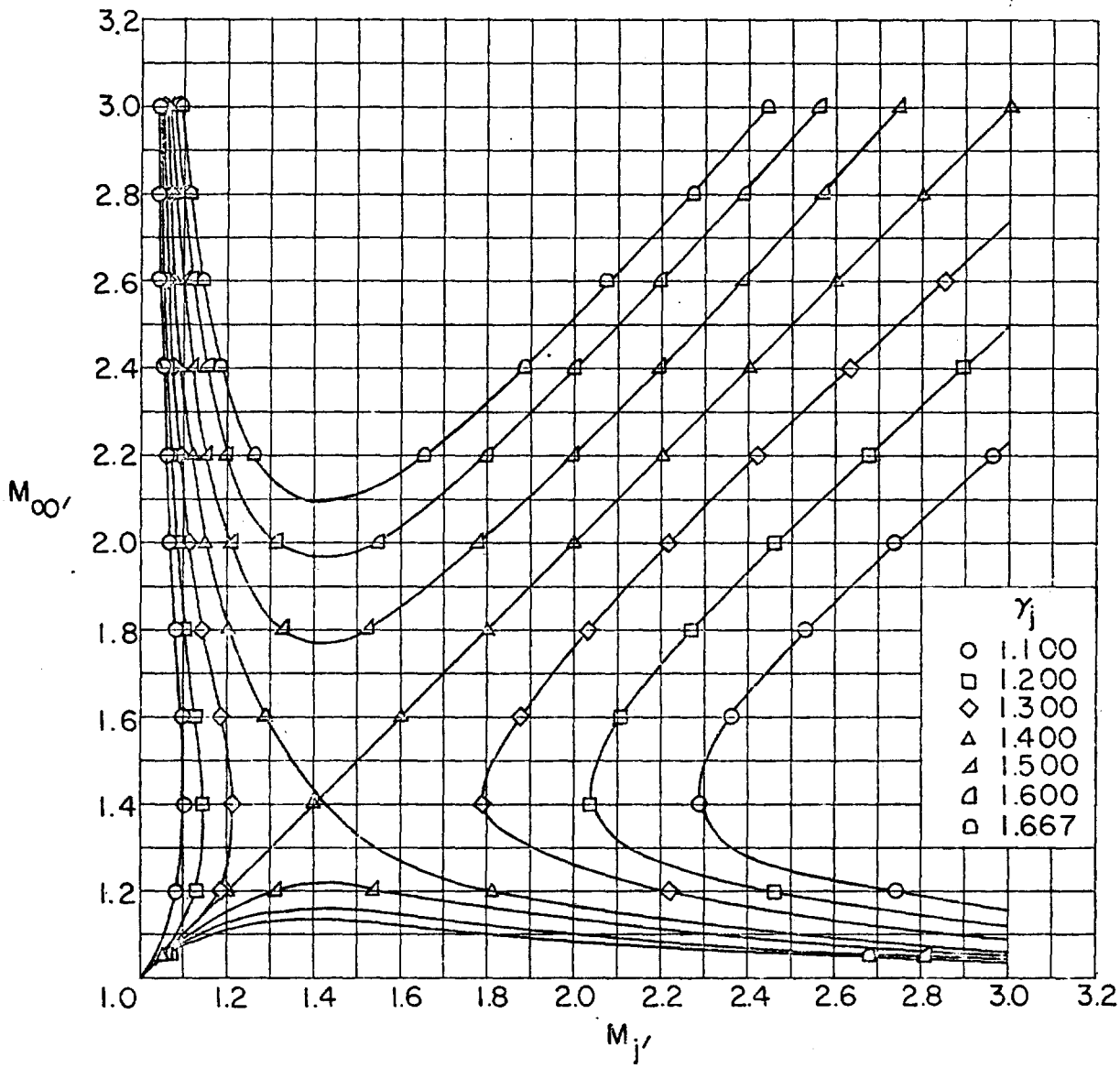

FIGURE 65.—Relation between the ratio of specific heats of the jet and the local Mach numbers at the boundary in the free jet and in the free stream for no reflection.

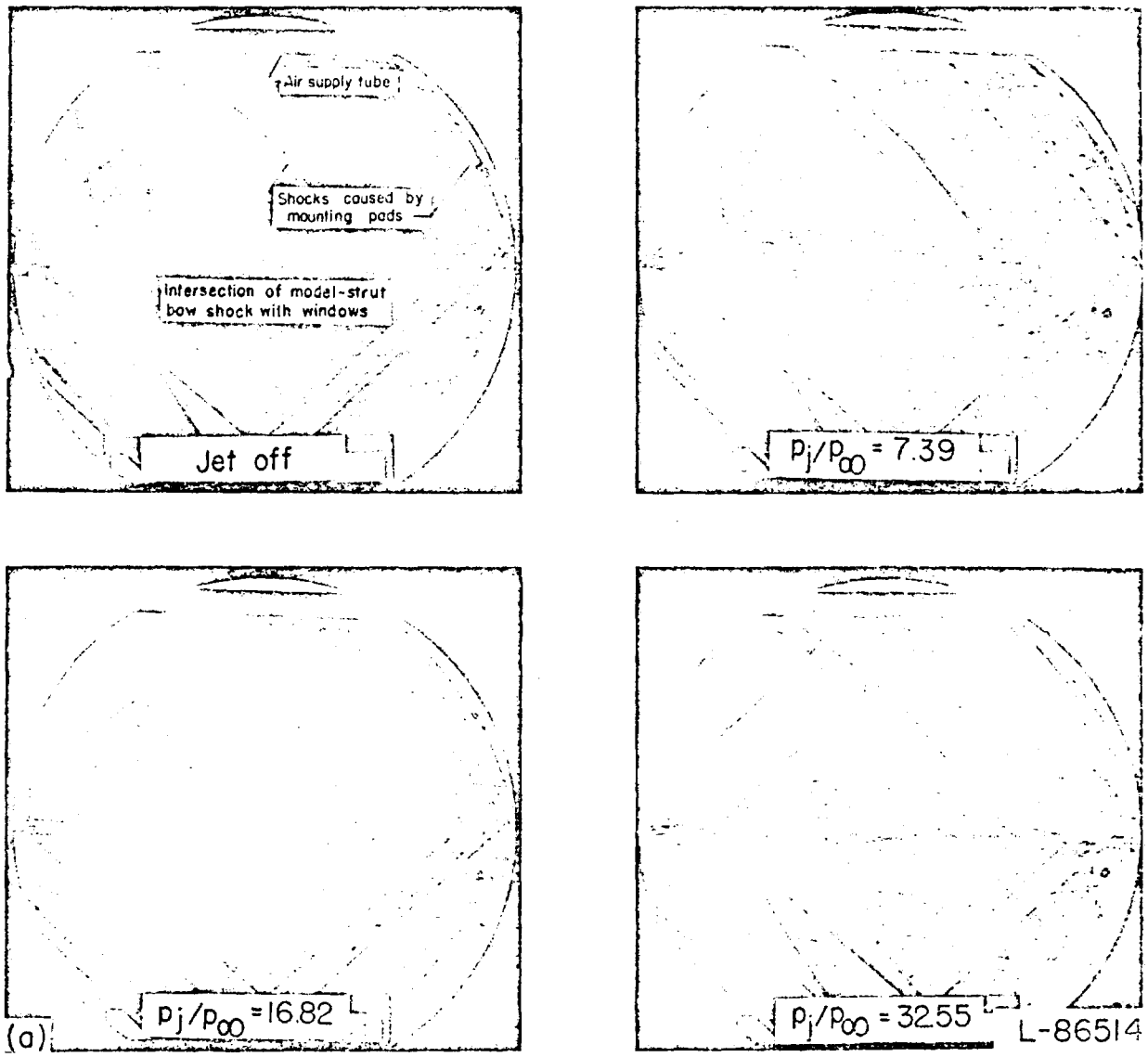

(a) $M_j = 1.00$; $\theta_N = 0°$.

FIGURE 66.—Schlieren photographs at a free-stream Mach number of 1.62 of jet exhausting from sonic and supersonic nozzle at varying jet pressure ratio.

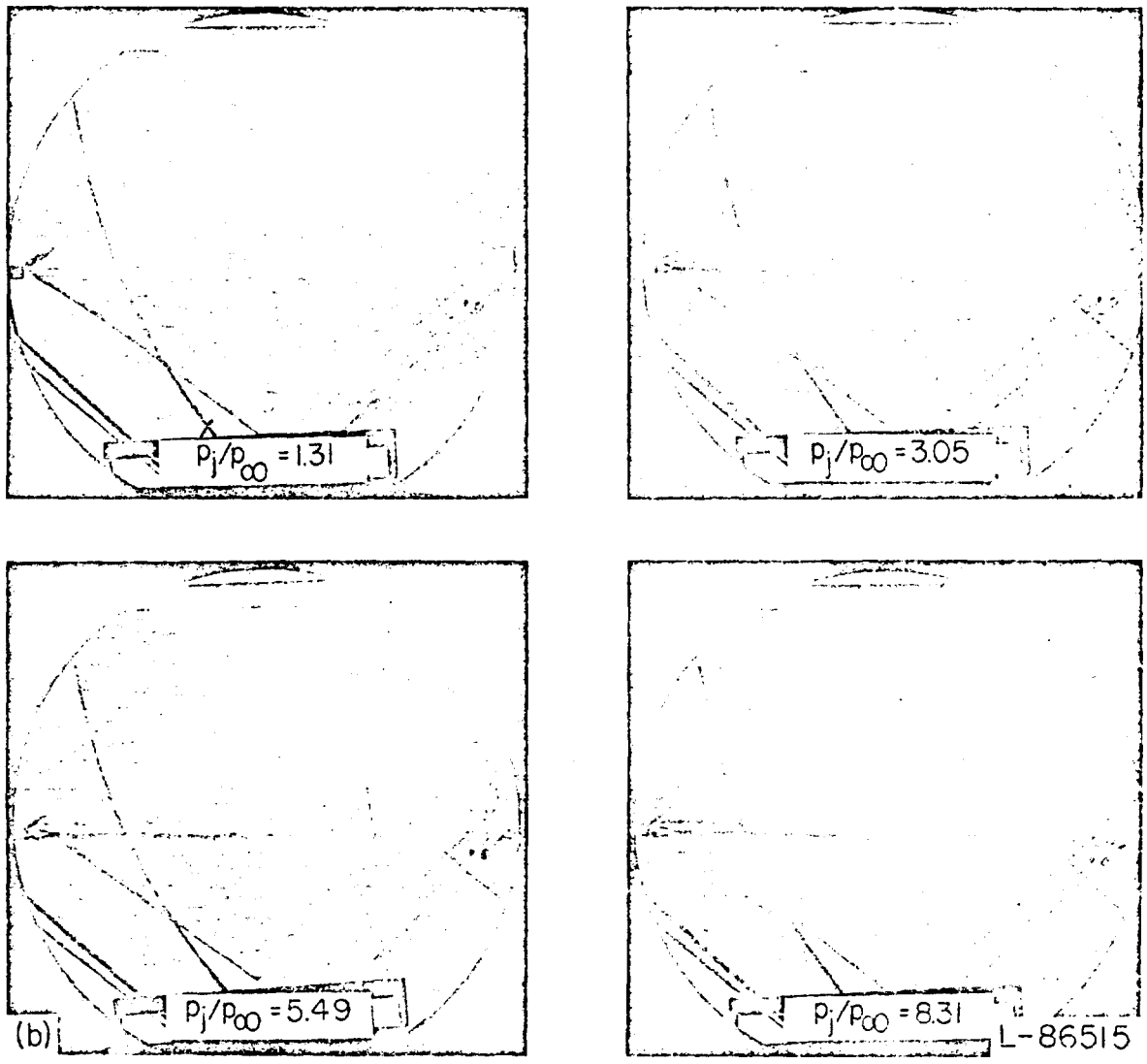

(b) $M_j = 2.50$; $\theta_N = 10°$.

FIGURE 66.—Concluded.

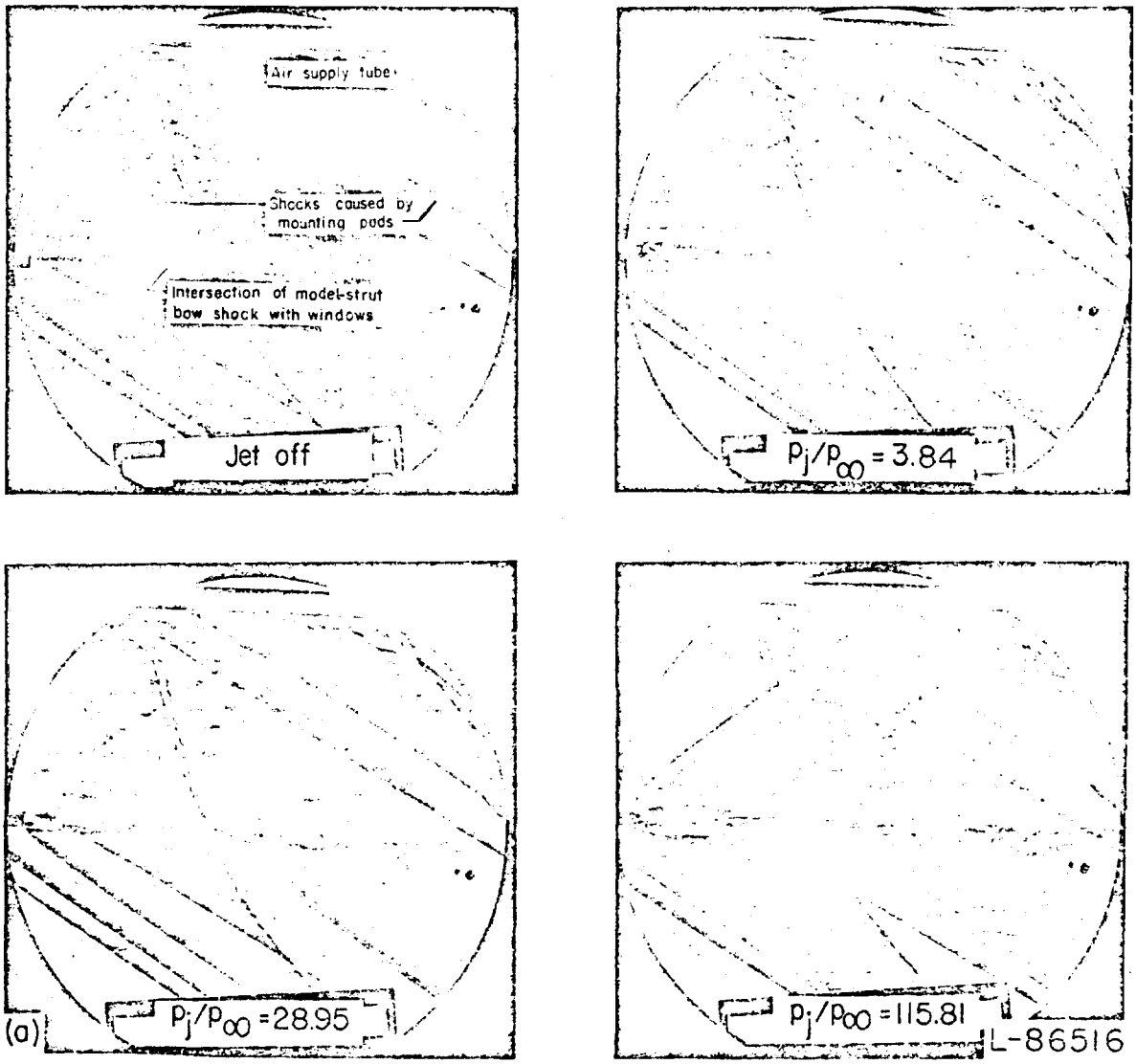

(a) $M_j = 1.00$; $\theta_N = 0°$.

FIGURE 67.—Schlieren photographs at a free-stream Mach number of 1.94 of jet exhausting from sonic and supersonic nozzle at varying jet pressure ratio.

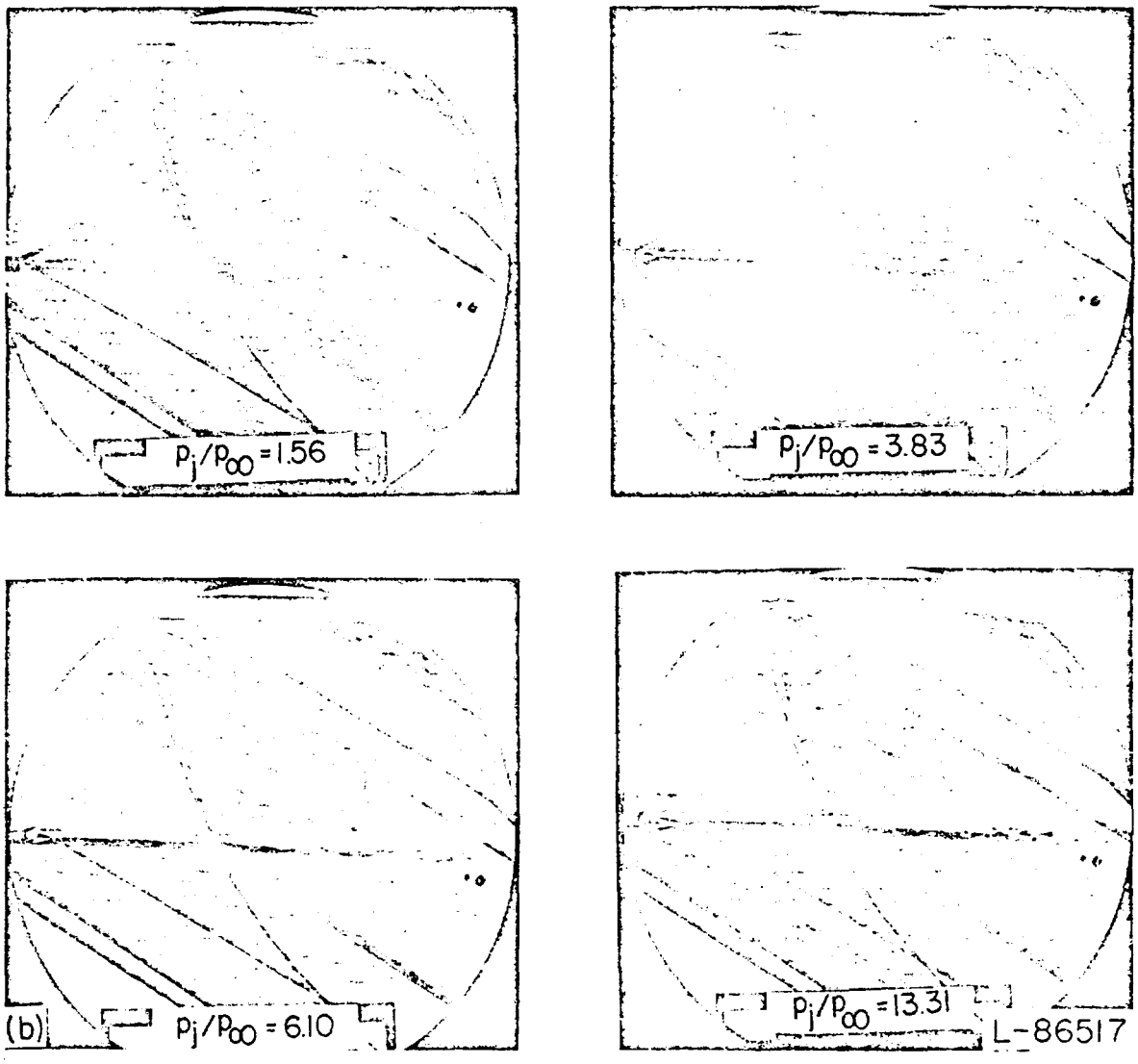

(b) $M_j = 2.50$; $\theta_N = 10°$.

FIGURE 67.—Concluded.

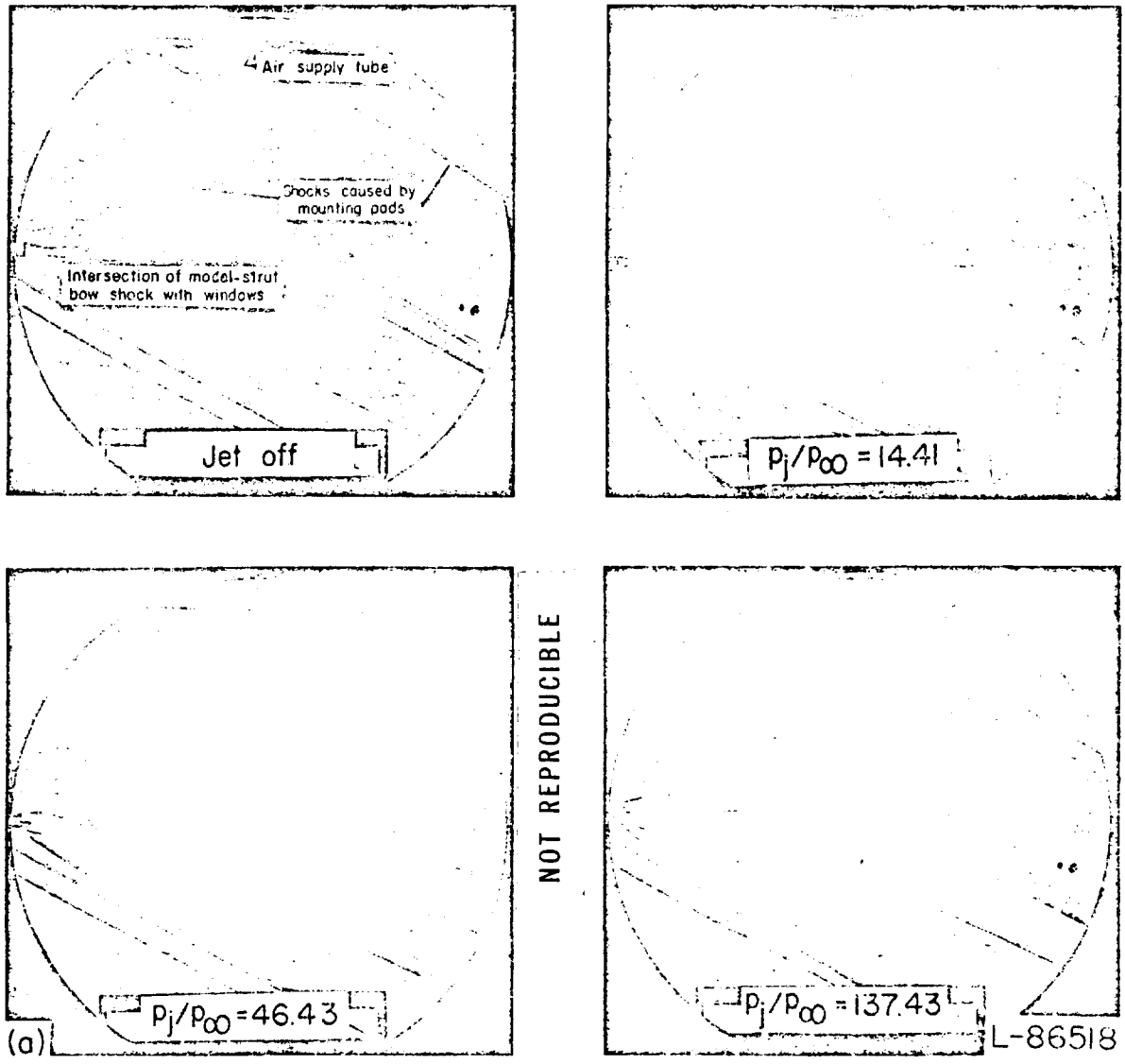

(a) $M_j = 1.00$; $\theta_N = 0°$.

FIGURE 68.—Schlieren photographs at a free-stream Mach number of 2.41 of jet exhausting from sonic and supersonic nozzle at varying jet pressure ratio.

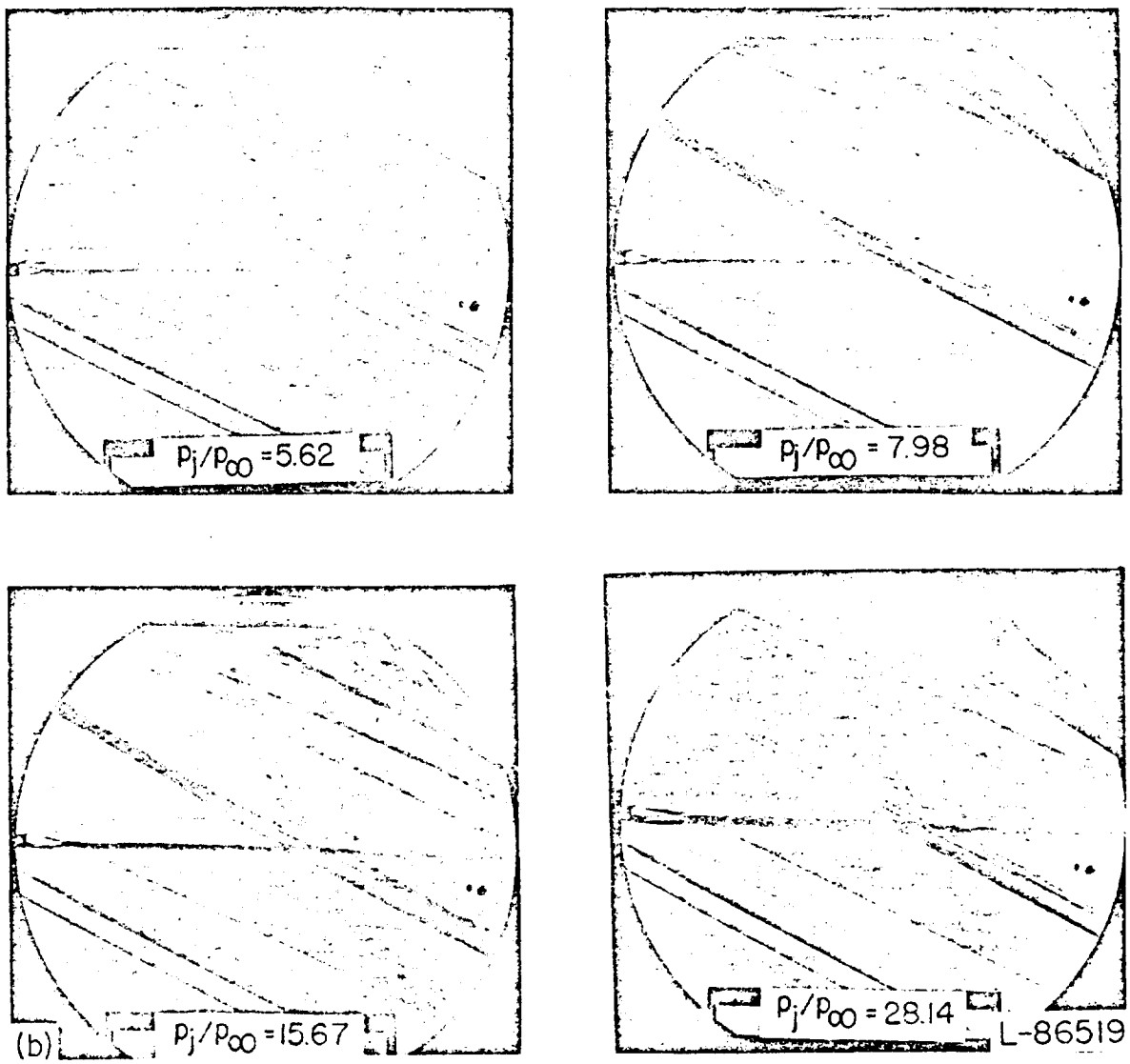

(b) $M_j = 2.50$; $\theta_N = 10°$.

FIGURE 68.—Concluded.

502683 O—59——19

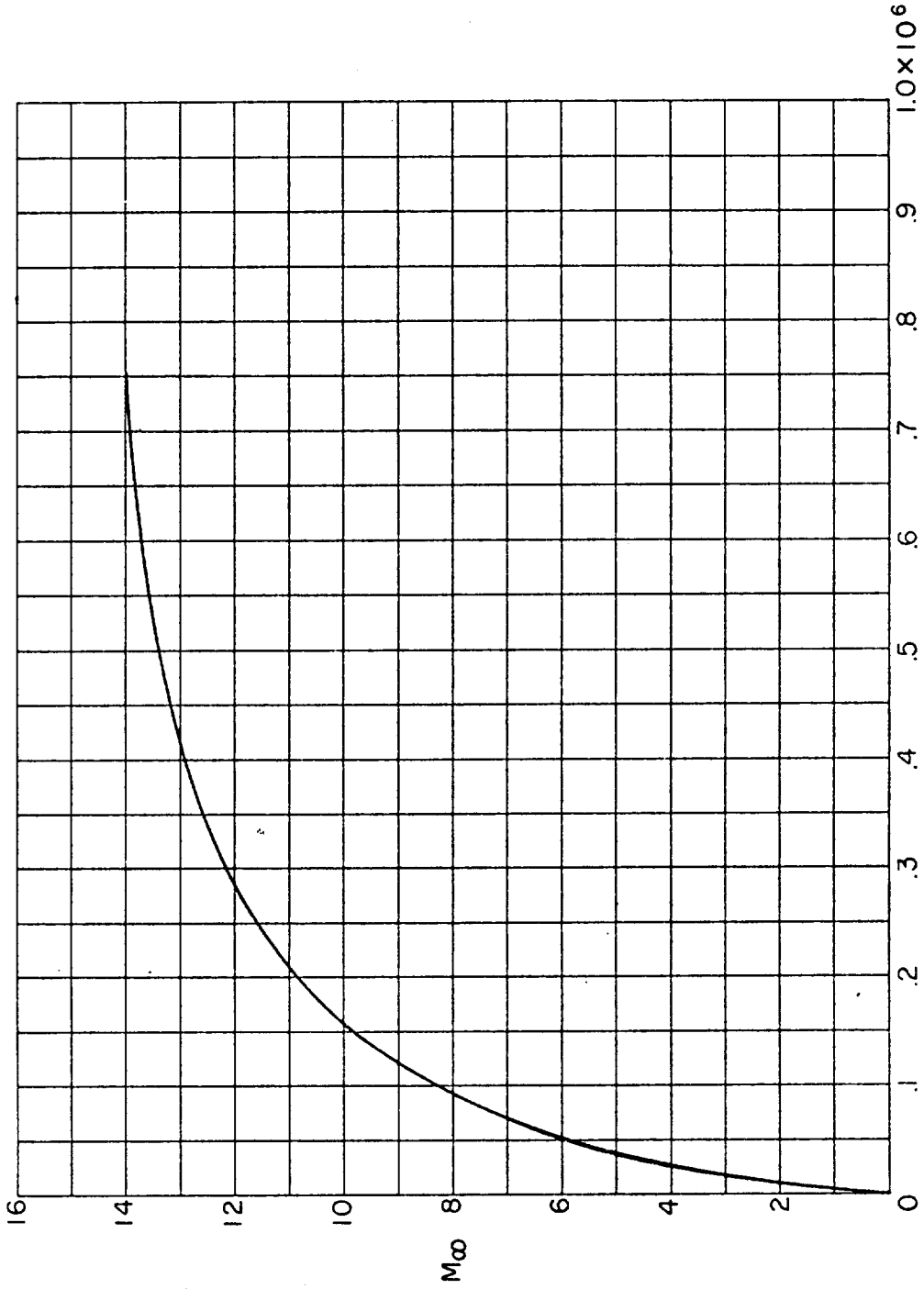

FIGURE 69.—Assumed Mach number—altitude variation of hypothetical vehicle.

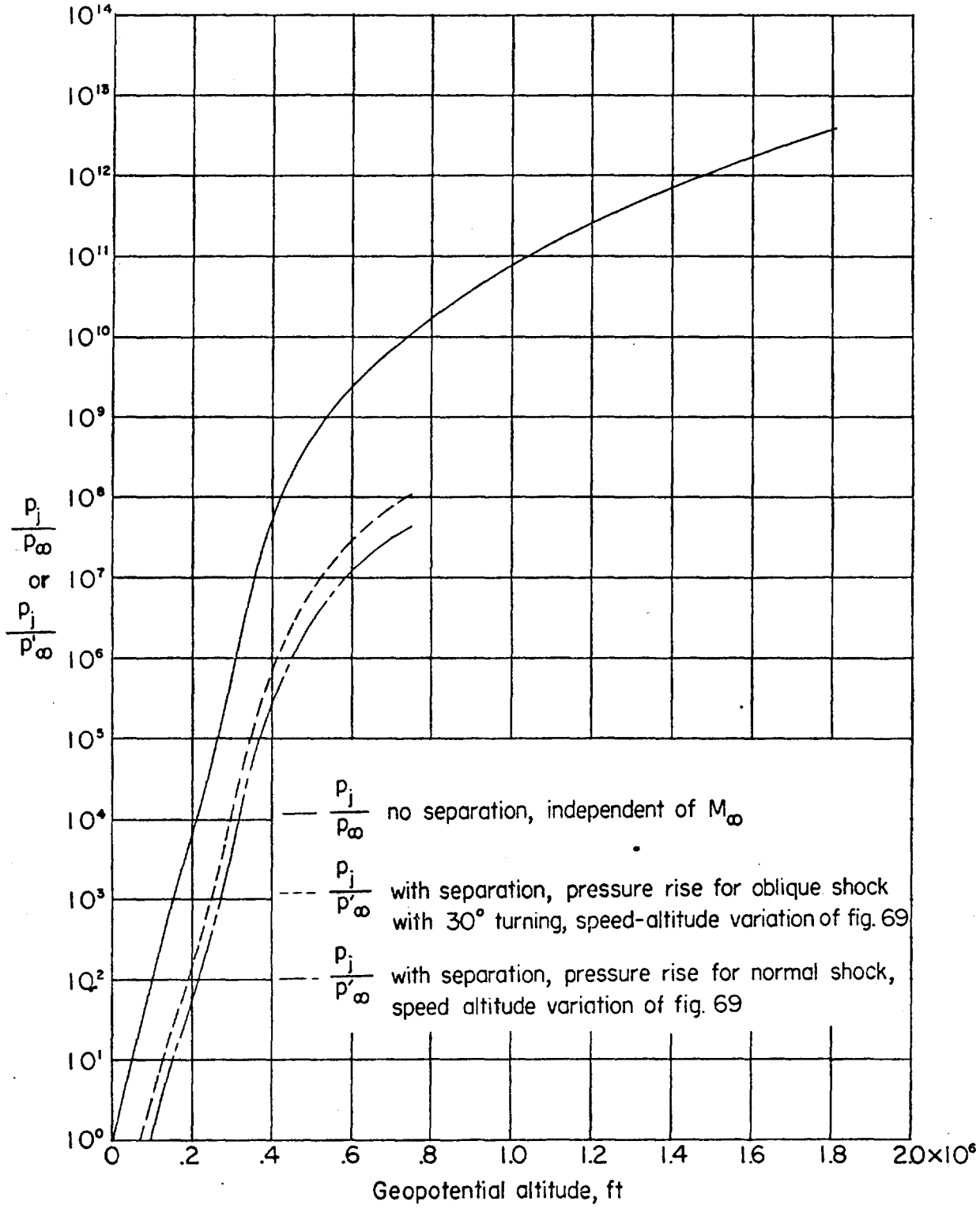

FIGURE 70.—Variation of pressure ratio with altitude. For all curves $p_i/p_\infty = 1$ at sea level, p_i is invariant with altitude, and p_∞ equals pressure at altitude.

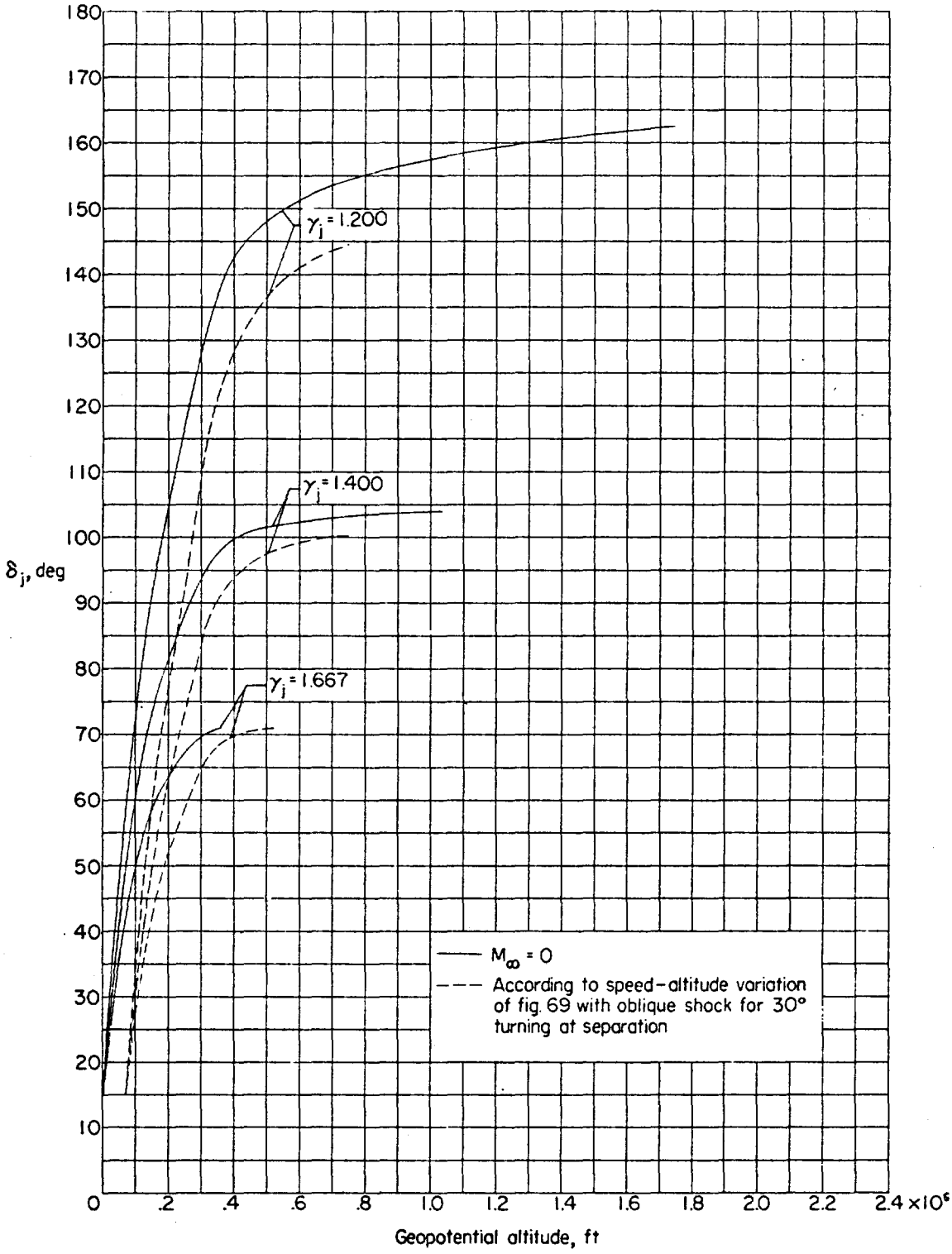

FIGURE 71.—Variation of initial inclination of boundary with altitude. $M_i = 2.5$; $\theta_N = 15°$.

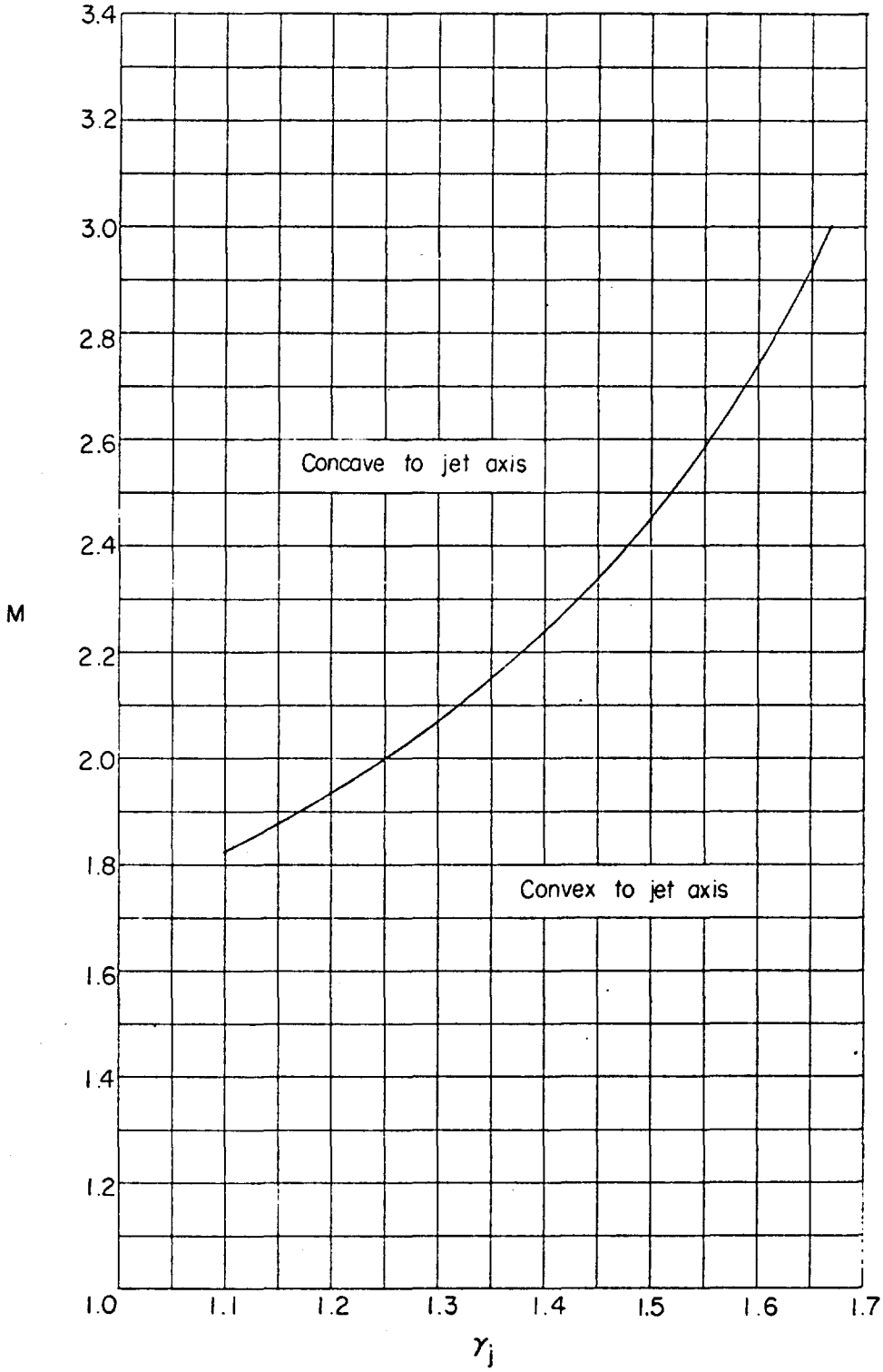

FIGURE 72.—Curvature of leading characteristic line in expansion of flow from conically divergent nozzles.

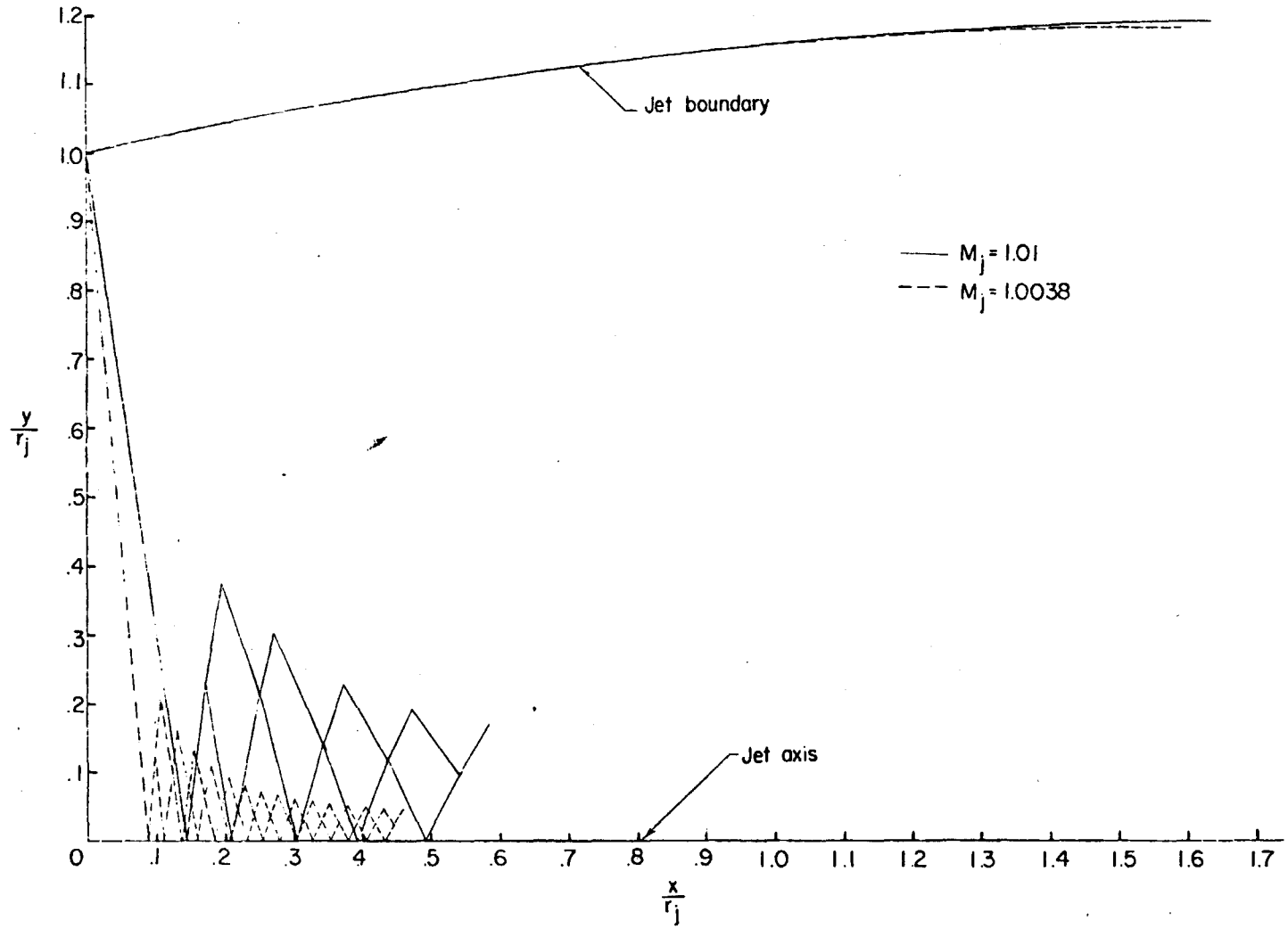

Figure 73.—Comparison of characteristic calculations for near-sonic exit to show effect of errors in flow field near jet axis upon jet boundary $\gamma_j = 1.400$; $p_j/p_\infty = 2$.

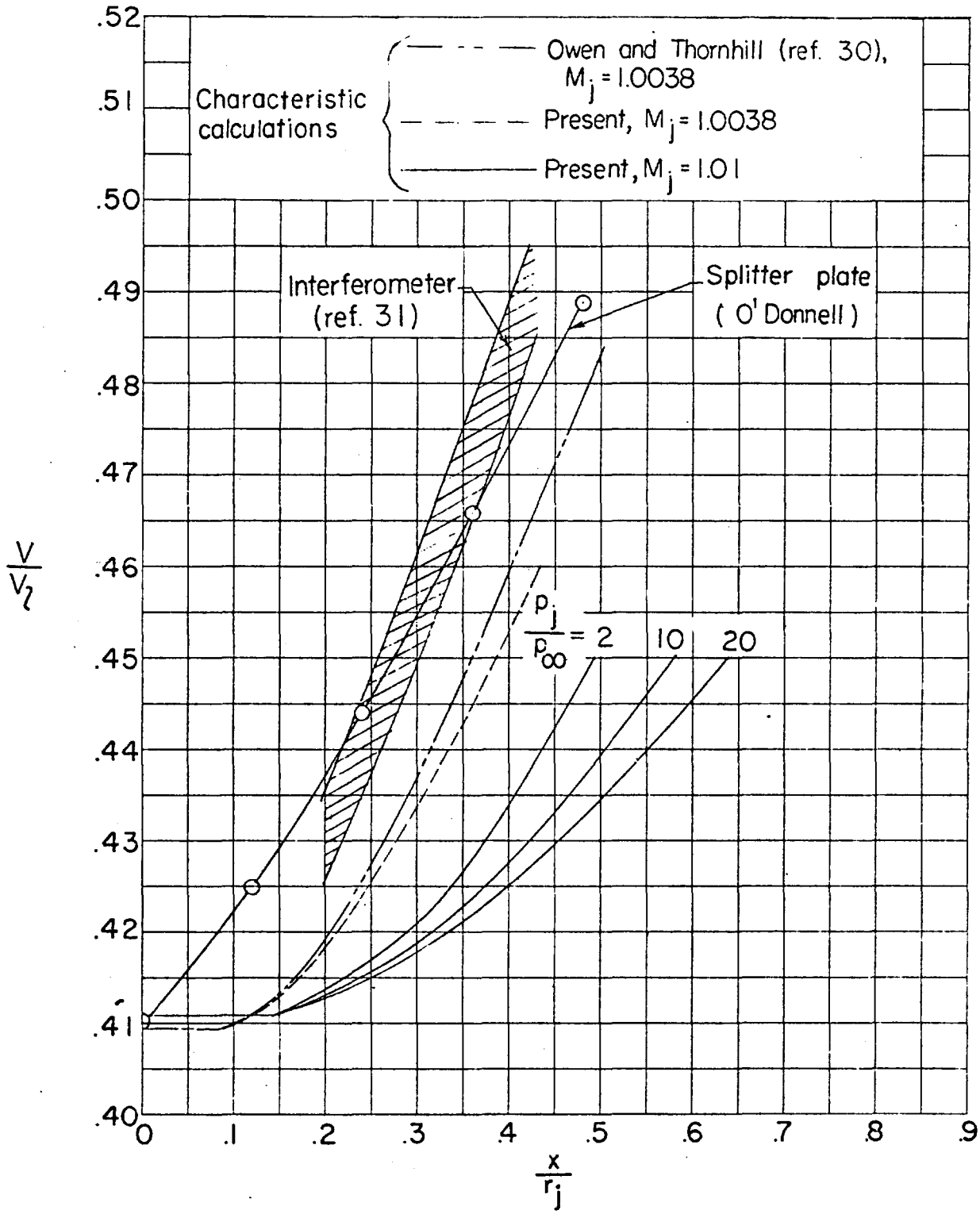

FIGURE 74.—Comparison of nondimensional velocity distributions along jet axis for sonic or near-sonic exits.

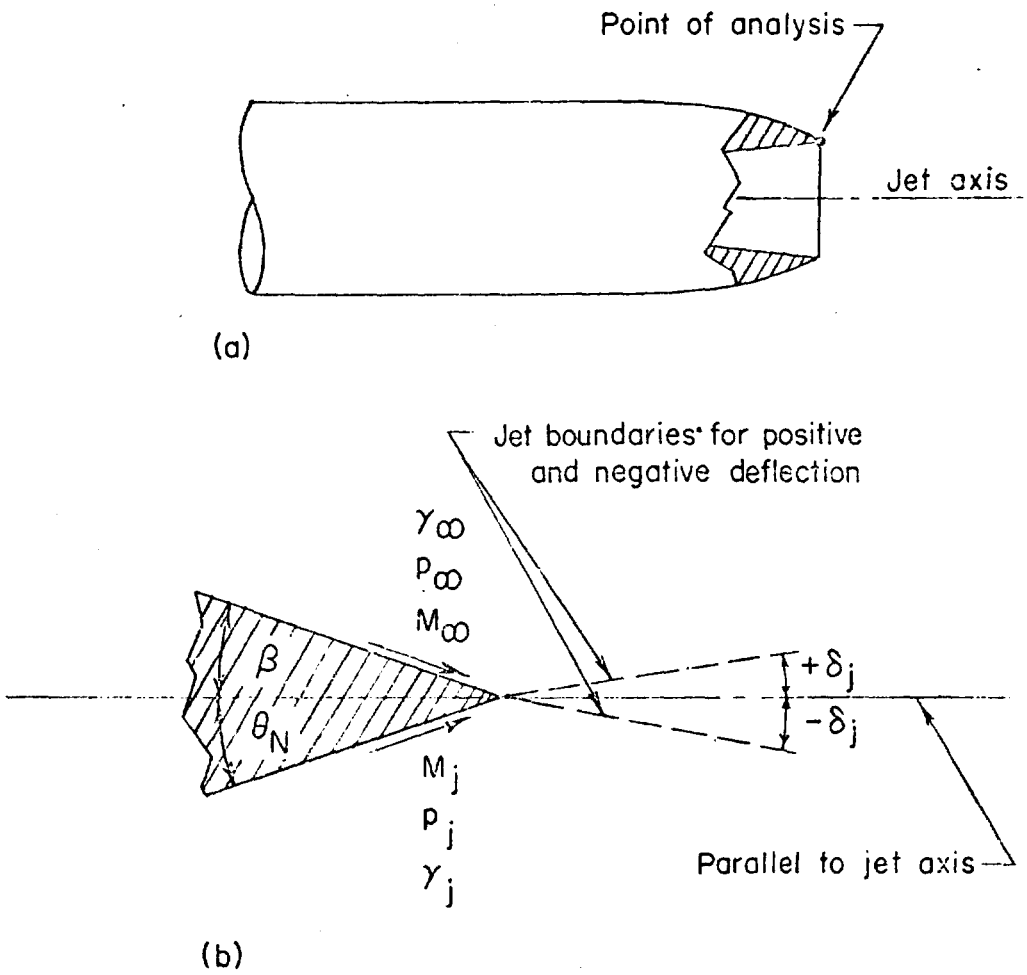

(a) Location of point of analysis.
(b) Magnification of point of analysis.

FIGURE 75.—Conditions of analysis used in present calculations.

U.S. GOVERNMENT PRINTING OFFICE : 1960 O—502601